



Université de Sherbrooke

**Étude de la modulation de l'épissage alternatif cellulaire lors de  
l'infection par réovirus**

Par  
Simon Boudreault  
Programme de biochimie

Thèse présentée à la Faculté de médecine et des sciences de la santé  
en vue de l'obtention du grade de philosophiae doctor (Ph.D.) en biochimie

Sherbrooke, Québec, Canada  
Septembre 2022

Membres du jury d'évaluation

Pr Martin Bisailon, département de biochimie et de génomique fonctionnelle  
Pr Guy Lemay, département de microbiologie, infectiologie et immunologie, Faculté  
de Médecine, Université de Montréal  
Pr François Bachand, département de biochimie et de génomique fonctionnelle  
Pr Nathalie Rivard, département d'immunologie et de biologie cellulaire  
Pr Tommy Alain, Department of Biochemistry, Microbiology and Immunology,  
Faculty of Medicine, University of Ottawa

© Simon Boudreault, 2022

## RÉSUMÉ

### Étude de la modulation de l'épissage alternatif cellulaire lors de l'infection par réovirus

Par  
Simon Boudreault  
Programme de doctorat en biochimie

Thèse présentée à la Faculté de médecine et des sciences de la santé en vue de l'obtention du diplôme de philosophiae doctor (Ph.D.) en biochimie  
Faculté de médecine et des sciences de la santé, Université de Sherbrooke,  
Sherbrooke, Québec, Canada, J1H 5N4

L'épissage alternatif (ÉA) est un processus de maturation des ARNm permettant de diversifier le potentiel codant provenant d'un même gène. L'ÉA modifie la séquence codante des ARNm en retirant des exons ou des parties d'exons, ou même en conservant des introns au sein de l'ARNm mature. L'ÉA est crucial pour la cellule, car il permet la production d'isoformes protéiques ayant des localisations cellulaires, des stabilités ou des régulations différentes. Il a été récemment démontré que plusieurs virus peuvent modifier l'ÉA des transcrits cellulaires. Cependant, notre compréhension du rôle de ce phénomène dans les interactions virus-hôte est encore limitée. Nous avons investigué si réovirus, un virus à ARN double-brin prometteur comme traitement contre le cancer, module l'ÉA lors de l'infection, le mécanisme de cette modulation ainsi que l'impact possible dans les interactions virus-hôtes. Nous avons identifié 240 événements d'ÉA altérés durant l'infection avec réovirus, qui se situent majoritairement dans des transcrits codant pour des protéines impliquées dans la régulation de l'expression génique ainsi que le métabolisme des ARN. Nous avons aussi identifié la protéine virale  $\mu 2$  comme étant le principal déterminant des changements d'ÉA causé par réovirus, et démontré que la protéine  $\mu 2$  par elle-même peut influencer l'ÉA. De plus, nous avons établi que des composantes du splicéosome, et plus particulièrement EFTUD2, PRPF8 et SNRNP200 du complexe U5, interagissent avec  $\mu 2$  et sont requises pour que réovirus module l'ÉA cellulaire. Finalement, les niveaux de ces protéines sont réduits durant l'infection par la protéine  $\mu 2$ . Nous avons par la suite déterminé les rôles respectifs d'EFTUD2, de PRPF8 et de SNRNP200 dans la réplication de réovirus et découvert des rôles distincts et qui se recoupent partiellement sur la survie cellulaire, l'apoptose, la nécroptose, l'induction de la réponse interféron, et la réplication du virus. Ces résultats démontrent l'importance de l'ÉA dans les interactions virus-hôte ainsi que l'implication des protéines du complexe U5 dans la réplication de réovirus.

**Mots clés:** Épissage alternatif, virus, splicéosome, U5 snRNP, réovirus, séquençage d'ARN à haut-débit, apoptose, nécroptose.

## SUMMARY

### Deciphering the modulation of cellular alternative splicing during reovirus infection

By  
Simon Boudreault  
Biochemistry Doctoral Program

Thesis presented at the Faculty of medicine and health sciences for the obtention of Doctor degree diploma philosophiae doctor (Ph.D.) in biochemistry  
Faculty of medicine and health sciences, Université de Sherbrooke, Sherbrooke,  
Québec, Canada, J1H 5N4

Alternative splicing (AS) is an RNA maturation process allowing enhanced diversity in mature messenger RNA originating from the same gene. AS modifies the mRNA's coding potential by removing exons or parts of exon, or even retaining introns in the mature RNA. AS is crucial in cells as it enables the production of proteins isoforms with different cellular localization, stability, and regulation. Recent evidence suggests that viruses alter cellular AS during infection, although our understanding of the role of these changes remains limited. We investigated if mammalian orthoreovirus (MRV), a double-stranded RNA virus from the *Reoviridae* family presenting a promising activity as an oncolytic virus, alters the host cell AS during infection, the mechanism of this modulation, and the possible impacts of these virus-host interactions on MRV replication. We identified 240 altered AS events upon MRV infection which belong to transcripts involved in the regulation of gene expression and RNA metabolism. We identified the viral protein  $\mu 2$  as the main determinant of MRV's alterations in cellular AS, and we showed that  $\mu 2$ , by itself, could impact cellular AS. Moreover, we discovered that central components of the U5 snRNP of the spliceosome EFTUD2, PRPF8, and SNRNP200 interacts with  $\mu 2$ , and are required for MRV modulation of AS. Finally, these U5 snRNP components are reduced at the protein level during MRV infection by the  $\mu 2$  protein. We then deciphered the respective impact of EFTUD2, PRPF8, and SNRNP200 on MRV replication. We discovered distinct and partially overlapping novel roles for EFTUD2, PRPF8, and SNRNP200 in cell survival, apoptosis, necroptosis, and the induction of the interferon response pathway during MRV infection. Moreover, we demonstrated that EFTUD2 restricts viral replication of MRV, both in a single cycle and multiple cycles of viral replication. These findings provide additional insights into the importance of AS in the complexity of virus-host interactions and the implications of U5 snRNP proteins in MRV replication.

**Keywords:** Alternative splicing, virus, spliceosome, U5 snRNP, reovirus, high-throughput RNA-sequencing, apoptosis, necroptosis.

## TABLE DES MATIERES

<b>Résumé</b> .....	<b>ii</b>
<b>Summary</b> .....	<b>iii</b>
<b>Table des matières</b> .....	<b>iv</b>
<b>Liste des figures</b> .....	<b>vii</b>
<b>Liste des tableaux</b> .....	<b>ix</b>
<b>Liste des abréviations</b> .....	<b>x</b>
<b>Introduction</b> .....	<b>1</b>
<b>Avant-propos</b> .....	<b>1</b>
<b>Les virus</b> .....	<b>1</b>
Interaction virus-hôte .....	2
Réponse antivirale cellulaire .....	3
Mort cellulaire programmée .....	4
Apoptose .....	4
Nécroptose .....	5
Pathologies causées par des virus .....	7
Cancer .....	8
Utilisation des virus .....	9
Virus oncolytiques .....	10
Vecteurs viraux .....	12
<b>Réovirus</b> .....	<b>13</b>
Généralités .....	13
Cycle de réplication .....	14
La protéine $\mu 2$ .....	17
Activité oncolytique de réovirus .....	20
<b>L'épissage</b> .....	<b>22</b>
L'épissage constitutif et alternatif .....	22
Le spliceosome et la réaction d'épissage .....	25
Importance des régions régulatrices dans l'épissage alternatif .....	27
Épissage alternatif et maladies .....	29
Cancer .....	29
Analyse de l'épissage alternatif .....	30

Approches ciblées .....	31
Approches non ciblées/à haut débit.....	33
Outils moléculaires permettant l'analyse fonctionnelle de l'épissage alternatif.....	35
<b>Les virus et l'épissage alternatif.....</b>	<b>36</b>
Utilisation de la machinerie d'épissage pour épisser les ARN viraux .....	36
Impact des virus sur l'épissage alternatif cellulaire .....	36
<b>Hypothèse/problématique.....</b>	<b>42</b>
Objectifs .....	42
<b>Résultats .....</b>	<b>43</b>
<b>Article 1: Global Profiling of the Cellular Alternative RNA Splicing Landscape during Virus-Host Interactions .....</b>	<b>43</b>
<b>Article 2: Reovirus <math>\mu</math>2 protein modulates host cell alternative splicing by reducing protein levels of U5 snRNP core components.....</b>	<b>113</b>
<b>Article 3: U5 snRNP core proteins are key components of the defense response against viral infection through their roles in programmed cell death and interferon induction.....</b>	<b>190</b>
<b>Discussion.....</b>	<b>243</b>
<b>Implication des protéines cellulaires dans la réplication de réovirus.....</b>	<b>244</b>
CCAR2 et RBM14 .....	245
Le complexe TRiC.....	247
CAMK2D et CAMK2G .....	248
ESRP1 .....	250
<b>Rôle et dynamique de la protéine <math>\mu</math>2 et du polymorphisme P208S .....</b>	<b>253</b>
Dynamique d'import nucléaire et d'export de $\mu$ 2.....	253
Ubiquitylation de $\mu$ 2 .....	255
Structure .....	257
Expression ectopique .....	258
<b>Modulation et rôle de l'épissage alternatif dans la réplication virale.....</b>	<b>261</b>
Modulation de l'épissage alternatif par réovirus.....	262
Rôle de la modulation de l'épissage alternatif par réovirus.....	264
Implication dans l'activité oncolytique.....	265
Modulation et rôle de l'épissage alternatif dans la réplication d'autres virus.....	266
<b>Le complexe U5.....</b>	<b>267</b>
Importance d'U5 dans la modulation de l'épissage alternatif par réovirus et $\mu$ 2 .....	267
Rôle de protéines de complexe U5 dans la mort cellulaire programmée.....	271

<b>Conclusion</b> .....	<b>275</b>
<b>Remerciements</b> .....	<b>276</b>
<b>Liste des références</b> .....	<b>278</b>
<b>Annexes</b> .....	<b>313</b>

## LISTE DES FIGURES

### Introduction

Figure 1. Schéma de la voie de signalisation menant à la nécroptose.....	6
Figure 2. Morphologie filamenteuse ou globulaire des VF de réovirus .....	17
Figure 3. Schéma et structure de la protéine $\mu 2$ .....	18
Figure 4. Schéma de l'épissage alternatif du gène <i>BCL2L</i> .....	23
Figure 5. Schéma des différents types d'épissage alternatif.....	24
Figure 6. Schéma de la réaction d'épissage ainsi que des régions requises dans l'ARN pré-messager.....	26
Figure 7. Schéma des régions régulatrices de l'épissage alternatif.....	28
Figure 8. Schéma des différentes manières de placer des amorces pour analyser l'épissage alternatif.....	32

### Chapitre 1

Figure 1. Transcriptomic studies of cells infected with reovirus.....	50
Figure 2. Global profiling of the cellular alternative splicing landscape and identification of differentially spliced ASEs during virus-host interactions.....	52
Figure 3. Validation of ASEs dysregulated in infected cells.....	54
Figure 4. Characterization of the ASEs that are modified upon viral infection .....	57
Figure 5. Proteomic analysis of uninfected and reovirus-infected cells. ....	59
Figure 6. Proteins involved in RNA splicing. ....	60

### Chapitre 2

Figure 1. The interferon response is not necessary nor sufficient to trigger AS changes during MRV infection.....	131
Figure 2. The modulation of AS occurs in a time-dependent manner during MRV infection .....	133
Figure 3. Strain-dependent modulation of AS segregates with the M1 gene segment and is dictated by a polymorphism at position 208 in $\mu 2$ .....	135
Figure 4. $\mu 2$ directly impacts the AS of minigene reporters in ectopic expression through both nuclear-dependent and nuclear-independent mechanisms.....	139
Figure 5. IP-MS of GFP-tagged $\mu 2$ reveals interaction with core components of the U5 spliceosomal snRNP .....	142
Figure 6. U5 core components are required for MRV modulation of cellular AS and are reduced during infection by $\mu 2$ .....	145
Figure 7. Model depicting how MRV infection leads to alterations in the host cell AS ..	148

### Chapitre 3

Figure 1. <i>EFTUD2</i> and <i>SNRNP200</i> KD protect cells from death after MRV infection.....	198
Figure 2. <i>EFTUD2</i> and <i>SNRNP200</i> depletion hamper apoptosis .....	201
Figure 3. Depletion of <i>EFTUD2</i> and <i>SNRNP200</i> impacts necroptosis.....	203
Figure 4. Depletion of U5 snRNP core components impacts the mRNA level, protein levels, and alternative splicing of necroptotic regulators .....	205



Figure 5. <i>EFTUD2 and PRPF8 control the interferon response during MRV infection...</i>	207
Figure 6. <i>EFTUD2 restricts MRV's replication in both single cycle and multiple cycles of replication.....</i>	210
Figure 7. <i>Summary of the involvement of U5 snRNP core proteins in virus-host interactions.....</i>	213

## **Discussion**

Figure 1. <i>Interaction de <math>\mu 2</math> avec CCAR2 et RBM14 et localisation de RBM14 durant l'infection avec réovirus.....</i>	246
Figure 2. <i>ESRP1 est un ISG induit par l'interéron durant l'infection avec réovirus.....</i>	252
Figure 3. <i>Impact de la co-expression de <math>\mu NS</math> sur la localisation cellulaire de <math>\mu 2</math> .....</i>	256
Figure 4. <i>Impact du polymorphisme P208S sur l'ubiquitylation et la structure de <math>\mu 2</math> .....</i>	257
Figure 5. <i>Impact des séquences déstabilisatrices dans la région codante de <math>\mu 2</math> sur le niveau d'ARNm .....</i>	260
Figure 6. <i>Impact des constructions <math>\mu 2</math>-GFP sur l'épissage alternatif en absence des protéines EFTUD2, PRPF8 et SNRNP200.....</i>	269
Figure 7. <i>Impact de la déplétion de CFLAR sur la mort cellulaire médiée par réovirus</i>	272

## LISTE DES TABLEAUX

### Introduction

Tableau 1. Liste des gènes et protéines de réovirus ainsi que leur rôles et activités....	14
Tableau 2. Résumé des principaux mécanismes connus de modulation de l'épissage alternatif par des virus .....	39

### Chapitre 1

Table 1. Protein families found in the 240 transcripts that are differentially spliced upon viral infection .....	53
---	----

## LISTE DES ABRÉVIATIONS

ADN	Acide désoxyribonucléique
ARN	Acide ribonucléique
ARNm	Acide ribonucléique messenger
ASO	Oligonucléotide antisens ( <i>antisense oligonucleotide</i> )
AS-PCR	PCR spécifique à l'épissage alternatif ( <i>alternative splicing PCR</i> )
db	Double brin
DISC	Complexe de signalisation induisant la mort ( <i>death-inducing signaling complex</i> )
ESE	<i>Exonic splicing enhancer</i>
ESS	<i>Exonic splicing silencer</i>
kDa	Kilodalton
kb	Kilobase
ISE	<i>Intronic splicing enhancer</i>
ISG	Gènes stimulés par l'interféron ( <i>interferon stimulated genes</i> )
ISS	<i>Intronic splicing silencer</i>
ISVP	Particule infectieuse subvirale ( <i>infectious subviral particle</i> )
ITAM	<i>Immunoreceptor tyrosine-based activation motif</i>
NES	Séquence d'export nucléaire ( <i>nuclear export signal</i> )
NLS	Séquence de localisation nucléaire ( <i>nuclear localisation sequence</i> )
pb	Paire de bases
PCR	Réaction de polymérisation en chaîne ( <i>polymerase chain reaction</i> )
PKR	Protéine kinase R
PSI ( $\Psi$ )	Pourcentage d'inclusion ( <i>percent spliced in</i> )
pré-ARNm	ARN messagers non matures
qPCR	PCR quantitatif ( <i>quantitative PCR</i> )
RLR	<i>RIG-I-like receptor</i>

sb	Simple brin
siRNA	Petit ARN interférent ( <i>small interfering RNA</i> )
snRNA	Petit ARN nucléaire ( <i>small nuclear RNA</i> )
snRNP	Petite ribonucléoprotéine nucléaire ( <i>small nuclear ribonucleoprotein</i> )
TLR	<i>Toll-like receptor</i>
TOES	Oligonucléotide ciblé favorisant l'épissage ( <i>targeted oligonucleotide enhancer of splicing</i> )
TOSS	Oligonucléotide ciblé défavorisant l'épissage ( <i>targeted oligonucleotide silencer of splicing</i> )
VEB	Virus Epstein-Barr
VF	Usines de réplifications virales ( <i>viral factories</i> )
VIH	Virus de l'immunodéficience humaine
VPH	Virus du papillome humain
VSV	Virus de la stomatite vésiculeuse
WB	Buvarbage de type Western ( <i>Western Blot</i> )

## **INTRODUCTION**

### **Avant-propos**

La thèse suivante se situe à l'interface de la virologie et de la biologie des ARN, et couvre donc un large éventail de savoirs allant des virus à l'épissage constitutif et alternatif. Afin de faciliter la compréhension de l'introduction, qui se doit ainsi de couvrir plusieurs thèmes de recherche relativement disparates, cet avant-propos se veut un court résumé des différentes sections de l'introduction ainsi que de leur lien avec la présente thèse. Dans un premier temps, j'aborderai les virus, et plus particulièrement les interactions virus-hôtes. Je discuterai de la réponse antivirale cellulaire, ainsi que de deux mécanismes de mort cellulaire programmée, soit l'apoptose et la nécroptose, puisque ce sont les trois phénomènes durant l'infection que nous avons approfondis lors de mes travaux de recherche. Par la suite, j'introduirai le virus sur lequel j'ai travaillé lors de cette thèse, soit réovirus. Nous discuterons ensuite plus en profondeur d'une des protéines de réovirus, la protéine  $\mu 2$ , sur laquelle nos efforts se sont concentrés de par son implication dans les changements d'épissage alternatif lors de l'infection avec réovirus. Finalement, je ferai une introduction de l'épissage, autant constitutif qu'alternatif, ainsi que la machinerie cellulaire responsable de ce phénomène de maturation des ARN. L'accent sera plus particulièrement mis sur le complexe U5 et ses protéines EFTUD2, PRPF8 et SNRNP200, sur lesquelles mes travaux ont porté, encore une fois en raison de leur implication dans les interactions virus-hôte lors de l'infection avec réovirus. Nous terminerons par la suite l'introduction avec la littérature sur l'importance de l'épissage alternatif lors des infections virales, avant de poursuivre avec les résultats de recherche et la discussion.

### **Les virus**

Les virus sont des entités biologiques acellulaires se reproduisant obligatoirement à l'intérieur d'une cellule-hôte en usurpant sa machinerie. Ils constituent donc une

classe à part n'appartenant pas au domaine du vivant, bien que partageant en partie ou totalement certaines caractéristiques propres au vivant, tels que la reproduction ainsi que l'organisation et l'adaptation (Moreira et López-García, 2009). Les virus sont composés d'un génome dont la nature peut être d'acides désoxyribonucléiques (ADN) ou d'acides ribonucléiques (ARN). Ce génome peut se présenter sous la forme simple brin (sb) ou double brin (db) et être circulaire, linéaire ou bien encore segmenté. Ce génome est entouré d'une capsid, une structure protéique permettant de protéger le génome. Finalement, certains virus possèdent aussi une enveloppe, c'est-à-dire une membrane lipidique dérivée de la membrane plasmique ou d'autres organelles membranaires lors de la sortie du virus de la cellule-hôte par bourgeonnement (Fields *et al.*, 2013). La particule virale constituée du génome viral, de la capsid ainsi que de l'enveloppe (si applicable) se nomme aussi virion, sauf lorsqu'elle est en train d'infecter une cellule-hôte, où le terme virus est préférable. Le cycle de reproduction des virus nécessite d'entrer dans une cellule-hôte, via des récepteurs présents à sa surface. Une fois à l'intérieur de la cellule, le virus va prendre contrôle de la machinerie ribosomale et la forcer à produire des protéines à partir des ARN viraux, permettant l'assemblage de nouvelles particules virales, ou virions. La relâche de ces particules complète le cycle et les virions peuvent alors aller réinfecter une nouvelle cellule pour recommencer le processus (Fields *et al.*, 2013). L'importance des virus dans notre environnement est impressionnante; les estimations chiffrent le nombre de particules virales dans l'océan à  $10^{30}$ , soit environ 15 fois plus que le nombre de bactéries et d'archées. Les virus sont l'organisme le plus abondant sur Terre, et, dans le cas des océans, le plus grand réservoir de diversité génétique (Suttle, 2007).

### ***Interaction virus-hôte***

La relation intime qui existe entre un virus et la cellule qu'il infecte provient du partage de la machinerie cellulaire, d'un côté afin d'assurer la réplication virale, et de l'autre, afin d'établir une réponse adéquate pour enrayer l'infection. En ce sens, l'équilibre entre le virus et la cellule peut être vu comme une partie de souque à la

corde, où chacun tente de prendre avantage sur l'autre de manière contrôlée (Boudreault *et al.*, 2019 - Voir Annexe 1). Pour la cellule, une réponse démesurée entrainera une réponse disproportionnée du système immunitaire pouvant avoir des conséquences graves pour l'organisme. Dans le même ordre d'idée, un virus se répliquant de manière incontrôlée entrainera rapidement l'apoptose de la cellule-hôte, limitant ainsi sa réplication. Les interactions virus-hôtes sont donc finement régulées, et ont évolué en parallèle afin de toujours contrecarrer efficacement l'ennemi.

### ***Réponse antivirale cellulaire***

Lors d'une infection virale, la première étape pour la cellule-hôte est la reconnaissance du pathogène. Les PAMP (*pathogen-associated molecular patterns*), tels que l'ARNdb et les ARN possédant une extrémité 5' non coiffée, seront reconnus par les RLR (*RIG-I-like receptor*), présents dans le cytoplasme, dont la protéine RIG-I est le modèle prototypique. Les PAMP peuvent aussi être reconnus par les TLR (*toll-like receptors*) dont certains sont à la surface des cellule (dans la membrane cytoplasmique) et d'autres en position intracellulaire (dans la membrane de l'endosome). Cette reconnaissance initiera une cascade de signalisation menant à la translocation du complexe IRF3/IRF7 dans le noyau et la production de la première vague d'interféron de type I, constituée de l'IFN- $\beta$  et de l'IFN- $\alpha$ 4 principalement (Fensterl *et al.*, 2015). Suite à la sécrétion de l'interféron dans le milieu extracellulaire, celui-ci peut aller stimuler la cellule sécrétrice de manière autocrine, ainsi que les cellules non infectées aux alentours de celle-ci de manière paracrine. La liaison de l'interféron à son récepteur à la surface de la cellule et la voie de signalisation subséquente entraine la formation du complexe ISGF3, formé de STAT1, STAT2 ainsi que d'IRF9 (Honda et Taniguchi, 2006). Ce complexe transloque au noyau où il se lie aux éléments de réponse à la stimulation par l'interféron dans le promoteur d'environ 300 gènes (Samarajiwa *et al.*, 2009; Sen et Sarkar, 2007). Ces gènes, nommés gènes stimulés par l'interféron (*Interferon stimulated genes*, ISG), sont les effecteurs permettant la réponse à l'infection (Fensterl et Sen, 2015;

Teijaro, 2016). L'interféron est lui-même un gène stimulé par l'interféron et permet donc d'amplifier dans une boucle de rétroaction positive sa production, via une deuxième vague caractérisée par une panoplie d'interféron- $\alpha$  (Fensterl *et al.*, 2015; Samarajiwa *et al.*, 2009). L'intégrité de cette signalisation est cruciale pour répondre à l'infection virale; une mutation affectant l'épissage dans *STAT1*, par exemple, empêche la production des gènes stimulés par l'interféron, et rend le patient extrêmement sensible aux infections virales (Vairo *et al.*, 2011). Bien évidemment, les virus ont évolué des mécanismes ingénieux leur permettant d'altérer cette réponse cellulaire, ainsi que de bloquer les effecteurs nuisant à la réplication virale (Fensterl *et al.*, 2015; Honda et Taniguchi, 2006). Un de ces effecteurs, la protéine kinase R (PKR), est activé par l'ARNdb et induit un arrêt de la traduction pour freiner l'infection (Sherry, 2009). Cependant, de nombreux virus ont développé des contres mécanismes, par exemple en produisant des protéines liant l'ARNdb et le masquant, ce qui empêche ainsi l'activation de PKR (Saunders et Barber, 2003).

### ***Mort cellulaire programmée***

Il existe une multitude de mécanismes de mort cellulaire programmée; on peut penser à l'apoptose, la nécroptose, la pyroptose, la ferroptose, etc (Galluzzi *et al.*, 2018). Cependant, dans le cadre de l'étude des interactions virus-hôtes, les deux phénomènes de mort cellulaire programmée les plus étudiés et les plus pertinents sont l'apoptose et la nécroptose.

#### ***Apoptose***

L'apoptose est probablement le programme de mort cellulaire le plus connu et le mieux étudié. Le stimulus provoquant l'apoptose peut être intracellulaire ou extracellulaire, ce qui correspond à l'apoptose induite par voie intrinsèque ou extrinsèque, respectivement (Galluzzi *et al.*, 2018). Pour l'apoptose induite par voie intrinsèque, l'apoptose est déclenchée par un déséquilibre dans les protéines pro-apoptotiques et anti-apoptotiques, qui peut lui-même être causé par de nombreux processus cellulaires. Ce déséquilibre induit la perméabilisation de la membrane externe des mitochondries et conséquemment la relâche du cytochrome C ainsi que



de la protéine SMAC. Le cytochrome C peut alors aller lier les protéines APAF1 et la caspase 9 pour former l'apoptosome, le complexe qui permet l'activation de la caspase 9. Pour l'apoptose induite par voie extrinsèque, le signal provient de la liaison des récepteurs de mort à leur ligand à la membrane plasmique, ce qui permet l'assemblage du complexe de signalisation induisant la mort (*death-inducing signaling complex*, DISC). Le DISC est notamment composé de la caspase 8, de la protéine c-FLIP, et parfois de la caspase 10, et permet l'activation de la caspase 8 via sa protéolyse. À partir de l'activation de la caspase 9 (intrinsèque) ou de la caspase 8 (extrinsèque), les deux voies convergent à ce moment par l'activation des deux caspases effectrices, les caspases 3 et 7. Les caspases 3 et 7 vont couper de nombreuses protéines cellulaires, déclenchant notamment la fragmentation de l'ADN cellulaire et l'exposition extracellulaire de la phosphatidylsérine. Lors de la réplication de plusieurs virus, l'apoptose, autant intrinsèque qu'extrinsèque, est induite et est la plupart du temps un phénomène nuisible au virus en mettant un frein à la réplication virale (Danthi, 2016). D'ailleurs, de nombreux virus possèdent des protéines anti-apoptotiques très semblables à celles présentes dans la cellule (Best, 2008). Finalement, puisque l'apoptose culmine avec la formation de corps apoptotiques qui peuvent être éliminés par les macrophages sans relâche du contenu cytoplasmique, les nouveaux virions qui sont encore à l'intérieur de la cellule seront détruits sans pouvoir aller infecter de nouvelles cellules, et avec un minimum de potentiel inflammatoire.

### *Nécroptose*

À l'inverse, la nécroptose est un programme de mort cellulaire moins connu qui émerge présentement comme crucial pour le système immunitaire de par son potentiel inflammatoire (Galluzzi *et al.*, 2018). Effectivement, la nécroptose se caractérise par la fuite du contenu cytoplasmique, extrêmement immunogène, dans le milieu extracellulaire via des pores membranaires formés par la protéine MLKL. Il existe plusieurs senseurs de la nécroptose qui répondent à une vaste diversité de stimuli (Figure 1). Premièrement, l'activation de RIPK1 est médiée par les récepteurs

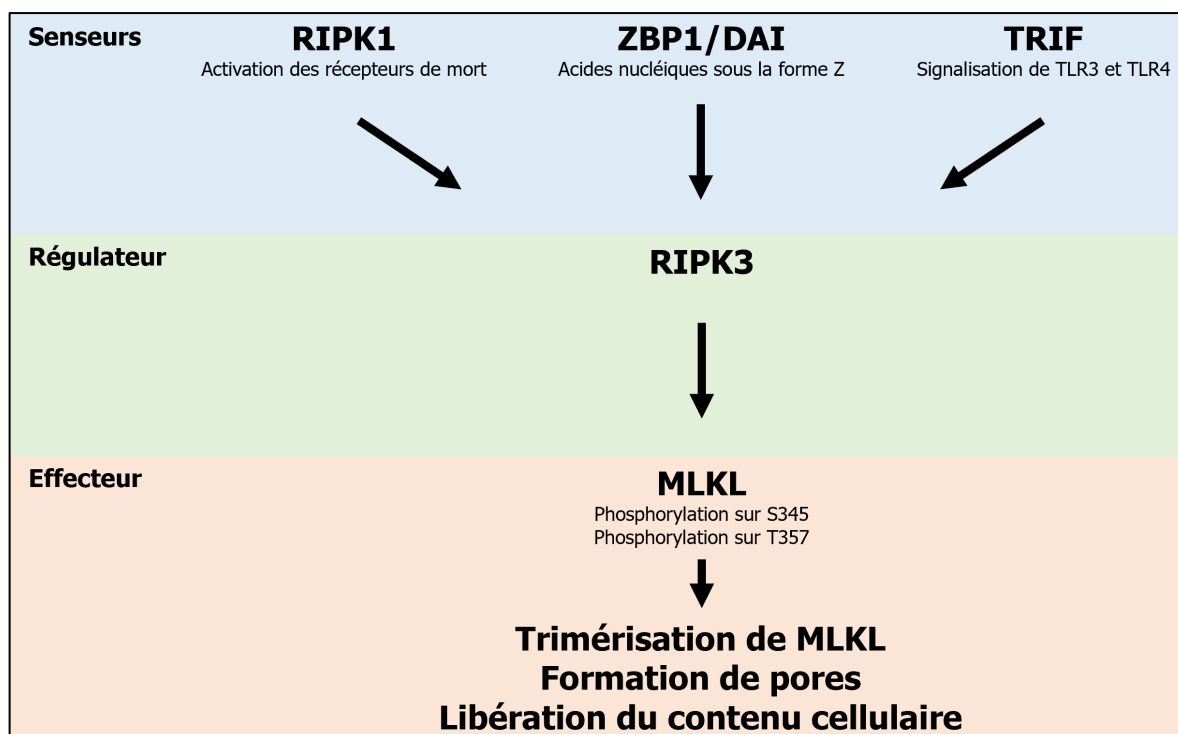


Figure 1. Schéma de la voie de signalisation menant à la nécroptose. Les positions de phosphorylation sur MLKL présentées sont celles chez la souris.

de mort, comme le récepteur du TNF $\alpha$ . RIPK1 interagit notamment avec le même complexe de signalisation induisant la mort (*death-inducing signaling complex*, DISC) que présenté précédemment pour l'apoptose induite par voie extrinsèque, et souligne donc que la régulation de ces deux phénomènes de mort cellulaire peut être étroitement reliée. Deuxièmement, ZBP1 (aussi appelée DAI par le passé) reconnaît des acides nucléiques sous la forme Z, et est notamment un ISG exprimé en réponse à l'interféron (Samarajiva *et al.*, 2009). Troisièmement, TRIF, une protéine adaptatrice de la réponse immunitaire cellulaire, répond aux signaux provenant de TLR3 qui détecte l'ARNdb dans l'endosome et TLR4 qui reconnaît les lipopolysaccharides bactériens à la membrane plasmique. Ces deux dernières parties de la voie de signalisation sont donc intimement liées à la réponse interféron discutée précédemment (Schock *et al.*, 2017). Autant RIPK1, ZBP1 que TRIF vont permettre la phosphorylation de RIPK3, qui régule la nécroptose. La phosphorylation de RIPK3 déclenche son activité kinase, et elle peut à son tour phosphoryler MLKL, l'effecteur de la nécroptose. Lorsque MLKL est phosphorylée, elle forme des trimères qui vont

aller s'insérer dans la membrane cellulaire et y former des pores. Le contenu de la cellule pourra donc s'écouler par ces pores. De nombreux virus, tel que réovirus, rotavirus, le virus Sendai, ainsi que le virus de l'influenza peuvent causer de la nécroptose durant l'infection (Berger *et al.*, 2017; Berger et Danthi, 2013; Mukhopadhyay *et al.*, 2022; Schock *et al.*, 2017; Soliman *et al.*, 2022; Zhang *et al.*, 2020). Cependant, il semble que la plupart des virus ont développé au cours de leur évolution des protéines bloquant la nécroptose, suggérant que la nécroptose puisse nuire à la réplication virale. Par exemple, chez le virus de la vaccine, de l'ARN sous forme Z est produit lors de la réplication et peut-être reconnu par ZBP1 (Koehler *et al.*, 2021). Cependant, le virus possède une protéine, E3, qui compétitionne ZBP1 pour la liaison à l'ARN sous forme Z et empêche ainsi ZBP1 de déclencher la nécroptose (Koehler *et al.*, 2017, 2021).

### ***Pathologies causées par des virus***

L'importance de l'étude des virus et de leur compréhension repose bien évidemment sur le danger qu'ils représentent ainsi que sur la vaste étendue des problèmes qu'ils nous causent. Les virus sont les agents étiologiques de nombreuses maladies humaines, telles que le syndrome d'immunodéficience acquise (virus de l'immunodéficience humaine, VIH), la mononucléose (virus Epstein-Barr, VEB) ainsi que des rhumes et syndromes gastro-intestinaux divers (rotavirus, norovirus, coronavirus) (Black, 2008). Les virus ont aussi le potentiel de causer de graves épidémies, telles qu'illustrées par la pandémie de grippe espagnole en 1918 (virus de l'influenza), l'épidémie d'Ebola de 2013-2016 (virus de l'Ebola) ainsi que la pandémie de COVID-19 de 2019-2022 (SARS-CoV-2) (Andersen *et al.*, 2020; Lever et Whitty, 2016; Wright *et al.*, 2013). Au niveau de l'industrie agroalimentaire, la monoculture dans nos champs les rend particulièrement vulnérables à la venue d'un pathogène, et les virus infectant les plants de haricots, de poivrons et de concombres sont responsables à chaque année de pertes monétaires substantielles (Laliberté et Zheng, 2014; Mandadi et Scholthof, 2015; Martin *et al.*, 2016; Zhu *et al.*, 2018).

## *Cancer*

Les virus sont un agent étiologique majeur des cancers, pour lesquels on estime qu'environ de 10% à 20% sont d'origine virale (Parkin, 2006). Certains cancers ont même une étiologie majoritairement virale, comme le cancer du col de l'utérus qui est associé à l'infection avec le virus du papillome humain (VPH) dans 99,7% des cas (Lehoux *et al.*, 2009; Parkin, 2006). Il y a présentement sept virus dont l'infection a été associée avec le processus de carcinogenèse chez l'humain, soit le VEB ainsi que le virus de l'herpès associé au sarcome de Kaposi, tous deux des *Herpesviridae*; le virus de l'hépatite B, un *Hepadnaviridae*; le virus de l'hépatite C, un *Flaviviridae*; le VPH, un *Papillomaviridae*; le polyomavirus de Merkel, un *Polyomaviridae*; et finalement, le virus T-lymphotropique humain-1, un *Retroviridae* (Ajiro et Zheng, 2014; Morales-Sánchez et Fuentes-Pananá, 2014; White *et al.*, 2014). Ces virus produisent tous des protéines ayant une activité oncogénique, ayant pour but d'aider la réplication virale (Ajiro et Zheng, 2014; Boudreault *et al.*, 2016). Par exemple, le VPH possède deux protéines oncogènes, E6 et E7, qui ont des rôles importants dans la réplication du virus. E6 interagit avec p53 et induit sa dégradation avec l'aide de l'ubiquitine ligase E6-AP (Huibregtse *et al.*, 1991; Mesplède *et al.*, 2012; Scheffner *et al.*, 1990, 1993). E7 interagit quant à elle avec pRB, brisant le complexe formé avec le facteur de transcription E2F et induisant la dégradation par le protéasome de pRB (Chellappan *et al.*, 1992; Gonzalez *et al.*, 2001; Huh *et al.*, 2007). La dégradation de p53 et de pRB permet à la cellule infectée de progresser anormalement dans son cycle cellulaire et de ne pas entrer en apoptose, établissant ainsi un environnement optimal pour la progression du cycle de réplication du VPH qui se termine dans des kératinocytes différenciés et donc normalement quiescents. Cependant, lors du processus de carcinogenèse, le génome du virus est fréquemment intégré dans le génome de la cellule-hôte (Annunziata *et al.*, 2012). Cette intégration brise la séquence codante de la protéine virale E2, qui régule négativement l'expression d'E6 et E7; les cancers positifs au VPH présentent donc une surexpression d'E6 et d'E7 en comparaison à des cellules infectées par le virus (Annunziata *et al.*, 2012). La plupart des cancers d'origine virale sont caractérisés

par ce phénomène d'infection virale allant de travers et où les oncogènes viraux ont favorisé l'émergence d'un phénotype cancéreux plutôt que de seulement supporter la réplication virale. L'infection chronique et/ou latente, souvent accompagnée d'inflammation, fait aussi partie des caractéristiques des virus causant des cancers (Ajiro et Zheng, 2014; Boudreault, *et al.*, 2016; Morales-Sánchez et Fuentes-Pananá, 2014; White *et al.*, 2014). Les études transcriptomiques de ces cancers ont démontré qu'ils sont moléculairement différents des cancers d'origine non virale, et l'avènement de la médecine de précision a amené l'hypothèse qu'il serait avantageux de traiter ces cancers différemment des cancers d'origine non virale (Armero *et al.*, 2017; Hernandez-Lopez et Graham, 2012; Tremblay *et al.*, 2016).

### ***Utilisation des virus***

Les virus sont le résultat d'une évolution extrêmement complexe et rapide, poussée par la génération de millions de particules virales à chaque nouvelle infection. À la fois très simples et extrêmement complexes, les virus représentent le paradigme parfait de ce qu'on pourrait qualifier de *biomachine*, c'est-à-dire un assemblage moléculaire de protéines, ADN ou ARN ayant un seul but, soit dans leur cas, la réplication. Par exemple, l'élégance de l'assemblage de certaines protéines formant des capsides virales a notamment influencé le domaine du génie et des nanotechnologies (Perlmutter et Hagan, 2015). Malgré la menace que représentent certains virus pour l'humain, l'idée de détourner les virus et de les utiliser à notre avantage réside dans les caractéristiques mêmes qu'ils possèdent. Par exemple, ils sont dotés d'un tropisme, autrement dit la capacité d'infecter certaines cellules de manière spécifique (Fields *et al.*, 2013). Certains ont aussi la capacité de réaliser des processus biochimiques complexes, comme intégrer leur génome au sein de la cellule-hôte (Fields *et al.*, 2013). Deux exemples d'utilisations de virus seront abordés plus en détail, soit le traitement de cancer par des virus ainsi que l'utilisation des virus comme vecteurs pour transporter du matériel génétique.

### *Virus oncolytiques*

L'idée d'utiliser des virus comme traitement contre le cancer peut sembler irrationnelle, surtout lorsque l'on sait que plusieurs de ces mêmes virus sont des facteurs importants pour le développement de la maladie (Boudreault, *et al.*, 2016). Néanmoins, les premières observations d'une capacité oncolytique (c'est-à-dire de destruction des cellules cancéreuses) de certains virus remontent déjà à plus de 100 ans. Dès le début du 20<sup>e</sup> siècle, il avait été remarqué que certains patients se remettaient de leur cancer suite à des infections d'origine naturelle ou une vaccination (Kelly et Russell, 2007; Sinkovics, 2004). Malheureusement, l'échec des premiers essais chez l'humain ainsi que l'avènement des premières chimiothérapies, à une période où tout était encore inconnu des virus, a détourné l'intérêt de l'activité oncolytique des virus (Kuruppu et Tanabe, 2005). Le développement des systèmes de génétique inverse, permettant la génération rapide de virus mutants, ainsi que la découverte de nouveaux virus oncolytiques candidats, tel que réovirus, a relancé le domaine des virus oncolytiques depuis la fin des années 90. Mais quelles caractéristiques confèrent une réplication préférentielle de certains virus dans les cellules cancéreuses? En fait, il faut se tourner vers les processus mis en place dans les cellules saines pour se défendre lors d'une infection virale pour bien comprendre. Lors d'une infection virale, la plupart des cellules vont mettre en place un programme de défense bien rodé : sécrétion d'interféron et de cytokines pour alerter le système immunitaire, arrêt du cycle cellulaire pour bloquer la réplication virale, arrêt de la formation de nouveaux vaisseaux sanguins pour éviter la dissémination du virus à travers l'organisme et apoptose en dernier recours (Pikor *et al.*, 2015). Or, ces mêmes phénomènes sont dérégulés dans le processus de carcinogenèse. Effectivement, une cellule cancéreuse tente par plusieurs moyens d'éviter la reconnaissance par le système immunitaire, prolifère de manière incontrôlée, induit la formation de nouveaux vaisseaux sanguins de manière anarchique et ne peut entrer en apoptose (Hanahan et Weinberg, 2011). Donc, le processus de carcinogenèse est incompatible avec le programme de défense immunitaire cellulaire, ce qui fait des cellules cancéreuses des cellules beaucoup moins bien

défendues et beaucoup plus permissives à la réplication de plusieurs virus (Pikor *et al.*, 2015). Au-delà de la réplication accrue dans les cellules cancéreuses et de leur lyse qui peut-être causée directement par la réplication ou par certaines protéines virales, les virus oncolytiques ont aussi la capacité de stimuler le système immunitaire à reconnaître la tumeur et à développer une réponse immunitaire antitumorale (Ilkow *et al.*, 2015; Kamta *et al.*, 2017). Il est effectivement connu que le système immunitaire détruit constamment des lésions précancéreuses dans notre organisme, et que certains patients entrent en rémission spontanément dû à un bris de tolérance de leur système immunitaire envers la tumeur (Hanahan et Weinberg, 2011). Les virus, en induisant la sécrétion de cytokines, d'interféron et en stimulant l'infiltration et la prolifération de cellules immunitaire dans le microenvironnement tumoral, contribuent eux aussi à ce bris de tolérance (Kuruppu et Tanabe, 2005). Les virus oncolytiques sensibilisent aussi les cellules cancéreuses à des traitements classiques, tels que la radiothérapie ou la chimiothérapie (Arulanandam *et al.*, 2015; Bourgeois-Daigneault *et al.*, 2016). Présentement, l'activité des virus oncolytiques seule n'est pas suffisante, et donc la plupart des études cliniques investiguent la combinaison d'un virus oncolytique et d'un traitement classique comme la chimiothérapie ou la radiothérapie. Cependant, beaucoup d'efforts sont présentement déployés pour mieux comprendre ces virus oncolytiques et en améliorer leur efficacité. Par exemple, il est possible d'ajouter un gène au sein du virus pour augmenter la dissémination du virus, la mort cellulaire et la stimulation du système immunitaire ou même pour activer une prodrogue au sein des cellules infectées (Le Boeuf *et al.*, 2017). Le virus peut aussi être affaibli, par exemple, en le rendant plus sensible aux défenses cellulaires antivirales, ce qui augmente sa spécificité pour les cellules de la tumeur. C'est une technique qui a été utilisée avec succès pour le virus de la stomatite vésiculeuse (VSV), pour lequel le retrait de l'acide aminé à la position 51 dans la protéine M (VSV $\Delta$ 51) rend le virus plus sensible à la réponse de la voie de l'interféron, et donc incapable de se répliquer dans des cellules saines ayant une réponse antivirale normale (Stojdl *et al.*, 2003). Il a aussi été démontré qu'il est possible de combiner certains virus afin de créer une synergie

entre eux (Alkassar *et al.*, 2011). De nombreux virus ont démontré une activité oncolytique, que ce soit avec le virus de type sauvage ou une version modifiée du virus. Par exemple, réovirus, VSV, le virus de Maraba, le virus de l'herpès simple, adénovirus, le virus de la vaccine et même le virus Zika ont démontré des propriétés oncolytiques (Kamta *et al.*, 2017; Zhu *et al.*, 2017). Puisque les déterminants de leur activité oncolytique ne sont toujours pas compris en profondeur, l'approche préconisée dans plusieurs études est de comparer plusieurs virus oncolytiques ensemble afin de trouver celui qui possède le meilleur effet dans le système à l'étude (Martin *et al.*, 2019).

### *Vecteurs viraux*

Certains virus, comme les *retroviridae*, possèdent la capacité d'intégrer leur génome au sein de la cellule-hôte. Cette capacité a rapidement intéressé les chercheurs, leur donnant un outil moléculaire permettant de faire de la thérapie génique, c'est-à-dire d'aller corriger un défaut génétique en réintégrant le gène de type sauvage à l'intérieur du génome de la cellule (Benskey *et al.*, 2019). Bien que prometteur, les défis de la thérapie génique n'ont toujours pas permis de percée significative et l'avènement de la technologie CRISPR-Cas9 permet maintenant une correction à la base près du génome qui risque de supplanter l'intégration aléatoire des vecteurs viraux (Ran *et al.*, 2013). De plus, certaines questions de sécurité avec l'intégration aléatoire, notamment des défauts d'épissage alternatif provenant de l'ajout au sein du génome de nouveaux sites d'épissage, avaient déjà été soulevées (Cesana *et al.*, 2012; Moiani *et al.*, 2012). Les vecteurs viraux ont aussi un intérêt accru en vaccination, où par exemple la production d'un virus fortement immunogène présentant une protéine d'un autre virus peut permettre d'élucider une réponse immunitaire inatteignable avec un pathogène faiblement immunogène (Ewer *et al.*, 2016). Ils peuvent aussi servir à transporter du matériel génétique permettant à la cellule de produire par elle-même un antigène. Par exemple, le ChAdOx1 nCoV-19, un vaccin développé par AstraZeneca ainsi que l'Université d'Oxford, est basé sur un adénovirus simien qui porte la séquence en ADN de la protéine spicule du virus



SARS-CoV-2, permettant à la cellule de produire l'antigène auquel l'organisme doit répondre par elle-même (Folegatti *et al.*, 2020).

## **Réovirus**

### *Généralités*

Dans le cadre des travaux de cette thèse, réovirus, un virus de la famille des *Reoviridae*, a été étudié. La famille des *Reoviridae* est une large famille de virus à ARNdb segmenté, ne possédant pas d'enveloppe lipidique, mais possédant plusieurs capsides protéiques concentriques afin de protéger leur génome. Cette famille de virus infecte un large spectre d'hôtes, tels que les animaux, les insectes et les plantes (Mertens, 2004). On retrouve parmi cette famille les rotavirus, un important pathogène humain causant des diarrhées chez l'enfant (Sherry, 2009). Le genre orthoréovirus inclut des virus dont les hôtes naturels sont les vertébrés, et dont l'espèce orthoréovirus de mammifères (référé comme réovirus tout au long de cette thèse) infecte les mammifères dont l'humain et la souris. Les réovirus possèdent dix segments d'ARNdb, codant pour douze protéines, dont huit protéines structurales et quatre protéines non structurales (Tableau 1). Les segments d'ARN sont classés selon leur longueur : les S (pour *small*) sont d'environ 1,2 à 1,4 kilobases (kb); les M (pour *medium*) sont d'environ 2,2 kb et les L (pour *large*) sont d'environ 4 kb. Les protéines qu'ils encodent suivent un classement similaire; les segments S encodent pour les protéines  $\sigma$  qui sont d'environ 40 kilodaltons (kDa) ; les M, pour les  $\mu$  qui sont d'environ 80 kDa; et finalement les L, les  $\lambda$ , qui font environ 140 kDa (Tableau 1). Il est à souligner que les segments d'ARN et les protéines ont été respectivement nommés selon leur migration sur gel; c'est pourquoi le segment M1 encode pour  $\mu_2$ , et le segment L3,  $\lambda_1$ . Les réovirus se sous-divisent en 4 sérotypes, soit le type 1 Lang (T1L), le type 2 Jones (T2J), le type 3 Dearing (T3D) et le type 4 Ndelle (T4N). Ces virus ont longtemps été des virus-modèles pour comprendre la réplication des virus à ARNdb (Gomatos, 1967; Watanabe *et al.*, 1968). La popularité de réovirus a

Tableau 1. *Liste des gènes et protéines de réovirus ainsi que leur rôles et activités.*

Segment	Protéine(s)	Localisation	Rôle ou activité
L1	$\lambda 3$	Capside interne	Polymérase d'ARN dépendante de l'ARN
L2	$\lambda 2$	Tourelle transcapside	Synthèse de la structure coiffe (guanynyltransférase, méthyltransférase) Tourelle transcapside permettant l'extrusion des ARNm synthétisés par la capsid interne Déterminant de la sensibilité à l'interféron
L3	$\lambda 1$	Capsid interne	Déterminant de l'induction d'interféron ARN triphosphatase (RTPase) Hélicase
M1	$\mu 2$	Capsid interne	Participation aux VF Lie les microtubules et ancre les VF à ceux-ci Déterminant de la sensibilité à l'interféron Déterminant de l'induction d'interféron ARN triphosphatase (RTPase) et nucléotides triphosphatase (NTPase) Complexe de réplication avec $\lambda 3$ Lie des ARNs et des ARNdb Interagit avec elle-même (dimères ou oligomères?)
M2	$\mu 1$	Capsid externe	Pénétration transmembranaire Induction de l'apoptose
M3	$\mu NS$	Non structurale	Formations des VF Séquestration d'IRF3 dans les VF? Interaction avec les granules de stress
	$\mu NS-C$	Non structurale	?
S1	$\sigma 1$	Capsid externe	Attachement à la cellule Apoptose
	$\sigma 1s$	Non structurale	Arrêt du cycle cellulaire? Apoptose? Déterminant de la sensibilité à l'interféron?
S2	$\sigma 2$	Capsid interne	Structurale
S3	$\sigma NS$	Non structurale	Participation aux VF Lie l'ARN et stabilise les ARN viraux Chaperone d'ARN?
S4	$\sigma 3$	Capsid externe	Lie l'ARNdb Bloque l'activation de PKR?

fortement augmenté au début des années 2000, lors de la démonstration de son potentiel oncolytique (Coffey *et al.*, 1998).

### ***Cycle de réplication***

Le cycle de réplication de réovirus commence par l'adsorption du virus à la surface de la cellule et est médiée par l'interaction entre la protéine  $\sigma 1$  et les sucres, principalement l'acide sialique chez plusieurs souches, dont celle utilisée au cours du travail de cette thèse (Barton *et al.*, 2003). Dans un deuxième temps, la protéine  $\sigma 1$  s'attache au récepteur JAM-A, bien que d'autres récepteurs semblent être en mesure de médier l'attachement (Aravamudhan *et al.*, 2022; Barton *et al.*, 2001; Konopka-

Anstadt *et al.*, 2014; Lemay, 2018). L'entrée du virus par endocytose est médiée par les intégrines  $\beta 1$  (Danthi *et al.*, 2010). Une fois à l'intérieur de l'endosome, plusieurs étapes de digestion protéolytique vont permettre la relâche de la capsid interne dans le cytoplasme. Premièrement, la perte de la protéine  $\sigma 3$ , le clivage de la protéine  $\mu 1$  en ses fragments  $\delta$  et  $\Phi$  médiée entre autres par les cathepsines B et L qui ont été les plus étudiées, ainsi que le changement de conformation de la protéine  $\sigma 1$  vont faire transitionner le virus vers sa forme de particule infectieuse subvirale (*infectious subviral particle*, ISVP) (Danthi *et al.*, 2013). Il est à noter que les ISVP peuvent aussi directement infecter les cellules, et ce de manière plus rapide et efficace que les virions. Il s'agit de la voie d'entrée principale du virus dans le tractus gastro-intestinal, où les protéases dans la lumière catalysent la conversion de virions à ISVP (Stanifer *et al.*, 2016). Dans un deuxième temps, les IVSP seront converties en ISVP\*, caractérisée par la perte de la protéine  $\sigma 1$ , un changement de conformation dans le fragment  $\delta$  de  $\mu 1$ , une augmentation dans l'hydrophobicité de la particule et la relâche du fragment  $\mu 1N$ . Produit à partir d'un site de clivage autocatalytique dans  $\mu 1$ , le groupement myristoylé de  $\mu 1N$  induit la formation de pores dans la membrane de l'endosome tardif et le relâche de la capsid interne dans le cytoplasme (Danthi *et al.*, 2010, 2013). Cette dernière étape requiert aussi la chaperonne cellulaire HSC70 ainsi que certains lipides membranaires spécifiques (Ivanovic *et al.*, 2007; Snyder et Danthi, 2016). La capsid interne, ou nucléoïde (*core*), est formée des protéines  $\lambda 1$ ,  $\lambda 2$ ,  $\lambda 3$ ,  $\mu 2$  et  $\sigma 2$  et est transcriptionnellement active lors de sa relâche dans le cytoplasme. Elle produira donc les dix ARNm du virus, portant une structure coiffe et sans queue poly-A, et les relâchera dans le cytoplasme à travers les tourelles formées par  $\lambda 2$  (Lemay, 1988, 2018). De cette manière, l'ARNdb est protégé de la détection par la cellule en restant à l'intérieur de la capsid interne. Cependant, ce mécanisme n'est pas infaillible, et il a été récemment démontré que l'ARNdb de réovirus est bien exposé et détecté par les senseurs d'ARNdb de la cellule, comme RIG-I, notamment lors du transit endosomal du virus (Abad et Danthi, 2022; Mohamed, Konda, *et al.*, 2020). Les ARNm viraux seront traduits par les ribosomes de la cellule-hôte, produisant ainsi les protéines

virales. Très tôt dans l'infection, les usines de réplication virales (*viral factories*, VF) apparaissent dans le cytoplasme des cellules infectées. Ces structures sont le site de réplication du virus et sont formées par la protéine non structurale  $\mu$ NS, qui est capable de former par elle-même en expression transitoire des structures ressemblant fortement aux VF (Broering *et al.*, 2002; Miller *et al.*, 2007, 2010). La protéine non structurale  $\sigma$ NS ainsi que la protéine structurale  $\mu$ 2 sont cependant aussi nécessaires à leur formation et leur maturation (Arnold *et al.*, 2008; Kobayashi *et al.*, 2006). Les VF sont considérées comme des centres organisationnels de la réplication virale, permettant de coordonner la production des ARNm viraux et leur traduction, la réplication du génome, sa répartition ainsi que son empaquetage dans les virions nouvellement produits, ainsi que l'assemblage de ces nouveaux virions (Tenorio *et al.*, 2019). La compréhension globale de la manière dont tous ces phénomènes sont coordonnés nous échappe encore cependant. De manière intéressante, il a été remarqué il y a longtemps que les VF chez réovirus pouvaient adopter deux différentes morphologies : une morphologie globulaire, typiquement retrouvée chez les souches du sérotype T3D, ou une morphologie filamenteuse, retrouvée typiquement chez les souches du sérotype T1L (Figure 2). Cette différence de morphologie est reliée au segment M1, encodant la protéine  $\mu$ 2 (voir la section *La protéine  $\mu$ 2* pour plus de détails) (Broering *et al.*, 2002; Eichwald *et al.*, 2017, 2018; Parker *et al.*, 2002). Très rapidement après leur formation, les VF recrutent les nucléoïdes ayant permis l'infection initiale, afin de circonscrire la réplication virale en leur sein (Broering *et al.*, 2004). Les ribosomes sont aussi recrutés à la périphérie des VF afin d'assurer la traduction des ARNm viraux (Desmet *et al.*, 2014). À l'intérieur des VF, la réplication de réovirus se passe selon les étapes suivantes. Les ARNm sont traduits; les protéines s'assemblent afin de former la capsid interne, qui est transcriptionnellement active et qui possède les dix segments d'ARN, sous forme simple-brin puis double-brin suite à l'action du complexe de réplication. Ces capsides internes produisent à leur tour des ARNm qui participent à augmenter la réplication virale. Les capsides internes cessent la transcription lors de l'ajout de la capsid externe; les virions sont alors matures. Leur relâche se fera généralement

par mort cellulaire et/ou rupture de la membrane plasmique, bien que le phénomène n'ait pas été particulièrement bien étudié; il a d'ailleurs été récemment suggéré que la sortie du virus soit possible par des voies non-lytiques (Lemay, 1988, 2018; Santiana *et al.*, 2018). Il est à noter qu'il a été démontré que réovirus induit l'apoptose et la nécroptose lors de l'infection, bien que leurs rôles respectifs dans la relâche des virions et dans le cycle viral soient encore mal compris (DeAntoneo *et al.*, 2022).

### ***La protéine $\mu 2$***

La protéine  $\mu 2$ , codée par le segment M1, est une protéine structurale de 83 kDa et une composante mineure de la capsid interne, où elle est présente de 20 à 24 copies par virion sur la face interne (Coombs, 1998). Durant l'infection, elle est hautement abondante et se localise dans les VF (Dermody *et al.*, 2013; Kobayashi *et al.*, 2009). En expression transitoire, la protéine est observée liée aux microtubules cellulaires, ainsi que dans le noyau des cellules, et plus particulièrement dans des organelles sans membrane nommées *nuclear speckles*; l'importance de cette localisation nucléaire est toujours inconnue, puisque  $\mu 2$  n'a jamais été observée dans le noyau durant l'infection (Kobayashi *et al.*, 2009; Rivera-Serrano *et al.*, 2017). Elle possède les activités enzymatiques ARN triphosphatase (RTPase) et

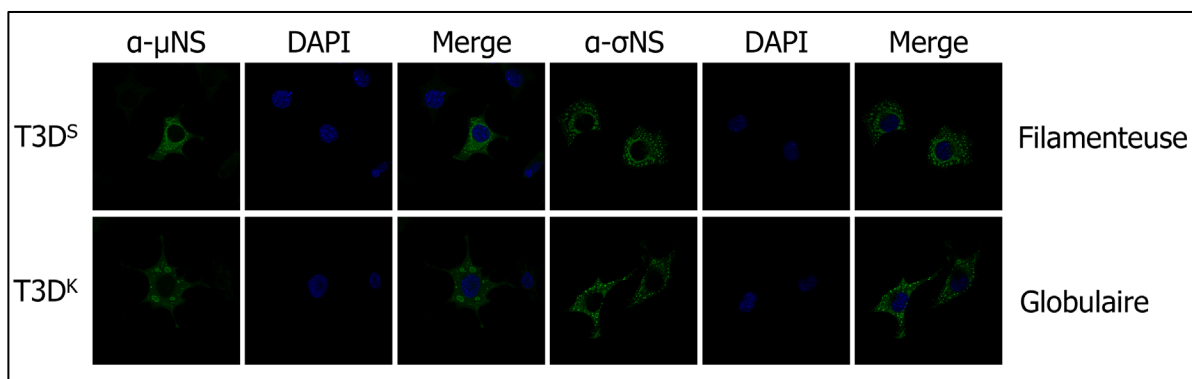


Figure 2. *Morphologie filamenteuse ou globulaire des VF de réovirus.* Des cellules L929 ont été infectées à une multiplicité d'infection (MOI) de 50 virus/cellule pendant 16 heures, puis une immunofluorescence a été réalisée contre les protéines virales  $\mu$ NS et  $\sigma$ NS. T3D<sup>S</sup>, le virus principalement utilisé pour cette thèse, bien qu'appartenant au sérotype T3D, possède la P208 dans sa protéine  $\mu 2$ , et forme donc des VF ayant une morphologie filamenteuse. T3D<sup>K</sup>, provenant du système de génétique inverse, est prototypique du sérotype T3D, sa protéine  $\mu 2$  possédant une sérine à la position 208; ce virus forme donc des VF globulaires.

nucléotides triphosphatase (NTPase) *in vitro*, qui sont nécessaires à la synthèse d'une structure coiffe en 5' des ARNm viraux (Kim *et al.*, 2004; Noble et Nibert, 1997). Cependant, dans le cadre du cycle de répllication viral, la protéine responsable de l'activité ARN triphosphatase de réovirus n'a toujours pas été déterminée, puisque la protéine de la capsid interne  $\lambda 1$  possède aussi cette activité (Bisaillon et Lemay, 1997). La protéine  $\mu 2$  est aussi un déterminant de l'efficacité transcriptionnelle de la capsid interne; elle est donc impliquée dans le complexe de répllication avec  $\lambda 3$ , la polymérase d'ARN dépendante de l'ARN qui interagit avec  $\mu 2$  (Yin *et al.*, 1996, 2004). Elle possède aussi la capacité de lier des ARNsb et des ARNdb, et l'hypothèse principale est que cette liaison est impliquée dans son rôle au sein du complexe de répllication (Brentano *et al.*, 1998). Elle peut aussi interagir avec elle-même, suggérant qu'elle existe sous forme de dimères ou d'oligomères durant l'infection (Eichwald *et al.*, 2017). Un résumé des différentes régions de la protéine décrites dans la littérature est schématisé à la figure 3A. Dans les VF,  $\mu 2$  interagit avec la protéine  $\mu NS$  et les microtubules cellulaires, et ancre ainsi les VF au réseau de

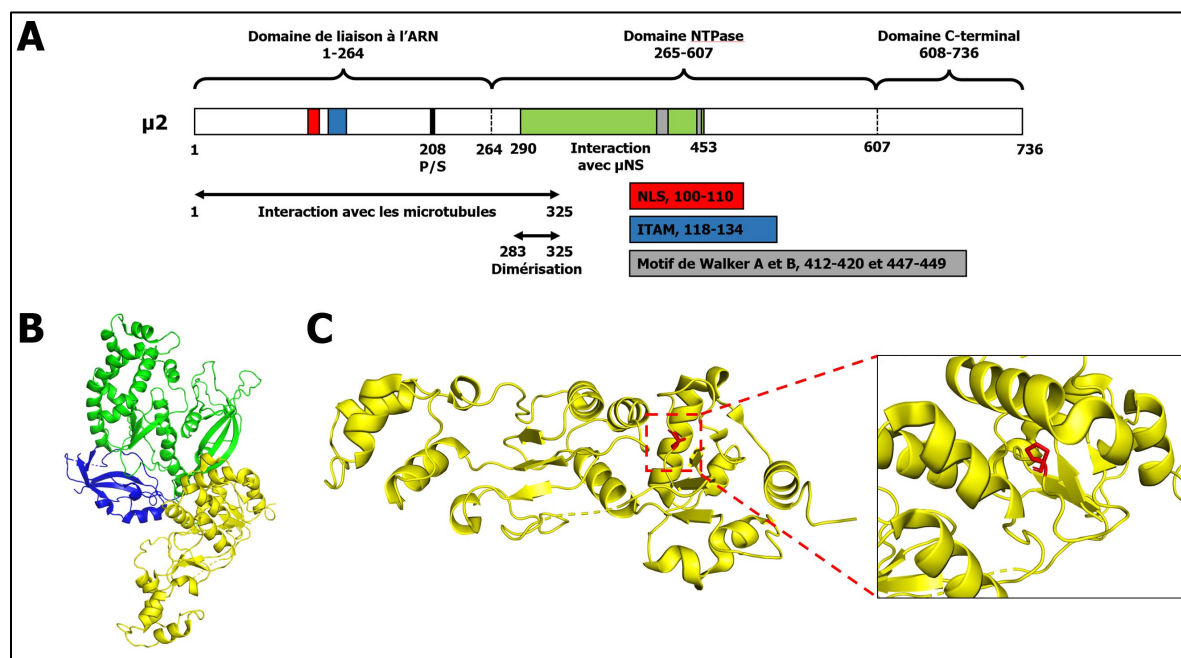


Figure 3. Schéma et structure de la protéine  $\mu 2$ . (A) Schéma de la protéine  $\mu 2$ , avec ses principaux domaines ainsi que les régions décrites dans la littérature. NLS: *nuclear localisation sequence*, ITAM: *Immunoreceptor tyrosine-based activation motif*. (B) Structure de la protéine  $\mu 2$  déterminée dans le virion par cryomicroscopie électronique (7elh). Le domaine de liaison à l'ARN a été coloré en jaune, le domaine NTPase en vert et le domaine C-terminal en bleu. (C) Vue du domaine de liaison à l'ARN ainsi que la proline 208 (P208), en rouge.

microtubules cellulaires (Arnold *et al.*, 2008, p. 2; Kobayashi *et al.*, 2006, 2009). Tel que mentionné précédemment, les VF peuvent présenter deux morphologies différentes selon le génotype de réovirus étudié : une morphologie globulaire (associée principalement aux souches T3D) et une morphologie filamenteuse (associée principalement aux souches T1L; Figure 2). Cette différence de morphologie est déterminée par le segment M1, et donc la protéine  $\mu 2$  (Broering *et al.*, 2002; Parker *et al.*, 2002). Les études subséquentes ont démontré que l'acide aminé à la position 208 de  $\mu 2$  est critique pour la morphologie des VF; un virus avec une proline à la position 208 présente des VF ayant une morphologie filamenteuse, alors qu'un virus avec une sérine à cette position présente des VF ayant une morphologie globulaire (Parker *et al.*, 2002; Yin *et al.*, 2004). Puisque la structure de la protéine  $\mu 2$  n'a été que très récemment résolue, et seulement dans le contexte de la particule virale, il est difficile de prédire la conséquence de ce polymorphisme sur sa structure (Pan *et al.*, 2021) (Figure 3B, 3C). La compréhension actuelle suggère que la protéine  $\mu 2$  ayant la S208 possède un défaut partiel de repliement, amenant une augmentation de son ubiquitination, de sa dégradation et donc une perte de sa fonction (Miller *et al.*, 2004). Il a aussi été suggéré que ce défaut de repliement soit thermosensible, puisque lors que la protéine  $\mu 2$  ayant la S208 est produite à plus basse température, elle regagne partiellement sa capacité à lier les microtubules et est moins ubiquitinylée (Miller *et al.*, 2004). Le polymorphisme à la position 208 de  $\mu 2$  a été relié à beaucoup d'autres phénotypes liés au segment M1, comme le blocage de la voie de l'interféron dans les cardiomyocytes (Irvin *et al.*, 2012; Zurney *et al.*, 2009), la capacité de  $\mu 2$  à se localiser aux *nuclear speckles* (Rivera-Serrano *et al.*, 2017), l'ubiquitinylation de la protéine (Miller *et al.*, 2004) et récemment, le potentiel oncolytique de réovirus (Mohamed, Clements, *et al.*, 2020). Dans tous ces exemples, la version de  $\mu 2$  possédant la P208 démontre la capacité d'induire un phénotype (bloquer la voie de l'interféron, se localiser aux *nuclear speckles*, etc), alors que sa contrepartie possédant la S208 est incapable d'accomplir cette action, appuyant l'hypothèse d'un défaut de repliement induisant une perte de fonction (Miller *et al.*, 2004). Très peu de partenaires d'interaction cellulaires ont été

démontrés pour les protéines de réovirus, ce qui limite très fortement notre compréhension des facteurs cellulaires qui sont nécessaires à la réplication de réovirus. Le seul partenaire cellulaire connu de  $\mu 2$  est le facteur d'épissage cellulaire SRSF2, avec lequel  $\mu 2$  interagit pour se localiser dans le noyau et aux *nuclear speckles* (Rivera-Serrano *et al.*, 2017). SRSF2 semble limiter la réplication du virus, puisque sa déplétion entraîne une augmentation, bien que limitée, de la réplication virale (Rivera-Serrano *et al.*, 2017).

### ***Activité oncolytique de réovirus***

Les balbutiements de l'utilisation de réovirus comme agent anticancéreux remontent aux années 90. Il a tout d'abord été démontré que réovirus se réplique préférentiellement dans les cellules transformées dont la voie RAS est suractivée (Strong *et al.*, 1993; Strong et Lee, 1996). Cette réplication préférentielle est due à l'absence d'activation de la protéine kinase R (PKR), qui a lieu normalement dans les cellules normales, et qui inhibe la traduction et par le fait même la réplication du virus. Dans les cellules dont la voie de RAS est suractivée, cette activation de PKR est inhibée ou renversée et la réplication virale n'est pas inhibée (Norman *et al.*, 2004; Strong *et al.*, 1998). Dans une étude clé publiée dans la revue *Science*, le groupe du Pr Patrick Lee a démontré qu'il est possible d'implanter des cellules transformées chez la souris et d'induire la régression de la tumeur à l'aide d'une injection intratumorale du virus (Coffey *et al.*, 1998). La course à l'utilisation de réovirus comme traitement contre le cancer venait de débuter. Des études subséquentes ont démontré qu'il n'y a pas que la synthèse protéique du virus qui est augmentée dans les cellules suractivant RAS; la digestion de la capsid externe, la production de particules virales infectieuses et leur relâche sont aussi augmentées et participent à la réplication accrue dans ce contexte cellulaire (Gong et Mita, 2014; Marcato *et al.*, 2007). Il est à souligner que l'implication de la voie de RAS dans l'activité oncolytique de réovirus a été débattue; il semble que le statut de RAS n'explique pas complètement l'activité oncolytique de réovirus. L'explication la plus probable vient probablement des réovirus utilisés dans ces études; nous savons



maintenant que les réovirus de la plupart des laboratoires n'ont pas exactement le même génotype et que ces changements peuvent fortement influencer certains phénotypes étudiés (Lanoie et Lemay, 2018). La sensibilité à l'interféron, et possiblement la capacité d'induire cette voie, serait aussi impliquée dans la capacité à discriminer les cellules saines des cellules transformées et varie grandement selon le réovirus utilisé par différents laboratoires (Lanoie et Lemay, 2018; Rudd et Lemay, 2005; Shmulevitz *et al.*, 2010). La compagnie Oncolytics Biotech basée en Alberta développe le Pelareorep™ (précédemment Reolysin™), un réovirus de type sauvage de sérotype T3D comme agent thérapeutique pour traiter les cancers. Réovirus possède d'ailleurs une activité oncolytique contre un large éventail de cancers : le cancer du sein (Norman *et al.*, 2004), ses cellules souches cancéreuses (Marcato *et al.*, 2009) ainsi que ses métastases (Yang *et al.*, 2004), le glioblastome (Alkassar *et al.*, 2011), le cancer de la prostate (Gujar *et al.*, 2011), le myélome (Thirukkumaran *et al.*, 2014), le cancer de la tête et du cou (Twigger *et al.*, 2012), le cancer du poumon et le mélanome (Campion *et al.*, 2016) et le cancer de l'ovaire (Gujar *et al.*, 2013). Bien que capable de directement détruire le cancer via sa réplication, nous savons maintenant qu'une grande partie de son activité thérapeutique passe par la stimulation du système immunitaire et le développement d'une réponse immunitaire antitumorale (Campion *et al.*, 2016; Errington *et al.*, 2008; Gujar *et al.*, 2013, 2010, 2011, 2014; Prestwich *et al.*, 2008, 2009). Au début, le régime de traitement utilisé était de combiner réovirus avec des traitements classiques tels que la chimiothérapie et la radiothérapie (Hamano *et al.*, 2015; Sobotkova *et al.*, 2008; Twigger *et al.*, 2008). Malgré le bénéfice d'une telle combinaison, ces régimes de traitements conservaient une toxicité élevée, ce qui a progressivement amené à une transition vers des combinaisons avec des inhibiteurs de point de contrôle immunitaire, afin de diminuer la tolérance du système immunitaire envers la tumeur et de potentialiser la réponse immunitaire antitumorale stimulée par réovirus (Chakrabarty *et al.*, 2015; Mahalingam *et al.*, 2020). Malgré tout, les avancées cliniques sont lentes et la transition vers une utilisation approuvée et standardisée en clinique demeure incertaine, ce qui encourage la recherche afin de développer de nouveaux réovirus

ayant un potentiel oncolytique accru (Bourhill *et al.*, 2018; Gong *et al.*, 2016; Mohamed *et al.*, 2015; Shmulevitz *et al.*, 2005). Plusieurs voies d'optimisation ont déjà été investiguées, telles que trouver les gènes viraux impliqués dans une activité oncolytique accrue et créer des réovirus réassortants présentant les meilleurs gènes (Mohamed, Clements, *et al.*, 2020; Mohamed *et al.*, 2019; Shmulevitz *et al.*, 2012), atténuer le virus pour le rendre plus spécifique aux cellules transformées (Kim *et al.*, 2011), cibler le virus aux cellules transformées (Brochu-Lafontaine et Lemay, 2012; Wollenberg *et al.*, 2008) et le combiner avec d'autres virus oncolytiques (Alkassar *et al.*, 2011). Malgré tous ces efforts, notre compréhension globale incomplète des facteurs cellulaires dictant la réplication de réovirus, autant dans des cellules saines que transformées, nuit à la conception rationnelle de meilleurs réovirus comme agents virothérapeutiques.

## **L'épissage**

### ***L'épissage constitutif et alternatif***

Suite à la transcription des ARN messagers (ARNm) dans le noyau, les cellules eucaryotes doivent modifier les ARN messagers non matures (pré-ARNm) via de nombreuses étapes avant de pouvoir les exporter dans le cytoplasme pour leur traduction sous leur forme mature. Une structure coiffe est notamment ajoutée en 5' de l'ARN, une queue poly-A en 3' et les introns sont retirés par un processus nommé épissage. Les ARN peuvent aussi être édités ou certaines bases de l'ARN méthylées (Cross *et al.*, 2019). Parmi ces étapes, l'épissage est un processus vital chez les eucaryotes supérieurs. D'une part, l'épissage constitutif permet le retrait des introns des ARN pré-messagers, laissant seulement les exons codants flanqués de leurs régions 5' et 3' non traduites dans l'ARNm mature (Merkhofer *et al.*, 2014). D'autre part, certains exons ou parties d'exons peuvent aussi être retirés du pré-ARNm par un processus qu'on appelle l'épissage alternatif (Wang *et al.*, 2015; Woodley et Valcárcel, 2002). Des introns peuvent aussi être conservés au sein de l'ARNm mature par le même mécanisme. L'épissage alternatif est un processus de maturation crucial pour permettre une diversité protéique accrue, puisque les ARNm

provenant d'un même gène peuvent encoder pour des isoformes différentes de la même protéine. Ainsi, même si on retrouve un peu plus de 20 000 gènes chez l'humain, le nombre de protéines différentes pouvant être produites est beaucoup plus élevé (Modrek et Lee, 2002). Il s'agit d'un processus quasi ubiquitaire, alors que les estimations provenant d'études à haut débit démontrent qu'entre 92% et 94% des gènes humains sont épissés alternativement (Pan *et al.*, 2008; Wang *et al.*, 2008). Ces multiples isoformes peuvent être régulées différemment via l'inclusion ou l'exclusion de domaines spécifiques, et aident donc la cellule à peaufiner le niveau et l'activité de ses protéines (Dörner *et al.*, 2004; Hardy et O'Neill, 2004; Labbé *et al.*, 2017). Un exemple classique de régulation de l'activité protéique via l'épissage alternatif provient du gène *BCL2L1* (Figure 4). Ce gène possède un site d'épissage alternatif en 5' à l'intérieur de son 2<sup>e</sup> exon, qui permet la production d'une version courte ou longue de l'ARNm (Boise *et al.*, 1993). La forme courte de l'ARNm produit la protéine Bcl-xS, qui possède un rôle pro-apoptotique, alors que la forme longue

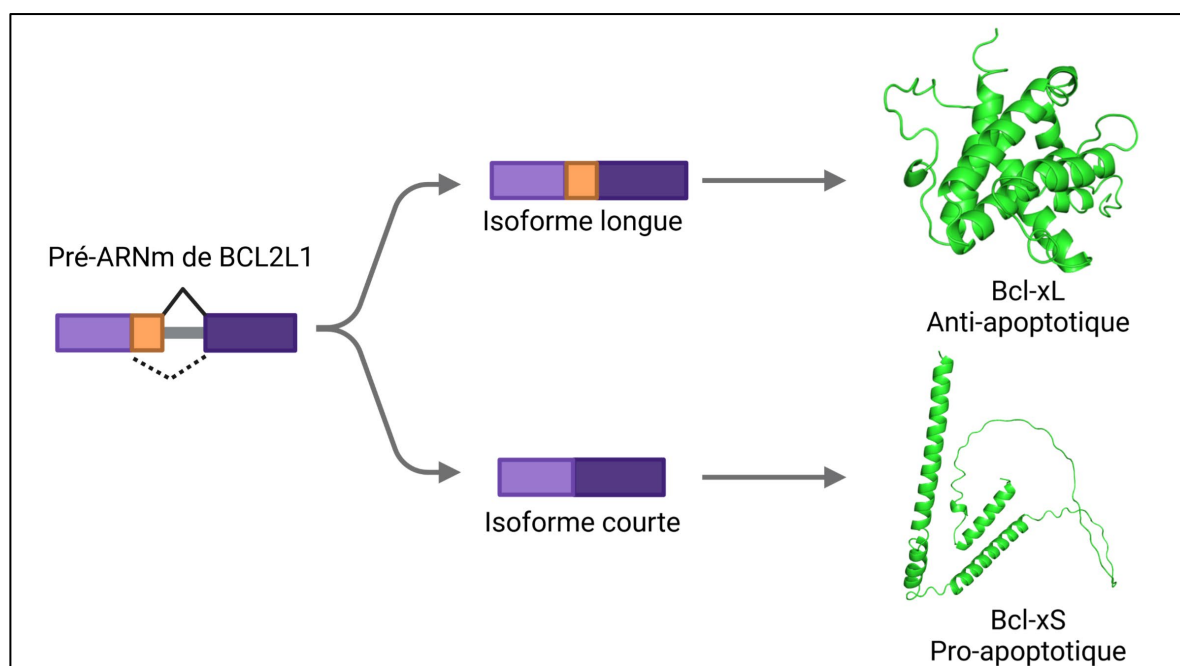


Figure 4. Schéma de l'épissage alternatif du gène *BCL2L1*. L'utilisation d'un site d'épissage en 5' permet de produire deux isoformes, une anti-apoptotique, Bcl-xL, et une pro-apoptotique, Bcl-xS. La structure pour Bcl-xL est la structure déterminée par spectroscopie de résonance magnétique nucléaire (1bxl). Pour Bcl-xS, puisqu'aucune structure n'a été déterminée, il s'agit de la structure prédite par AlphaFold2. Fait avec BioRender.

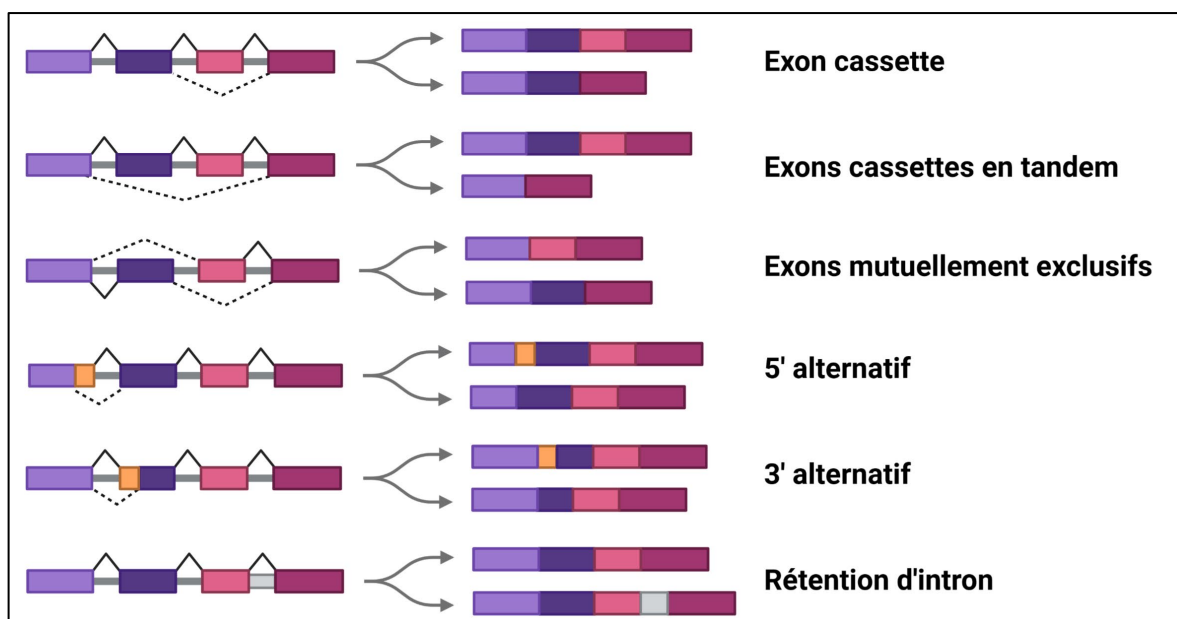


Figure 5. Schéma des différents types d'épissage alternatif. Fait avec BioRender.

produit plutôt la protéine Bcl-xL, qui a plutôt un rôle anti-apoptotique (Boise *et al.*, 1993). Il est donc possible d'apprécier qu'avec l'aide de l'épissage alternatif, la cellule peut complètement inverser l'activité de la protéine produite, sans avoir recours à la transcription de nouveau, lui conférant donc une capacité d'adaptation très rapide. Il existe plusieurs types d'évènements d'épissage alternatif dont les conséquences fonctionnelles diffèrent grandement en fonction de leur nature (Figure 5) (Keren *et al.*, 2010). Tout d'abord, il est possible d'inclure ou d'exclure un seul exon; cet exon est alors nommé exon cassette. Plusieurs exons consécutifs peuvent aussi être retirés ou conservés ensemble; on les nommera alors exons cassettes en tandem. Certains exons peuvent être incompatibles ensemble; lorsqu'un sera retiré, l'autre sera conservé, et vice-versa. Il s'agit d'exons mutuellement exclusifs. Des portions d'exons en amont ou en aval de l'intron peuvent aussi être retirées, si l'exon en question présente un deuxième site d'épissage pouvant être reconnu par le spliceosome (voir la section *Le spliceosome et la réaction d'épissage*). Ces évènements seront nommés 5' alternatif si la partie de l'exon retirée est en amont de l'intron (le site d'épissage alternatif est en 5'), et 3' alternatif si la partie de l'exon retirée est en aval de l'intron (le site d'épissage alternatif est en 3'). Finalement, des introns peuvent aussi être incorrectement reconnus par la machinerie d'épissage et

conservés au sein de l'ARNm mature, cet évènement d'épissage alternatif est nommé rétention d'intron. Il est à souligner que des signaux de polyadénylation peuvent être présents de manière différentielle dans les régions épissées en 3' de l'ARN, promouvant ainsi l'utilisation de différents sites de polyadénylation dans différentes isoformes du même pré-ARNm. De la même manière, différents sites d'initiation de la transcription peuvent aussi être utilisés pour initier la transcription, amenant différents exons en 5' de l'ARNm. Ces deux derniers cas ne sont pas à proprement parler des évènements d'épissage alternatif, mais soulignent plutôt les conséquences sur l'ARNm mature de l'épissage alternatif ainsi que l'impact du site d'initiation de la transcription sur l'arrangement final de l'ARNm mature.

### ***Le spliceosome et la réaction d'épissage***

L'épissage, qu'il soit constitutif ou alternatif, est catalysé par un large complexe ribonucléoprotéique, nommé spliceosome, constitué de 5 petits ARN nucléaires (snRNA, *small nuclear RNA*), soit U1, U2, U4, U5 et U6, et de plus de 200 protéines auxiliaires chez les eucaryotes pluricellulaires. Chacun de ces snRNA s'assemble avec certaines protéines pour former les cinq petites ribonucléoprotéines nucléaires du même nom (snRNP, ou *small nuclear ribonucleoprotein*) (Lee et Rio, 2015). Le spliceosome reconnaît les jonctions d'épissage et catalyse deux réactions de transestérification pour permettre l'excision de l'intron et la liaison des deux exons ensemble (Boudreault *et al.*, 2019 - Voir Annexe 1; Kim *et al.*, 2008; Lee et Rio, 2015; Merkhofer *et al.*, 2014). Les principaux éléments nucléotidiques nécessaires à l'épissage sont le site d'épissage en 5' et le site d'épissage en 3', qui lui-même comporte une chaîne de plusieurs pyrimidines à la toute fin de l'intron ainsi que le point de branchement qui va permettre la première réaction de transestérification (Figure 6A) (Garrett *et al.*, 2013; Kim *et al.*, 2008; Lee et Rio, 2015; Ule et Blencowe, 2019; Wang *et al.*, 2015). Premièrement, le site d'épissage en 5' et le point de branchement sont reconnus par les complexes U1 et U2, respectivement (Figure 6B). Ensuite, le complexe formé par U4, U5 et U6 (U4/U6.U5) est recruté. Cela entraîne une réorganisation structurelle et la relâche d'U1 et d'U4, et permet

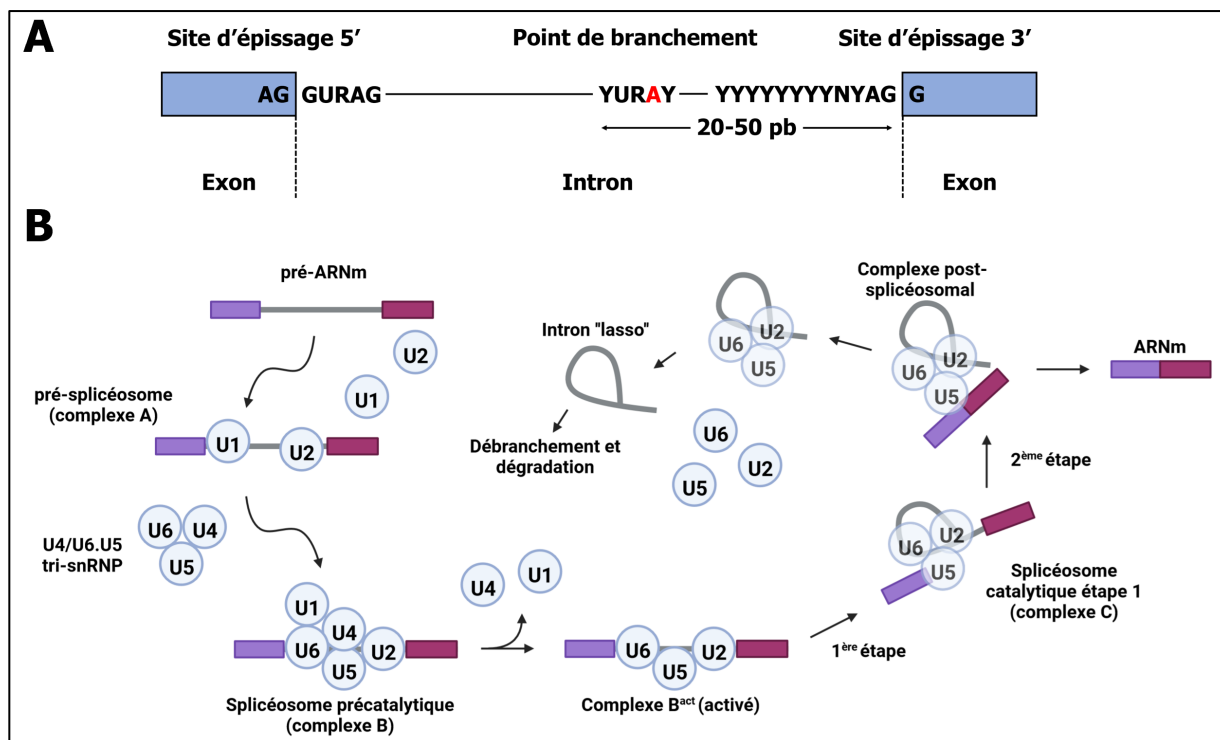


Figure 6. Schéma de la réaction d'épissage ainsi que des régions requises dans l'ARN pré-messager. (A) Régions requises dans l'ARN pré-messager pour l'épissage et reconnues par les snRNP. (B) Schéma de la réaction d'épissage. Fait avec BioRender.

l'activation du complexe B. Cette réorganisation du complexe permettant l'activation requière notamment les protéines EFTUD2, une GTPase, et la protéine SNRNP200, une hélicase, du complexe U5 (Newman, 1997; Wood *et al.*, 2021). Le point de branchement est maintenant tout près du site d'épissage en 5' grâce à la nouvelle connexion entre les complexes U6 et U2. Durant la première étape, le groupement 2' hydroxyle de l'adénosine du point de branchement réalise une attaque nucléophile sur le 5' phosphate du premier nucléotide de l'intron dans le site d'épissage en 5', habituellement une guanine. L'attaque nucléophile brise la liaison entre l'exon en amont et l'intron, et en forme une nouvelle entre l'intron et le point de branchement. Dans la deuxième étape, le groupement 3' OH à l'extrémité 5', maintenant libre, attaque le dernier nucléotide de l'intron, habituellement aussi une guanine. Cela permet de lier les deux exons ensemble et relâche l'intron sous forme de lasso. La protéine PRPF8, principale composante du complexe U5, est critique pour ces deux dernières étapes, notamment en liant les sites d'épissage en 5' et en 3' (Wahl *et al.*,

2009). Normalement, l'épissage constitutif se fait de manière cotranscriptionnelle; l'intron est retiré peu après sa transcription par la polymérase à ARN II (Merkhofer *et al.*, 2014; Wang *et al.*, 2015). Dans le cas de l'épissage alternatif, ce processus peut-être couplé de manière très serrée à la transcription, ou plutôt découplé; effectivement, si on imagine un exon cassette pouvant être retiré, il faut alors que les deux introns le ceinturant aient été transcrits pour permettre son excision (Vargas *et al.*, 2011). L'implication de plusieurs séquences régulatrices, autant introniques qu'exoniques et en aval de l'évènement expliquent aussi souvent le découplage entre transcription et épissage alternatif. De plus, l'épissage n'est pas exclusivement nucléaire; plusieurs exemples d'introns retenus dans les transcrits et épissés dans le cytoplasme existent (Buckley *et al.*, 2014). Bien que l'activité du spliceosome dans le cytoplasme soit débattue, certains de ces introns sont épissés par d'autres mécanismes, tels que l'ARNm codant pour la protéine XBP1. Cette protéine est notamment impliquée dans la réponse au stress liée aux protéines mal repliées et permet l'expression de chaperonnes et de protéases via son activité de facteur de transcription (Yoshida, 2007). Suite à ce stress, l'activation d'IRE1, une kinase et endonucléase, permet de retirer un petit intron de 26 nucléotides dans l'ARNm de XBP1 dans le cytoplasme grâce à son activité endonucléase. Le retrait de cet intron induit un changement du cadre de lecture dans l'ARNm de XBP1, permettant de produire l'isoforme XBP1s de 40 kDa, plutôt que l'isoforme XBP1u de 33 kDa lorsque l'intron est présent. L'isoforme XBP1s possède une plus grande activité pour permettre l'expression des gènes de réponse face à la réponse au stress liée aux protéines mal repliées (Yoshida, 2007).

### ***Importance des régions régulatrices dans l'épissage alternatif***

L'épissage alternatif émerge de la capacité du spliceosome à s'assembler ou non à différentes jonctions d'épissage. Bien évidemment, la force intrinsèque des sites d'épissage dicte en partie si le spliceosome peut s'assembler à cette jonction ou non. Cependant, de nombreuses jonctions d'épissage sont considérées comme faibles, et des séquences régulatrices en amont et en aval dans l'ARN et liées par des protéines,

les facteurs d'épissage, vont soit stabiliser l'assemblage du spliceosome ou le déstabiliser (Berget, 1995; Black, 1995, 2003; Boudreault *et al.*, 2019 - Voir Annexe 1; Wang *et al.*, 2015; Woodley et Valcárcel, 2002). Les protéines SR, comme SRSF1, SRSF2 et SRSF3, se lient à des régions activatrices introniques ou exoniques et vont stabiliser le spliceosome dans sa formation (Figure 7). À l'opposé, les facteurs inhibiteurs, tels que les protéines hnRNP comme hnRNPA1 et hnRNPA2B1, vont se lier à des régions inhibitrices introniques ou exoniques et déstabiliser l'assemblage du spliceosome (Figure 7). La somme de tous ces signaux dictera la capacité du spliceosome à s'assembler, ou non, à la jonction d'épissage. En fait, il faudrait plutôt parler de fréquence d'assemblage, puisque les différents sites d'épissages sont en compétition entre eux pour l'assemblage du spliceosome. De ce fait, il est très rare de n'observer que l'espèce X pour un événement d'épissage alternatif dans la condition basale et que l'espèce Y suite à un traitement ou un stimulus; soit un nouveau site sera maintenant utilisé, amenant l'apparition de l'espèce Y suite au traitement, soit les deux formes seront présentes dans les deux conditions, mais leur ratio va varier. Il est aussi important de souligner que malgré l'activité classique activatrice des protéines SR et inhibitrice des hnRNP sur l'assemblage du spliceosome, ces classes de protéines peuvent aussi avoir une activité déstabilisatrice et stabilisatrice, respectivement, en fonction de l'endroit qui sera lié au sein du pré-ARNm. Donc, la classe de protéine, sa position par rapport au site

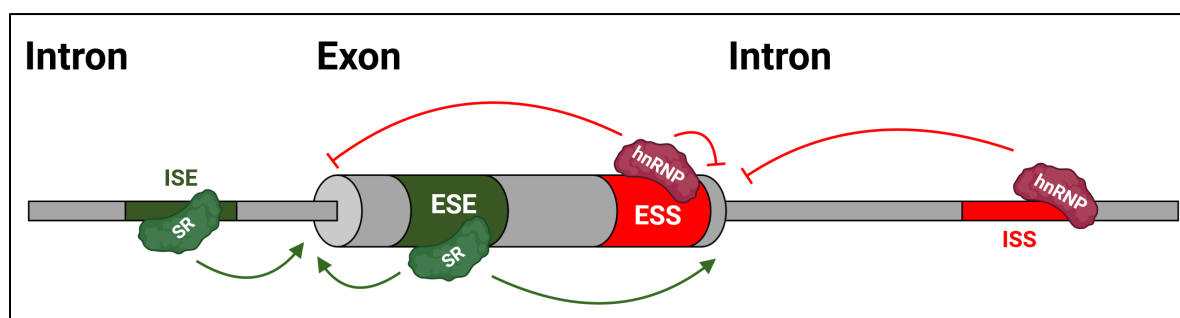


Figure 7. Schéma des régions régulatrices de l'épissage alternatif. Les régions activatrices, qu'elles soient introniques (*intronic splicing enhancer*, ISE) ou exoniques (*exonic splicing enhancer*, ESE), sont liées principalement par les protéines de type SR, qui vont favoriser l'assemblage du spliceosome. Les régions inhibitrices, qu'elles soient introniques (*intronic splicing silencer*, ISS) ou exoniques (*exonic splicing silencer*, ESS) sont liées principalement par les protéines de type hnRNP, qui vont déstabiliser l'assemblage du spliceosome. Fait avec BioRender et adapté de Boudreault et al., 2019.



d'épissage, ainsi que l'ensemble des autres protéines et leur position respective permettent de dicter ce qui est reconnu comme un exon et conservé au sein de l'ARNm mature (Lee et Rio, 2015). La plupart de ces protéines sont stockées dans les *nuclear speckles*, des compartiments nucléaires sans membrane servant de réserves et se localisant souvent à proximité des sites de transcription actifs (Galganski *et al.*, 2017).

### ***Épissage alternatif et maladies***

De nombreuses maladies présentent des dérégulations de l'épissage alternatif, soulignant ainsi le rôle central de l'épissage alternatif dans le maintien des fonctions cellulaires normales dans les cellules saines. Des dérégulations de l'épissage alternatif sont présentes dans la maladie de Parkinson (Soreq *et al.*, 2014), l'arthrite rhumatoïde (Turkkila *et al.*, 2015) et la sclérose latérale amyotrophique (Prudencio *et al.*, 2015). L'exemple le mieux caractérisé reste cependant le cancer et sera abordé dans la section suivante.

#### *Cancer*

Les cellules cancéreuses accumulent au cours du processus de carcinogenèse de nombreuses aberrations au niveau de leur épissage alternatif, qui contribuent à leur transformation (David et Manley, 2010; Oltean et Bates, 2014; Shkreta *et al.*, 2013). L'exemple du gène *BCL2L1* est un exemple classique (abordé à la section *L'épissage constitutif et alternatif*), mais de nombreux autres gènes tels que *CCND1*, *PKM2*, *CD44* et *VEGFA* possèdent aussi des isoformes surexprimées dans les cancers qui participent à tous les processus caractéristiques dérégulés par la carcinogenèse comme le cycle cellulaire, l'évasion du système immunitaire, le métabolisme et l'angiogenèse (David et Manley, 2010). Vers la fin des années 2000, l'accent a été mis particulièrement sur l'identification d'évènements d'épissage alternatif dérégulés dans les cancers, qui pourraient servir de biomarqueurs ou aider notre compréhension dans le rôle de l'épissage alternatif dans le processus de carcinogenèse (Klinck *et al.*, 2008; Venables *et al.*, 2009; Venables, Klinck, *et al.*, 2008). De plus, de nombreux facteurs d'épissage participent activement au

processus de carcinogenèse. Par exemple, la protéine SRSF1 agit comme un oncogène en favorisant des variants d'épissage de *BIM*, *BIN1* et *BCL2L1* inhibant l'apoptose et en interagissant avec MYC (Anczuków *et al.*, 2012). À l'inverse, RBM4, un autre facteur d'épissage, possède une activité de suppresseur de tumeur favorisant l'isoforme Bcl-xS au lieu de Bcl-xL de *BCL2L1* et antagonisant l'effet oncogénique de SRSF1 (Wang *et al.*, 2014). De nombreuses petites molécules permettant d'altérer l'épissage ont fait l'objet d'études pré-cliniques et cliniques afin de traiter différents types de cancers (Eymin, 2021; Hsu *et al.*, 2015; Salton et Misteli, 2016). L'approche par oligonucléotides ciblés (voir section *Outils moléculaires permettant l'analyse fonctionnelle de l'épissage alternatif*) a elle aussi été utilisée afin d'investiguer le rôle fonctionnel de ces changements d'épissage dans le processus de carcinogenèse et la survie de ces cellules cancéreuses (Brosseau, 2018).

### ***Analyse de l'épissage alternatif***

Il existe plusieurs méthodologies permettant l'analyse et la compréhension de l'épissage alternatif, comportant chacune leurs avantages et leurs inconvénients. Un résumé des principales approches est présenté dans la section suivante, en classant les approches qu'elles soient ciblées, non ciblées et/ou à haut débit, et finalement les outils moléculaires à notre disposition pour interroger le rôle fonctionnel de ces évènements d'épissage. Avant d'entrer plus en détail dans les techniques, la notion de pourcentage d'inclusion,  $\Psi$  (PSI, *percent spliced in*) doit cependant être abordée. Le PSI est la mesure la plus couramment utilisée pour caractériser l'épissage alternatif d'une région différentiellement épissée (Katz *et al.*, 2010). Cette mesure représente le pourcentage de la forme longue de l'évènement, donc la forme où la région différentiellement épissée est incluse, et sa formule est la suivante :

$$\Psi = \frac{\text{Forme longue}}{\text{Forme longue} + \text{forme courte}} * 100$$

Il s'agit donc d'une mesure variant de 0% à 100%; 0% signifiant que seulement la forme courte est présente, et 100%, seulement la forme longue. Cette mesure peut être utilisée avec toutes les approches décrites dans les prochaines sections pour caractériser le comportement d'une région différentiellement épissée.

### *Approches ciblées*

Les approches ciblées principalement utilisées sont basées sur la technique de réaction de polymérisation en chaîne (*polymerase chain reaction*, PCR) (Brosseau, 2018). Premièrement, il est possible d'adapter la conception des amorces de PCR quantitative (*quantitative PCR*, qPCR) pour amplifier de manière spécifique la forme longue ou la forme courte d'un évènement d'épissage alternatif, et ainsi de bénéficier de la précision quantitative du qPCR (Brosseau, 2018). Dans cette approche, la forme longue est amplifiée avec une amorce dans la région partagée par les deux formes et l'autre amorce dans la région différentiellement épissée, permettant l'amplification seulement de la forme longue (Figure 8A) (Brosseau *et al.*, 2010). La forme courte, quant à elle, est plutôt amplifiée par la même amorce dans la région partagée, et une amorce chevauchant la jonction exon-exon spécifique à la forme courte (Figure 8B) (Brosseau *et al.*, 2010). Il est à noter qu'il est aussi concevable dans certains cas d'avoir deux amorces ne chevauchant pas une jonction exon-exon, par exemple si l'évènement analysé consiste en deux exons mutuellement exclusifs (Figure 8C). Deuxièmement, une approche par PCR spécifique à l'épissage alternatif (*alternative splicing PCR*, AS-PCR) peut aussi être utilisée (Brosseau, 2018). Dans cette approche, les amorces sont plutôt placées de part et d'autre de l'évènement d'épissage alternatif, de telle sorte que deux amplicons seront produits : un amplicon court, correspondant à la forme courte de l'évènement (par exemple lorsque l'exon cassette est retiré), et un amplicon long, correspondant à la forme longue de l'évènement (lorsque l'exon cassette est inclus) (Figure 8D). Une PCR en point final (*endpoint PCR*) est ensuite réalisée et les amplicons peuvent être résolus sur gel d'agarose; cependant, ils sont la plupart du temps résolus en électrophorèse capillaire, permettant à la technique d'avoir un débit beaucoup plus élevé (Klinck *et*

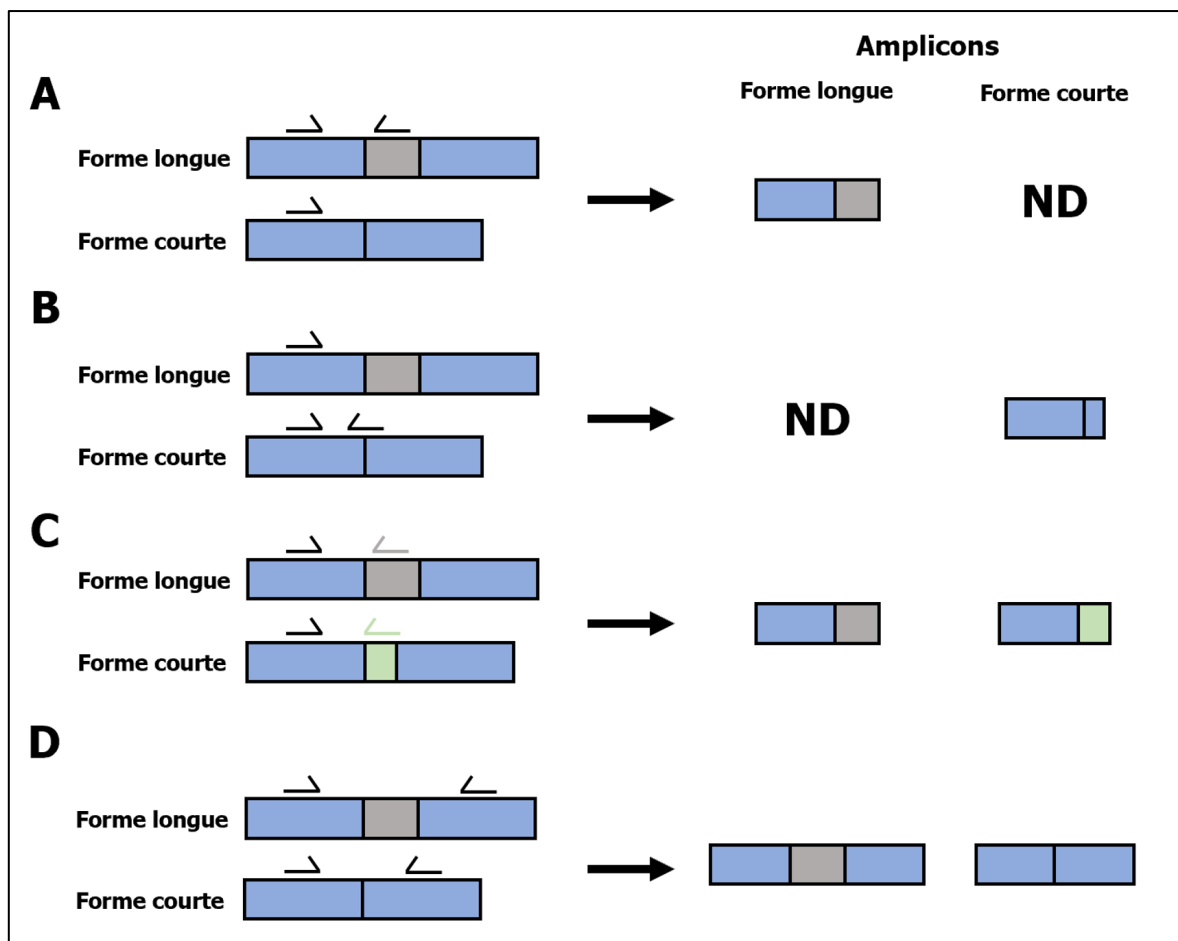


Figure 8. *Schéma des différentes manières de placer des amorces pour analyser l'épissage alternatif.* (A) En qPCR, on place une amorce spécifique à la forme longue dans la région différenciellement épissée, et l'autre amorce dans une région commune. (B) En qPCR, on place une amorce spécifique à la forme courte sur la jonction exon-exon spécifique à cette forme, et l'autre amorce dans une région commune. (C) Il est aussi possible, par exemple ici dans le cas de deux exons mutuellement exclusifs, d'avoir une amorce spécifique à chaque région unique, et l'autre amorce dans une région commune. (D) En AS-PCR, on place des amorces de part et d'autre de la région différenciellement épissée, de manière à obtenir deux amplicons de tailles différentes. Ces amplicons peuvent être résolus par la suite sur gel ou par électrophorèse capillaire.

*al.*, 2008; Venables *et al.*, 2009; Venables, Klinck, *et al.*, 2008; Venables, Koh, *et al.*, 2008). La quantification de la forme longue ou courte se fait via la fluorescence respective induite par un agent intercalant sur gel d'agarose, ou par rapport à un marqueur connu par électrophorèse capillaire; c'est pourquoi on considère que cette technique est semi-quantitative. Bien que sur gel il n'y a théoriquement pas de limite supérieure de séparation de tailles d'amplicons, il est recommandé pour l'électrophorèse capillaire de séparer des fragments de 50 à 600 pb. Ce ne sont donc pas tous les événements d'épissage qui se prêtent à cette technique. Finalement,

autant sur gel que par électrophorèse capillaire, des changements de petite taille (de quelques nucléotides jusqu'à quelques dizaines) seront très difficilement détectables grâce à cette technique. L'utilisation de l'hybridation *in situ* en fluorescence de molécule seule (*single molecule fluorescence in situ hybridization*, smFISH) est aussi compatible avec l'analyse de l'épissage alternatif pour visualiser en cellule la forme longue et la forme courte d'un évènement d'épissage (Vargas *et al.*, 2011; Waks *et al.*, 2011). En utilisant des sondes couplées à un fluorophore pour une région constante et des sondes couplées à un fluorophore différent pour la région différenciellement épissée, deux couleurs seront obtenues : la couleur du premier fluorophore pour la version courte, et un mélange des deux fluorophores pour la version longue. Cette technique permet d'avoir l'information concernant la localisation spatiale de l'ARN dans la cellule, mais nécessite d'avoir une région différenciellement épissée dans les alentours de 700 pb pour accommoder les sondes permettant de visualiser des molécules seules. Cette approche peut être adaptée en créant une construction comportant l'évènement d'épissage d'intérêt ainsi qu'un aptamère d'ARN permettant la détection, comme par exemple l'aptamère MS2 (Rino *et al.*, 2015). Finalement, il est aussi possible d'aller directement cibler les isoformes protéiques encodées par la forme courte et longue d'un transcrit, comme par exemple par buvardage de type Western (*Western-Blot*, WB) (Brosseau, 2018; Brosseau *et al.*, 2014; Ku *et al.*, 2011). L'avantage de cette technique est qu'elle permet d'aller directement évaluer l'impact de l'épissage alternatif sur l'effecteur, soit la protéine produite. Cependant, il est aussi important de suivre l'épissage au niveau de l'ARN en utilisant une des techniques présentées précédemment.

#### *Approches non ciblées/à haut débit*

L'arrivée des technologies de séquençage à haut débit et la diminution progressive des coûts associés à ces expériences ont considérablement changé notre approche de l'analyse de l'épissage. Même avant cette démocratisation du séquençage à haut-débit, l'apparition des micropuces à ADN sondant de nombreux isoformes d'ARN permettait d'analyser de manière plus exhaustive l'épissage alternatif dans plusieurs

conditions expérimentales (Woodley et Valcárcel, 2002). Cette approche a été utilisée avec succès dans plusieurs études, notamment pour caractériser l'impact du VIH et du VEB sur l'épissage alternatif cellulaire (Homa *et al.*, 2013; Imbeault *et al.*, 2012; Wilhelm *et al.*, 2008). Cette approche restait ciblée, bien que permettant l'analyse d'un très grand nombre d'isoformes d'ARN à la fois. L'utilisation des technologies de séquençage à haut débit appliqué au transcriptome, ou séquençage d'ARN (RNA-Seq), a véritablement permis une approche non ciblée et permettant d'aller interroger l'épissage alternatif de tous les gènes de la cellule (Metzker, 2010). L'apport de la bio-informatique à cette approche a été crucial, puisque l'obtention des lectures du séquençage n'apporte aucune information sans leur analyse par bio-informatique. Par exemple, les adaptateurs doivent être retirés des lectures obtenues, la qualité des lectures validée et les lectures amputées de leur fragment de moins bonne qualité, ces lectures alignées sur le génome ou le transcriptome et ensuite comptées pour obtenir une idée de l'abondance des gènes desquels elles proviennent. De nombreux programmes bio-informatiques ont été développés pour effectuer ces étapes de manière optimale (Alamancos *et al.*, 2014; Bray *et al.*, 2015; Fang *et al.*, 2012; Katz *et al.*, 2010; Kvam *et al.*, 2012; Li et Dewey, 2011; Li *et al.*, 2014; Shen *et al.*, 2014; Vaquero-Garcia *et al.*, 2016). Récemment, de nouvelles approches basées sur le séquençage, mais plus ciblées permettant notamment d'enrichir la librairie de séquençage pour les gènes d'intérêt, tels que le RASL-Seq et le MPE-Seq, sont apparues afin de permettre des analyses plus ciblées et ainsi augmenter le pourcentage d'information d'intérêt suite au séquençage (Li *et al.*, 2012; Thompson *et al.*, 2018; Xu *et al.*, 2019). Finalement, l'avènement de la technologie de séquençage de longues lectures, notamment le séquençage par nanopores principalement développé par Oxford Nanopore Technologies, permet maintenant une lecture complète et directe de la molécule d'ARN d'une extrémité à l'autre (Leonardi et Leger, 2021). Cette technologie rend donc possible le séquençage de chaque transcrit dans son ensemble, avec ses différentes régions d'épissage, et contourne le problème de la division de l'information liée à la fragmentation dans le séquençage de lecture courte de type Illumina.

### *Outils moléculaires permettant l'analyse fonctionnelle de l'épissage alternatif*

Les outils moléculaires permettant de changer la proportion des formes relatives d'un évènement d'épissage sont absolument cruciaux afin d'interroger la fonction de ces différentes isoformes. Les premières approches ont utilisé des oligonucléotides antisens (ASO, *antisense oligonucleotide*) complémentaires au site d'épissage aberrant en 5' dans le gène de la  $\beta$ -globine afin de le masquer et rediriger l'épissage vers le site 5' canonique (Dominski et Kole, 1993). Cette approche a été utilisée de nombreuses fois depuis afin de corriger l'épissage anormal provenant de mutations et, plus récemment, afin d'interroger le rôle de l'épissage alternatif durant l'infection avec le virus de l'influenza (Garcia-Blanco, 2006; Kole *et al.*, 2012; Thompson *et al.*, 2020; Zammarchi *et al.*, 2011). Dans le même ordre d'idée, il a aussi été remarqué que des petits ARN interférents (siRNA, *small interfering RNA*) se liant près d'un exon alternatif influencent son épissage (Alló *et al.*, 2009). Des travaux menés à l'Université de Sherbrooke durant les années 2000 ont permis de développer des oligonucléotides bifonctionnels permettant de moduler spécifiquement l'épissage à un site précis (Brosseau *et al.*, 2014; Villemare *et al.*, 2003). Ces oligonucléotides sont formés d'une partie s'hybridant à la région d'intérêt, permettant ainsi le ciblage spécifique de l'oligonucléotide à sa cible, ainsi que d'une queue flottante, permettant de recruter des facteurs d'épissage permettant d'aider ou de déstabiliser l'assemblage du spliceosome, comme les sites de liaison pour TDP-43 ou hnRNP A1, respectivement (Brosseau *et al.*, 2014). Il est donc possible de favoriser la forme longue de l'évènement d'épissage; un tel oligonucléotide sera nommé TOES (oligonucléotide ciblé favorisant l'épissage, *targeted oligonucleotide enhancer of splicing*). À l'inverse, un oligonucléotide favorisant la forme courte de l'épissage sera nommé TOSS, pour oligonucléotide ciblé défavorisant l'épissage (*targeted oligonucleotide silencer of splicing*). Finalement, l'avènement de la technologie d'édition du génome CRISPR-Cas9 permet maintenant d'aller effectuer l'invalidation génique de manière précise (Ran *et al.*, 2013). Dans un contexte où le gène d'intérêt est invalidé, il serait alors possible de réintroduire de manière exogène chaque

isoforme dont on veut étudier la fonction, bien que cette technique n'ait pas encore été utilisée à ma connaissance.

## **Les virus et l'épissage alternatif**

### *Utilisation de la machinerie d'épissage pour épisser les ARN viraux*

Le lien entre l'épissage et les infections virales est très impressionnant; les premières observations de l'épissage ont été faites notamment sur les ARN d'adénovirus à la fin des années 70 (Berget *et al.*, 1977; Chow *et al.*, 1977). Avant que nous soyons conscients de l'importance de l'épissage chez l'humain, nous savions déjà que certains virus pouvaient épisser leurs propres ARN. Il s'agit en effet d'une machinerie cellulaire extrêmement intéressante à usurper pour les virus. La pression sélective sur ceux-ci les force à maintenir le plus petit génome possible, afin de conserver une taille minimale et d'éviter plus efficacement la détection par l'hôte. Cependant, cette même pression réduit ainsi la diversité génique au sein du virus. Usurper la machinerie d'épissage de la cellule-hôte permet donc à certains virus d'augmenter le potentiel codant de leur génome (Meyer, 2016). Les exemples les plus connus sont bien sûr les adénovirus, ainsi que le VIH et le VPH (Akusjarvi, 2008; Dowling *et al.*, 2008; Fukuhara *et al.*, 2006; Johansson et Schwartz, 2013). La dépendance de certains virus à l'utilisation de cette machinerie peut même être exploitée afin de mettre au point des antiviraux ciblant des facteurs de la cellule-hôte, une approche qui a été récemment utilisée pour développer de nouvelles classes de médicaments contre le VIH (Shkreta *et al.*, 2017).

### *Impact des virus sur l'épissage alternatif cellulaire*

Si la découverte de l'épissage en étudiant des ARN viraux nous permettait déjà d'apprécier leur capacité à usurper le spliceosome il y a plus de 40 ans, il aura fallu attendre une trentaine d'années supplémentaires avant que la question inverse, soit l'impact des virus sur l'épissage alternatif de leur cellule-hôte, ne commence à être posée de manière généralisée. L'avènement des technologies de séquençage a notamment permis aux chercheurs d'interroger de manière non biaisée le



transcriptome de cellules infectées avec des virus. Les premières études s'intéressaient bien sûr à l'impact des virus sur l'expression génique de la cellule-hôte suite à l'infection (Chang *et al.*, 2011; Tempera *et al.*, 2016; Xu *et al.*, 2016, p. 6), mais avec le développement d'outils bio-informatiques et la facilité d'interroger ces mêmes données pour l'épissage alternatif, de plus en plus d'études strictement transcriptomiques se sont intéressées à l'impact des virus sur l'épissage (Gao *et al.*, 2018; Hu *et al.*, 2016, 2017; Martin *et al.*, 2016; Niu *et al.*, 2017; Zhu *et al.*, 2018). Bien évidemment, de telles études n'apportent que peu d'explications sur les raisons biologiques ainsi que les mécanismes de cette modulation. Des revues exhaustives sur le sujet ont d'ailleurs été publiées récemment (Ashraf *et al.*, 2019; Boudreault *et al.*, 2019 - Voir Annexe 1; Chauhan *et al.*, 2019; Cross *et al.*, 2019); la section suivante se veut donc plutôt un résumé des différents mécanismes qui sont utilisés par les virus pour moduler l'épissage alternatif ainsi que de nos connaissances actuelles sur son rôle dans les interactions virus-hôtes plutôt qu'une liste exhaustive des exemples connus.

Certaines protéines virales possèdent de manière intrinsèque la capacité de moduler l'épissage alternatif cellulaire. Deux exemples intéressants sont les polymérases d'ARN dépendante de l'ARN NS5 du virus de la Dengue de la famille des *Flaviviridae*, ainsi que 3D<sup>pol</sup> du virus EV71 de la famille *Picornaviridae*. Malgré que la réplication de ces deux virus soit exclusivement cytoplasmique, leur polymérase se localise aussi dans le noyau de la cellule infectée, où elle interagit avec des composantes du complexe U5 du spliceosome pour déstabiliser l'épissage dans la cellule-hôte (Liu *et al.*, 2014; Maio *et al.*, 2016). La protéine SM du VEB, interagissant avec l'ARNm de *STAT1* pour déplacer SRSF1 et recruter SRSF3, est un autre exemple d'interaction directe avec les ARN cellulaires ainsi que des facteurs d'épissage pour en moduler l'activité (Verma *et al.*, 2010; Verma et Swaminathan, 2008). L'exemple le plus étudié reste cependant la protéine ICP27 du *Herpes Simplex virus 1*, un *Herpesviridae*. Cette protéine inhibe l'épissage *in vitro* et interagit avec SF3B2, une protéine impliquée dans le complexe U2 du spliceosome (Bryant *et al.*, 2001; Hardy

et Sandri-Goldin, 1994; Lindberg et Kreivi, 2002). Elle cause aussi la redistribution dans le noyau des snRNP et du facteur d'épissage SRSF2 avec lequel elle interagit directement (Phelan *et al.*, 1993; Sandri-Goldin *et al.*, 1995). Finalement, elle interagit avec SRPK1, une kinase responsable de phosphoryler de nombreux facteurs d'épissage de la famille SR, ce qui induit leur hypophosphorylation (Sciabica *et al.*, 2003). Malgré toutes ces études, il n'est toujours pas clair par quel(s) mécanisme(s) ICP27 altère l'épissage cellulaire (Sandri-Goldin, 1994, 1998, 2008; Smith *et al.*, 2005). Beaucoup de virus possèdent aussi des ARN non codants (micro-ARN, long ARN non codants, etc.) qui peuvent aussi avoir un effet sur l'épissage alternatif cellulaire. Par exemple, le VEB possède aussi deux petits ARN non codants, EBER1 et EBER2, qui s'accumulent dans le noyau des cellules infectées en très grande quantité. Il a été démontré que l'expression de ces deux ARN dans des cellules induisait des changements dans l'épissage alternatif et qu'EBER1 est en mesure d'interagir avec le facteur d'épissage AUF1/hnRNP D (Lee *et al.*, 2012; Pimienta *et al.*, 2015). Un autre exemple intéressant est le virus Sindbis, de la famille des *Togaviridae*. Ce virus possède deux sites de liaison pour la protéine cellulaire HuR dans la région non traduite en 3' de ses ARN subgénomiques, permettant de séquestrer la protéine dans le cytoplasme lors de l'infection (Barnhart *et al.*, 2013; Dickson *et al.*, 2012). Cette séquestration induit notamment des changements dans l'épissage alternatif de deux gènes régulés par HuR, *PCBP2* et *DST*. Ces exemples ainsi que d'autres sont résumés dans le tableau 2. Plusieurs virus à ARN se répliquent à l'intérieur de structures spécialisées d'origine virale, comme les VF chez réovirus. Chez rotavirus, un autre *Reoviridae*, il a été démontré que les usines de réplication, nommées viroplasmes, peuvent séquestrer de nombreuses hnRNP ainsi que des protéines liant des séquences AU-riches, telles que HuR (Dhillon *et al.*, 2018). De manière plus générale, de nombreux virus perturbent l'import et l'export nucléaire, pouvant mener à la relocalisation du noyau vers le cytoplasme de certains facteurs d'épissage; c'est le cas de rhinovirus, un *Picornaviridae*, qui relocalise SFPQ dans le

Tableau 2. *Résumé des principaux mécanismes connus de modulation de l'épissage alternatif par des virus.* Adapté de Boudreault et al., 2019.

Virus	Famille	Génome	Mécanisme
Herpes Simplex virus II	<i>Herpesviridae</i>	ADNdb	Liaison directe d'ICP27 à certains pré-ARNm
Virus de la maladie de Marek	<i>Herpesviridae</i>	ADNdb	Interaction probable d'ICP27 avec SRSF3
Virus Epstein-Barr	<i>Herpesviridae</i>	ADNdb	La protéine SM déplace SRSF1 du pré-ARNm et recrute SRSF3
Cytomegalovirus humain	<i>Herpesviridae</i>	ADNdb	Surexpression de CPEB1 durant l'infection
Virus sindbis	<i>Togaviridae</i>	ARNsb de polarité positive	Les ARN subgénomiques du virus contiennent des sites de liaison à la protéine HuR dans leur 3' UTR, ce qui induit la séquestration d'HuR dans le cytoplasme
Virus de la dengue	<i>Flaviviridae</i>	ARNsb de polarité positive	NS5 interagit avec CD2BP2 et DDX23 du complexe U5 du spliceosome
EV71	<i>Picornaviridae</i>	ARNsb de polarité positive	3D <sup>pol</sup> interagit avec PRPF8 pour bloquer la seconde étape catalytique de la réaction d'épissage
Poliovirus	<i>Picornaviridae</i>	ARNsb de polarité positive	2A <sup>pro</sup> bloque la seconde étape catalytique de la réaction d'épissage 2A <sup>pro</sup> induit une redistribution nucléo-cytoplasmique sélective de HuR et TIA1/TIAR
Virus de l'influenza (type A)	<i>Orthomyxoviridae</i>	ARNsb de polarité négative	Interaction de NS1 avec CPSF4 L'interaction de NS1 avec hnRNP K induit sa relocalisation à l'intérieur des <i>nuclear speckles</i>

cytoplasme suite à son clivage par une protéase virale (Flather *et al.*, 2018). Les virus peuvent aussi moduler les niveaux d'expression de ces mêmes facteurs d'épissage. Un exemple bien connu est le VPH, qui dépend de l'expression de facteurs d'épissage tels que SRSF2 et SRSF3 à des étapes précises de son cycle de réplication qui se fait en même temps que la différenciation des kératinocytes (Klymenko *et al.*, 2016; McPhillips *et al.*, 2004; Mole, McFarlane, *et al.*, 2009; Mole, Milligan, *et al.*, 2009). Plusieurs facteurs d'épissage, dont les protéines SR, sont dépendantes de modifications post-traductionnelles, comme la phosphorylation. Les adénovirus (*adenoviridae*) et le virus de la vaccine (*poxviridae*) induisent tous deux l'hypophosphorylation des protéines SR suite à l'infection (Huang *et al.*, 2002; Kanopka *et al.*, 1998). Ces divers exemples résument les différents mécanismes qui peuvent permettre aux virus d'interférer avec l'épissage au sein de la cellule qu'ils infectent.

Bien entendu, le fait que plusieurs virus provenant de familles différentes et ayant des hôtes et des tropismes différents causent tous des changements de l'épissage alternatif cellulaire suppose un bénéfice pour la réplication virale d'induire de tels changements ou un mécanisme de défense de la cellule-hôte. De plus, la présence

de macromolécules d'origine virale comme responsables de ces changements supporte plutôt la première hypothèse. Malheureusement, l'état de la recherche actuelle démontre un manque criant de résultats pouvant nous renseigner sur le rôle fonctionnel de ces changements dans la réplication virale. Cependant, les quelques exemples connus où le rôle de ces changements a été analysé confirment un bénéfice pour la réplication virale (Kuo *et al.*, 2016; Maio *et al.*, 2016; Thompson *et al.*, 2020). L'exemple le plus parlant à ce jour est certainement le virus de l'influenza, pour lequel le groupe de la Pr. Kristen Lynch à l'University of Pennsylvania a démontré que les gènes dont l'épissage est modifié par le virus ont un impact sur sa réplication (Thompson *et al.*, 2020). Dans un deuxième temps, ils ont directement modulé l'épissage alternatif de ces gènes avec des ASO et démontré que cette modulation était requise pour une réplication optimale du virus. Finalement, ils ont aussi démontré que cet effet était additif et que rétablir l'épissage alternatif de plusieurs gènes en même temps augmentait l'effet délétère sur la réplication du virus. Un autre exemple est l'infection avec *Herpes Simplex virus 1*, qui favorise un variant d'épissage du gène *MX1* (Ku *et al.*, 2011). Malgré l'activité antivirale de la protéine MxA encodée par ce gène, ce variant d'épissage produit plutôt une isoforme de MxA qui favorise la réplication du virus, soulignant encore une fois la possibilité d'inverser complètement la fonctionnalité d'une protéine grâce à l'épissage alternatif. Malheureusement, il s'agit des seuls exemples que nous ayons présentement afin de comprendre le rôle de l'épissage alternatif dans les interactions virus-hôte.

De plus, de nombreux gènes du système antiviral cellulaire permettant de combattre l'infection possèdent plusieurs isoformes ayant différentes activités en fonction de leur épissage alternatif (Dörner *et al.*, 2004; Hardy et O'Neill, 2004; van Eyndhoven *et al.*, 1998, 1999). Il serait donc logique de penser que les virus modulent l'épissage alternatif de ces gènes de manière préférentielle. Cependant, les études transcriptomiques montrent plutôt un enrichissement dans les gènes impliqués dans les processus de maturation des ARN, tels que l'épissage, l'ajout d'une structure coiffe ou la polyadénylation (Fabozzi *et al.*, 2018; Han *et al.*, 2018; Hu *et al.*, 2016,

2017; Rivera-Serrano *et al.*, 2017). Encore une fois, de plus amples études seront nécessaires afin de bien comprendre pourquoi et comment ces gènes sont ciblés préférentiellement. Finalement, de nombreux facteurs d'épissage ont été démontrés comme étant nécessaires à la réplication des virus (Brunetti *et al.*, 2015; Dechtawewat *et al.*, 2015; Friedrich *et al.*, 2014; Jagdeo *et al.*, 2015; Kuo *et al.*, 2016; Lawrence *et al.*, 2012; Lin *et al.*, 2015; Shwetha *et al.*, 2015; Zhao *et al.*, 2012); le seul exemple connu d'un facteur d'épissage limitant la réplication est SRSF2 dans la réplication de réovirus (Rivera-Serrano *et al.*, 2017). De manière intéressante, il a aussi été démontré que SRSF2 limite l'activité oncolytique de KM-100, une des versions oncolytiques du *Herpes Simplex virus 1* (Workenhe *et al.*, 2016). Bien que ces résultats suggèrent des impacts potentiels sur l'épissage alternatif cellulaire, ils soulignent surtout que ces protéines sont souvent détournées par les virus afin d'aider à leur réplication, et donc qu'il est possible que le partage de la machinerie cellulaire vienne avec un coût sur la capacité de la cellule à maintenir son épissage alternatif.

## **Hypothèse/problématique**

Nous avons émis l'hypothèse que réovirus, un virus oncolytique prometteur comme traitement contre le cancer, induit des changements d'épissage alternatif durant l'infection. Ces changements seraient le résultat d'un mécanisme d'origine virale, et présenteraient un avantage pour le virus dans son combat contre la cellule-hôte. Il était donc primordial d'investiguer ces changements et leur rôle dans les interactions virus-hôtes, afin de mieux comprendre réovirus et potentiellement de développer de nouvelles avenues pour optimiser son potentiel oncolytique.

### *Objectifs*

#### **Objectif #1**

Investiguer et caractériser, grâce au séquençage d'ARN à haut-débit, les changements d'épissage alternatif induits par réovirus dans la cellule-hôte lors de l'infection.

#### **Objectif #2**

Advenant le cas où de tels changements pourraient être mis en évidence, identifier la protéine virale responsable de ces changements d'épissage alternatif et caractériser son mécanisme d'action et les protéines cellulaires impliquées.

#### **Objectif #3**

Advenant le cas où des protéines cellulaires seraient identifiées comme impliquées dans ces changements, interroger le rôle des protéines cellulaires ciblées par réovirus pour induire ces changements d'épissage alternatif dans les interactions virus-hôte.

## RÉSULTATS

### ARTICLE 1

#### **Global Profiling of the Cellular Alternative RNA Splicing Landscape during Virus-Host Interactions**

**Auteurs de l'article:** Boudreault S, Martenon-Brodeur C, Caron M, Garant JM, Tremblay MP, Armero VES, Durand M, Lapointe E, Thibault P, Tremblay-Létourneau M, Perreault JP, Scott MS, Lemay G, Bisailon M.

**Statut de l'article :** Article publié dans PLoS One en septembre 2016, 11(9): e0161914.

**Avant-propos:** J'ai participé à la conception du projet et j'ai effectué la majorité des expériences ainsi que l'analyse des résultats (>90%). J'ai généré les figures et j'ai participé à l'écriture du manuscrit avec l'aide des Pr Bisailon et Lemay. J'ai aussi participé à la réponse aux évaluateurs en écrivant la lettre de réponse.

**Résumé :** L'épissage alternatif est un mécanisme central de régulation génique qui modifie la séquence codante des transcrits d'ARN chez les eucaryotes supérieurs. L'épissage alternatif permet d'augmenter la variabilité ainsi que la diversité du protéome cellulaire en changeant la composition des protéines résultantes à travers le choix différentiel d'exons étant inclus dans l'ARNm mature. Dans la présente étude, les altérations de l'épissage alternatif cellulaire suite à l'infection virale ont été investigués en utilisant réovirus comme modèle. Notre étude fournit le premier portrait compréhensif des changements globaux de l'épissage alternatif qui sont induits dans les cellules eucaryotes suite à l'infection avec un virus humain. Nous avons identifié 240 évènements d'épissage alternatif modulés suite à l'infection qui

appartiennent à des transcrits impliqués dans la régulation de l'expression génique ainsi que dans le métabolisme des ARN. En utilisant la spectrométrie de masse, nous avons confirmé des changements dans les peptides provenant de transcrits spécifiques résultant de l'épissage alternatif dans les cellules infectées. Ces découvertes apportent davantage d'éclairage sur la complexité des interactions virus-hôtes alors que ces variants d'épissage gonflent la diversité et la fonction protéique durant les infections virales.



## **Global Profiling of the Cellular Alternative RNA Splicing Landscape During Virus-host Interactions**

### Alternative Splicing and Viral Infection

Simon Boudreault<sup>1</sup>, Camille Martenon-Brodeur<sup>1</sup>, Marie Caron<sup>1</sup>, Jean-Michel Garant<sup>1</sup>, Marie-Pier Tremblay<sup>1</sup>, Victoria E.S. Armero<sup>1</sup>, Mathieu Durand<sup>2</sup>, Elvy Lapointe<sup>2</sup>, Philippe Thibault<sup>2</sup>, Maude Tremblay-Létourneau<sup>1</sup>, Jean-Pierre Perreault<sup>1</sup>, Michelle S Scott<sup>1</sup>, Guy Lemay<sup>3</sup>, Martin Bisailon<sup>1,\*</sup>

<sup>1</sup> Département de biochimie, Faculté de médecine et des sciences de la santé, Université de Sherbrooke, Sherbrooke, Quebec, Canada J1E 4K8.

<sup>2</sup> Laboratoire de Génomique Fonctionnelle, Université de Sherbrooke, Sherbrooke, Quebec, Canada J1E 4K8.

<sup>3</sup> Département de microbiologie, infectiologie et immunologie, Faculté de médecine, Université de Montréal, Montreal, Quebec, Canada H3C 3J7.

\*Correspondence:

Martin Bisailon  
Département de biochimie  
Pavillon de recherche appliquée sur le cancer  
Faculté de médecine et des sciences de la santé  
Université de Sherbrooke  
3201 Jean-Mignault  
Sherbrooke, Qc J1E 4K8 Canada  
Martin.Bisailon@USherbrooke.ca

**Abstract**

Alternative splicing (AS) is a central mechanism of genetic regulation which modifies the sequence of RNA transcripts in higher eukaryotes. AS has been shown to increase both the variability and diversity of the cellular proteome by changing the composition of resulting proteins through differential choice of exons to be included in mature mRNAs. In the present study, alterations to the global RNA splicing landscape of cellular genes upon viral infection were investigated using mammalian reovirus as a model. Our study provides the first comprehensive portrait of global changes in the RNA splicing signatures that occur in eukaryotic cells following infection with a human virus. We identify 240 modified alternative splicing events upon infection which belong to transcripts frequently involved in the regulation of gene expression and RNA metabolism. Using mass spectrometry, we also confirm modifications to transcript-specific peptides resulting from AS in virus-infected cells. These findings provide additional insights into the complexity of virus-host interactions as these splice variants expand proteome diversity and function during viral infection.

## Introduction

Virus-host studies of a wide range of human viruses have identified many changes that occur in host cells upon viral infection, including modulation of host DNA/RNA/protein synthesis, induction of various anti-viral pathways, and sequestration/degradation of cellular proteins [1-3]. Viruses rely on host cell proteins and their associated mechanisms to replicate [4,5]. Numerous virus-host interactions therefore occur during infection, which enable both partners to respond to each other. Identifying the modifications that result from virus-host interactions is currently a crucial frontier in understanding viral infection.

Alternative RNA splicing is a central mode of genetic regulation found in higher eukaryotes which changes the sequence of an RNA transcript, thereby influencing gene expression on several levels [6]. Alternative splicing (AS) increases the variability of the cellular proteome by changing the composition of transcribed genes through differential choice of exons to be included in mature mRNAs. AS is therefore a critical determinant of protein diversity by producing multiple transcripts and, as a consequence, various proteins from a single gene [7,8]. Many splice variants have distinct and sometimes opposing functions. For instance, the Bcl-x RNA transcript can be alternatively spliced to produce two isoforms: Bcl-x(L), which has anti-apoptotic effects, and Bcl-x(S), which promotes apoptosis [9]. Not surprisingly, changes in pre-mRNA splicing patterns have been associated with many human diseases including cancer and amyotrophic lateral sclerosis [10-13]. The variety of alternative mRNA isoforms in the transcriptomes of higher eukaryotes suggests the presence of a complex interplay between *cis* elements and *trans* factors in order to regulate splicing decisions [14]. Splicing factors often bind specific pre-mRNA sequences to promote or repress splice-site recognition [15]. The role of some of these specific mRNA isoforms in disease biology is starting to emerge, and recent evidences indicate that some of these can be used as prognostic or diagnostic biomarkers [16-19]. The identification of molecules capable of correcting and/or

inhibiting pathological splicing events is also an important issue for future therapeutic approaches [17,20,21].

Human viruses can utilize RNA splicing to facilitate the expression of their own genes. Modulation of AS of viral mRNA by viral-encoded factors is well established in such classical examples as papillomavirus, adenovirus and HIV, among others [22-24]. In contrast, the study of AS in mRNAs encoded by cellular genes during infection by human viruses remains sparse. Recent studies have shown that significant changes can be observed in the AS patterns of two cellular pre-mRNAs (i.e. PCBP2 and DST) as a result of the sequestration of the cellular HuR protein by Sindbis virus [25]. Similarly, the Poliovirus protease 2A (2Apro) induces a selective nucleocytoplasm translocation of several important RNA binding proteins and splicing factors which might lead to modifications in AS [26]. In the case of Epstein-Barr virus, a viral noncoding RNA (EBER1) interacts with splicing factor AUF1/hnRNP D, leading to a modification of cellular AS patterns [27]. In addition, previous studies reported the inhibition of pre-mRNA splicing by the Herpes simplex virus 1 (HSV-1) ICP27 protein. This viral protein is thought to contribute to HSV-1 host protein synthesis shut-off by interfering with cellular splicing machinery [28,29]. ICP27 interacts with components of the splicing machinery and causes a redistribution of splicing factors [30,31]. However, a recent transcriptomic study found no evidence of generalized inhibition of splicing upon HSV-1 infection [32].

In the present study, possible alterations to the global RNA splicing landscape of cellular genes upon viral infection were investigated using mammalian orthoreovirus, representative of a large family of viruses with a segmented double-stranded RNA genome, such as pathogenic rotaviruses. A non-pathogenic strain of mammalian itself is presently under clinical trials as a virotherapy agent against various cancers [33,34], while possible emergence of new pathogenic orthoreoviruses has been accumulating over the last few years [35]. There is thus major incentives to a better fundamental understanding of viral and cellular determinants that could affect reovirus replication and its effect on the host cells.

Our study reveals both the transcriptomic and AS landscapes of reovirus-infected cells. This study provides the first comprehensive portrait of global changes in the RNA splicing signatures that occur in eukaryotic cells following infection with a human virus. We identify modifications in 240 AS events of transcripts frequently involved in the regulation of gene expression and RNA metabolism. These findings provide additional insights into the complexity of virus-host interactions as these splice variants significantly expand proteome diversity and function during viral infection.

## **Results**

### **Transcriptome of Reovirus-infected Cells**

Reoviruses have long served as a model system for studying viral pathogenesis and virus-host interactions [36]. In the present study, high-throughput RNA sequencing (RNA-seq) was used in order to analyze both the cellular isoform-level mRNA abundances and AS patterns that are altered during reovirus infection. Murine L929 fibroblasts were mock-infected or infected with mammalian orthoreovirus (serotype T3/Human/Ohio/Dearing/55). Although initially isolated from human, this virus strain is generally used as a representative of mammalian reoviruses that exhibit a very large host-range. The mouse is generally used as an animal model while the murine L929 cell line is most currently used for propagation and study of reovirus in cell culture; this cell line was thus chosen for studies presented herein. In order to capture AS changes preceding the cytopathic effect, RNA-seq was performed on infected cells at 14 hrs post-infection, and viral infection was confirmed by qRT-PCR using specific primers for three viral genes (Figure A in S1 Appendix). More than 132 million reads were obtained for each of the uninfected (mock-infected) and reovirus-infected cell samples (sequencing was done in triplicate, Table A in S1 Appendix). Reads were then mapped to the reference genome, followed by transcript assembly and analysis of cellular gene expression and RNA isoform abundance. The overview of all the analyses performed in this study is outlined in Fig 1A. The gene list (23,343

genes) was initially filtered to keep only data detected in at least two replicates for both virus-infected and mock-infected cells (16,044 genes). To ensure higher reproducibility, only genes with expression levels higher than one transcript-per-million (TPM) in either dataset were conserved. More than 12,500 genes were expressed at  $>1$  TPM. Fold changes were then calculated between infected and uninfected cells (average TPM from the triplicate). Q-values (false-discovery rate) were calculated in order to correct for multiple statistical hypothesis testing, and results under 0.05 were considered significant. Our analysis revealed that the expression of a large number of cellular genes was modified upon viral infection (Fig 1B and figure B in S1 Appendix). The 569 genes for which the expression was the most significantly modified (which represent 5% of genes with the highest fold-change) were used for further analysis. The complete list and the corresponding

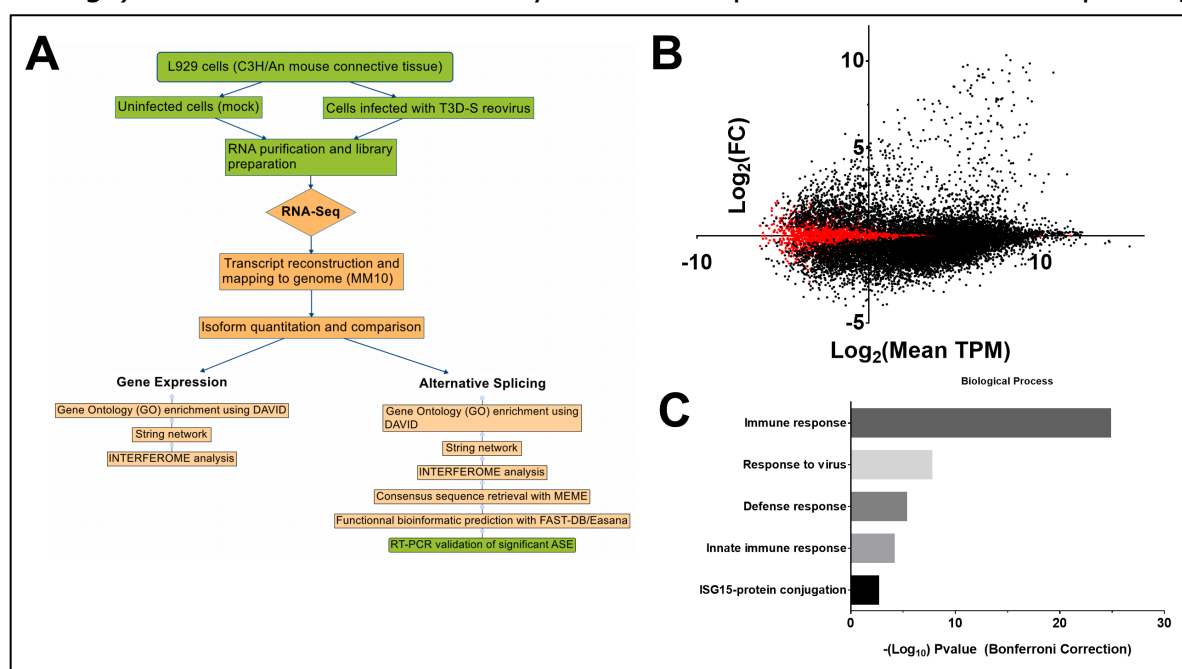


Figure 1. *Transcriptomic studies of cells infected with reovirus.* (A) Overview of the strategy used to identify the changes in both the cellular transcriptome and alternative splicing landscape upon reovirus infection. RNA-seq analysis was performed on infected cells at 14 hours post-infection. (B) MA-plot of cellular gene expression levels upon viral infection as compared to uninfected cells. The graph shows the fold-change (FC) in base 2 logarithm between infected and mock cells according to the mean expression of the gene in transcripts per million (TPM, also presented in  $\text{log}_2$ ). A cluster of over-expressed genes during viral infections with high TPM value can be seen on the upper right corner. (C) Gene ontology analyses of the 569 genes for which the expression was the most significantly modified following viral infection. Up- and down-regulated genes were imported into the DAVID gene ontology suite of programs at the NIAID. Ontological functions were determined for biological processes, and background of all detected genes was used.

expression profiles of these 569 genes (380 up-regulated and 189 down-regulated) is presented in figure C in S1 Appendix. As expected, gene ontology analysis revealed that the immune response is the most enriched function in the group of genes whose expression is upregulated upon infection (Fig 1C). Many of these immunomodulatory proteins (70/380, 18.4%) form a major interacting cluster and interact either directly or indirectly with each other (Figure D in S1 Appendix). It should be noted that a recent study by Schurch and Al showed that at least six replicates should be used in differential gene expression analysis [37]. However, they also concluded that genes with a fold change higher than two are well detected with three replicates. Since our aim was to focus on genes with the highest fold change, a number of three replicates is acceptable to validate the biological interpretation of our results.

### **Modification of the Cellular AS Landscape Upon Viral Infection**

In order to identify the cellular AS patterns that are altered during reovirus infection, we evaluated modification to discrete splicing region on isoforms by quantifying all alternative splicing events (ASEs) using the percent spliced-in (PSI) metric. For every ASEs detected, quantitation was carried on based on the percentage on the long form on total form present for a specific ASE. (Fig 2A-2B) (see Materials and methods). The ASE list (19,125 events) was initially filtered to keep only data detected in at least two replicates for both virus-infected and mock cells (8,482 genes). The ASEs that differed between mock-infected and infected cells with a P-value of less than 0.05 were conserved (1,732 events). To ensure higher stringency, the ASEs were further filtered with a cutoff Q-value of less than 0.05 (416 events). From these events, only those with a difference higher than 10% in |PSI| were considered biologically relevant. Using such an approach, we identified 240 splicing events belonging to 194 genes for which the AS pattern was significantly modified upon viral infection ( $Q < 0.05$ ,  $\Delta|PSI| > 10$ ) (Fig 2C and figure E in S1 Appendix) including 42 events which had  $\Delta|PSI|$  values higher than 30% (Table B in S1 Appendix). To identify cellular pathways for the differential ASEs associated with

viral infection, we performed a functional enrichment analysis on the 240 selected ASEs. The analysis revealed significantly enriched ( $P < 0.05$ , Bonferroni correction) terms in both RNA metabolism (22.3%) and gene expression (25.1%) (Figure F in S1 Appendix). A significant number of the modified ASEs are encoded by genes with important roles in viral infection/immunity. For instance, alterations in the splicing

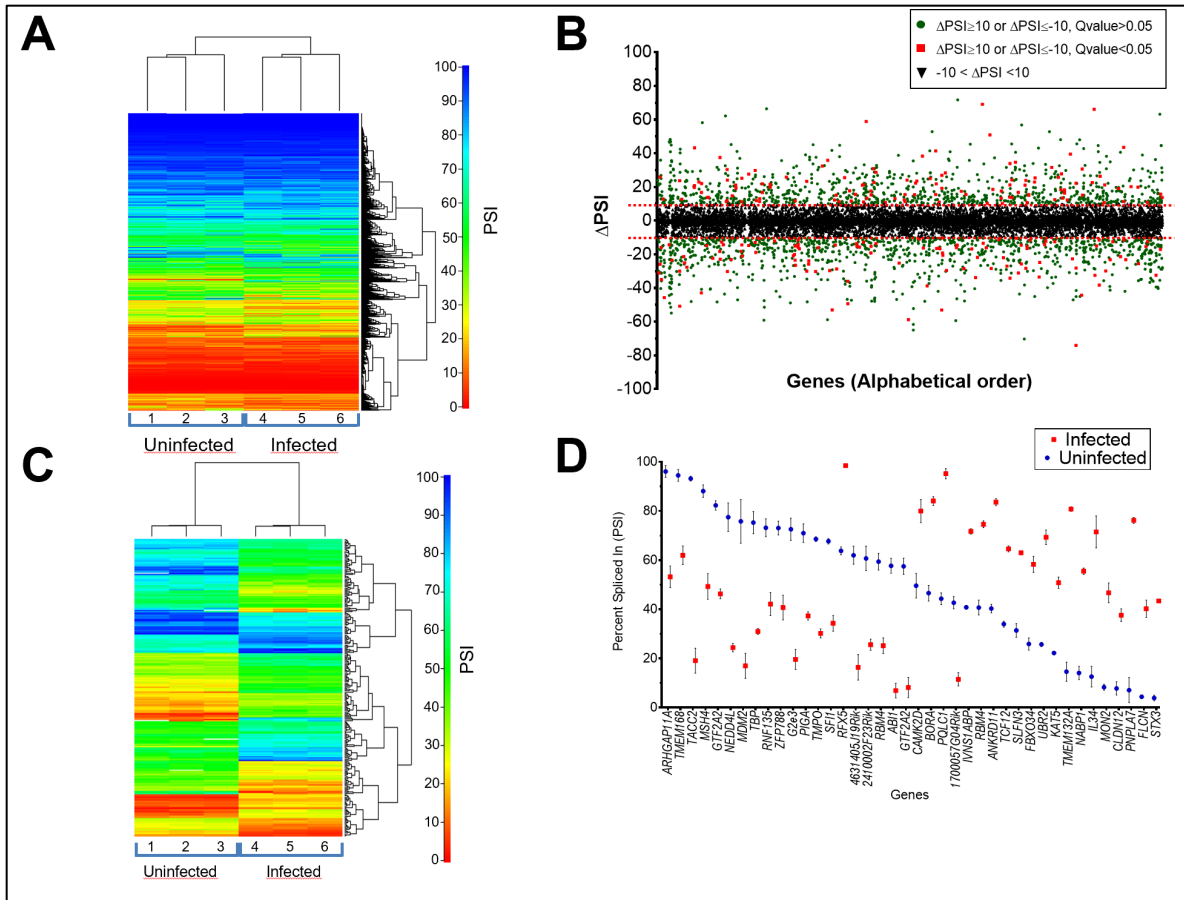


Figure 2. *Global profiling of the cellular alternative splicing landscape and identification of differentially spliced ASEs during virus-host interactions.* (A) Heatmap representation of isoform ratios for cellular transcripts in both uninfected and infected (mock) cells. RNA sequencing was done in triplicate for each condition. The map represents the percent-spliced-in (PSI) values based on isoform expression for the long and the short ASEs (see Materials and methods). Blue indicates high PSI values and red indicates low PSI values. (B) Alternative splicing events (ASEs) in cells infected with reovirus. ASEs were detected and quantified using the percent-spliced-in (PSI) metric. The graph shows an analysis of the difference in PSI values (Delta PSI) of the cellular genes following viral infection. Black triangles indicate Delta PSI values between -10 and 10, red squares indicate Delta PSI values greater than 10 or less than -10 with a Q value under 0.05, and green circles indicate same Delta PSI values but with a Q value above 0.05. (C) Heatmap representation of the 240 ASEs that are differentially spliced upon viral infection. RNA sequencing was done in triplicate for both the uninfected (mock) and infected cells. Blue indicates high absolute PSI values and red indicates low absolute PSI values. (D) PSI distribution of the 40 primary ASEs for which AS is the most significantly altered upon viral infection. The PSI values for the respective ASEs are indicated both for the uninfected and infected cells. Error bars indicate standard deviation.



patterns of *RFX5*, which encodes for a protein involved in MHC-II expression, *MDM2*, a key cellular component of the signaling pathway used by reovirus for infection, and *RFN135*, which encodes a RING finger protein involved in the RIG-I/MDA5-mediated induction of IFN-alpha/beta pathways were observed upon viral infection. Through manual curation of functional annotations, we also identified 23 transcription factors, 7 proteases, 5 kinases, 23 hydrolases, and 9 splicing factors for which AS is significantly modified upon viral infection (Table 1). An example of a differentially spliced transcript is presented in Fig 3A-3B, illustrating the modifications in isoform usage in transcripts encoded by the *ABI1* gene upon viral infection. Additional examples of alterations in splicing profiles are displayed in figure G in S1 Appendix. The variations in AS of the 40 ASEs for which AS is the most

Table 1. *Protein families found in the 240 transcripts that are differentially spliced upon viral infection*

<b>Protein Classification</b>	<b>Frequency</b>	<b>Percentage</b>
Calcium-binding protein (PC00060)	1	0.5%
Cell adhesion molecule (PC00069)	2	1.0%
Cell junction protein (PC00070)	1	0.5%
Chaperone (PC00072)	1	0.5%
Cytoskeletal protein (PC00085)	10	5.1%
Defense/immunity protein (PC00090)	3	1.5%
Enzyme modulator (PC00095)	23	11.7%
Extracellular matrix protein (PC00102)	2	1.0%
Hydrolase (PC00121)	19	9.7%
Kinase (PC00137)	5	2.6%
Ligase (PC00142)	10	5.1%
Membrane traffic protein (PC00150)	4	2.0%
Nucleic acid binding (PC00171)	47	24.0%
Oxidoreductase (PC00176)	2	1.0%
Phosphatase (PC00181)	2	1.0%
Protease (PC00190)	7	3.6%
Receptor (PC00197)	4	2.0%
Signaling molecule (PC00207)	2	1.0%
Splicing Factors	9	4.6%
Structural protein (PC00211)	1	0.5%
Transcription factor (PC00218)	23	11.7%
Transfer/carrier protein (PC00219)	3	1.5%
Transferase (PC00220)	11	5.6%
Transporter (PC00227)	4	2.0%

significantly altered upon viral infection are presented in Fig 2D, and the complete list of the differential ASEs associated with viral infection is shown in figure H in S1 Appendix. Finally, we used RT-PCR analysis in order to experimentally validate the differential ASEs that were observed through RNA-seq studies. Specific primers were

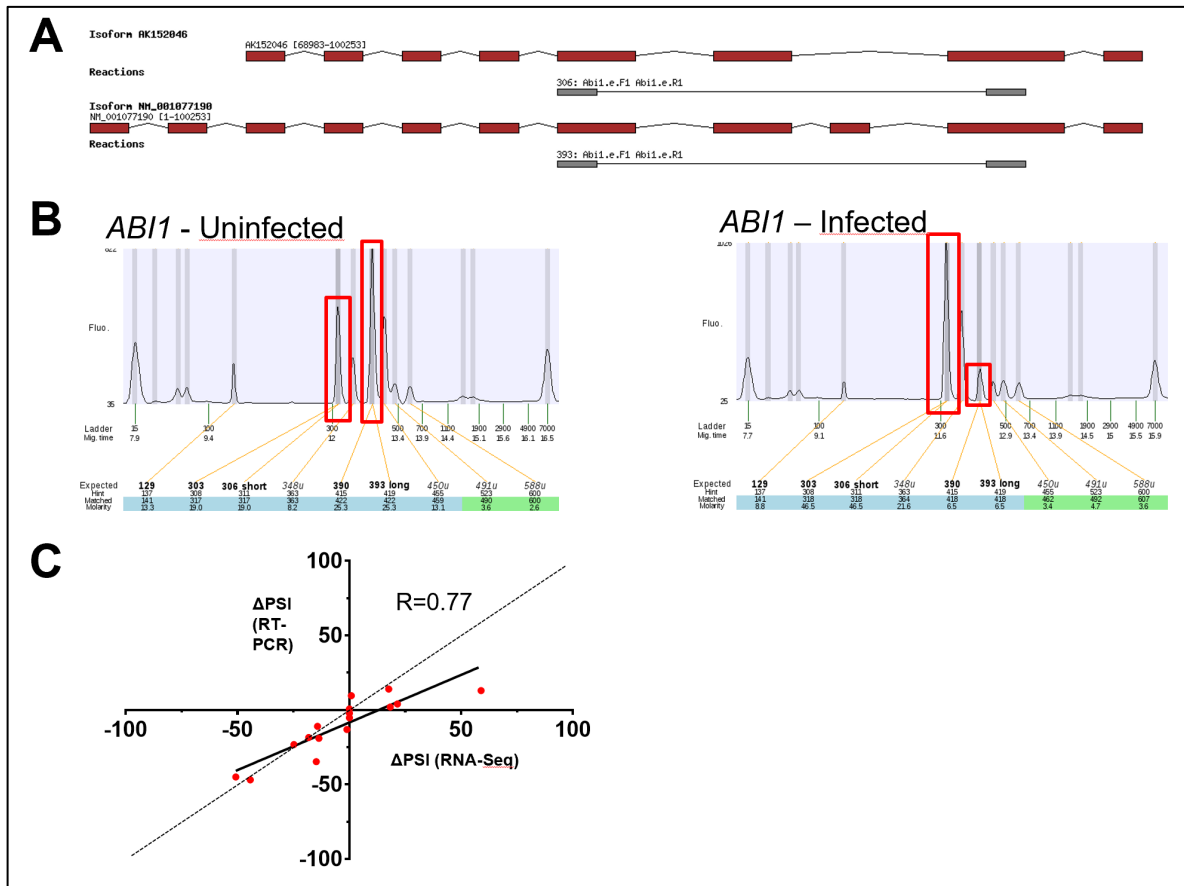


Figure 3. Validation of ASEs dysregulated in infected cells. (A) Overview of two isoforms encoded by the ABI1 gene. Exons are depicted in red and the intervening introns are shown as thin black lines (not to scale). The primers used to detect the ASE by RT-PCR assays are shown in gray and the sizes of the expected amplicons (306 nt and 393 nt) are also indicated. The genomic coordinates of these two representative isoforms are also indicated. (B) Cellular mRNAs isolated from both uninfected and infected cells were analyzed by RT-PCR using specific primers to detect both forms of the modified ASE encoded by the ABI1 gene. The amplified products were analyzed by automated chip-based microcapillary electrophoresis. Capillary electropherograms of the PCR reactions are shown. The positions and the amplitude of the detected amplicons are highlighted by red boxes. The positions of the internal markers are also indicated. The data shows the increase in the relative abundance of the short form (306 nt) and a decrease in the abundance of the long form (393 nt) upon viral infection. (C) Correlation between PSI values obtained from RNA-Seq and RT-PCR data. The analysis was performed on 16 selected ASEs (Abi1, Cwc22, Eif4a2, Hnrnpa2b1, Il34, Srsf3, Srsf5, Alkbh1, Cdkn2aip, Cflar, Hif1a, Mdm2, Serbp1, Sfswap, Smc2, Tbp). In all cases, the changes in AS levels detected by RT-PCR and the ones revealed through transcriptome sequencing displayed high levels of correlation ( $r > 0.77$ ). Sanger sequencing was also realized on several ASEs to confirm that RT-PCR reaction is specific and amplifies predicted ASE.

designed to allow detection of sixteen predicted ASEs by PCR. Our results demonstrated that the changes in AS levels detected by RT-PCR were similar to the ones revealed through transcriptome sequencing, and displayed high levels of correlation ( $r = 0.77$ ) (Fig 3C). Sanger sequencing was also realized on several ASEs to confirm that RT-PCR reactions are specific and amplify the predicted ASEs (Table C in S1 Appendix).

It should also be noted that we also identified the cellular AS pattern that is altered during infection with a mutant reovirus harboring a single amino acid substitution in the mRNA capping enzyme  $\lambda 2$  (P4L-12 mutant). This mutant has been previously shown to display an increase in interferon sensitivity [38,39]. Analysis of the ASEs revealed almost identical modifications to the cellular AS patterns than with the wild-type reovirus (Figure I in S1 Appendix). Indeed, upon infection with the mutant virus, we identified similar changes to the AS of cellular transcripts i.e. the AS of the same events were modified and displayed similar  $\Delta$ PSI values. The only notable exception was for an ASE on the ATAT1 gene (Alpha Tubulin Acetyltransferase 1) which showed a considerable  $\Delta$ PSI shift from WT virus ( $\Delta$ PSI=13.8) to mutant ( $\Delta$ PSI=-10.4). However, RT-PCR validation failed to validate this shift, hence pointing toward a sequencing artifact rather than a mutant virus-specific change of alternative splicing.

### **Characterization of the ASEs that are Modified Upon Viral Infection**

We next compared the profiles of the 240 selected ASEs that are differentially spliced upon viral infection against all the ASEs that were detected in our RNA-seq experiments. Among the different types of AS changes noted in the 240 selected ASEs, exon cassette events were the most common and represented a significant proportion of total changes ( $p < 0.0001$ ; Fig 4A) as compared to all the ASEs identified in our assay. In addition, a significant decrease in alternative 5' end usage was observed in the selected ASEs in comparison to all ASEs ( $p < 0.0001$ ). The vast majority of the ASEs that are modified upon viral infection were found at a level of

one splicing event per gene (Fig 4B). Interestingly, analysis of the correlation between AS and gene expression indicated stable expression of most of the transcripts harboring ASEs that are differentially spliced upon viral infection (Fig 4C). Notable exceptions included GVIN1, an interferon-inducible GTPase, and the apolipoprotein 9a (APOI9A) which are both significantly over-expressed upon viral infection and differentially spliced.

Among the 240 ASEs for which AS was significantly affected upon viral infection, many splicing events we documented affect known protein domains. Table D in S1 Appendix displays the predicted consequences of the differentially spliced transcripts on protein function for 110 transcripts that are differentially spliced upon viral infection. Among the differential ASEs associated with viral infection, at least 10 ASEs resulted in the addition or loss of predicted nuclear localization signals (NLS) including the CDC-Like Kinase 4 (CLK4), the e2F3 transcription factor, and the Influenza Virus NS1A Binding Protein (IVNS1ABP). Other ASEs were associated with key functional domains in proteins such as the loss of the RhoGAP domain in the Rho GTPase activating protein 11A (ARHGAP11a), and the loss of death-effector domains (DED) in the CASP8 And FADD-Like Apoptosis Regulator (CFLAR).

### **Proteomic Analysis of Reovirus-Infected Cells**

Since we identified changes at the transcriptomic level, we were interested to know if those ASEs have functional consequences at the proteome level during reovirus infection. To assess this question, we infected L929 cells with reovirus and conducted proteomic analysis using LC-MS/MS. Since our informatics analysis predicted that protein localization could be altered in infected cells, nuclear and cytoplasm cell fractionations were realized prior to MS analysis. 42,489 peptides belonging to 4521 genes were detected, of which 100 genes were also previously identified to have altered splicing (100/194: 51.5%). In order to confirm predicted functional changes caused by AS, we used the SpliceVista program which allows visualization and characterization of spliced protein isoforms. The identification of transcripts-specific

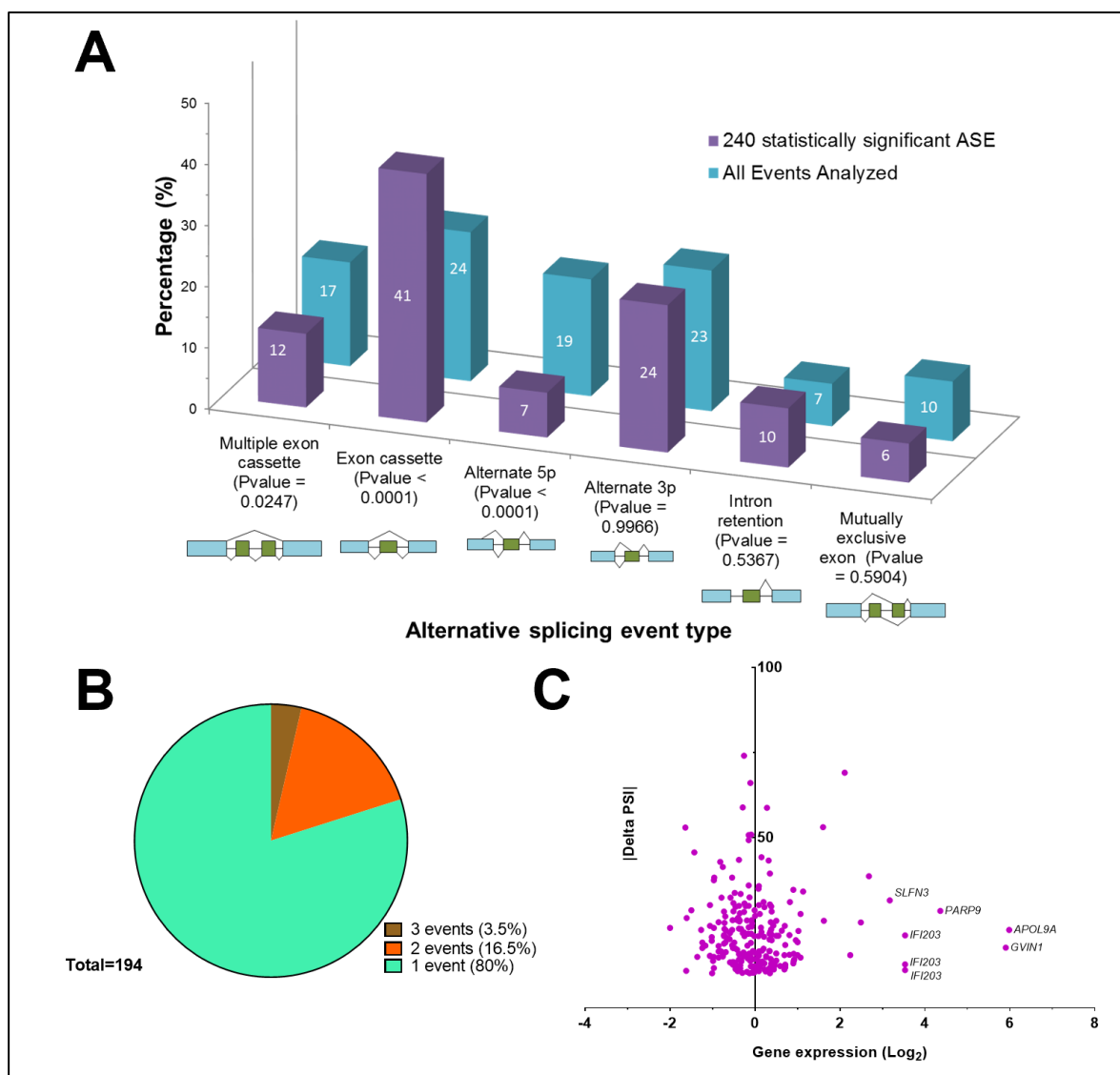


Figure 4. *Characterization of the ASEs that are modified upon viral infection.* (A) The percentage of splicing profiles found in cells and in the 240 differentially spliced transcripts are presented. Schematic representations of the various splicing profiles are also indicated as well as the statistical significance (chi-square with Yates' correction). (B) Distribution of the number of ASEs per gene. The vast majority of the ASEs that are modified upon viral infection were found at a level of one splicing event per gene. (C) Gene expression levels of the 240 differentially spliced transcripts. The graph displays both the modifications in gene expression and alternative splicing of the 240 ASEs that are differentially spliced upon viral infection. The variations in gene expression are presented in a logarithmic scale (Log<sub>2</sub>).

peptides confirmed that AS modifications in infected cells can modify protein isoform expression from the *MACF1*, *TPP2*, *LRRFIP1*, *PRPF39* and *SON* genes (Fig 5A). For instance, peptide B originating from the *LRRFIP1* short transcript isoform was detected by mass spectrometry only in the cytoplasm fraction of the uninfected cells

(Fig 5B). A similar pattern was also observed for the peptide originating from the PRPF39 short transcript. The molecular investigation concerning these changes and their impact in alternative splicing and viral-host interaction will be required.

### **Conserved RNA Motif and RNA Splicing Factors**

The observed differences in the AS landscape of uninfected versus infected cells raised the possibility that AS might be driven by common RNA motifs responding to specific splicing factors. Consequently, the presence of over-represented nucleotide sequences near the splicing regions of the selected ASEs was analyzed. Sequences of the alternative exons and the flanking introns were selected for analysis since they have previously been shown to harbor AS control elements. Notably, we found a significant enrichment of a 41 nt motif in the vicinity of many splice regions of transcripts for which AS was altered upon viral infection (e-value =  $1.3e-10^{49}$ ) (Figure J in S1 Appendix). The motif was found in 93 of the 240 ASEs that were differentially spliced upon viral infection. Although the exact role of this motif is currently unknown, bioinformatic analyses did not reveal the potential binding of splicing factors to this RNA sequence (data not shown). The AS landscape modification in infected cells could also result from the direct and/or indirect action of specific viral proteins. For instance, a viral protein could be interacting with specific sequences on cellular mRNAs thereby altering normal splicing process. Alternatively, a viral protein could also interact with splicing factors to alter the splicing reaction in the cell nucleus. Previous studies have shown a partial nuclear localization for certain reovirus proteins, namely  $\mu 2$ ,  $\sigma 1s$  and  $\sigma 3$  [40-47], although other proteins were not necessarily examined, especially in the context of infected cells. Interestingly, our proteomics analysis of infected cells revealed nuclear enrichment for  $\mu 2$ ,  $\lambda 3$  and  $\sigma NS$  (Fig 5C). The potential role of these viral proteins in the virus-induced modification of cellular AS will need to be investigated in future studies.

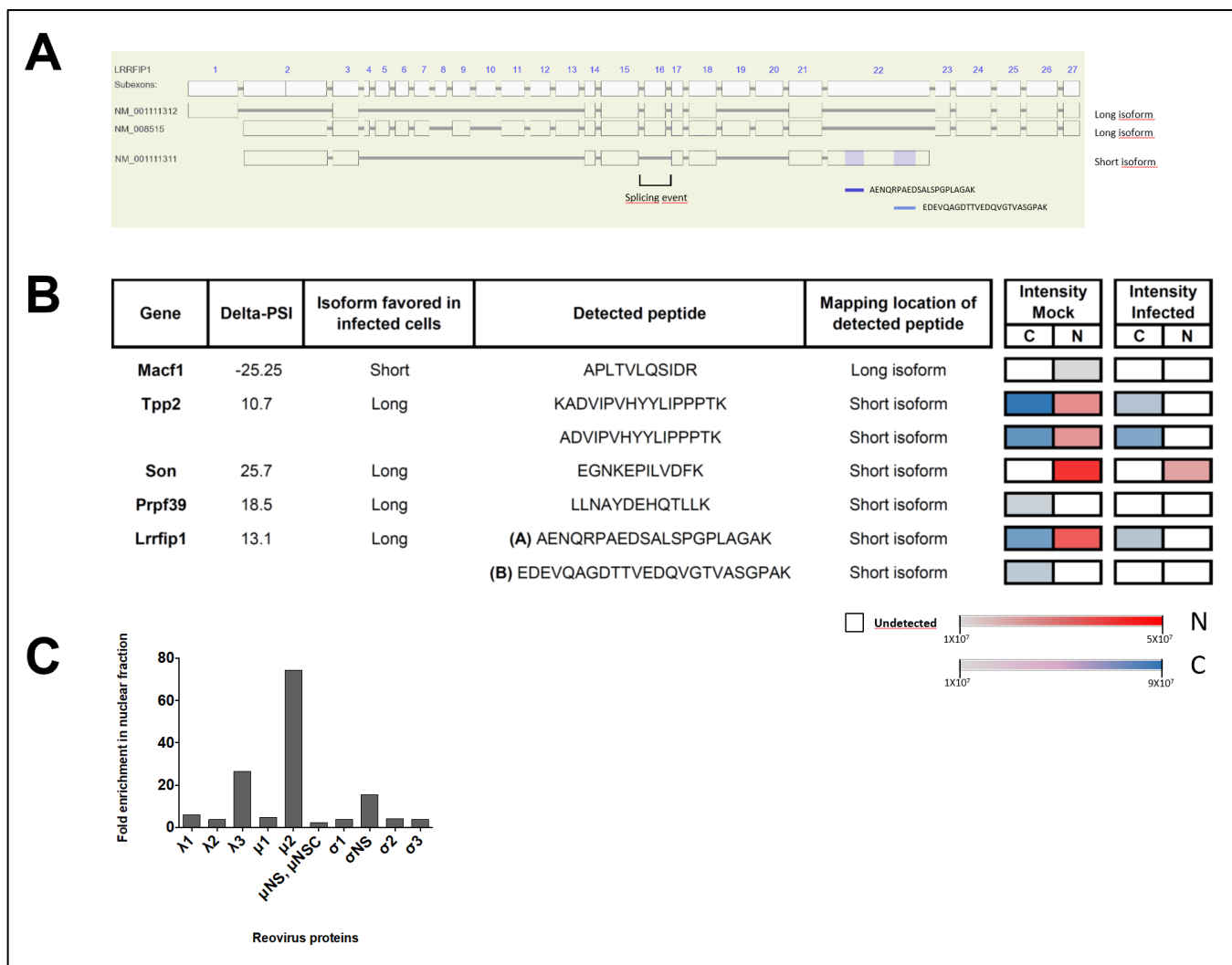


Figure 5. *Proteomic analysis of uninfected and reovirus-infected cells.* (A) LRRFIP1 coding exon structure and localization of peptides detected for this gene. Two long isoform transcripts (NM\_001111312; NM\_008515) and one short isoform transcript (NM\_001111311) are also represented. Other short (BC144955; AK044174) and long (BC145642) isoforms analyzed in the RNA-Seq process were omitted. (B) Transcript-specific peptides detected for the long/short transcript. The intensities of peptide detection for both uninfected (mock) and infected cells in the cytoplasm/nucleus fractions are displayed as color gradation (Cytoplasm: grey = weakly detected, blue = strongly detected, white=undetected; Nucleus: grey: lightly detected, red = strongly detected; white=undetected). For Lrrfip1, two peptides (A and B) are presented. (C) Fold enrichment of reovirus proteins in nuclear fraction over the cytoplasmic one. Proteins  $\mu$ 2 (74.5x),  $\lambda$ 3 (26.5x) and  $\sigma$ NS (15.4x) were found to be above the background level of other viral proteins.

The precise mechanism by which viral infection leads to modifications of the AS landscape in infected cells is currently unknown. Changes in splice site choice frequently arise from modifications in the assembly of the spliceosome or by altering the binding of splicing factors to the RNA transcripts [48]. Although splicing is regulated by an abundant and yet incompletely characterized set of splicing factors,

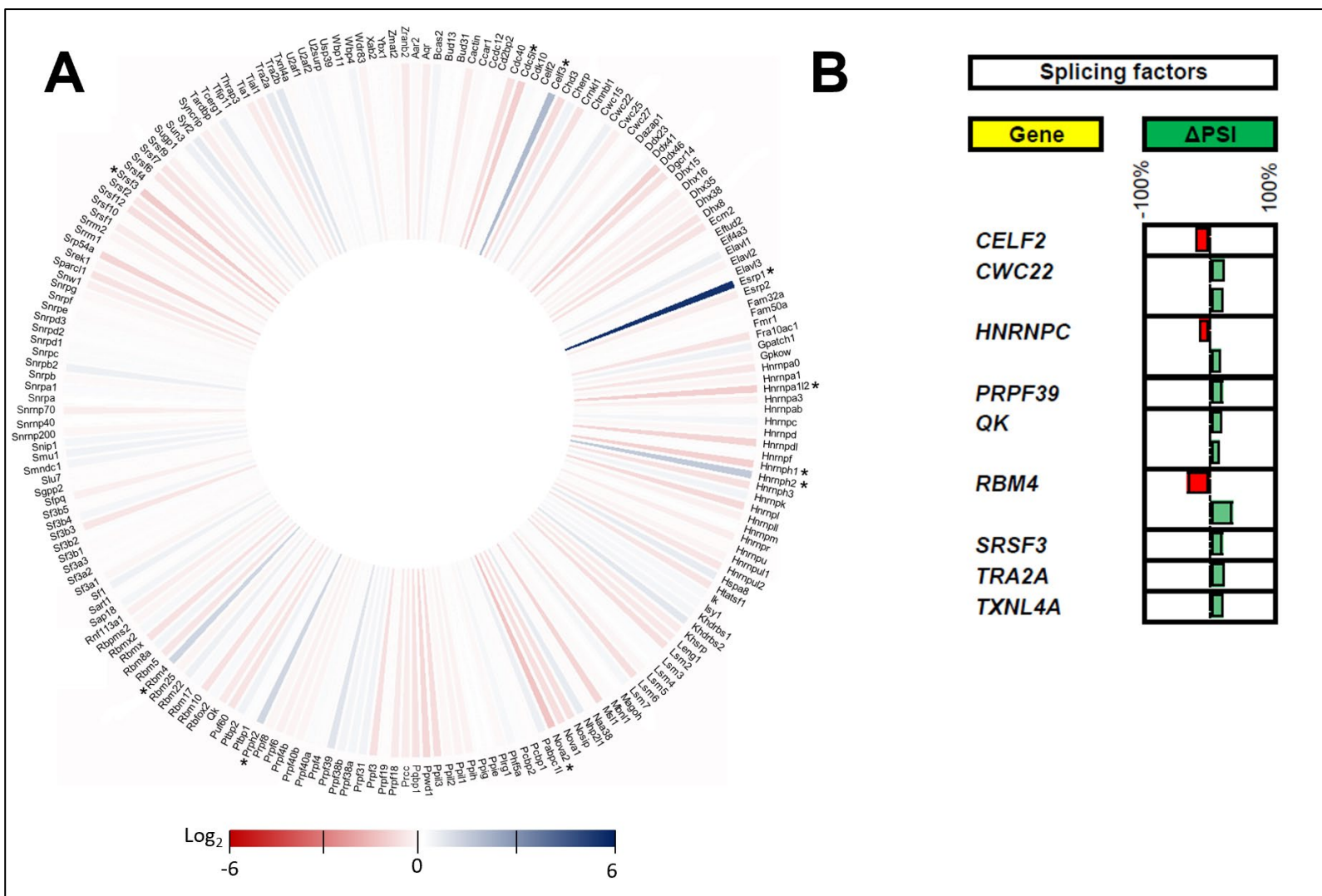


Figure 6. *Proteins involved in RNA splicing*. (A) Iris graph displaying the expression profile of proteins involved in RNA splicing. Differences in gene expression levels are shown on a logarithmic color scale (Log<sub>2</sub>). The expression of only 10 proteins involved in splicing was modulated by more than 2-fold upon infection (indicated by an asterisk). (B) Modifications to the splicing profiles of proteins involved in RNA splicing upon viral infection. Nine splicing factors were differentially spliced following viral infection. The changes in PSI values are indicated in red (negative delta PSI) or green (positive delta PSI).

dysregulated expression of individual splicing factors has been shown to frequently result in aberrant splicing [49]. In light of these findings, we therefore monitored both the expression profiles and the modifications in the AS patterns of transcripts encoding spliceosomal proteins and RNA splicing factors. As shown in Fig 6A, the expression of a very limited number of splicing factors and spliceosomal proteins is indeed affected upon viral infection. The expression of only 10 proteins involved in splicing was modulated by more than 2-fold upon infection. Interestingly, the expression of ESRP1, a splicing factor known to regulate diverse types of alternative



splicing events [50], was apparently increased by more than 32-fold in infected cells. The ability of reovirus to alter the splicing patterns of transcripts encoding proteins involved in splicing (splicing factors and proteins of the spliceosome) was also investigated. Our study identified 9 splicing factors that were differentially spliced upon viral infection (Fig 6B). One example is the RNA Binding Motif Protein 4 (RBM4), a known modulator of alternative 5' splice site and exon selection [51]. Modifications to both the expression level and AS of splicing factors likely contribute to the observed modifications in the cellular AS landscape during viral infection.

## **Discussion**

The present study demonstrated that viral infection can extensively modify the splicing patterns of numerous cellular transcripts involved in gene expression and RNA processing. These splice variants significantly expand proteome diversity and function during viral infection by encoding altered proteins that could influence gene expression and defense homeostasis. These data raise very interesting questions and open new avenues of research for a better understanding of post-transcriptional events during virus infection and possible new targets for the development of antiviral agents.

Many viruses can modify the host cell nuclear functions in order to promote an ideal environment for viral replication. These effects on host cell nuclear functions can be mediated by a variety of mechanisms including the alteration of nuclear architecture [52-55], the interruption of nucleocytoplasmic transport pathways [56-59], and the induction of nuclear herniations [60]. It may come as a surprising observation that infection by a cytoplasmic RNA virus alters the alternative splicing of specific cellular transcripts in the nucleus. In the case of poliovirus, for which alterations to a limited number of transcripts has previously been demonstrated, visible morphological alterations of the nucleus have long been known to occur during viral infection [61]. Such changes are more subtle with reovirus, although "herniations" has been reported in the nucleus of infected cells [42]. Altered DNA

synthesis and cell cycle is also observed at least in some cell types and with some reovirus strains [36]. The presence of viral proteins in the nucleus of reovirus-infected cells also supports the idea that this cytoplasmic virus could alter the nuclear splicing machinery. Two likely mechanistic scenarios involve the binding of viral proteins to specific splicing factors thereby hindering their processing activity, and/or the binding of viral proteins to specific sequences on cellular transcripts preventing both binding of splicing factors and subsequent processing.

Dysregulated expression of splicing factors has been shown to be involved in human diseases. For instance, the Serine/Arginine-Rich Splicing Factor 1 (SRSF1) was found to be over-expressed in several tumor types [62], and fibroblasts overexpressing SRSF1 caused tumor formation when injected into mice [63]. Similarly, upregulation of the splicing factor hnRNPH has been shown to drive splicing switches of oncogenic target genes in gliomas [64]. Recently, RBM4, an RNA-binding factor involved in multiple aspects of cellular processes such as AS, was also demonstrated to control cancer-related splicing events affecting cellular processes such as apoptosis, proliferation, and migration [65]. Very few changes in the expression levels and/or splicing patterns of splicing factors were detected in our study upon viral infection. One notable exception is the transcript encoded by *ESRP1* which seemed significantly over-expressed following viral infection (32-fold increase). How the altered expression dynamics of *ESRP1* (and other splicing regulators) contribute to AS homeostasis during virus infection remains to be investigated. Interestingly, a previous study identified ASEs regulated by *Esrp1* using RNA silencing technology in a human epithelial cell line [50]. Using such a strategy, the authors identified 148 alternative splicing events in a total of 134 different genes that were regulated by *Esrp1*. In the present study, the splicing of eight of these *Esrp1*-regulated transcripts are also found to be differentially spliced upon viral infection (*ASPH*, *JMJD1C*, *MACF1*, *NASP*, *NEDD4L*, *RBM39*, *TRA2A*, *WSB1*) suggesting, at least in part, that some of the observed splicing alterations observed upon viral infection could be related to *Esrp1* over-expression.

Among the 240 ASEs that were differentially spliced upon viral infection, many have predicted changes in their protein function. Among the latter, the expression of the full-length Mdm2 transcript was found to be significantly reduced and replaced by a shorter form that is predicted to encode a truncated Mdm2 protein deficient in its ability to bind p53. The true relevance of this modification needs to be further confirmed by functional studies. Binding of Mdm2 to p53 has been shown to induce degradation of this key regulator of cell proliferation [66]. Interestingly, stabilization of p53, as is predicted to occur by truncation of the MDM2 protein resulting from alternative splicing modification, was previously shown to increase reovirus oncolytic activity [67]. Indeed, reovirus has been shown to exploit altered Ras signaling pathways in a myriad of cancers [68,69], and this has led to current clinical trials of reovirus as an oncolytic agent [33,34]. Unfortunately, mass spectrometry analysis did not allow the detection of the Mdm2 protein in both uninfected and reovirus-infected cells. Altered splicing pattern of *MDM2* upon viral infection could be another factor contributing to reovirus oncolytic activity and a possible new target to further optimize its therapeutic potential.

Modifications to the global landscape of cellular AS has been thoroughly studied in cancer [10-12]. Various studies are starting to reveal the extent of changes that occur at the splicing level in different types of cancer. Strategies to modulate AS by splice-switching oligonucleotides in order to correct aberrant events, or to induce expression of therapeutic splice variants are being developed [17,20,21]. For instance, the splicing of Bcl-x(L) in cancer cells can be redirected towards the pro-apoptotic variant Bcl-x(S), which has been shown to reduce the tumor load in xenografts of metastatic melanoma [70]. It is therefore tempting to speculate that such a strategy could likely be utilized to limit viral replication. The current identification of extensive changes in the cellular AS landscape during virus-host interactions likely represents a first step toward the development of antiviral agents based on the modulation of AS during viral infections. Molecular tools such as splice-switching oligonucleotides that can specifically alter the proportion of splice

variants are also essential to assess the function of these splice variants during viral infection.

## **Experimental Procedures**

### **Cells and Viruses**

Murine L929 fibroblasts were obtained from the American Type Culture Collection (ATCC) and were routinely grown in minimal Eagle medium (Wisent) containing 5% fetal bovine serum (FBS Gold, PAA Laboratories). Mammalian orthoreovirus serotype 3 strain Dearing (T3/Human/Ohio/Dearing/55) also originally obtained from ATCC was propagated and titrated by TCID<sub>50</sub> on L929 fibroblasts, as routinely used in the laboratory [71]. This laboratory stock was recently completely sequenced (NCBI accession numbers KP208804 to KP208813) and rescued by plasmid-based reverse genetics [39]; this virus is referred to as T3D-S. Mutant PL4-12 reovirus was obtained through chemical mutagenesis as described before [38,39].

### **Viral Infection**

L929 cells were plated at a density of  $7 \times 10^4$  cells per square centimeter the day before infection at an MOI of 50TCID<sub>50</sub> units per cell using standard procedures [71]. Control L929 cells were seeded at the same density and uninfected. Cells were collected 14 hrs post-infection, at which time visible cytopathic effect was still minimal. For RNA-Seq analysis, total RNA was extracted with Trizol<sup>®</sup> as recommended by the manufacturer (Life Technologies).

### **RNA-seq Library Preparation**

Messenger RNAs were isolated from 5 ug total RNA using New England Biolabs magnetic mRNA isolation kit (S1550S), as per manufacturer's protocol, and then eluted in 25  $\mu$ l. Quality and quantity assessments were performed on Agilent Nano Chip (Catalog number 5067-1511); all RIN-Value were equal or above 9.7. The RNA-seq library was then built using Illumina SSV21106 kit from 9  $\mu$ l isolated mRNA.

Library quality was assessed using Agilent DNA HS Chip (Catalog number 5067-4626). Library quantification was performed by qPCR following Illumina Kappa library quantification protocol. WT and P4L-12 reovirus-infected and mock libraries were multiplexed and sequencing was done in triplicate. Pooled libraries were sequenced at 100bp paired-end reads using Illumina HiSeq 2000 at McGill University and Génome Québec Innovation Centre Sequencing Service.

### **RNA-seq Data Analysis**

Sequence reads were aligned on a transcriptome reference sequence database (UCSCGene MM10) using Bowtie v2 aligner (default parameters) and all valid mapping positions were kept. Associated gene isoforms were quantified in transcript-per-million (TPM) using RSEM for each sequenced sample [72,73]. RSEM uses an Expectation-Maximization (EM) algorithm as its statistical model, allowing reads mapping to multiple transcripts to be also part of the quantification; this huge advantage has lead groups such as the Cancer Genome Atlas (TCGA) to use RSEM in their pipelines. A maximum of two mismatches in the seed (25 bases) was allowed (default parameter). The estimated number of fragments that originate from a specific isoform/gene and the estimated fraction of transcripts corresponding to an isoform/gene are returned by RSEM. Alternative splicing events were automatically detected and quantified using the percent-spliced-in (PSI,  $\Psi$ ) metric based on long (L) and short (S) forms of all splicing events presents (equation shown below). Briefly, for each splicing events in one given gene (cassette-exon, mutually exclusive exons, alternative 5' and 3' splice site, etc), a PSI value was given according to the ratio of the long form on total form present (short form and long form) to characterize inclusion of exon, differential splice-site choice, intron retention, etc. For example, the long form of a cassette-exon would be its inclusion, and short form would be its exclusion from the mature transcript. Events resulting in no change in size (e.g. mutually exclusive exon with the same size) were arbitrary given the long and the short forms.

$$\psi = \frac{L}{L+S}$$

## **Gene Expression Analysis**

The gene list was initially filtered to keep only data present in at least two replicates for both virus-infected and mock cells. To ensure higher reproducibility, only genes with expression levels higher than one transcript per million (TPM) in either dataset were conserved. Fold changes in base 2 logarithm were then calculated between infected and mock average TPM. Q-values were calculated to take into account multiple statistical hypothesis testing and results under 0.05 were considered significant.

## **Alternative Splicing Analysis**

The alternative splicing event (ASE) list was filtered to keep only data with at least two replicates for both virus-infected and mock cells (16,044 genes). Events with a P-value less than 0.05 were conserved (1,732 events). To ensure higher stringency, the ASEs were further filtered with a cutoff Q-value of less than 0.05. From these events, only those with a difference higher than 10% in PSI were considered biologically relevant. The same process was applied to P4L-12 mutant reovirus and mock cells.

## **Statistical Analysis**

Welch's t-test (Student's t-test with unequal sample sizes and unequal variances) was calculated through the GSL library (<http://www.gnu.org/software/gsl/>) integrated to Perl system analysis for gene expression and alternative splicing data. Also, false discovery rate was calculated with the Q-value package in R (<https://cran.r-project.org/src/contrib/Archive/qvalue/>) based on [74]. For all other analysis, Graph Pad Prism version 6.05 was used to run statistics.

## **Data Availability**

The data discussed in this publication have been deposited in NCBI's Gene Expression Omnibus [75] and are accessible through GEO Series accession number GSE81017 (<https://www.ncbi.nlm.nih.gov/geo/query/acc.cgi?acc=GSE81017>).

### **Gene Ontology Analysis**

The Database for Annotation, Visualization and Integrated Discovery (DAVID) [76] version 6.7 was used and Bonferroni correction was applied to obtained P-values. Reference background was composed of all genes or splicing events analyzed to take into account any bias from the experimental analysis.

### **String Networks**

Using the STRING database [77] (version 10), genes were submitted for generation of protein-protein interaction network from the *Mus musculus* interactome. High-resolution evidence views were created and saved.

### **Consensus Sequence Retrieval**

The MEME suite [78] (version 4.10.1) was run against the intron-exon-intron sequence of the selected alternative splicing events, looking for a conserved motif up to 75 nucleotides long. A cutoff of 5 sequences was used to obtain only relevant motifs.

### **Functional ASE Prediction**

Using the FAST-DB or EASANA suite, the splicing patterns of a gene of interest was visualized. DNA sequences of representative transcripts presenting long and short isoforms were downloaded and translated into proteins using ExPASy translation tool [79]. Counter verification using Genome Browser was done to ensure expression of transcripts and good protein sequence. Predicted proteins were then compared using Multalin (truncation and frameshift event) [80], PFAM and Interpro (loss or

appearance of a functional domain) [81,82] and NLS Mapper (loss or gain of nuclear localization signal) [83].

### **RT-PCR Validation**

Reverse transcription was performed on 2.2 µg total RNA with Transcriptor reverse transcriptase, random hexamers, dNTPs (Roche Diagnostics), and 10 units of RNase OUT (Invitrogen) following the protocol of the manufacturer in a total volume of 20 µl. All the forward and reverse primers were individually resuspended to 20–100 µM in Tris-EDTA buffer and diluted as a primer pair to 1 µM in RNase DNase-free water (IDT). Quantitative PCR (qPCR) reactions were performed in 10 µl in 96 well plates on a CFX-96 thermocycler (BioRad) with 5 µL of 2X iTaq Universal SYBR Green Supermix (BioRad), 10 ng (3 µl) cDNA, and 200 nM final (2 µl) primer pair solutions. The following cycling conditions were used: 3 min at 95°C; 50 cycles: 15 sec at 95°C, 30 sec at 60°C, 30 sec at 72°C. Relative expression levels were calculated using the qBASE framework. For every PCR run, control reactions performed in the absence of template were performed for each primer pair and these were consistently negative. The amplified products were analyzed by automated chip-based microcapillary electrophoresis on Caliper LC-90 instruments (Caliper LifeSciences). Amplicon sizing and relative quantitation were performed by the manufacturer's software.

### **Cell Fractionation**

Cells were harvested and pelleted by centrifugation at 1000 RPM for 2 minutes. They were then resuspended in 100 µL magnesium-free PBS; 100 µL of nuclear extraction buffer (40mM Tris-HCl pH 7.5, 20mM MgCl<sub>2</sub>, 4 % Triton X-100, 1.28M sucrose) was added with 300 µL of ultrapure water, with all solutions at 4°C. Incubation was carried on ice with occasional agitation by inversion for 20 minutes. Nuclei were retrieved by centrifugation at 5000 RPM, 4°C during 15 minutes; the supernatant was kept as the cytoplasmic fraction. Nuclei were resuspended in 100 µL of low salt buffer (20mM Hepes-KOH pH 7.9, 20mM KCl, 1.5mM MgCl<sub>2</sub>, 20mM EDTA, 0.5mM



DTT, 25 % glycerol) and 100 uL of KCl 1.2 M was added before harsh agitation. Nuclear lysis was carried for one hour on ice with vigorous vortexing at every 10 minutes. Chromatin was then eliminated by centrifugation at 13 000 RPM for 15 minutes at 4°C and the supernatant represented the nuclear soluble fraction.

### **LC-MS/MS Analysis**

Proteomic analysis of infected and mock cells was carried out as previously described [84]. Briefly, 50 ug of protein from each fraction (nucleus and cytoplasm of infected and mock cells) were reduced in 10 mM DTT and alkylated in 50 mM iodoacetamide. Protein mixture was then separated by one-dimensional SDS-PAGE precast Mini-PROTEAN TGX gel (Bio-Rad). Upon separation, each lane was cut into 4 slices, trypsin-digested and subjected to LC-MS/MS analysis. MaxQuant was used to identify peptide-spectrum match (PSM) against either Uniprot *Mus Musculus* and Reovirus proteins, or against ENSEMBL *Mus musculus* proteins for SpliceVista analysis.

### **SpliceVista Isoform Analysis**

*Mus musculus* ENSEMBL ID and gene names were retrieved using BioMart to create the initial database. The code converter.py was modified to permit retrieval of *Mus musculus* gene ID from the ENSEMBL ID database previously created. The SpliceVista program was then run using all default parameters under Linux [85].

### **Acknowledgments**

S.B. contributed to experimental design and analysis of the data, performed validation experiments and helped in writing the manuscript; M.C., and C.M.B. helped in data analysis; J.M.G. performed RNA sequence analyses and protein isoform detection using SpliceVista; M.P.T. and V.E.S.A. helped in the generation of figures; E.L and M.D. performed RNA extraction and library construction; P.T. performed informatics analyses;; M.T.L., M.S., and J.P.P contributed to experimental design and analysis; G.L. performed viral infection, contributed to experimental

design and writing of the manuscript; M.B. contributed to experimental design, data analysis and wrote the manuscript with contributions from all the authors.

## Supporting Information

### S1 Appendix. Supplemental data (tables and figures)

<b>Table A. RNA-sequencing data</b>		
<b>Sample</b>	<b>Number of bases</b>	<b>HiSeq Reads</b>
Mock 1	9 270 066 200	46 350 331
Mock 2	9 400 946 800	47 004 734
Mock 3	7 880 753 600	39 403 768
Reovirus 1	10 499 367 400	52 496 837
Reovirus 2	10 352 922 800	51 764 614
Reovirus 3	8 850 997 600	44 254 988

RNA-seq was performed on uninfected (mock-infected) cells, and cells infected with reovirus (14 hours post-infection). Sequencing was done in triplicate.

Table B. *Distribution of  $\Delta PSI$  values in the 240 differentially spliced ASEs*

<b><math>\Delta PSI</math></b>	<b>Number of ASEs modified</b>
[-80,-70[	1
[-70,-60[	0
[-60,-50[	4
[-50,-40[	4
[-40,-30[	15
[-30,-20[	35
[-20,-10[	60
]10,20]	64
]20,30]	39
]30,40]	11
]40,50]	3
]50,60]	2
]60,70]	2

<b>Gene</b>	<b>ASE Form</b>	<b>Splicing junction</b>	<b>Predicted sequence</b>	<b>Sequencing results</b>
<i>II34</i>	Short	5-7	CAGCGGAGCCT CATGGATGTGG AGATTGGC	CAGCGGAGCCT CATGGATGTGG AGATTGGC
	Long	5-6	NA	NA
	Long	6-7	NA	NA
<i>hnRNPA2B1</i>	Short	8-10	GAGGAGGACCT GGAGGAAATTA TGGAAGTG	GAGGAGGACCT GGAGGAAATTA TGGAAGTG
	Long	8-9	GAGGAGGACCT GGAGGTGGCAA TTTTGGAG	GAGGAGGACCT GGAGGTGGCAA TTTTGGAG
	Long	9-10	ACAACTATGGA GGAGGAAATTA TGGAAGTG	ACAACTATGGA GGAGGAAATTA TGGAAGTG

NA: Splicing junction expressed at levels too low to allow sequencing

**Table D. Bioinformatic prediction of functional changes caused by some identified ASEs**

Gene	Delta-PSI	Event Type	Full name	Predicted residue variation caused by alternative splicing modification ( $\Delta$ AA)	Predicted functional consequence
<b>Abi1</b>	-50.8	exon-cassette+alternate-3p+multiple-exon-cassette	abl-interactor 1	-29	Unknown
<b>Adar</b>	-25.1	alternate-5p	adenosine deaminase, RNA-specific	-26	Unknown
<b>Agfg1</b>	-27.6	alternate-3p	ArfGAP with FG repeats 1	-19	Unknown
<b>Apol9a</b>	22.9	alternate-5p	apolipoprotein L 9a	0	No predicted functional change
<b>Arhgap11a</b>	-42.9	exon-cassette+alternate-3p+intron-retention	Rho GTPase activating protein 11A	-515	NLS and RhoGAP domain loss in short isoform
<b>Arhgap11a</b>	16.7	exon-cassette+alternate-3p+intron-retention	Rho GTPase activating protein 11A	-489	Premature stop codon introduced by intron retention in long isoform
<b>Asph</b>	13.8	exon-cassette	aspartate-beta-hydroxylase	83	Unknown
<b>Atat1</b>	13.8	exon-cassette	alpha tubulin acetyltransferase 1	23	Unknown
<b>Atxn711</b>	-22.4	exon-cassette	ataxin 7-like 1	-51	Unknown
<b>Bnip2</b>	-18.3	exon-cassette	BCL2/adenovirus E1B interacting protein 2	-6	Unknown
<b>Bora</b>	37.5	exon-cassette	bora, aurora kinase A activator	-251	Premature stop codon in long isoform
<b>Bptf</b>	-22.9	alternate-5p	bromodomain PHD finger transcription factor	-281	Unknown
<b>Calu</b>	13.3	mutually-exclusive-exon	Calumenin	0	Unknown
<b>Cbwd1</b>	-23.1	alternate-5p	COBW domain containing 1	-121	CobW/HypB/UreG domain truncated in short isoform
<b>Ccdc136</b>	-10.2	exon-cassette	coiled-coil domain containing 136	-47	Unknown
<b>Ccdc15</b>	14.8	alternate-5p	coiled-coil domain containing 15	116	Unknown
<b>Cdkn2aip</b>	-18.2	alternate-5p	CDKN2A interacting protein	-444	Premature stop codon inducing a NLS loss in short isoform
<b>Celf1</b>	11.2	alternate-3p	CUGBP, Elav-like family member 1	1	Unknown

Gene	Delta-PSI	Event Type	Full name	Predicted residue variation caused by alternative splicing modification ( $\Delta$ AA)	Predicted functional consequence
<b>Cflar</b>	-14.8	exon-cassette	CASP8 and FADD-like apoptosis regulator	-186	Loss of the two DED domains in short isoform
<b>Cflar</b>	27.6	exon-cassette	CASP8 and FADD-like apoptosis regulator	-186	Loss of the two DED domains in long isoform
<b>Clip1</b>	-18.9	alternate-5p	CAP-GLY domain containing linker protein 1	-76	Unknown
<b>Clk4</b>	11.9	exon-cassette+intron-retention	CDC like kinase 4	180	Gain of 10 NLS and full-length Pkinase domain in long isoform
<b>Cwc22</b>	21.5	alternate-5p	CWC22 spliceosome-associated protein homolog (S, cerevisiae)	-6	Unknown
<b>Cwc22</b>	19.9	exon-cassette	CWC22 spliceosome-associated protein homolog (S, cerevisiae)	6	Unknown
<b>E2f3</b>	-20.9	alternate-3p	E2F transcription factor 3	-6	Additional NLS in short isoform
<b>Edc3</b>	-26.5	exon-cassette	enhancer of mRNA decapping 3 homolog (S, cerevisiae)	-183	Loss of Edc3-linker domain, LSM14 domain and truncation of YjwF_N domain in short isoform
<b>Eif4a2</b>	-11.4	exon-cassette	eukaryotic translation initiation factor 4A2	-95	Truncation of DEAD box helicase domain in short isoform
<b>Eif4h</b>	-16.7	exon-cassette	eukaryotic translation initiation factor 4H	-20	Unknown
<b>ErbB2ip</b>	-30.0	exon-cassette+alternate-3p+multiple-exon-cassette+mutually-exclusive-exon	ErbB2 interacting protein	-39	Unknown
<b>ErbB2ip</b>	23.3	exon-cassette+alternate-3p+multiple-exon-cassette+mutually-exclusive-exon	ErbB2 interacting protein	-384	Premature stop codon, C-Term PDZ domain loss in short isoform
<b>Fam179b</b>	-30.2	exon-cassette	family with sequence similarity 179, member B	-50	Unknown

Gene	Delta-PSI	Event Type	Full name	Predicted residue variation caused by alternative splicing modification ( $\Delta$ AA)	Predicted functional consequence
<b>Ficn</b>	35.8	alternate-3p	folliculin	-129	Premature stop codon, resulting in Folliculin domain truncation (174AA, C-term)
<b>Foxk2</b>	-29.7	exon-cassette	forkhead box K2	-401	Unknown
<b>G2e3</b>	-53.0	exon-cassette+alternate-3p+multiple-exon-cassette	G2/M-phase specific E3 ubiquitin ligase	116	Unknown
<b>Gdap2</b>	15.1	alternate-3p	ganglioside-induced differentiation-associated-protein 2	256	Complete CRAL and TRIO domains in long isoform
<b>Gen1</b>	-28.7	exon-cassette	Gen homolog 1, endonuclease (Drosophila)	-10	Earlier start codon in long isoform; Short isoform loses its XPG_N domain in N-term
<b>Gls</b>	11.3	alternate-3p	glutaminase	-376	Unknown
<b>Gpbp1</b>	25.6	exon-cassette	GC-rich promoter binding protein 1	20	Unknown
<b>Hmga1</b>	15.6	exon-cassette+alternate-5p+intron-retention	high mobility group AT-hook 1	0	5'UTR sequence change
<b>Hnrnpa2b1</b>	-13.6	exon-cassette	heterogeneous nuclear ribonucleoprotein A2/B1	-40	Additional HnRNPA1 domain in N-term of short isoform
<b>Il34</b>	58.9	exon-cassette	interleukin 34	-16	Frameshift introducing a premature stop codon in exon 8; truncation of Il34 domain
<b>Ilf3</b>	13.2	exon-cassette	interleukin enhancer binding factor 3	13	Unknown
<b>Iqce</b>	17.6	exon-cassette	IQ motif containing E	17	Unknown
<b>Iqce</b>	-19.2	exon-cassette	IQ motif containing E	-17	Unknown
<b>Ivns1abp</b>	30.8	exon-cassette+alternate-3p	influenza virus NS1A binding protein	-281	NLS and BTB domains loss in long isoform

Gene	Delta-PSI	Event Type	Full name	Predicted residue variation caused by alternative splicing modification ( $\Delta$ AA)	Predicted functional consequence
<b>Kat5</b>	28.7	exon-cassette	K(lysine) acetyltransferase 5	52	Long isoform have two NLS instead of only one in the short isoform
<b>Kat6a</b>	-13.6	exon-cassette	K(lysine) acetyltransferase 6A	130	Unknown
<b>Kmt2e</b>	10.8	exon-cassette	lysine (K)-specific methyltransferase 2E	-1602	Loss of 6 NLS and SET and PHD domains in long isoform
<b>Lrrfip1</b>	13.1	exon-cassette	leucine rich repeat (in FLII) interacting protein 1	24	Truncation in double-stranded RNA binding protein DUF2051 in long isoform
<b>Macf1</b>	-25.2	multiple-exon-cassette	microtubule-actin crosslinking factor 1	-2027	Loss of all 9 Plectin repeat domains in short isoform
<b>Matr3</b>	12.3	alternate-5p	matrin 3	0	No predicted functional change
<b>Max</b>	11.3	exon-cassette	Max protein	-122	NLS and Helix-Loop-Helix domain loss in long isoform
<b>Mbnl2</b>	24.1	exon-cassette	muscleblind-like 2	18	Unknown
<b>Mdm2</b>	-58.8	exon-cassette+alternate-5p	transformed mouse 3T3 cell double minute 2	-197	SWIB domain in N-Term loss in short isoform
<b>Mon2</b>	38.3	exon-cassette	MON2 homolog (yeast)	7	6 residue gap in Mon2 domain in short isoform
<b>Morn1</b>	-16.3	alternate-5p	MORN repeat containing 1	-245	Loss of 4 MORN domain out of 8 in short isoform
<b>Msh4</b>	-38.7	alternate-5p	mutS homolog 4 (E. coli)	404	Premature stop codon in long isoform
<b>Mtif3</b>	25.0	exon-cassette+alternate-5p	mitochondrial translational initiation factor 3	0	Unknown
<b>Nabp1</b>	41.4	alternate-5p+intron-retention	nucleic acid binding protein 1	-91	Unknown
<b>Naip2</b>	21.8	exon-cassette	NLR family, apoptosis inhibitory protein 2	56	Unknown



Gene	Delta-PSI	Event Type	Full name	Predicted residue variation caused by alternative splicing modification ( $\Delta$ AA)	Predicted functional consequence
<b>Nasp</b>	-16.5	exon-cassette	nuclear autoantigenic sperm protein (histone-binding)	-325	Unknown
<b>Nde1</b>	-16.6	alternate-3p	nuclear distribution gene E homolog 1 (A nidulans)	27	Unknown
<b>Nek1</b>	26.9	exon-cassette	NIMA (never in mitosis gene a)-related expressed kinase 1	29	Unknown
<b>Neurl4</b>	-19.2	exon-cassette	neuralized homolog 4 (Drosophila)	-22	Unknown
<b>Nfx1</b>	28.3	alternate-3p	nuclear transcription factor, X-box binding 1	-14	Unknown
<b>Odf2l</b>	-16.0	exon-cassette	outer dense fiber of sperm tails 2-like	-96	Unknown
<b>Opa1</b>	-14.5	exon-cassette	optic atrophy 1	-37	Unknown
<b>Pan3</b>	17.4	exon-cassette	PAN3 polyA specific ribonuclease subunit homolog (S, cerevisiae)	258	Unknown
<b>Pcgf5</b>	15.5	exon-cassette	polycomb group ring finger 5	20	C-term RAWUL domain truncated in long isoform
<b>Phactr4</b>	-16.8	exon-cassette	phosphatase and actin regulator 4	-27	RPEL repeat domain loss in short isoform
<b>Piga</b>	-33.8	alternate-5p	phosphatidylinositol glycan anchor biosynthesis, class A	-316	PIGA domain loss in short isoform
<b>Pitpnb</b>	-21.8	exon-cassette	phosphatidylinositol transfer protein, beta	-1	Unknown
<b>Pnpla7</b>	69.1	alternate-5p	patatin-like phospholipase domain containing 7	-886, -52, -454 or +380	Unknown
<b>Polg2</b>	-13.5	alternate-5p	polymerase (DNA directed), gamma 2, accessory subunit	-44	Unknown
<b>Ppfibp1</b>	-16.1	exon-cassette+intron-retention	PTPRF interacting protein, binding protein 1 (liprin beta 1)	-11	Unknown

Gene	Delta-PSI	Event Type	Full name	Predicted residue variation caused by alternative splicing modification ( $\Delta$ AA)	Predicted functional consequence
<b>Ppp1r12a</b>	10.2	exon-cassette	protein phosphatase 1, regulatory (inhibitor) subunit 12A	422	Unknown
<b>Pqlc1</b>	50.9	exon-cassette	PQ loop repeat containing 1	18	Unknown
<b>Prpf39</b>	18.5	exon-cassette+multiple-exon-cassette	PRP39 pre-mRNA processing factor 39 homolog (yeast)	-201, -239	Loss of part of Tetratricopeptide-like helical domain and HAT repeats in both C- and N-term
<b>Pum2</b>	-11.2	exon-cassette	pumilio RNA-binding family member 2	-79	Unknown
<b>Ranbp3</b>	-27.0	exon-cassette+multiple-exon-cassette	RAN binding protein 3	331	NLS loss and full RanBP1 domain in long isoform
<b>Rfx5</b>	34.7	exon-cassette+alternate-5p	regulatory factor X, 5 (influences HLA class II expression)	185	NLS gain and full-length RFX5 DNA-binding domain in long isoform
<b>Rnf135</b>	-31.1	exon-cassette	ring finger protein 135	-216	Zinc finger of C3HC4-type domain loss in short isoform
<b>Rnps1</b>	-25.7	exon-cassette+multiple-exon-cassette	ribonucleic acid binding protein S1	-23	Unknown
<b>Rnps1</b>	-14.6	exon-cassette+multiple-exon-cassette	ribonucleic acid binding protein S1	-23	Unknown
<b>Scaf11</b>	-11.6	alternate-5p	SR-related CTD-associated factor 11	-16	Unknown
<b>Senp1</b>	22.9	exon-cassette	SUMO1/sentrin specific peptidase 1	-142	Unknown
<b>Sfswap</b>	-24.8	alternate-5p	splicing factor, suppressor of white-apricot family	-724	47 AA truncation in Alternative splicing regulator domain and 2 Surp module domain loss in short isoform
<b>Skil</b>	-14.2	alternate-5p	SKI-like	-35	Unknown

Gene	Delta-PSI	Event Type	Full name	Predicted residue variation caused by alternative splicing modification ( $\Delta$ AA)	Predicted functional consequence
<b>Slc23a2</b>	-12.2	alternate-3p	solute carrier family 23 (nucleobase transporters), member 2	-308	208 AA loss in the N-term of Xan_ur_permease domain in short isoform
<b>Son</b>	25.7	exon-cassette+alternate-5p	Son DNA binding protein	-2198	Premature stop codon in long isoform, introducing 4 NLS and G-patch, Arginine/Serine-Rich protein 1 and double-stranded RNA binding domain loss
<b>Spef2</b>	18.4	exon-cassette	sperm flagellar 2	923	Unknown
<b>Spopl</b>	27.8	exon-cassette	speckle-type POZ protein-like	56	Unknown
<b>Stx3</b>	39.5	exon-cassette+mutually-exclusive-exon	syntaxin 3	97	75 AA truncation of Syntaxin domain in long isoform
<b>Tbp</b>	-44.3	exon-cassette	TATA box binding protein	-56	TBP domain loss and truncation of first TBP domain's end in short isoform
<b>Tcf12</b>	30.7	exon-cassette+intron-retention	transcription factor 12	24	Unknown
<b>Tmem132a</b>	66.1	alternate-3p	transmembrane protein 132A	29	Unknown
<b>Tmem168</b>	-32.5	exon-cassette	transmembrane protein 168	-384	Unknown
<b>Tmem19</b>	-15.0	alternate-5p	transmembrane protein 19	12	Full length DUF92 integral membrane domain in long isoform
<b>Tmpo</b>	-38.3	exon-cassette+multiple-exon-cassette	thymopoietin	-40	Unknown
<b>Tmpo</b>	-11.5	exon-cassette+multiple-exon-cassette	thymopoietin	-72	Unknown
<b>Thpp2</b>	10.7	exon-cassette	tripeptidyl peptidase II	-130	Unknown
<b>Tra2a</b>	21.2	exon-cassette	transformer 2 alpha homolog (Drosophila)	97	Full-length RNA recognition motif in long isoform

Gene	Delta-PSI	Event Type	Full name	Predicted residue variation caused by alternative splicing modification ( $\Delta$ AA)	Predicted functional consequence
<b>Trappc13</b>	-29.9	exon-cassette	trafficking protein particle complex 13	-6	DUF974 domain truncation of 6 AA in short isoform
<b>Ubap1</b>	-21.4	exon-cassette	ubiquitin-associated protein 1	-61	Unknown
<b>Ubr3</b>	11.3	alternate-3p	ubiquitin protein ligase E3 component n-recognin 3	4	Unknown
<b>Upf1</b>	-23.4	alternate-5p	UPF1 regulator of nonsense transcripts homolog (yeast)	-11	Unknown
<b>Wsb1</b>	19.9	alternate-3p	WD repeat and SOCS box-containing 1	-177	Premature stop codon in long isoform, resulting in a truncated protein containing only a WD, G-beta domain instead of 4 WD, G-beta domain and a SOCS box domain
<b>Xdh</b>	-25.6	alternate-5p	xanthine dehydrogenase	-599	NLS appearance in short isoform
<b>Zfp207</b>	-12.5	exon-cassette	zinc finger protein 207	-6	Unknown
<b>Zfp788</b>	-32.4	exon-cassette+alternate-3p+multiple-exon-cassette	zinc finger protein 788	-532	Unknown
<b>Zmynd11</b>	-17.1	exon-cassette	zinc finger, MYND domain containing 11	-54	Unknown
<b>Zyx</b>	13.8	exon-cassette	zyxin	31	Unknown
<b>1700057G04Rik</b>	-31.1	exon-cassette	RIKEN cDNA 1700057G04 gene	-76	Truncation in Scramblase domain in short isoform
<b>2310057M21Rik</b>	-15.9	alternate-5p	RIKEN cDNA 2310057M21 gene	77	Unknown
<b>4631405J19Rik</b>	-45.7	alternate-3p	RIKEN cDNA 4631405J19 gene	-100	Unknown
<b>4930511M06Rik</b>	-23.6	exon-cassette	RIKEN cDNA 4930511M06 gene	NA	Non-coding RNA

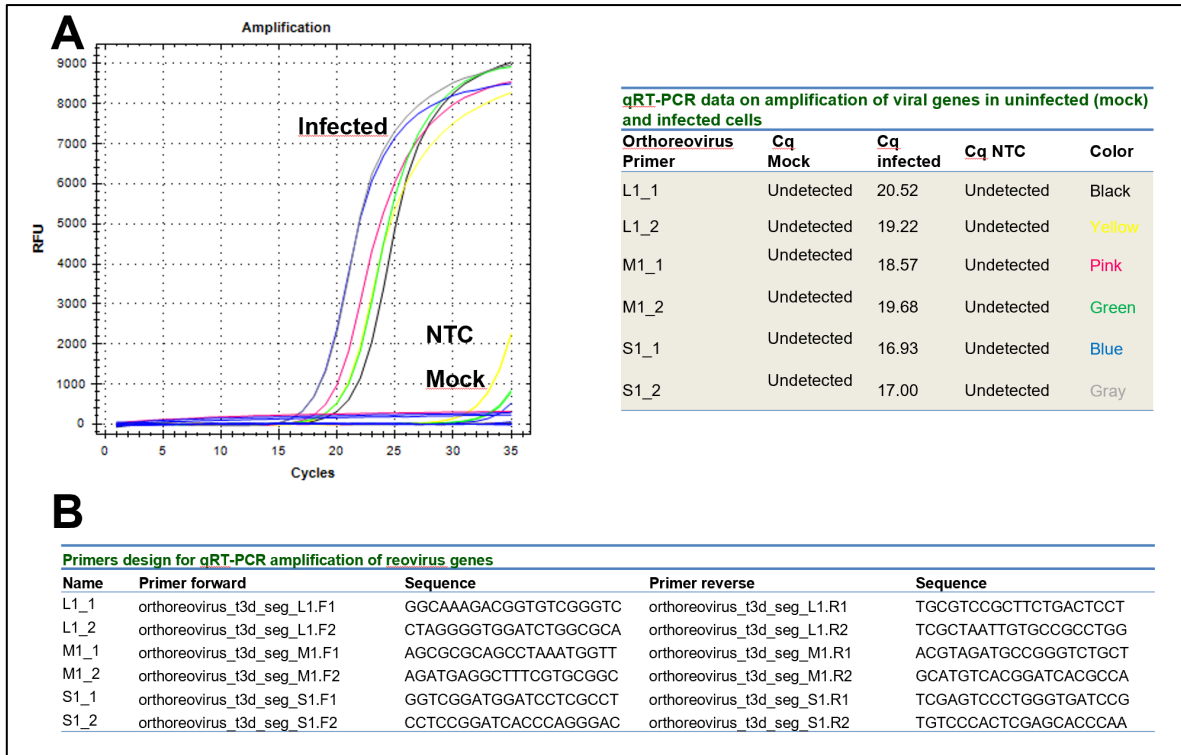


Figure A. *Detection of reovirus genes in infected cells by qRT-PCR.* (A) Total RNA was extracted from both uninfected and infected cells (14 h post-infection). Viral infection was confirmed by qRT-PCR using specific primers for three viral genes (M1, S1, L1). A control reaction without template (NTC: no template control) was also performed. All three viral genes were detected in the infected cells samples but were undetectable in the uninfected (mock) samples (absence of amplification or nonspecific amplification). Cq: quantification cycle. (B) Primers used for qPCR detection.

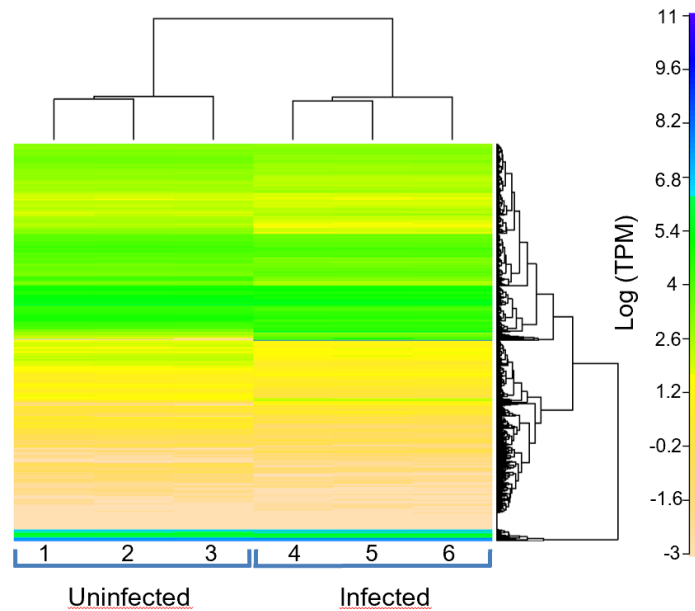
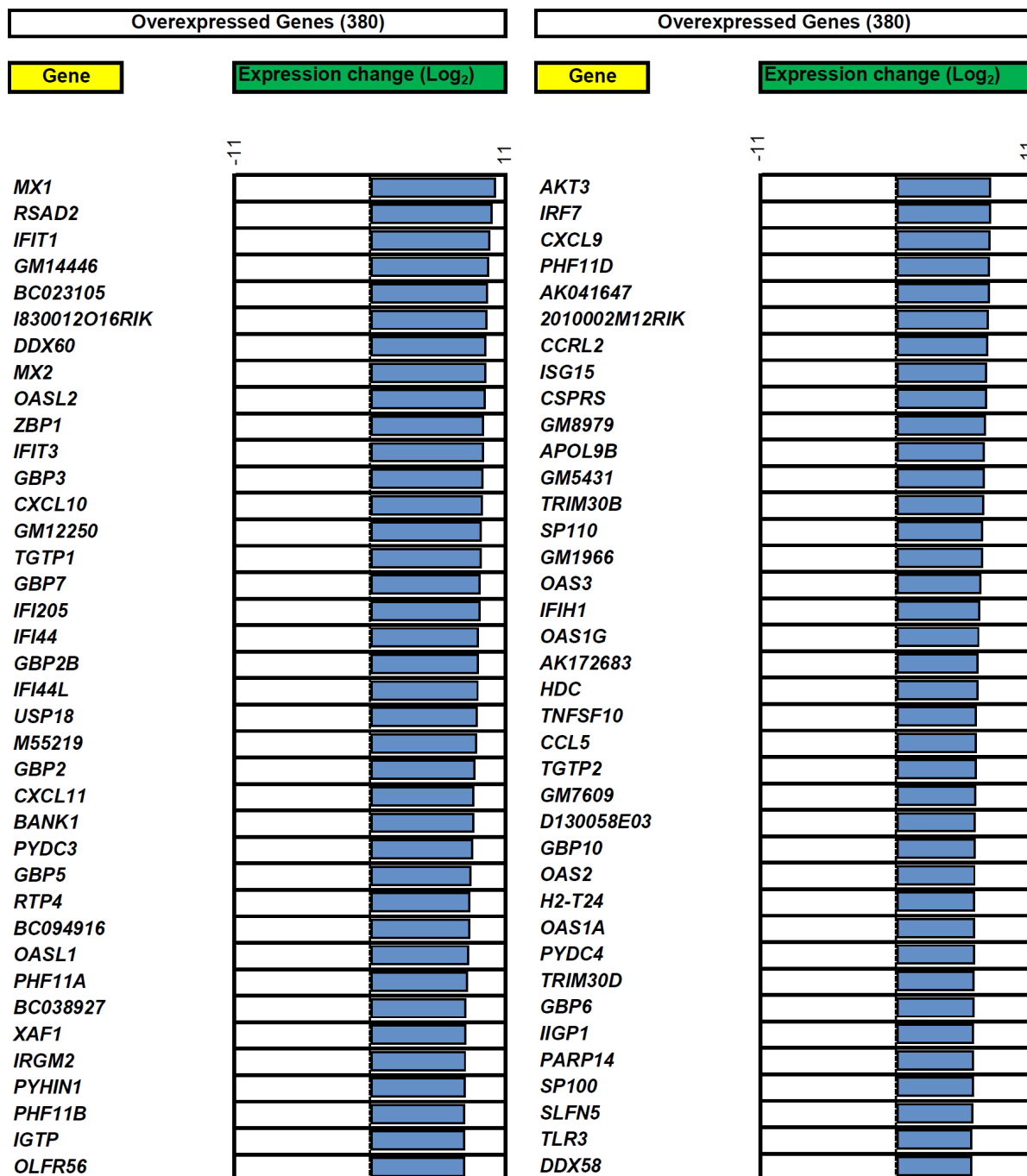
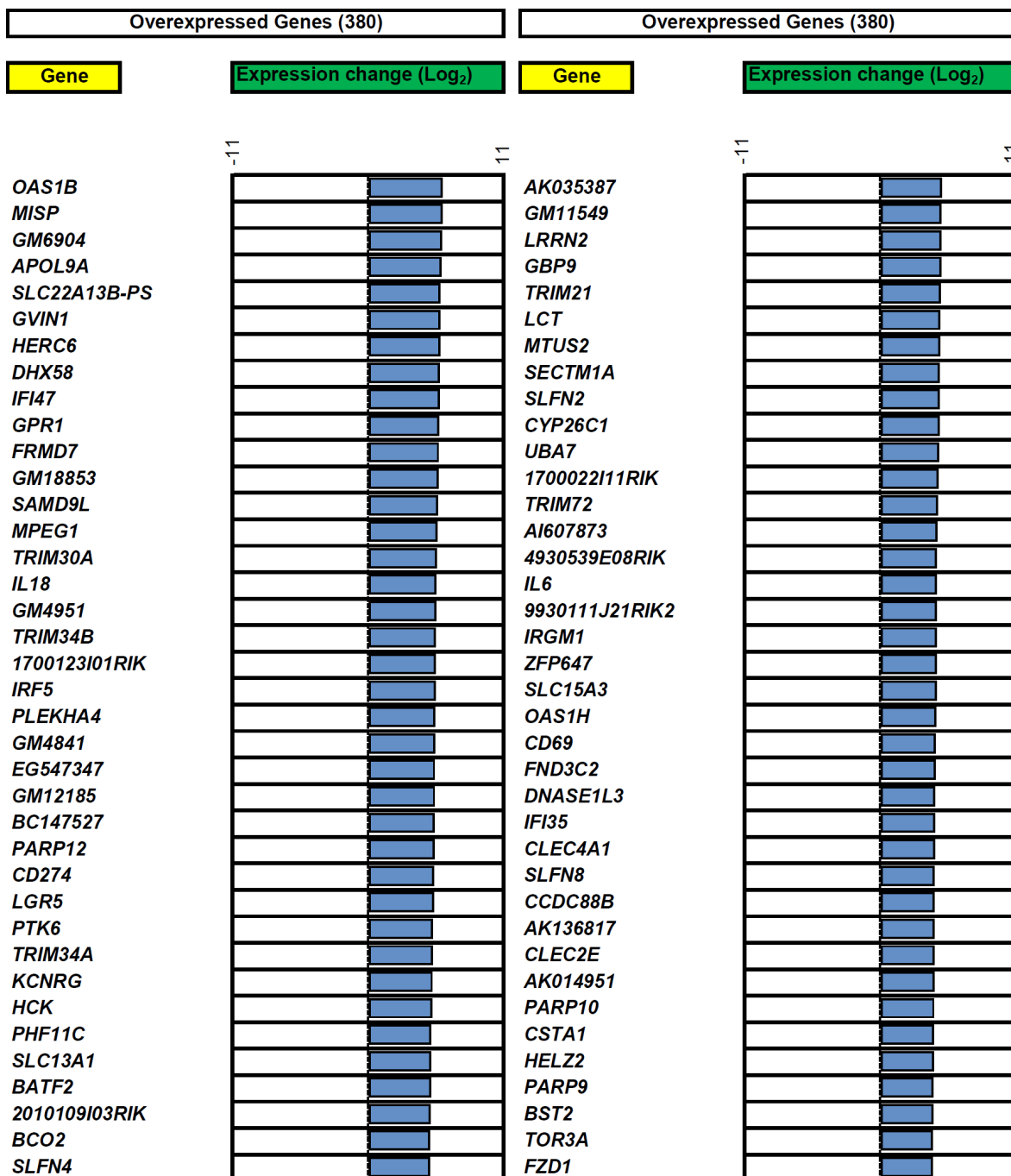
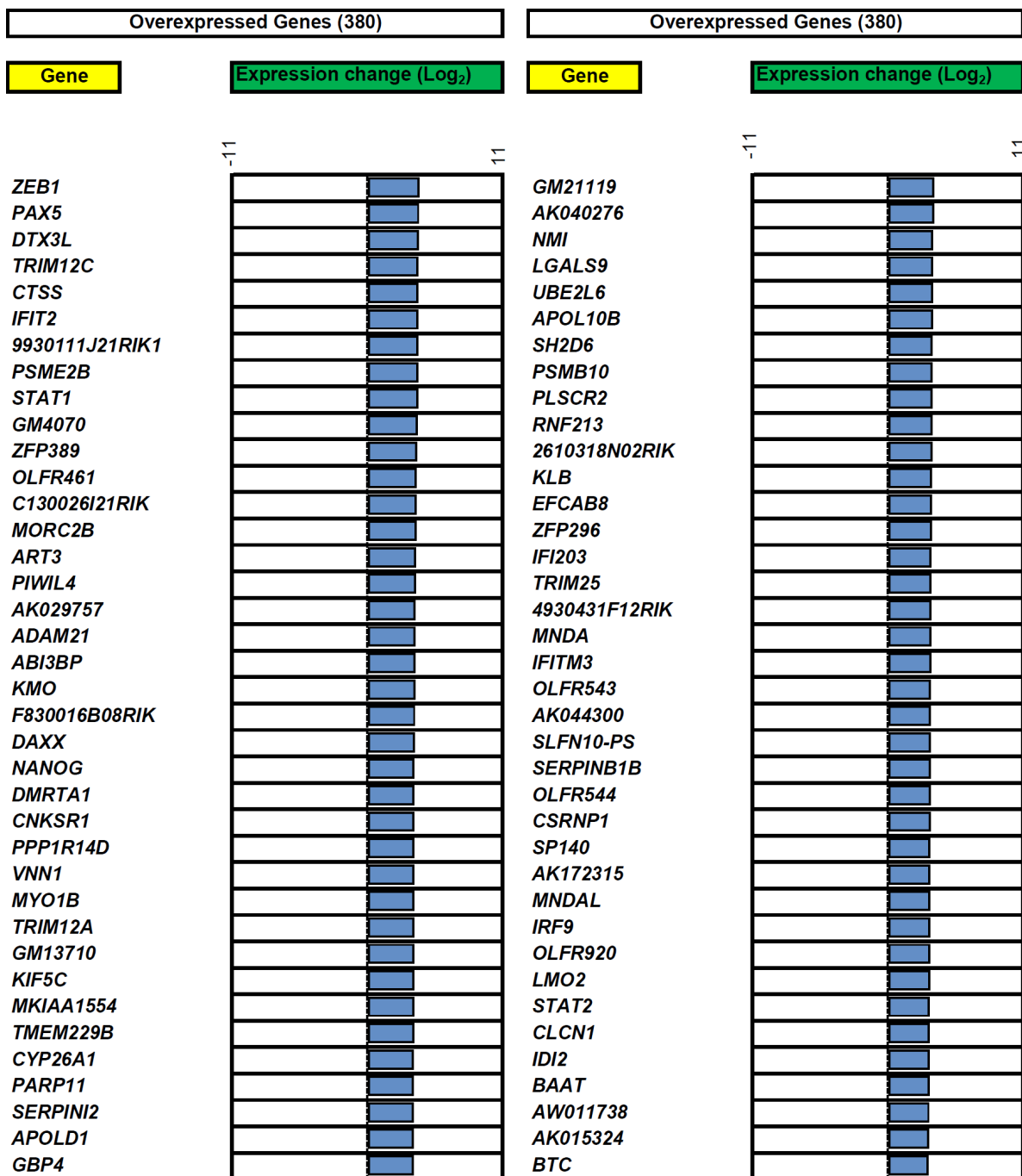


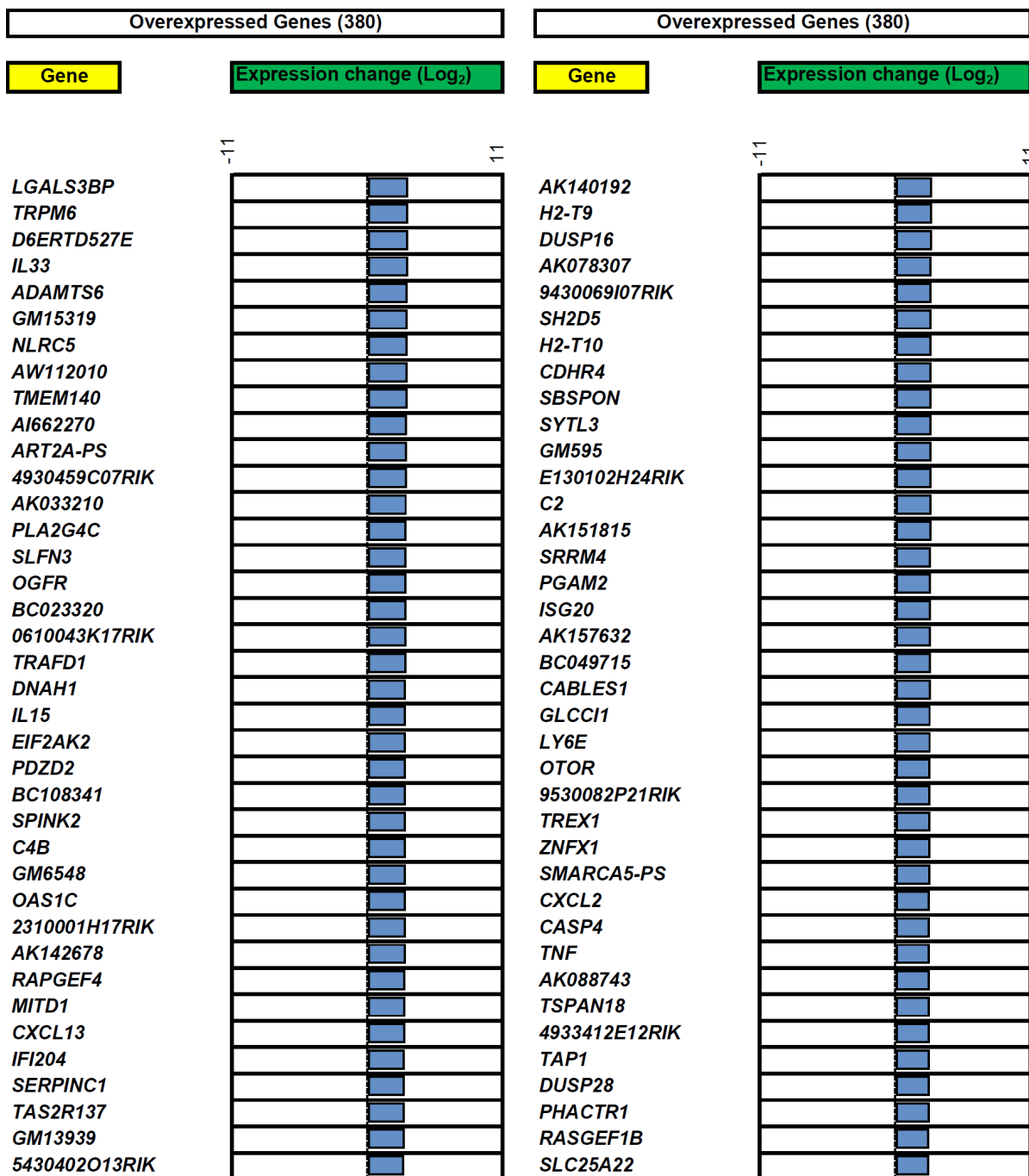
Figure B. *Heatmap representation of gene expression of total cellular genes in both infected and uninfected (mock) cells.* RNA sequencing was done in triplicate for each condition. The map represents the number of transcripts sequences (TPM: transcripts per million) in a color-coded logarithmic scale. Blue and green indicates high levels of gene expression while yellow indicates low levels of gene expression.

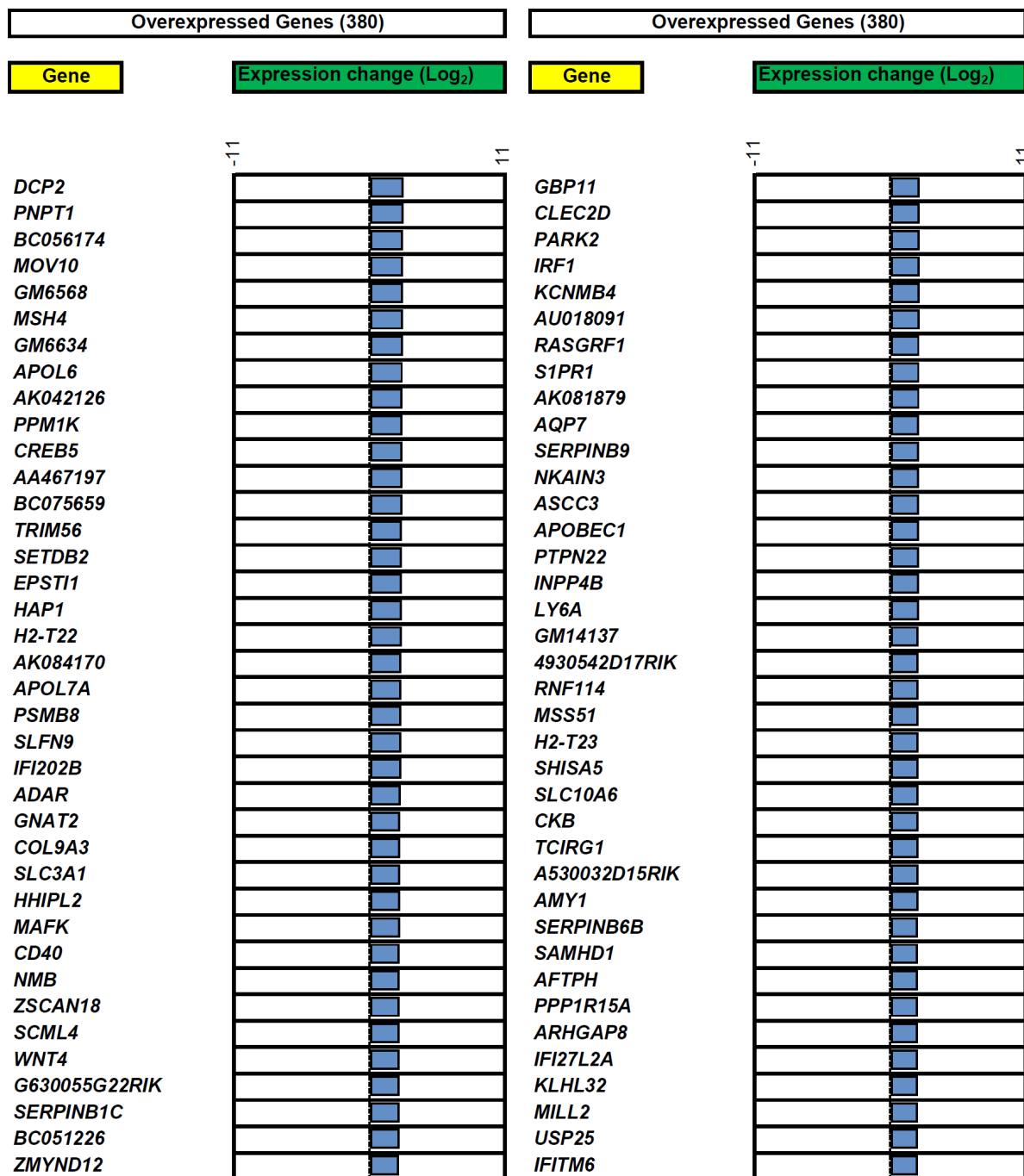


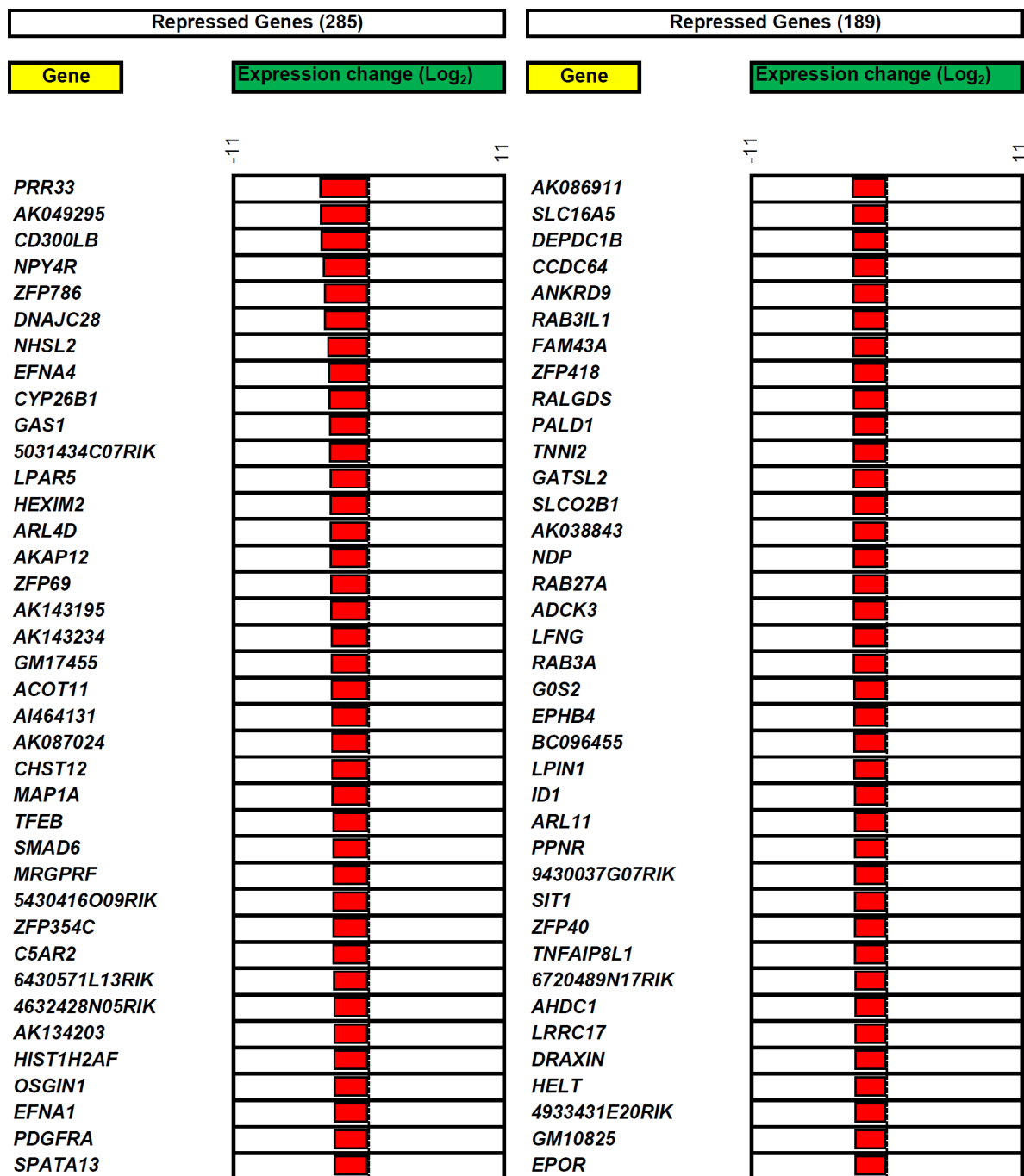


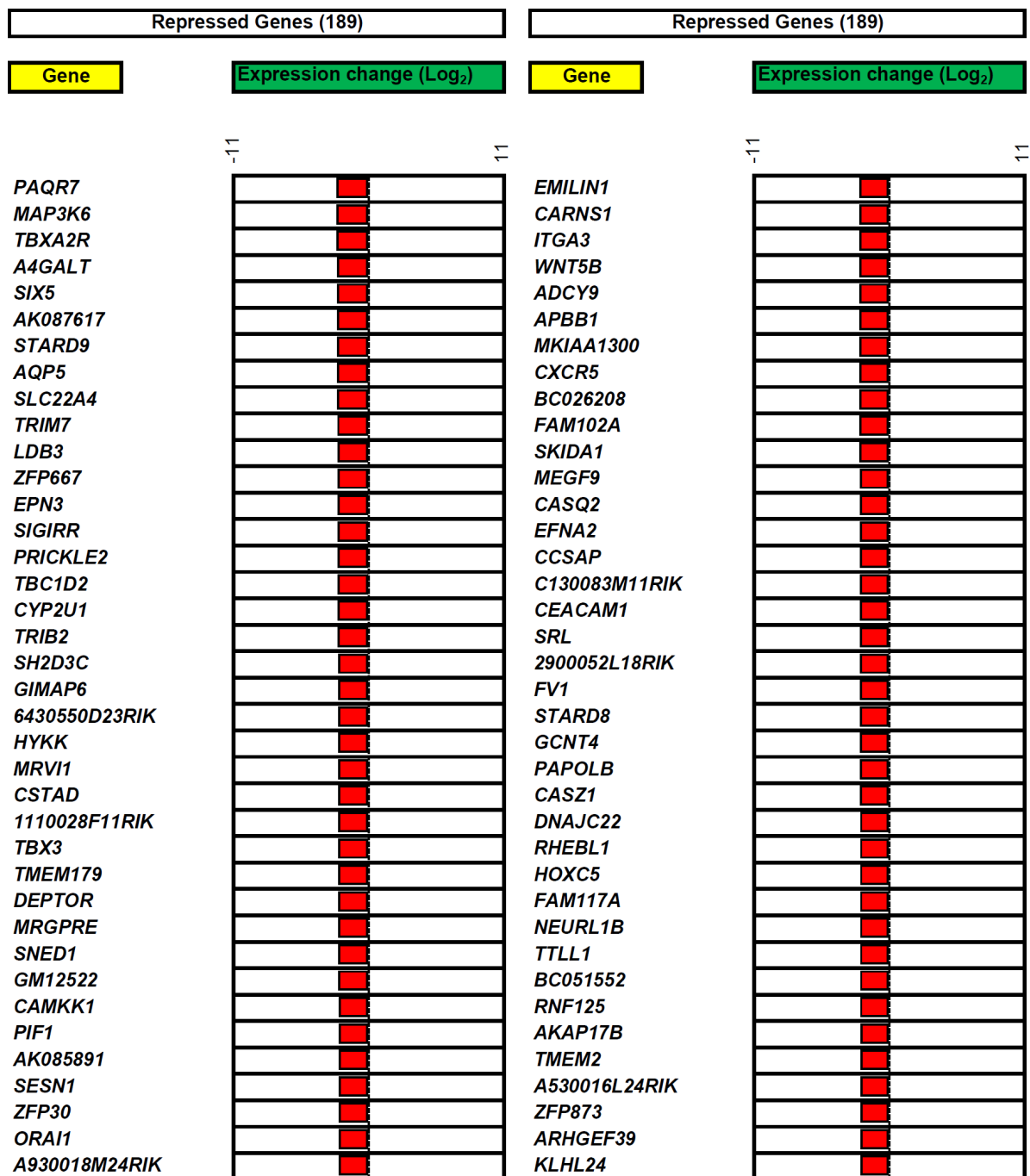












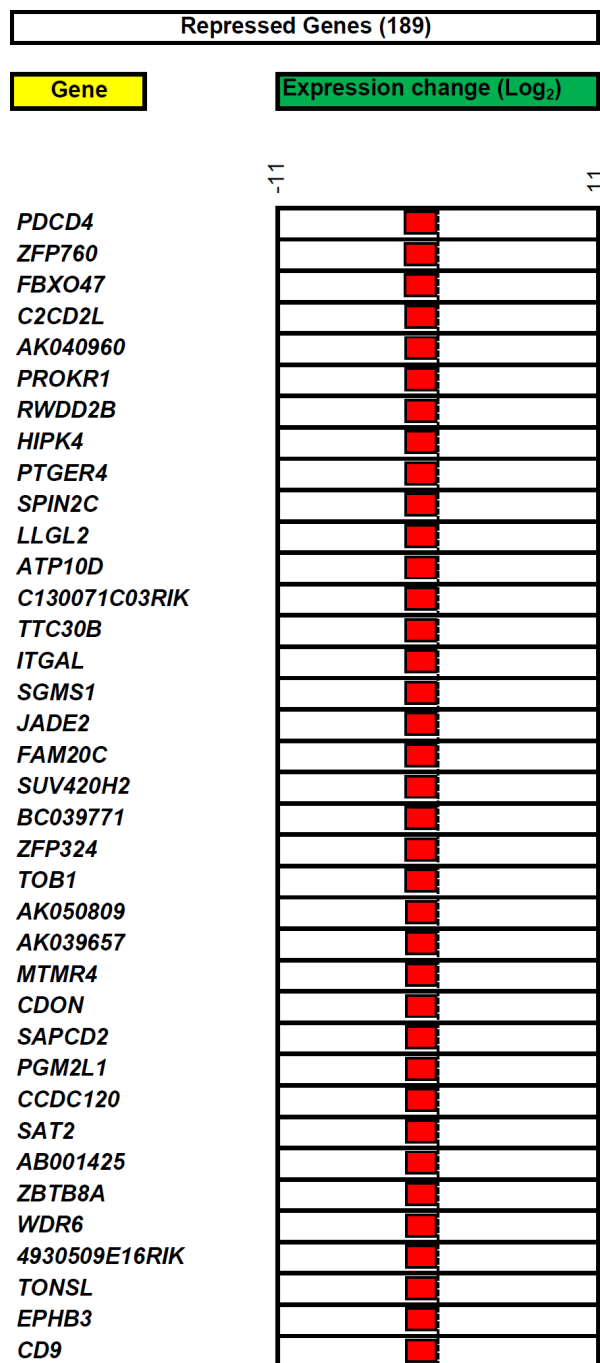


Figure C. List of the 570 genes for which the expression was the most significantly modified following viral infection. The list of genes is shown with the corresponding expression profile of each gene. The level of gene expression is presented on a logarithmic scale (Log<sub>2</sub>).

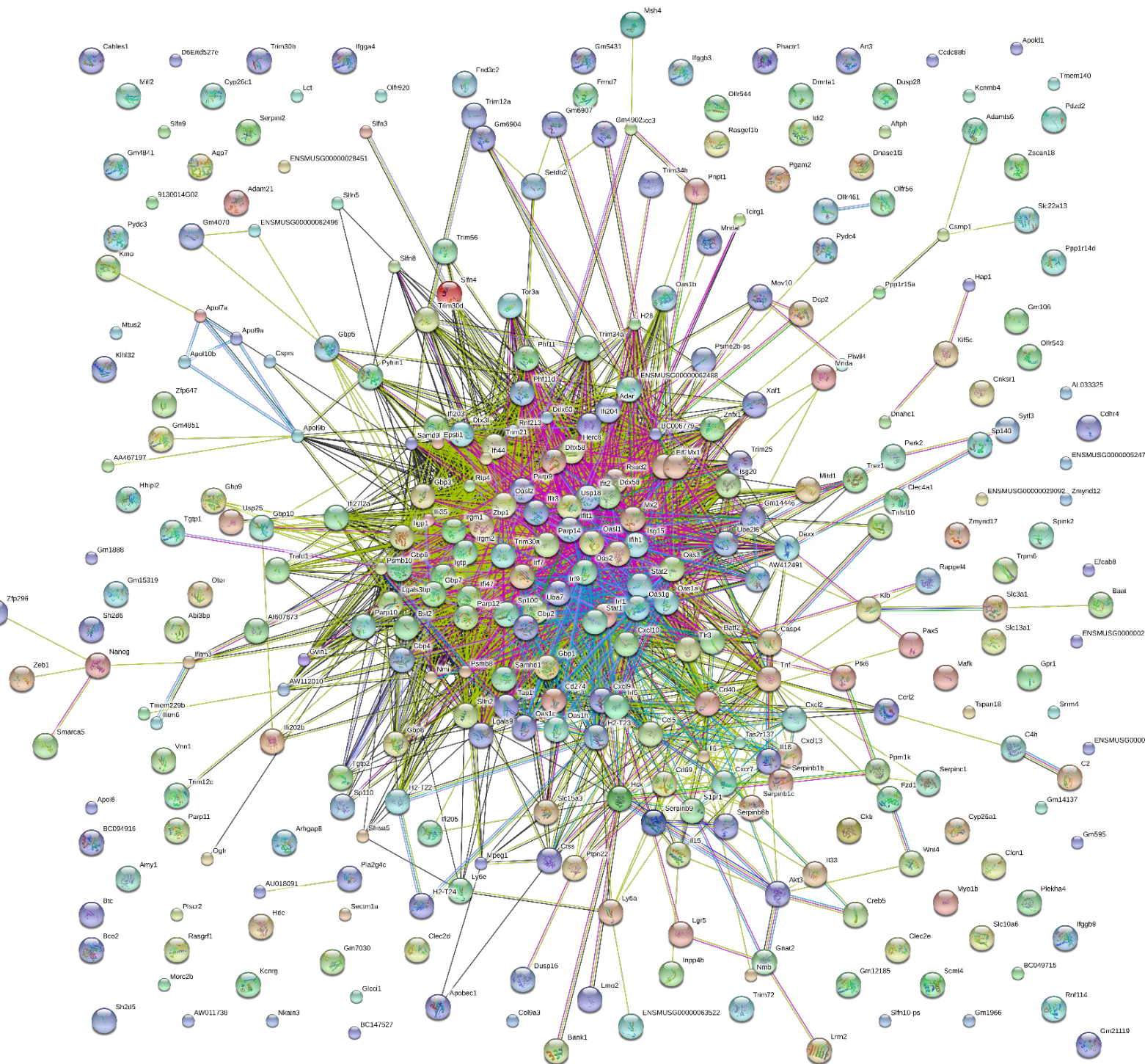


Figure D. *Overexpressed genes interaction network during reovirus infection.* Interaction network for the 380 cellular genes for which the expression was upregulated upon viral infection. The network was determined by uploading the genes into STRING. Solid lines: direct known interactions; dashed lines: suspected or indirect interactions.

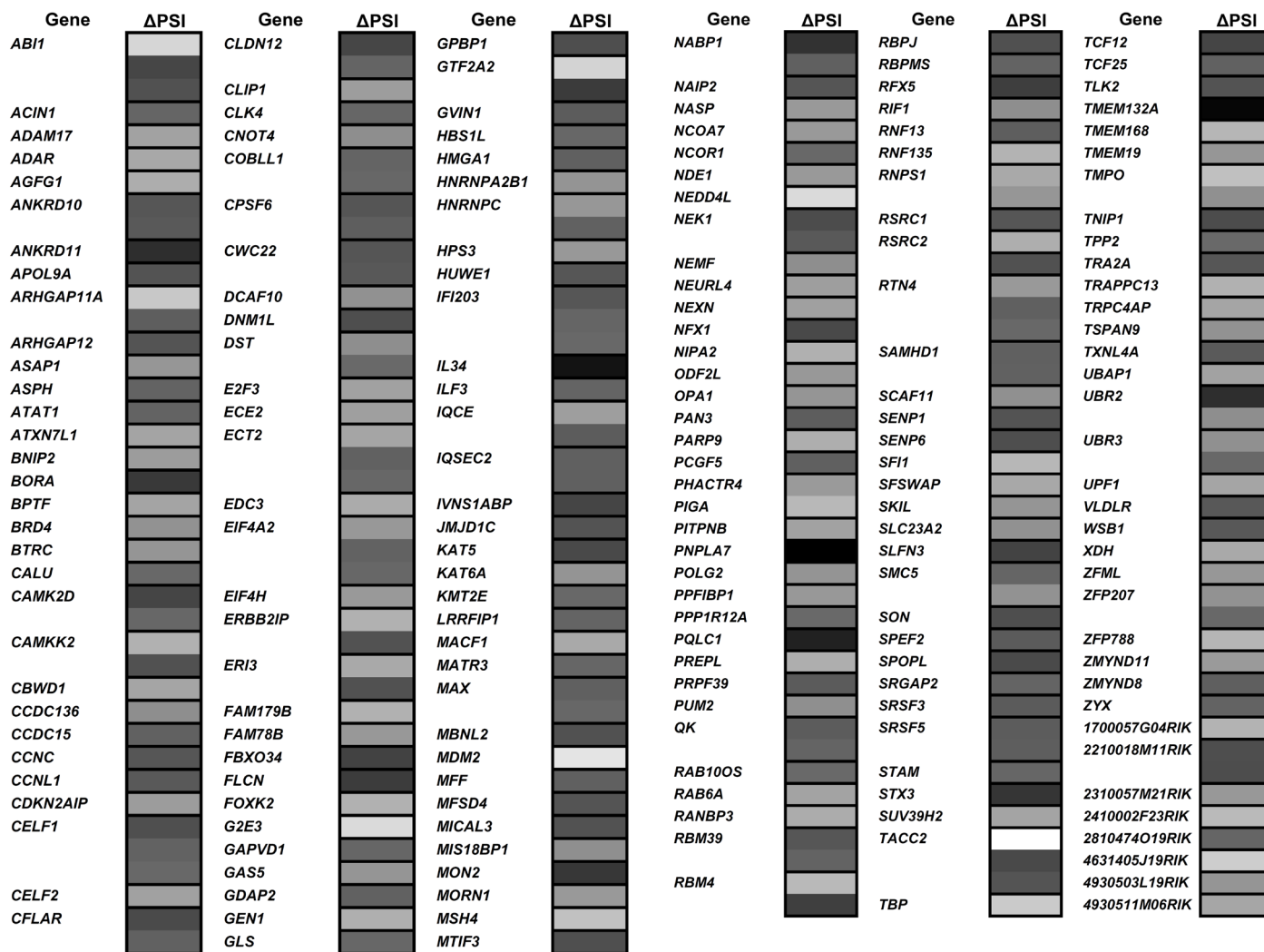


Figure E. 240 ASEs are modified during viral infection with reovirus. Heatmap representation with a sequential color scale of the 240 ASEs that are differentially spliced upon viral infection. RNA sequencing was done in triplicate for both the uninfected (mock) and infected cells. Darker shades indicates high  $\Delta$ PSI values and lighter shades indicates low  $\Delta$ PSI values between infected and mock cells. More than one ASEs can impact the same gene.



A

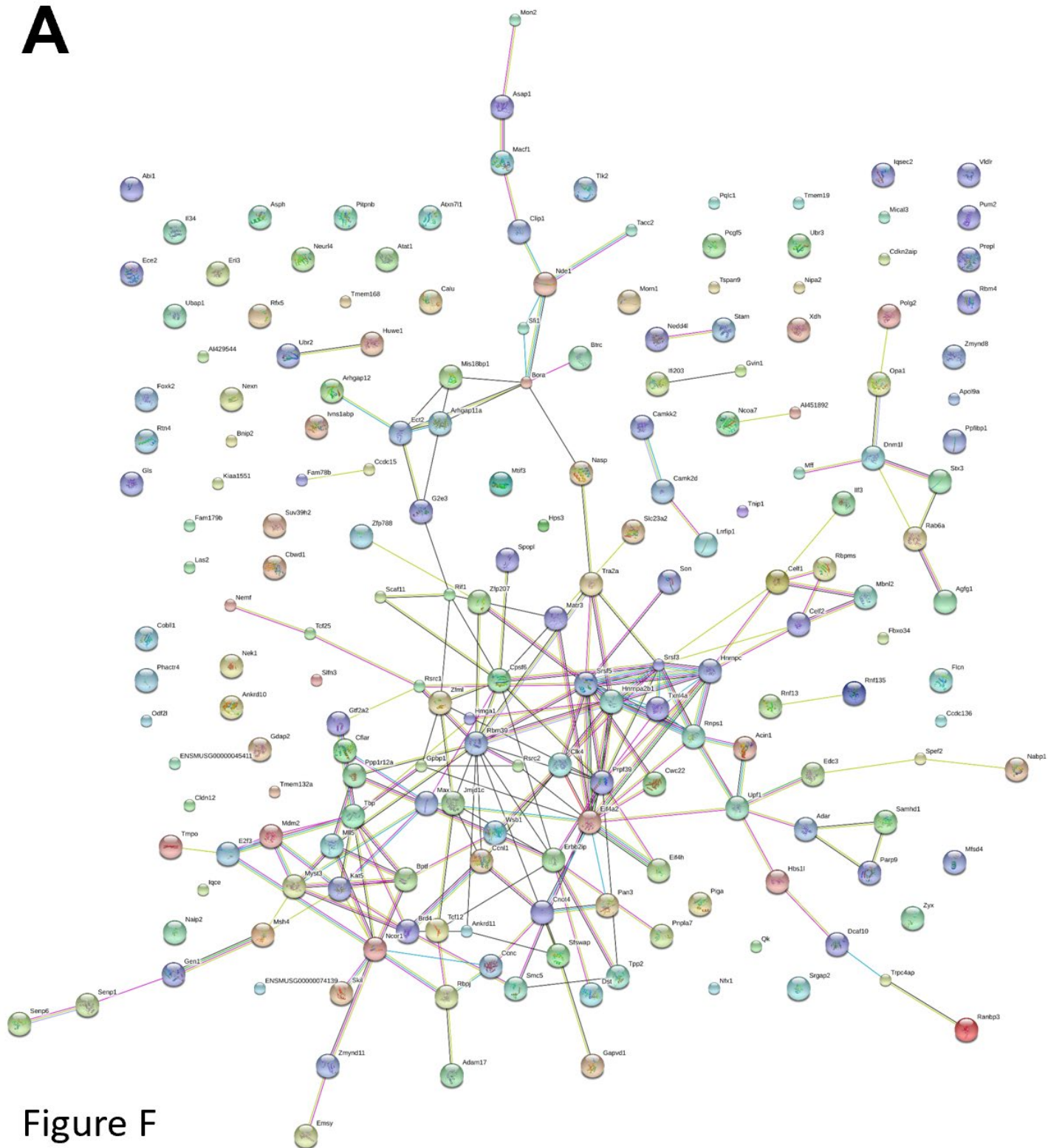


Figure F

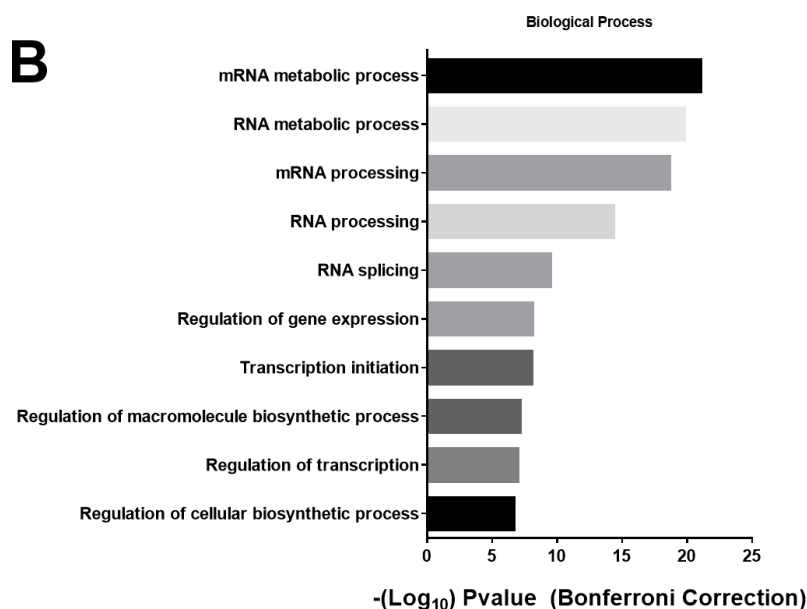
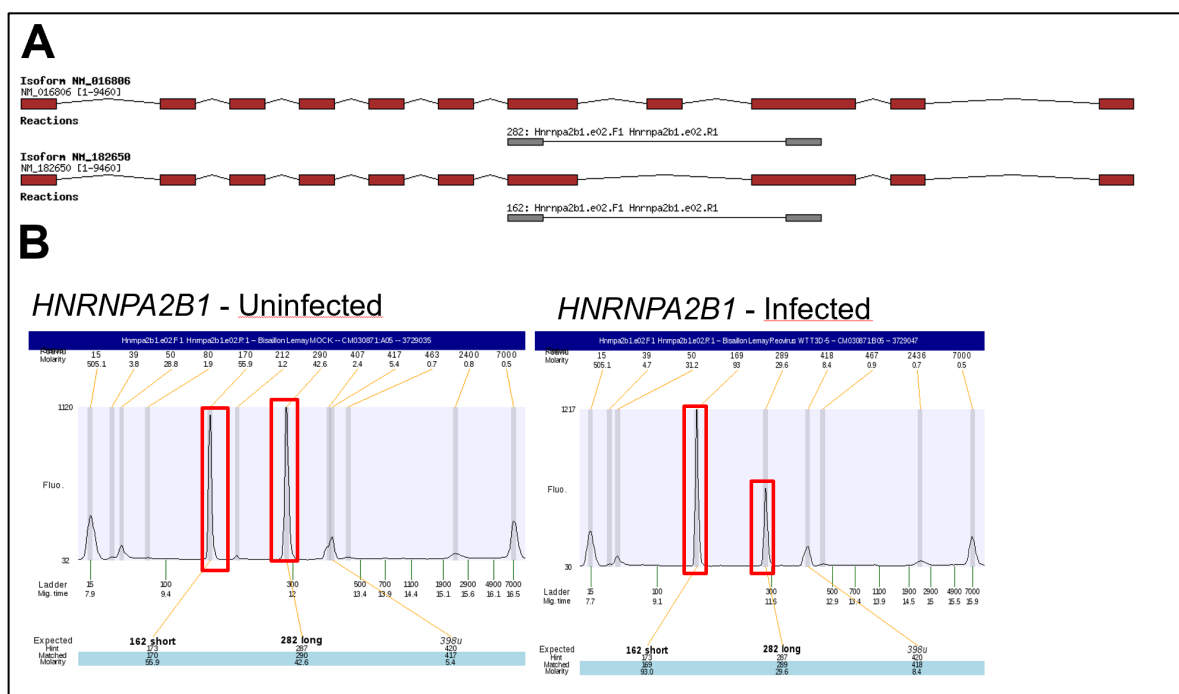


Figure F (cont'd)

Figure F. Profiling of the cellular alternative splicing landscape during reovirus infection. (A) Interaction network for genes encoding the 240 differentially spliced transcripts upon viral infection. The network was determined by uploading the corresponding genes into STRING. Solid lines: direct known interactions; dashed lines: suspected or indirect interactions. (B) Gene ontology analysis of the 240 differentially spliced transcripts upon viral infection. The corresponding genes were imported into the DAVID gene ontology suite of programs at the NIAID. Ontological functions were determined for biological processes using all ASEs characterized as background.



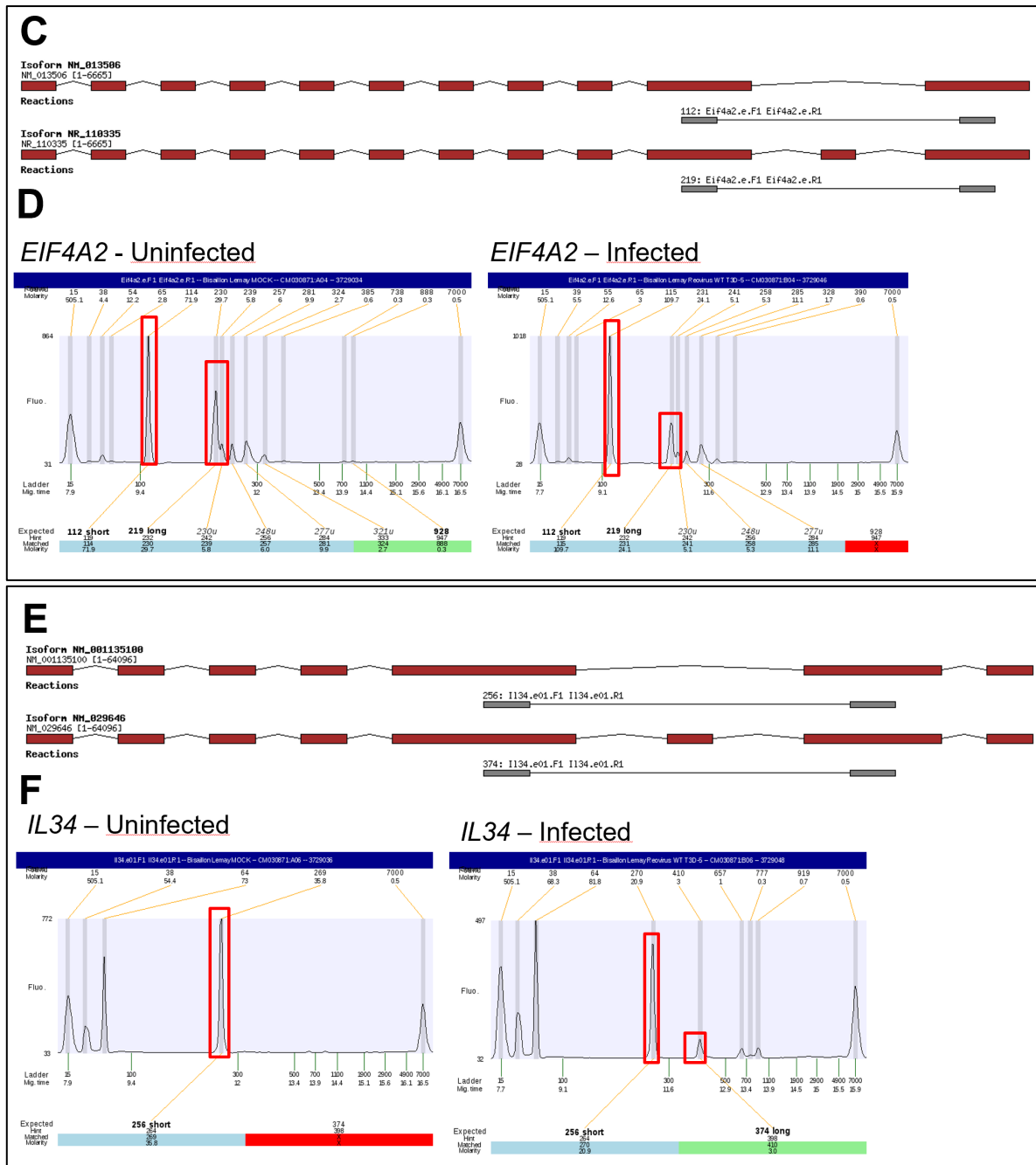
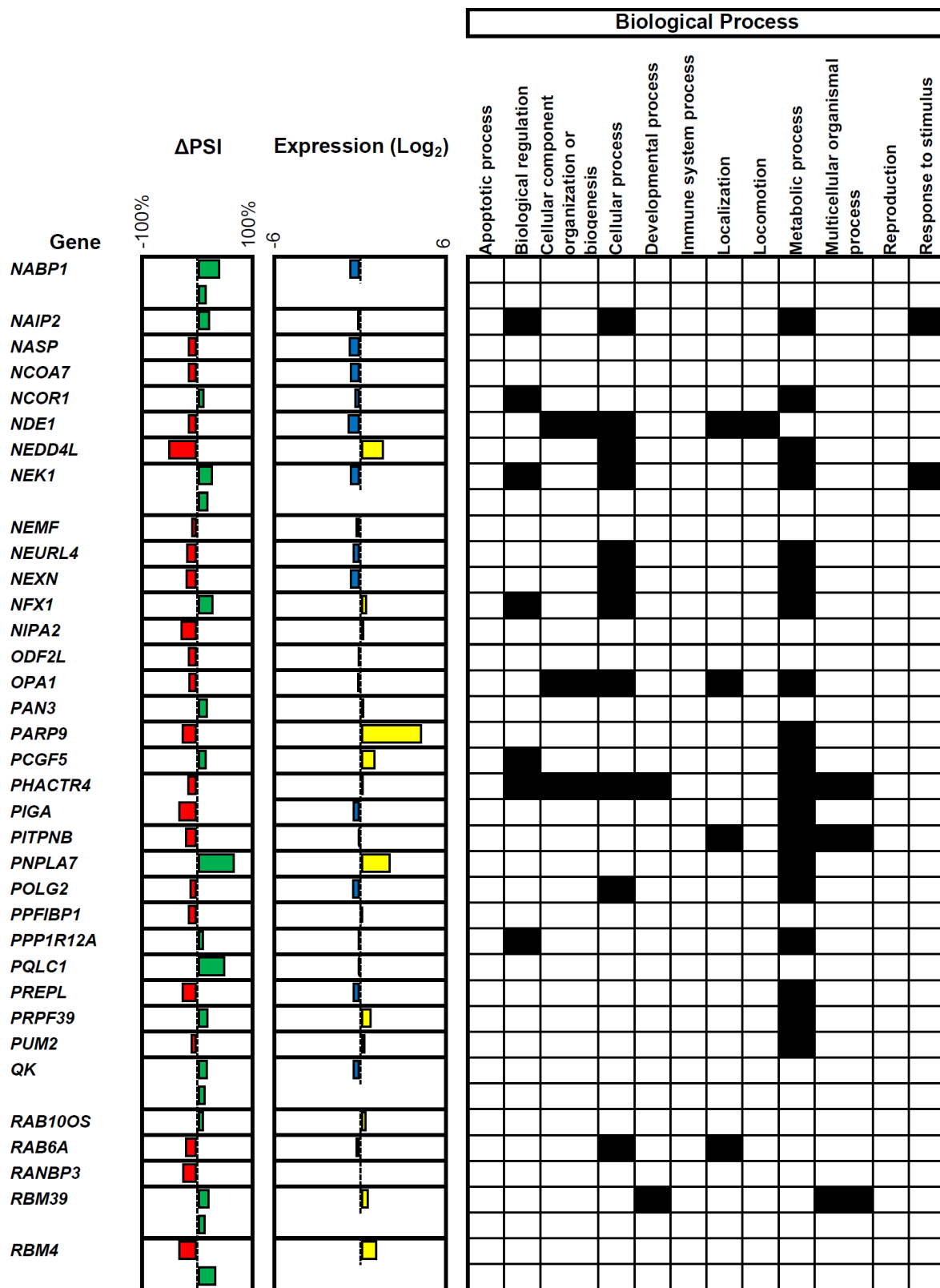


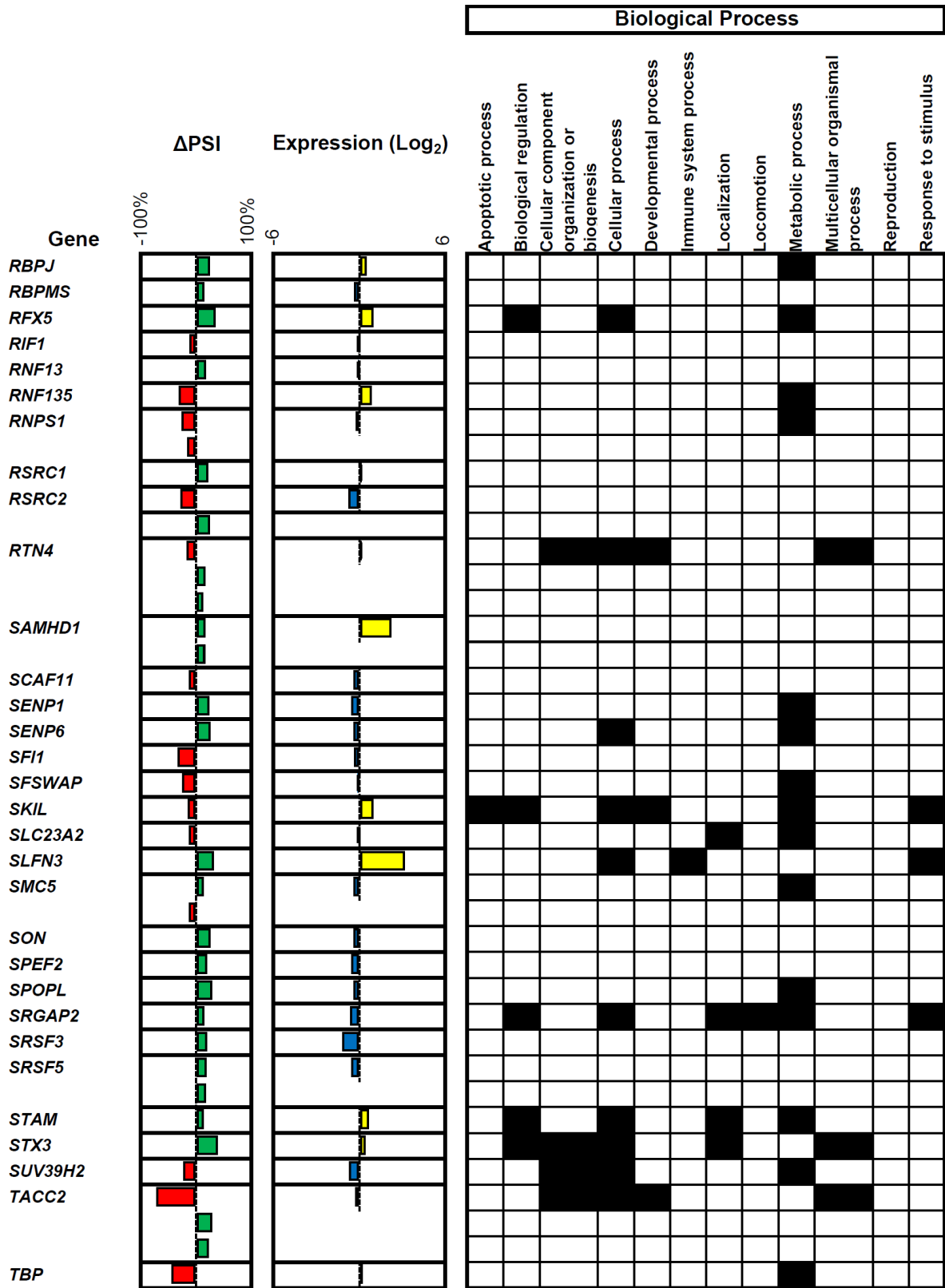
Figure G. Additional validation of ASEs dysregulated in infected cells. (A, C, E) Overview of two isoforms encoded by the *HNRNPA2B1*, *EIF4A2*, and *IL34* genes. Exons are depicted in red and the intervening introns are shown as thin black lines (not to scale). The primers used to detect the ASEs by RT-PCR assays are shown in gray and the sizes of the expected amplicons (162 nt and 282 nt, 112 nt and 219 nt, 256 nt and 374 nt, respectively) are also indicated. The genomic coordinates of the two isoforms are also indicated. (B, D, F) Cellular mRNAs isolated from both uninfected and infected cells were analyzed by RT-PCR using specific primers to detect both forms of the ASE encoded on various genes. The amplified products were analyzed by automated chip-based microcapillary electrophoresis. Capillary electrophoregrams of the PCR reactions are shown. The positions and the amplitude of the detected amplicons are highlighted by red boxes. The positions of the internal markers are also indicated.













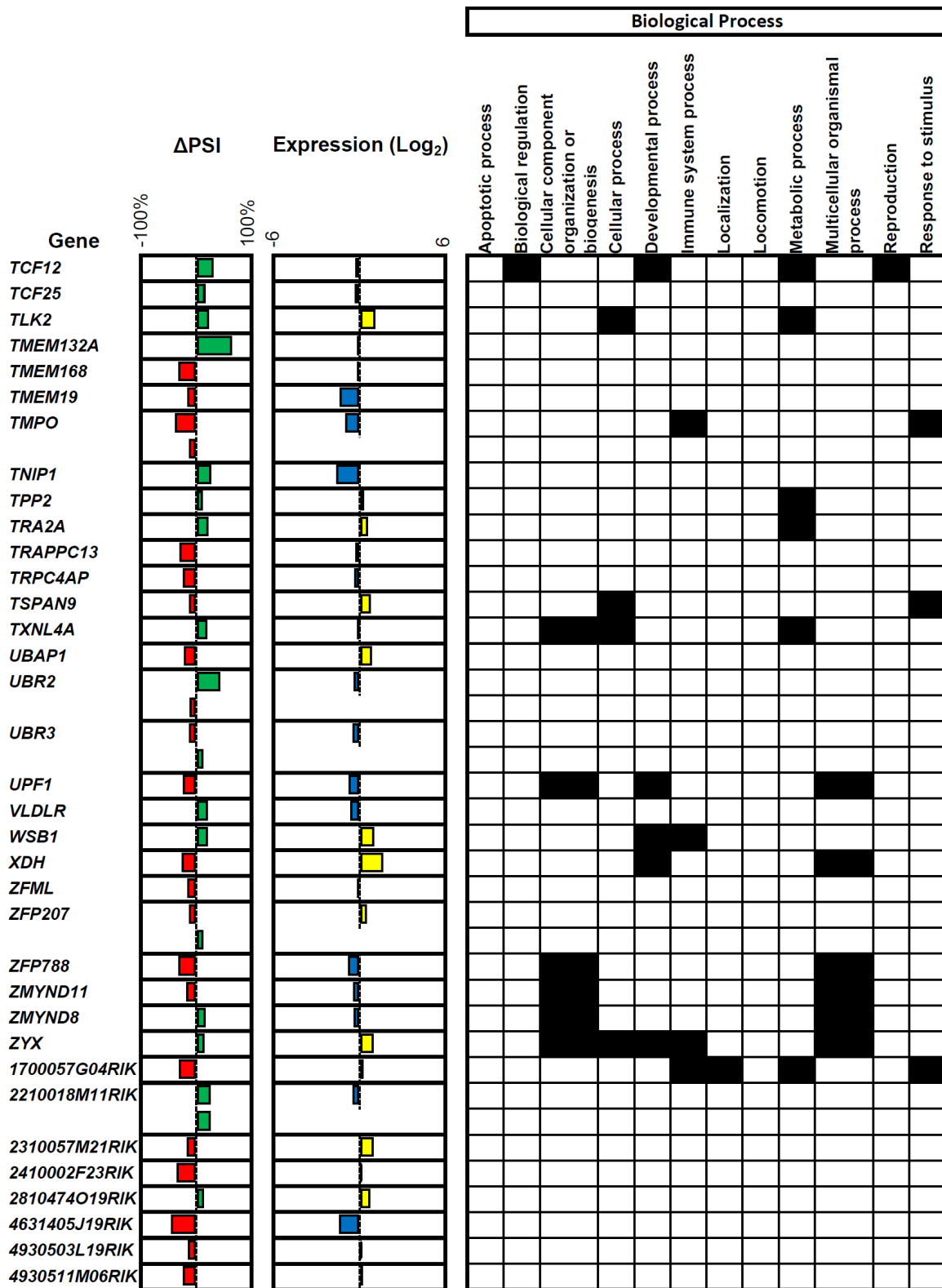


Figure H. List of the differentially ASEs associated with viral infection. The list displays the 240 differentially spliced transcripts with the corresponding Delta PSI values, the associated gene expression (in Log<sub>2</sub>), and the associated biological processes.

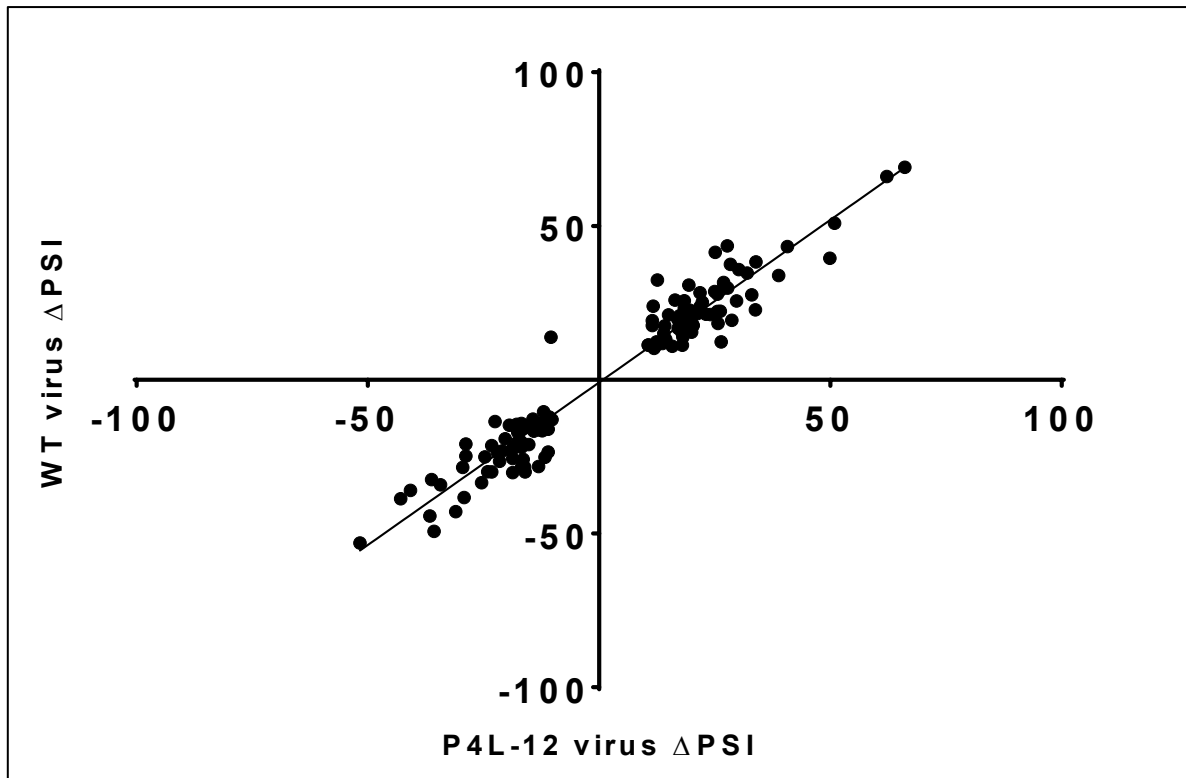


Figure I. *Common ASEs modified between WT reovirus and P4L-12 mutant show a strong correlation. Correlation between PSI values for WT and P4L-12 mutant reovirus.*

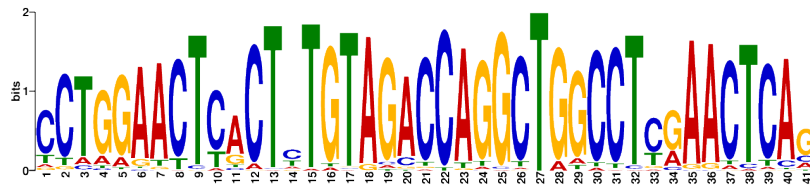


Figure J. *Analysis of the 240 differentially spliced transcripts highlights a consensus sequence. A significant enrichment of a 41 nt motif in the vicinity of many splice regions was found in transcripts for which AS was altered upon viral infection. The motif was found in 93 of the 240 transcripts that were differentially spliced upon viral infection (e value =  $1,3e-10^{49}$ ). The differentially spliced exon and its flanking introns were used to search for this motif.*

## References

1. McCormick AL, Mocarski Jr. ES. Viral modulation of the host response to infection. In: Arvin A, Campadelli-Fiume G, Mocarski E, Moore PS, Roizman B, Whitley R, et al., editors. *Human Herpesviruses: Biology, Therapy, and Immunoprophylaxis*. Cambridge: Cambridge University Press; 2007. Available from: <http://www.ncbi.nlm.nih.gov/books/NBK47417/>
2. Nagy PD, Pogany J. The dependence of viral RNA replication on co-opted host factors. *Nat Rev Microbiol*. 2012;10(2):137–49.
3. Walsh D, Mathews MB, Mohr I. Tinkering with translation: Protein synthesis in virus-infected cells. *Cold Spring Harb Perspect Biol*. 2013;5(1):a012351.
4. Hao L, Sakurai A, Watanabe T, Sorensen E, Nidom CA, Newton MA, et al. *Drosophila* RNAi screen identifies host genes important for influenza virus replication. *Nature*. 2008;454(7206):890–3.
5. Kushner DB, Lindenbach BD, Grdzlishvili VZ, Noueiry AO, Paul SM, Ahlquist P. Systematic, genome-wide identification of host genes affecting replication of a positive-strand RNA virus. *Proc Natl Acad Sci*. 2003;100(26):15764–9.
6. Black DL. Mechanisms of alternative pre-messenger RNA splicing. *Annu Rev Biochem*. 2003;72:291–336.
7. Pan Q, Shai O, Lee LJ, Frey BJ, Blencowe BJ. Deep surveying of alternative splicing complexity in the human transcriptome by high-throughput sequencing. *Nat Genet*. 2008;40(12):1413–5.
8. Wang ET, Sandberg R, Luo S, Khrebtkova I, Zhang L, Mayr C, et al. Alternative isoform regulation in human tissue transcriptomes. *Nature*. 2008;456(7221):470–6.

9. Boise LH, González-García M, Postema CE, Ding L, Lindsten T, Turka LA, et al. *bcl-x*, a *bcl-2*-related gene that functions as a dominant regulator of apoptotic cell death. *Cell*. 1993;74(4):597–608.
10. Biamonti G, Catillo M, Pignataro D, Montecucco A, Ghigna C. The alternative splicing side of cancer. *Semin Cell Dev Biol*. 2014;32:30–6.
11. Faustino NA, Cooper TA. Pre-mRNA splicing and human disease. *Genes Dev*. 2003;17(4):419–37.
12. Germann S, Gratadou L, Dutertre M, Auboeuf D, Germann S, Gratadou L, et al. Splicing Programs and Cancer, *J Nucleic Acids*. 2012:e269570.
13. Prudencio M, Belzil VV, Batra R, Ross CA, Gendron TF, Pregent LJ, et al. Distinct brain transcriptome profiles in C9orf72-associated and sporadic ALS. *Nat Neurosci*. 2015;18(8):1175–82.
14. Wang Z, Burge CB. Splicing regulation: From a parts list of regulatory elements to an integrated splicing code. *RNA*. 2008;14(5):802–13.
15. Matera AG, Wang Z. A day in the life of the spliceosome. *Nat Rev Mol Cell Biol*. 2014;15(2):108–21.
16. Klinck R, Bramard A, Inkel L, Dufresne-Martin G, Gervais-Bird J, Madden R, et al. Multiple alternative splicing markers for ovarian cancer. *Cancer Res*. 2008;68(3):657–63.
17. Oltean S, Bates DO. Hallmarks of alternative splicing in cancer. *Oncogene*. 2014;33(46):5311–8.
18. Venables JP, Klinck R, Bramard A, Inkel L, Dufresne-Martin G, Koh C, et al. Identification of alternative splicing markers for breast cancer. *Cancer Res*. 2008;68(22):9525–31.

19. Venables JP, Klinck R, Koh C, Gervais-Bird J, Bramard A, Inkel L, et al. Cancer-associated regulation of alternative splicing. *Nat Struct Mol Biol.* 2009;16(6):670–6.
20. Alló M, Buggiano V, Fededa JP, Petrillo E, Schor I, Mata M de la, et al. Control of alternative splicing through siRNA-mediated transcriptional gene silencing. *Nat Struct Mol Biol.* 2009;16(7):717–24.
21. Brosseau J-P, Lucier J-F, Lamarche A-A, Shkreta L, Gendron D, Lapointe E, et al. Redirecting splicing with bifunctional oligonucleotides. *Nucleic Acids Res.* 2014;42(6):e40–e40.
22. Akusjarvi G. Temporal regulation of adenovirus major late alternative RNA splicing. *Front Biosci J Virtual Libr.* 2008;13:5006–15.
23. Johansson C, Schwartz S. Regulation of human papillomavirus gene expression by splicing and polyadenylation. *Nat Rev Microbiol.* 2013;11(4):239–51.
24. Dowling D, Nasr-Esfahani S, Tan CH, O'Brien K, Howard JL, Jans DA, et al. HIV-1 infection induces changes in expression of cellular splicing factors that regulate alternative viral splicing and virus production in macrophages. *Retrovirology.* 2008;5:18.
25. Barnhart MD, Moon SL, Emch AW, Wilusz CJ, Wilusz J. Changes in cellular mRNA stability, splicing and polyadenylation through HuR protein sequestration by a cytoplasmic RNA virus. *Cell Rep.* 2013;5(4):909-17.
26. Álvarez E, Castelló A, Carrasco L, Izquierdo JM. Poliovirus 2A protease triggers a selective nucleo-cytoplasmic redistribution of splicing factors to regulate alternative pre-mRNA splicing. *PLoS ONE.* 2013;8(9):e73723.
27. Pimienta G, Fok V, Haslip M, Nagy M, Takyar S, Steitz JA. Proteomics and transcriptomics of BJAB cells expressing the Epstein-Barr virus noncoding RNAs EBER1 and EBER2. *PLoS ONE.* 2015;10(6):e0124638.

28. Lindberg A, Kreivi J-P. Splicing inhibition at the level of spliceosome assembly in the presence of herpes simplex virus protein ICP27. *Virology*. 2002;294(1):189–98.
29. Sciabica KS. ICP27 interacts with SRPK1 to mediate HSV splicing inhibition by altering SR protein phosphorylation. *EMBO J*. 2003;22(7):1608–19.
30. Bryant HE, Wadd SE, Lamond AI, Silverstein SJ, Clements JB. Herpes simplex virus IE63 (ICP27) protein interacts with spliceosome-associated protein 145 and inhibits splicing prior to the first catalytic step. *J Virol*. 2001;75(9):4376–85.
31. Sandri-Goldin RM, Hibbard MK, Hardwicke MA. The C-terminal repressor region of herpes simplex virus type 1 ICP27 is required for the redistribution of small nuclear ribonucleoprotein particles and splicing factor SC35; however, these alterations are not sufficient to inhibit host cell splicing. *J Virol*. 1995;69(10):6063–76.
32. Rutkowski AJ, Erhard F, L'Hernault A, Bonfert T, Schilhabel M, Crump C, et al. Widespread disruption of host transcription termination in HSV-1 infection. *Nat Commun*. 2015;6:7126.
33. Lee P, Clements D, Helson E, Gujar S. Reovirus in cancer therapy: an evidence-based review. *Oncolytic Virotherapy*. 2014;3:69-82
34. Chakrabarty R, Tran H, Selvaggi G, Hagerman A, Thompson B, Coffey M. The oncolytic virus, pelareorep, as a novel anticancer agent: a review. *Invest New Drugs*. 2015;33(3):761–74.
35. Kohl C, Kurth A. Bat reoviruses. In: Wang L-F, Cowled C, editors. *Bats and Viruses: A New Frontier of Emerging Infectious Diseases*. John Wiley & Sons, Inc.; 2015. pp. 203-205.
36. Tyler KL, Clarke P, DeBiasi RL, Kominsky D, Poggioli GJ. Reoviruses and the host cell. *Trends Microbiol*. 2001;9(11):560–4.

37. Schurch NJ, Schofield P, Gierliński M, Cole C, Sherstnev A, Singh V, et al. How many biological replicates are needed in an RNA-seq experiment and which differential expression tool should you use? *RNA*. 2016;22(6):839-51.
38. Rudd P, Lemay G. Correlation between interferon sensitivity of reovirus isolates and ability to discriminate between normal and Ras-transformed cells. *J Gen Virol*. 2005;86(5):1489–97.
39. Sandekian V, Lemay G. A single amino acid substitution in the mRNA capping enzyme  $\lambda 2$  of a mammalian orthoreovirus mutant increases interferon sensitivity. *Virology*. 2015;483:229–35.
40. Bergeron J, Mabrouk T, Garzon S, Lemay G. Characterization of the thermosensitive ts453 reovirus mutant: increased dsRNA binding of sigma 3 protein correlates with interferon resistance. *Virology*. 1998;246(2):199–210.
41. Boehme KW, Hammer K, Tollefson WC, Konopka-Anstadt JL, Kobayashi T, Dermody TS. Nonstructural protein  $\sigma 1s$  mediates reovirus-induced cell cycle arrest and apoptosis. *J Virol*. 2013;87(23):12967–79.
42. Hoyt CC, Bouchard RJ, Tyler KL. Novel nuclear herniations induced by nuclear localization of a viral protein. *J Virol*. 2004;78(12):6360–9.
43. Yue Z, Shatkin AJ. Regulated, stable expression and nuclear presence of reovirus double-stranded RNA-binding protein sigma3 in HeLa cells. *J Virol*. 1996;70(6):3497–501.
44. Zurney J, Kobayashi T, Holm GH, Dermody TS, Sherry B. Reovirus  $\mu 2$  Protein Inhibits Interferon Signaling through a Novel Mechanism Involving Nuclear Accumulation of Interferon Regulatory Factor 9. *J Virol*. 2009;83(5):2178–87.

45. Ooms LS, Jerome WG, Dermody TS, Chappell JD. Reovirus Replication Protein  $\mu$ 2 Influences Cell Tropism by Promoting Particle Assembly within Viral Inclusions. *J Virol.* 2012;86(20):10979–87.
46. Ooms LS, Kobayashi T, Dermody TS, Chappell JD. A Post-entry Step in the Mammalian Orthoreovirus Replication Cycle Is a Determinant of Cell Tropism. *J Biol Chem.* 2010;285(53):41604–13.
47. Kobayashi T, Ooms LS, Chappell JD, Dermody TS. Identification of functional domains in reovirus replication proteins  $\mu$ NS and  $\mu$ 2. *J Virol.* 2009;83(7):2892–906.
48. Grosso AR, Martins S, Carmo-Fonseca M. The emerging role of splicing factors in cancer. *EMBO Rep.* 2008;9(11):1087–93.
49. Fackenthal JD, Godley LA. Aberrant RNA splicing and its functional consequences in cancer cells. *Dis Model Mech.* 2008;1(1):37–42.
50. Warzecha CC, Shen S, Xing Y, Carstens RP. The epithelial splicing factors ESRP1 and ESRP2 positively and negatively regulate diverse types of alternative splicing events. *RNA Biol.* 2009;6(5):546.
51. Lu C-C, Chen T-H, Wu J-R, Chen H-H, Yu H-Y, Tarn W-Y. Phylogenetic and molecular characterization of the splicing factor RBM4. *PLoS ONE.* 2013;8(3):e59092.
52. Gustin KE. Effects of poliovirus infection on nucleo-cytoplasmic trafficking and nuclear pore complex composition. *EMBO J.* 2001;20(1):240–9.
53. Gustin KE, Sarnow P. Inhibition of nuclear import and alteration of nuclear pore complex composition by rhinovirus. *J Virol.* 2002;76(17):8787–96.
54. Muranyi W, Haas J, Wagner M, Krohne G, Koszinowski UH. Cytomegalovirus recruitment of cellular kinases to dissolve the nuclear lamina. *Science.* 2002;297(5582):854–7.



55. Scott ES, O'Hare P. Fate of the inner nuclear membrane protein lamin B receptor and nuclear lamins in herpes simplex virus type 1 infection. *J Virol.* 2001;75(18):8818–30.
56. Enninga J, Levy DE, Blobel G, Fontoura BMA. Role of nucleoporin induction in releasing an mRNA nuclear export block. *Science.* 2002;295(5559):1523–5.
57. Fortes P, Beloso A, Ortín J. Influenza virus NS1 protein inhibits pre-mRNA splicing and blocks mRNA nucleocytoplasmic transport. *EMBO J.* 1994;13(3):704–12.
58. Petersen JM, Her L-S, Varvel V, Lund E, Dahlberg JE. The matrix protein of vesicular stomatitis virus inhibits nucleocytoplasmic transport when it is in the nucleus and associated with nuclear pore complexes. *Mol Cell Biol.* 2000;20(22):8590–601.
59. Petersen JM, Her L-S, Dahlberg JE. Multiple vesiculoviral matrix proteins inhibit both nuclear export and import. *Proc Natl Acad Sci.* 2001;98(15):8590–5.
60. Noronha CMC de, Sherman MP, Lin HW, Cavrois MV, Moir RD, Goldman RD, et al. Dynamic disruptions in nuclear envelope architecture and integrity induced by HIV-1 Vpr. *Science.* 2001;294(5544):1105–8.
61. Reissig M, Howes DW, Melnick JL. Sequence of morphological changes in epithelial cell cultures infected with poliovirus. *J Exp Med.* 1956;104(3):289–304.
62. Anczuków O, Rosenberg AZ, Akerman M, Das S, Zhan L, Karni R, et al. The splicing factor SRSF1 regulates apoptosis and proliferation to promote mammary epithelial cell transformation. *Nat Struct Mol Biol.* 2012;19(2):220–8.
63. Karni R, Stanchina E de, Lowe SW, Sinha R, Mu D, Krainer AR. The gene encoding the splicing factor SF2/ASF is a proto-oncogene. *Nat Struct Mol Biol.* 2007;14(3):185–93.

64. Lefave CV, Squatrito M, Vorlova S, Rocco GL, Brennan CW, Holland EC, et al. Splicing factor hnRNPH drives an oncogenic splicing switch in gliomas. *EMBO J*. 2011;30(19):4084–97.
65. Wang Y, Chen D, Qian H, Tsai YS, Shao S, Liu Q, et al. The splicing factor RBM4 controls apoptosis, proliferation, and migration to suppress tumor progression. *Cancer Cell*. 2014;26(3):374–89.
66. Okoro DR, Rosso M, Bargonetti J. Splicing Up Mdm2 for Cancer Proteome Diversity. *Genes Cancer*. 2012;3:311–9.
67. Pan D, Pan L-Z, Hill R, Marcato P, Shmulevitz M, Vassilev LT, et al. Stabilisation of p53 enhances reovirus-induced apoptosis and virus spread through p53-dependent NF- $\kappa$ B activation. *Br J Cancer*. 2011;105(7):1012–22.
68. Gong J, Mita MM. Activated Ras signaling pathways and reovirus oncolysis: an update on the mechanism of preferential reovirus replication in cancer cells. *Mol Cell Oncol*. 2014;4:167.
69. Yang D. RNA Viruses: Host Gene Responses to Infections. World Scientific; 2009. 722 p.
70. Bauman JA, Kole R. Modulation of RNA splicing as a potential treatment for cancer. *Bioeng Bugs*. 2011;2(3):125–8.
71. Danis C, Lemay G. Protein synthesis in different cell lines infected with orthoreovirus serotype 3: inhibition of host-cell protein synthesis correlates with accelerated viral multiplication and cell killing. *Biochem. Cell Biol*. 1993;71(1–2):81–5.
72. Langmead B, Salzberg SL. Fast gapped-read alignment with Bowtie 2. *Nat Methods*. 2012;9(4):357–9.

73. Li B, Dewey CN. RSEM: accurate transcript quantification from RNA-Seq data with or without a reference genome. *BMC Bioinformatics*. 2011;12(1):323.
74. Storey JD, Tibshirani R. Statistical significance for genomewide studies. *Proc Natl Acad Sci*. 2003;100(16):9440–5.
75. Edgar R, Domrachev M, Lash AE. Gene Expression Omnibus: NCBI gene expression and hybridization array data repository. *Nucleic Acids Res*. 2002;30(1):207–10.
76. Jiao X, Sherman BT, Huang DW, Stephens R, Baseler MW, Lane HC, et al. DAVID-WS: a stateful web service to facilitate gene/protein list analysis. *Bioinformatics*. 2012;28(13):1805–6.
77. Szklarczyk D, Franceschini A, Wyder S, Forslund K, Heller D, Huerta-Cepas J, et al. STRING v10: protein–protein interaction networks, integrated over the tree of life. *Nucleic Acids Res*. 2015;43(D1):D447–52.
78. Bailey TL, Boden M, Buske FA, Frith M, Grant CE, Clementi L, et al. MEME Suite: tools for motif discovery and searching. *Nucleic Acids Res*. 2009;37(suppl 2):W202–8.
79. Artimo P, Jonnalagedda M, Arnold K, Baratin D, Csardi G, Castro E de, et al. ExPASy: SIB bioinformatics resource portal. *Nucleic Acids Res*. 2012;40(W1):W597–603.
80. Corpet F. Multiple sequence alignment with hierarchical clustering. *Nucleic Acids Res*. 1988;16(22):10881–90.
81. Finn RD, Bateman A, Clements J, Coggill P, Eberhardt RY, Eddy SR, et al. Pfam: the protein families database. *Nucleic Acids Res*. 2014;42(D1):D222–30.

82. Mitchell A, Chang H-Y, Daugherty L, Fraser M, Hunter S, Lopez R, et al. The InterPro protein families database: the classification resource after 15 years. *Nucleic Acids Res.* 2015;43(D1):D213–21.
83. Kosugi S, Hasebe M, Tomita M, Yanagawa H. Systematic identification of cell cycle-dependent yeast nucleocytoplasmic shuttling proteins by prediction of composite motifs. *Proc Natl Acad Sci U S A.* 2009;106(25):10171–6.
84. Drissi R, Dubois M-L, Douziech M, Boisvert F-M. Quantitative proteomics reveals dynamic interactions of the minichromosome maintenance complex (MCM) in the cellular response to etoposide induced DNA damage. *Mol Cell Proteomics.* 2015;14(7):2002–13.
85. Zhu Y, Hultin-Rosenberg L, Forshed J, Branca RMM, Orre LM, Lehtiö J. SpliceVista, a tool for splice variant identification and visualization in shotgun proteomics data. *Mol Cell Proteomics.* 2014;13(6):1552–62.

### **Perspectives**

Ces travaux ont permis, pour la première fois, de démontrer des changements de l'épissage alternatif cellulaire lors de l'infection avec réovirus. Cependant, les mécanismes moléculaires sous-jacents qui expliquent cette modulation nous étaient encore inconnus. C'est pourquoi nous avons alors voulu nous intéresser à comment ces changements d'épissage sont déclenchés lors de l'infection virale, les protéines virales qui sont impliquées dans ces changements et leur mécanisme d'action. Les résultats de ces travaux seront approfondis dans le prochain chapitre.

## ARTICLE 2

### **Reovirus $\mu$ 2 protein modulates host cell alternative splicing by reducing protein levels of U5 snRNP core components**

**Auteurs de l'article:** Boudreault S, Durand M; Martineau, CA; Perreault JP, Lemay G, Bisailon M.

**Statut de l'article:** Article publié dans Nucleic Acids Research en avril 2022, 50, 5263–5281.

**Avant-propos:** J'ai participé à la conception du projet et j'ai effectué la majorité des expériences ainsi que l'analyse des résultats (>90%). J'ai généré les figures et j'ai écrit le manuscrit sous la supervision des Pr Bisailon et Lemay. J'ai aussi participé à la réponse aux évaluateurs en écrivant la lettre de réponse.

**Résumé :** L'orthoréovirus de mammifère (réovirus) est un virus à ARN bicaténaire segmenté de la famille des *Reoviridae* présentant une activité oncolytique prometteuse. Des études récentes ont souligné la capacité de réovirus à induire des changements d'épissage alternatif cellulaire pendant l'infection, avec une compréhension limitée des mécanismes en jeu. Dans cette étude, nous avons investigué comment réovirus module l'épissage alternatif cellulaire. En utilisant une combinaison de biologie cellulaire et d'expériences de génétique inverse, nous avons démontré que le segment viral *M1*, produisant la protéine  $\mu$ 2, est le déterminant principal de la capacité de réovirus à moduler l'épissage alternatif, et que l'acide aminé à la position 208 dans  $\mu$ 2 est critique pour induire ces changements. De plus, nous avons démontré que l'expression de  $\mu$ 2 par elle-même est suffisante pour déclencher ces changements d'épissage, et que son habilité à se localiser au noyau n'est pas requise pour tous ces changements. Par la suite, nous avons identifié les

composantes principales du complexe U5 (EFTUD2, PRPF8 et SNRNP200) comme des interacteurs de  $\mu 2$  qui sont requises pour la modulation de l'épissage alternatif par réovirus. Finalement, ces composantes principales du complexe U5 sont réduites au niveau protéique autant par l'infection avec réovirus que par l'expression de  $\mu 2$ . Ces découvertes identifient la réduction des composantes principales du complexe U5 comme un nouveau mécanisme par lequel les virus peuvent altérer l'épissage alternatif cellulaire.

## **Reovirus $\mu$ 2 protein modulates host cell alternative splicing by reducing protein levels of U5 snRNP core components**

Simon Boudreault<sup>1</sup>, Mathieu Durand<sup>2</sup>, Carole-Anne Martineau<sup>1</sup>, Jean-Pierre Perreault<sup>1</sup>, Guy Lemay<sup>3</sup>, Martin Bisailon<sup>1,\*</sup>

<sup>1</sup> Département de biochimie et de génomique fonctionnelle, Faculté de médecine et des sciences de la santé, Université de Sherbrooke, Sherbrooke, Québec, J1E 4K8, Canada

<sup>2</sup> Plateforme de RNomique, Université de Sherbrooke, Sherbrooke, Québec, J1E 4K8, Canada

<sup>3</sup> Département de microbiologie, infectiologie et immunologie, Faculté de médecine, Université de Montréal, Montréal, Québec, H3C 3J7, Canada

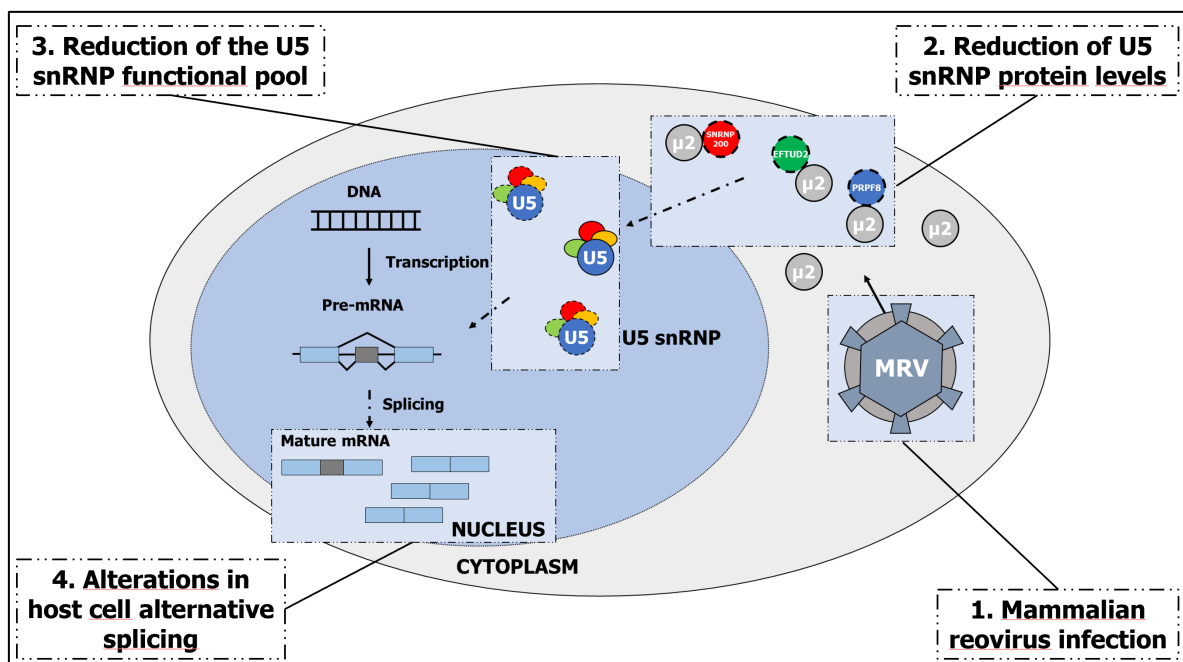
\*To whom correspondence should be addressed. Tel: +1-819-821-8000 (Ext 75904); Email:

Martin.Bisailon@USherbrooke.ca

## ABSTRACT

Mammalian orthoreovirus (MRV) is a double-stranded RNA virus from the *Reoviridae* family presenting a promising activity as an oncolytic virus. Recent studies have underlined MRV's ability to alter cellular alternative splicing (AS) during infection, with a limited understanding of the mechanisms at play. In this study, we investigated how MRV modulates AS. Using a combination of cell biology and reverse genetics experiments, we demonstrated that the *M1* gene segment, encoding the  $\mu 2$  protein, is the primary determinant of MRV's ability to alter AS, and that the amino acid at position 208 in  $\mu 2$  is critical to induce these changes. Moreover, we showed that the expression of  $\mu 2$  by itself is sufficient to trigger AS changes, and its ability to enter the nucleus is not required for all these changes. Moreover, we identified core components of the U5 snRNP (i.e., EFTUD2, PRPF8, and SNRNP200) as interactors of  $\mu 2$  that are required for MRV modulation of AS. Finally, these U5 snRNP components are reduced at the protein level by both MRV infection and  $\mu 2$  expression. Our findings identify the reduction of U5 snRNP components levels as a new mechanism by which viruses alter cellular AS.

## GRAPHICAL ABSTRACT





## INTRODUCTION

Mammalian orthoreovirus (MRV) is a double-stranded (dsRNA) virus from the *Reoviridae* family which has been instrumental to our understanding of the basis of virus replication, such as internalization, uncoating, transcription, and translation (1-3). MRV genome is composed of ten dsRNA segments that produce 8 structural proteins ( $\lambda 1$ ,  $\lambda 2$ ,  $\lambda 3$ ,  $\mu 1$ ,  $\mu 2$ ,  $\sigma 1$ ,  $\sigma 2$ ,  $\sigma 3$ ) that form both the outer and the inner capsid (or core), and 4 non-structural proteins ( $\mu$ NS,  $\mu$ NSC,  $\sigma$ NS, and  $\sigma 1s$ ) involved in replication (4). MRV replication happens in cytoplasmic inclusions named viral factories (VF), which are structures acting as organizing centers to coordinate translation of viral mRNA, genome replication, gene segment assortment, genome packaging, and assembly of newly produced viral particles (5,6). VF are formed primarily by the non-structural protein  $\mu$ NS, but  $\mu 2$  and  $\sigma$ NS are also necessary for their genesis and maturation (7,8). In VF,  $\mu 2$  binds to both  $\mu$ NS and cellular microtubules, and thus anchors VF to cellular microtubules (7-9). The  $\mu 2$  protein is a 83 kDa structural protein encoded by the M1 segment, and a minor component of the core (10). The  $\mu 2$  protein possesses both ssRNA- and dsRNA-binding activities (11); nucleoside triphosphatase (NTPase) and RNA 5'-triphosphatase (RTPase) enzymatic activities *in vitro* (12), and can also form homodimers (13). Interest in MRV has exploded since the discovery of its natural ability to preferentially replicate in and destroy cancer cells, making it one of the few naturally oncolytic viruses (14). Despite initial promises, clinical trials have not been as successful as hoped, suggesting that improvement to WT MRV might enhance its oncolytic potential (15). Notably, polymorphisms in  $\mu 2$  have been linked to the MRV's oncolytic potential (16).

The interferon (IFN) pathway is the main cellular response to fight viral infection and alert the immune system (17). Viral determinants, such as dsRNA, are recognized by pattern-recognition receptors (e.g. RIG-I), triggering a signaling cascade leading to the production of IFN, key components of the innate immune response to fight viral infection. Once secreted, IFN can act on uninfected cells in a paracrine fashion to shield them from infection, or on the infected cell in an autocrine

manner to help them fight the virus. The binding of IFN to its receptor induces the expression of a myriad of interferon-stimulated genes (ISG), which produces the effectors of the cellular antiviral response (17,18). This pathway is notably dysregulated in cancer cells (19,20), and is involved in the ability of certain viruses to infect and kill them preferentially (21-23).

Upon transcription of the RNA in the nucleus, eukaryotic cells need to process pre-mature RNA through numerous steps before exporting them into the cytoplasm for translation. Amongst those maturation processes, constitutive splicing allows the removal of non-coding introns, and ligation of the coding exons in the mature mRNA. The spliceosome is a large ribonucleoprotein (RNP) complex assembled from five small nuclear ribonucleoproteins complexes (snRNP; U1, U2, U4, U5, and U6) responsible for recognizing key sequences in introns (i.e., branch point and polypyrimidine tract) and exons (5' splice site and 3' splice site) to catalyze the removal of introns. These snRNP are recruited to the intron in a sequential fashion, culminating in the reorganization of the precatalytic spliceosome and formation of an activated B complex committed to excising the intron (reviewed in (Boudreault, Roy, *et al.*, 2019b)). Remarkably, the U5 snRNP plays a critical role in the reorganization and in the subsequent steps allowing the removal of the intron (25-27). On the other hand, alternative splicing (AS) results in the formation of a mixed populations of mature mRNAs (28-31). AS arises from stimulatory and inhibitory signals coming from multiple splicing factors bound to pre-mature RNA near weak splice sites, either helping or destabilizing spliceosome assembly at this location. This allows for the removal of exon or part of exons, and introns to be retained in the mRNA, altering the coding potential of the RNA. AS is a pivotal RNA processing step to allow increased protein diversity since mRNA arising from the same gene can encode different isoforms of the same protein. These isoforms can be differentially regulated through the inclusion of specific domains, and thus help the cell fine-tune the levels and activity of its proteins (32-34). Notably, numerous proteins involved

in the innate immune response, such as IRF7, are regulated through their AS (34-36).

Many viruses usurp the cellular splicing machinery to splice their own genes and increase protein diversity (37). However, the impact of viruses on the AS landscape of their host cells has been overlooked until recently. This field has been rapidly expanding in the last ten years, with mounting evidence showing that viral infection indeed impacts the AS of the infected cell (38-41); reviewed in (24, 42, 43). Previously, we and others have demonstrated that MRV infection induces drastic changes in cellular AS (44,45). For example, infection of murine L929 fibroblasts with MRV leads to a dysregulation in 240 alternative splicing events (ASE) at 16 h post-infection (PI) (44). This modulation of cellular AS is an entirely novel actor in MRV-host interaction, and these changes in AS have the potential to reshape the proteome of infected cells. Moreover, cancer cells present dysregulated AS compared to normal cells, and it is thus tempting to speculate that MRV modulation of AS could be involved in the specificity of the virus towards cancer cells or its ability to destroy them preferentially.

In the present study, we investigated the mechanism used by MRV to induce changes in cellular AS during infection. Using a combination of cell biology, reverse genetics experiments, AS minigene reporter assays, and IP-MS, we demonstrated that the MRV  $\mu 2$  protein is the main determinant of MRV modulation of AS, and interacts with core components of the U5 snRNP. These U5 components are required for MRV modulation of AS and are reduced at the protein level during MRV infection. Our findings identify this reduction of U5 snRNP components as a new mechanism by which viruses alter cellular AS during infection.

## **MATERIAL AND METHODS**

### **Cells and Viruses**

Murine L929 fibroblasts were originally obtained from the American Type Culture Collection (ATCC). The baby hamster kidney (BHK) cell line stably expressing the T7 RNA polymerase (BSR-T7 cells) has been described (46) and was a generous gift from the laboratory of Dr. John Hiscott (Lady Davis Research Institute, Montréal, Canada). The Vero cell line was obtained from the laboratory of Dr. Lee-Hwa Tai (Université de Sherbrooke, Sherbrooke, Canada). The COS-7 cell line was acquired from the laboratory of Dr. Xavier Roucou (Université de Sherbrooke, Sherbrooke, Canada). The 293T cell line was a generous gift from the laboratory of Dr. Nathalie Rivard (Université de Sherbrooke, Sherbrooke, Canada). L929, Vero and BHK-T7 cells were routinely grown in Eagle's minimal essential medium (EMEM, Wisent) containing 5% fetal bovine serum (Wisent) and supplemented in 1% glutamine; 293T and COS-7 cells were routinely grown in Dulbecco's modified Eagle's medium (DMEM, Wisent) containing 10% fetal bovine serum (Wisent). MRV serotype 3 strain Dearing (T3/Human/Ohio/Dearing/55) was also originally obtained from ATCC and was propagated and titrated by TCID<sub>50</sub> on L929 fibroblasts, as routinely used in the laboratory (47). The WT laboratory stock of MRV type 3 (T3D<sup>S</sup>) was previously described (48,49), and rescued by reverse genetics following the introduction of the appropriate mutations in the plasmids encoding the WT virus from the original reverse genetics system, T3D<sup>K</sup> (50). T3D<sup>K</sup> was rescued using the original reverse genetics system. Other viruses, harboring various combinations of genes from T3D<sup>K</sup> or T3D<sup>S</sup> in either background, were obtained by reverse genetics, as described below.

### **Viral Infection**

L929 cells were plated at a density of  $7 \times 10^4$  cells per square centimeter the day before infection at a multiplicity of infection (MOI) of 50 TCID<sub>50</sub> units per cell using standard procedures (47). Control L929 cells were seeded at the same density and

mock infected. For AS-PCR experiments described below, cells were collected 16 h post-infection, at which time visible cytopathic effect was still minimal, with the exception of the time course experiment where RNA was harvested at indicated times.

### **Bystander Experiment**

L929 cells were plated on 0.4  $\mu\text{m}$  pore-diameter Transwell™ (top) and in a 6-well plate (bystander; bottom) the day before the experiment. The next day, cells on the Transwell™ filters were either infected or mock infected using the procedure described above. After adsorption, medium was added, and cells were incubated 1 h at 37°C to allow internalization of the viral particles. In parallel, the medium in the 6-well plate was replaced by the same medium containing 1% rabbit neutralizing antireovirus antiserum (a generous gift from Dr. Earl G. Brown, University of Ottawa). After 1 h of internalization, the medium on the Transwell™ was replaced by fresh medium, and then the Transwell™ was laid atop of the second layer of cells for 15 h.

### **siRNA transfection**

L929 cells were plated in a 12-well plate at 75,000 cells/well and transfected on the following morning using 50 pmol of siRNA and 3.75  $\mu\text{L}$  of RNAiMAX (ThermoFisher) as per the manufacturer's protocol. Ambion Silencer® Select (catalog number 4390771) siRNA were used against RIG-I (#1; ID: s106374 and #2; ID: s106375); EFTUD2 (ID: s74089); PRPF8 (ID: s101224); and SNRNP200 (ID: s115821). Cells were incubated for 56 h before being infected or mock-infected as previously described and further incubated for 16 h before harvesting RNA or proteins.

### **Production of reassortant MRV by reverse genetics**

The plasmids corresponding to the ten genes of MRV serotype 3 Dearing, T3D<sup>K</sup>, under the transcriptional control of the T7 promoter were originally obtained from the laboratory of Dr. Terence Dermody (UPMC Children's Hospital of Pittsburgh,

Pittsburgh, Pennsylvania) (50). To generate point mutations in the *M1* gene segment, standard QuikChange site-directed mutagenesis was performed. All constructions were validated using Sanger sequencing. Sequences of all primers used in mutagenesis are available upon request. Plasmids were then used to recover infectious virus by the improved reverse genetics approach using transfection in BHK cells expressing the T7 RNA polymerase with some modifications (51-53). Briefly, the ten plasmids (100 ng of each) were simultaneously introduced alongside plasmids encoding the cytoplasmic Vaccinia Virus capping proteins D1R and D12L into semi-confluent 35 mm-diameter petri dish of BHK21-T7 cells using Fugene 6 (Roche). pCAG-D1R and pCAG-D12L were a gift from Takeshi Kobayashi (Addgene plasmid #89160; <http://n2t.net/addgene:89160>; RRID:Addgene\_89160 and Addgene plasmid #89161; <http://n2t.net/addgene:89161>; RRID:Addgene\_89161, respectively). Upon confluency (3-4 days), the medium was recovered, cells trypsinized and plated in a P100 dish with the medium recovered previously and completed with complete medium containing 5% heat-inactivated fetal bovine serum. Upon confluency (3-4 days), cells and their medium were subjected to three freeze-thaw cycles (-80°C/37°C) and used as starting virus stocks. Reassortant viruses were first propagated in Vero cells in the presence of chymotrypsin, as previously described (52). Upon sufficient cell lysis (2-3 days), cells and their medium were again subjected to three freeze-thaw cycles (-80°C/37°C) and used to further propagate the viruses in L929 cells.

### **Molecular cloning**

The genomic sequence encoding the  $\mu 2$  protein (T3D<sup>s</sup> strain) was amplified from the reverse genetics plasmid and cloned using HindIII and XhoI into the pEGFPN1 and pEGFPC1 plasmid. For pEGFPN1, the stop codon was removed to ensure the GFP was translated together with  $\mu 2$ ; for pEGFPC1, two nucleotides (CG) were added before  $\mu 2$  start codon to conserve the open reading frame with GFP. The P208S mutant was realized from these plasmids using the same QuikChange primers as described for the reverse genetics' mutants. Mutants unable to accumulate in the

nucleus were generated using KLD mutagenesis (New England Biolabs). To clone AS minigenes, L929 genomic DNA was harvested using DNeasy Blood & Tissue kit (Qiagen). The amplicons were amplified by PCR and cloned using KpnI and NotI (*ALKBH1*, *SERBP1*) or by Gibson assembly (NEB) for the remaining by opening the plasmid with the same enzymes. All constructions were validated using Sanger sequencing; sequences are available upon demand.

### **RNA extraction**

Total RNA samples were extracted with Qiazol® as recommended by the manufacturer (Qiagen).

### **Reverse transcription**

Reverse transcription was performed on 2.2 µg total RNA with Transcriptor reverse transcriptase, random hexamers, dNTPs (Roche Diagnostics), and 10 units of RNase OUT (Invitrogen) following the manufacturer's protocol in a total volume of 20 µL.

### **qPCR**

All forward and reverse primers were individually resuspended to 20–100 µM stock solution in Tris-EDTA buffer (IDT) and diluted as a primer pair to 1 µM in RNase DNase-free water (IDT). The complete list of primers used in this study is available in Supplementary Table S1. Quantitative PCR (qPCR) reactions were performed in 10 µL in 96 well plates on a CFX-96 thermocycler (BioRad) with 5 µL of 2X iTaq Universal SYBR Green Supermix (BioRad), 10 ng (3 µl) cDNA, and 200 nM final (2 µL) primer pair solutions. The following cycling conditions were used: 3 min at 95°C; 50 cycles: 15 sec at 95°C, 30 sec at 60°C, 30 sec at 72°C. Relative expression levels were calculated using the qBASE framework using PSMC4, PUM1, and TXNL4B as housekeeping genes. For all PCR run, control reactions performed in the absence of template were performed for each primer pair, and these were consistently negative. All qPCR data were generated following the MIQE guidelines (54).

### **Alternative splicing PCR (AS-PCR)**

PCR primer sequences were designed at the Université de Sherbrooke Rnomics Platform using a custom software designed to optimize standard primer design criterias, and to certify target specificity using embedded NCBI Blast software (<https://blast.ncbi.nlm.nih.gov/>). The primers were placed on exons flanking the alternative region to amplify both isoforms in the same PCR reaction. All forward and reverse primers were individually resuspended to 20–100  $\mu\text{M}$  stock solution in Tris-EDTA buffer (IDT) and diluted as a primer pair to 1.2  $\mu\text{M}$  in RNase DNase-free water (IDT). End-point PCR reactions were done on 10 ng cDNA in 10  $\mu\text{L}$  final volume containing 0.2 mmol/L each dNTP, 1.5 mmol/L  $\text{MgCl}_2$ , 0.6  $\mu\text{mol/L}$  each primer, and 0.2 units of Platinum Taq DNA polymerase (Invitrogen). An initial incubation of 2 min at 95°C was followed by 35 cycles at 94°C 30 sec, 55°C 30 sec, and 72°C 60 sec. The amplification was completed by a 2 min incubation at 72°C. PCR reactions were carried on thermocyclers GeneAmp PCR System 9700 (ABI), and the amplified products were analyzed by automated chip-based microcapillary electrophoresis on LabChip GX Touch HT Nucleic Acid Analyzer (PerkinElmer). Amplicon sizing and relative quantitation were performed by the manufacturer's software, before being uploaded to the LIMS database. The percent spliced-in (PSI) metric was used to quantitate the level of inclusion in these alternative splicing events. It represents the percent of the long form over total abundance for both the long and short forms. The formula is as follows:

$$PSI = \frac{\textit{Long form}}{\textit{Long form} + \textit{Short form}}$$

For the minigene reporters, the reverse primer was substituted for the BGH primer from the pcDNA3.1+ plasmid alongside the usual forward primer, only allowing the monitoring of the RNA derived from the plasmid and not from the endogenous gene. The only exception was *SERBP1* for which the forward primer was substituted for another primer in the 2<sup>nd</sup> exon to generate shorter amplicons to correctly separate the two forms in capillary electrophoresis.



### **Plasmid transfection**

293T cells were plated in a 12-well plate at 400,000 cells/well (24 h) or 300,000 cells/well (48 h) and transfected on the following morning using Lipofectamine2000 (ThermoFisher) and 1.5 µg of plasmid DNA. Only 75 ng (20x less) of the control empty plasmid encoding only GFP (pEGFPN1) was transfected to normalize the expression of the GFP alone to GFP-µ2 proteins; empty pcDNA3.1+ was used to fill the remaining 1.5 µg of plasmid DNA. AS minigenes were co-transfected altogether with the plasmid of interest at 10 ng per AS minigene.

### **Western blot**

The linearity of all antibodies used in this study was first experimentally determined to allow for an adequate quantification in the linear range of both samples analyzed and the antibody used. Cells were rinsed with PBS and lysed in RIPA Buffer (1% Triton X-100, 1% sodium deoxycholate, 0.1% SDS, 1 mM EDTA, 50 mM Tris-HCl pH 7.5 and complete protease inhibitor (ROCHE)) on ice. Upon transfer in a microtube, DNA was fragmented using ultrasound on ice at 13% amplitude for 5 sec, two to four times. Debris were then pelleted at 13,000 RPM, 4°C, 10 min. Lysates were dosed for total protein in triplicate using standard Bradford assay (Thermo Scientific Coomassie Protein Assay). The appropriate quantity of protein was diluted with water and Laemmli 4x buffer. Samples were heated 5 min at 95°C. Samples were loaded on 10% or 6% SDS-polyacrylamide gels and electrophoresis was carried out at 150 volts. The Bluelif protein ladder was used as a molecular weight marker (FroggaBio). Gels were transferred onto a polyvinylidene difluoride (PVDF) membrane at 4°C, 75 min, 100 volts. Membranes were blocked in 5% non-fat milk in TBS-T (10 mM Tris-HCl pH 8.0, 220 mM NaCl, 0.1% Tween 20), 1 h at room temperature. Membranes were incubated overnight with the appropriate antibody in 2.5% milk/PBS. The commercial antibodies used in this study are the following: Actin (Sigma, A5441, 1:10,000), CAMK2D (Abcam, ab181052, 1:2,000), CAMK2G (Abcam, ab201966, 1:500), EFTUD2 (Abcam, ab188327, 1:2,000), GAPDH (Sigma, G9545, 1:12,000), GFP (Santa Cruz Biotechnology, sc-9996, 1:8,000), RIG-I (Cell Signaling

Technology, #3743, 1:1,000), PRPF6 (Abcam, ab99292, 1:2,000), PRPF8 (Abcam, ab79237, 1:1,000), SNRNP200 (Abcam, ab241589, 1:1,000), U2AF35 (Abcam, ab172614, 1:2,000), Vinculin (Santa Cruz Biotechnology, sc-73614, 1:1,000). The anti- $\mu$ 2 T1L is a rabbit antiserum (55) and was diluted 1:1,000; the  $\sigma$ 3 antibody is the supernatant from a mouse hybridoma cells expressing the monoclonal antibody 4F2 (56) and was diluted 1:100. Membranes were washed 3x in TBS-T and incubated with a horse anti mouse-HRP secondary antibody 1:5,000 (Cell Signaling Technologies, 7076) or goat anti rabbit-HRP secondary antibody 1:10,000 (Abcam, ab205718) during 1 h at room temperature. Membranes were washed again 3 times with TBS-T and once with PBS. Bound antibodies were revealed using Clarity ECL western blotting substrates (BIO RAD) except for the lowly expressed CAMK2G that required the Clarity Max ECL western blotting substrates (BIO RAD) and scanned on an ImageQuant LAS4000 (GE Healthcare Life Science). For quantification, HRP was inactivated using 30% H<sub>2</sub>O<sub>2</sub> for 30 min, followed by 2x PBS washing, and membranes were blocked again and probed for the relevant loading control. All western blots were performed three times, and a representative result is presented in the article. All uncropped western blots are available in the Supplementary Figure S32.

### **Immunoprecipitation (IP)**

293T cells were seeded at  $6 \times 10^6$  cells/100 mm dish and transfected on the following morning with 10  $\mu$ g of plasmid DNA and Lipofectamine2000 (ThermoFisher) as per the manufacturer's protocol. After 24 h incubation, cells were washed with PBS and 1 mL lysis buffer (1% Triton X-100; 150 mM NaCl; 20 mM Tris-HCl, pH 7.5; 0.1 mg/ml PMSF) and incubated 5 min on ice. Petri dishes were scraped, and protein lysis was completed by a couple up and down. Lysates were sonicated on ice at 25% amplitude, 5 sec for four times. Debris were then pelleted at 13,000 RPM, 4°C for 10 min. Lysates were dosed for total protein in triplicate using standard Bradford assay (Thermo Scientific Coomassie Protein Assay). One milligram of lysate was DNase and RNase treated using 5  $\mu$ g of DNase I (Sigma) and 5  $\mu$ g of RNase A (Bio Basic), 10 min at room temperature. GFP-trap beads (Chromotek) were washed

twice in lysis buffer; 20  $\mu$ L were added per IP and IP reactions were completed at 1 mL with lysis buffer. IP was performed for 4 h at 4°C on a tube rotator. Tubes were then spun at 2,000 RPM, the supernatant was removed, and beads were washed three times with lysis buffer and twice with PBS. Immunoprecipitates were subjected to mass spectrometry preparation, or resuspended in 1x Laemmli buffer, boiled, and submitted to western blotting.

### **LC-MS/MS preparation and analysis**

All solutions for this section were prepared in MS-grade water. Beads were washed five times with 20 mM ammonium bicarbonate in LoBind eppendorfs. Proteins were then reduced with 10 mM DTT in 20 mM ammonium bicarbonate for 30 min with shaking at 1,250 RPM, 60°C. Proteins were then alkylated by adding an equal volume of 15 mM chloroacetamide in 20 mM ammonium bicarbonate in the dark with shaking at 1,250 RPM for 1 h. Proteins were digested with 1  $\mu$ g of trypsin at 37°C overnight with shaking at 1,250 RPM. Trypsin digestion was stopped by acidifying to a final concentration of 1% formic acid (FA) and supernatant was harvested upon centrifugation at 2,000 g for 3 min. Beads were washed again in 100  $\mu$ L of a 60% acetonitrile/1% formic acid solution for 5 min with shaking at 1,250 RPM at room temperature and centrifuged at 2,000 g for 3 min. This second supernatant was pooled with the first and dried in a speed vac. The peptides were resuspended in 30  $\mu$ L of 0.1% trifluoroacetic acid (TFA) to desalt on ZipTip. Desalted peptides were dried again with a speed vac and resuspended in 30  $\mu$ L of 1% formic acid. Peptides were quantified using a nanodrop at 205 nm and 250 ng of each sample were injected into a nanoElute HPLC (Bruker Daltonics); loaded onto a trap column with a constant flow of 4  $\mu$ L/min (Acclaim PepMap100 C18 column, 0.3 mm id x 5 mm, Dionex Corporation); and eluted onto an analytical C18 Column (1.9  $\mu$ m beads size, 75  $\mu$ m x 25 cm, PepSep). A 2 h gradient of acetonitrile (5-37%) in 0.1% FA at 500 nL/min was used to elute peptides and inject them into a TimsTOF Pro ion mobility mass spectrometer equipped with a CaptiveSpray nano electrospray source (Bruker Daltonics). Data was acquired using data-dependent auto-MS/MS with a 100-1,700

m/z mass range, with PASEF enabled with a number of PASEF scans set at 10 (1.27 sec duty cycle) and a dynamic exclusion of 0.4 min, m/z dependent isolation window and collision energy of 42.0 eV. The target intensity was set to 20,000, with an intensity threshold of 2,500.

### **Protein Identification by MaxQuant**

The raw files were analyzed using MaxQuant (version 1.6.17.0, (57)) and the Uniprot human proteome database (21/03/2020, 75,776 entries) supplemented with both  $\mu$ 2 and  $\mu$ 2-P208S sequences. The settings used for the MaxQuant analysis (with TIMS-DDA type in group-specific parameters) were: 2 miscleavages allowed; fixed modification: carbamidomethylation on cysteine; enzyme was trypsin (K/R not before P); variable modifications included were methionine oxidation, and protein N-terminal acetylation. The mass tolerance were 10 ppm (precursor ions) and 20 ppm (fragment ions). FDR (PSM and protein) and site decoy fraction were set to 0.05; minimum peptide count was set to 1. Label-Free-Quantification (LFQ) was also allowed with minimal ratio count of 2. The "Second peptides" and "Match between runs" options were both allowed. Following the analysis, proteins positive for at least either one of the "Reverse", "Only.identified.by.site" or "Potential.contaminant" categories were eliminated, as well as proteins identified from a single peptide.

### **Indirect immunofluorescence in COS-7 cells**

COS-7 cells were seeded at  $1 \times 10^4$  cells/well in 24-well plates on glass coverslips and transfected on the next morning. After a 24 h incubation period, cells were washed with PBS and fixed 20 min using 4% paraformaldehyde and 4% sucrose in PBS at room temperature. Cells were then permeabilized with 0.15 % triton X-100 in PBS for 5 min at room temperature and blocked in 10% normal goat serum (Wisent) for 20 min. Anti-GFP antibody (1:1,000) was incubated 4 h at room temperature to increase the GFP signal. Cells were washed three times in 10% normal goat serum for 5 min and incubated 1 h in the dark with AlexaFluor 488-labelled goat anti-mouse secondary antibody (Invitrogen, 1:1,000). Cells were washed three time in PBS, and

nucleus staining was performed using 1  $\mu\text{g/ml}$  Hoechst for 15 min at room temperature. Coverslips were mounted on slides with SlowFade Diamond mounting medium (Life Technologies), then confocal microscopy imaging was done using a confocal Zeiss LSM 880 2 photons microscope.

### **Data analysis and statistical analyses**

Image quantitation was done using the ImageJ software (Fiji). All statistical analyses were conducted with the GraphPad software. All results presented in this article are mean  $\pm$  standard deviation.

## **RESULTS**

### **The interferon response is not necessary nor sufficient to trigger AS changes during MRV infection**

Upon infection of L929 murine cells with MRV, we and others have previously demonstrated that drastic changes in cellular AS occur 16 h post-infection (PI) (44,45). These changes could either be (1) induced directly by the presence of the virus; (2) triggered by the host cell as a defense mechanism; or (3) linked to the antiviral state mediated through secreted factors, such as IFN, cytokines or other ISG. We initially wanted to address if IFN induction is required for MRV modulation of cellular AS. To do so, we targeted RIG-I, one of the principal cytoplasmic sensors of viral dsRNA and ssRNA allowing IFN production during MRV infection (58, 59). siRNA-mediated knockdown (KD) of RIG-I using two different siRNA completely abrogated its expression in MRV-infected L929 at 16 h PI (Figure 1A). Further validation by measuring mRNA levels of IFN- $\beta$  and two ISG (*DDX60* and *MX1*) confirmed an 80-90% reduction in IFN- $\beta$  mRNA levels and a 60% (siRIG-I #1) to 80-90% (siRIG-I #2) reduction in ISG induction (Supplementary Figure S1). Next, we harvested RNA from both mock and infected cells at 16 h PI in either siCTRL or siRIG-I conditions, and submitted them to alternative splicing PCR (AS-PCR) coupled to capillary electrophoresis to quantitate potential changes in AS (60-64). Alternative splicing events (ASE) were selected from the 240 ASE previously shown to be

modulated during MRV infection and validated using AS-PCR (44). All pertinent information regarding the primers and the amplicon quantitated are available in Supplementary Table S2, and design maps for every ASE analyzed are depicted in Supplementary Figure S2. The percent spliced-in (PSI) metric was used to quantitate the level of intron inclusion in these ASE; it represents the percent of the long form over total abundance (both long and short forms). In the control siRNA transfection, MRV drastically changed the AS of the ASE we monitored, as we have previously demonstrated (44) (Figure 1B). We also analyzed an ASE in the *SERBP1* gene, which is not modulated by MRV, as a negative control to confirm that MRV's impact on cellular AS is targeted to specific transcripts, as we previously described (44). Upon RIG-I KD, the capacity of MRV to alter the splicing of these events was not affected, indicating that the interferon response is not necessary for MRV modulation of these ASE (Figure 1B). However, a very limited number of ASE, such as in *CKDN2AIP* and *EIF4A2*, were affected by the status of the IFN response. For instance, in the case of *CKDN2AIP*, RIG-I KD limits MRV ability to alter AS. For *EIF4A2*, the AS in uninfected cells is modulated by the RIG-I KD (Supplementary figure S3). As controls, we also monitored viral *M1* and *S1* RNA levels (Supplementary Figure S4) and viral protein levels (Supplementary Figure S5) to ensure that knocking RIG-I was indeed increasing viral RNA and protein levels.

We next wondered if soluble factors secreted upon infection were sufficient to trigger the observed AS changes. To do so, we designed a bystander experiment aimed at answering this question (Figure 1C). First, L929 cells were plated on a 0.4 mM semi-permeable membrane and infected by MRV, before being laid atop a second layer of uninfected cells in 1% anti-MRV antibody. In such a system, the first layer of cells is infected, but not the second layer, and no virus is present in these bystander cells nor the mock experiment as determined by measuring the levels of *M1* and *S1* viral RNA by qPCR (Supplementary Figure S6). However, bystander cells are stimulated by secreted factors from infected cells, as demonstrated by the levels of induction

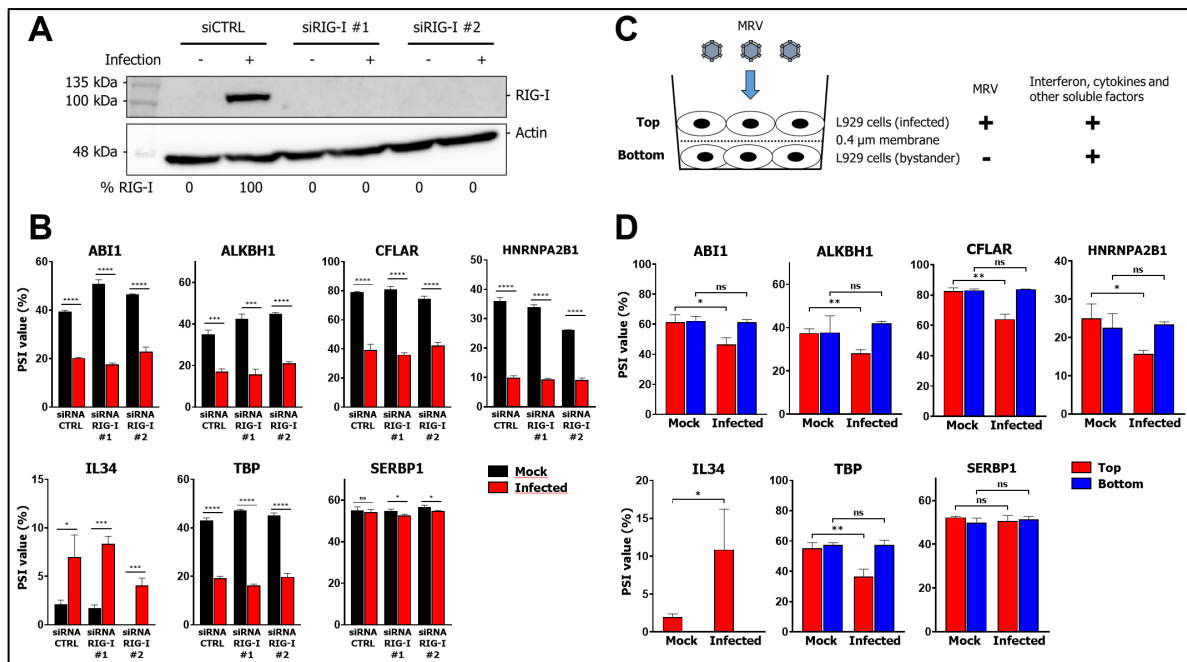


Figure 1. *The interferon response is not necessary nor sufficient to trigger AS changes during MRV infection.* (A) Validation by western blot of RIG-I knockdown in mock- and MRV- (T3DS) L929 infected cells. The membrane was H<sub>2</sub>O<sub>2</sub>-inactivated and probed against actin as a loading control. (B) Percent spliced in (PSI) values for numerous ASE modulated by MRV in siCTRL and siRIG-I mock (black) and infected (red) L929 cells. SERBP1 was included as a negative control ASE. n=3, biological replicates, unpaired two-tailed Student's t-test (ns, P>0.05; \*, P≤0.05; \*\*, P≤0.01; \*\*\*, P≤0.001; \*\*\*\*, P≤0.0001) comparing mock and infected cells for each siRNA condition. (C) Overview of the bystander experiment. (D) PSI values of the same ASE as B in the membrane (top, red) or the bystander (bottom, blue) cells when the top layer was infected or mock-infected with MRV. SERBP1 was included as a negative control ASE. n=3, biological replicates, unpaired two-tailed Student's t-test (ns, P>0.05; \*, P≤0.05; \*\*, P≤0.01) comparing mock and infected cells on the membrane (top, red) or bystander (bottom, blue).

of two ISG at the RNA level (Supplementary Figure S6). Upon analysis of the same ASE as Figure 1B, the bystander experiment in the uninfected control condition showed no change in AS, whether cells were on the membrane (top) or bystander (bottom) to those cells (Figure 1D). In the infected condition, a change in AS can be observed in cells cultured on the membrane (top, red); however, no impact on AS can be observed in bystander cells (bottom, blue) for all ASE tested (Figure 1D, Supplementary Figure S7). The *SERBP1* negative control ASE was constant in all tested conditions. These results indicate that secreted factors are not sufficient to mediate changes in these ASE in bystander cells. To further rule out any possibility that IFN signaling might affect AS, we directly treated L929 cells with 10, 100, or 1,000 U/mL of recombinant mouse IFN-β and demonstrated that all concentrations

of IFN- $\beta$  do not impact the AS of selected ASE (Supplementary Figure S8). Taken together, these data suggest the IFN response is neither necessary (RIG KD) nor sufficient (bystander experiment) for MRV's impact on these cellular ASE.

### **The modulation of AS happens in a time-dependent manner during MRV infection**

Since the preceding results suggested that MRV presence is necessary to induce changes in AS, we next assessed the kinetics of these changes observed during infection. Changes in AS early in infection could point towards early replication steps, such as internalization or uncoating of the viral particle, to be involved. On the other hand, changes appearing later during infection would suggest that the translation of viral RNA and production of viral proteins are required, thereby suggesting the involvement of newly produced viral proteins. A time-course experiment was performed where RNA was harvested directly after adsorption (0 h) and up to 24 h PI (Figure 2A). The splicing profile of ASE modulated during infection was then assessed using AS-PCR. The time-course experiment revealed that upon adsorption and early during infection (4 h and 8 h), no significant modulation in the AS profiles of *ABI1*, *CFLAR*, and *IL34* could be detected (Figure 2B). However, at 12 h, the splicing profile started to shift and peaked at 16 h post-infection for the three ASE analyzed. These splicing changes were not further modulated at 24 h, and some PSI values were even returning towards the basal level in some case (*CFLAR*, *IL34*). Monitoring the AS profile of the negative control ASE (*SERBP1*) showed no change throughout the infection, hence showing that the modulation of AS is specific and timely regulated (Figure 2B). Additional ASE were analyzed and showed similar profiles; however, some rare examples, such as the one in *EIF4A2*, were modulated using a different kinetic (Supplementary Figure S9). We monitored viral replication by following levels of *M1* and *S1* RNA by qPCR during the same time course and confirmed that MRV replication peaks at 16 h post-infection (Figure 2C), as previously described under similar conditions (65). Since these AS changes happen in a coordinated fashion with the peak of viral replication, the simultaneous timing



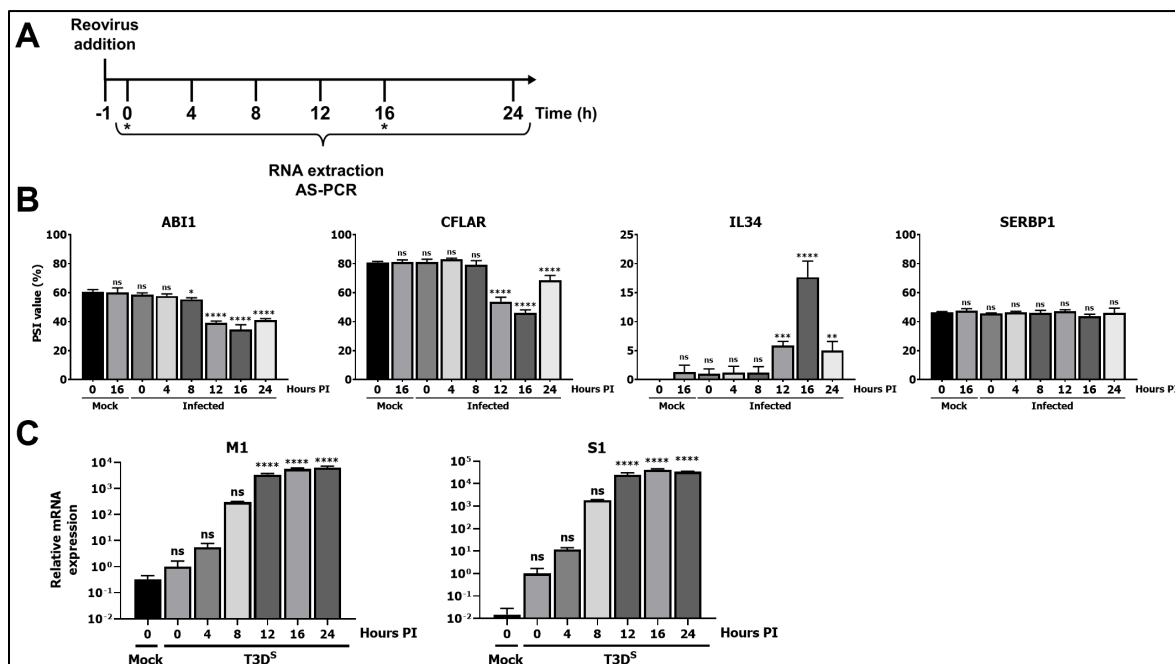


Figure 2. *The modulation of AS occurs in a time-dependent manner during MRV infection.* (A) Overview of the time-course experiment. Mock cells were harvested at the 0 h and 16 h time point (denoted by an asterisk). (B) Splicing profiles (PSI) of the ABI1, CFLAR, IL34, and negative control SERBP1 ASE throughout infection. PCR amplicons were resolved using capillary electrophoresis and quantified using relative fluorescence.  $n=3$ , biological replicates, one-way ANOVA with Dunnett's multiple comparisons test against the 0 h mock condition (ns,  $P>0.05$ ; \*,  $P\leq 0.05$ ; \*\*,  $P\leq 0.01$ ; \*\*\*,  $P\leq 0.001$ ; \*\*\*\*,  $P\leq 0.0001$ ). (C) Relative levels of M1 and S1 RNA as determined by qPCR throughout the time-course experiment and up to 24h. The first time point upon adsorption (0h post-infection, T3D<sup>S</sup>) was used to normalize the RNA level to the input RNA that was present to infect cells. PSMC4, PUM1, and TXNL4B were used as housekeeping genes for normalization.  $n=3$ , biological replicates, one-way ANOVA with Dunnett's multiple comparisons test against the 0 h mock condition (ns,  $P>0.05$ ; \*\*\*\*,  $P\leq 0.0001$ ).

of these two events suggests that the production of some viral protein(s), reaching a critical peak at this time point (65), is involved in this modulation.

### The $\mu 2$ protein is the main determinant of the modulation of cellular AS during MRV infection

In an effort to identify which protein(s) could be involved, we decided to assess the ability of another MRV T3D strain to modulate AS. The rationale is that if a strain-dependent phenotype is present, then mapping that phenotype to one of the ten gene segments, each encoding one or two proteins, should be possible. To do so, we compared our MRV laboratory stock, T3D<sup>S</sup>, with the one from the original reverse genetics system, T3D<sup>K</sup> (50). There are a dozen single amino acid polymorphisms between these two virus strains, leading to drastic differences in some phenotypes

such as the induction of interferon and the morphology of the viral factories (5, 48, 66). L929 cells were infected with either T3D<sup>S</sup>, T3D<sup>K</sup>, or mock-infected, and RNA was harvested 16 h post-infection. Following AS-PCR, T3D<sup>K</sup> appeared to be a less-potent modulator of AS than T3D<sup>S</sup> for the various ASE analyzed (Figure 3). For example, the AS of *ABI1*, *CFLAR*, and *IL34* is efficiently modulated by T3D<sup>S</sup>, but not by T3D<sup>K</sup>. Both T3D<sup>S</sup> and T3D<sup>K</sup> modulate the splicing of *TBP*; however, T3D<sup>K</sup> induces the accumulation of the long form instead of the short form of the ASE as seen with T3D<sup>S</sup>. Again, additional ASE analyzed are shown in Supplementary Figure S10 and further confirmed the different impact of T3D<sup>S</sup> and T3D<sup>K</sup> on cellular AS. The negative control ASE *SERPBI* shows that the two viruses are not broadly impacting AS but rather modulating only specific ASE.

Since the two laboratory strains present striking differences in their ability to modulate the splicing of these ASE, recombinant viruses were produced to map this strain-specific phenotype to one or more of their gene segments. It has been previously observed that the  $\mu 2$  protein from another MRV strain (T1L) interacts with the splicing factor SRSF2 (45). Involvement of the *M1* gene segment, encoding for the  $\mu 2$  protein, was thus first questioned by swapping the *M1* gene segment from T3D<sup>K</sup> into the genetic background of T3D<sup>S</sup> (M1T3D<sup>K</sup>[T3D<sup>S</sup>]), or reciprocally (M1T3D<sup>S</sup>[T3D<sup>K</sup>]). L929 cells were then infected using these two viruses and the splicing profiles characterized by AS-PCR, as before. Upon infection with either virus, their splicing profiles were mimicking the one from which the *M1* gene segment comes from, i.e., the splicing of M1T3D<sup>K</sup>[T3D<sup>S</sup>] was the same as the WT T3D<sup>K</sup>, and the same observation can be made for M1T3D<sup>S</sup>[T3D<sup>K</sup>] and T3D<sup>S</sup> (Figure 3). This experiment confirmed that the strain-dependent phenotype in the ability to modulate these ASE mostly segregates with the *M1* gene segment, and thus suggests the involvement of the  $\mu 2$  protein. Again, additional ASE analyzed are shown in Supplementary Figure S10 and confirmed that ability to modulate the AS of these genes is linked to the *M1* gene segment. However, it is also possible to observe some effects of the genetic background. For example, in the M1T3D<sup>S</sup>[T3D<sup>K</sup>]

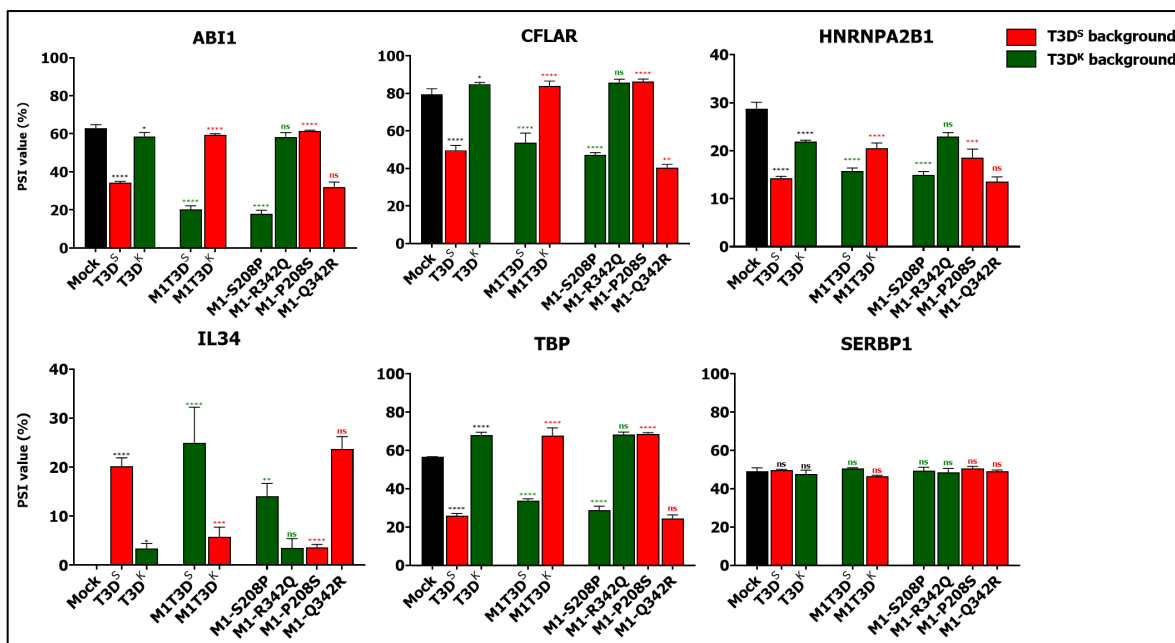


Figure 3. Strain-dependent modulation of AS segregates with the *M1* gene segment and is dictated by a polymorphism at position 208 in  $\mu 2$ . Splicing profile (PSI) of the ASE in the *ABI1*, *CFLAR*, *HNRNPA2B1*, *IL34* and *TBP* gene upon infection with (1), T3DS or T3DK MRV; (2), T3DS harboring the *M1* gene segment from T3DK (M1T3DK[T3DS]) or T3DK harboring the *M1* gene segment from T3DS (M1T3DS[T3DK]); and (3), single amino acid mutant in  $\mu 2$  S208P or R342Q in T3DK and P208S or Q342R in T3DS. PCR amplicons were resolved using capillary electrophoresis and quantified using relative fluorescence. The negative control ASE in *SERPBI* was also analyzed.  $n=3$ , biological replicates, one-way ANOVA with Dunnett's multiple comparisons test against the mock condition for T3DS/T3DK (in black); two-way ANOVA with Šidák's multiple comparisons test against the parental virus (T3DS in red and T3DK in green) for the reassortant and mutant viruses (ns,  $P>0.05$ ; \*,  $P\leq 0.05$ ; \*\*,  $P\leq 0.01$ ; \*\*\*,  $P\leq 0.001$ ; \*\*\*\*,  $P\leq 0.0001$ ).

infection, the modulation of *ABI1* and *TBP* ASE is respectively increased and decreased as compared to WT T3D<sup>S</sup>. Other genetic determinants might thus be involved, either helping or restricting  $\mu 2$  impact on AS. The same negative control as previously used, *SERPBI*, was also analyzed. Once again, this ASE was not modulated in all the viruses tested. To rule out any possibility that slower replication kinetics might be explaining these results, we monitored the levels of *M1* and *S1* RNA at 16 h PI as a general indicator of viral replication. All viruses tested only show slight significant differences in their levels of *M1* and *S1* RNA (Supplementary Figure S11). This indicates that these different virus strains replicate efficiently and do not exhibit gross defects in replication. Moreover, even the lower replicating viruses, such as M1T3D<sup>S</sup>[T3D<sup>K</sup>], induced changes in AS, indicating that small differences in replication levels cannot explain the differences in the ability to induce changes in

cellular AS. Monitoring viral  $\sigma 3$  protein levels also confirmed similar replication for all viruses tested (Supplementary Figure S12). Altogether, these results clearly established that the strain-dependent phenotype in the modulation of these ASE is caused by the *M1* gene segment, and that the  $\mu 2$  protein from T3D<sup>S</sup> and T3D<sup>K</sup> possesses drastically different capacities to alter AS during infection.

Interestingly, there are only two amino acid differences in  $\mu 2$  between T3D<sup>S</sup> and T3D<sup>K</sup>. In the case of T3D<sup>S</sup>, position 208 is a proline, and position 342 is a glutamine; in the case of T3D<sup>K</sup>, these positions are occupied by a serine and an arginine, respectively (48). The position 208 has already been involved in numerous strain-dependent phenotype attributed to  $\mu 2$ , such as the blockade of the IFN response and morphology of the viral factories (5, 67, 68). No strain-dependent phenotype has been linked to the position 342. We thus assessed which polymorphism (i.e., position 208 or 342) is responsible for this differential ability to modulate the cellular AS of these ASE by substituting the amino acid at these positions with the one from the other strain. Site-directed mutagenesis was conducted on the reverse genetic plasmid encoding the T3D<sup>K</sup> *M1* gene segment to introduce individually S208P or R342Q mutation in the T3D<sup>K</sup>  $\mu 2$  protein. This process was also done using the T3D<sup>S</sup>  $\mu 2$ -encoding plasmid to introduce reciprocal mutations, P208S or Q342R. T3D<sup>S</sup> or T3D<sup>K</sup> viruses harboring these single amino acid mutations in the  $\mu 2$  protein were rescued by reverse genetics, L929 cells were infected as before, and their ability to modulate the AS of target ASE evaluated using AS-PCR. Mutating the proline to serine at position 208 in  $\mu 2$  from T3D<sup>S</sup> abrogates its ability to strongly modulate these ASE; reciprocally mutating the serine to proline at this position in T3D<sup>K</sup>  $\mu 2$  rescue this phenotype (Figure 3). Mutating the arginine to glutamine or vice versa at position 342 has no effect on the modulation of AS for these genes. Once again, some influence from the genetic background can be observed for certain ASE. For example, the M1-S208P T3D<sup>K</sup> virus induces a bigger change in the splicing of the *ABI* ASE than WT T3D<sup>S</sup>, indicating that additional factors in the background can influence  $\mu 2$ 's impact on AS. Additional ASE analyzed are presented in

Supplementary Figure S10 and support both the involvement of the amino acid at position 208 in  $\mu 2$  and the importance of MRV genetic background in the modulation of cellular AS. The AS of the negative control *SERBP1* was the same in all viruses tested. Once again, viral RNA levels (Supplementary Figure S11) and protein levels (Supplementary Figure S12) confirmed only minor differences in replication levels that cannot explain the impact on cellular AS. Taken together, these results show that the amino acid at position 208 in  $\mu 2$  is critical for its impact on AS, and is mainly responsible for the strain-dependent phenotype previously described.

### **$\mu 2$ directly impacts cellular AS of reporter minigenes in ectopic expression through both nuclear-dependent and nuclear-independent mechanisms**

Our results so far demonstrate that MRV  $\mu 2$  protein is the main determinant of MRV modulation of AS during infection, at least for the ASE we analyzed. However, we cannot conclude solely from these results that the  $\mu 2$  protein is directly able to trigger these changes during infection, as all other viral proteins are expressed and might be indirectly necessary for the  $\mu 2$ -dependent alterations of AS. We thus needed to assess the ability of  $\mu 2$  by itself to modulate cellular AS in the absence of other viral proteins. However, ectopic expression of  $\mu 2$  was previously described to be challenging, especially in L929 cells classically used for MRV infection studies (55, 69). To circumvent this problem, HEK293 and 293T cells have been shown to be suitable for the transient expression of the  $\mu 2$  protein alone (9, 45, 68, 70). We found that SV40 large T antigen harboring cells such as 293T and COS-7 were the most efficient for  $\mu 2$  expression harboring either a N- or C-terminal GFP moiety (Supplementary Figure S13).

We first monitored the cellular localization of the  $\mu 2$  protein harboring a N- or C-terminal GFP moiety, or corresponding mutants where the proline at 208 was substituted for a serine (P208S) in COS-7 cells (Figure 4A). As previously shown, the WT  $\mu 2$  showed filamentous localization in the cytoplasm by binding to cellular microtubules (5), and broad nuclear staining with bright foci described previously as

nuclear speckles (9, 45). Moreover, the P208S mutants showed a diffuse cytoplasmic staining, as it cannot bind to microtubules (5). Surprisingly, the P208S mutant was devoid of any nuclear accumulation, both in terms of the number of cells presenting nuclear  $\mu 2$  as well as when quantifying the fluorescent signal inside the cells (Supplementary Figure S14A, S14B). Moreover, the same results were obtained in 293T cells (Supplementary Figure S15). This raises the possibility that incorrect import into the nucleus for the P208S mutant might be responsible for its reduced impact on cellular AS. To test this hypothesis, we monitored the ability of these constructions to alter AS in ectopic expression. Since AS is not very well conserved between mouse and human (71), we derived AS minigene reporters from the murine L929 cells for *ALKBH1*, *CFLAR*, *HNRNPA2B1*, *TBP*, and *SERBP1* ASE (Figure 4B). These constructs encompass the spliced region known to be modulated by MRV that we previously monitored (Figures 1B, 1D, 2B, and 3) into the pcDNA3.1+ vector. All pertinent information regarding the primers and the amplicon quantitated are available in Supplementary Table S3A. These constructs allowed the monitoring of the AS of these five ASE when co-transfected in 293T cells together with the different  $\mu 2$  constructs. Western blotting (Supplementary Figure S16) and epifluorescence microscopy (Supplementary Figure S17) confirmed that all the constructions tested were correctly expressed. We first assessed the ability of WT  $\mu 2$  or P208S- $\mu 2$  to alter the splicing of these minigenes. The PSI in the *CFLAR* ASE was reduced upon WT  $\mu 2$  expression but not when the proline was substituted for a serine, recapitulating the phenotypes observed during MRV infection (Figure 3). Surprisingly, the PSI for the *ALKBH1* was strongly increased by the WT  $\mu 2$  harboring the C-term GFP or both P208S mutants (Figure 4C), as opposed to the reduction in inclusion of this ASE previously observed during infection (Figure 1B, Supplementary Figure S10). However, this event is more complex than the other ones, as two long forms are present (exons 1-2-4 and exons 1-2-3-4) that might complexify the interpretation. As a control, the AS of the 3'-SS from the *SERBP1* minigene was not altered by the expression of any of these constructions. Together, these three minigenes reveal that  $\mu 2$  protein expression alone specifically alters the AS profiles of ASE targeted

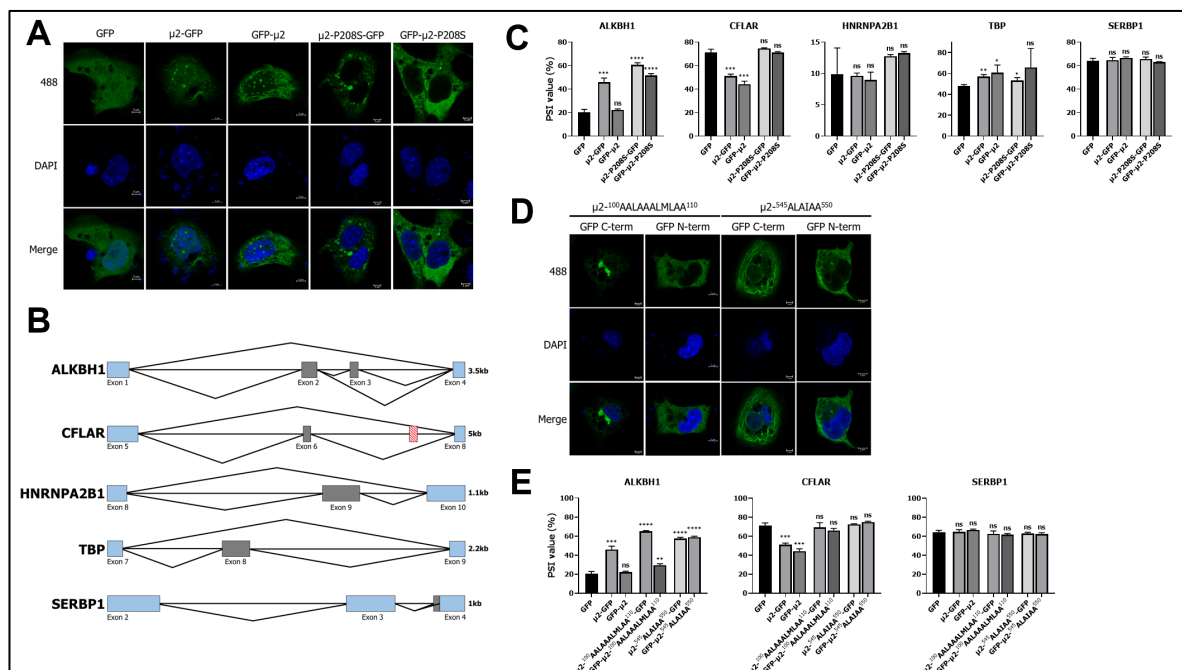


Figure 4.  $\mu 2$  directly impacts the AS of minigene reporters in ectopic expression through both nuclear-dependent and nuclear-independent mechanisms. (A) Cellular localization of GFP, N-term or C-term GFP- $\mu 2$ , and N-term or C-term GFP- $\mu 2$  harboring the single amino acid polymorphism P208S in COS-7 cells. The white scale bar represents 5  $\mu$ m. (B) Schematic representation of the selected ASE cloned into the pcDNA3.1+ plasmid to act as AS reporters. Black lines represent introns and rectangles denote exons; in blue are the constitutive ones and in gray are the alternatively spliced ones. All selected ASE modulated by MRV are single exon cassette, except for the ASE in ALKBH1 where there are two consecutive cassette exons. The negative control SERBP1 is an alternative 3' splice site (+18 nucleotides) that was previously monitored; although the exon 3 is annotated as a cassette exon, we have never observed the skipping of this exon in L929 cells. Introns and exons are to scale (for each ASE separately) and the length of the cloned fragment is denoted on the right. The red hatched exon in CFLAR denotes the 7th exon, which is an alternative transcription initiation site and is only included when transcription begins at this exon. (C) Splicing profiles (PSI) of the ALKBH1, CFLAR, HNRNPA2B1, TBP, and the negative control SERBP1 AS minigenes reporters upon expression of the different  $\mu 2$  constructs.  $n=3$ , biological replicates, unpaired two-tailed Student's t-test (ns,  $P>0.05$ ; \*,  $P\leq 0.05$ ; \*\*,  $P\leq 0.01$ ; \*\*\*,  $P\leq 0.001$ ; \*\*\*\*,  $P\leq 0.0001$ ) against the GFP alone condition. (D) Cellular localization of N-term or C-term GFP- $\mu 2$  mutants 100-AALAAALMLAA-110 and 545-ALAIAA-550 unable to accumulate in the nucleus in COS-7 cells. The white scale bar represents 5  $\mu$ m. (E) Splicing profiles (PSI) of the ABI1, CFLAR, and the negative control SERBP1 AS minigene reporters upon expression of the different  $\mu 2$  constructs.  $n=3$ , biological replicates, unpaired two-tailed Student's t-test (ns,  $P>0.05$ ; \*,  $P\leq 0.05$ ; \*\*,  $P\leq 0.01$ ; \*\*\*,  $P\leq 0.001$ ; \*\*\*\*,  $P\leq 0.0001$ ) against the GFP alone condition.

during MRV infection. However, we failed to observe any changes in the splicing of the *HNRNPA2B1* and *TBP* reporters; these results will be addressed below in section *U5 core components are required for MRV modulation of cellular AS and are reduced by  $\mu 2$* . Finally, we also exploited two conserved ASE between mouse and human dysregulated during MRV infection, namely *ABI1*, *CDKN2AIP*, in addition to the *SERBP1* negative control which is also conserved (Supplementary Table S3B), and

analyzed their splicing upon the expression of the  $\mu 2$  constructs (Supplementary Figure S18). The ASE in *ABI1* and *CDKN2AIP* were both modulated efficiently by  $\mu 2$ -GFP and  $\mu 2$ -P208S-GFP, but not when the GFP moiety was fused to the N-terminus of  $\mu 2$ . Once again, the negative control ASE was not impacted by  $\mu 2$  expression. These results suggest an involvement of the N-terminus of  $\mu 2$  in the modulation of the ASE in *ABI1*, *CDKN2AIP*, and *ALKBH1*. Taken together, only the ASE in *CFLAR* (minigene) was not modulated by the P208S mutants; ASE in *ALKBH1* (minigene), *ABI* (endogenous), and *CDKN2AIP* (endogenous) were all affected in the same fashion by the mutant than the WT  $\mu 2$ .

These previous results support that  $\mu 2$  is altering cellular AS through both nuclear-dependent and nuclear-independent mechanisms. However, substituting the P208 for a serine might affect other aspects of  $\mu 2$  than the localization, and we thus wanted to specifically target the ability of  $\mu 2$  to enter the nucleus. One nuclear localization sequence (NLS) in  $\mu 2$ , 100-RRLRKRLMLKK-110, was previously described (9). However, it was never mutated in the context of the endogenous protein, but rather studied when grafted alone to GFP moiety (9). We also identified another potential NLS, 545-RLKIPY-550, satisfying the R/H/K-X<sub>(2-5)</sub>P-Y rule for PY-NLS recognized by Kap $\beta$ 2 (72) (Supplementary Figure S19). In all these sequences, all basic residues were substituted for alanine, and the resulting mutants tested for their ability to accumulate in the nucleus in transiently-transfected COS-7 cells. All these mutations severely impaired nuclear localization, indicating that altering either of these sequences is sufficient to restrain the  $\mu 2$  protein to the cytoplasm (Figure 4D, Supplementary Figure S14A, S14B). Next, we assess the ability of these mutants to alter cellular AS of the reporter minigenes for *ALKBH1*, *CFLAR*, and *SERBP1*. All mutants were still able to alter the splicing of the *ALKBH1* minigene and unable to alter the splicing of *CFLAR* (Figure 4E). Moreover, the mutations restraining  $\mu 2$ 's ability to accumulate in the nucleus also had no impact on the capacity to alter the endogenous ASE in *ABI1* and *CDKN2AIP* (Supplementary Figure S18). Altogether, these data clearly established that MRV  $\mu 2$  protein by itself is sufficient to alter



cellular AS, and that  $\mu 2$  is able to alter cellular AS through both nuclear-dependent and nuclear-independent mechanisms.

### **IP-MS of GFP-tagged $\mu 2$ reveals interaction with core components of the U5 spliceosomal snRNP**

We next sought to determine which molecular mechanism(s) is (are) used by this viral protein to trigger such changes. Since numerous viral proteins interact with spliceosomes and splicing factors through direct protein-protein interaction (38, 39, 73, 74), we first determined the cellular interactome of both  $\mu 2$  and  $\mu 2$ -P208S using IP-MS. GFP-tagged constructions of  $\mu 2$  and  $\mu 2$ -P208S in both C- and N- terminus were transfected in 293T cells alongside control GFP alone, and submitted to GFP pulldown. These constructions were readily expressed in 293T cells (Supplementary Figure S15, S16) and were efficiently pulled down using GFP-Trap beads (Figure 5A). Since the  $\mu 2$  protein binds RNA (11), lysates were DNase and RNase treated prior to IP to ensure interactions mediated by nucleic acids were not identified. Next, the immunoprecipitated proteins were subjected to tandem mass-spectrometry in three independent replicates to identify bound proteins. Each replicate was analyzed independently using SAINT (75), and interactors with a Saint score above 0.9 were considered statistically significant (Supplementary Figure S20). To ensure that only true partners were identified, we added an additional criterion of independent identification in at least two replicates, which allowed the identification of between 51 and 195 cellular partners for the four different constructs (Figure 5B). Moreover, each dataset had an important overlap with one another, as 39% of identified interactors were represented more than once (Figure 5B). Of those 61% that were unique, 46% percent belonged to the GFP- $\mu 2$ -P208S dataset, which contained 2.5 to 4 times more identified proteins than the three other ones. The complete list of identified interactors is available in Supplementary Figure S21. To further validate our experimental procedure, we confirmed CAMK2D and CAMK2G as interacting partners of both WT and P208S mutant  $\mu 2$ , but only when the GFP moiety was fused

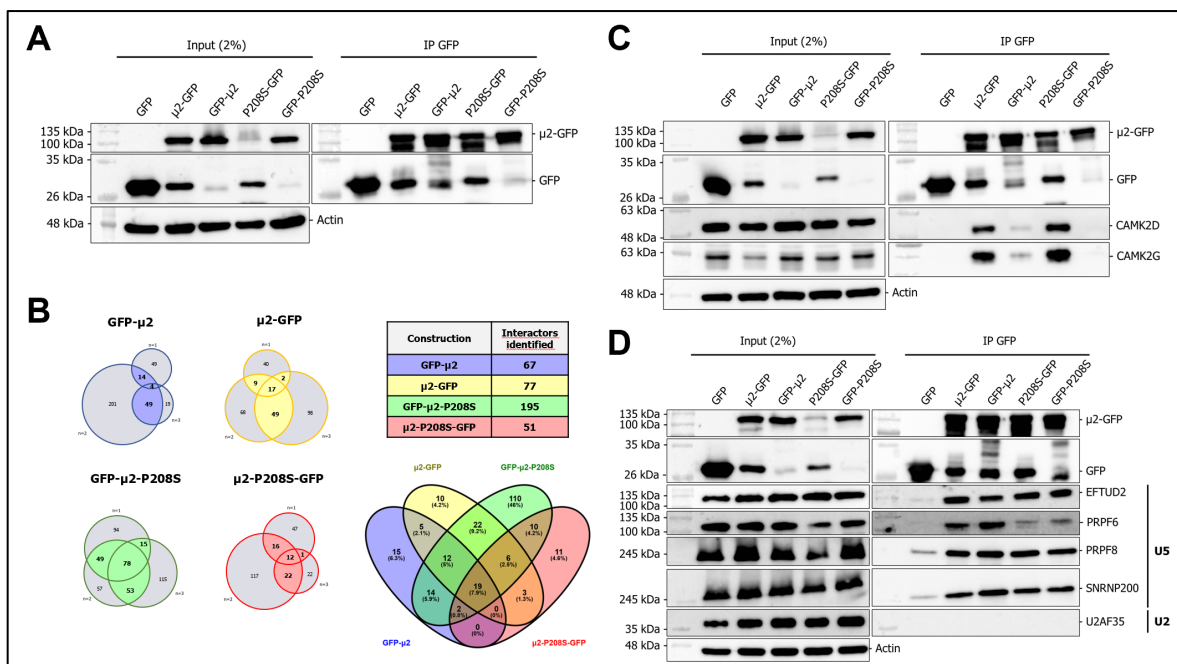


Figure 5. IP-MS of GFP-tagged  $\mu 2$  reveals interaction with core components of the U5 spliceosomal snRNP. (A) Validation of the immunoprecipitation of the different  $\mu 2$ -GFP constructions. (B) Summary of the IP-MS results. On the left, the three independent replicates are shown for each construction, alongside the overlap between them. Only proteins identified in two or three independent replicates were selected as hits. On the top right, the number of identified hits for each construction is denoted. On the bottom right, the protein overlap between the different constructions is depicted using a Venn diagram. (C) Validation of the experimental  $\mu 2$  IP-MS design using the CAMK2D and CAMK2G potential interactors by Co-IP and western blot. (D) Validation of the co-immunoprecipitation of MRV  $\mu 2$  protein with components of the U5 snRNP by Co-IP and western blot. Input or IP fractions were resolved on SDS-page gels and submitted to a WB against GFP, EFTUD2, PRPF6, PRPF8, SNRNP200, U2AF35 or the loading control actin.

in C-terminus, as determined in the MS results (Figure 5C; Supplementary Figure S21). These results underline the pertinence of analyzing interactors by tagging both ends of  $\mu 2$ , as in this case, the N-terminus GFP moiety is likely blocking the interaction interface of  $\mu 2$  with these partners.

Having validated the experimental approach, we searched the interactome data for potential splicing factors and spliceosomal components involved in AS. The aforementioned overlap between the WT protein and the mutant suggests the P208S mutation has a limited impact on the interactome of the  $\mu 2$  protein, and thus a difference in interacting partners might not be the explanation for their different impacts on AS. In light of these results, we focused our attention on the 19 proteins

that were common between all constructions, which included the three core components of the U5 snRNP, i.e. EFTUD2, PRPF8, and SNRNP200 (Supplementary Figure S22). This strongly suggested that  $\mu 2$  interacts with spliceosomal proteins, which could explain its impact on cellular AS. We validated that the different  $\mu 2$  constructs indeed co-immunoprecipitated EFTUD2, PRPF8, and SNRNP200, with no impact of the P208S mutation on these interactions (Figure 5D). Moreover, another component of the U5 snRNP, PRPF6, which was identified in the GFP- $\mu 2$ -P208S IP (Supplementary Figure S21), also immunoprecipitated with the WT  $\mu 2$ , albeit to a lesser extent (Figure 5D). However,  $\mu 2$  failed to pulldown the U2AF35 protein, an auxiliary factor required for the recruitment of the U2 snRNP to the branch point, showing that  $\mu 2$  specifically interacts with components from the U5 snRNP (Figure 5D). Finally, we also tested the ability of  $\mu 2$  to pulldown the RNA components of the different snRNP in RIP-ddPCR experiment, and  $\mu 2$  failed to pulldown the U5 RNA (Supplementary Figure S23). These data, taken together with the dispensable nuclear localization of  $\mu 2$  for the modulation of some ASE (Figure 4E, Supplementary Figure S18), suggest that  $\mu 2$  does not interact with the assembled snRNP in the nucleus, but rather with individual components in the cytoplasm before their import in the nucleus and assembly into a functional snRNP.

### **U5 core components are required for MRV modulation of cellular AS and are reduced during infection by $\mu 2$**

The interaction of  $\mu 2$  with multiple central components of the U5 snRNP, namely EFTUD2, PRPF8, and SNRNP200, suggests that  $\mu 2$  might exert its impact on cellular AS by affecting this crucial complex in the splicing reaction (38). To test this hypothesis, we individually depleted EFTUD2, PRPF8, and SNRNP200 in L929 cells using siRNA, and then infected the cells 16 h before harvesting the RNA to assess the ability of MRV to modulate AS in the absence of these components of the splicing machinery. We could readily reduce the levels of the three proteins between 50 to 75% (Figure 6A). Then, we calculated the difference in cellular AS upon infection by subtracting the PSI in infected cells from the PSI in control cells for each siRNA

condition ( $\Delta$ PSI). By doing so, we could isolate MRV's impact in the experiment with no regard on the impact of the siRNA on these ASE. A drastic reduction of MRV's ability to induce changes in the studied ASE was observed when either EFTUD2, PRPF8 or SNRNP200 was reduced (Figure 6B). However, knockdown of U5 core components did not enhance or affect the capacity of the virus to alter the splicing of the *SERBP1 ASE* negative control. Moreover, we monitored *M1* and *S1* viral RNA levels (Supplementary Figure S24), and  $\mu$ 2 and  $\sigma$ 3 viral protein levels (Supplementary Figure S25) in infected cells to ensure that the knockdown of U5 components did not reduce viral replication under these conditions. Taken together, these data suggest that  $\mu$ 2 exerts its ability to alter the splicing of these ASE through components of the U5 snRNP.

To further understand the importance of the U5 snRNP in the control of AS for these ASE, we analyzed the impact of the reduction of these U5 components in uninfected cells. As shown for some of these ASE, depleting core components of the U5 snRNP led to more skipping of the ASE, as the PSI decreases (Supplementary Figure S26). This was particularly marked for the ASE in *ALKBH1* and *TBP*, with reduction of 10% to 20% in PSI upon knockdown. Interestingly, these ASE all show a reduction in inclusion and more exon skipping during infection (Figure 3 and 6B), which suggests MRV and  $\mu$ 2 might alter normal U5 snRNP function to alter the splicing of these ASE. We validated in immunofluorescence that there was no drastic relocalization of these proteins during MRV infection (Supplementary Figure S27). Next, we monitored protein levels for the main U5 components (EFTUD2, PRPF8, SNRNP200) in control and L929-infected cells, comparing again T3D<sup>S</sup> with T3D<sup>K</sup> as a prototypic virus harboring the P208S mutation in  $\mu$ 2. Surprisingly, T3D<sup>S</sup> infection led to a striking reduction in PRPF8 (80%) protein levels, and a more modest reduction in EFTUD2 (35%) and SNRNP200 (25%). (Figure 6C). Interestingly, T3D<sup>K</sup> reduced SNRNP200 and EFTUD2 levels in a similar fashion, but had only a modest impact on PRPF8, further strengthening our hypothesis that these two viruses affect the U5 snRNP differently, which lead them to also affect cellular AS in a different fashion (Figure

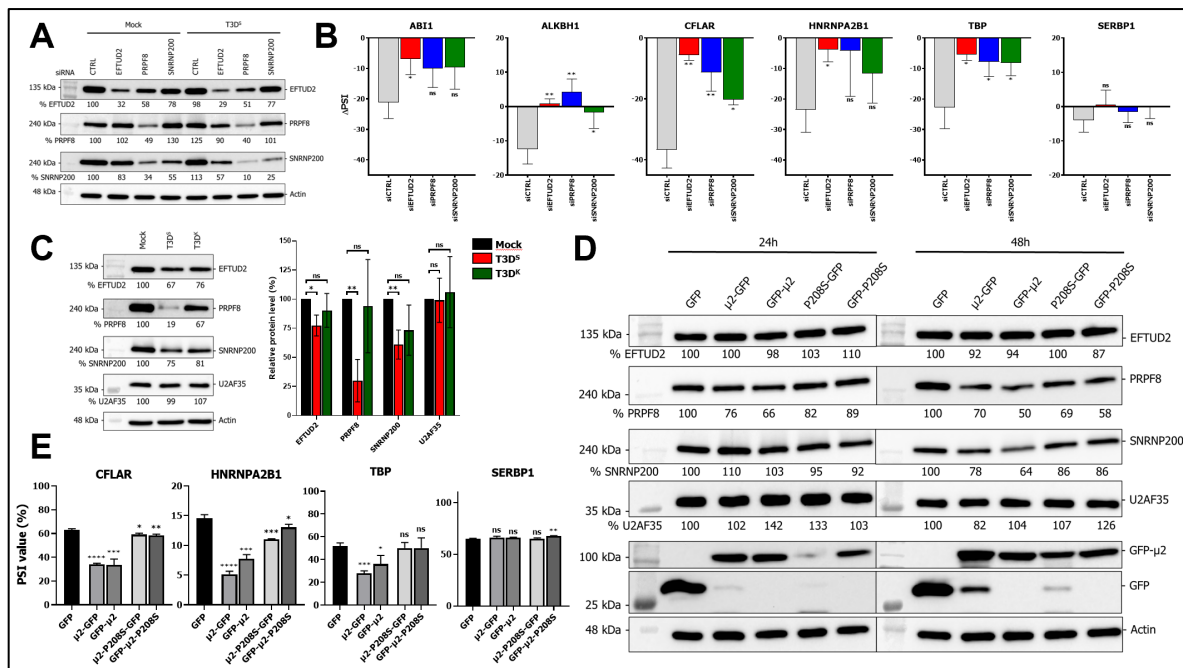


Figure 6. *U5* core components are required for MRV modulation of cellular AS and are reduced during infection by  $\mu 2$ . (A) Validation of the KD efficiency for EFTUD2, PRPF8 and SNRNP200 by western blot in mock- and T3DS-infected L929 cells. (B) Difference in splicing ( $\Delta$ PSI) between infected and mock L929 cells in control siRNA or EFTUD2, PRPF8, and SNRNP200 siRNA-treated cells. Respective standard deviation for the mock and infected cells were added when calculating the standard deviation for the  $\Delta$ PSI.  $n=3$ , biological replicates, unpaired two-tailed Student's t-test (ns,  $P>0.05$ ; \*,  $P\leq 0.05$ ; \*\*,  $P\leq 0.01$ ) comparing each condition against the control siRNA. (C) Protein levels of U5 snRNP components EFTUD2, PRPF8 and SNRNP200 in mock, T3DS and T3DK infected L929 cells. The membranes were H<sub>2</sub>O<sub>2</sub>-inactivated and probed again against actin (EFTUD2, U2AF35) or vinculin (PRPF8, SNRNP200) as a loading control; a representative loading control is shown. On the right, the cumulative results for three western blots are summarized in a bar graph. The U2 snRNP protein U2AF35 was probed as a control.  $n=3$ , biological replicates, unpaired two-tailed Student's t-test (ns,  $P>0.05$ ; \*,  $P\leq 0.05$ ; \*\*,  $P\leq 0.01$ ) comparing infected cells against control cells. (D) Impact of the ectopic expression of  $\mu 2$  on U5 components protein levels at 24h and 48h in 293T cells. The U2 snRNP protein U2AF35 was probed as a control. The membranes were H<sub>2</sub>O<sub>2</sub>-inactivated and probed again against actin (EFTUD2, U2AF35) or vinculin (PRPF8, SNRNP200) as a loading control; a representative loading control is shown. (E) Splicing profiles (PSI) of the HNRNPA2B1, TBP, and the negative control SERBP1 AS minigene reporters upon expression of the different  $\mu 2$  constructs at 48 h. PCR amplicons were resolved using capillary electrophoresis and quantified using relative fluorescence.  $n=3$ , biological replicates, unpaired two-tailed Student's t-test (ns,  $P>0.05$ ; \*,  $P\leq 0.05$ ; \*\*,  $P\leq 0.01$ ; \*\*\*,  $P\leq 0.001$ ; \*\*\*\*,  $P\leq 0.0001$ ) against the GFP alone condition.

3). These differences in levels upon T3D<sup>S</sup> infection were all statistically significant with three independent biological replicates, but not for the T3D<sup>K</sup> infection (Figure 6C). Monitoring protein levels for U2AF35 revealed no reduction in this auxiliary spliceosomal protein, underlining that MRV specifically affect the levels of only some spliceosomal components in the U5 snRNP. Moreover, the U5 snRNA was the only spliceosomal RNA affected at the RNA level by MRV infection, further confirming that

we identified the precise snRNP affected by MRV infection (Supplementary Figure S28).

Since U5 components were reduced in MRV-infected cells, we directly tested if the expression of  $\mu 2$  was sufficient to alter the protein levels of those U5 proteins. GFP alone,  $\mu 2$ -GFP or the P208S mutants were transfected in 293T cells, and cells were harvested at 24 h and 48 h to test EFTUD2, PRPF8, and SNRNP200 protein levels. At 24 h, a 20% reduction of PRPF8 levels could already be detected (Figure 6D). This reduction was further increased at 30-50% after 48 h for PRPF8, and SNRNP200 protein level was also reduced 15-35% by  $\mu 2$  expression at that time point. The P208S mutation did not affect the reduction of either PRPF8 or SNRNP200, suggesting the P208S mutant retains its ability to reduce PRPF8 levels, as seen during T3D<sup>K</sup> infection (Figure 6C). Once again, we could not detect any difference in the U2 auxiliary protein U2AF35. Quantification of three independent experiments confirmed a statistically significant reduction at 24 h for PRPF8 and for both PRPF8 and SNRNP200 at 48 h (Supplementary Fig S29). Taken together, these data suggest that  $\mu 2$  is the main MRV protein responsible for reducing protein levels of the U5 snRNP core components during infection. Furthermore, the increased reduction at 48 h of U5 snRNP PRPF8 and SNRNP200 protein levels suggests the impact of the ectopic expression of  $\mu 2$  on AS might be increased at this time point. As we previously monitored  $\mu 2$ 's impact on AS minigenes at 24h, we reassessed this ability at 48 h with the previously inconclusive *HNRNPA2B1* and *TBP* reporters (Figure 4C). Very reminiscent of the case of the *CFLAR* minigene (Figure 4C),  $\mu 2$  expression alone modulated the AS of both these minigenes, but the P208S had a much more limited impact (Figure 6E), highlighting that the reduction of U5 snRNP components are correlated with an increased impact on cellular AS attributable to the  $\mu 2$  protein. The impact on the *CFLAR* minigene was also increased at 48 h compared to 24 h (Figure 4C, 6E). Altogether, these results reveal that MRV modulation of these ASE involves the reduction of core components of the U5 snRNP through the action of the  $\mu 2$  protein.

## **DISCUSSION**

### *Involvement of $\mu$ 2 in reducing U5 snRNP components during MRV infection to modulate cellular AS*

In this study, we demonstrated that the  $\mu$ 2 protein is a key determinant for the modulation of AS during MRV infection. We showed that upon MRV infection, the  $\mu$ 2 protein exerts its effect on some specific ASE by reducing the levels of core components of the U5 snRNP (Figure 7). The  $\mu$ 2 protein is not sequestering U5 snRNP protein in the cytoplasm, as immunofluorescence of MRV-infected cells failed to show any defect in localization for EFTUD2, PRPF8, and SNRNP200 (Supplementary Figure S27). Although we demonstrated that the reduction of U5 snRNP core components protein levels during infection was attributable to  $\mu$ 2, and that  $\mu$ 2 interacts with these proteins, how  $\mu$ 2 exerts this effect on these U5 snRNP proteins remains elusive. However, the data presented herein supports the hypothesis that  $\mu$ 2 is not able to induce the degradation of U5 components assembled in the mature U5 snRNP in the nucleus, but suggests it rather impairs the renewal of these proteins. First,  $\mu$ 2 mutants unable to accumulate in the nucleus remain capable of altering AS (Figure 4E, Supplementary Figure S18), suggesting nuclear localization is not required for all the modulation of AS. Second, transient expression of  $\mu$ 2 shows a very limited reduction of these components at 24h and a modest reduction at 48h (Figure 6D), arguing against the degradation of the bulk nuclear pool of these proteins. This suggests that the reduction requires time, and supports a defect in renewal as more probable than the degradation of already translated proteins. Third,  $\mu$ 2 does not interact with the assembled U5 snRNP (Supplementary Figure S23). Altogether, the data presented in this study suggest that  $\mu$ 2 affects either the transcription, stability, export, or translation of the RNA for these U5 proteins, or degradation of the newly synthesized proteins in the cytoplasm before their nuclear import.

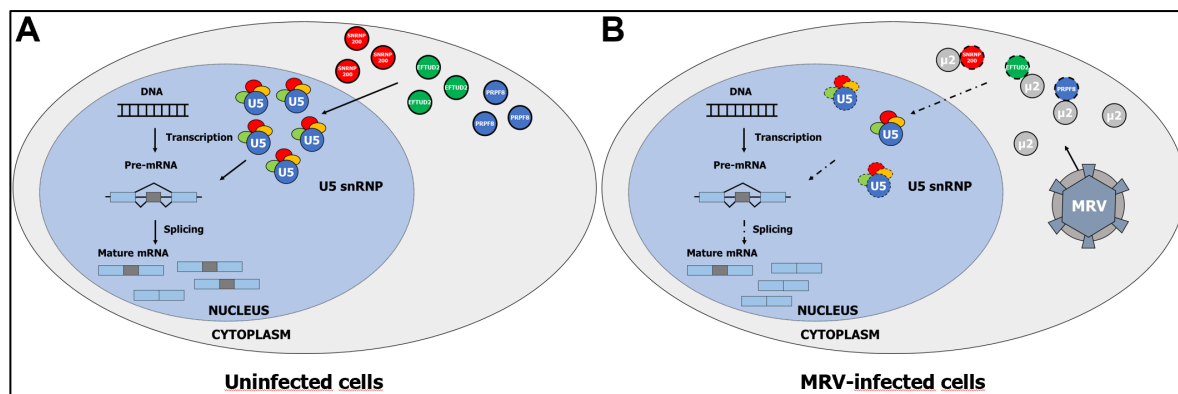


Figure 7. Model depicting how MRV infection leads to alterations in the host cell AS. In normal conditions (A), U5 main components EFTUD2, PRPF8, and SNRNP200 are translated in the cytoplasm and imported in the nucleus. The U5 snRNP levels are decreased due to the normal turnover of the complex, but this decrease is balanced by the import of the protein components and assembly of new U5 snRNP, allowing the functional U5 snRNP level to stay at equilibrium. Upon infection (B), expression of MRV viral protein  $\mu 2$  in the cytoplasm disturbs the capacity of the cell to produce EFTUD2, PRPF8, and SNRNP200 protein through a yet to define mechanism. This shutdown prevents the cell from replenishing the diminution of the U5 snRNP due to the normal turnover, and functional U5 snRNP level diminishes. This affects the capacity of the cell to regulate its AS, and leads to AS changes observed during MRV infection.

Since  $\mu 2$  mutants unable to accumulate in the nucleus also exert an activity on AS (Figure 4E, Supplementary Figure S18), transcription and nuclear export of the RNA seems less likely than RNA stability in the cytoplasm, translation, or degradation of the newly synthesized proteins. In the RIP-ddPCR experiment, we saw that  $\mu 2$  was bound non-specifically to all cellular mRNA that we tested (Supplementary Figure S30). This result supports the RNA binding activity of  $\mu 2$  demonstrated before (11), and further suggests it might impair translation by interacting with cellular mRNA. A translational block was shown long ago in MRV-infected cells (1,2) that favours MRV RNA to the detriments of cellular mRNA. Although it was attributed to  $\sigma 3$  and its antagonism of the PKR protein (76,77), a contribution of the  $\mu 2$  protein might have been overlooked. Supporting this hypothesis is the identification of numerous proteins from the large ribosomal subunit in the  $\mu 2$  IP-MS (i.e. *RPL3*, *RPL5*, *RPL7A*, *RPL8*, *RPL9*, *RPL10A*, *RPL12*, *RPL28*, *RPL31*, and *RPL35A*; Supplementary Figure S21). Care must be taken as ribosomal proteins are frequent contaminants in IP-MS (78), but this result warrants further study to determine if  $\mu 2$  does indeed contact the large subunit of the ribosome and affects translation. Interestingly, the  $\mu 2$



protein itself is ubiquitinated (79), and  $\mu 2$  pulldowns numerous E3 ubiquitin ligases (i.e. *MYCBP2*, *HERC2*, *UBR5*, *PRPF19*, *UBE3C*, and *TRIM27*; Supplementary Figure S21). Since ubiquitination is the principal pathway of degradation for nuclear proteins (80), this raises the hypothesis that  $\mu 2$  might contact E3 ubiquitin ligases and U5 snRNP components to induce their degradation.

One limitation of our IP-MS approach is that it is very likely that some of the U5 proteins we identified (EFTUD2, PRPF8, and SNRNP200; Figure 5D) are direct interactors of  $\mu 2$ , and some are co-immunoprecipitated by the direct interactors bound with  $\mu 2$ . However, our data clearly involve the U5 snRNP in MRV modulation of cellular AS, as KD of any of U5 snRNP core proteins reduce the ability of MRV to alter AS (Figure 6B). Surprisingly, one might expect that this would result in complete abrogation of both constitutive and alternative splicing, as U5 is required for the splicing reaction. This study thus points towards a possible implication of the U5 snRNP in controlling AS, and a high tolerance to reduction of the U5 snRNP levels without any drastic effect on constitutive splicing. Recent ENCODE data bolsters this hypothesis, as only between 15% to 25% of affected ASE following KD of EFTUD2, PRPF8, or SNRNP200, are retained introns (81). Therefore, the impact of reducing specific components of U5 snRNP and/or reducing the total U5 snRNP functional pool translates principally to an impact on AS, and not on constitutive splicing. Further studies will need to address the precise role of the U5 snRNP in regulating AS, and how this allows MRV to modulate cellular AS during infection.

### ***Importance of the U5 snRNP in viral infection***

The identification of components of the U5 snRNP as interactors of MRV  $\mu 2$  protein might seem surprising, as these cellular components are mainly nuclear, whereas MRV replicates in the cytoplasm. However, some examples of cytoplasmic virus proteins interacting with U5 snRNP components exist, such as the NS5 protein from Dengue virus. This RNA-dependent RNA polymerase (RdRp) interacts with CD2BP2 and DDX23 from the U5 snRNP, allowing modulation of cellular AS during infection

benefiting the replication of Dengue virus (38). Another RdRp, 3D<sup>pol</sup> from EV71 (a picornavirus), directly interacts with PRPF8 to also induce changes in cellular AS (39). In both cases, these RdRp are directly located in the nucleus of the cell during infection. In the case of MRV, our data support that the usurpation of these components is not nuclear, but rather cytoplasmic, suggesting a new mechanism never described before (see *Insight into the molecular impact of the P208S substitution on  $\mu$ 2 activity on cellular AS* for further explanations). Moreover, it is intriguing that the two known examples of viral proteins interacting with U5 components are RdRp, as  $\mu$ 2 is forming the MRV replicase complex alongside  $\lambda$ 3, MRV's RdRp. The fact that multiple proteins from different RNA viruses interact with U5 proteins suggests that U5 might play an important role in virus-host interactions. PRPF8 has previously been demonstrated to influence viral replication, as during influenza infection, it is induced by viral proteins and act as a proviral factor increasing viral production (82). Moreover, numerous studies support the involvement of U5 snRNP proteins in the interferon pathway (83). Indeed, both EFTUD2 and SNRNP200 have been shown to act as RNA sensors in the cytoplasm to allow the induction of the IFN response pathway during viral infection (84, 85). Furthermore, EFTUD2 also controls the splicing of *MYD88*, which is crucial in allowing the transduction signal from Toll-like receptors to the nucleus to induce IFN production (86). The role of U5 core components (EFTUD2, PRPF8, SNRNP200) in MRV replication and IFN induction could be further addressed in follow-up studies. Nevertheless, we did notice in the present work a small increase in  $\mu$ 2 protein levels (Supplementary Figure S25) and S1 viral RNA levels (Supplementary Figure S24) upon KD of PRPF8, suggesting it might exert an antiviral role. The suspected implication of U5 snRNP proteins in MRV replication is further strengthened by the recent identification of multiple components of the U5 snRNP (*EFTUD2*, *PRPF8*, *SNRNP200*, and *TXNL4A*) in a CRISPR-screen of host factors required for MRV replication and cell killing (87).

### ***Insight into the molecular impact of the P208S substitution on $\mu$ 2 activity on cellular AS***

We identified a key polymorphism in  $\mu$ 2, the serine or proline at position 208, that drastically alters the impact of  $\mu$ 2 on cellular AS (Figure 3). This position has been linked to a number of phenotypes before. Indeed, the P208S polymorphism controls the viral factories morphology (5-9, 66), the blockade of the IFN signaling in cardiomyocytes (67, 68), the ability of  $\mu$ 2 to locate to nuclear speckles (45), the ubiquitination of  $\mu$ 2 (79), and the oncolytic potential of MRV (16). Since we identified a new phenotype linked to this position, we sought to understand how this position affected the impact on cellular AS. Our data showed no drastic impact of the P208S substitution on the interactome of  $\mu$ 2 (Figure 5B), nor on  $\mu$ 2's ability to reduce PRPF8 and SNRNP200 protein levels in transient expression (Figure 6D). However, we did show that the P208S impairs the ability of  $\mu$ 2 to accumulate in the nucleus during transient transfection (Figure 4A), although our results with  $\mu$ 2 mutants showed that nuclear localization was not necessary for the modulation of all ASE tested (Figure 4E and Supplementary Figure S18). The significance of the accumulation of  $\mu$ 2 in the nucleus during transient transfection is unclear, as we and others have failed to locate the  $\mu$ 2 in the nucleus during infection using immunofluorescence (9). An additional explanation for the P208S defective mutation could be that this mutation simply decreases the levels of  $\mu$ 2 during infection, likely through increased ubiquitination, and thus insufficient  $\mu$ 2 levels could lead to all these aforementioned loss-of-function phenotypes. We did observe that viruses harboring a P208 present higher  $\mu$ 2 levels than the ones harboring a S208 (Supplementary Figure S31), supporting this hypothesis. Further studies will be required to adequately compare biochemical properties of  $\mu$ 2 proteins bearing P208 or S208, and the impact of  $\mu$ 2 levels on its activities during viral replication.

We have also generated mutants of the  $\mu$ 2 protein with an impaired nuclear localization (Figure 4D) that are useful molecular tools to define the role of nuclear localization in  $\mu$ 2 activity. We do not claim to have mutated the nuclear localization

signal of  $\mu 2$ , as several different mutants present impaired nuclear localization; we rather think we affected the structure of the protein sufficiently to impair the nuclear accumulation. For instance, the 100-AALAAALMLAA-110 mutant is no longer binding to microtubules; it is also the case of the 545-ALAIIAA-550 mutant bearing the GFP in N-terminus (Figure 4D) which supports a more global misfolding rather than a specific mutation to the nuclear localization signal. Designing such mutants have been challenging in the absence of a structure for  $\mu 2$ , but the structure has been recently solved using Cryo-EM in the viral particle (88). The structural information will greatly help the designing of molecular tools such as truncation mutants and isolated  $\mu 2$  domains that will help a better understanding of the  $\mu 2$  protein and the impact of the P208S substitution.

Finally, one last remark must be made concerning the impact of the P208S on cellular AS. As the RNA-Seq data have been generated using T3D<sup>S</sup> that harbors the P208 (44), the selection of ASE to analyze was biased for events modulated strongly by  $\mu 2$  with a proline at 208. The limited impact of the  $\mu 2$ -S208 on these ASE must be regarded in light of how ASE were selected; it is highly possible that some events (such as CDKN2AIP, Supplementary Figure S10) are modulated more efficiently by  $\mu 2$ -S208 but were not further studied because of the limited impact of T3D<sup>S</sup> on them. Future work could be done to get a thorough understanding by comparing the impact on AS for T3D<sup>S</sup>, T3D<sup>K</sup>, and their isogenic virus with the P208S and S208P substitution, respectively, by a non-biased approach such as RNA-Seq. Furthermore, we concentrated our efforts on some ASE that were modulated by MRV through the U5 snRNP. To which extent this mechanism accounts for the other AS changes observed previously, and if additional mechanisms are at play during MRV infection to alter AS, remains to be further studied.

### **Concluding remarks**

This study underlines a novel mechanism utilized by viruses to modulate cellular AS during infection involving the U5 snRNP of the spliceosome. The identification of a

polymorphism in  $\mu 2$  that controls both the impact of MRV on cellular AS and its oncolytic potential raises the possibility that the ability to impact cellular AS might be beneficial for the oncolytic potential (16). It has previously been shown that SRSF2 splicing factor restrict herpes simplex virus type 1 oncolytic activity, further suggesting cellular AS might dictate the oncolytic potential of viruses (89). Further studies should increase our understanding of the ability of other viruses to alter cellular AS by reducing spliceosomal protein levels, and if this modulation shape MRV therapeutic potential as an oncolytic virus.

### **DATA AVAILABILITY**

The mass spectrometry proteomics data have been deposited to the ProteomeXchange Consortium via the PRIDE (90) partner repository with the dataset identifier PXD029701. The Venn diagram was produced using Venny2.1 (*Oliveros, J.C. (2007-2015) Venny. An interactive tool for comparing lists with Venn's diagram; <https://bioinfogp.cnb.csic.es/tools/venny/index.html>*).

## SUPPLEMENTARY DATA

Table S1. *qPCR and ddPCR primers*

Target	Housekeeping gene	Species	Assays	Primers	
				Fw	Rv
DDX60		Mouse	qPCR – RIG-I KD, bystander	5'-CCACCACAGTTCATGAGTGCC-3'	5'-TGATTCCCAAAGCGAGTGTCCA-3'
IFNB1		Mouse	qPCR – RIG-I KD, bystander	5'-ACACTGCCCTTGCCATCCAAGA-3'	5'-ACACTGCTGCTGGTGGAGTTCA-3'
MX1		Mouse	qPCR – RIG-I KD, bystander	5'-GAAGGAGAGGAGTGGAGAGCA-3'	5'-GCTTATCACTGATCCCCAGGCC-3'
Rnu1a1 (U1)		Mouse	qPCR – infected cells (S28)	5'-TTTTCCAGGGCGAGGCTTA-3'	5'-CCCCACTACCACAAATATGCA-3'
Rnu2-10 (U2)		Mouse	qPCR – infected cells (S28)	5'-TGGTATTGCAGGGCTAAGATCA-3'	5'-CAGTGCATCGTGGAGT-3'
Gm24265 (U4)		Mouse	qPCR – infected cells (S28)	5'-CTTTGCGCAGTGGCAGTATC-3'	5'-CCAATGCCGACTATATTGCAAGTC-3'
Rnu5g (U5)		Mouse	qPCR – infected cells (S28)	5'-CCTTGTCAGACAAGGCCTC-3'	5'-CTCTGGTTTCTCTCAGATCGTATAAATC-3'
Gm25064 (U6)		Mouse	qPCR – infected cells (S28)	5'-CGCTTCGGCAGCACATATAC-3'	5'-AATATGGAACGCTTACGAATTTGC-3'
PSMC4	✓	Mouse	qPCR – RIG-I KD, bystander, time course, reassortant viruses, U5 KD	5'-CCCAGGAGGAGTGAAGCGG-3'	5'-GGTCGATGGTACTCAGGATGCC-3'
PUM1	✓	Mouse	qPCR – RIG-I KD, bystander, time course, reassortant viruses, U5 KD	5'-TGCCAGTCTCTCCAGCAGCA-3'	5'-TGATTTGGGGTCAAAGGACGTTGG-3'
TXNL4B	✓	Mouse	qPCR – RIG-I KD, bystander, time course, reassortant viruses, U5 KD	5'-CCCTCTACCGTATTTTCTCAATGGGC-3'	5'-AGTTTTCCCTCATCGCTCCCC-3'
S1		MRV	qPCR – RIG-I KD, bystander, time course, reassortant viruses, U5 KD	5'-AGCGCGCAGCCTAAATGGTT-3'	5'-ACGTAGATGCCGGTCTGCT-3'
M1		MRV	qPCR – RIG-I KD, bystander, time course, reassortant viruses, U5 KD, RIP-ddPCR	5'-GGTCGGATGGATCCTCGCCT-3'	5'-TCGAGTCCCTGGGTGATCCG-3'

Target	Housekeeping gene	Species	Assays	Primers	
				Fw	Rv
ABI1		Human	RIP-ddPCR	5'-TCAGAAACCGCAAGTCTCTCC-3'	5'-GCTGACTCCAAGCCTAGCAGG-3'
ACTB		Human	RIP-ddPCR	5'-AACCCCAAGGCCAACCGCA-3'	5'-GGCCAGAGGCGTACAGGGATAG-3'
ALKBH1		Human	RIP-ddPCR	5'-GGGGTCATCGACTTCTCGGC-3'	5'-CACTTGCTGACGGGCTGAAGAC-3'
CFLAR		Human	RIP-ddPCR	5'-GGCAGAGATTGGTGAGGATTTGGA-3'	5'-CCAACTCAACCACAAGTCCAAGA-3'
GAPDH		Human	RIP-ddPCR	5'-CGAGCCACATCGCTCAGACAC-3'	5'-ATGGCAACAATATCCACTTTACCAGAGT-3'
HNRNPA2B1		Human	RIP-ddPCR	5'-GCAGGAAGTTCAGAGTTCTAGGAGTG-3'	5'-AAATTTCCACGCCACCACG-3'
IL34		Human	RIP-ddPCR	5'-GCCCTTGACGAGAATGAGGAG-3'	5'-ACGTTGGCGATTCTGAACACCC-3'
MRPL19	✓	Human	RIP-ddPCR	5'-AAGGAGAAAAGTACTCCACATTCAGAG-3'	5'-TGGGTGAGCTGTAGTAACACGA-3'
RNU1-1		Human	RIP-ddPCR	5'-TCACGAAGGTGGTTTCCA-3'	5'-GAACGCAGTCCCCACTACC-3'
RNU2-1		Human	RIP-ddPCR	5'-TTTTGGCTAAGATCAAGTGTAG-3'	5'-AGCTCCTATTCATCTCCCT-3'
RNU4-1		Human	RIP-ddPCR	5'-CAGTATCGTAGCCAATGAGGTC-3'	5'-TGTCAAAAATTGCCAGTGC-3'
RNU5D-1		Human	RIP-ddPCR	5'-GCTCTGGTTTCTCTTCAAATC-3'	5'-AAAAATTTGCTTGAAACTCAA-3'
RNU6-1		Human	RIP-ddPCR	5'-TGCTCGCTTCGGCAGCAC-3'	5'-ATGGAACGCTTACGAATTTGC-3'
SERBP1		Human	RIP-ddPCR	5'-AAGACCAGAAAGGCGACCACCT-3'	5'-GCCCTTCGACTCTTCCA-3'
TBP		Human	RIP-ddPCR	5'-GGGTGCTCGACTTCTCGGC-3'	5'-CACTTGCTGACGGGCTGAAGAC-3'

Table S2. *Primers and peaks analyzed by AS-PCR in mouse cells*

Gene	Primers		ASE present in this region	Expected peak(s) (bp)	Detected peak(s) (bp)	ASE quantified	Corresponding detected peak(s) (bp)
	Fw	Rv					
ABI1	5'-TGGAAGTAGTG GAGGAAGCGGA-3'	5'-GGTGGTGGTG GAGTTGGGCTAT-3'	Multiple exon cassette (2) 3'-SS	129, 303, 306, 390, 393	138, 313, 366, 424, 468, 564, 688, 894	Exon cassette	313, 424
ALKBH1	5'-GGAAGCTTTTC CGTTCTACCG-3'	5'-GTTCAAGTCCC ACCCTCTCGG-3'	Multiple exon cassette (2)	180, 318, 391	191, 323, 419	Multiple exon cassette (2)	191, 323
CDKN2AIP	5'-GCTCCAATCC ATACCACACGA-3'	5'-AACAAATGAC GCTGAACCACG-3'	5'-SS	371, 402	388, 425, 482	5'-SS	388, 425
CFLAR	5'-CAGAGTGAGGC GGTTTGACCTT-3'	5'-TGGACTGGGTG TACTTCTGGAT-3'	Exon cassette	238, 344, 704, 869	244, 355	Exon cassette	244, 355
EIF4A2	5'-GGGATTGACG TGCAACAAGTG-3'	5'-CCACACCTTTCC TCCCAATCG-3'	Exon cassette Intron retention	112, 219, 928	115, 232, 243, 264, 302	Exon cassette	115, 232
HNRNPA2B1	5'-ATGGATACGGA AGTGGACGTGG-3'	5'-TCTGCTACCCC CAAAGTTTC-3'	Exon cassette	162, 282	170, 290, 549	Exon cassette	170, 290
IL34	5'-ACGTGAGTGA GCGAGACTTC-3'	5'-AAGCAGTTGTC CAGCAAGGCT-3'	Exon cassette	256, 374	272, 417	Exon cassette	272, 417
SERBP1	5'-AAGGCGAGTTGG AAGAAGACCC-3'	5'-TTCCCCAGTTGTG AGAGCCG-3'	Exon cassette Intron retention 5'-SS, 3'-SS	172, 341, 359, 470	356, 381, 443, 491	3'-SS	356, 381
TBP	5'-ACGGACAACCTGC GTTGATTTTC-3'	5'-AGGAGAACAATT CTGGGTTGATCA-3'	Exon cassette	120, 288	121, 288, 481	Exon cassette	121, 288

Table S3A. *Primers and peaks analyzed by AS-PCR in human cells - AS minigene reporters*

Gene	Primer		ASE present in this region	Expected peak(s) (bp)	Detected peak(s) (bp)	ASE quantified	Corresponding detected peak(s) (bp)
	Fw	Rv					
ALKBH1	5'-GGAAGCTTTTC CGTTCTACCG-3'	5'-TAGAAGGCACA GTCGAGG-3'	Multiple exon cassette (2)	284, 422, 495	284, 426, 489	Exon cassette	284, 422
CFLAR	5'-CAGAGTGAGGC GGTTTGACCTT-3'	5'-TAGAAGGCACA GTCGAGG-3'	Exon cassette	294, 400	292, 420	Exon cassette	292, 420
HNRNPA2B1	5'-ATGGATACGGA AGTGGACGTGG-3'	5'-TAGAAGGCACA GTCGAGG-3'	Exon cassette	201, 362	241, 255, 400	Exon cassette	255, 400
TBP	5'-ACGGACAACCTGC GTTGATTTTC-3'	5'-TAGAAGGCAC AGTCGAGG-3'	Exon cassette	173, 376	219, 392	Exon cassette	219, 392
SERBP1	5'-GGTGAAGGAG GTGAATTTTCAGT TGATAG-3'	5'-TAGAAGGCACA GTCGAGG-3'	Exon cassette Intron retention 5'-SS, 3'-SS	304, 322	298, 331	3'-SS	298, 331

Table S3B. *Primers and peaks analyzed by AS-PCR in human cells – Endogenous human ASE*

Gene	Primer		ASE present in this region	Expected peak(s) (bp)	Detected peak(s) (bp)	ASE quantified	Corresponding detected peak(s) (bp)
	Fw	Rv					
ABI1	5'-TCGAGAAAACA GTGGTAGCAGT-3'	5'-CGGTGGAGTTG GACTATCAGCA-3'	Multiple exon cassette 3'-SS	100, 181, 187, 268, 274, 277, 355, 358, 361, 364, 442, 445, 491	105, 283, 360, 395, 458, 473, 667	Multiple exon cassette	105, 395
CDKN2AIP	5'-CAAAGTGACA GATGCTCCAACC-3'	5'-TGGCAGAGGTT TTTGCGTGATC-3'	5'-SS	139, 170	150, 187, 274, 284	5'-SS	150, 187
SERBP1	5'-AGACGAGTTGG AAGAAGACCTG-3'	5'-TTCCCCAGTTGT GAGATCCGC-3'	3'-SS	340, 358	179, 372, 393, 498, 599	3'-SS	372, 393

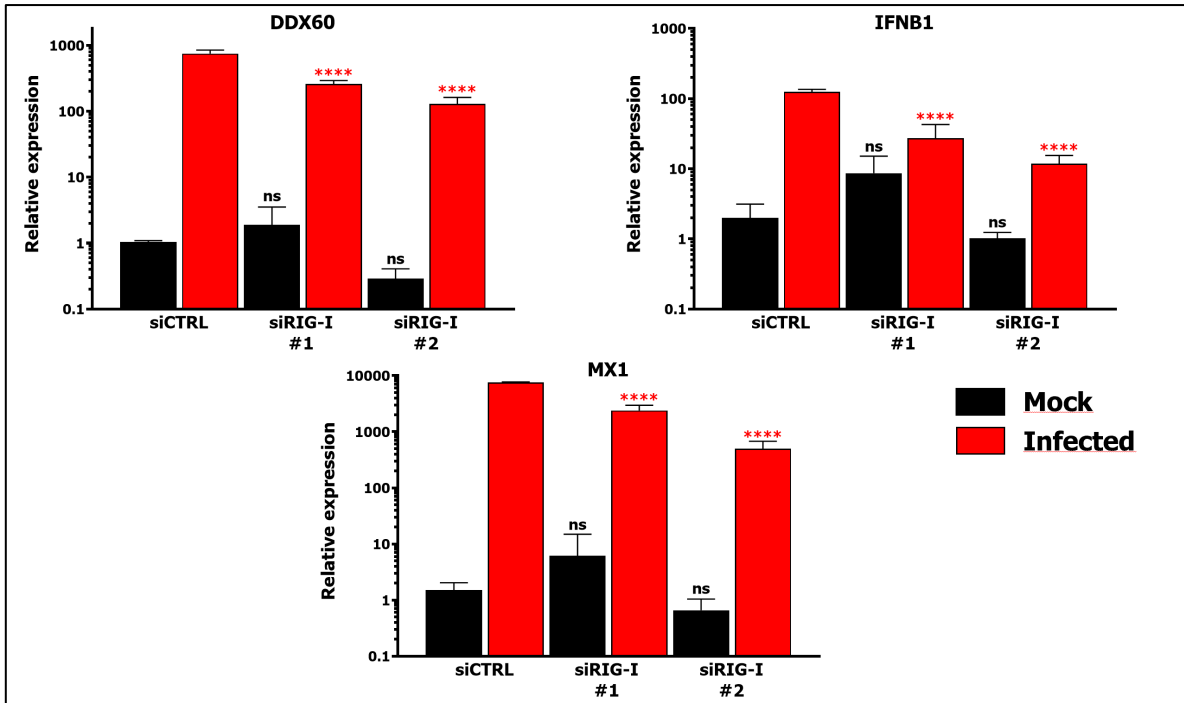
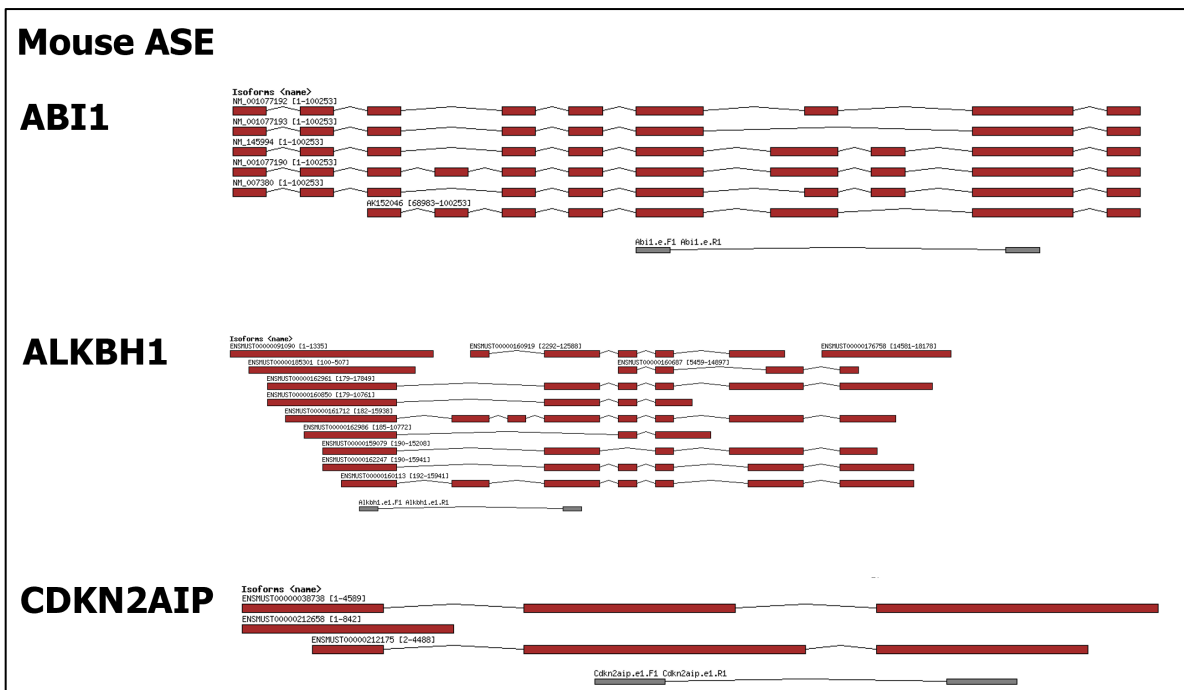
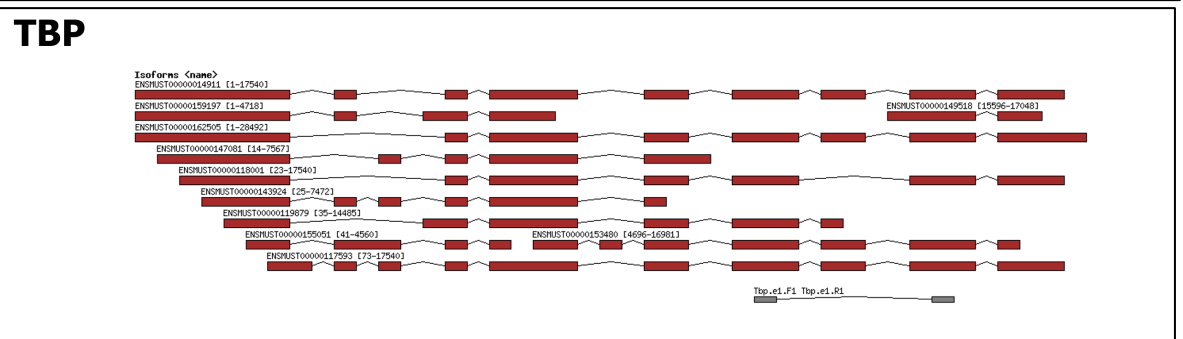
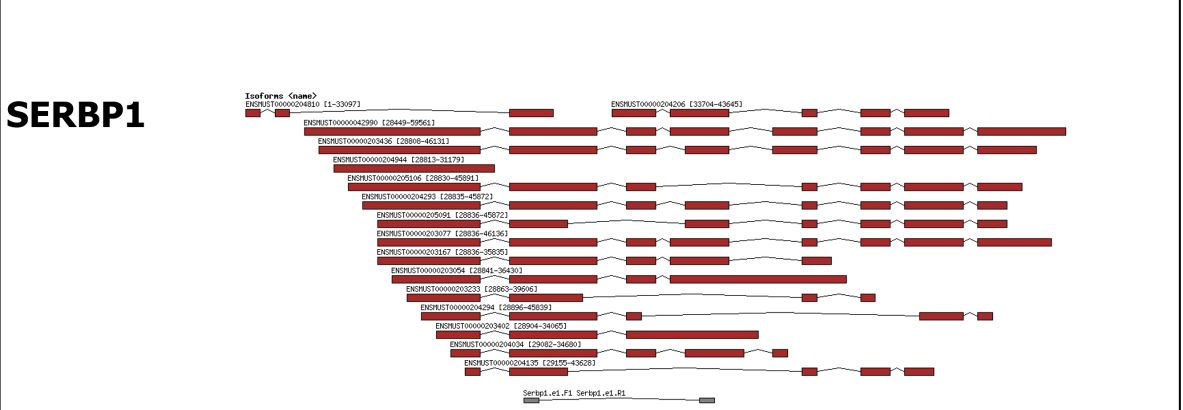
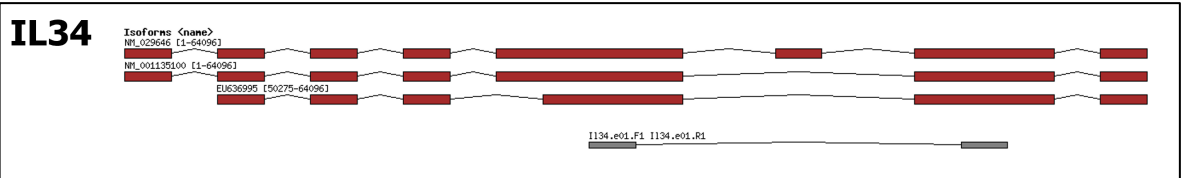
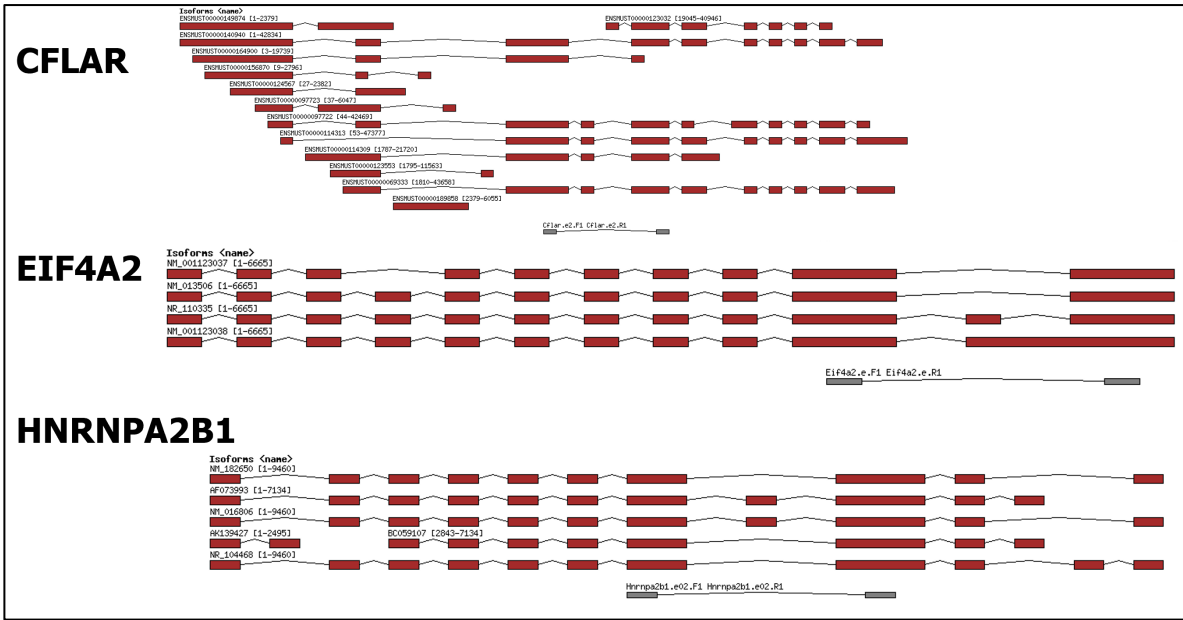


Figure S1. *Relative mRNA levels for IFNB1, DDX60, and MX1 in siCTRL and siRIG-I mock and infected L929 cells.* siRNA were transfected using RNAiMAX, and 56 h post-transfection, cells were infected with MRV (T3D<sup>S</sup>) at a MOI of 50, or mock-infected. Cells were further incubated for 16 h before RNA was harvested using Qiazol, reverse-transcribed, and subjected to qPCR for IFNB1, DDX60, and MX1 with PSMC4, PUM1, and TXNL4B used as housekeeping genes. The first replicate in the mock siCTRL condition was fixed at 1, and the relative mRNA expression was calculated for all other samples relative to that one. n=3, biological replicates, two-way ANOVA with Dunnett's multiple comparisons test against the siCTRL condition for mock (in black) or infected cells (in red); (ns, P>0.05; \*\*\*\*, P≤0.0001).







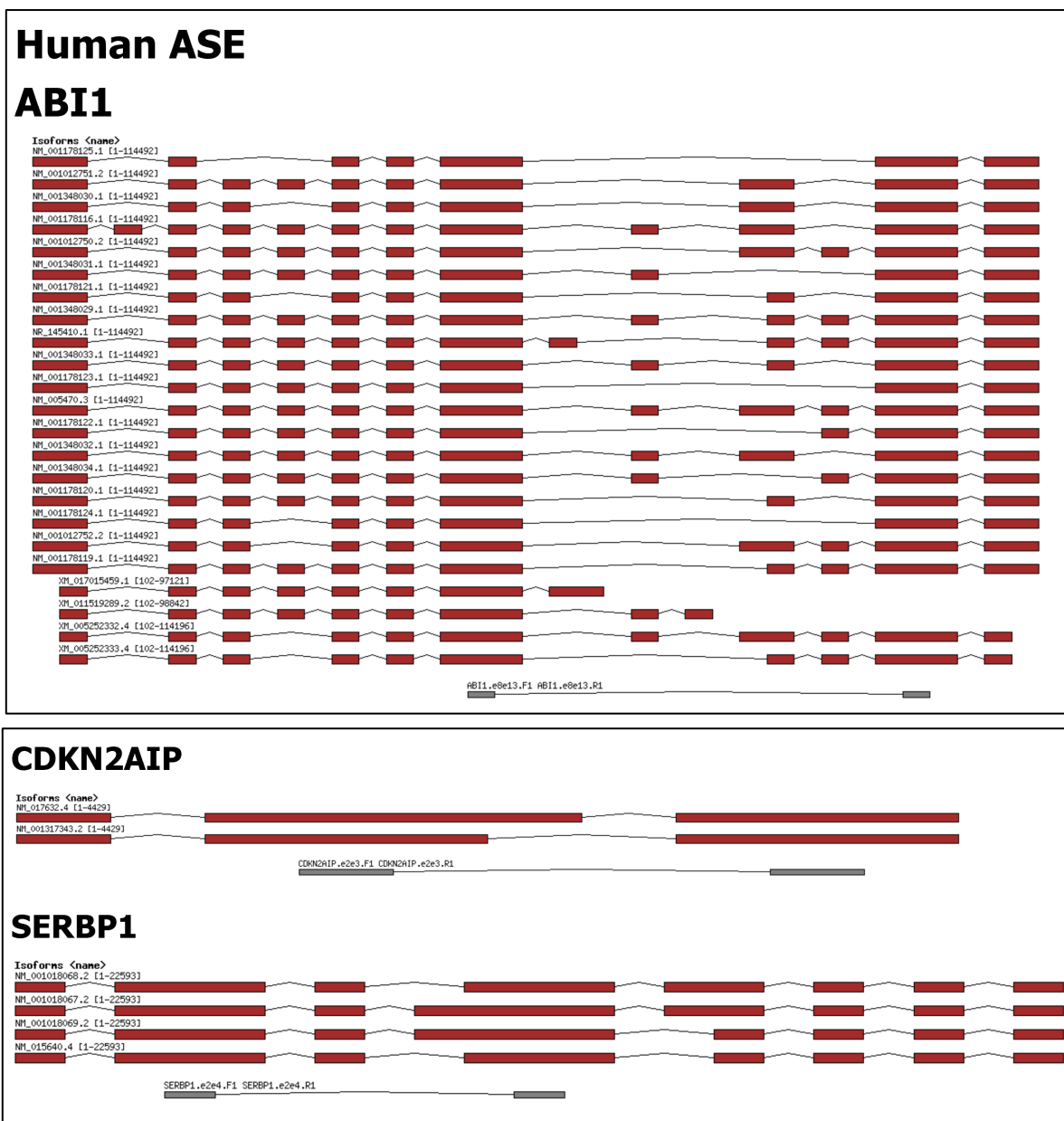


Figure S2. Design maps for the ASE analyzed by AS-PCR in mouse and human cells. All RNA isoforms for each gene is depicted, with the region alternatively spliced where the primers bind. The ENSEMBL assembly MM88.GRCm38 (mouse) and Hg38.p12.109.20191206 (human) were used to generate the maps.

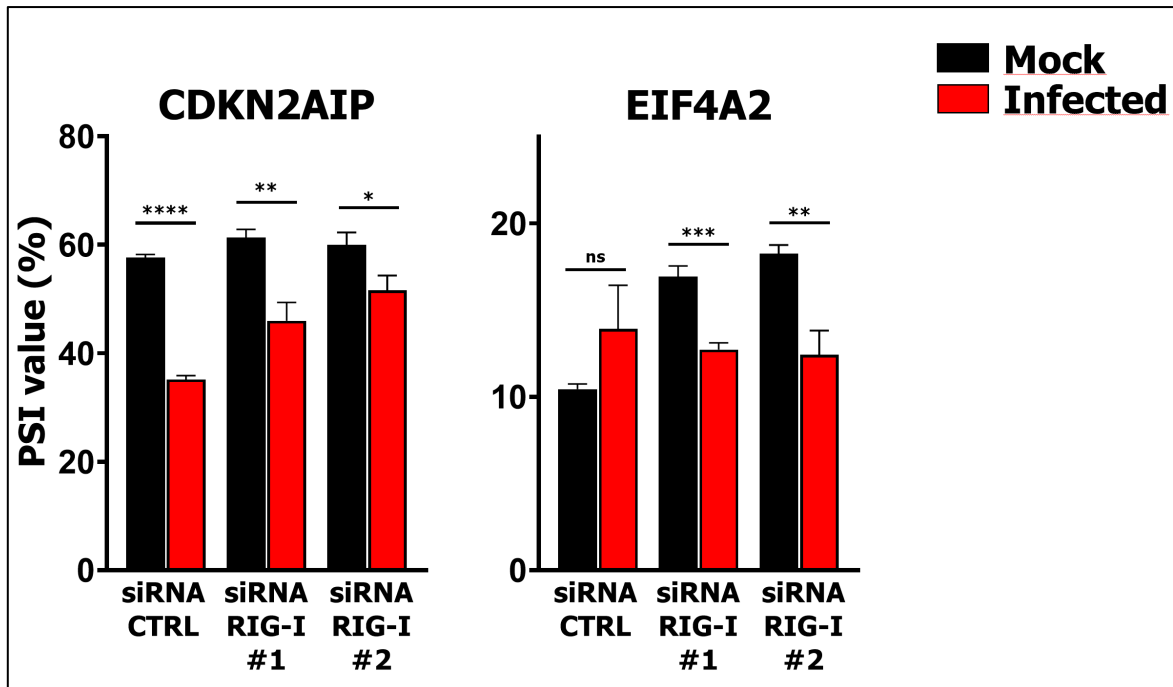


Figure S3. Splicing profiles of the *CDKN2AIP* and *EIF4A2* ASE in *siCTRL* and *siRIG-I* mock and infected L929 cells. siRNA were transfected using RNAiMAX, and 56 h post-transfection, cells were infected with MRV (T3D<sup>5</sup>) at a MOI of 50, or mock-infected. Cells were further incubated for 16 h before RNA was harvested using Qiazol, reverse-transcribed, and subjected to AS-PCR for the *CDKN2AIP* and *EIF4A2* ASE. PCR amplicons were resolved using capillary electrophoresis and quantified using relative fluorescence. n=3, biological replicates, unpaired two-tailed Student's t-test (ns, P>0.05; \*, P≤0.05; \*\*, P≤0.01; \*\*\*, P≤0.001; \*\*\*\*, P≤0.0001).

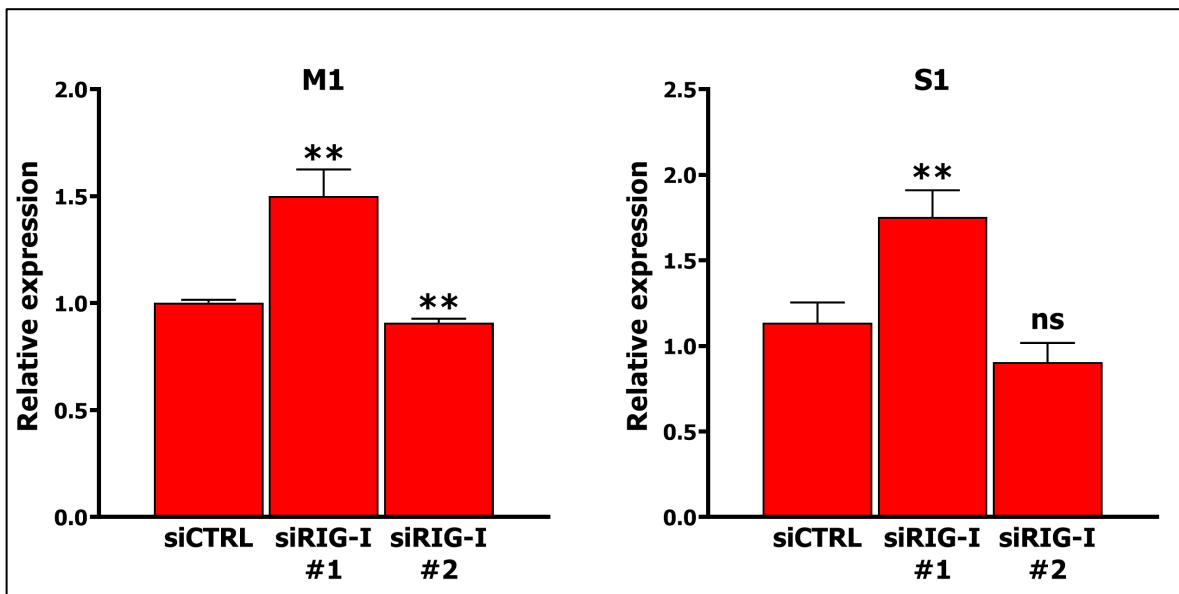


Figure S4. Relative mRNA levels for *S1* and *M1* viral genes in *siCTRL* and *siRIG-I* mock and infected L929 cells. siRNA were transfected using RNAiMAX, and 56 h post-transfection, cells were infected with MRV (T3D<sup>5</sup>) at a MOI of 50. Cells were further incubated for 16 h before RNA was harvested using Qiazol, reverse-transcribed, and subjected to qPCR for the *S1* and *M1* viral gene segment with *PSMC4*, *PUM1*, and *TXNL4B* used as housekeeping genes. The first replicate in the *siCTRL* condition was fixed at 1 and the relative mRNA expression was calculated for all other samples relative to that one. n=3, biological replicates, unpaired two-tailed Student's t-test (ns, P>0.05; \*\*, P≤0.01).

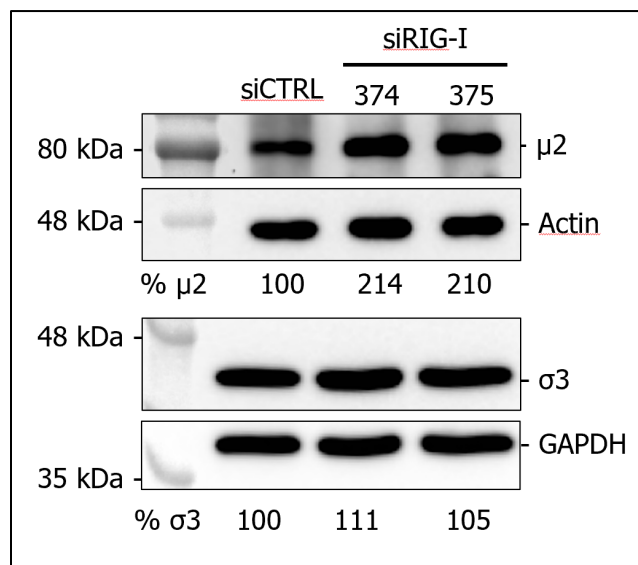


Figure S5. *Viral protein levels for  $\sigma 3$  and  $\mu 2$  in siCTRL and siRIG-I infected L929 cells.* siRNA were transfected using RNAiMAX, and 56 h post-transfection, cells were infected with MRV (T3D<sup>S</sup>) at a MOI of 50. Cells were further incubated for 16 h before being lysed in RIPA. Protein lysates were dosed by Bradford assay, and western blots against  $\sigma 3$  and  $\mu 2$  were realized. Membranes were H<sub>2</sub>O<sub>2</sub>-inactivated and probed against the loading controls actin ( $\mu 2$ ) and GAPDH ( $\sigma 3$ ). The relative protein level was calculated using Image J.

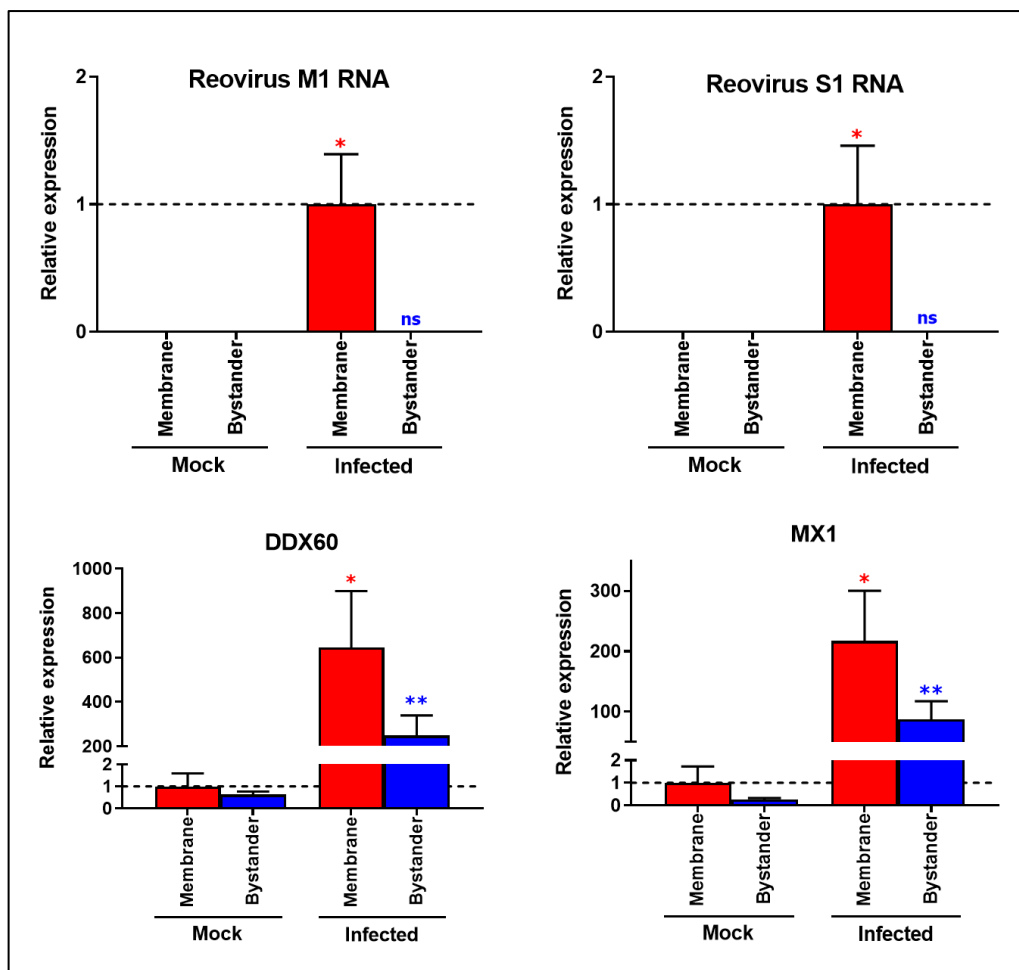


Figure S6. Relative mRNA level for the S1 and M1 viral RNA and two ISG (DDX60 and MX1) by qPCR as controls for the bystander experiment. RNA was harvested at 16h post-infection from either the membrane (top, red) or the bystander (bottom, blue) cells when the top layer was infected or mock-infected with MRV (T3D<sup>5</sup>) at a MOI of 50. PSMC4, PUM1, and TXNL4B were used as housekeeping genes for normalization. n=3, biological replicates, unpaired two-tailed Student's t-test comparing membrane (in red) and bystander (in blue; ns, P>0.05; \*, P≤0.05; \*\*, P≤0.01).

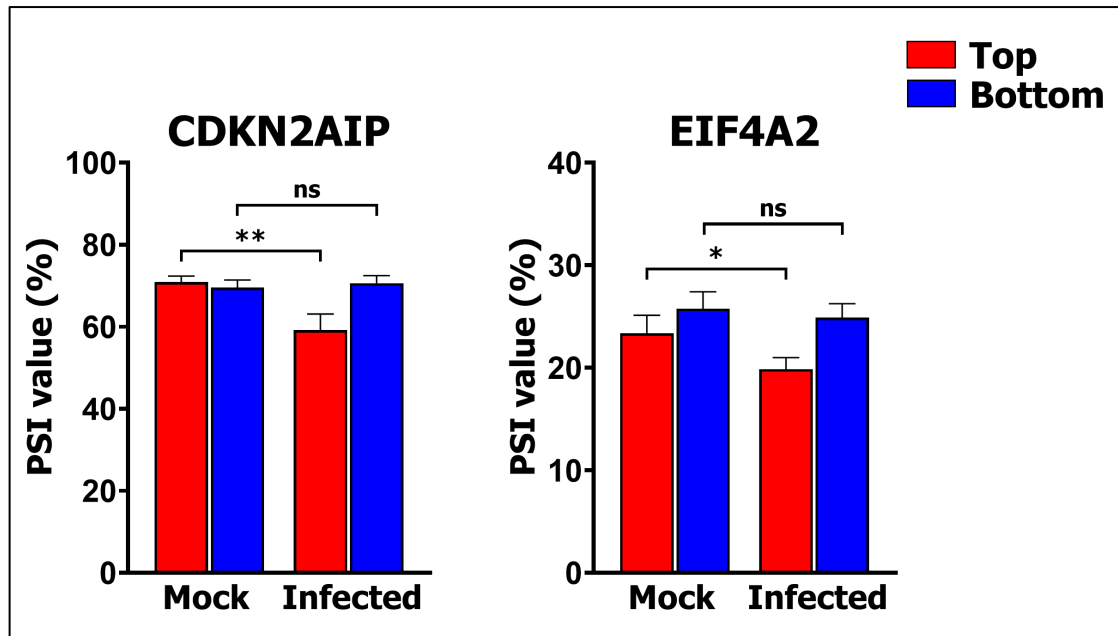


Figure S7. Splicing profiles of the *CDKN2AIP* and *EIF4A2* ASE in the bystander experiment. RNA was harvested at 16 h post-infection from either the membrane (red) or the bystander (blue) cells when the top layer was infected or mock-infected with MRV (T3D<sup>5</sup>) at a MOI of 50. n=3, biological replicates, unpaired two-tailed Student's t-test (ns, P>0.05; \*, P≤0.05; \*\*, P≤0.01; \*\*\*, P≤0.001; \*\*\*\*, P≤0.0001).

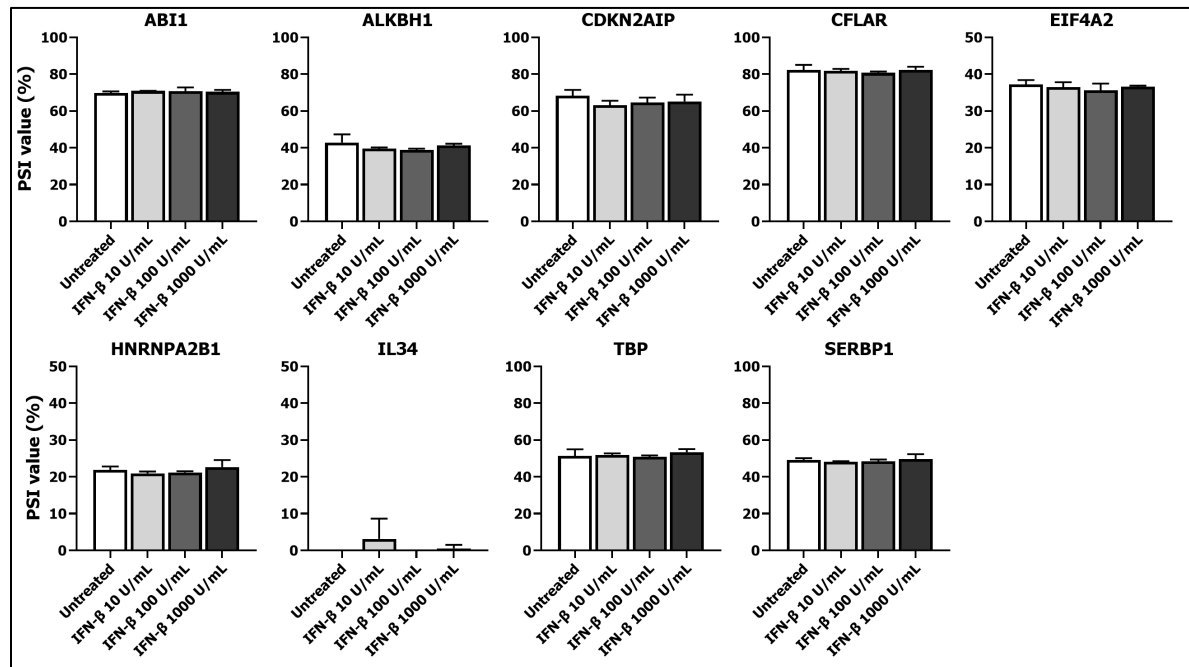


Figure S8. Impact of *IFN-β* treatment on the studied ASE. L929 cells were plated at  $2.5 \times 10^5$  cells per well in 12-well plates, and treated the following morning with 10, 100 or 1,000 U/mL of recombinant mouse interferon beta (PBL Assay Science, #12401-1) for 5 h. RNA was extracted using Qiazol, reverse-transcribed, and subjected to AS-PCR for the different ASE analyzed. PCR amplicons were resolved using capillary electrophoresis and quantified using relative fluorescence. All treated results were not statistically different from the untreated condition using an unpaired two-tailed Student's t-test. n=3, biological replicates.

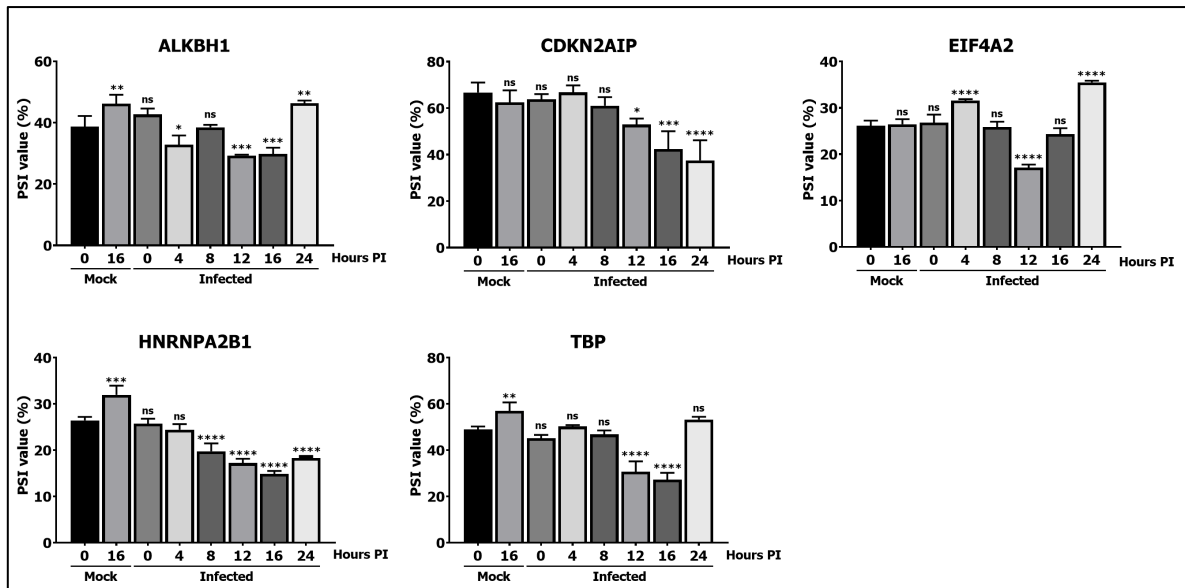


Figure S9. *Splicing profiles of additional ASE modulated by reovirus throughout infection.* L929 cells were infected with T3D<sup>S</sup> at a MOI of 50, RNA was extracted at indicated time point using Qiazol, reverse-transcribed, and subjected to AS-PCR for the different ASE analyzed. PCR amplicons were resolved using capillary electrophoresis and quantified using relative fluorescence. n=3, biological replicates, one-way ANOVA with Dunnett's multiple comparisons test against the 0 h mock condition (ns, P>0.05; \*, P≤0.05; \*\*, P≤0.01; \*\*\*, P≤0.001; \*\*\*\*, P≤0.0001).

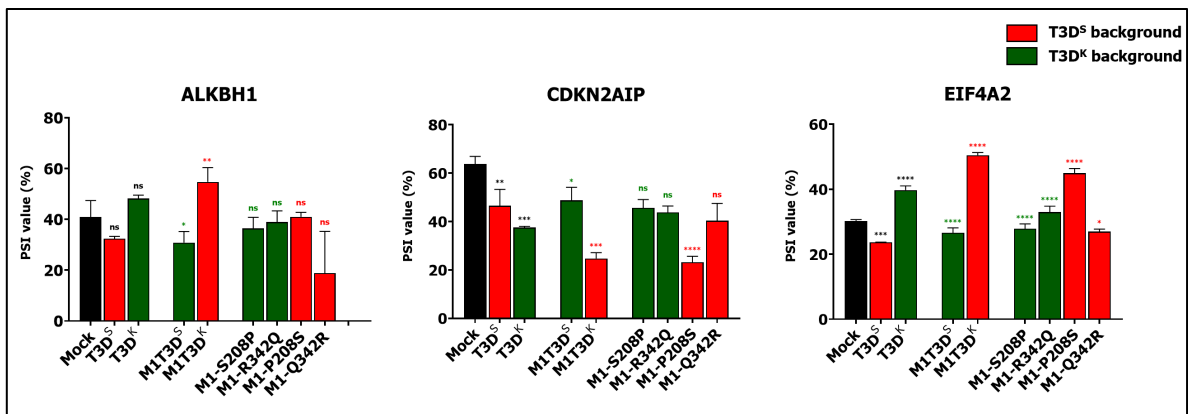


Figure S10. *Splicing profiles of the ALKBH1, CDKN2AIP, and EIF4A2 ASE upon infection with all wild-type/reassortant/single amino acid mutant MRV viruses.* Single amino acid mutants, M1T3D<sup>K</sup>[T3D<sup>S</sup>], and M1T3D<sup>S</sup>[T3D<sup>K</sup>] reassortant viruses were rescued by reverse genetics. L929 cells were infected with respective reovirus at a MOI of 50, or mock-infected. RNA was extracted at 16 h PI using Qiazol, reverse-transcribed, and subjected to AS-PCR for the different ASE analyzed. PCR amplicons were resolved using capillary electrophoresis and quantified using relative fluorescence. n=3, biological replicates, one-way ANOVA with Dunnett's multiple comparisons test against the mock condition for T3D<sup>S</sup>/T3D<sup>K</sup> (in black); two-way ANOVA with Šídák's multiple comparisons test against the parental virus (T3D<sup>S</sup> in red and T3D<sup>K</sup> in green) for the reassortant and mutant viruses (ns, P>0.05; \*, P≤0.05; \*\*, P≤0.01; \*\*\*, P≤0.001; \*\*\*\*, P≤0.0001).

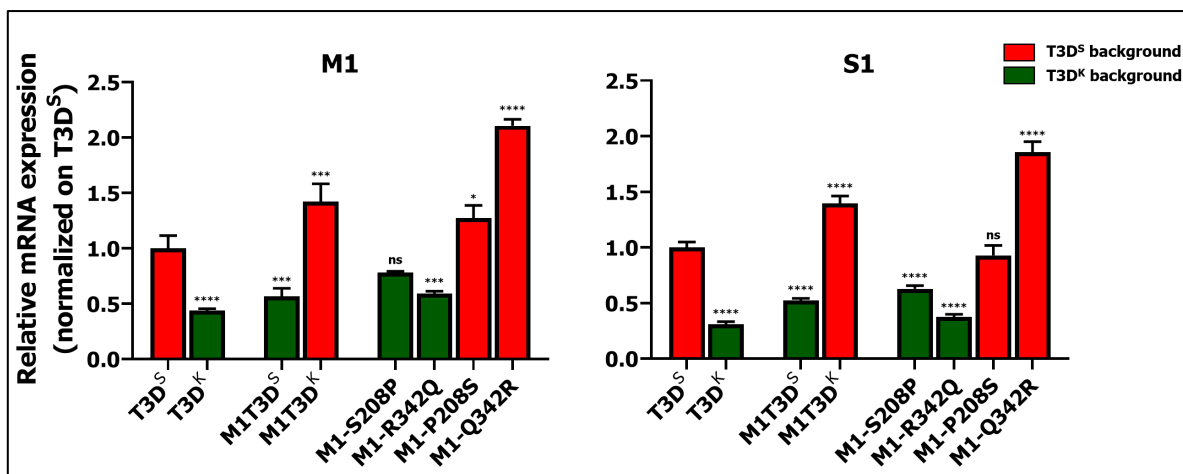


Figure S11. *Relative mRNA levels of S1 and M1 viral genes in all wild-type/reassortant/single amino acid mutant MRV viruses.* L929 cells were infected with the respective virus at a MOI of 50, RNA was extracted at 16 h PI using Qiazol, reverse-transcribed, and subjected to qPCR for either the M1 or S1 RNA with PSMC4, PUM1, and TXNL4B as housekeeping genes for normalization. Results were normalized against T3D<sup>S</sup>, to allow for an easier comparison of RNA levels between the different viruses. n=3, biological replicates, two-way anova with Tukey's multiple comparisons test where all groups were compared; results of the comparison against T3D<sup>S</sup> are shown (ns, P>0.05; \*, P≤0.05; \*\*\*, P≤0.001; \*\*\*\*, P≤0.0001).

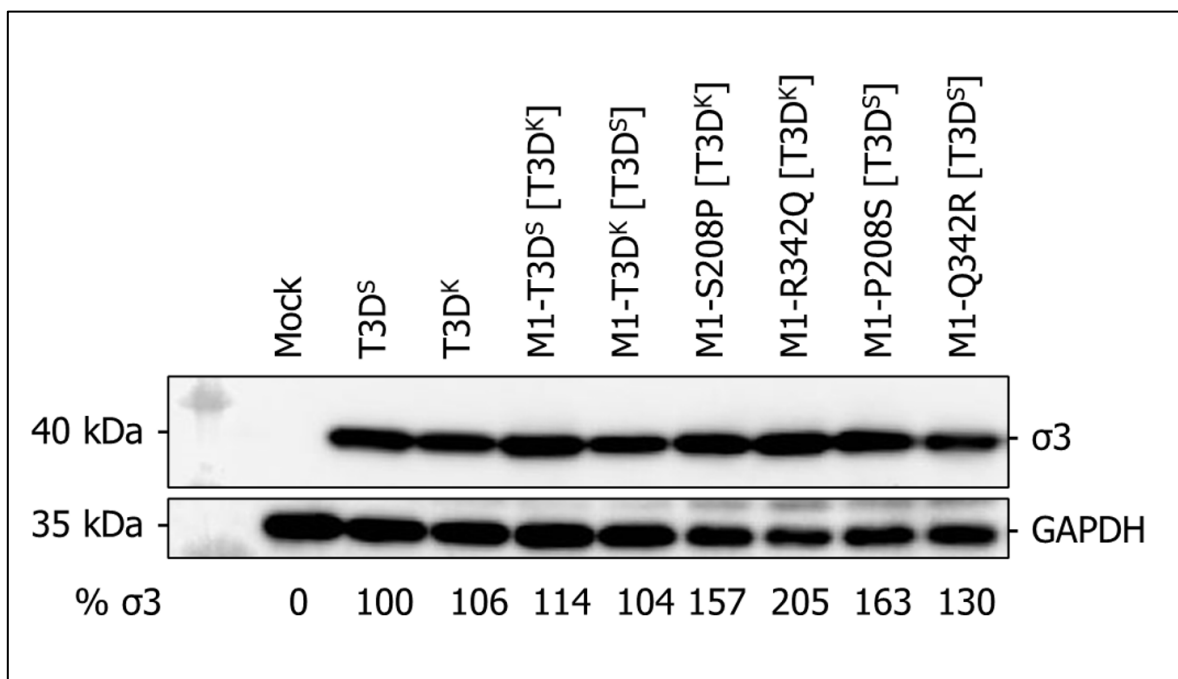


Figure S12. *Viral protein levels of  $\sigma_3$  in all wild-type/reassortant/single amino acid mutant MRV viruses.* L929 cells were infected with the respective virus at a MOI of 50 and incubated for 16 h before being lysed in RIPA. Protein lysates were dosed by Bradford assay and a western blot against  $\sigma_3$  was realized. The membrane was H<sub>2</sub>O<sub>2</sub>-inactivated and probed against the loading control GAPDH. Relative protein level was calculated using Image J.



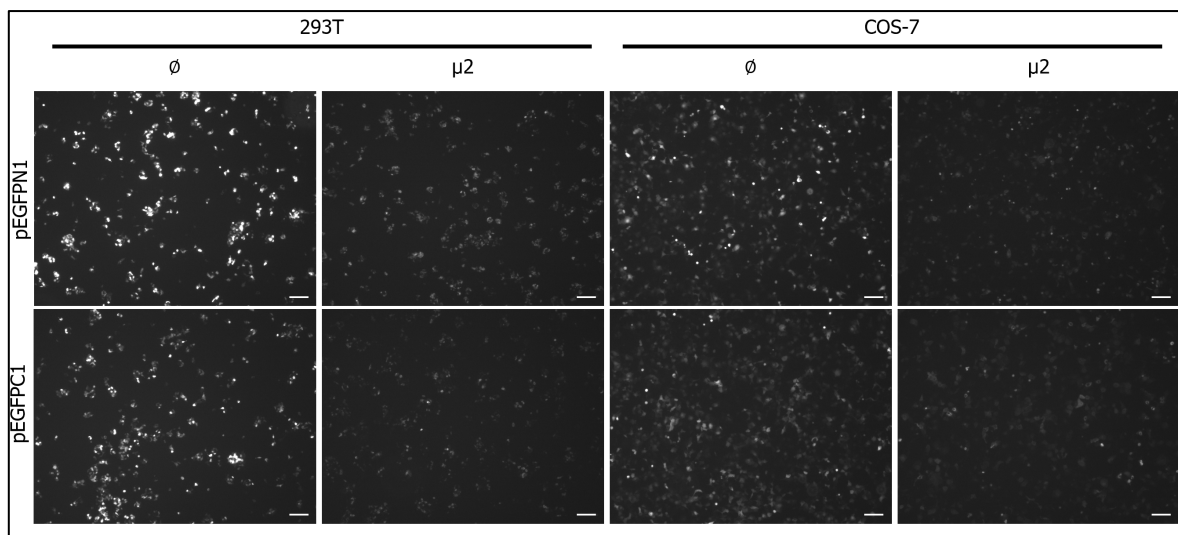


Figure S13. Live cell imaging of GFP alone or GFP-tagged  $\mu 2$  in SV40 large T antigen harboring 293T and COS-7 cells. Cells were transfected with either Lipofectamine2000 (293T cells) or LipofectamineLTX (COS-7) following the manufacturer's protocol and incubated for 24 h. Cells were then directly imaged using a Nikon TE2000E epifluorescence microscope at 488 nm, 4x objective and a 500 ms exposure time. The scale bars represent 100  $\mu\text{m}$ .

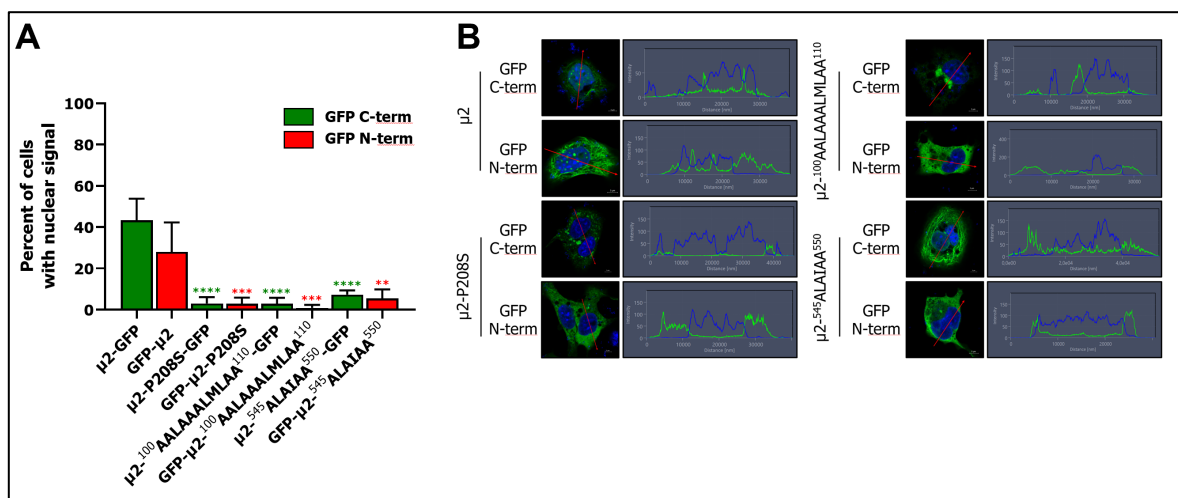


Figure S14. Quantification of the nuclear signal for the different  $\mu 2$  constructions. (A) Percent of COS-7 cells with clear nuclear signal over all cells presenting the expression of the  $\mu 2$  constructs. Cells were transfected for 24 h, and at least 10 fields for an average of 100 cells were quantified using epifluorescence microscopy. Fields were randomly separated into three groups to form three independent quantification replicates. Two-way ANOVA with Dunnett's multiple comparisons test against  $\mu 2$ -GFP (in green) or GFP- $\mu 2$  (in red) (\*\*,  $P \leq 0.01$ ; \*\*\*,  $P \leq 0.001$ ; \*\*\*\*,  $P \leq 0.0001$ ). (B) The histograms display the fluorescence intensity along the red arrow in the panels from Figure 4A and 4D. Scale bar, 5  $\mu\text{m}$ .

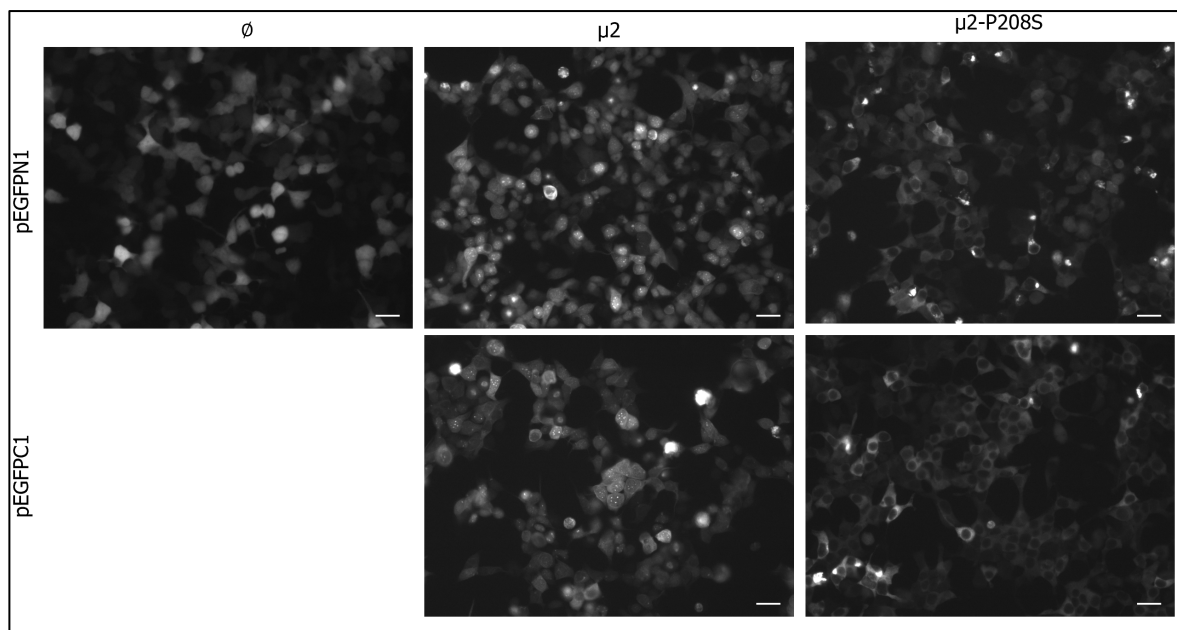


Figure S15. *Cellular localization of GFP- $\mu$ 2 constructs in 293T cells.* 293T cells were transfected with GFP-tagged  $\mu$ 2 or  $\mu$ 2-P208S using Lipofectamine2000, and directly imaged using epifluorescence microscopy 24 h after transfection. A Nikon TE2000E epifluorescence microscope was used with a 20X objective at 488 nm and a 100 ms exposure time.  $\emptyset$  denotes an empty control plasmid encoding only the GFP moiety. The scale bars represent 20  $\mu$ m.

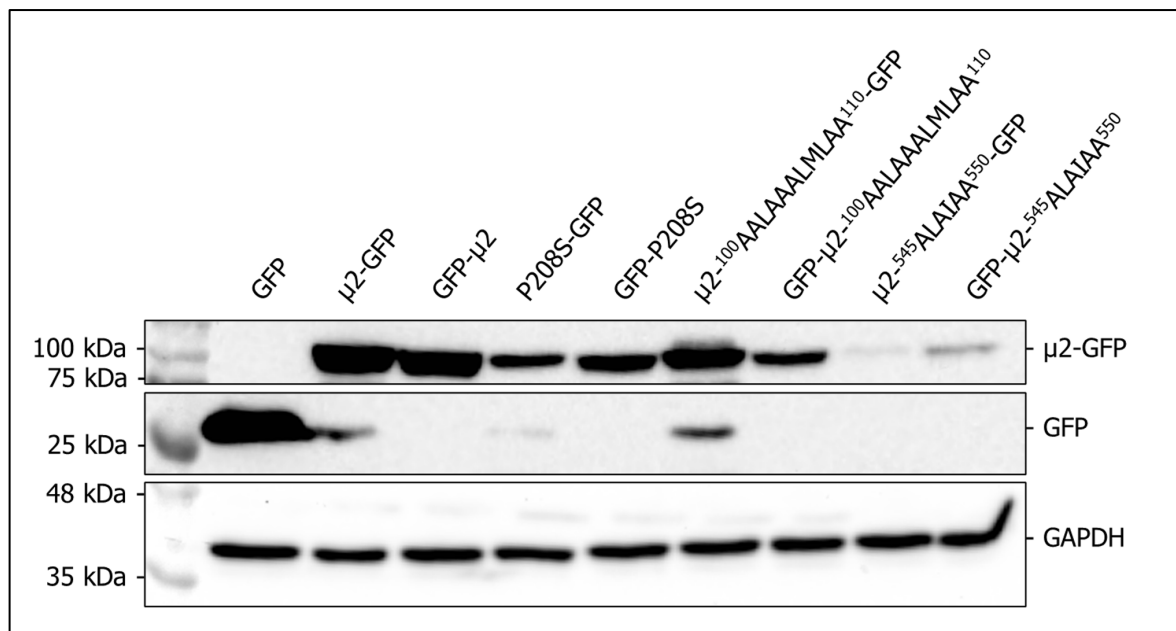


Figure S16. *Western blot validation of the expression of different  $\mu$ 2-GFP constructs.* 293T cells were transfected with Lipofectamine2000, incubated for 24 h before being lysed in RIPA. Soluble protein lysates were dosed by Bradford assay, and a western blot against GFP was realized. The membrane was  $H_2O_2$ -inactivated and probed against the loading control GAPDH.

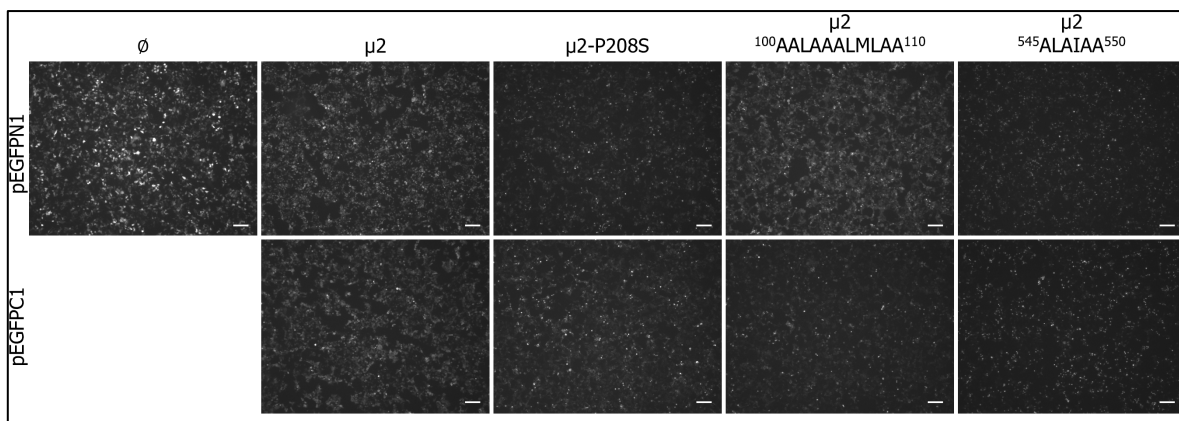


Figure S17. *Epifluorescence validation of the expression of different  $\mu 2$ -GFP constructs.* 293T cells were transfected with Lipofectamine2000, incubated for 24 h and directly imaged using epifluorescence microscopy. A Nikon TE2000E epifluorescence microscope was used with a 4X objective at 488 nm and a 500 ms exposure time.  $\emptyset$  denotes an empty control plasmid encoding only the GFP moiety. The scale bars represent 100  $\mu$ m.

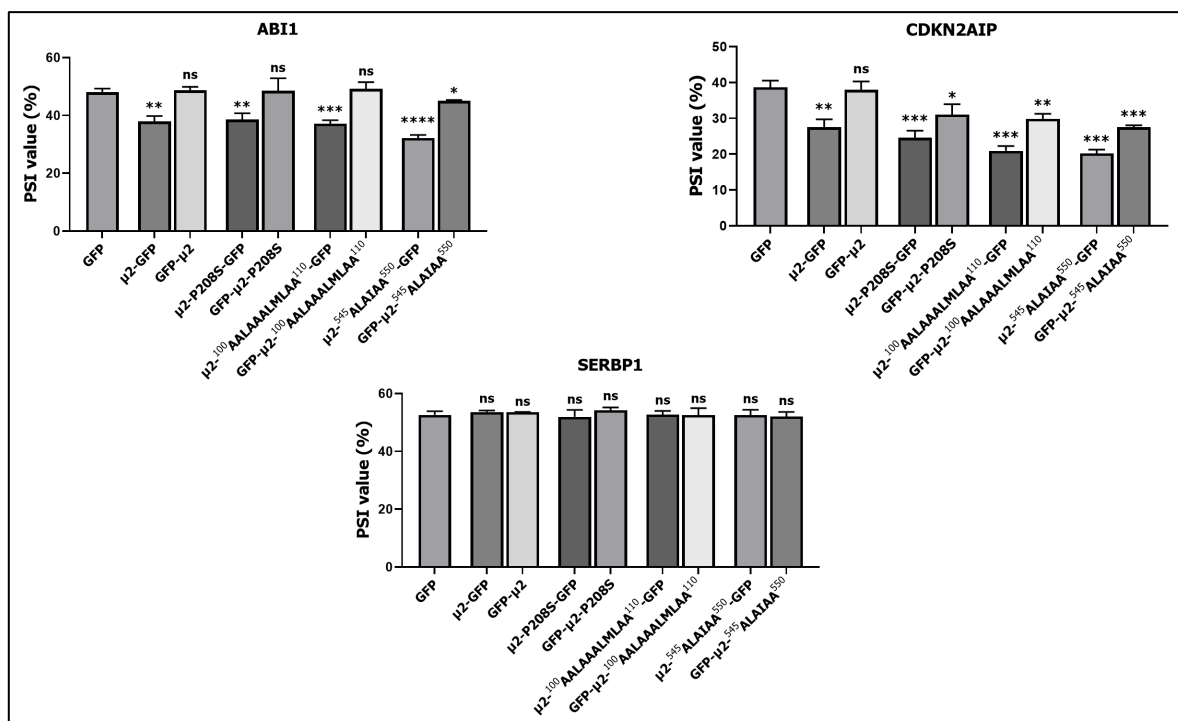


Figure S18. *Splicing profiles of endogenous human ASE in the ABI1, CDKN2AIP, and SERBP1 upon expression of different  $\mu 2$ -GFP constructs.* 293T cells were transfected with Lipofectamine2000, incubated for 24 h and RNA was extracted using Qiazol, reverse-transcribed, and subjected to AS-PCR for the different ASE analyzed. PCR amplicons were resolved using capillary electrophoresis and quantified using relative fluorescence. n=3, biological replicates, unpaired two-tailed Student's t-test (ns,  $P > 0.05$ ; \*,  $P \leq 0.05$ ; \*\*,  $P \leq 0.01$ ; \*\*\*,  $P \leq 0.001$ ; \*\*\*\*,  $P \leq 0.0001$ ) against the GFP alone condition.

MAYI AVPAVDSRSSEAI GLLSFGVDAGADANDVSYQDHDYVLDQLQYMLDGYEAGDVI  
 DALVHKNWLHHSVYCLLPKSQLLEYWKSNP SAI PDNVD**RRLRKRLMLKK**DLRKDDEYNQ  
 LARAFKISDVYAPLISSTTSPMTMIQN LNQGEIVYTTTDRVIGARILLYAPRKY YASTLS  
 FTMTKCIIPFGKEVGRVPHSRFNVGTF **P**SIATPKCFVMSGVDIESIPNEFIKLFYQRVKS  
 VHANILNDISPQIVSDMINRKRLRVHTPSDRRAAQLMHLPHYVVKRGASHVDVYKVDVDM  
 LFEVVDVADGLRNVSRKLTMHTV PVCILEMLGIEIADY CIRQEDGMLTDWFLLLTMLS DG  
 LTDRRTHCQYLINPSSVPPDVILNISITGF INRHTIDVMPDIYDFVKPIGAVLPKGSFKS  
 TIMRVLDSISILGIQIMPRAHVDSDEVGEQMEPTFEQAVMEIYKGIAGVDSLDDLIKWV  
 LNSDLIPHDDR LGQLFQAF LPLAKDLLAPMARKFYDNSMSEGRLLTFAHADSELLNANYF  
 GHLL**RRLKIPY**ITEVNL MIRKNREGGELFQLVLSYLYKMYATSAQPKWFGSLLRLLICPWL  
 HMEKLI GEADPASTSAEIGWHI PREQLMQDGWCGCEDGFIPYVSIRAPRLVIEELMEKNW  
 GQYHAQVIVTDQLVVGEP RRVSAKAVIKGNHLPVKLVSRFACFTLTAKYEMRLSCGHSTG  
 RGAAYSARLAFRSDLA

Figure S19. Sequence of the  $T3D^S$   $\mu 2$  protein and relevant potential NLS involved in the nuclear localization. Potential NLS are underlined and basic residues are shown bold. The P208 position is indicated in red.

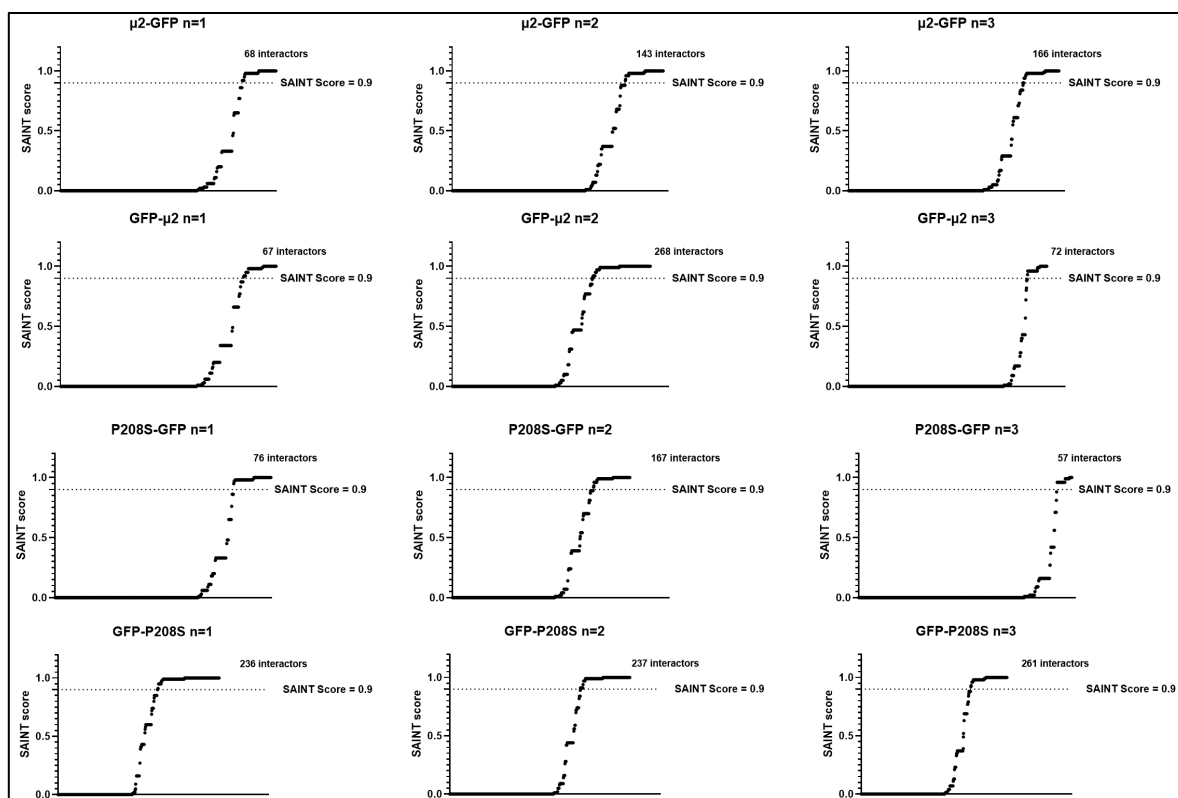


Figure S20. Individual SAINT scores for each IP-MS replicates. Each independent replicate was analyzed using SAINT against the corresponding control GFP IP. Identified proteins (x-axis) are sorted in increasing SAINT score (y-axis). SAINT scores above 0.9 were considered a hit; the number of hits for each independent replicates are depicted.



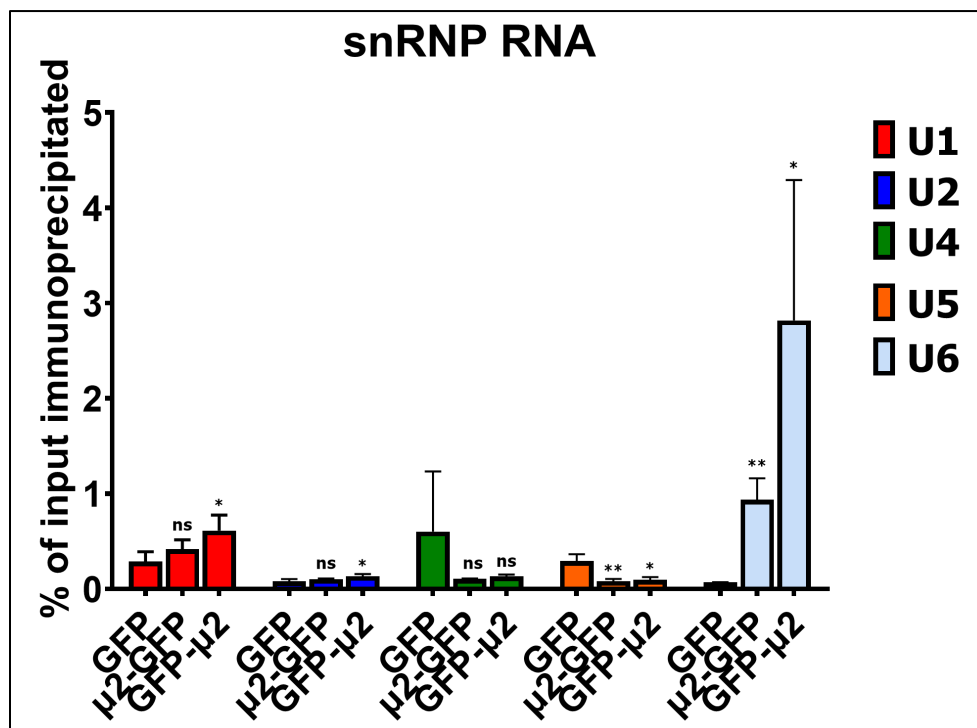


Figure S23. RIP-ddPCR of GFP,  $\mu$ 2-GFP and GFP- $\mu$ 2 assessing the immunoprecipitation of all spliceosomal snRNA. 293T cells were transfected with pEGFPN1 (GFP), pEGFPN1- $\mu$ 2 ( $\mu$ 2-GFP), or pEGFPC1- $\mu$ 2 (GFP- $\mu$ 2), and incubated for 24 h. RIP was performed as previously described (Boudreault et al. (2019) *Virology Journal* 16, pg. 29, reference 41 in the manuscript) and inputs and IP fractions were submitted to ddPCR. A percent of input immunoprecipitated was calculated based on quantity of the target before IP and after IP.  $n=3$ , biological replicates, unpaired two-tailed Student's t-test (ns,  $P>0.05$ ; \*,  $P\leq 0.05$ ; \*\*,  $P\leq 0.01$ ) against the GFP alone IP. Input fractions were normalized using the MRPL19 housekeeping gene.

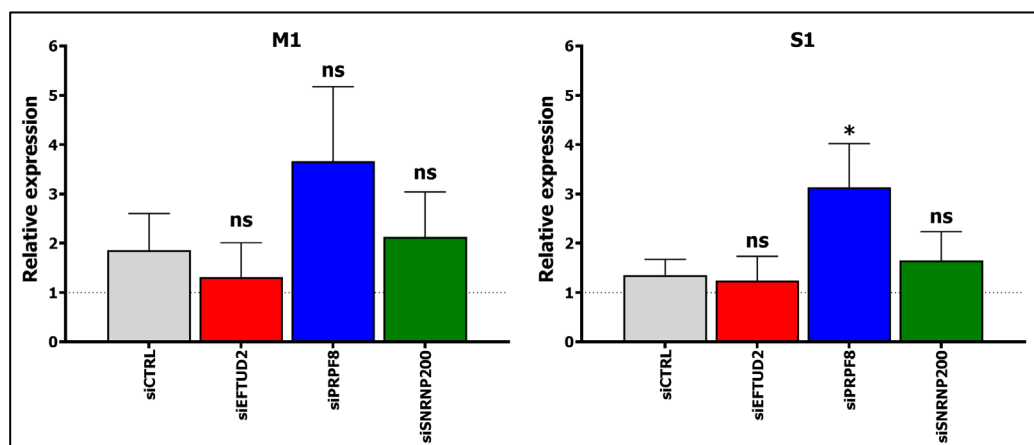


Figure S24. Relative mRNA levels for M1 and S1 viral genes during infection upon silencing of EFTUD2, PRPF8 and SNRNP200. L929 cells were transfected with the respective siRNA using RNAiMAX, and 56 h post-transfection, cells were infected with MRV (T3D<sup>S</sup>) at a MOI of 50. Cells were further incubated for 16 h before RNA was harvested using Qiazol, reverse-transcribed, and subjected to qPCR for the S1 and M1 viral gene segment with PSMC4, PUM1, and TXNL4B as housekeeping genes for normalization. The first replicate in the siCTRL condition was fixed at 1 and the relative mRNA expression was calculated for all other samples relative to that one.  $n=3$ , biological replicates, unpaired two-tailed Student's t-test (ns,  $P>0.05$ ; \*,  $P\leq 0.05$ ) against the siCTRL condition.

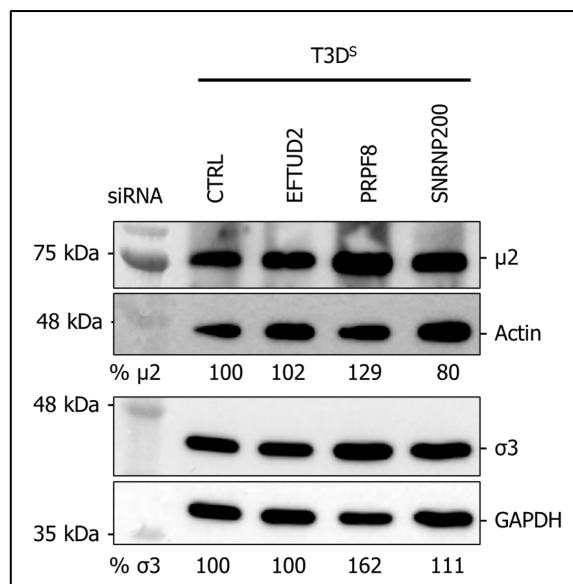


Figure S25. *Viral protein levels of  $\mu 2$  and  $\sigma 3$  during infection upon silencing of EFTUD2, PRPF8 and SNRNP200.* L929 cells were transfected with the respective siRNA using RNAiMAX, and 56 h post-transfection, cells were infected with MRV (T3D<sup>S</sup>) at a MOI of 50. Cells were further incubated for 16 h before being lysed in RIPA. Protein lysates were dosed by Bradford assay, and western blots against  $\sigma 3$  and  $\mu 2$  were realized. Membranes were H<sub>2</sub>O<sub>2</sub>-inactivated and probed against the loading controls actin ( $\mu 2$ ) and GAPDH ( $\sigma 3$ ). The relative protein level was calculated using Image J.

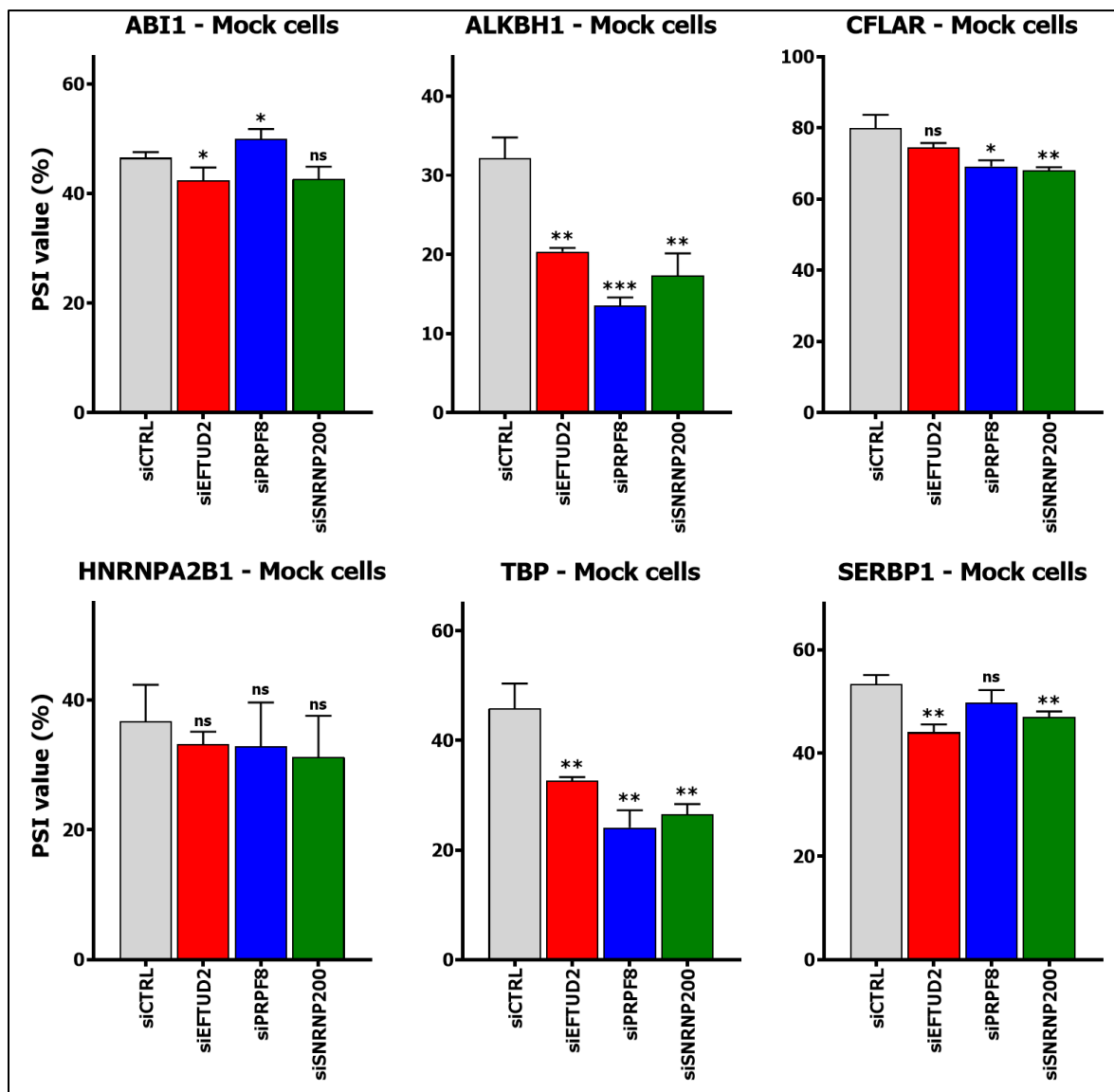


Figure S26. *Impact of silencing core U5 proteins EFTUD2, PRPF8, and SNRNP200 on cellular AS.* L929 cells were transfected with the respective siRNA using RNAiMAX, and 56 h post-transfection, cells were mock-infected, and further incubated for 16 h before RNA was harvested using Qiazol, reverse-transcribed, and subjected to AS-PCR for the different ASE analyzed. PCR amplicons were resolved using capillary electrophoresis and quantified using relative fluorescence. n=3, biological replicates, unpaired two-tailed Student's t-test (ns, P>0.05; \*, P≤0.05; \*\*, P≤0.01; \*\*\*, P≤0.001; \*\*\*\*, P≤0.0001) against the control siRNA condition.



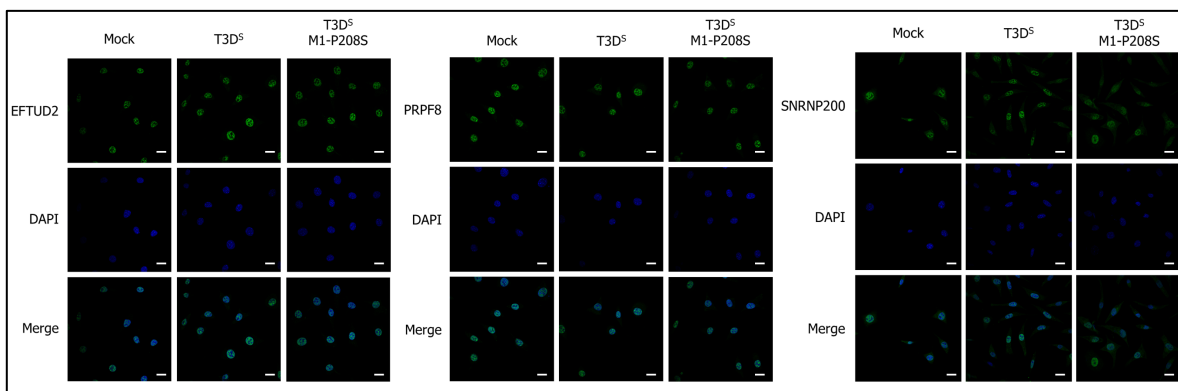


Figure S27. Immunofluorescence of U5 spliceosomal components *EFTUD2*, *SNRNP200*, and *PRPF8* in mock-, *T3D<sup>S</sup>*- and *T3D<sup>S</sup> M1-P208S*-infected cells. L929 cells were infected at a MOI of 50, fixed at 16 h post-infection and imaged using protein-specific antibodies against *EFTUD2*, *SNRNP200*, and *PRPF8* using standard immunofluorescence technique. Slides were imaged using a confocal Zeiss LSM 880 2-Photon microscope. The scale bars represent 20  $\mu$ m.

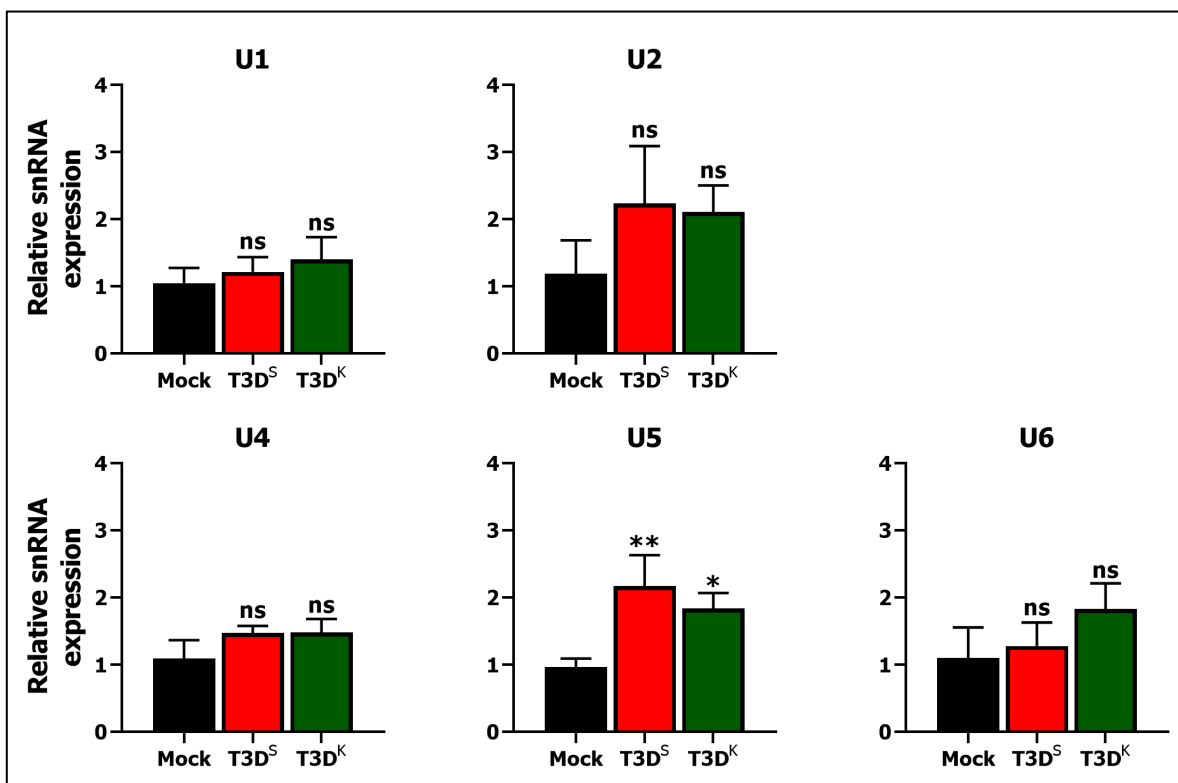


Figure S28. Relative RNA level for all spliceosomal snRNA upon infection with *T3D<sup>S</sup>* and *T3D<sup>K</sup>*. L929 cells were mock-infected or infected with MRV (*T3D<sup>S</sup>* or *T3D<sup>K</sup>*) at a MOI of 50, incubated for 16 h before RNA was harvested using Qiazol, reverse-transcribed, and subjected to qPCR for U1, U2, U4, U5, and U6 snRNA with *PSMC4*, *PUM1*, and *TXNL4B* used as housekeeping genes. The first replicate in the mock siCTRL condition was fixed at 1, and the relative mRNA expression was calculated for all other samples relative to that one.  $n=3$ , biological replicates, one-way ANOVA with Dunnett's multiple comparisons test against the mock condition (ns,  $P>0.05$ ; \*,  $P\leq 0.05$ ; \*\*,  $P\leq 0.01$ ).

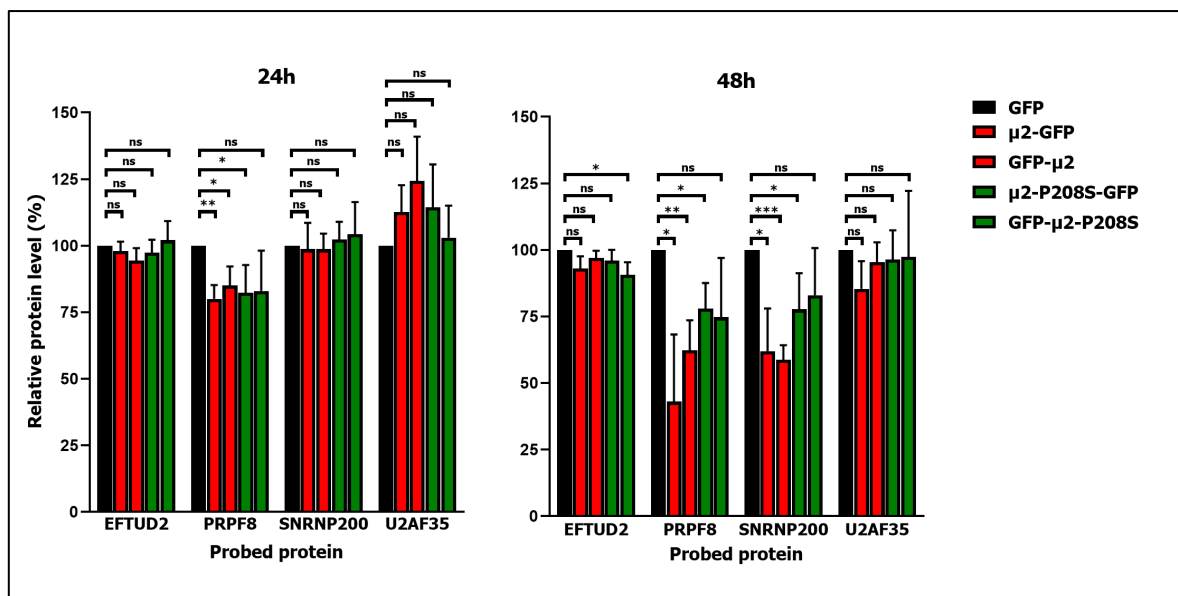


Figure S29. *Relative quantitation of U5 snRNP protein levels upon expression of different  $\mu$ 2-GFP constructs.* 293T cells were transfected with pEGFPN1 (GFP), pEGFPN1- $\mu$ 2 ( $\mu$ 2-GFP), pEGFPC1- $\mu$ 2 (GFP- $\mu$ 2), or P208S mutants and incubated for 24 h or 48 h before being lysed in RIPA. Protein lysates were dosed by Bradford assay, and western blots against EFTUD2, PRPF8, SNRNP200 or U2AF35 were realized. The membranes were H<sub>2</sub>O<sub>2</sub>-inactivated and probed again against actin (EFTUD2, U2AF35) or vinculin (PRPF8, SNRNP200) as a loading control. The cumulative results for three western blots are summarized in bar graph. The U2 auxiliary factor U2AF35 was probed as a control. n=3, biological replicates, unpaired two-tailed Student's t-test (ns, P>0.05; \*, P≤0.05; \*\*, P≤0.01; \*\*\*, P≤0.001) comparing against GFP alone control cells.

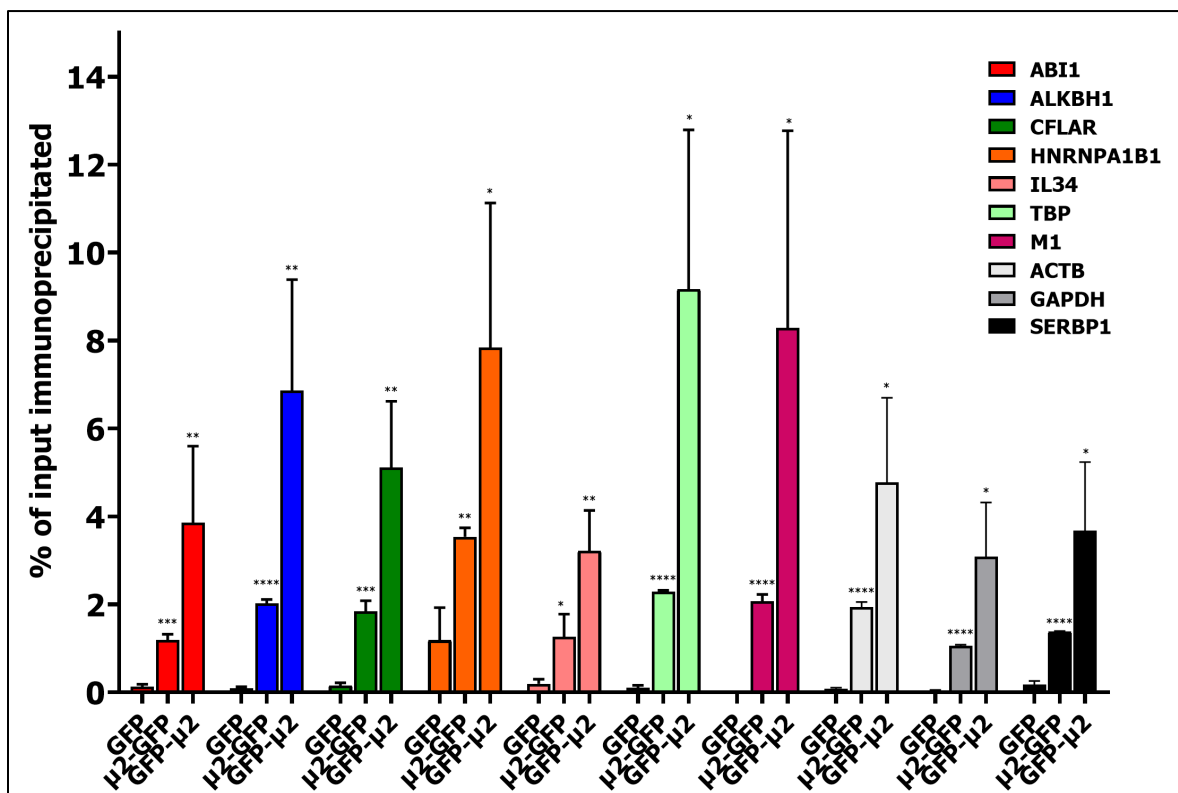


Figure S30. RIP-ddPCR of GFP,  $\mu$ 2-GFP, and GFP- $\mu$ 2 assessing the immunoprecipitation of cellular mRNA. 293T cells were transfected with pEGFPN1 (GFP), pEGFPN1- $\mu$ 2 ( $\mu$ 2-GFP), or pEGFPC1- $\mu$ 2 (GFP- $\mu$ 2), and incubated for 24 h. RIP was performed as previously described (Boudreault et al. (2019) *Virology Journal* 16, pg. 29, reference 41 in the manuscript) and both input and IP fractions were submitted to ddPCR. A percent of input immunoprecipitated was calculated based on quantity of the target before IP and after IP. Input fractions were normalized using the MRPL19 housekeeping gene. n=3, biological replicates, unpaired two-tailed Student's t-test (\*,  $P \leq 0.05$ ; \*\*,  $P \leq 0.01$ ; \*\*\*,  $P \leq 0.001$ ; \*\*\*\*,  $P \leq 0.0001$ ) against the GFP alone IP.

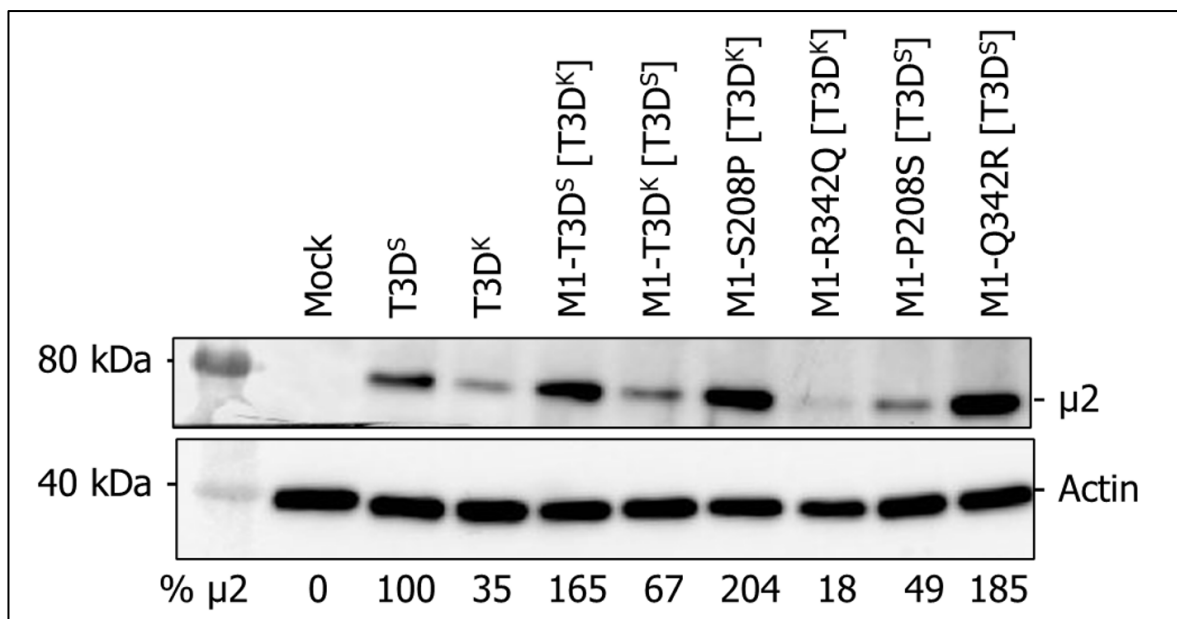


Figure S31.  $\mu 2$  protein levels in all wild-type/reassortant/single amino acid mutant MRV viruses. L929 cells were infected with the respective virus at a MOI of 50 and incubated for 16 h before being lysed in RIPA. Protein lysates were dosed by Bradford assay and a western blot against  $\mu 2$  was realized. The membrane was H<sub>2</sub>O<sub>2</sub>-inactivated and probed against the loading control actin. Relative protein level was calculated using Image J.

## **AUTHOR CONTRIBUTIONS**

S.B., J.P.P., G.L., and M.B. conceived the study and the experimental frame. S.B. performed most of the experiments, analyzed the data, generated the figures, and wrote the manuscript with G.L. and M.B. M.D. performed the RT, qPCR, AS-PCR, and ddPCR experiments. C.A.M. helped with experiments during the revision process. The manuscript was reviewed by all the authors

## **ACKNOWLEDGEMENTS**

We thank Dominique Lévesque and Pr. François-Michel Boisvert for the help with mass spectrometry experiments; Edna Amoah for the molecular cloning of some minigenes; Philippe Thibault and Danny Bergeron for the design of qPCR and AS-PCR primers; and Marie Brunet for the help with statistical analysis.

## **FUNDING**

This work was supported by funding from the Natural Sciences and Engineering Research Council of Canada (NSERC) to M.B. [grant number RGPIN-2016-03916] and G.L. [grant number RGPIN-2017-05482]. S.B is now supported by the Fonds de recherche du Québec – Santé (FRQS), and previously by a Vanier scholarship from the Canadian Institutes of Health Research (CIHR). J.P.P. holds the Research Chair of the Université de Sherbrooke in RNA Structure and Genomics. M.B. and J.P.P. are members of the Centre de Recherche du CHUS.

*Conflict of interest statement.* The authors declare no conflict of interest. The funders had no role in the design of the study; in the collection, analyses, or interpretation of data; in the writing of the manuscript, or in the decision to publish the results.

## **REFERENCES**

1. Lemay,G. (1988) Transcriptional and translational events during reovirus infection. *Biochem. Cell Biol.*, **66**, 803–812.

2. Lemay,G. (2018) Synthesis and Translation of Viral mRNA in Reovirus-Infected Cells: Progress and Remaining Questions. *Viruses*, **10**, 671.
3. Danthi,P., Holm,G.H., Stehle,T. and Dermody,T.S. (2013) Reovirus receptors, cell entry, and proapoptotic signaling. *Adv. Exp. Med. Biol.*, **790**, 42–71.
4. Dermody,T.S., Parker,J.S. and Sherry,B. (2013) Orthoreoviruses. In *Dans David M. Knipe, Peter Howley (Éds). Fields virology*. Lippincott Williams & Wilkins, Philadelphia.
5. Parker,J.S.L., Broering,T.J., Kim,J., Higgins,D.E. and Nibert,M.L. (2002) Reovirus Core Protein  $\mu$ 2 Determines the Filamentous Morphology of Viral Inclusion Bodies by Interacting with and Stabilizing Microtubules. *J. Virol.*, **76**, 4483–4496.
6. Broering,T.J., Parker,J.S.L., Joyce,P.L., Kim,J. and Nibert,M.L. (2002) Mammalian Reovirus Nonstructural Protein  $\mu$ NS Forms Large Inclusions and Colocalizes with Reovirus Microtubule-Associated Protein  $\mu$ 2 in Transfected Cells. *J. Virol.*, **76**, 8285–8297.
7. Kobayashi,T., Chappell,J.D., Danthi,P. and Dermody,T.S. (2006) Gene-Specific Inhibition of Reovirus Replication by RNA Interference. *J. Virol.*, **80**, 9053–9063.
8. Arnold,M.M., Murray,K.E. and Nibert,M.L. (2008) Formation of the factory matrix is an important, though not a sufficient function of nonstructural protein  $\mu$ NS during reovirus infection. *Virology*, **375**, 412–423.
9. Kobayashi,T., Ooms,L.S., Chappell,J.D. and Dermody,T.S. (2009) Identification of Functional Domains in Reovirus Replication Proteins  $\mu$ NS and  $\mu$ 2. *J. Virol.*, **83**, 2892–2906.
10. Coombs,K.M. (1998) Stoichiometry of Reovirus Structural Proteins in Virus, ISVP, and Core Particles. *Virology*, **243**, 218–228.

11. Brentano,L., Noah,D.L., Brown,E.G. and Sherry,B. (1998) The Reovirus Protein  $\mu$ 2, Encoded by the M1 Gene, Is an RNA-Binding Protein. *J. Virol.*, **72**, 8354–8357.
12. Kim,J., Parker,J.S.L., Murray,K.E. and Nibert,M.L. (2004) Nucleoside and RNA Triphosphatase Activities of Orthoreovirus Transcriptase Cofactor  $\mu$ 2. *J. Biol. Chem.*, **279**, 4394–4403.
13. Eichwald,C., Kim,J. and Nibert,M.L. (2017) Dissection of mammalian orthoreovirus  $\mu$ 2 reveals a self-associative domain required for binding to microtubules but not to factory matrix protein  $\mu$ NS. *PLoS One*, **12**, e0184356.
14. Coffey,M.C., Strong,J.E., Forsyth,P.A. and Lee,P.W.K. (1998) Reovirus Therapy of Tumors with Activated Ras Pathway. *Science*, **282**, 1332–1334.
15. Chakrabarty,R., Tran,H., Selvaggi,G., Hagerman,A., Thompson,B. and Coffey,M. (2015) The oncolytic virus, pelareorep, as a novel anticancer agent: a review. *Invest New Drugs*, **33**, 761–774.
16. Mohamed,A., Clements,D.R., Gujar,S.A., Lee,P.W., Smiley,J.R. and Shmulevitz,M. (2020) Single Amino Acid Differences between Closely Related Reovirus T3D Lab Strains Alter Oncolytic Potency In Vitro and In Vivo. *J. Virol.*, **94**.
17. Fensterl,V., Chattopadhyay,S. and Sen,G.C. (2015) No Love Lost Between Viruses and Interferons. *Annu. Rev. Virol.*, **2**, 549–572.
18. Sen,G.C. and Sarkar,S.N. (2007) The interferon-stimulated genes: targets of direct signaling by interferons, double-stranded RNA, and viruses. *Curr. Top. Microbiol. Immunol.*, **316**, 233–250.
19. Katsoulidis,E., Kaur,S. and Plataniias,L.C. (2010) Deregulation of Interferon Signaling in Malignant Cells. *Pharmaceuticals*, **3**, 406–418.
20. Cheon,H., Borden,E.C. and Stark,G.R. (2014) Interferons and their stimulated genes in the tumor microenvironment. *Semin. Oncol.*, **41**, 156–173.

21. Matveeva,O.V. and Chumakov,P.M. (2018) Defects in interferon pathways as potential biomarkers of sensitivity to oncolytic viruses. *Rev. Med. Virol.*, **28**, e2008.
22. Ebrahimi,S., Ghorbani,E., Khazaei,M., Avan,A., Ryzhikov,M., Azadmanesh,K. and Hassanian,S.M. (2017) Interferon-Mediated Tumor Resistance to Oncolytic Virotherapy. *J. Cell. Biochem.*, **118**, 1994–1999.
23. Rudd,P. and Lemay,G. (2005) Correlation between interferon sensitivity of reovirus isolates and ability to discriminate between normal and Ras-transformed cells. *J. Gen. Virol.*, **86**, 1489–1497.
24. Boudreault,S., Roy,P., Lemay,G. and Bisailon,M. (2019) Viral modulation of cellular RNA alternative splicing: A new key player in virus–host interactions? *Wiley Interdiscip. Rev. RNA*, **10**, e1543.
25. Liu,S., Rauhut,R., Vornlocher,H.-P. and Lührmann,R. (2006) The network of protein–protein interactions within the human U4/U6.U5 tri-snRNP. *RNA*, **12**, 1418–1430.
26. Wood,K.A., Eadsforth,M.A., Newman,W.G. and O’Keefe,R.T. (2021) The Role of the U5 snRNP in Genetic Disorders and Cancer. *Front. Genet*, **12**.
27. Newman,A.J. (1997) The role of U5 snRNP in pre-mRNA splicing. *EMBO J.*, **16**, 5797–5800.
28. Black,D.L. (2003) Mechanisms of alternative pre-messenger RNA splicing. *Annu. Rev. Biochem.*, **72**, 291–336.
29. Lee,Y. and Rio,D.C. (2015) Mechanisms and Regulation of Alternative Pre-mRNA Splicing. *Annu. Rev. Biochem.*, **84**, null.
30. Kim,E., Goren,A. and Ast,G. (2008) Alternative splicing: current perspectives. *BioEssays*, **30**, 38–47.



31. Keren,H., Lev-Maor,G. and Ast,G. (2010) Alternative splicing and evolution: diversification, exon definition and function. *Nat. Rev. Genet.*, **11**, 345–355.
32. Dörner,A., Xiong,D., Couch,K., Yajima,T. and Knowlton,K.U. (2004) Alternatively Spliced Soluble Coxsackie-adenovirus Receptors Inhibit Coxsackievirus Infection. *J. Biol. Chem.*, **279**, 18497–18503.
33. Labbé,P., Faure,E., Lecointe,S., Le Scouarnec,S., Kyndt,F., Marrec,M., Le Tourneau,T., Offmann,B., Duplaà,C., Zaffran,S., *et al.* (2017) The alternatively spliced LRRFIP1 Isoform-1 is a key regulator of the Wnt/ $\beta$ -catenin transcription pathway. *Biochim Biophys Acta Mol Cell Res*, **1864**, 1142–1152.
34. Hardy,M.P. and O’Neill,L.A.J. (2004) The Murine Irak2 Gene Encodes Four Alternatively Spliced Isoforms, Two of Which Are Inhibitory. *J. Biol. Chem.*, **279**, 27699–27708.
35. Frankiw,L., Majumdar,D., Burns,C., Vlach,L., Moradian,A., Sweredoski,M.J. and Baltimore,D. (2019) BUD13 Promotes a Type I Interferon Response by Countering Intron Retention in Irf7. *Mol. Cell*, **73**, 803-814.e6.
36. Frankiw,L., Mann,M., Li,G., Joglekar,A. and Baltimore,D. (2020) Alternative splicing coupled with transcript degradation modulates OAS1g antiviral activity. *RNA*, **26**, 126–136.
37. Meyer,F. (2016) Chapter Eight - Viral interactions with components of the splicing machinery. In San Francisco,M., San Francisco,B. (eds), *Progress in Molecular Biology and Translational Science*, Host-Microbe Interactions. Academic Press, Vol. 142, pp. 241–268.
38. Maio,F.A.D., Risso,G., Iglesias,N.G., Shah,P., Pozzi,B., Gebhard,L.G., Mammi,P., Mancini,E., Yanovsky,M.J., Andino,R., *et al.* (2016) The Dengue Virus NS5 Protein Intrudes in the Cellular Spliceosome and Modulates Splicing. *PLoS Pathog.*, **12**, e1005841.

39. Liu,Y.-C., Kuo,R.-L., Lin,J.-Y., Huang,P.-N., Huang,Y., Liu,H., Arnold,J.J., Chen,S.-J., Wang,R.Y.-L., Cameron,C.E., *et al.* (2014) Cytoplasmic Viral RNA-Dependent RNA Polymerase Disrupts the Intracellular Splicing Machinery by Entering the Nucleus and Interfering with Prp8. *PLoS Pathog.*, **10**, e1004199.
40. Batra,R., Stark,T.J., Clark,E., Belzile,J.-P., Wheeler,E.C., Yee,B.A., Huang,H., Gelboin-Burkhart,C., Huelga,S.C., Aigner,S., *et al.* (2016) RNA-binding protein CPEB1 remodels host and viral RNA landscapes. *Nat. Struct. Mol. Biol.*, **23**, 1101.
41. Boudreault,S., Armero,V.E.S., Scott,M.S., Perreault,J.-P. and Bisailon,M. (2019) The Epstein-Barr virus EBNA1 protein modulates the alternative splicing of cellular genes. *Viol. J.*, **16**, 29.
42. Ashraf,U., Benoit-Pilven,C., Lacroix,V., Navratil,V. and Naffakh,N. (2019) Advances in Analyzing Virus-Induced Alterations of Host Cell Splicing. *Trends Microbiol.*, **27**, 268–281.
43. Chauhan,K., Kalam,H., Dutt,R. and Kumar,D. (2019) RNA Splicing: A New Paradigm in Host-Pathogen Interactions. *J. Mol. Biol.*, **431**, 1565–1575.
44. Boudreault,S., Martenon-Brodeur,C., Caron,M., Garant,J.-M., Tremblay,M.-P., Armero,V.E.S., Durand,M., Lapointe,E., Thibault,P., Tremblay-Létourneau,M., *et al.* (2016) Global Profiling of the Cellular Alternative RNA Splicing Landscape during Virus-Host Interactions. *PLoS One*, **11**, e0161914.
45. Rivera-Serrano,E.E., Fritch,E.J., Scholl,E.H. and Sherry,B. (2017) A Cytoplasmic RNA Virus Alters the Function of the Cell Splicing Protein SRSF2. *J. Virol.*, **91**, e02488-16.
46. Buchholz,U.J., Finke,S. and Conzelmann,K.-K. (1999) Generation of Bovine Respiratory Syncytial Virus (BRSV) from cDNA: BRSV NS2 Is Not Essential for Virus Replication in Tissue Culture, and the Human RSV Leader Region Acts as a Functional BRSV Genome Promoter. *J. Virol.*, **73**, 251–259.

47. Danis,C. and Lemay,G. (1993) Protein synthesis in different cell lines infected with orthoreovirus serotype 3: inhibition of host-cell protein synthesis correlates with accelerated viral multiplication and cell killing. *Biochem. Cell Biol.*, **71**, 81–85.
48. Lanoie,D. and Lemay,G. (2018) Multiple proteins differing between laboratory stocks of mammalian orthoreoviruses affect both virus sensitivity to interferon and induction of interferon production during infection. *Virus Res.*, **247**, 40–46.
49. Sandekian,V. and Lemay,G. (2015) A single amino acid substitution in the mRNA capping enzyme  $\lambda 2$  of a mammalian orthoreovirus mutant increases interferon sensitivity. *Virology*, **483**, 229–235.
50. Kobayashi,T., Antar,A.A.R., Boehme,K.W., Danthi,P., Eby,E.A., Guglielmi,K.M., Holm,G.H., Johnson,E.M., Maginnis,M.S., Naik,S., *et al.* (2007) A Plasmid-Based Reverse Genetics System for Animal Double-Stranded RNA Viruses. *Cell Host Microbe*, **1**, 147–157.
51. Kobayashi,T., Ooms,L.S., Ikizler,M., Chappell,J.D. and Dermody,T.S. (2010) An improved reverse genetics system for mammalian orthoreoviruses. *Virology*, **398**, 194–200.
52. Brochu-Lafontaine,V. and Lemay,G. (2012) Addition of exogenous polypeptides on the mammalian reovirus outer capsid using reverse genetics. *J. Virol. Methods*, **179**, 342–350.
53. Eaton,H.E., Kobayashi,T., Dermody,T.S., Johnston,R.N., Jais,P.H. and Shmulevitz,M. (2017) African Swine Fever Virus NP868R Capping Enzyme Promotes Reovirus Rescue during Reverse Genetics by Promoting Reovirus Protein Expression, Virion Assembly, and RNA Incorporation into Infectious Virions. *J. Virol.*, **91**, e02416-16.

54. Taylor,S., Wakem,M., Dijkman,G., Alsarraj,M. and Nguyen,M. (2010) A practical approach to RT-qPCR—Publishing data that conform to the MIQE guidelines. *Methods*, **50**, S1–S5.
55. Zou,S. and Brown,E.G. (1996) Stable Expression of the Reovirus  $\mu$ 2 Protein in Mouse L Cells Complements the Growth of a Reovirus ts Mutant with a Defect in Its M1 Gene. *Virology*, **217**, 42–48.
56. Virgin,H.W., Mann,M.A., Fields,B.N. and Tyler,K.L. (1991) Monoclonal antibodies to reovirus reveal structure/function relationships between capsid proteins and genetics of susceptibility to antibody action. *J. Virol.*, **65**, 6772–6781.
57. Tyanova,S., Temu,T. and Cox,J. (2016) The MaxQuant computational platform for mass spectrometry-based shotgun proteomics. *Nat Protoc*, **11**, 2301–2319.
58. Mohamed,A., Konda,P., Eaton,H.E., Gujar,S., Smiley,J.R. and Shmulevitz,M. (2020) Closely related reovirus lab strains induce opposite expression of RIG-I/IFN-dependent versus -independent host genes, via mechanisms of slow replication versus polymorphisms in dsRNA binding  $\sigma$ 3 respectively. *PLoS Pathog.*, **16**, e1008803.
59. Thoresen,D., Wang,W., Galls,D., Guo,R., Xu,L. and Pyle,A.M. (2021) The molecular mechanism of RIG-I activation and signaling. *Immunol. Rev.*, **304**, 154–168.
60. Armero,V.E.S., Tremblay,M.-P., Allaire,A., Boudreault,S., Martenon-Brodeur,C., Duval,C., Durand,M., Lapointe,E., Thibault,P., Tremblay-Létourneau,M., *et al.* (2017) Transcriptome-wide analysis of alternative RNA splicing events in Epstein-Barr virus-associated gastric carcinomas. *PLoS One*, **12**, e0176880.
61. Tremblay,M.-P., Armero,V.E.S., Allaire,A., Boudreault,S., Martenon-Brodeur,C., Durand,M., Lapointe,E., Thibault,P., Tremblay-Létourneau,M., Perreault,J.-P., *et al.* (2016) Global profiling of alternative RNA splicing events provides insights into

molecular differences between various types of hepatocellular carcinoma. *BMC Genet.*, **17**, 683.

62. Venables,J.P., Koh,C.-S., Froehlich,U., Lapointe,E., Couture,S., Inkel,L., Bramard,A., Paquet,É.R., Watier,V., Durand,M., *et al.* (2008) Multiple and Specific mRNA Processing Targets for the Major Human hnRNP Proteins. *Mol. Cell. Biol.*, **28**, 6033–6043.

63. Venables,J.P., Klinck,R., Bramard,A., Inkel,L., Dufresne-Martin,G., Koh,C., Gervais-Bird,J., Lapointe,E., Froehlich,U., Durand,M., *et al.* (2008) Identification of Alternative Splicing Markers for Breast Cancer. *Cancer Res*, **68**, 9525–9531.

64. Venables,J.P., Klinck,R., Koh,C., Gervais-Bird,J., Bramard,A., Inkel,L., Durand,M., Couture,S., Froehlich,U., Lapointe,E., *et al.* (2009) Cancer-associated regulation of alternative splicing. *Nat. Struct. Mol. Biol.*, **16**, 670–676.

65. Zarbl,H. and Millward,S. (1983) The Reovirus Multiplication Cycle. In Joklik,W.K. (ed), *The Reoviridae*, The Viruses. Springer US, Boston, MA, pp. 107–196.

66. Yin,P., Keirstead,N.D., Broering,T.J., Arnold,M.M., Parker,J.S., Nibert,M.L. and Coombs,K.M. (2004) Comparisons of the M1 genome segments and encoded  $\mu 2$  proteins of different reovirus isolates. *Viol. J.*, **1**, 6.

67. Irvin,S.C., Zurney,J., Ooms,L.S., Chappell,J.D., Dermody,T.S. and Sherry,B. (2012) A Single-Amino-Acid Polymorphism in Reovirus Protein  $\mu 2$  Determines Repression of Interferon Signaling and Modulates Myocarditis. *J. Virol.*, **86**, 2302–2311.

68. Zurney,J., Kobayashi,T., Holm,G.H., Dermody,T.S. and Sherry,B. (2009) Reovirus  $\mu 2$  Protein Inhibits Interferon Signaling through a Novel Mechanism Involving Nuclear Accumulation of Interferon Regulatory Factor 9. *J. Virol.*, **83**, 2178–2187.

69. Mbisa,J.L., Becker,M.M., Zou,S., Dermody,T.S. and Brown,E.G. (2000) Reovirus  $\mu$ 2 Protein Determines Strain-Specific Differences in the Rate of Viral Inclusion Formation in L929 Cells. *Virology*, **272**, 16–26.
70. Stebbing,R.E., Irvin,S.C., Rivera-Serrano,E.E., Boehme,K.W., Ikizler,M., Yoder,J.A., Dermody,T.S. and Sherry,B. (2014) An ITAM in a Nonenveloped Virus Regulates Activation of NF- $\kappa$ B, Induction of Beta Interferon, and Viral Spread. *J. Virol.*, **88**, 2572–2583.
71. Yeo,G.W., Nostrand,E.V., Holste,D., Poggio,T. and Burge,C.B. (2005) Identification and analysis of alternative splicing events conserved in human and mouse. *Proc. Natl. Acad. Sci. U.S.A.*, **102**, 2850–2855.
72. Lee,B.J., Cansizoglu,A.E., Süel,K.E., Louis,T.H., Zhang,Z. and Chook,Y.M. (2006) Rules for Nuclear Localization Sequence Recognition by Karyopherin $\beta$ 2. *Cell*, **126**, 543–558.
73. Pozzi,B., Bragado,L., Mammi,P., Torti,M.F., Gaioli,N., Gebhard,L.G., García Solá,M.E., Vaz-Drago,R., Iglesias,N.G., García,C.C., *et al.* (2020) Dengue virus targets RBM10 deregulating host cell splicing and innate immune response. *Nucleic Acids Res.*, **48**, 6824–6838.
74. Beyleveld,G., Chin,D.J., Olmo,E.M.D., Carter,J., Najera,I., Cillóniz,C. and Shaw,M.L. (2018) Nucleolar Relocalization of RBM14 by Influenza A Virus NS1 Protein. *mSphere*, **3**.
75. Choi,H., Larsen,B., Lin,Z.-Y., Breitzkreutz,A., Mellacheruvu,D., Fermin,D., Qin,Z.S., Tyers,M., Gingras,A.-C. and Nesvizhskii,A.I. (2011) SAINT: Probabilistic Scoring of Affinity Purification - Mass Spectrometry Data. *Nat Methods*, **8**, 70–73.
76. Schmechel,S., Chute,M., Skinner,P., Anderson,R. and Schiff,L. (1997) Preferential Translation of Reovirus mRNA by a  $\sigma$ 3-Dependent Mechanism. *Virology*, **232**, 62–73.

77. Imani,F. and Jacobs,B.L. (1988) Inhibitory activity for the interferon-induced protein kinase is associated with the reovirus serotype 1 sigma 3 protein. *Proc. Natl. Acad. Sci. U.S.A.*, **85**, 7887–7891.
78. Mellacheruvu,D., Wright,Z., Couzens,A.L., Lambert,J.-P., St-Denis,N., Li,T., Miteva,Y.V., Hauri,S., Sardiù,M.E., Low,T.Y., *et al.* (2013) The CRAPome: a Contaminant Repository for Affinity Purification Mass Spectrometry Data. *Nat Methods*, **10**, 730–736.
79. Miller,C.L., Parker,J.S.L., Dinoso,J.B., Piggott,C.D.S., Perron,M.J. and Nibert,M.L. (2004) Increased Ubiquitination and Other Covariant Phenotypes Attributed to a Strain- and Temperature-Dependent Defect of Reovirus Core Protein  $\mu$ 2. *J. Virol.*, **78**, 10291–10302.
80. Enam,C., Geffen,Y., Ravid,T. and Gardner,R.G. (2018) Protein Quality Control Degradation in the Nucleus. *Annu Rev Biochem*, **87**, 725–749.
81. Van Nostrand,E.L., Freese,P., Pratt,G.A., Wang,X., Wei,X., Xiao,R., Blue,S.M., Chen,J.-Y., Cody,N.A.L., Dominguez,D., *et al.* (2020) A large-scale binding and functional map of human RNA-binding proteins. *Nature*, **583**, 711–719.
82. Yang,C.-H., Li,H.-C., Shiu,Y.-L., Ku,T.-S., Wang,C.-W., Tu,Y.-S., Chen,H.-L., Wu,C.-H. and Lo,S.-Y. (2017) Influenza A virus upregulates PRPF8 gene expression to increase virus production. *Arch. Virol.*, **162**, 1223–1235.
83. Patzina,C., Botting,C.H., García-Sastre,A., Randall,R.E. and Hale,B.G.Y. 2017 Human interactome of the influenza B virus NS1 protein. *J. Gen. Virol.*, **98**, 2267–2273.
84. Tremblay,N., Baril,M., Chatel-Chaix,L., Es-Saad,S., Park,A.Y., Koenekoop,R.K. and Lamarre,D. (2016) Spliceosome SNRNP200 Promotes Viral RNA Sensing and IRF3 Activation of Antiviral Response. *PLoS Pathog.*, **12**, e1005772.

85. Zhu,C., Xiao,F., Hong,J., Wang,K., Liu,X., Cai,D., Fusco,D.N., Zhao,L., Jeong,S.W., Brisac,C., *et al.* (2015) EFTUD2 Is a Novel Innate Immune Regulator Restricting Hepatitis C Virus Infection through the RIG-I/MDA5 Pathway. *J. Virol.*, **89**, 6608–6618.
86. De Arras,L., Laws,R., Leach,S.M., Pontis,K., Freedman,J.H., Schwartz,D.A. and Alper,S. (2014) Comparative Genomics RNAi Screen Identifies Eftud2 as a Novel Regulator of Innate Immunity. *Genetics*, **197**, 485–496.
87. Urbanek,K., Sutherland,D.M., Orchard,R.C., Wilen,C.B., Knowlton,J.J., Aravamudhan,P., Taylor,G.M., Virgin,H.W. and Dermody,T.S. (2020) Cytidine Monophosphate N-Acetylneuraminic Acid Synthetase and Solute Carrier Family 35 Member A1 Are Required for Reovirus Binding and Infection. *J. Virol.*, **95**, e01571-20.
88. Pan,M., Alvarez-Cabrera,A.L., Kang,J.S., Wang,L., Fan,C. and Zhou,Z.H. (2021) Asymmetric reconstruction of mammalian reovirus reveals interactions among RNA, transcriptional factor  $\mu 2$  and capsid proteins. *Nat. Commun.*, **12**, 4176.
89. Workenhe,S.T., Ketela,T., Moffat,J., Cuddington,B.P. and Mossman,K.L. (2016) Genome-wide lentiviral shRNA screen identifies serine/arginine-rich splicing factor 2 as a determinant of oncolytic virus activity in breast cancer cells. *Oncogene*, **35**, 2465–2474.
90. Perez-Riverol,Y., Csordas,A., Bai,J., Bernal-Llinares,M., Hewapathirana,S., Kundu,D.J., Inuganti,A., Griss,J., Mayer,G., Eisenacher,M., *et al.* (2019) The PRIDE database and related tools and resources in 2019: improving support for quantification data. *Nucleic Acids Res.*, **47**, D442–D450.



## **Perspectives**

Ces travaux ont permis de mettre en évidence l'implication des protéines EFTUD2, PRPF8 et SNRNP200 du complexe U5 dans la modulation de l'épissage alternatif cellulaire causée par réovirus. De plus, nos résultats ont démontré que le niveau de ces protéines est réduit lors de l'infection, notamment par l'action de la protéine virale  $\mu 2$ . Outre le contrôle de l'épissage alternatif, existe-t-il d'autres rôles à ces protéines du spliceosome lors de l'infection virale? Quel bénéfice réovirus retire-t-il de diminuer le niveau de ces protéines? Ces questions ont motivé les travaux présentés au chapitre suivant, qui s'intéressent aux rôles des protéines du complexe U5 dans les interactions virus-hôtes lors de l'infection avec réovirus.

## **ARTICLE 3**

### **U5 snRNP core proteins are key components of the defense response against viral infection through their roles in programmed cell death and interferon induction**

**Auteurs de l'article:** Boudreault S, Lemay G, Bisailon M.

**Statut de l'article:** Article soumis à Scientific Reports.

**Avant-propos:** J'ai participé à la conception du projet et j'ai effectué la majorité des expériences ainsi que l'analyse des résultats (>90%). J'ai généré les figures et j'ai écrit le manuscrit sous la supervision des Prs Bisailon et Lemay.

**Résumé :** Le splicéosome est un complexe ribonucléoprotéique massif composé de cinq petites ribonucléoprotéines nucléaires qui catalyse le retrait des introns des pré-ARNm durant l'épissage constitutif et alternatif. EFTUD2, PRPF8 et SNRNP200 sont les composantes principales du complexe U5, qui est crucial pour la fonction du splicéosome puisqu'il coordonne et effectue les dernières étapes de la réaction d'épissage. Plusieurs études ont démontré que les protéines du complexe U5 sont ciblées durant l'infection virale, avec une compréhension limitée de leur rôle dans les interactions virus-hôte. Dans la présente étude, nous avons déchiffré l'impact respectif d'EFTUD2, de PRPF8 et de SNRNP200 sur la réplication virale en utilisant réovirus comme virus modèle. En utilisant une combinaison d'interférence par ARN, d'analyse de cellules en temps réel, d'essais de mort cellulaire et de réplication virale, nous avons découvert des rôles distincts et se recoupant pour EFTUD2, PRPF8 et SNRNP200 dans la survie cellulaire, l'apoptose, la nécroptose, et l'induction de la voie de réponse à l'interféron. Par exemple, nous avons démontré qu'EFTUD2 et SNRNP200 sont requises pour la mort cellulaire programmée via l'apoptose et la nécroptose, alors qu'EFTUD2 et PRPF8 sont requises pour une réponse interféron

optimale contre l'infection virale. De plus, nous avons démontré qu'EFTUD2 restreint la réplication virale, autant sur un cycle que plusieurs cycles de réplication. Ces résultats établissent les composantes principales du complexe U5 comme étant des éléments clés de la réponse antivirale cellulaire.

**U5 snRNP core proteins are key components of the defense response against viral infection through their roles in programmed cell death and interferon induction**

Simon Boudreault<sup>1</sup>, Guy Lemay<sup>2</sup>, Martin Bisailon<sup>1,\*</sup>

<sup>1</sup> Département de biochimie et de génomique fonctionnelle, Faculté de médecine et des sciences de la santé, Université de Sherbrooke, Sherbrooke, Québec, J1E 4K8, Canada

<sup>2</sup> Département de microbiologie, infectiologie et immunologie, Faculté de médecine, Université de Montréal, Montréal, Québec, H3C 3J7, Canada

\*To whom correspondence should be addressed.

Tel: +1-819-821-8000 (Ext 75904)

Email: [Martin.Bisailon@USherbrooke.ca](mailto:Martin.Bisailon@USherbrooke.ca)

**ABSTRACT**

The spliceosome is a massive ribonucleoprotein structure composed of five small nuclear ribonucleoprotein (snRNP) complexes that catalyzes the removal of introns from pre-mature RNA during constitutive and alternative splicing. EFTUD2, PRPF8, and SNRNP200 are core components of the U5 snRNP, which is crucial for spliceosome function as it coordinates and performs the last steps of the splicing reaction. Several studies have demonstrated U5 snRNP proteins as targeted during viral infection, with a limited understanding of their involvement in virus-host interactions. In the present study, we deciphered the respective impact of EFTUD2, PRPF8, and SNRNP200 on viral replication using mammalian reovirus as a model. Using a combination of RNA silencing, real-time cell analysis, cell death and viral replication assays, we discovered distinct and partially overlapping novel roles for EFTUD2, PRPF8, and SNRNP200 in cell survival, apoptosis, necroptosis, and the induction of the interferon response pathway. For instance, we demonstrated that EFTUD2 and SNRNP200 are required for both apoptosis and necroptosis, whereas EFTUD2 and PRPF8 are required for optimal interferon response against viral infection. Moreover, we demonstrated that EFTUD2 restricts viral replication, both in a single cycle and multiple cycles of viral replication. Altogether, these results establish U5 snRNP core components as key elements of the cellular antiviral response.

## **INTRODUCTION**

During viral infection, the interferon (IFN) pathway is the principal cellular response to fight back viruses and signal an infection to the immune system<sup>1</sup>. Pathogen-associated molecular patterns (PAMP), such as double-stranded RNA (dsRNA) and 5'-triphosphate single-stranded RNA, are detected by pattern-recognition receptors (e.g. RIG-I, MDA5, TLR3, etc.), and through a complex signaling cascade culminate with the production of IFN. Upon secretion, IFN can act in a paracrine fashion on uninfected cells to prepare them prior to getting infected, or in an autocrine fashion on infected cells to stimulate them in their fight against viral infection. The interaction of IFN with its receptor triggers the expression of hundreds of interferon-stimulated genes (ISG), which are the effectors of the cellular antiviral response<sup>1,2</sup>. On the other end of the spectrum, programmed cell death is another means for the cell to hamper viral replication by killing the cell before the virus can replicate efficiently. Diverse programs of cell death allow cells to perform this altruistic death in favor of overall survival of the greater number<sup>3</sup>. The most well-known is apoptosis, characterized by caspase activation and shrinkage of the cell<sup>3</sup>. Apoptosis is notably recognized as a "clean" death, as there is no leakage of the cellular content, and the remaining apoptotic bodies are swallowed by macrophages with limited inflammation. Conversely, necroptosis is emerging as a key programmed cell death to trigger inflammation, as it results in leakage of the cellular content, which is highly immunogenic<sup>3</sup>. The sensors of necroptosis (i.e., RIPK1, ZBP1 (formerly DAI), and TLR3/TRL4) all activate RIPK3, which is the primary regulator of this cell death program. Upon phosphorylation, RIPK3 is activated and phosphorylates MLKL, the main effector of necroptosis. MLKL phosphorylation leads to its trimerization and the formation of pores in the cellular membrane, which results in the leakage of the cytoplasmic content into the extracellular space.

Recently, several viruses were shown to interact with the splicing machinery components and interfere with the splicing process during infection, with a limited understanding of the role of these spliceosomal proteins and splicing factors in virus-

host interactions<sup>4-7</sup>. The spliceosome is a large ribonucleoprotein (RNP) structure composed of five small nuclear ribonucleoproteins complexes (snRNP; U1, U2, U4, U5, and U6), each formed by one small nuclear RNA and numerous proteins components. The spliceosome catalyzes the removal of introns for mRNA processing through constitutive splicing by recognizing key sequences in introns, such as the branch point and the polypyrimidine tract, and in exons, such as the 5' splice site (5'-SS) and the 3' splice site (3'-SS). The snRNP are sequentially recruited to the intron, starting with U1 binding the 5'-SS and U2 binding the branch point. Then, the U4/U6.U5 tri-snRNP is recruited to the assembling spliceosome, forming the precatalytic spliceosome, or complex B. U5 proteins EFTUD2 and SNRNP200 are critical to drive the reorganization of the complex, the release of U1 and U4 snRNP, and activation to excise the intron (B<sup>act</sup>)<sup>8-10</sup>. Two nucleophilic attacks, one from the branch site to the 5'-SS, and then from the 5'-SS to the 3'-SS, allow the removal of the intron. During these attacks, U5's central protein PRPF8's role is crucial, as it binds both the 5'-SS and 3'-SS<sup>11</sup>. Alternative splicing (AS), as opposed to constitutive splicing, arises from spliceosome assembly being stabilized or destabilized near weak splice sites by splicing factors bound to the pre-mRNA. These inhibitory and stimulatory signals allow the removal of exons, parts of exon, and even introns to be retained in the mature RNA. AS thus modifies the coding potential of the mRNA, and results in the formation of a mixed population of mature mRNAs arising from the same gene<sup>12-15</sup>. Emerging evidence seems to implicate U5 in cellular AS, as opposed to the previous vision that the B<sup>act</sup> complex is committed to removing the intron and that U5 can thus only control constitutive splicing<sup>5,16</sup>.

In the past few years, numerous viruses have been shown to modulate cellular AS upon infection<sup>7,17-19</sup>. The increasing importance of the impact of viruses on cellular AS has prompted us to study the impact of mammalian reovirus (MRV) infection on cellular AS. MRV is a dsRNA virus from the Reoviridae family which has been fundamental to our comprehension of the basis of virus replication, such as internalization, uncoating, transcription, RNA cap synthesis, translation, and virus-

host interactions<sup>20-23</sup>. The genome of MRV is composed of ten dsRNA segments encoding eight structural proteins and four non-structural proteins and is protected by a double-layered capsid. Previously, we and others have demonstrated that MRV infection induces drastic changes in cellular AS, identifying more than 200 cellular AS events impacted by MRV infection<sup>23,24</sup>. We recently showed that MRV's  $\mu 2$  protein is the primary viral protein involved in this modulation<sup>5</sup>.  $\mu 2$  impacts cellular AS by interacting with U5 snRNP proteins EFTUD2, PRPF8, and SNRNP200, and reducing their levels during infection<sup>5</sup>. However, how are these U5 snRNP proteins involved in the fundamental aspect of viral replication, and what is the benefit for the virus to reduce these spliceosomal components remain unknown.

In the present study, we deciphered the impact of EFTUD2, PRPF8, and SNRNP200 silencing on viral replication using MRV as a model and discovered novel roles for EFTUD2 and SNRNP200 in cell survival, apoptosis, and necroptosis during viral infection. Moreover, EFTUD2 and PRPF8 control the induction of the IFN response pathway, establishing the U5 snRNP as a potent target for viruses to abrogate the cellular response mounted against infection. Finally, we demonstrated that EFTUD2 restricts the replication of MRV, both in a single cycle and multiple cycles of viral replication. Overall, these results establish U5 snRNP core components as key elements of the cellular antiviral response.



## RESULTS

### **EFTUD2 and SNRNP200 are required for cell death after infection**

As a first step towards understanding the role of U5 snRNP core proteins in viral replication, we used real-time cell analysis (RTCA) to profile the dynamics of MRV replication in siCTRL or EFTUD2, PRPF8, and SNRNP200 knocked-down (KD) cells. We previously demonstrated efficient KD of these proteins ranging from 50 to 70% using the same experimental conditions<sup>5</sup>. Nevertheless, we still validated using an orthogonal assay, namely qPCR, that the depletion was still both efficient and specific (Supplementary Figure S1). To perform RTCA, L929 cells were seeded and allowed to adhere overnight before transfecting them with the appropriate siRNA. After an incubation of 24 h with the siRNA, cells were mock-infected or infected with MRV at a multiplicity of infection (MOI) of 3, and the normalized cell index was followed throughout the infection. As seen in the control condition, the normalized cell index is stable up to 30 h, after which an increase is apparent before a constant decrease corresponding to the lysis of cells after infection is observed (Figure 1A). This curve is typical of infected cells<sup>25–29</sup>. However, when components of the U5 snRNP were depleted, the curves were shifted towards the right, suggesting that cells were surviving longer after infection. Moreover, the effect of SNRNP200 was still observable at a MOI of 50; however, the impact for EFTUD2 and PRPF8 at higher MOI was less clear (Supplementary Figure S2). We also validated that the depletion of EFTUD2, PRPF8, and SNRNP200 was not decreasing cell viability, and that cell survived and even expanded throughout the course of the experiment in the absence of infection (Figure 1B). These results suggest that U5 snRNP proteins might control cell death and/or cell survival during MRV infection. To validate these results, we quantified cell viability using FACS by staining with Hoechst (nucleus) and propidium iodide (dead cells) (Figure 1C). This assay confirmed a significant increase in cell survival, as measured by the percentage of cells negative for propidium iodide compared to total cell count, upon KD of EFTUD2 and SNRNP200 and no effect of PRPF8 on cell survival during MRV infection.

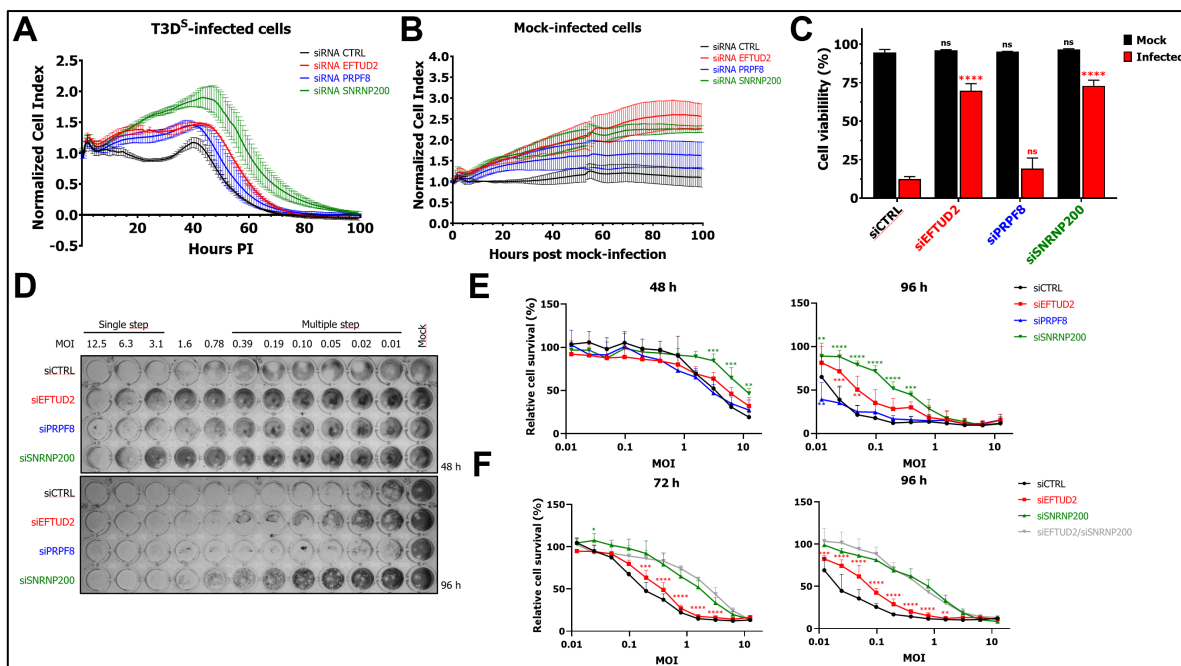


Figure 1. *EFTUD2* and *SNRNP200* KD protect cells from death after MRV infection. (A) RTCA of T3D<sup>S</sup>-infected L929 cells (MOI of 3) transfected with a control siRNA or *EFTUD2*, *PRPF8*, or *SNRNP200* specific siRNA. Measurements were made every 10 min. n=3, biological replicates. (B) RTCA of mock-infected L929 cells transfected with a control siRNA or *EFTUD2*, *PRPF8*, or *SNRNP200* specific siRNA. Measurements were made every 10 min. n=3, biological replicates. (C) Cell viability in mock- or T3D<sup>S</sup>-infected L929 cells. Cells were treated with the siRNA for 55 h before being mock-infected or infected at a MOI of 3 for 65 h. Cell viability was measured using FACS by staining with Hoechst and propidium iodide; live cells were selected as Hoechst positive and propidium iodide negative. n=3, biological replicates, two-way ANOVA with Dunnett's multiple comparisons test against the siCTRL treated cells for each condition (mock in black, infected in red; ns, P>0.05; \*\*\*\*, P≤0.0001). (D) Representative images of methylene blue staining of control or *EFTUD2*, *PRPF8*, or *SNRNP200*-depleted L929 cells infected with binary dilutions of T3D<sup>S</sup> at 48 h or 96 h post-infection. (E) Quantification of cell-bound methylene blue stain for three independent experiments. n=3, biological replicates, two-way ANOVA with Dunnett's multiple comparisons test against the control siRNA condition (\*\*, P≤0.01; \*\*\*, P≤0.001; \*\*\*\*, P≤0.0001); if not indicated, results are non-statistically significant. (F) Methylene blue staining of control, *EFTUD2*, *SNRNP200*, or *EFTUD2*/*SNRNP200*-depleted L929 cells infected with binary dilutions of T3D<sup>S</sup> at 72 h or 96 h post-infection. Twice the quantity of siRNA was transfected to perform DKD; in the case of single KD, siCTRL was added to match the total siRNA quantity of the DKD. The quantification of cell-bound methylene blue stain is shown for three independent experiments. n=3, biological replicates, two-way ANOVA with Dunnett's multiple comparisons test against the DKD condition, in gray (\*, P≤0.05; \*\*, P≤0.01; \*\*\*, P≤0.001; \*\*\*\*, P≤0.0001). If not indicated, results are non-statistically significant. The results of the comparison against the control siRNA are not indicated for clarity purposes.

To further validate the effect of *EFTUD2* and *SNRNP200* on cell survival, we exploited a previously described methylene blue staining assay using binary MRV dilutions<sup>30–33</sup>. L929 cells were treated with control, *EFTUD2*, *PRPF8*, or *SNRNP200* siRNA, and then infected with MRV binary dilutions, ranging from a MOI of approximately 0.01 to 12.5. This experimental workflow allows profiling of both a single cycle of

replication (MOI of 3 to 12.5) and multiple cycles (MOI<0.1) by changing the incubation time. At 48 h, most cells treated with siCTRL or siPRPF8 were dead at the highest MOI; however, cells were surviving better when treated with the siRNA against SNRNP200 and EFTUD2 (Figure 1D). This protection from cell death was even more striking at 96 h when looking at multiple cycles of replication; cells knocked-down for SNRNP200 and EFTUD2 survived several binary dilutions higher than siCTRL or siPRPF8-treated cells (Figure 1D). To quantify this phenomenon, we measured cell-bound methylene blue using spectrophotometry in biological triplicates, both at 48 h and 96 h (Figure 1E). In average, 20-30% of cells survived at the highest MOI when treated with siCTRL, siEFTUD2, or siPRPF8 at 48 h. This survival increased to 45% in the case of the siSNRNP200. At 96 h, 90% (siSNRNP200) and 75% (siEFTUD2) of cells at the lowest MOI were still alive, compared to 35% with the siRNA against the control or PRPF8. Finally, we wondered if these effects of EFTUD2 and SNRNP200 were independent or merely reflecting the involvement of both proteins in the same cellular process. To ask this question, we KD EFTUD2, SNRNP200, and both proteins altogether and looked if the double knock-down (DKD) could confer synergetic protection from MRV-mediated cell death. Since twice the amount of siRNA was transfected to perform DKD, cells survived longer than in the previous assay at earlier timepoints; we thus performed the DKD at 72 h and 96 h. The DKD of EFTUD2 and SNRNP200 did not protect cells from death more than the simple KD of SNRNP200 at both 72 h and 96 h (Figure 1F). This experiment led us to conclude that the impact of EFTUD2 and SNRNP200 on cell survival are redundant and likely to involve a similar mechanism. Together, these data show that U5 snRNP proteins EFTUD2 and SNRNP200 are involved in cell survival and/or cell death after infection with MRV.

### **EFTUD2 and SNRNP200 knock-down affects apoptosis**

After infection with MRV, both apoptosis<sup>34-36</sup> and necroptosis<sup>37,38</sup> can be induced and result in cell death and lysis. We first questioned if KD of EFTUD2 and SNRNP200 impacted apoptosis to enhance cell survival after MRV infection by using a high-

throughput microscopy-based assay. L929 cells were treated with the appropriate siRNA and infected with MRV for 40 h, just before cells started to die under these conditions (see Figure 1A). Cells were then stained with Annexin-V conjugated to AlexaFluor-647 (early apoptosis), propidium iodide (dead cells), calcein AM (cytoplasm) and Hoechst (nucleus) in 96-well plates, as previously described<sup>39,40</sup>. Plates were imaged using a 96-well plate microscope, and positive cells were automatically counted. In mock condition, cells exhibited low levels of apoptosis, with only a modest but significant impact of the PRPF8 siRNA (Figure 2A, 2B). Moreover, when cells were infected with MRV, there was no significant reduction of apoptotic positive cells, as measured by this assay, with any of the siRNA transfected compared to the control siRNA (Figure 2A, 2B). This result suggests that apoptosis normally proceeds, even in EFTUD2- and SNRNP200-depleted cells. In addition, staining for dead cells using propidium iodide revealed a significant decrease in dead cells when EFTUD2 and SNRNP200 were KD, further strengthening our previous finding that these KD protect cells from MRV-mediated death (Figure 1C, 2A and 2C). Once again, a small but significant impact could be observed in PRPF8-depleted mock cells and also in the SNRNP200-depleted condition (Figure 2C). To validate that apoptosis was indeed induced, we further quantified the activity of caspase 3 and 7, the effector caspases of apoptosis, using a luminescence-based assay. Surprisingly, this assay revealed a 75% reduction in Cas3/7 activity in MRV-infected cells when either EFTUD2 or SNRNP200 was depleted (Figure 2D). Since the extracellular exposure of phosphatidylserine is induced in other programmed cell death pathways than apoptosis<sup>41,42</sup>, this latest result suggests that even though cells present extracellular phosphatidylserine (Figure 2B), the activity of effector caspases are actually reduced. Apoptosis is thus impaired upon EFTUD2 and SNRNP200 depletion in MRV-infected cells, and both the depletion of EFTUD2 and SNRNP200 likely protects cells from MRV's induced apoptosis.

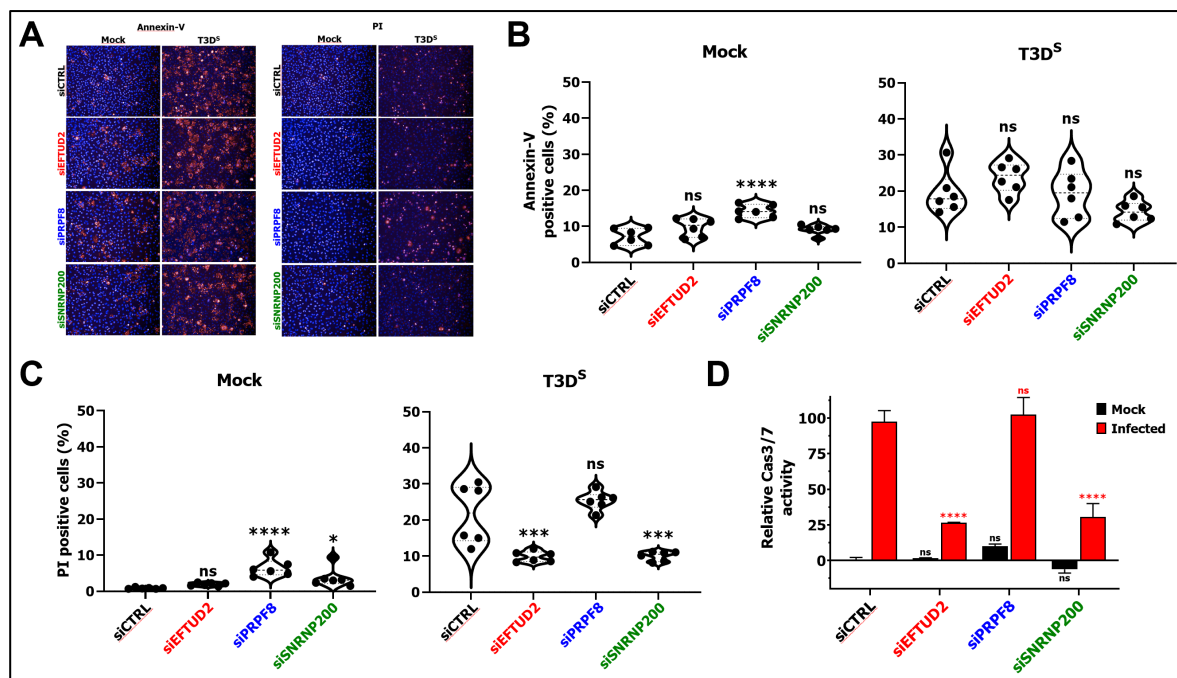


Figure 2. *EFTUD2* and *SNRNP200* depletion hamper apoptosis. (A) Representative set of images for the high-throughput multiplex microscopy-based apoptosis assay. On the left, Annexin-V signal is shown in red, representative of apoptotic cells. On the right, propidium iodide signal is shown in red, representative of dead cells. On both sides, the nuclei are stained with Hoechst and shown in blue. (B) Percent of mock- or T3DS-infected L929 cells staining positive for Annexin-V upon depletion of *EFTUD2*, *PRPF8*, or *SNRNP200*. Cells were infected (MOI of 3) or mock-infected, and the percent of Annexin-V positive cells was calculated 40 h later.  $n=6$ , biological replicates, one-way ANOVA with Dunnett's multiple comparisons test against the siCTRL treated cells (ns,  $P>0.05$ ; \*\*\*\*,  $P\leq 0.0001$ ). (C) Percent of dead cells upon depletion of *EFTUD2*, *PRPF8*, or *SNRNP200*. Cells were infected (MOI of 3) or mock-infected, and the percent of propidium iodide positive cells was calculated at 40 h post infection.  $n=6$ , biological replicates, one-way ANOVA with Dunnett's multiple comparisons test against the siCTRL treated cells (ns,  $P>0.05$ ; \*,  $P\leq 0.05$ ; \*\*\*,  $P\leq 0.001$ ; \*\*\*\*,  $P\leq 0.0001$ ). (D) Relative Cas3/7 activity for mock- and T3DS-infected L929 cells. Cells were treated with the siRNA for 55 h before being infected or mock-infected at a MOI of 3 for 40 h. Cas3/7 activity was measured using the Caspase-Glo® 3/7 Assay System. The first replicate of the siCTRL in the mock condition was fixed at 0%, and the first replicate of the siCTRL in the infected condition was fixed at 100%.  $n=3$ , biological replicates, two-way ANOVA with Dunnett's multiple comparisons test against the siCTRL treated cells for each condition (mock in black, infected in red; ns,  $P>0.05$ ; \*\*\*\*,  $P\leq 0.0001$ ).

### **EFTUD2 and SNRNP200 are required for necroptosis**

Next, we turned to the potential impact of *EFTUD2* and *SNRNP200* on necroptosis, which is also induced in MRV-infected cells<sup>37,38</sup>. The striking effect of U5 snRNP proteins KD on cell survival during MRV infection suggests that these proteins of the U5 snRNP (i.e., *EFTUD2* and *SNRNP200*) might affect more than simply apoptosis to confer such a drastic enhancement in cell survival. The effector of necroptosis, MLKL, is phosphorylated on S345 by RIPK3, which allows its trimerization and the formation

of pores that leak the cellular content into the extracellular space<sup>43,44</sup>. We thus quantitated the levels of phosphorylated MLKL (pMLKL) as an indicator of necroptosis in mock- and T3D<sup>S</sup>-infected cells treated with control or EFTUD2, PRPF8 or SNRNP200 specific siRNA (Figure 3A). Upon EFTUD2 or SNRNP200 KD, there was a defect in the phosphorylation of MLKL in infected cells. Quantification of multiple western blots (WB) confirmed this significant absence of pMLKL induction in EFTUD2 and SNRNP200-depleted cells after MRV infection (Figure 3B). Surprisingly, PRPF8 KD led to a considerable amount of pMLKL in the absence of infection, revealing that the enhanced cell death observed with this KD (Figure 2B) could be attributable, at least in part, to necroptosis (Figure 3A, 3B). These results place U5 snRNP core components as regulators of necroptosis. We also observed some variations in the total protein levels of MLKL (Figure 3A), although there was significantly less MLKL only in the PRPF8 KD after MRV infection (Figure 3B).

Considering MRV-induced necroptosis is, at least in part, dependent on RIPK1<sup>37,38</sup>, we tested the impact of U5 core components KD with another RIPK1-dependent necroptosis stimulus. Necroptosis can be elicited in L929 cells by first blocking apoptosis using the pan-caspase inhibitor zVAD-fmk, and then stimulating the tumor necrosis factor receptor (TNFR) using TNF $\alpha$ , which elicits RIPK1-dependent necroptosis<sup>43,44</sup>. We first monitored EFTUD2-, PRPF8-, and SNRNP200-depleted cells treated with zVAD-fmk/TNF $\alpha$  using RTCA and observed results consistent with increased survival when EFTUD2 and PRPF8 levels were reduced (Figure 3C). However, using this stimulus, the depletion of SNRNP200 did not seem to confer any protection from necroptotic cell death when monitoring using RTCA. We then monitored EFTUD2-, PRPF8-, and SNRNP200-depleted cells treated with zVAD-fmk/TNF $\alpha$  using microscopy and confirmed that EFTUD2 depletion protected cells against zVAD-fmk/TNF $\alpha$ -mediated cell death, whereas SNRNP200 KD had no protective effect using this stimulus and even seemed to sensitize cells (Supplementary Figure S3). Using live-cell microscopy, we could not observe any impact of PRPF8 on cell survival following zVAD-fmk/TNF $\alpha$  necroptotic stimulus. To

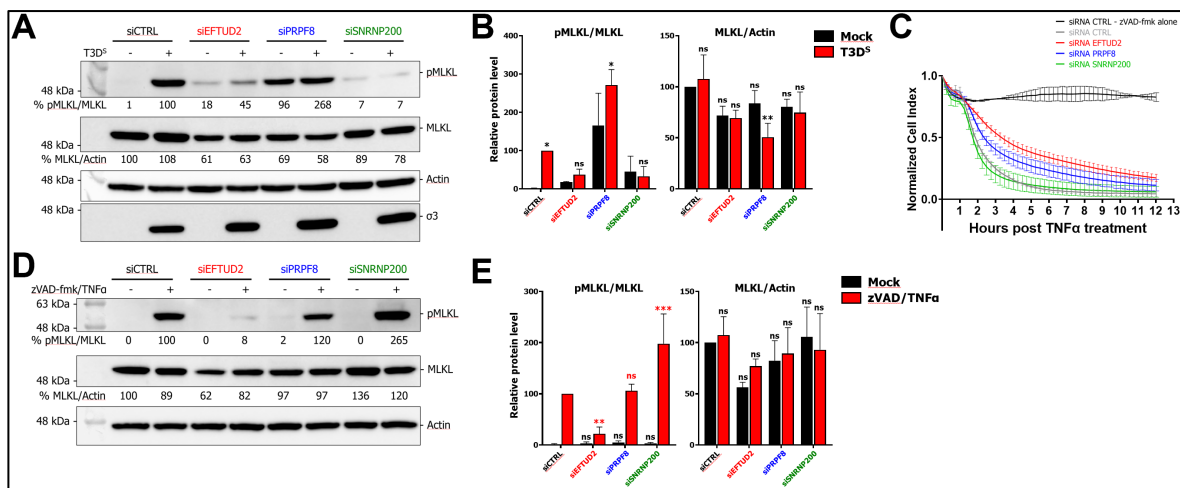


Figure 3. *Depletion of EFTUD2 and SNRNP200 impacts necroptosis.* (A) Western blot of phosphorylated MLKL (pMLKL) and total MLKL in mock- or T3DS-infected L929 cells treated with control or EFTUD2, PRPF8, or SNRNP200 specific siRNA. Cells were infected at an MOI of 3 and incubated for 40 h before proteins were harvested. Actin was used as a loading control and the MRV  $\sigma 3$  viral protein was used to validate the infection. Relative quantitation is shown for pMLKL/MLKL and MLKL/Actin. (B) Quantification and statistical analysis of three independent western blots. For pMLKL/MLKL, the infected cells were compared to their respective non-infected siRNA condition using a two-way ANOVA with Šídák's multiple comparisons test; for MLKL/Actin, all conditions were compared to the siCTRL mock condition using a one-way ANOVA with Dunnett's multiple comparisons test.  $n=3$ , biological replicates (ns,  $P>0.05$ ; \*,  $P\leq 0.05$ ; \*\*,  $P\leq 0.01$ ). (C) RTCA of zVAD-fmk/TNF $\alpha$  treated L929 cells transfected with a control siRNA or EFTUD2, PRPF8, or SNRNP200 specific siRNA. A siCTRL condition was treated with only zVAD-fmk to confirm no cell death was induced in the absence of TNF $\alpha$ . Measurements were made every 15 min for 12 h.  $n=3$  for all conditions except for siRNA CTRL - zVAD-fmk alone ( $n=2$ ), biological replicates. (D) Western blot of phosphorylated MLKL (pMLKL) and total MLKL in control or EFTUD2, PRPF8, or SNRNP200-depleted L929 cells untreated or treated 4h with zVAD/TNF $\alpha$  to induce necroptosis. Actin was used as a loading control. Relative quantitation is shown for pMLKL/MLKL and MLKL/Actin. (E) Quantification and statistical analysis of three independent western blot. For pMLKL/MLKL, the zVAD/TNF $\alpha$  treated cells were compared to the zVAD/TNF $\alpha$  siCTRL condition (in red) and the same was done for the untreated cells (in black) using a two-way ANOVA with Šídák's multiple comparisons test; for MLKL/Actin, all conditions were compared to the siCTRL mock condition using a one-way ANOVA with Dunnett's multiple comparisons test.  $n=3$ , biological replicates (ns,  $P>0.05$ ; \*\*,  $P\leq 0.01$ ; \*\*\*,  $P\leq 0.001$ ).

validate these results, we quantified the levels of pMLKL upon zVAD-fmk/TNF $\alpha$  stimulation in cells treated with control or EFTUD2, PRPF8, or SNRNP200 siRNA. The results revealed EFTUD2 depletion hampered the phosphorylation of MLKL upon zVAD-fmk/TNF $\alpha$  treatment, and that SNRNP200 enhanced MLKL phosphorylation (Figure 3D). Quantification of multiple WB confirmed a significant decrease of phosphorylated MLKL in EFTUD2-depleted cells, a significant increase in SNRNP200-depleted cells, while no impact of the PRPF8 depletion could be observed (Figure 3E). These results underline the opposite effect of SNRNP200 depletion depending

on the necroptotic stimulus, and the reproducible effect of EFTUD2 previously observed during MRV infection. Once again, we observed variations in the total level of MLKL (Figure 3D), although there was no statistically significant difference when multiple WB were analyzed (Figure 3E). EFTUD2 and SNRNP200 are thus required for induction of necroptosis during MRV infection while EFTUD2's importance for necroptosis appears to be generalized to other necroptotic stimuli, such as zVAD-fmk/TNF $\alpha$ .

### **KD of U5 snRNP core components impacts mRNA levels, protein levels, and alternative splicing of necroptotic regulators**

The preceding results suggest that EFTUD2 KD is protecting cells against necroptosis from MRV infection and zVAD/TNF $\alpha$  treatment, whereas SNRNP200 KD is only able to block necroptosis arising from MRV infection. To understand the impact of depleting the U5 snRNP core components on necroptosis, we first investigated the impact of these depletions on mRNA levels of the main regulators of necroptosis, i.e., RIPK1, RIPK3, and MLKL (Figure 4A). RIPK3 mRNA levels were unaffected by the KD, while MLKL mRNA levels were significantly decreased by all KD. RIPK1 mRNA levels were only reduced upon EFTUD2 KD, pointing to a specific impact of EFTUD2 depletion on RIPK1 mRNA. Then, we profiled the relative protein levels of RIPK1, RIPK3 and MLKL upon depletion of EFTUD2, PRPF8 and SNRNP200. EFTUD2 and PRPF8 depletion reduced the protein levels of all the necroptotic regulators tested, whereas SNRNP200 depletion only reduced MLKL levels (Figure 4B). Quantification of three independent WB revealed no significant reduction of RIPK1 upon U5 core proteins KD, and a significant reduction of RIPK3 upon both EFTUD2 and PRPF8 KD (Figure 4C). Since there is no change in RIPK3 mRNA level upon EFTUD2 and PRPF8 silencing (Figure 4A), these results suggest EFTUD2 and PRPF8 regulate RIPK3 level post-transcriptionally, such as through alternative splicing or post-translationally. Moreover, there was a significant reduction of MLKL protein levels upon KD of all three proteins (Figure 4C). This was previously observed in other experiments (Figure 3B, 3E), although not statistically significant in these experiments. These



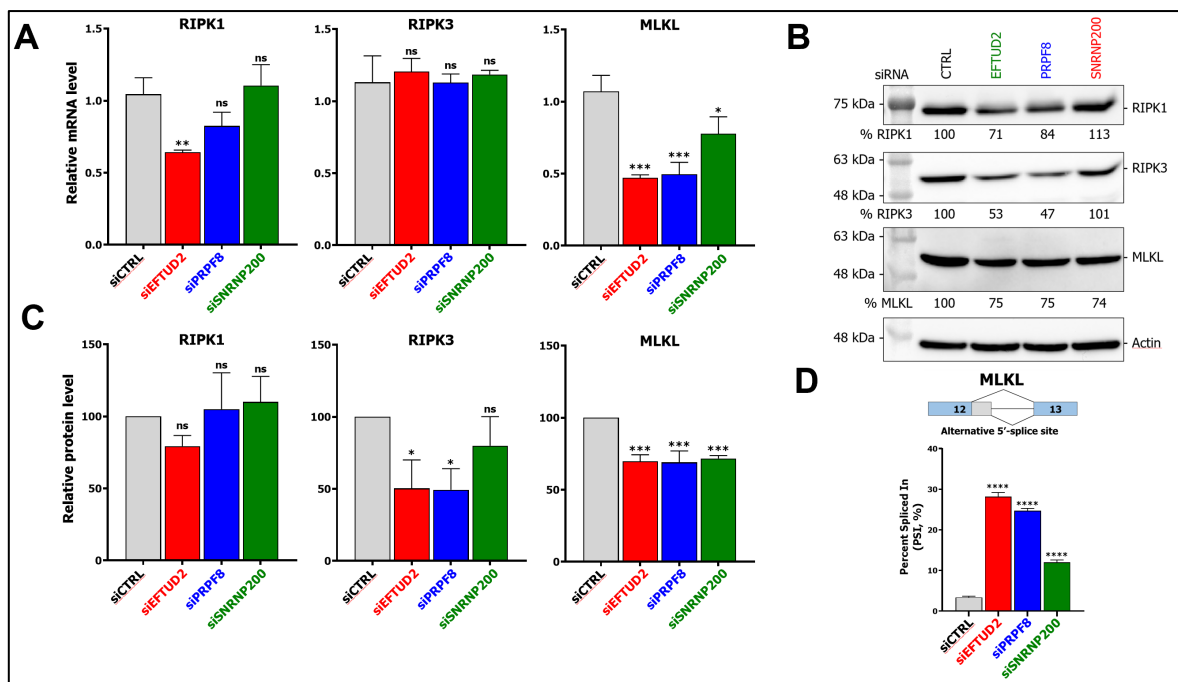


Figure 4. Depletion of U5 snRNP core components impacts the mRNA level, protein levels, and alternative splicing of necroptotic regulators. (A) Relative mRNA levels for RIPK1, RIPK3, and MLKL in control or EFTUD2, PRPF8, or SNRNP200-depleted L929 cells as determined by qPCR. L929 cells were transfected with the appropriate siRNA for 72 h before RNA was harvested, reverse transcribed, and subjected to qPCR. PSMC4, PUM1, and TXNL4B were used as housekeeping genes for normalization.  $n=3$ , biological replicates, one-way ANOVA with Dunnett's multiple comparisons test against the control siRNA condition (ns,  $P>0.05$ ; \*,  $P\leq 0.05$ ; \*\*,  $P\leq 0.01$ ; \*\*\*,  $P\leq 0.001$ ). (B) Western blot of the main necroptotic regulators (RIPK1, RIPK3, MLKL) in L929 cells treated with control or EFTUD2, PRPF8, or SNRNP200 specific siRNA. Cells were incubated for 72 h after transfection before proteins were harvested for western blot. Actin was used as a loading control. Relative quantitation is shown compared to the siCTRL condition. (C) Quantification and statistical analysis of three independent western blot for RIPK1, RIPK3 and MLKL.  $n=3$ , biological replicates, one-way ANOVA with Dunnett's multiple comparisons test against the siCTRL treated cells (ns,  $P>0.05$ ; \*,  $P\leq 0.05$ ; \*\*\*,  $P\leq 0.001$ ). (D) Percent Spliced In (PSI) values for the AS event (alternative 5' splice site) in MLKL upon depletion of EFTUD2, PRPF8, and SNRNP200. The AS event is depicted on the top.  $n=3$ , biological replicates, one-way ANOVA with Dunnett's multiple comparisons test against the control siRNA condition (\*\*\*\*,  $P\leq 0.0001$ ).

results emphasize that U5 snRNP core components control both the mRNA levels and proteins levels of critical proteins involved in necroptosis. Since the impact of EFTUD2 and PRPF8 KD on RIPK3 and MLKL levels are similar, whereas PRPF8 do not protect from necroptosis, these differences in protein levels cannot solely explain the involvement of EFTUD2 and SNRNP200 in necroptosis, and other mechanisms are likely involved. Finally, we wondered if the alternative splicing of RIPK1, RIPK3, and MLKL might be affected by manipulating the levels of the U5 snRNP core components since recent studies have suggested that the U5 snRNP controls cellular

AS<sup>5,16</sup>. The only annotated AS event in MLKL, an alternative 5' splice site, was strongly regulated by the depletion of all U5 snRNP proteins studied herein (Figure 4D). Two AS events in RIPK1, and two AS events in RIPK3, were also analyzed and revealed not to be the subject of AS under the conditions studied (Supplementary Figure S4). These results establish U5 snRNP proteins EFTUD2, PRPF8, and SNRNP200 as important for the necroptotic pathway, through their roles in regulating the mRNA levels, the protein levels, and the AS of key necroptotic proteins RIPK1, RIPK3, and MLKL.

### **EFTUD2 and PRPF8 are required for optimal induction of the IFN response**

Since an increasing amount of evidence suggests that some U5 snRNP proteins control the interferon response<sup>45–48</sup>, which is also involved in necroptosis<sup>49</sup>, we next investigated whether EFTUD2, PRPF8, and SNRNP200 are required for the IFN response. First, we tested if the reduction of U5 core components impacted the basal mRNA levels of IFN- $\beta$  and three interferon-stimulated genes (ISG; DDX60, MX1, MX2) by qPCR (Figure 5A). A significant reduction of DDX60 and MX2 mRNA levels was observed with all U5-directed siRNA, while MX1 mRNA was also significantly reduced except in the SNRNP200 depletion. This suggests the U5 snRNP is important for the processing and maturation of ISG, even in the absence of viral infection and IFN signaling. In the case of IFNB1, only the EFTUD2 KD significantly impacted its mRNA level. Next, we investigated if U5 snRNP core components are required for the IFN response in the context of MRV infection. Control and EFTUD2-, PRPF8- and SNRNP200-depleted cells were infected with MRV, and RNA was harvested at 24 h post-infection. To correct for the impact of these siRNA on the basal levels of ISG, a fold-change was calculated between infected and mock cells for each siRNA to allow adequate quantification of the induction of these genes during infection without the effect of the siRNA. The depletion of EFTUD2 and PRPF8 significantly reduced the IFN response after MRV infection (Figure 5B). In contrast, SNRNP200 had limited effect on the cell's ability to respond to infection through the IFN response pathway, highlighting once again the specific and different roles of these proteins belonging

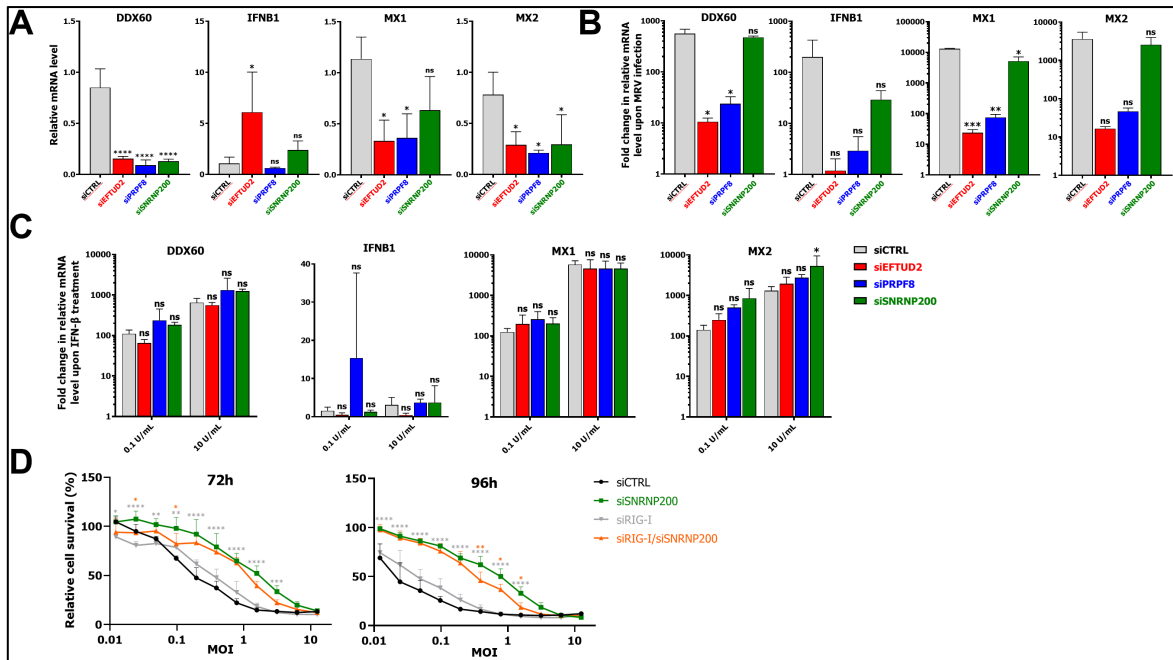


Figure 5. *EFTUD2* and *PRPF8* control the interferon response during MRV infection. (A) Relative mRNA levels for DDX60, IFNB1, MX1, and MX2 in control or EFTUD2, PRPF8, or SNRNP200-depleted L929 cells. L929 cells were transfected with the appropriate siRNA for 72 h before RNA was harvested, reverse transcribed, and subjected to qPCR. PSMC4, PUM1, and TXNL4B were used as housekeeping genes for normalization.  $n=3$ , biological replicates, one-way ANOVA with Dunnett's multiple comparisons test against the control siRNA condition (ns,  $P>0.05$ ; \*,  $P\leq 0.05$ ; \*\*\*\*,  $P\leq 0.0001$ ). (B) Relative fold induction upon MRV infection for DDX60, IFNB1, MX1, and MX2 in control or EFTUD2, PRPF8, or SNRNP200-depleted L929 cells. L929 cells were transfected with the appropriate siRNA for 55 h before being either mock-infected or infected with T3DS at a MOI of 3 for 24 h. Each replicate was arbitrarily attributed an uninfected control sample to calculate a fold-change upon infection.  $n=3$ , biological replicates, Brown-Forsythe and Welch one-way ANOVA with Dunnett's T3 multiple comparisons test against the control siRNA condition (ns,  $P>0.05$ ; \*,  $P\leq 0.05$ ; \*\*,  $P\leq 0.01$ ; \*\*\*,  $P\leq 0.001$ ). (C) Relative fold induction upon IFN- $\beta$  treatment for DDX60, IFNB1, MX1, and MX2 in control or EFTUD2, PRPF8, or SNRNP200-depleted L929 cells. L929 cells were transfected with the appropriate siRNA for 72 h, and then IFN- $\beta$  was added for 5 h before RNA was harvested, reverse transcribed and subjected to qPCR. PSMC4, PUM1, and TXNL4B were used as housekeeping genes for normalization.  $n=3$ , biological replicates, two-way ANOVA with Šidák's multiple comparisons test against the control siRNA treated with the same IFN- $\beta$  concentration (ns,  $P>0.05$ ; \*,  $P\leq 0.05$ ). (D) Methylene blue staining of control, SNRNP200, RIG-I, or RIG-I/ SNRNP200-depleted L929 cells infected with binary dilutions of T3DS at 72 h or 96 h post-infection. Twice the quantity of siRNA was transfected to perform DKD; in the case of single KD, siCTRL was added to match the total siRNA quantity of the DKD. The quantification of cell-bound methylene blue stain is shown for three independent experiments.  $n=3$ , biological replicates, two-way ANOVA with Dunnett's multiple comparisons test against the SNRNP200 KD condition (in red; \*,  $P\leq 0.05$ ; \*\*,  $P\leq 0.01$ ; \*\*\*,  $P\leq 0.001$ ; \*\*\*\*,  $P\leq 0.0001$ ). If not indicated, results are not statistically significant. The results of the comparison against the control siRNA (in black) are not indicated for clarity purposes.

to the same snRNP. Although quantitatively different, similar effects on the interferon response were also observed upon infection at a higher MOI

(Supplementary Figure S5).

The IFN response pathway is divided in two parts: recognition of viral PAMP and production of IFN, and then signaling through the IFN receptor (IFNAR) and induction of ISG. To address whether the involvement of EFTUD2 and PRPF8 is in the first or second part of the pathway, we repeated the preceding experiment, but this time we stimulated the cells using IFN- $\beta$  instead of using MRV. By doing so, the first part of the pathway is bypassed, and only the IFNAR signaling and ISG induction are involved. First, we treated L929 cells with 10-fold dilutions of recombinant IFN- $\beta$  and measured the induction of ISG to determine the right concentration of IFN- $\beta$  to use (Supplementary Figure S6). None of the IFN- $\beta$  concentrations tested could induce the IFNB1 gene, highlighting that the observed effect is strictly driven by the exogenous IFN- $\beta$  added to the medium. Based on these titration curves, we selected 10 U/mL of IFN- $\beta$ , since this concentration was inducing the maximal effect, and 0.1 U/mL, a concentration sufficient to induce ISG a little less than a 100-fold. Control and EFTUD2-, PRPF8- and SNRNP200-depleted cells were then treated with IFN- $\beta$ , and RNA was harvested 5 h later. In the absence of EFTUD2, PRPF8, and SNRNP200, the fold induction of DDX60, MX1, and MX2 was not significantly reduced in comparison to the control condition (Figure 5C). This supports the idea that the impact previously observed in MRV-infected cells (Figure 5B) of EFTUD2 and PRPF8 is not on the second part of the pathway (signaling through IFNAR and induction of ISGs), but rather lies before, probably during recognition of viral PAMP and production of IFN.

Having shown that SNRNP200 had little effect on IFN induction during MRV infection, we further validated that its impact on cell survival is not dependent on the interferon pathway. To do so, we depleted RIG-I, one of the principal cytoplasmic sensors of viral dsRNA and ssRNA during MRV infection that allows the production of primary IFN and subsequent induction of ISG<sup>50,51</sup>. The depletion of RIG-I in L929 using siRNA was previously shown to be highly efficient<sup>5</sup> and validated again using qPCR

(Supplementary Figure S1). We depleted RIG-I and SNRNP200 individually, or in combination, and looked at overall cell survival using methylene blue staining as before. The DKD is slightly reduced compared to KD of SNRN200, but still presents an overall increased survival compared to the single RIG-I KD (Figure 5D). We thus conclude that only a marginal part of the effect of SNRNP200 is mediated by the IFN response pathway, as KD of RIG-I minimally decreases its protective effect. Similar experiments were performed for EFTUD2; however, the interpretation of the results was much more complex since the survival induced by EFTUD2 is much closer to the control condition than SNRNP200 in this assay (Supplementary Figure S7). From these experiments, we conclude that both EFTUD2 and PRPF8 control the IFN response during MRV infection, and SNRNP200's requirement for cell death during MRV infection is mainly not IFN-mediated.

### **EFTUD2 restricts MRV's replication in both single cycle and multiple cycles of replication**

The results presented herein highlight novel roles of U5 snRNP proteins EFTUD2, PRPF8, and SNRNP200 in apoptosis, necroptosis, and interferon induction, using MRV as a model for viral infection. However, one last question remains to this point: are these U5 snRNP proteins antiviral? Since they are involved in critical aspects of the battle between the virus and the cell (i.e., the interferon response and cell death), one could hypothesize that they indeed contribute to limit viral replication, since they are required for cell death and induction of the interferon response. To answer this question, we infected L929 cells with MRV at a MOI of 3 upon KD of EFTUD2, PRPF8, and SNRNP200 and followed viral replication by TCID<sub>50</sub> at 24 h, 48 h and 72 h. In the control siRNA condition, maximal viral replication was already obtained at 24 h (Figure 6A), as expected during MRV's replication cycle<sup>52</sup>. When PRPF8 or SNRNP200 were depleted, no increase in viral replication could be detected at these time points (Figure 6A). However, EFTUD2 KD significantly enhanced the replication at 72 h by 10-fold (Figure 6A). Since EFTUD2-depleted cells survive longer

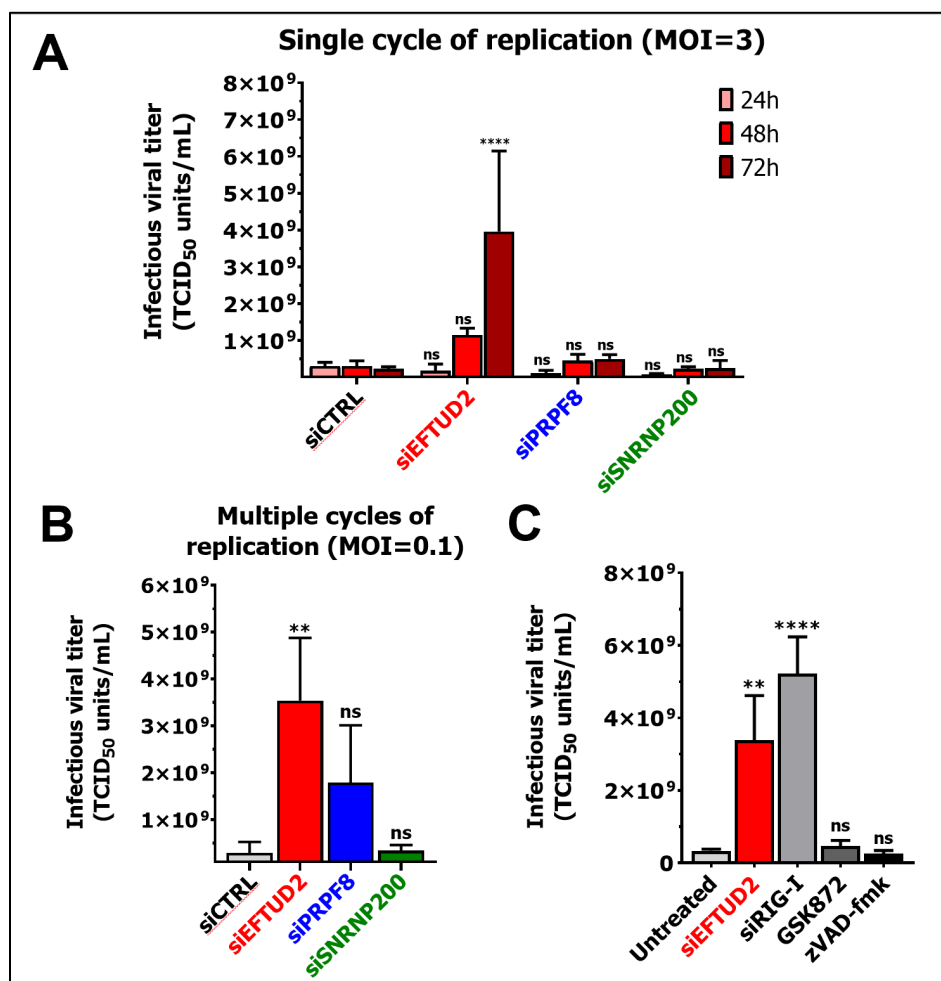


Figure 6. *EFTUD2* restricts MRV's replication in both single cycle and multiple cycles of replication. (A) MRV viral titers from siCTRL, siEFTUD2, siPRPF8, and siSNRNP200-treated L929 cells infected cells at 24 h, 48 h, and 72 h. Cells were infected at a MOI of 3, and viral titers were determined by TCID<sub>50</sub> on L929 cells. n=3, biological replicates, two-way ANOVA with Dunnett's multiple comparisons test against the siCTRL matched timepoint (ns, P>0.05; \*\*\*\*, P≤0.0001). (B) MRV viral titers from siCTRL, siEFTUD2, siPRPF8 and siSNRNP200-treated L929 cells infected cells at 96 h. Cells were infected at a MOI of 0.1, and viral titers were determined by TCID<sub>50</sub> on L929 cells. n=3, biological replicates, one-way ANOVA with Dunnett's multiple comparisons test against the siCTRL condition (ns, P>0.05; \*\*, P≤0.01). (C) MRV viral titers in L929 cells untreated, transfected with a siRNA against EFTUD2 or RIG-I, or treated with GSK872 (3 μM) or zVAD-fmk (50 μM) to block necroptosis and apoptosis, respectively. L929 cells were infected at a MOI of 3, and viral titers were determined by TCID<sub>50</sub> on L929 cells at 72 h post-infection. n=3, biological replicates, one-way ANOVA with Dunnett's multiple comparisons test against the untreated condition (ns, P>0.05; \*\*, P≤0.01; \*\*\*\*, P≤0.0001).

after infection (Figure 1A, 1C, 1D, and 1E), this increased survival is also accompanied by prolonged viral replication beyond the normal replication cycle. This effect is also specific for EFTUD2, since there is no increase in viral replication in

fSNRNP200-depleted cells that also present the cell-survival phenotype (Figure 1A, 1C, 1D, and 1E). We next wanted to assess if the same increase in viral replication is maintained during multiple replication cycles, since EFTUD2-depleted cells could potentially exert a protective effect by keeping the virus intracellular and preventing its release through increased survival. L929 cells were thus infected with MRV at a MOI of 0.1 upon KD of EFTUD2, PRPF8, and SNRNP200, and viral replication was quantified at 96 h. Once again, only the EFTUD2 KD enhanced viral replication significantly by 10-fold (Figure 6B). Since the same increase is observed in both single cycle and multiple replication cycles, we conclude that EFTUD2 KD does not block the release of MRV from infected cells beyond the normal replication cycle, and that EFTUD2 restricts MRV replication, both in a single cycle and multiple cycles of replication. We previously showed that EFTUD2 is required for apoptosis (Figure 2D), necroptosis (Figure 3A, 3B, 3E, and 3F), and efficient interferon response (Figure 5B) during MRV infection; we finally wondered if the antiviral effect of EFTUD2 is mediated through its role in apoptosis, necroptosis, or the interferon response. First, we assessed the best way to chemically block necroptosis during MRV infection by using GSK963 (targeting RIPK1) or GSK872 (targeting RIPK3) (Supplementary Figure S8). GSK872 could completely abrogate MLKL phosphorylation in MRV-infected cells; however, GSK963 could only reduce the levels of p-MLKL by approximately 50%. We thus utilized GSK872 to block necroptosis, zVAD-fmk to block apoptosis, and a siRNA against RIG-I to limit the interferon response and monitored viral replication at 72 h to decipher the respective role of apoptosis, necroptosis and the interferon response on MRV replication. Both zVAD-fmk and GSK872 did not significantly impact MRV's viral titers, suggesting that apoptosis and necroptosis have little influence on MRV replication (Figure 6C). However, limiting the interferon response using a siRNA against RIG-I significantly enhanced MRV replication, in a range similar to the EFTUD2 depletion. This result suggests the antiviral activity of EFTUD2 is principally mediated by its impact on the interferon response, and minimally by its role in apoptosis and necroptosis.

## DISCUSSION

In this study, we demonstrated distinct and overlapping crucial roles of U5 snRNP core components EFTUD2, PRPF8, and SNRNP200 on apoptosis, necroptosis, and interferon induction during viral infection, using MRV as a model virus. We demonstrated that EFTUD2 and SNRNP200 are required for both apoptosis and necroptosis, whereas EFTUD2 and PRPF8 are required for optimal interferon response against viral infection. These results are summarized in Figure 7A. Previous studies had already hinted at the role of U5 snRNP core components in apoptosis. Expression of pathogenic PRPF8 variants responsible for retinitis pigmentosa induced apoptosis<sup>53</sup>. Retinitis pigmentosa is a genetic disorder of the eyes characterized by a loss of vision and is sometimes caused by mutations in specific spliceosomal proteins, such as PRPF8 and SNRNP200. Moreover, increased PRPF8 protein levels in ovarian cancer cells protect cells from apoptosis<sup>54</sup>. Our results support these findings, as depleting PRPF8 led to enhanced annexin V staining (Figure 2B) and enhanced cell death (Figure 2C) in uninfected cells. However, we did not observe any defect in cell proliferation by RTCA (Figure 1B), any difference in cell death by FACS (Figure 1C), nor any significant enhancement in Cas3/7 activity when silencing PRPF8 in the absence of infection (Figure 2D). It thus indicates that the effect of PRPF8 on apoptosis is minor, at least in L929 cells, and might be challenging to observe, especially if cells are already dead by the time the assay is performed. Other studies have demonstrated that EFTUD2 performs a similar role, where depletion of EFTUD2 leads to enhanced apoptosis in developmental models and cancer cell lines<sup>55-58</sup>. EFTUD2 depletion also impacts the splicing of mRNA encoding survival and cell death proteins, suggesting that the involvement of EFTUD2 in apoptosis might be, at least in part, splicing-dependent<sup>58</sup>. Our results do not point to any impact of EFTUD2 depletion on apoptosis in the absence of MRV infection in L929 cells (Figure 1B, 1C, 2B, 2C, and 2D). The impact of EFTUD2 on apoptosis might depend on other determinants, such as the status of p53, as previously demonstrated by others<sup>56,58</sup>. Further research should clarify the involvement of



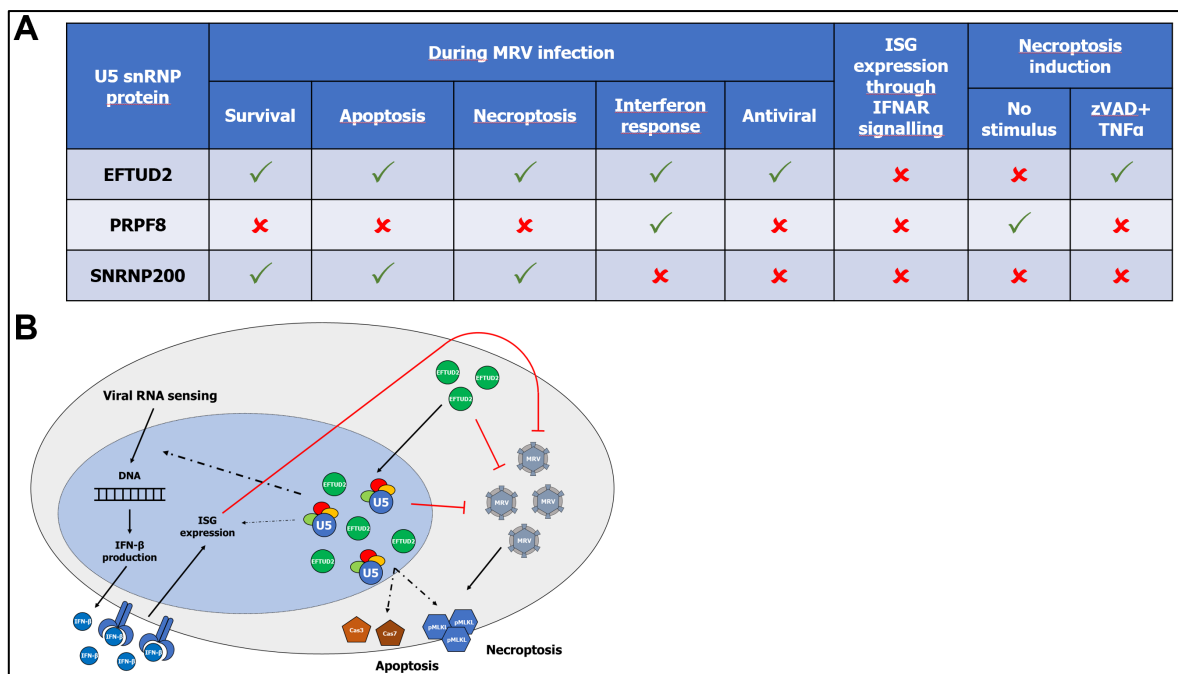


Figure 7. *Summary of the involvement of U5 snRNP core proteins in virus-host interactions.* (A) Table depicting the respective roles of EFTUD2, PRPF8, and SNRNP200 in the interferon response pathway, apoptosis, and necroptosis. (B) Model depicting the roles of EFTUD2 during MRV infection. EFTUD2 (either cytoplasmic or nuclear, and when nuclear, either in the U5 snRNP or by itself) exerts an antiviral role on MRV replication. MRV infection elicits both apoptosis and necroptosis, which require the presence of EFTUD2 to normally proceed. EFTUD2 is also required for the basal expression of ISG, but its principal impact on the IFN response pathway during infection lies somewhere between the sensing of viral RNA and the production of IFN.

EFTUD2 and PRPF8 in apoptosis in different cellular contexts, both in the absence and presence of apoptosis triggers, and the determinants that might influence these roles.

Since the link between apoptosis and some U5 snRNP core components had already been established, we focused our experiments on necroptosis, which had never been previously linked to U5 proteins. Once again, both EFTUD2 and SNRNP200 protected L929 cells from MRV-induced necroptosis. Moreover, EFTUD2 also protected from zVAD/TNF $\alpha$ -mediated necroptosis, whereas with this stimulus, SNRNP200 exerted no protective effect, and even sensitized cells to necroptosis (Figure 3C, 3D, and 3E). The opposite effects of SNRNP200 on necroptosis based on the stimulus triggering necroptosis is interesting; determining how SNRNP200 protects cells from MRV-mediated necroptosis will help understand why during zVAD/TNF $\alpha$  treatment

necroptosis is enhanced in the absence of SNRNP200 whereas its depletion protects against MRV-mediated necroptosis. Once again, we observed the induction of cell death, this time necroptosis, when PRPF8 is depleted (Figure 2A and 2B), very similarly to apoptosis. However, this effect is not always observed, notably during zVAD/TNF $\alpha$  treatment (Figure 3D). The difference between these two experiments is the time allowed to accumulate dead cells in the medium; in Figure 3A, cells were harvested 40 h after infection, a very long incubation time that could lead to a significant accumulation of dead cells in the medium. In contrast, zVAD/TNF $\alpha$  treatment is much shorter (4 h), and cells are rinsed before zVAD-fmk pretreatment. This thus suggests that the number of necroptotic cells when PRPF8 is depleted is low and requires long incubation times to accumulate sufficiently for detection. Nevertheless, the observation that depletion of PRPF8 triggers necroptosis raises further important questions. Which cells are actively undergoing necroptosis? Are these the ones that have the most drastic reduction of PRPF8? And what is sensed in those cells as the trigger for necroptosis, and through which sensor? This raises the interesting hypothesis that misspliced RNA might somehow be sensed and trigger necroptosis, or at least could be involved in necroptosis regulation. Available interactome data for MLKL, RIPK1, and RIPK3 seem to support this hypothesis, as MLKL interactors are enriched for RNA binding protein and splicing factors as well as for nuclear proteins, which is not the case for RIPK1 and RIPK3 (Supplementary Figure S9). Notably, six proteins from the U5 snRNP (DDX23, EFTUD2, PRPF6, PRPF8, SNRNP40, and SNRNP200) are amongst the interactors of MLKL, suggesting that these U5 snRNP proteins, either alone or assembled in the mature snRNP, might interact with MLKL, and point to some U5-driven regulation of necroptosis. The importance of nuclear-driven phenomenon during necroptosis further hints at a nuclear component of its regulation<sup>59-61</sup>. During apoptosis, some caspases, such as caspase-7, are notably regulated through RNA to target RNA binding proteins, further emphasizing the critical role of RNA in the regulation of programmed cell death<sup>62,63</sup>.

Both apoptosis and necroptosis are triggered during MRV infection<sup>35,38</sup>. However, the roles of these respective programmed cell death pathways and how they are intertwined have not been systemically deciphered. For rotavirus, a closely related pathogenic virus causing diarrhea in infants, recent work revealed that apoptosis and necroptosis are balanced together, and when one cell death pathway is chemically blocked, the other takes over<sup>64,65</sup>. The absence of cell death is detrimental during multiple viral replication cycles, supporting the vision that cell death allows the release of the progeny virions from the host cell and viral spread<sup>64</sup>. However, in a single replication cycle, the effects of both necroptosis and apoptosis are less clear; a study showed no impact of necroptosis on viral replication<sup>64</sup>, whereas another suggested apoptosis is antiviral and necroptosis is proviral<sup>65</sup>. MRV's determinants of apoptosis have been well-studied, with the involvement of viral proteins  $\sigma 1$ ,  $\sigma 3$ ,  $\mu 1$ , and possibly  $\sigma 1s$ <sup>22,35,66,67</sup>. However, determinants of MRV-mediated necroptosis are much less known and require further studies. Viral replication is required, and chemically blocking RIPK1 seems to reduce MRV-driven necroptosis<sup>37,38</sup>. In this study, we observed that blocking RIPK1 using GSK963 could not completely abrogate MLKL phosphorylation, whereas blocking RIPK3 using GSK872 efficiently suppresses all phosphorylation of MLKL (Supplementary Figure S8). This result suggests that MRV-induced necroptosis is not strictly sensed by RIPK1, and that other necroptotic sensors might be involved. MRV's cell entry is notably endosomal, where another necroptotic sensor, TRL3, is located<sup>21,22</sup>. TRL3 recognizes dsRNA, such as the one present in MRV's internal capsid and recently shown to be exposed during entry, and thus could likely trigger necroptosis from the endosome by sensing MRV's dsRNA<sup>68,69</sup>. The role of TLR3 in MRV's infection requires further studies, as its involvement is still unclear<sup>70-73</sup>. More research should also be performed to determine if MRV's proteins are directly triggering necroptosis. In the case of rotavirus, NSP4 is directly responsible for both apoptosis and necroptosis<sup>65</sup>. We have shown previously that MRV's  $\mu 2$  protein interacts with EFTUD2, PRPF8, and SNRNP200<sup>5</sup>, and we now demonstrate that some of these proteins are required for

induction of necroptosis. Whether the  $\mu 2$  protein might be involved in the induction of necroptosis during MRV infection warrants further studies.

We also demonstrated that the silencing of EFTUD2 and PRPF8 significantly limits both interferon- $\beta$  and ISG induction during MRV infection (Figure 5B). These results support other studies that have suggested a role of U5 proteins in the interferon pathway<sup>45-48</sup>. Indeed, both EFTUD2 and SNRNP200 have been shown to sense viral RNA in the cytoplasm, setting off the interferon response<sup>46,47</sup>. Furthermore, EFTUD2 also controls the AS of MYD88, a key player of the signal transduction upstream IFN production<sup>48</sup>. However, in MRV-infected L929 cells, SNRNP200 exerted no control over the IFN response, whereas PRPF8 had an effect very similar to EFTUD2, albeit to a lesser extent. Further studies should clarify if these discrepancies are cell line specific or arise through an indirect effect of one of the KD. Nonetheless, the aforementioned mechanism of viral RNA sensing in the cytoplasm of U5 snRNP core components was also confirmed in this study, as directly treating cells with IFN- $\beta$  completely abrogated EFTUD2 and PRPF8 control of the IFN response. This raises the interesting question as to where in the cell is the U5 snRNP and/or the U5 components controlling the IFN response. Are individual components in the cytoplasm having this second role before their loading in the mature U5 snRNP and import into the nucleus, as shown previously for EFTUD2 and SNRNP200<sup>46,47</sup>? Is this role linked to the mature U5 snRNP and AS-dependent, as it was demonstrated for MYD88<sup>48</sup>? Finally, we cannot rule out that the U5 snRNP complex fully assembled in the nucleus might control the induction of IFN and ISG not linked to AS. All these possibilities warrant further studies into the role of the U5 snRNP in the IFN response. Finally, we also demonstrated that EFTUD2 restrict MRV's replication, both in a single cycle and multiple cycles of replication. Neither blocking apoptosis or necroptosis alone could enhance MRV's titers, but limiting the IFN response could enhance MRV's titer to levels similar to the depletion of EFTUD2, suggesting EFTUD2 exerts its antiviral activity mainly by its role in the IFN pathway. EFTUD2's roles during MRV infection are summarized in Figure 7B.

We previously demonstrated that MRV reduces the protein levels of EFTUD2, PRPF8, and SNRNP200 through the action of the  $\mu 2$  protein during infection<sup>5</sup>. We now show a direct benefit for MRV to induce this reduction, which allows enhanced cell survival through reduced apoptosis and necroptosis, diminished IFN response, and enhanced viral replication. As U5 snRNP emerged recently as a targeted cellular component during viral infection<sup>4-6</sup>, the study presented herein further strengthens our understanding of the benefit for viruses to destabilize the U5 snRNP through its crucial role in regulating apoptosis, necroptosis, and the IFN response pathway.

## **METHODS**

### **Cells, viruses, and treatments**

Mouse L929 fibroblasts were originally obtained from the American Type Culture Collection (ATCC) and were grown in Eagle's minimal essential medium (EMEM, Wisent) containing 5% fetal bovine serum (Wisent) and supplemented with 1% glutamine. MRV serotype 3 strain Dearing (T3/Human/Ohio/Dearing/55) was also originally obtained from ATCC and was propagated and titrated by TCID<sub>50</sub> on L929 fibroblasts<sup>74</sup>. The laboratory stock of MRV type 3 (T3DS) was previously described<sup>30,31</sup>, and rescued by reverse genetics following the introduction of the appropriate mutations in the plasmids encoding the virus from the original reverse genetics system<sup>75</sup>. The pan-caspase inhibitor zVAD-fmk (AdooQ Bioscience), the RIPK3 inhibitor GSK872 (Abcam) and the RIPK1 inhibitor GSK963 (Sigma) were resuspended at 10 mM in DMSO and used at final concentrations of 100  $\mu$ M (necroptosis induction) or 50  $\mu$ M (viral titers), 3  $\mu$ M, and 3  $\mu$ M, respectively. To elicit RIPK1-mediated necroptosis in L929 cells, cells were pretreated with zVAD-fmk at 100  $\mu$ M for 1 h, and then recombinant murine TNF- $\alpha$  (Peprotech) was directly added to the medium at 25 ng/mL. Recombinant mouse interferon- $\beta$  (PBL Assay Science, #12401-1) was diluted in complete medium to the indicated concentration and cells were treated for 5 h.

## **Viral Infection**

L929 cells were plated at a density of  $7 \times 10^4$  cells per square centimeter the day before being infected at a multiplicity of infection (MOI) of 0.1 or 3 TCID<sub>50</sub> units per cell using standard procedures<sup>74</sup>. Control L929 cells were seeded at the same density and mock-infected. Whenever cells needed to be transfected using siRNA first, the number of cells at the time of infection was evaluated based on the number of cells seeded for transfection, the time since transfection, and apparent confluency of the cells.

## **siRNA transfection**

L929 cells were plated in a 12-well plate at 100,000 cells/well and transfected on the following morning using 50 pmol of siRNA and 3.75  $\mu$ L of RNAiMAX (ThermoFisher Scientific) as per the manufacturer's protocol. Ambion Silencer® Select (catalog number 4390771) siRNA were used against EFTUD2 (ID: s74089); PRPF8 (ID: s101224); SNRNP200 (ID: s115821); and RIG-I (ID: s106375). The Silencer™ Select Negative Control No. 1 siRNA (#4390843) was used as a negative control. Cells were incubated for 72 h before harvesting RNA or proteins for downstream analyses. For double knock-down (DKD), twice the quantity of siRNA was transfected to perform DKD alongside twice the volume of RNAiMAX; in the case of a single KD, siCTRL was added to match the total siRNA quantity of the DKD.

## **Real-time cell analysis (RTCA)**

The xCELLigence system (ACEA Biosciences) was used to monitor cell adherence and morphology in real time. E-plates were filled with 50  $\mu$ L of complete culture medium per well, and the plates incubated for several hours at 37°C with 5% CO<sub>2</sub> to allow equilibration. Then, L929 cells were seeded at 5000 cells/well in 50  $\mu$ L of complete medium and allowed to adhere overnight. The next morning, siRNA were transfected and the monitoring was resumed. 24 h later, the medium containing the siRNA complexes was removed and kept and cells were infected at a MOI of 3. Following adsorption, the medium containing the siRNA complexes was added back

to the wells and plates were allowed to equilibrate approximately 15 min at 37°C with 5% CO<sub>2</sub> before the monitoring was resumed. The relative cell index was normalized to the 0 h time point, right after infection. Measurements were taken every 10 min for up to 100 h after infection. For the zVAD-fmk/TNF $\alpha$  treatment, cells were incubated for 72 h after siRNA transfection to allow an efficient depletion of the targeted proteins. Then, cells were pretreated for 1 h with 100  $\mu$ M of zVAD-fmk, before medium was changed for zVAD-fmk (100  $\mu$ M) and TNF $\alpha$  (25 ng/mL). A siCTRL condition was treated with only zVAD-fmk to confirm no cell death was induced in the absence of TNF $\alpha$ . Plates were allowed to equilibrate approximately 20 min at 37°C with 5% CO<sub>2</sub> before the monitoring was resumed. The relative cell index was normalized to the 0 h time point, right after TNF $\alpha$  was added. Measurements were taken every 15 min.

### **FACS analysis**

The cell culture medium was transferred to a new tube, and cells were harvested by trypsinization before being pooled with the culture medium. Upon centrifugation, the cell pellet was resuspended in 100  $\mu$ L of annexin V binding buffer (10 mM HEPES, 140 mM NaCl, 2 mM CaCl<sub>2</sub>, pH 7.4) containing Hoechst (Invitrogen, 0.8 mg/mL) and propidium iodide (Invitrogen, 1  $\mu$ g/mL). The cells were stained for 30 min at 37°C with 5% CO<sub>2</sub> before 400  $\mu$ L of annexin V binding buffer was added and live cells were quantitated by FACS on a BD LSRFortessa. Cells were gated first using FSC/SSC to exclude cell debris, and then using Hoechst and SSC to only retain single cells. 10,000 events were acquired satisfying these criteria. Then, cell viability was quantitated by identifying live cells as both Hoechst positive and propidium iodide negative.

### **Methylene Blue Staining**

L929 cells were seeded at 20,000 cells/well and transfected the following day with the appropriate siRNA. 24 h later, binary dilutions of T3D<sup>S</sup> were prepared, starting from a MOI of 12.5 to  $\approx$ 0.01 (11 dilutions). A control well was left uninfected (mock).

The transfection medium was removed from the plate and kept at 37°C with 5% CO<sub>2</sub>; binary dilutions of the virus were added to the plates and followed by an incubation of 1 h at 4°C. Transfection medium was then added back to their original wells, and plates were incubated for 48 h, 72 h, or 96 h at 37°C with 5% CO<sub>2</sub>. Plates were fixed in 4% formaldehyde in PBS for 1 h, washed in PBS, and then stained with methylene blue (1% w/v methylene blue, 150 mM NaCl, 90% MeOH in water) for 1 h. Plates were washed once with PBS and twelve times with tap water and allowed to dry in a chemical hood. When dried, plates were imaged using a Quantum ST5 gel doc (Montreal Biotech, Vilber Lourmat). To allow for a precise quantification, cell bound methylene blue was resolubilized in 100 µL of 0.1 N HCl overnight and read at 665 nm in a 96-well plate reader. Normalization was realized by first setting the mock well in the siCTRL condition at 100% for each replicate; then, the mock for each other siRNA conditions was also normalized at 100%, to allow for correction of growth and confluency effects.

### **High-throughput multiplex microscopy-based apoptosis assay**

The multiplex cell death phenotypic assay was performed as previously described<sup>39,40</sup>. L929 cells were seeded at 10,000 cells/well in black 96-well plates and transfected the next morning with the appropriate siRNA. Thirty hours later, medium was removed, kept at 37°C with 5% CO<sub>2</sub> and cells were mock-infected or infected with T3D<sup>S</sup> at a MOI of 3. The initial medium was put back on the cells and infection was allowed to pursue for 40 h before the assay. The medium was removed and 50 µL of dye mix (Hoechst, Invitrogen, 0.8 mg/mL; calcein AM, Invitrogen, 0.5 µM; annexin V conjugated with Alexa Fluor 647, Invitrogen A23204, 2.85 µL/mL; propidium iodide, Invitrogen, 1 µg/mL; in annexin V binding buffer) was added to each well, and cells were stained 30 min at 37°C, 5% CO<sub>2</sub>. The dye mix was removed and 50 µL of new annexin V binding buffer was added prior to imaging using the Operetta CLS High Content Analysis System (Perkin Elmer). Nine different fields per well were imaged and imported into the Columbus software (PerkinElmer) for analysis. Each experiment included six biological replicates.



### **Caspase Activity Assay**

Cas3/7 activity was measured using the Caspase-Glo® 3/7 Assay System (Promega). Briefly, cells were treated with the siRNA for 55 h before being infected or mock-infected at a MOI of 3 for 40 h. Then, plates were allowed to equilibrate at room temperature for 10 min, and 100 µL of Caspase-Glo reagent was added to each well. Plates were shaken for 30 s, and read 30 min later in a TECAN SPARK multimode microplate reader for 5 s. First, mean background was subtracted to each measurement. Then, the first replicate of the siCTRL in the mock condition was fixed at 0%, and the first replicate of the siCTRL in the infected condition was fixed at 100%.

### **RNA extraction**

Total RNA samples were extracted with Qiazol® as recommended by the manufacturer (Qiagen).

### **Reverse transcription**

Reverse transcription was performed on 2.2 µg total RNA with Transcriptor reverse transcriptase, random hexamers, dNTPs (Roche Diagnostics), and 10 units of RNase OUT (Invitrogen) following the manufacturer's protocol in a total volume of 20 µL.

### **qPCR**

All forward and reverse primers were individually resuspended to 20–100 µM stock solution in Tris-EDTA buffer (IDT) and diluted as a primer pair to 1 µM in RNase DNase-free water (IDT). The complete list of qPCR primers used in this study is available in Supplementary Table S1. Quantitative PCR (qPCR) reactions were performed in 10 µL in 96-well plates on a CFX-96 thermocycler (BioRad) with 5 µL of 2X iTaq Universal SYBR Green Supermix (BioRad), 10 ng (3 µl) cDNA, and 200 nM final (2 µL) primer pair solutions. The following cycling conditions were used: 3 min at 95°C; 50 cycles: 15 s at 95°C, 30 s at 60°C, 30 s at 72°C. Relative expression levels were calculated using the qBASE framework using PSMC4, PUM1, and TXNL4B

as housekeeping genes. For all PCR run, control reactions performed in the absence of template were performed for each primer pair, and these were consistently negative. All qPCR data were generated following the MIQE guidelines<sup>76</sup>.

### **Alternative splicing PCR (AS-PCR)**

PCR primer sequences were designed at the Université de Sherbrooke's RNomics Platform using a custom software designed to optimize standard primer design criteria, and to certify target specificity using embedded NCBI Blast software. The primers were placed on exons flanking the alternative region to amplify both isoforms in the same PCR reaction. The complete list of AS-PCR primers used in this study is available in Supplementary Table S2. Design maps for the AS events analyzed in this study are shown in Supplementary Figure S10. All forward and reverse primers were individually resuspended to 20–100  $\mu\text{M}$  stock solution in Tris-EDTA buffer (IDT) and diluted as a primer pair to 1.2  $\mu\text{M}$  in RNase DNase-free water (IDT). End-point PCR reactions were done on 10 ng cDNA in 10  $\mu\text{L}$  final volume containing 0.2 mM each dNTP, 1.5 mM  $\text{MgCl}_2$ , 0.6  $\mu\text{M}$  each primer, and 0.2 units of Platinum Taq DNA polymerase (Invitrogen). An initial incubation of 2 min at 95°C was followed by 35 cycles at 94°C 30 s, 55°C 30 s, and 72°C 60 s. The amplification was completed by a 2 min incubation at 72°C. PCR reactions were carried on thermocyclers GeneAmp PCR System 9700 (ABI), and the amplified products were analyzed by automated chip-based microcapillary electrophoresis on LabChip GX Touch HT Nucleic Acid Analyzer (PerkinElmer). Amplicon sizing and relative quantitation were performed by the manufacturer's software, before being uploaded to the LIMS database. The percent spliced-in (PSI) metric was used to quantitate the level of inclusion in these alternative splicing events. It represents the percent of the long form over total abundance for both the long and short forms. The formula is as follows:

$$PSI = \frac{\textit{Long form}}{\textit{Long form} + \textit{Short form}}$$

## **Immunoblotting analysis**

The linearity of antibodies used in this study was first experimentally determined to allow the adequate quantification in the linear range of both the samples analyzed and the antibody used. Cells were scraped into the culture medium using the blunt end of a P1000 tip and pelleted at 3000 RPM for 10 min. Medium was removed and cells were lysed in RIPA Buffer (1% Triton X-100, 1% sodium deoxycholate, 0.1% SDS, 1 mM EDTA, 50 mM Tris-HCl pH 7.5 and complete protease inhibitor (ROCHE)) supplemented with 1X Halt™ Protease and Phosphatase Inhibitor Cocktail (ThermoFisher Scientific) right before use. Sonication at 13% amplitude for 5 s, twice on ice was used to complete cell lysis and enhance the solubility of the samples. Debris were then pelleted at 13,000 RPM, 4°C, 10 min. Lysates were dosed for total protein in triplicate using standard Bradford assay (ThermoFisher Scientific Pierce™ Coomassie (Bradford) Protein Assay Kit). The right amount of protein was diluted with water and Laemmli 4x buffer (200 mM Tris-HCl pH 6.8, 40% glycerol, 1.47 M β-mercaptoethanol, 4% SDS, bromophenol blue) and heated 5 min at 95°C. Samples were loaded on 10% SDS-polyacrylamide gels alongside BLUelf protein ladder (FroggaBio) and electrophoresis was carried out at 70 volts until samples entered the resolving gel. Electrophoresis was allowed to proceed at 100 volts until complete migration. Proteins were transferred onto a polyvinylidene difluoride (PVDF) membrane at 4°C, 75 min, 100 volts. Membranes were blocked in 5% non-fat milk in TBS-T (10 mM Tris-HCl pH 8.0, 220 mM NaCl, 0.1% Tween 20), 1 h at room temperature. The commercial antibodies used in this study are the following: Actin (Sigma, A5441, 1:10,000), MLKL phosphorylated on S345 (Cell Signaling Technology, #37333, 1:1000), MLKL (Cell Signaling Technology, #37705, 1:1000), RIPK1 (Cell Signaling Technology, #37333) and RIPK3 (Cell Signaling Technology, #37333). The σ3 antibody is the supernatant from a mouse hybridoma cell line expressing the monoclonal antibody 4F2 and was diluted 1:100<sup>77</sup>. Membranes were incubated overnight with the appropriate antibody in 2.5% milk/PBS, except for pMLKL and MLKL antibodies which were diluted with 5% bovine serum albumin in TBS-T. Membranes were washed three times in TBS-T and incubated with a horse

anti mouse-HRP secondary antibody diluted 1:5000 (Cell Signaling Technologies, 7076) or goat anti rabbit-HRP secondary antibody diluted 1:10,000 (Abcam, ab205718) during 1 h 30 min at room temperature. Membranes were washed again three times with TBS-T and once with PBS. Bound antibodies were revealed using Clarity ECL western blotting substrates (BIO RAD) and scanned with an ImageQuant LAS4000 (GE Healthcare Life Science). For quantification, HRP was inactivated using 30% H<sub>2</sub>O<sub>2</sub> for 30 min, washed twice in PBS, and membranes were blocked again and probed for actin. For pMLKL/MLKL WB, membranes were stripped after the actin to probe total MLKL. Membranes were incubated 15 min at 56°C in stripping buffer (7.25 mM Tris-HCL pH 7.5, 0.1% SDS, 0.1% β-mercaptoethanol) before being blocked again and follow the usual procedure. All western blots were performed three times, and a representative result is presented in the article. Uncropped western blots are available in the Supplementary Figure S11.

### **Infectious viral titers using TCID<sub>50</sub>**

For siRNA depletion, L929 cells were seeded in 24-well plates at 100,000 cells/well (MOI of 0.1) or 40,000 cells/well (MOI of 3). On the following morning, cells were transfected with the appropriate siRNA. Infections were performed 24 h later (MOI of 0.1); the transfection medium was kept and put back on the cell immediately after viral adsorption, or 55 h later (MOI of 3) and the transfection medium discarded. For chemical treatments, L929 cells were seeded in 24-well plates at 125,000 cells/well the day before infection, and respective concentration of the drugs were added after infection the following day. Upon incubation for the appropriate time at 37°C with 5% CO<sub>2</sub>, samples were harvested by three freezing-thawing cycle (-80°C, 37°C), aliquoted, and infectious viral titers were determined by TCID<sub>50</sub> on L929 fibroblasts, as described before<sup>74</sup>.

### **Data analysis and statistical analyses**

Image quantitation was done using the ImageJ software (Fiji). All statistical analyses were conducted with the GraphPad software. In some case, the variance ratio

between samples was superior to 1.5, and thus Brown-Forsythe and Welch one-way ANOVA was applied<sup>78</sup>. All results presented in this article are mean  $\pm$  standard deviation.

## Data availability

All data generated or analyzed during this study are included in this published article (and its Supplementary Information files).

## Supplementary Figures

Table S1. *qPCR primers*

Target	Housekeeping gene	Species	Primer	
			Fw	Rv
RIPK1		Mouse	5'-GCTTTGGCATTGCTCTTTGGGC-3'	5'-GGCTGATGATCTCCCTTGGACAG-3'
RIPK3		Mouse	5'-TACACAGCTTGAACCCCTCCGCT-3'	5'-ACCCTCCCTGAAACGTGGACAG-3'
MLKL		Mouse	5'-TGTCAGCCAGCCAGCATCCT-3'	5'-GGGTTTTGTTGATTCTCCACGCT-3'
DDX60		Mouse	5'-CCACCACAGTTCCATGAGTGCC-3'	5'-TGATTCCCAAAGCGAGTGTCCA-3'
IFNB1		Mouse	5'-ACACTGCCTTTGCCATCCAAGA-3'	5'-ACACTGTCTGTGGTGGAGTTCA-3'
MX1		Mouse	5'-GAAGGAGAGAGTGGAGAGGCA-3'	5'-GCTTATCACTGATCCCCAGGCC-3'
MX2		Mouse	5'-GGAAGCTGAGGAGGAGAAGAACA-3'	5'-GCTGGAGATGCGGTTGTGAGC-3'
DDX58		Mouse	5'-AACTTGCTTTGGAGAAGACAACAGC-3'	5'-CGCCTCCGCTCCATCATCCT-3'
EFTUD2		Mouse	5'-TCGGCTCAGTGAAGACAGCAT-3'	5'-GGGCAACCACAGCATCCAGT-3'
PRPF8		Mouse	5'-CCACCAGCCTTTGAGAGACAGTAG-3'	5'-GGCCAGTCGGTAGAGTGTGGAC-3'
SNRNP200		Mouse	5'-AACTGGAGCGAGAGGAGGAAGT-3'	5'-TGAGGCTGTTGGACTTGGCGT-3'
PSMC4	✓	Mouse	5'-CCCAGGAGGAGTGAAGCGG-3'	5'-GGTCGATGGTACTCAGGATGCG-3'
PUM1	✓	Mouse	5'-TGCCAGTCTCTCCAGCAGCA-3'	5'-TGATTGGGGTCAAAGGACGTTGG-3'
TXNL4B	✓	Mouse	5'-CCCTCTACCGTATTTTTCTCAATGGGC-3'	5'-AGTTTTCCCTCATCGCTCCCC-3'

Table S2. *AS-PCR primers*

Gene	Primers		ASE present in this region	Expected peak(s) (bp)	Detected peak(s) (bp)	ASE quantified	Corresponding detected peak(s) (bp)
	Fw	Rv					
MLKL	5'-CAGGATTGCCCTGAGTTGTTGC-3'	5'-CCTCTTACACCTCTTGTCCGT-3'	5'-SS	136, 160	136, 160, 261, 269	5'-SS	136, 160
RIPK1	5'-GGAAGTATTCGCTGGTATGGA-3'	5'-TGTCATTAGGTGTCGGGTGC-3'	Exon cassette	210, 348	348, 471	Exon cassette	348
RIPK1	5'-GCCCGTCCCTCCACCTAG-3'	5'-AACACAAGGACACCTTCCCGA-3'	Possible exon cassette of the alternative first exon	212, 292	212	Exon cassette	212
RIPK3	5'-CTCCCGACGATGCTTCTGTCA-3'	5'-ACTCCGAACCTCCTTTACCCA-3'	3'-SS	96, 113, 194	113, 382	3'-SS	113
RIPK3	5'-TTGAACCTCCGCTCCTGCA-3'	5'-CAGCCAGCACTGCCACACG-3'	Exon cassette	104, 262	262	Exon cassette	262

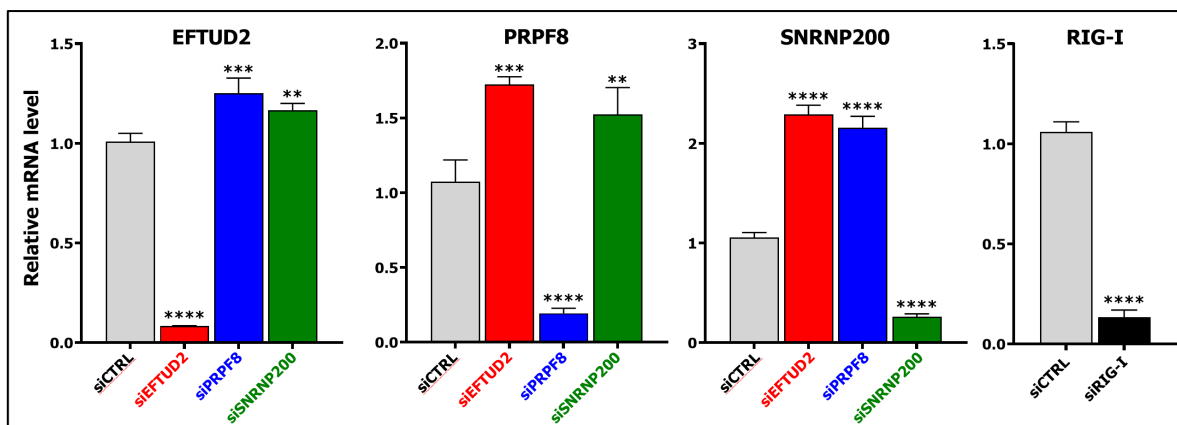


Figure S1. qPCR validation of the knock-down of *EFTUD2*, *PRPF8*, *SNRNP200* and *RIG-I* (*DDX58*). L929 were transfected with the appropriate siRNA for 72 h before RNA was harvested, reverse transcribed and subjected to qPCR. *PSMC4*, *PUM1*, and *TXNL4B* were used as housekeeping genes for normalization. n=3, biological replicates, one-way ANOVA with Dunnett's multiple comparisons test against the control siRNA condition for *EFTUD2*, *PRPF8*, and *SNRNP200*; unpaired two-tailed Student's t-test for *RIG-I* (ns,  $P > 0.05$ ; \*\*,  $P \leq 0.01$ ; \*\*\*,  $P \leq 0.001$ ; \*\*\*\*,  $P \leq 0.0001$ ).

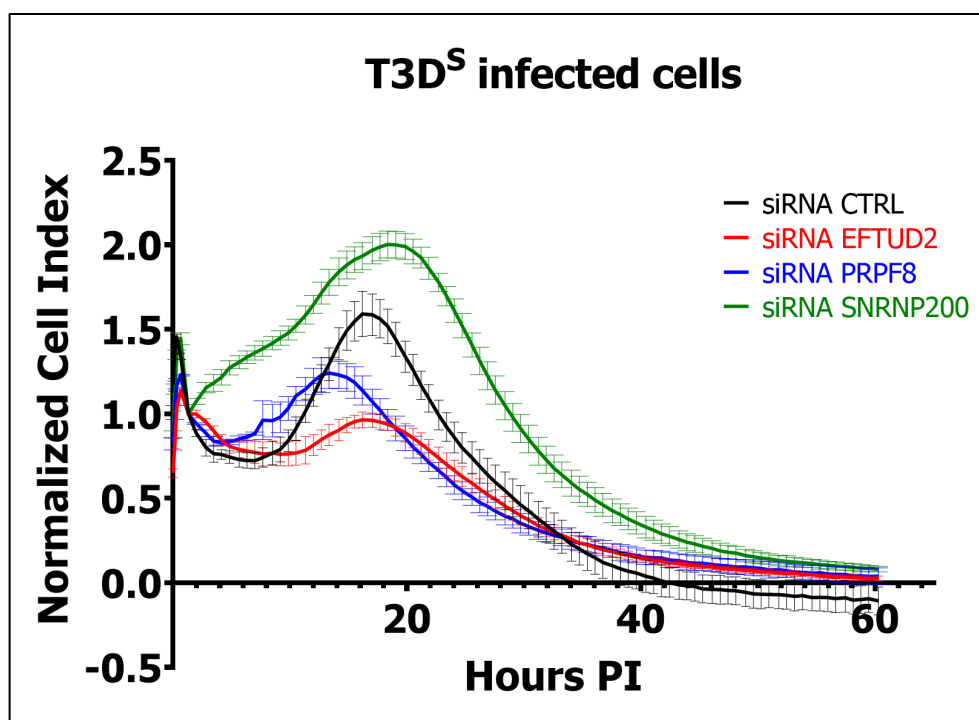


Figure S2. RTCA of *T3D<sup>S</sup>*-infected L929 cells transfected with a control siRNA or *EFTUD2*, *PRPF8*, or *SNRNP200* specific siRNA. L929 cells were seeded at 5000 cells/well in E-plates and transfected the next morning with the appropriate siRNA. 55 h later, cells were infected at a MOI of 50 and monitored using the xCELLigence system. The relative cell index was normalized to the 1 h 20 min timepoint after the monitoring resumed, because the monitoring in the first hour post-infection was not stable. Measurements were taken every 10 min for up to 90 h after infection; the graph was cut at 60h because lysis was already complete by that timepoint. n=3, biological replicates.

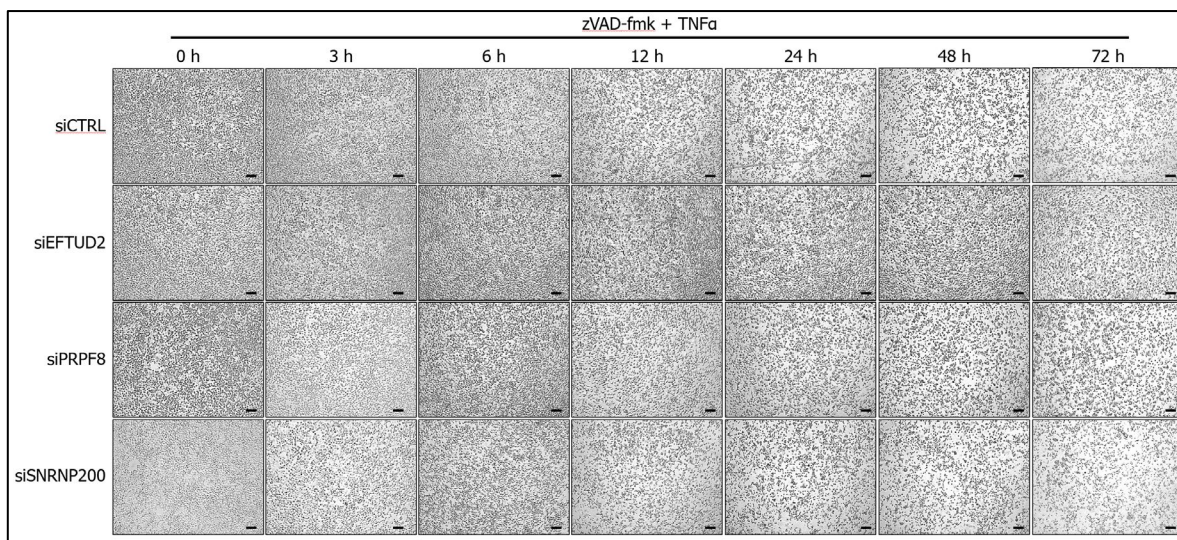


Figure S3. Live cell imaging of control or *EFTUD2*, *PRPF8*, or *SNRNP200*-depleted L929 cells treated with *zVAD*/*TNF-α* to induce necroptosis. Cells were transfected with the appropriate siRNA for 72 h. Then, they were pretreated for 1h with *zVAD-fmk* (100  $\mu$ M) before *TNF-α* (25 ng/mL) was added directly to the culture medium. Cells were then directly imaged using a Nikon TE2000E epifluorescence microscope using the differential interference contrast (DIC) channel, gain at 100, 4x objective and a 40 ms exposure time for a period of three days. The black scale bars represent 100  $\mu$ m.

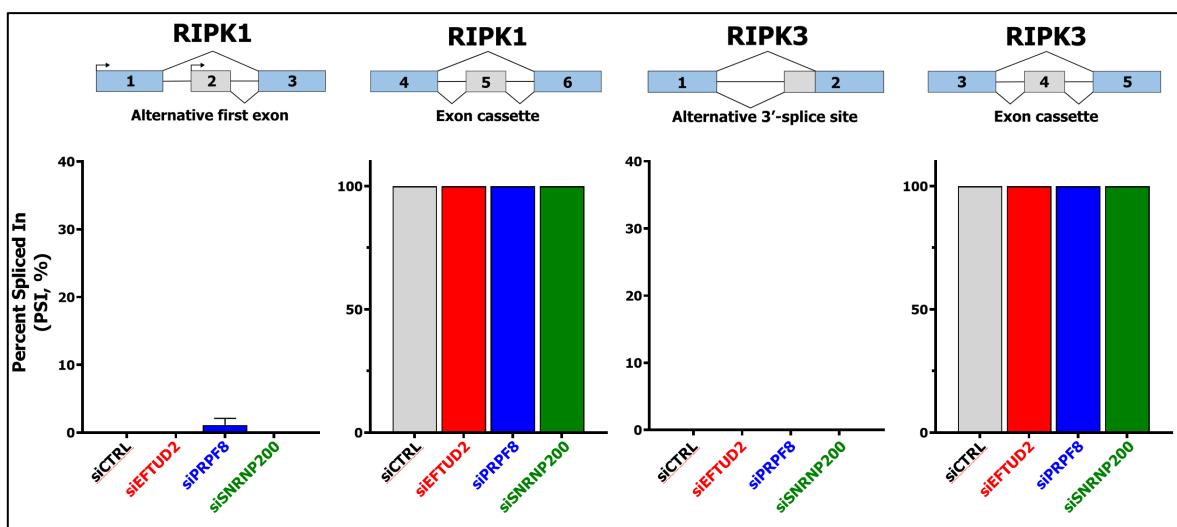


Figure S4. AS-PCR for the AS events in *RIPK1* and *RIPK3* upon *EFTUD2*, *PRPF8* and *SNRNP200* depletion. Percent Spliced In (PSI) values for the two AS event in *RIPK1* and the two AS events in *RIPK3* upon depletion of *EFTUD2*, *PRPF8* and *SNRNP200*. The AS events are depicted on the top of the graph. n=3, biological replicates.

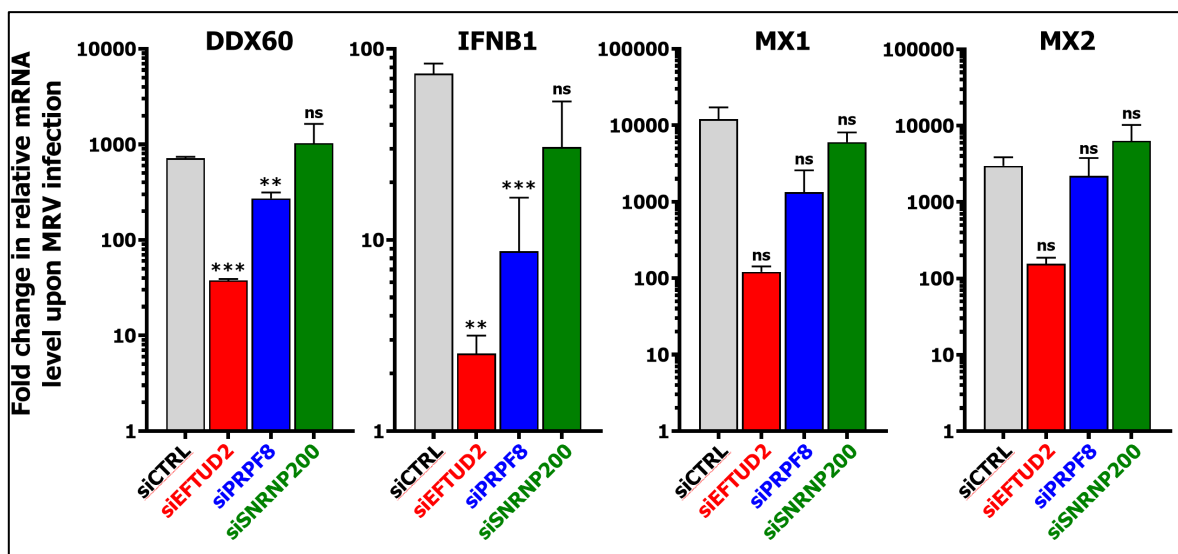


Figure S5. Relative fold induction upon MRV infection for *DDX60*, *IFNB1*, *MX1*, and *MX2* in control or *EFTUD2*, *PRPF8*, or *SNRNP200*-depleted L929 cells. L929 were transfected with the appropriate siRNA for 55 h before being either mock-infected or infected with T3D<sup>S</sup> at a MOI of 50 for 16 h. RNA was then harvested, reverse transcribed and subjected to qPCR. *PSMC4*, *PUM1*, and *TXNL4B* were used as housekeeping genes for normalization. Each replicate was arbitrarily attributed an uninfected control sample to calculate a fold-change upon infection. Since the variance ratio was superior to 1.5, Brown-Forsythe and Welch one-way ANOVA with Dunnett's T3 multiple comparisons test against the control siRNA condition was used for every comparison. The only exception was the comparison between siPRPF8 and siCTRL for *IFNB1*, where the variance ratio was inferior to 1.5 and one-way ANOVA with Dunnett's multiple comparisons test against the control siRNA condition was applied. n=3, biological replicates (ns, P>0.05; \*\*, P≤0.01; \*\*\*, P≤0.001).



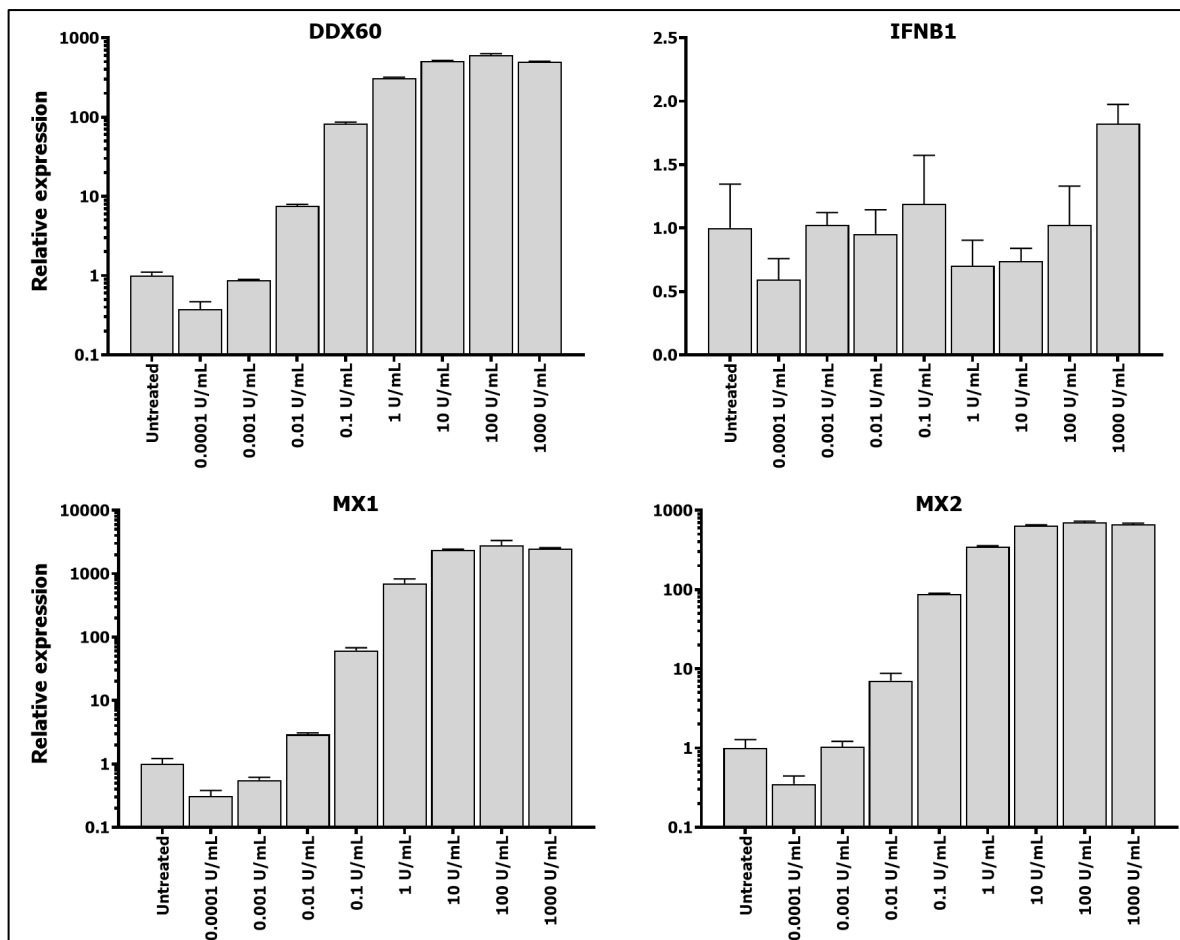


Figure S6. *Relative mRNA levels for DDX60, IFNB1, MX1, and MX2 in L929 cells treated with logarithmic dilutions of IFN- $\beta$ .* L929 were transfected with a control siRNA for 72 h before IFN- $\beta$  (0.0001 U/mL to 1000 U/mL) was added for 5 h. RNA was then harvested, reverse transcribed and subjected to qPCR. *PSMC4*, *PUM1*, and *TXNL4B* were used as housekeeping genes for normalization. n=1, technical triplicates.

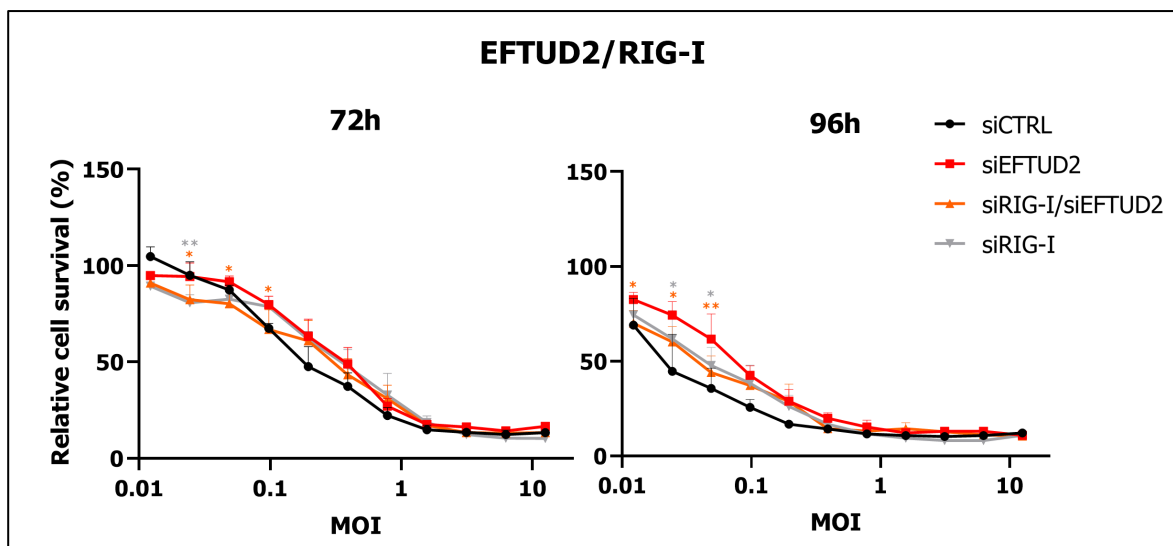


Figure S7. Methylene blue staining of control, EFTUD2, RIG-I, or RIG-I/EFTUD2-depleted L929 cells infected with binary dilutions of T3D<sup>S</sup> at 72 h or 96 h post-infection. Twice the quantity of siRNA was transfected to perform the DKD; in the case of a single KD, siCTRL was added to match the total siRNA quantity of the DKD. The quantification of cell-bound methylene blue stain is shown for three independent experiments. n=3, biological replicates, two-way ANOVA with Dunnett's multiple comparisons test against the EFTUD2 KD condition (in red; \*, P≤0.05; \*\*, P≤0.01). If not indicated, results are not statistically significant. The results of the comparison against the control siRNA (in black) are not indicated for clarity purpose.

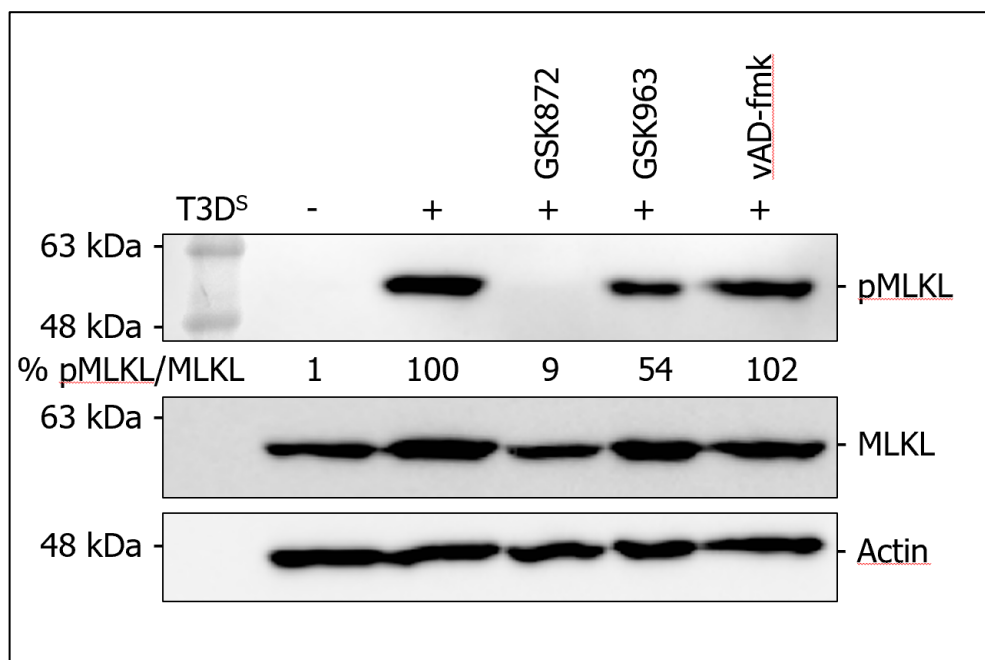


Figure S8. Western blot of phosphorylated MLKL (pMLKL) and total MLKL in mock- or T3D<sup>S</sup>-infected cells treated with necroptosis inhibitors (GSK872, GSK963) or apoptosis inhibitor (zVAD-fmk). L929 cells were infected at an MOI of 3 and left untreated or treated with the RIPK3 inhibitor GSK872 (3 μM), the RIPK1 inhibitor GSK963 (3 μM) or the pan-caspase inhibitor zVAD-fmk (100 μM) for 40 h before proteins were harvested. Relative quantitation is shown for pMLKL/MLKL.

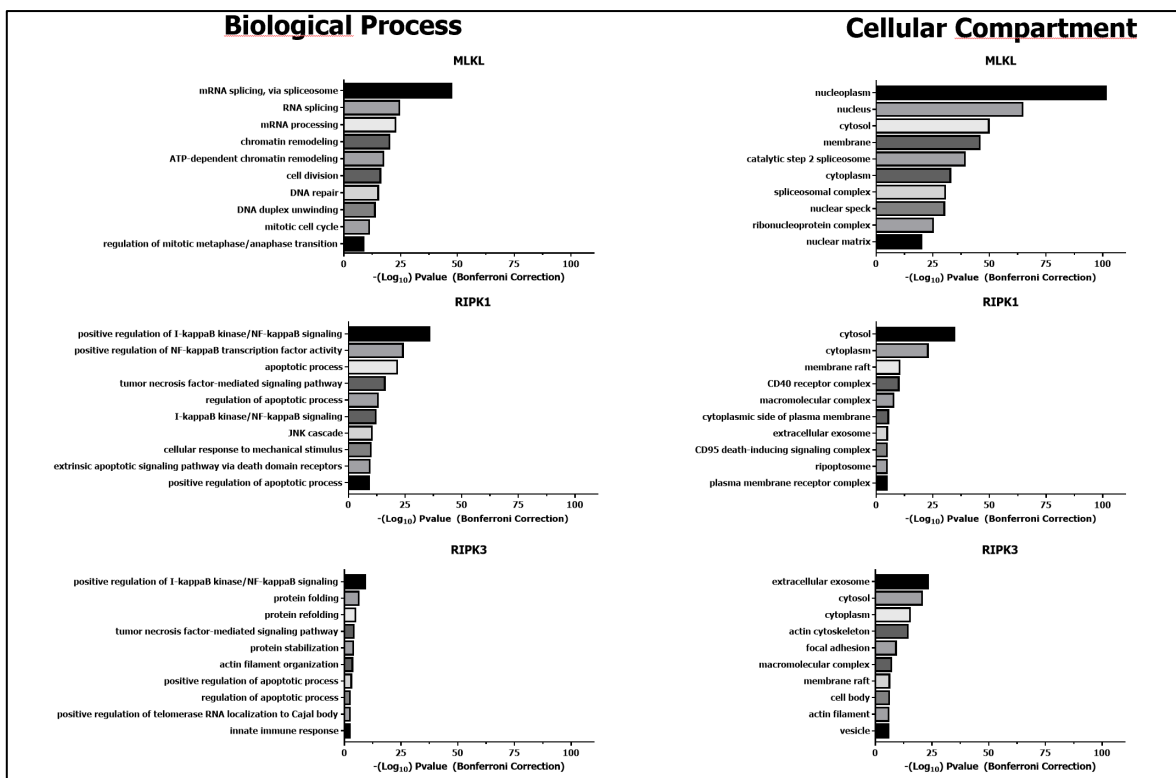


Figure S9. *Gene ontology (GO) analysis of the protein interactors for key necroptotic regulators RIPK1, RIPK3 and MLKL.* Protein interactors were retrieved from the Harmonizome database<sup>1</sup> (RIPK1, 137 interactors; RIPK3, 112 interactors; MLKL, 537 interactors). The gene ontology analysis of the interactors was performed using DAVID web server<sup>2</sup> with the gene ontology (biological process or cellular compartment) direct function. The complete list of human genes was used as the background. The Bonferroni correction was used to correct for multiple statistical tests.

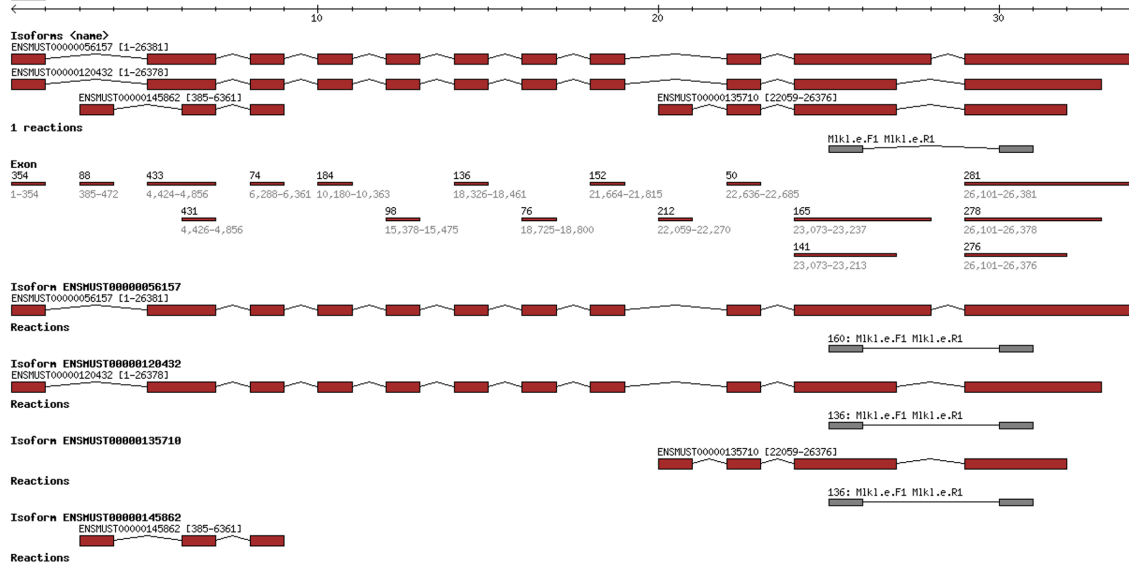
<sup>1</sup>Rouillard, A. D. *et al.* The harmonizome: a collection of processed datasets gathered to serve and mine knowledge about genes and proteins. *Database* 2016, baw100 (2016).

<sup>2</sup>Sherman, B. T. *et al.* DAVID: a web server for functional enrichment analysis and functional annotation of gene lists (2021 update). *Nucleic Acids Research* gkac194 (2022) doi:10.1093/nar/gkac194.

# MLKL

GeneTagGroup on 8- Mouse|NCBI|38.p1 (1 gene tags)

ENSMUSG00000012519(Mlkl)|Ensembl|Hm92.GRCv38Y



# RIPK1

GeneTagGroup on 13+ Mouse|NCBI|38.p1 (1 gene tags)

ENSMUSG00000021408(Ripk1)|Ensembl|Hm92.GRCv38Y



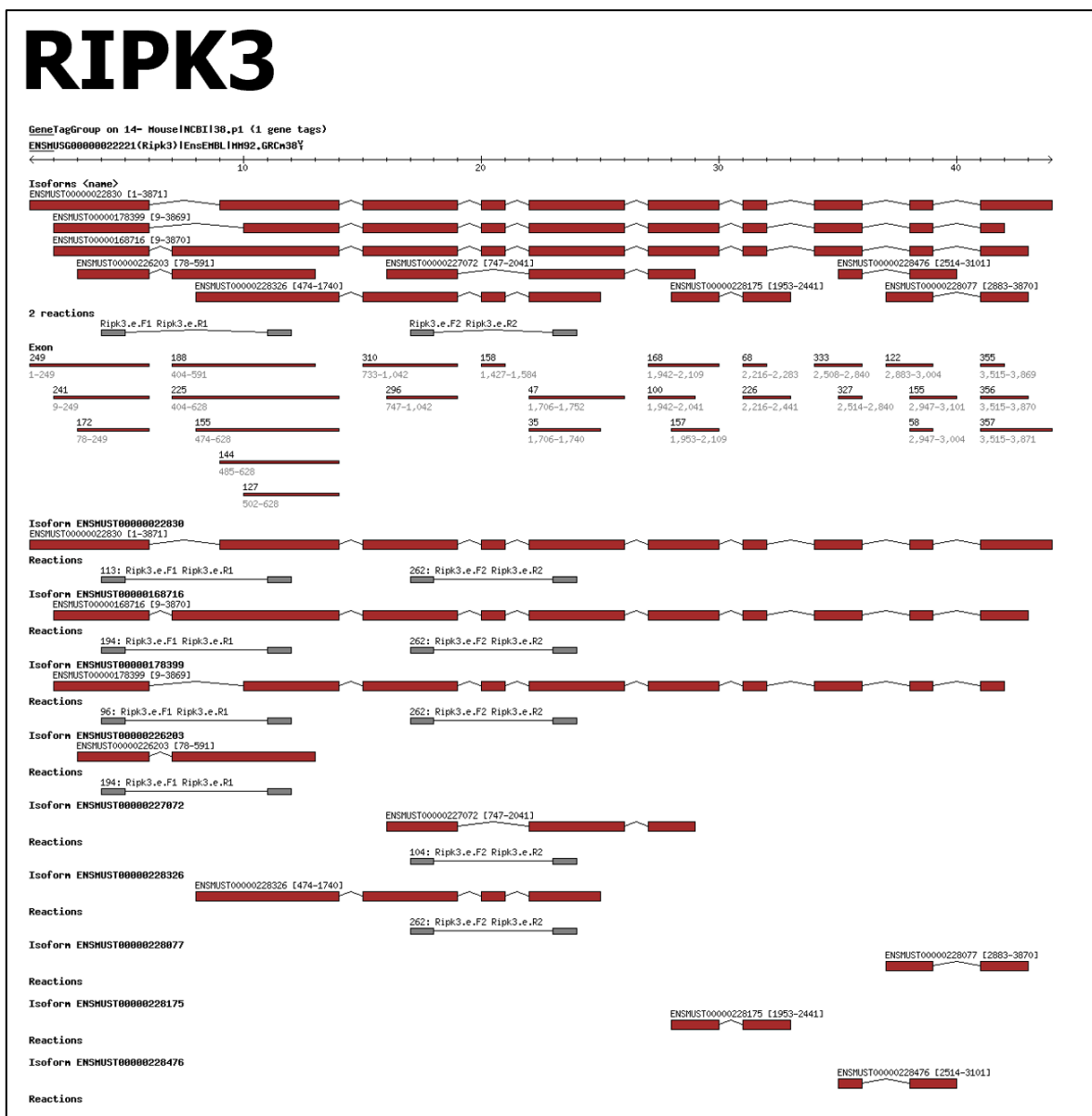


Figure S10. Design maps for the ASE analyzed by AS-PCR in L929 cells. All the RNA isoforms for each gene are depicted alongside their ENSEMBL transcript ID. The primers, designed to amplify the region alternatively spliced, are shown as gray rectangles. On the bottom, a predicted size for the PCR amplicon is given for each transcript. Maps were generated using the mouse assembly GRCm38 (v92) from Ensembl.

**REFERENCES**

1. Fensterl, V., Chattopadhyay, S. & Sen, G. C. No Love Lost Between Viruses and Interferons. *Annu. Rev. Virol.* 2, 549–572 (2015).
2. Sen, G. C. & Sarkar, S. N. The interferon-stimulated genes: targets of direct signaling by interferons, double-stranded RNA, and viruses. *Curr. Top. Microbiol. Immunol.* 316, 233–250 (2007).
3. Galluzzi, L. et al. Molecular mechanisms of cell death: recommendations of the Nomenclature Committee on Cell Death 2018. *Cell Death Differ.* 25, 486–541 (2018).
4. Maio, F. A. D. et al. The Dengue Virus NS5 Protein Intrudes in the Cellular Spliceosome and Modulates Splicing. *PLoS Pathog.* 12, e1005841 (2016).
5. Boudreault, S. et al. Reovirus  $\mu$ 2 protein modulates host cell alternative splicing by reducing protein levels of U5 snRNP core components. *Nucleic Acids Res.* 50, 5263–5281 (2022).
6. Liu, Y.-C. et al. Cytoplasmic Viral RNA-Dependent RNA Polymerase Disrupts the Intracellular Splicing Machinery by Entering the Nucleus and Interfering with Prp8. *PLoS Pathog.* 10, e1004199 (2014).
7. Boudreault, S., Roy, P., Lemay, G. & Bisailon, M. Viral modulation of cellular RNA alternative splicing: A new key player in virus–host interactions? *Wiley Interdiscip. Rev. RNA* 10, e1543 (2019).
8. Liu, S., Rauhut, R., Vornlocher, H.-P. & Lührmann, R. The network of protein–protein interactions within the human U4/U6.U5 tri-snRNP. *RNA* 12, 1418–1430 (2006).
9. Wood, K. A., Eadsforth, M. A., Newman, W. G. & O’Keefe, R. T. The Role of the U5 snRNP in Genetic Disorders and Cancer. *Front. Genet* 12, 636620 (2021).

10. Newman, A. J. The role of U5 snRNP in pre-mRNA splicing. *EMBO J.* 16, 5797–5800 (1997).
11. Wahl, M. C., Will, C. L. & Lührmann, R. The Spliceosome: Design Principles of a Dynamic RNP Machine. *Cell* 136, 701–718 (2009).
12. Black, D. L. Mechanisms of alternative pre-messenger RNA splicing. *Annu. Rev. Biochem.* 72, 291–336 (2003).
13. Lee, Y. & Rio, D. C. Mechanisms and Regulation of Alternative Pre-mRNA Splicing. *Annu. Rev. Biochem.* 84, 291–323 (2015).
14. Kim, E., Goren, A. & Ast, G. Alternative splicing: current perspectives. *BioEssays* 30, 38–47 (2008).
15. Keren, H., Lev-Maor, G. & Ast, G. Alternative splicing and evolution: diversification, exon definition and function. *Nat. Rev. Genet.* 11, 345–355 (2010).
16. Van Nostrand, E. L. et al. A large-scale binding and functional map of human RNA-binding proteins. *Nature* 583, 711–719 (2020).
17. Chauhan, K., Kalam, H., Dutt, R. & Kumar, D. RNA Splicing: A New Paradigm in Host-Pathogen Interactions. *J. Mol. Biol.* 431, 1565–1575 (2019).
18. Ashraf, U., Benoit-Pilven, C., Lacroix, V., Navratil, V. & Naffakh, N. Advances in Analyzing Virus-Induced Alterations of Host Cell Splicing. *Trends Microbiol.* 27, 268–281 (2019).
19. Cross, S. T., Michalski, D., Miller, M. R. & Wilusz, J. RNA regulatory processes in RNA virus biology. *Wiley Interdiscip. Rev. RNA* 10, e1536 (2019).
20. Lemay, G. Synthesis and Translation of Viral mRNA in Reovirus-Infected Cells: Progress and Remaining Questions. *Viruses* 10, 671 (2018).

21. Danthi, P. et al. From Touchdown to Transcription: The Reovirus Cell Entry Pathway. *Curr Top Microbiol Immunol* 343, 91–119 (2010).
22. Danthi, P., Holm, G. H., Stehle, T. & Dermody, T. S. Reovirus receptors, cell entry, and proapoptotic signaling. *Adv. Exp. Med. Biol.* 790, 42–71 (2013).
23. Boudreault, S. et al. Global Profiling of the Cellular Alternative RNA Splicing Landscape during Virus-Host Interactions. *PLoS One* 11, e0161914 (2016).
24. Rivera-Serrano, E. E., Fritch, E. J., Scholl, E. H. & Sherry, B. A Cytoplasmic RNA Virus Alters the Function of the Cell Splicing Protein SRSF2. *J. Virol.* 91, e02488-16 (2017).
25. Lebourgeois, S. et al. Development of a Real-Time Cell Analysis (RTCA) Method as a Fast and Accurate Method for Detecting Infectious Particles of the Adapted Strain of Hepatitis A Virus. *Front. Cell. Infect. Microbiol.* 8, 335 (2018).
26. Burmakina, G., Bliznetsov, K. & Malogolovkin, A. Real-time analysis of the cytopathic effect of African swine fever virus. *J. Virol. Methods* 257, 58–61 (2018).
27. Fang, Y., Ye, P., Wang, X., Xu, X. & Reisen, W. Real-time monitoring of flavivirus induced cytopathogenesis using cell electric impedance technology. *J. Virol. Methods* 173, 251–258 (2011).
28. Charretier, C. et al. Robust real-time cell analysis method for determining viral infectious titers during development of a viral vaccine production process. *J. Virol. Methods* 252, 57–64 (2018).
29. Teng, Z., Kuang, X., Wang, J. & Zhang, X. Real-time cell analysis – A new method for dynamic, quantitative measurement of infectious viruses and antiserum neutralizing activity. *J. Virol. Methods* 193, 364–370 (2013).



30. Lanoie, D. & Lemay, G. Multiple proteins differing between laboratory stocks of mammalian orthoreoviruses affect both virus sensitivity to interferon and induction of interferon production during infection. *Virus Res.* 247, 40–46 (2018).
31. Sandekian, V. & Lemay, G. A single amino acid substitution in the mRNA capping enzyme  $\lambda 2$  of a mammalian orthoreovirus mutant increases interferon sensitivity. *Virology* 483, 229–235 (2015).
32. Lanoie, D., Côté, S., Degeorges, E. & Lemay, G. A single mutation in the mammalian orthoreovirus S1 gene is responsible for increased interferon sensitivity in a virus mutant selected in Vero cells. *Virology* 528, 73–79 (2019).
33. Sandekian, V., Lim, D., Prud'homme, P. & Lemay, G. Transient high level mammalian reovirus replication in a bat epithelial cell line occurs without cytopathic effect. *Virus Res.* 173, 327–335 (2013).
34. Holm, G. H. et al. Retinoic Acid-inducible Gene-I and Interferon- $\beta$  Promoter Stimulator-1 Augment Proapoptotic Responses Following Mammalian Reovirus Infection via Interferon Regulatory Factor-3. *J. Biol. Chem.* 282, 21953–21961 (2007).
35. Tyler, K. L. et al. Differences in the capacity of reovirus strains to induce apoptosis are determined by the viral attachment protein sigma 1. *J. Virol.* 69, 6972–6979 (1995).
36. Clarke, P., DeBiasi, R. L., Meintzer, S. M., Robinson, B. A. & Tyler, K. L. Inhibition of NF- $\kappa$  B activity and cFLIP expression contribute to viral-induced apoptosis. *Apoptosis* 10, 513–524 (2005).
37. Berger, A. K. et al. Viral RNA at Two Stages of Reovirus Infection Is Required for the Induction of Necroptosis. *J. Virol.* 91, e02404-16 (2017).

38. Berger, A. K. & Danthi, P. Reovirus Activates a Caspase-Independent Cell Death Pathway. *mBio* 4, e00178-13 (2013).
39. Prinos, P. et al. Alternative splicing of SYK regulates mitosis and cell survival. *Nat. Struct. Mol. Biol.* 18, 673–679 (2011).
40. Faucher-Giguère, L. et al. High-grade ovarian cancer associated H/ACA snoRNAs promote cancer cell proliferation and survival. *NAR Cancer* 4, zcab050 (2022).
41. Nagata, S., Suzuki, J., Segawa, K. & Fujii, T. Exposure of phosphatidylserine on the cell surface. *Cell Death Differ* 23, 952–961 (2016).
42. Shlomovitz, I., Speir, M. & Gerlic, M. Flipping the dogma – phosphatidylserine in non-apoptotic cell death. *Cell Commun. Signal.* 17, 139 (2019).
43. Koehler, H. et al. Inhibition of DAI-dependent necroptosis by the Z-DNA binding domain of the vaccinia virus innate immune evasion protein, E3. *PNAS* 114, 11506–11511 (2017).
44. Koehler, H. et al. Vaccinia virus E3 prevents sensing of Z-RNA to block ZBP1-dependent necroptosis. *Cell Host Microbe* 29, 1266-1276.e5 (2021).
45. Patzina, C., Botting, C. H., García-Sastre, A., Randall, R. E. & Hale, B. G. Human interactome of the influenza B virus NS1 protein. *J. Gen. Virol.* 98, 2267–2273 (2017).
46. Tremblay, N. et al. Spliceosome SNRNP200 Promotes Viral RNA Sensing and IRF3 Activation of Antiviral Response. *PLoS Pathog.* 12, e1005772 (2016).
47. Zhu, C. et al. EFTUD2 Is a Novel Innate Immune Regulator Restricting Hepatitis C Virus Infection through the RIG-I/MDA5 Pathway. *J. Virol.* 89, 6608–6618 (2015).
48. De Arras, L. et al. Comparative Genomics RNAi Screen Identifies Eftud2 as a Novel Regulator of Innate Immunity. *Genetics* 197, 485–496 (2014).

49. Schock, S. N. et al. Induction of necroptotic cell death by viral activation of the RIG-I or STING pathway. *Cell Death Differ.* 24, 615–625 (2017).
50. Mohamed, A. et al. Closely related reovirus lab strains induce opposite expression of RIG-I/IFN-dependent versus -independent host genes, via mechanisms of slow replication versus polymorphisms in dsRNA binding  $\sigma 3$  respectively. *PLoS Pathog.* 16, e1008803 (2020).
51. Thoresen, D. et al. The molecular mechanism of RIG-I activation and signaling. *Immunol. Rev.* 304, 154–168 (2021).
52. Zarbl, H. & Millward, S. The Reovirus Multiplication Cycle. in *The Reoviridae* (ed. Joklik, W. K.) 107–196 (Springer US, 1983). doi:10.1007/978-1-4899-0580-2\_4.
53. Stanković, D., Claudius, A.-K., Schertel, T., Bresser, T. & Uhlirova, M. A *Drosophila* model to study retinitis pigmentosa pathology associated with mutations in the core splicing factor Prp8. *Dis. Model. Mech.* 13, dmm043174 (2020).
54. Xu, Q., Deng, B., Li, M., Chen, Y. & Zhuan, L. circRNA-UBAP2 promotes the proliferation and inhibits apoptosis of ovarian cancer through miR-382-5p/PRPF8 axis. *J. Ovarian Res.* 13, 81 (2020).
55. Tu, M. et al. EFTUD2 maintains the survival of tumor cells and promotes hepatocellular carcinoma progression via the activation of STAT3. *Cell Death Dis* 11, 1–12 (2020).
56. Lei, L. et al. Spliceosomal protein eftud2 mutation leads to p53-dependent apoptosis in zebrafish neural progenitors. *Nucleic Acids Res.* 45, 3422–3436 (2017).
57. Sato, N. et al. Inhibition of SNW1 association with spliceosomal proteins promotes apoptosis in breast cancer cells. *Cancer Med.* 4, 268–277 (2015).
58. Wood, K. A. et al. Disease modeling of core pre-mRNA splicing factor haploinsufficiency. *Hum. Mol. Genet.* 28, 3704–3723 (2019).

59. Zhang, T. et al. Influenza Virus Z-RNAs Induce ZBP1-Mediated Necroptosis. *Cell* 180, 1115-1129.e13 (2020).
60. Yoon, S., Bogdanov, K., Kovalenko, A. & Wallach, D. Necroptosis is preceded by nuclear translocation of the signaling proteins that induce it. *Cell Death Differ* 23, 253–260 (2016).
61. Weber, K., Roelandt, R., Bruggeman, I., Estornes, Y. & Vandenabeele, P. Nuclear RIPK3 and MLKL contribute to cytosolic necrosome formation and necroptosis. *Commun Biol* 1, 1–13 (2018).
62. Desroches, A. & Denault, J.-B. Caspase-7 uses RNA to enhance proteolysis of poly(ADP-ribose) polymerase 1 and other RNA-binding proteins. *Proc. Natl. Acad. Sci. U.S.A.* 116, 21521–21528 (2019).
63. Desroches, A. & Denault, J.-B. Characterization of caspase-7 interaction with RNA. *Biochem. J.* 478, 2681–2696 (2021).
64. Mukhopadhyay, U. et al. Rotavirus activates MLKL-mediated host cellular necroptosis concomitantly with apoptosis to facilitate dissemination of viral progeny. *Mol. Microbiol.* 117, 818–836 (2022).
65. Soliman, M. et al. Opposite Effects of Apoptotic and Necroptotic Cellular Pathways on Rotavirus Replication. *J Virol.* 96, e01222-21 (2022).
66. DeAntoneo, C., Danthi, P. & Balachandran, S. Reovirus Activated Cell Death Pathways. *Cells* 11, 1757 (2022).
67. Boehme, K. W. et al. Nonstructural Protein  $\sigma$ 1s Mediates Reovirus-Induced Cell Cycle Arrest and Apoptosis. *J. Virol.* 87, 12967–12979 (2013).
68. Alexopoulou, L., Holt, A. C., Medzhitov, R. & Flavell, R. A. Recognition of double-stranded RNA and activation of NF- $\kappa$ B by Toll-like receptor 3. *Nature* 413, 732–738 (2001).

69. Abad, A. T. & Danthi, P. Early Events in Reovirus Infection Influence Induction of Innate Immune Response. *J. Virol.* 96, e00917-22 (2022).
70. An, Y. et al. Oncolytic reovirus induces ovarian cancer cell apoptosis in a TLR3-dependent manner. *Virus Res.* 301, 198440 (2021).
71. Katayama, Y. et al. Oncolytic Reovirus Inhibits Immunosuppressive Activity of Myeloid-Derived Suppressor Cells in a TLR3-Dependent Manner. *J. Immunol.* 200, 2987–2999 (2018).
72. Long, S. et al. Reovirus enhances cytotoxicity of natural killer cells against colorectal cancer via TLR3 pathway. *J. Transl. Med.* 19, 185 (2021).
73. Edelmann, K. H. et al. Does Toll-like receptor 3 play a biological role in virus infections? *Virology* 322, 231–238 (2004).
74. Danis, C. & Lemay, G. Protein synthesis in different cell lines infected with orthoreovirus serotype 3: inhibition of host-cell protein synthesis correlates with accelerated viral multiplication and cell killing. *Biochem. Cell Biol.* 71, 81–85 (1993).
75. Kobayashi, T. et al. A Plasmid-Based Reverse Genetics System for Animal Double-Stranded RNA Viruses. *Cell Host Microbe* 1, 147–157 (2007).
76. Taylor, S., Wakem, M., Dijkman, G., Alsarraj, M. & Nguyen, M. A practical approach to RT-qPCR—Publishing data that conform to the MIQE guidelines. *Methods* 50, S1–S5 (2010).
77. Virgin, H. W., Mann, M. A., Fields, B. N. & Tyler, K. L. Monoclonal antibodies to reovirus reveal structure/function relationships between capsid proteins and genetics of susceptibility to antibody action. *J. Virol.* 65, 6772–6781 (1991).
78. Blanca, M. J., Alarcón, R. & Arnau, J. Non-normal data: Is ANOVA still a valid option? *Psicothema* 552–557 (2017) doi:10.7334/psicothema2016.383.

## **ACKNOWLEDGEMENTS**

We thank Laurence Faucher-Giguère and Pr. Sherif Abou Elela for the help with the xCELLigence system and the high-throughput apoptosis staining assay; Mathieu Catala for the help with FACS experiments; Mateusz Szczerba and Pr. Bertram Jacobs for helpful discussion and sharing their protocols and expertise with the necroptosis assays; Philippe Thibault and Danny Bergeron for the design of qPCR and AS-PCR primers; Mathieu Durand for the qPCR and AS-PCR; and Pr. Jean-Bernard Denault and Jean-Pierre Perreault for reviewing the manuscript.

## **AUTHOR CONTRIBUTIONS AND FUNDING**

S.B., G.L., and M.B. conceived the study and the experimental frame. S.B. performed all the experiments, analyzed the data, generated the figures, and wrote the manuscript with G.L. and M.B. The manuscript was reviewed by all the authors. This work was supported by funding from the Natural Sciences and Engineering Research Council of Canada (NSERC) to M.B. [grant number RGPIN-2016-03916] and G.L. [grant number RGPIN-2017-05482]. S.B is now supported by the Fonds de recherche du Québec – Santé (FRQS), and previously by a Vanier scholarship from the Canadian Institutes of Health Research (CIHR). M.B. is a member of the Centre de Recherche du CHUS.

## **COMPETING INTERESTS STATEMENT**

The authors declare no competing interests. The funders had no role in the design of the study; in the collection, analyses, or interpretation of data; in the writing of the manuscript, or in the decision to publish the results.

## DISCUSSION

Les travaux présentés dans cette thèse ont permis de mettre de l'avant l'impact de réovirus, un virus prometteur comme traitement contre le cancer, sur l'épissage alternatif de la cellule-hôte durant l'infection. Nous avons démontré que réovirus altère 240 événements d'épissage alternatif durant l'infection. Ces événements appartiennent à 194 gènes cellulaires dont les rôles sont principalement dans le métabolisme des ARN ainsi que dans la transcription. Nous avons caractérisé cette modulation et l'impact potentiel sur le protéome de la cellule-hôte.

Dans un deuxième temps, j'ai identifié un des mécanismes qui explique l'impact de réovirus sur l'épissage alternatif cellulaire. J'ai identifié la protéine virale  $\mu 2$  comme un des déterminants principaux de cette modulation, et identifié le polymorphisme à la position 208 dans  $\mu 2$  comme critique pour l'impact sur l'épissage alternatif. J'ai ensuite réalisé l'interactome de  $\mu 2$  pour la première fois et démontré que  $\mu 2$  interagit avec au moins trois protéines du complexe U5 du spliceosome, soit EFTUD2, PRPF8 et SNRNP200. La déplétion de ces protéines réduit l'impact du virus sur l'épissage alternatif, soulignant que ces changements sont médiés par le complexe U5. Réovirus, via l'action de la protéine  $\mu 2$ , réduit les niveaux de ces protéines durant l'infection, un mécanisme jamais décrit auparavant permettant la modulation de l'épissage alternatif cellulaire durant l'infection.

Dans un troisième temps, nous avons démontré des nouveaux rôles pour les protéines EFTUD2, PRPF8 et SNRNP200 durant l'infection avec réovirus. EFTUD2 et SNRNP200 sont requises pour la mort cellulaire programmée via l'apoptose et la nécroptose. EFTUD2 et PRPF8 sont requises pour une réponse antivirale cellulaire optimale via la voie de l'interféron. Finalement, EFTUD2 restreint la réplication virale de réovirus, principalement via son rôle dans la réponse interféron.

Les travaux que j'ai menés sur réovirus ainsi que la protéine  $\mu 2$  nous ont amenés à nous intéresser à de nombreux aspects de la réplication de ce virus et des activités cellulaires de la protéine  $\mu 2$ . L'importance des protéines cellulaires impliquées dans l'épissage sur la biologie de réovirus nous a plus particulièrement fasciné. Bien entendu, de nombreux résultats de mes travaux ainsi que certaines hypothèses très intéressantes n'ont pas pu faire partie d'une publication scientifique, faute de temps pour mener à terme ces embryons de projets et de lien avec les autres aspects déjà poursuivis. Cette discussion permettra donc de mettre de l'avant ces résultats préliminaires et les hypothèses restantes à étudier à la suite de mes travaux de doctorat.

### **Implication des protéines cellulaires dans la réplication de réovirus**

Mes travaux de doctorat se sont concentrés sur les protéines du complexe U5, principalement EFTUD2, PRPF8 et SNRNP200, de par leur implication dans la modulation de l'épissage alternatif durant l'infection avec réovirus (Boudreault *et al.*, 2022). La poursuite des travaux sur ces protéines nous a permis de mieux comprendre leurs rôles dans de multiples phénomènes importants durant l'infection avec réovirus, comme l'apoptose, la nécroptose, ainsi que la voie de l'interféron (Boudreault *et al.*, soumis à Scientific Reports). Cependant, nous avons identifié un très grand nombre d'interacteurs probables de la protéine  $\mu 2$  par IP-MS, dont la plupart reste inexplorés (Boudreault *et al.*, 2022). Par exemple, parmi les 19 protéines identifiées avec toutes nos constructions de  $\mu 2$ , seulement EFTUD2, PRPF8 et SNRNP200 ont été étudiées. D'autres protéines importantes pour le métabolisme des ARN (SON, PABPC1), les microtubules (SLAIN1) ainsi que le pore nucléaire (RANBP2, NUP153) ont été identifiés comme des interacteurs probables avec un haut taux de confiance. Ces protéines mériteraient certainement d'être validées par immunoprécipitation suivie d'un WB et leurs rôles durant la réplication de réovirus investigués. J'aborderai certaines protéines auxquelles nous nous sommes plus particulièrement intéressés de manière plus exhaustive dans les sous-sections suivantes.



### ***CCAR2 et RBM14***

Parmi les 19 interacteurs mentionnés précédemment, la protéine CCAR2 a tout d'abord retenu notre attention. À la fois facteur de transcription et protéine impliquée dans l'épissage, ses rôles principaux reposent dans le contrôle du cycle cellulaire et l'apoptose, et elle est notamment dérégulée lors de la carcinogenèse (Best *et al.*, 2017; Close *et al.*, 2012; Trauernicht *et al.*, 2007). Nous avons validé que  $\mu 2$  interagit avec CCAR2 par IP-WB, mais malheureusement nous n'avons pas pu aller plus loin dans la compréhension du rôle de CCAR2 durant l'infection avec réovirus (Figure 1A). Il serait intéressant d'utiliser la même approche que décrite au chapitre 3 pour EFTUD2, PRPF8 et SNRNP200, et d'investiguer le rôle de CCAR2 dans la réplication de réovirus et pourquoi  $\mu 2$  interagit avec cette protéine.

Une autre protéine qui nous a intrigué est RBM14. RBM14 régule l'épissage alternatif et est un composant important des *nuclear speckles*, ces structures nucléaires sans membranes enrichies pour des facteurs impliqués dans l'épissage, auxquelles notamment  $\mu 2$  se localise en expression transitoire (Boudreault *et al.*, 2022; Hirose *et al.*, 2019; Rivera-Serrano *et al.*, 2017). De plus, RBM14 a été identifié dans un complexe cytoplasmique responsable de la réponse interféron avec le long ARN non-codant NEAT1, principal composant ARN des *nuclear speckles* (Morchikh *et al.*, 2017). Conséquemment, de nombreux virus, dont le VIH et le virus de l'influenza, interagissent avec RBM14 (Beyleveld *et al.*, 2018; Budhiraja *et al.*, 2015; Lee *et al.*, 2016). Cette protéine était souvent identifiée dans nos résultats préliminaires de spectrométrie de masse; cependant, les résultats finaux de notre expérience d'IP-MS n'ont pas identifié RBM14 comme interacteur de  $\mu 2$  (Boudreault *et al.*, 2022). Nous avons tout de même testé si nous pouvions détecter RBM14 lors de l'immunoprécipitation de nos constructions  $\mu 2$ -GFP et nous avons pu valider que  $\mu 2$  interagit avec RBM14, et un peu moins lorsque l'on mute la proline en sérine à 208

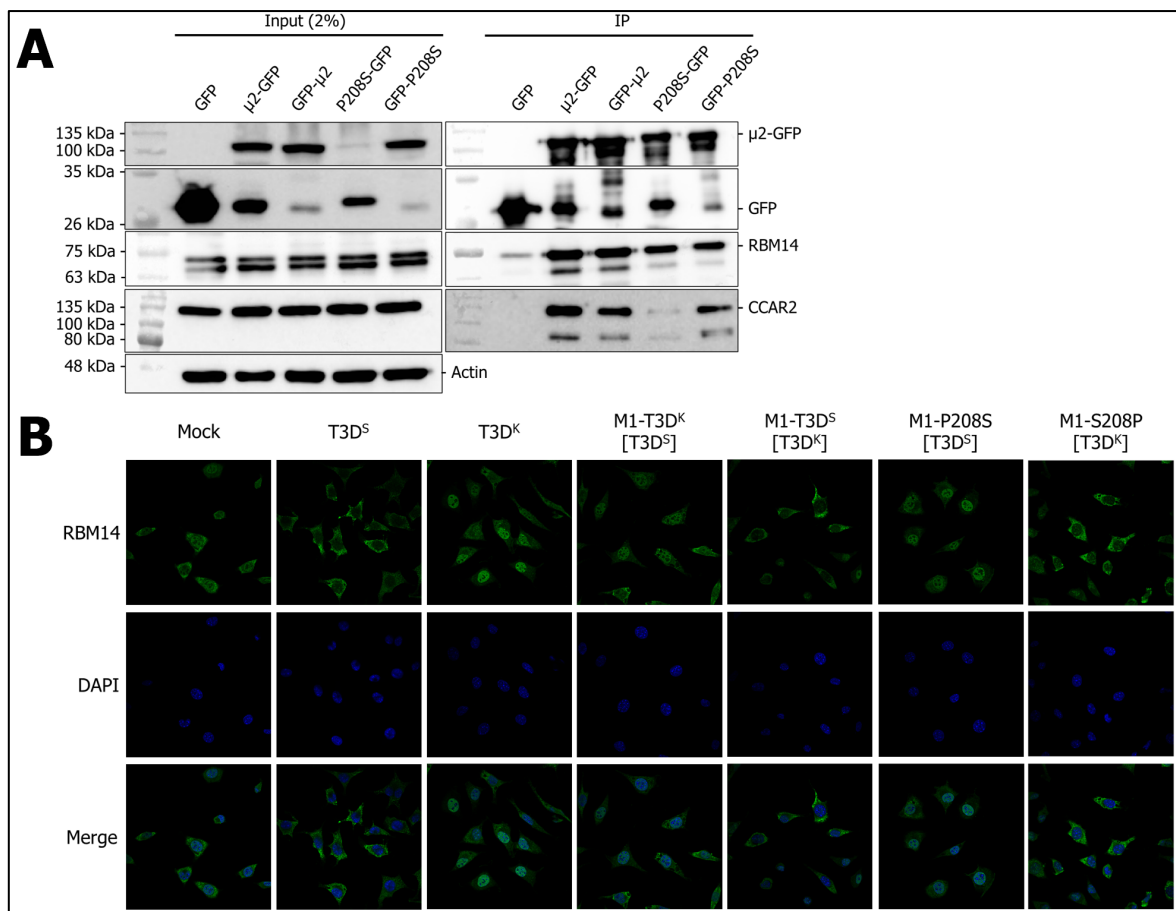


Figure 1. *Interaction de  $\mu$ 2 avec CCAR2 et RBM14 et localisation de RBM14 durant l'infection avec réovirus.* (A) Validation de la co-immunoprécipitation de CCAR2 et RBM14 avec différentes constructions de  $\mu$ 2 par IP et WB. (B) Des cellules L929 ont été infectées à une multiplicité d'infection (MOI) de 50 virus/cellule pendant 16 heures, puis une immunofluorescence a été réalisée contre la protéine RBM14.

(Figure 1A). Ce résultat souligne la stringence de nos résultats d'IP-MS et suggère qu'il existe de nombreux faux négatifs dans cette expérience, comme RBM14. Puisqu'il a été démontré que RBM14 peut être relocalisé suite à l'infection virale (Beyleveld *et al.*, 2018), nous avons par la suite investigué sa localisation par immunofluorescence avec différents virus réassortants. Nous avons pu démontrer que RBM14 est majoritairement pan-cellulaire, et que lors de l'infection avec T3D<sup>S</sup>, elle devient exclusivement cytoplasmique (Figure 1B). Cependant, lorsque des L929 sont infectées avec T3D<sup>K</sup>, la localisation de RBM14 est principalement nucléaire (Figure 1B). Nous avons pu démontrer que cette différence de localisation est due au segment viral M1, qui encode  $\mu$ 2, et que la P208 est requise pour la relocalisation

de RBM14 dans le cytoplasme (Figure 1B). Ces résultats suggèrent que l'interaction de  $\mu 2$  avec RBM14 induit sa relocalisation du noyau de la cellule vers le cytoplasme. L'absence de relocalisation lorsque  $\mu 2$  possède une sérine à 208 semble s'expliquer par l'interaction plus forte lorsqu'une proline est présente à 208 qu'une sérine (Figure 1A), combiné avec les niveaux de  $\mu 2$  plus élevés pour le P208 que le S208 (Boudreault *et al.*, 2022). Cette différence drastique de localisation suggère que RBM14 joue un rôle important durant la réplication de réovirus. Puisque RBM14 a été lié à la réponse interféron et que  $\mu 2$  contrôle cette réponse, il serait intéressant d'investiguer si RBM14 participe à la réponse interféron durant l'infection avec réovirus (Lanoie et Lemay, 2018; Morchikh *et al.*, 2017). Des expériences de réduction du niveau de RBM14 avec des siRNA ainsi que sa surexpression à partir d'un plasmide permettrait d'investiguer son rôle durant l'infection. Bien évidemment, il serait pertinent d'étudier RBM14 avec T3D<sup>S</sup> et T3D<sup>K</sup> ainsi que les virus réassortants P208S et S208P pour bien comprendre le rôle de RBM14 dans le noyau et le cytoplasme.

### ***Le complexe TRiC***

Parmi les 19 interacteurs communs aux quatre constructions de  $\mu 2$  mentionnés au début de cette section, deux appartiennent au complexe TRiC (*T-complex protein Ring Complex*, aussi connu comme *Chaperonin Containing TCP-1*, CCT), soit CCT2 et CCT8. De plus, de nombreux autres composants du complexe ont été retrouvés parmi les interacteurs de certaines constructions que nous avons testées : TCP1 (1 constructions/4 testées), CCT3 (1/4), CCT4 (3/4), CCT5 (3/4), CCT6A (1/4) et CCT7 (2/4) (Boudreault *et al.*, 2022). Nous avons donc détecté les 8 composantes de ce complexe à au moins une reprise et certaines dans toutes les constructions que nous avons testées, ce qui suggère fortement que  $\mu 2$  interagit avec TRiC. Le complexe TRiC est un complexe protéique agissant comme chaperone permettant le repliement des protéines, et il aide notamment au bon repliement de 10% des protéines du cytosol (Jin *et al.*, 2019). Ce complexe a déjà été démontré pour aider au repliement de la protéine  $\sigma 3$  de réovirus (Knowlton *et al.*, 2018, 2021), et chez

le réovirus aviaire, des protéines  $\sigma A$  ( $\sigma 2$  ou  $\sigma 3$  de réovirus),  $\sigma C$  ( $\sigma 1$  de réovirus) et  $\sigma NS$  (Huang *et al.*, 2022). Ces résultats suggèrent donc que  $\mu 2$  bénéficie aussi de l'aide du complexe TRiC pour se replier et que ce complexe est peut-être usurpé de manière plus globale par réovirus pour replier plusieurs de ses protéines. Il serait intéressant d'aller valider que  $\mu 2$  interagit avec ce complexe et que son repliement est dépendant du complexe TRiC. Il serait aussi intéressant d'aller questionner l'importance de ce complexe pour le repliement des autres protéines de réovirus. Des expériences d'immunofluorescence dans des cellules infectées pourraient être menées pour voir si le complexe TRiC se localise aux usines de réplication virales; si effectivement ce complexe replie plusieurs protéines de réovirus, alors le virus aurait intérêt à relocaliser le complexe à même ses usines de réplication, où l'essentiel de sa synthèse protéique est situé. Finalement, il serait intéressant de regarder l'impact de la P208/S208 dans  $\mu 2$  sur l'interaction avec ce complexe; peut-être qu'il serait possible d'apprendre des informations sur la nature de ce polymorphisme et son impact sur repliement de  $\mu 2$  en analysant comment le complexe TRiC interagit et replie ces deux versions de  $\mu 2$ .

### ***CAMK2D et CAMK2G***

Dans l'article publié dans *Nucleic Acids Research* (chapitre 2), nous avons démontré l'interaction de  $\mu 2$  avec les protéines CAMK2D et CAMK2G pour valider notre procédure expérimentale (Figure 5B, chapitre 2). Nous avons aussi identifié CAMK2B parmi les interacteurs de la construction  $\mu 2$ -GFP. Ces protéines sont des kinases dépendantes du  $Ca^{2+}$  et de la calmoduline, dont il existe 4 gènes : *CAMK2A*, *CAMK2B*, *CAMK2D* et *CAMK2G*. Elles sont régulées par le  $Ca^{2+}$  et la calmoduline, une protéine qui lie le calcium, et sont notamment importantes dans le cerveau où elles représentent 1 à 2% des protéines totales (CAMK2B, CAMK2G), dans le muscle squelettique (CAMK2B, CAMK2G) et dans le cœur (CAMK2D). L'importance de la signalisation médiée par le calcium pour les infections virales est de mieux en mieux comprise et suggère que  $\mu 2$  puisse être impliquée dans cette signalisation via CAMK2D, CAMK2G et possiblement CAMK2B (Saurav *et al.*, 2021). De plus, la

pathogénèse de réovirus chez la souris est principalement cardiaque et neurologique, suggérant que l'abondance des protéines CAMKII dans ces tissus puissent être impliquée dans les lésions d'origine virale (Aravamudhan *et al.*, 2022; Sherry, 1998). Rien n'est connu pour l'instant sur l'importance du  $\text{Ca}^{2+}$  lors de l'infection avec réovirus, mais plusieurs études supportent un rôle important de cette signalisation lors de l'infection avec un proche cousin de réovirus, rotavirus. Chez rotavirus, une élévation du calcium intracellulaire est observée, concomitante avec une diminution de l'expression de CAMKII (Chen *et al.*, 2017). Rotavirus produit une viroporine, la protéine NSP4, qui s'insère dans la membrane du réticulum endoplasmique et induit la relâche du  $\text{Ca}^{2+}$  dans le cytoplasme. Ce  $\text{Ca}^{2+}$  active les CAMKII, ce qui initie l'autophagie pour favoriser le transport des protéines virales du réticulum endoplasmique vers les VF (Crawford *et al.*, 2012; Crawford et Estes, 2013). Ce  $\text{Ca}^{2+}$  semble aussi important pour contrôler le cycle cellulaire, et notamment l'accumulation des cellules infectées en phase S du cycle cellulaire bénéfique pour la réplication virale (Bhowmick *et al.*, 2014). Il serait certainement très intéressant d'aller investiguer si l'infection avec réovirus induit une augmentation du  $\text{Ca}^{2+}$  cytoplasmique et le rôle de CAMK2B, CAMK2D et CAMK2G dans cette potentielle augmentation. De plus, puisque l'interaction de  $\mu 2$  avec CAMK2D et CAMK2G a déjà été validée et que l'interaction avec  $\mu 2$  peut induire une relocalisation intracellulaire (Figure 1B), il serait aussi intéressant d'analyser la localisation des protéines CAMKII par immunofluorescence lors de l'infection avec réovirus. Finalement, il faut aussi mentionner que les ARN codant pour les protéines CAMKII sont épissés alternativement de manière extensive et que nous avons déjà mis en lumière lors de l'infection avec réovirus des changements d'épissage dans le gène *CAMK2D* (2 évènements identifiés) et dans *CAMKK2* (2 évènements identifiés), une kinase responsable de la phosphorylation de CAMK2D (Boudreault *et al.*, 2016). Il serait donc particulièrement pertinent, dans un premier temps, de valider par AS-PCR les modulations de l'épissage alternatif dans ces gènes lors de l'infection. Par la suite, l'impact de ces potentiels changements d'épissage alternatif sur le niveau de protéines et les isoformes produites pourrait être investigué par WB. Une hypothèse

intéressante serait que  $\mu 2$  favorise une isoforme particulière de CAMK2D durant l'infection, et que  $\mu 2$  interagisse de manière préférentielle avec cette isoforme.

### ***ESRP1***

Lors de nos premières analyses de la modulation de l'épissage alternatif cellulaire par réovirus, nous avons regardé l'expression des facteurs d'épissage suite à l'infection (Boudreault *et al.*, 2016). Nous avons alors remarqué très peu de changements dans l'expression de ces protéines qui contrôlent l'épissage alternatif, hormis pour un gène, *ESRP1* (Figure 6A, chapitre 1). Alors que la plupart des facteurs d'épissage n'avait pas ou peu de changement de leur expression (au maximum, une augmentation de 3,7 fois), *ESRP1* était surexprimé 46,4 fois. Nous étions alors très intéressés à investiguer l'implication de la protéine ESRP1 dans les changements d'épissage causés par réovirus. ESRP1 est un facteur d'épissage peu caractérisé, dont le rôle premier est de contrôler un programme d'épissage alternatif spécifique aux cellules épithéliales (Dittmar *et al.*, 2012; Warzecha *et al.*, 2009). Elle semble cependant posséder des rôles beaucoup plus larges, par exemple dans la transition épithélio-mésenchymateuse, l'apoptose et la carcinogenèse (Qu *et al.*, 2020; Vadlamudi *et al.*, 2020; Vadlamudi et Kang, 2022). Il est donc surprenant d'observer une protéine décrite comme régulant un programme d'épissage alternatif caractéristique des cellules épithéliales lors de l'infection virale de cellules fibroblastiques, comme les L929 que nous utilisons. Nous avons donc investigué ce qui permet cette surexpression d'ESRP1, et découvert que des cellules non-infectées cultivées en présence de cellules infectées surexpriment aussi ESRP1 (Figure 2A). Puisque nous avons démontré que peu de changements d'épissage se produisent dans ces mêmes cellules non-infectées cultivées en présence de cellules infectées (Figure 1D, chapitre 2), il est clair que la surexpression d'ESRP1 n'explique pas une proportion élevée des changements d'épissage induits par réovirus. Cependant, ce dernier résultat suggérait que ce n'est pas l'infection avec réovirus directement, mais plutôt ce qui est sécrété par les cellules infectées, qui induit la surexpression d'ESRP1. Nous avons donc investigué cette possibilité en tirant profit de la dualité

T3D<sup>S</sup>/T3D<sup>K</sup>, puisque T3D<sup>K</sup> induit une plus forte sécrétion d'interféron lors de l'infection (Lanoie et Lemay, 2018). J'ai pu démontrer que T3D<sup>K</sup> induit effectivement une surexpression plus grande d'ESRP1 que T3D<sup>S</sup>, corrélant avec la quantité d'interféron relative que ces deux virus induisent (Figure 2B). Finalement, nous avons directement testé l'impact de traiter des cellules L929 avec de l'interféron- $\beta$  recombinant, et pu montrer que ce traitement induit aussi la surexpression d'ESRP1 (Figure 2C). ESRP1 est donc un ISG qui répond vraisemblablement à l'interféron- $\beta$  durant l'infection avec réovirus et dont l'expression est induite en réponse aux infections virales, en accord avec certaines évidences dans la littérature scientifique (Qu *et al.*, 2020). Puisque *ESRP1* est un gène qui répond à l'interféron, une implication de la protéine ESRP1 dans les interactions virus-hôte est à investiguer. Il serait intéressant de commencer en regardant l'impact d'ESRP1 sur la réplication de réovirus (ARN, protéines, titre viral) en condition de déplétion par siRNA et de surexpression de la protéine. Si un effet sur la réplication est détecté, il serait alors de mise d'identifier quelle étape de la réplication est affectée par ESRP1, et si cette inhibition est généralisable à d'autres virus. Il serait aussi intéressant d'identifier si le rôle d'ESRP1 est dépendant de son implication dans l'épissage alternatif ou indépendant de cette activité. Finalement, il est à noter qu'il existe deux isoformes d'ESRP1 qui se localise dans le noyau et le cytoplasme par l'ajout ou le retrait d'une séquence de localisation nucléaire (*nuclear localisation signal*, NLS) par épissage alternatif (Yang et Carstens, 2017). Évidemment, les hypothèses à émettre sur le rôle d'ESRP1 sont très différentes si la protéine est nucléaire ou cytoplasmique. Nous avons donc suivi l'épissage alternatif du site 5' de l'exon 12, responsable de l'inclusion du NLS, dans toutes nos expériences. Nous avons pu démontrer que les cellules L929 expriment en majeure partie la forme longue, et donc l'isoforme nucléaire possédant le NLS (Figure 2D). L'infection avec réovirus ou le traitement à l'interféron n'altérerait pas l'épissage alternatif d'ESRP1, et donc l'isoforme induite par l'interféron est donc aussi nucléaire (Figure 2D). Il est donc peu probable qu'ESRP1 soit une protéine antivirale qui agisse de manière directe contre réovirus durant

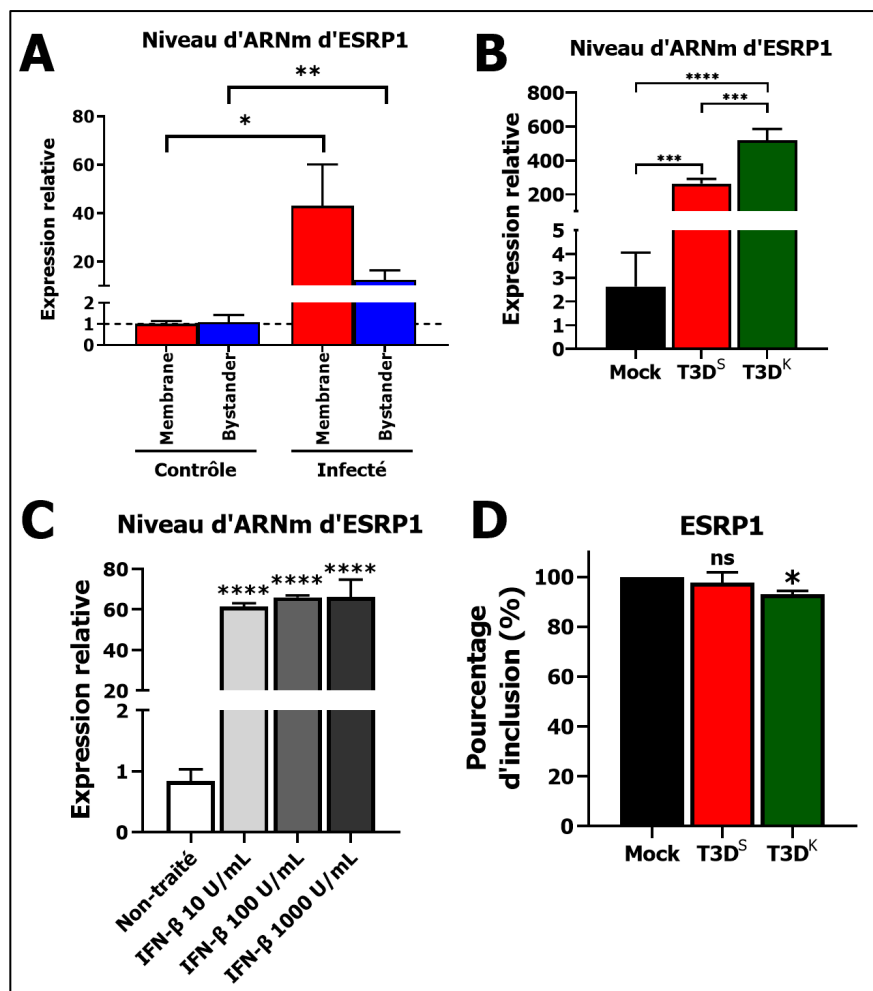


Figure 2. *ESRP1* est un ISG induit par l'interféron durant l'infection avec réovirus. (A) Expression relative de l'ARNm d'ESRP1 dans l'essai de bystander. Test T de Student bilatéral; \*,  $P \leq 0.05$ ; \*\*,  $P \leq 0.01$ . (B) Expression relative de l'ARNm d'ESRP1 suite à l'infection avec T3D<sup>S</sup> et T3D<sup>K</sup>. Des cellules L929 ont été infectées à une multiplicité d'infection (MOI) de 50 virus/cellule pendant 16 heures, puis l'ARN a été récolté pour faire un qPCR. ANOVA à un facteur; \*\*\*,  $P \leq 0.001$ ; \*\*\*\*,  $P \leq 0.0001$ . (C) Expression relative de l'ARNm d'ESRP1 suite à des traitements avec de l'IFN-β. Des cellules L929 ont traité avec les concentrations indiqués d'IFN-β pendant 5 heures, puis l'ARN a été récolté pour faire un qPCR. ANOVA à un facteur avec test de comparaison multiple de Dunnett. Chaque échantillon a été comparé au contrôle non-traité; \*\*\*\*,  $P \leq 0.0001$ . (D) Caractérisation de l'épissage alternatif du site 5' alternatif dans l'exon 12 d'ESRP1. Les mêmes conditions expérimentales qu'en B ont été utilisées, puis l'ARN a été soumis à un AS-PCR avec des amorces pour le site 5' de l'exon 12 dans ESRP1. ANOVA à un facteur avec test de comparaison multiple de Dunnett. Chaque échantillon a été comparé au contrôle non-infecté; ns,  $P > 0.05$ ; \*,  $P \leq 0.05$ .

l'infection, puisque la réplication de réovirus est cytoplasmique. Il est donc plus probable qu'ESRP1, en plus de contrôler un programme d'épissage alternatif pour



les cellules épithéliales, contrôle aussi un deuxième programme d'épissage alternatif en réponse à l'interféron.

### **Rôle et dynamique de la protéine $\mu 2$ et du polymorphisme P208S**

Mes travaux sur  $\mu 2$  et son implication dans la modulation de l'épissage alternatif cellulaire nous ont amené à démontrer que la position 208 dans  $\mu 2$  contrôle aussi la capacité à moduler l'épissage alternatif cellulaire. Puisque l'impact de ce polymorphisme à la position 208 sur  $\mu 2$ , sur ses activités et sur sa structure reste très mal compris, nous nous y sommes plus particulièrement intéressés.

#### *Dynamique d'import nucléaire et d'export de $\mu 2$*

Mes travaux supportent les résultats de la littérature qui démontrent que  $\mu 2$  est importée dans le noyau des cellules lorsqu'elle est exprimée de manière ectopique (Kobayashi *et al.*, 2009; Rivera-Serrano *et al.*, 2017). Cependant, nous avons mis en évidence, pour la première fois, que le polymorphisme à la position 208 contrôle aussi la localisation nucléaire de  $\mu 2$  dans ce même contexte (Figure 4A, chapitre 2). Néanmoins, l'impact de la sérine à 208 sur ce phénotype n'a pas encore été déterminé. Il est possible que cette mutation empêche la reconnaissance de  $\mu 2$  par l'importine responsable de l'amener dans le noyau. Une autre possibilité est que cette sérine augmente l'interaction avec une exportine, ce qui accélérerait son export du noyau. Effectivement, il est connu que  $\mu 2$  fasse la navette entre le noyau et le cytoplasme, notamment parce qu'il est possible d'empêcher son export du noyau en traitant les cellules avec de la leptomycine B, un inhibiteur de CRM1 (Rivera-Serrano *et al.*, 2017). Finalement, il est aussi possible que  $\mu 2$  avec la sérine à 208 n'interagissent pas ou peu avec certaines protéines nucléaires, ce qui empêcherait sa rétention dans le noyau par ces mêmes protéines. Il est certain qu'il serait pertinent de correctement caractériser le ou les NLS présents dans  $\mu 2$ . Celui décrit par le groupe du Pr. Dermody, 100-RRLRKRLMLKK-110, n'avait jamais été muté dans le contexte endogène de  $\mu 2$  (Kobayashi *et al.*, 2009). Quand nous avons muté ce NLS, nous avons remarqué que  $\mu 2$  ne se liait plus aux microtubules, ce qui suggère que la protéine n'est plus correctement repliée. Le groupe du Pr. Dermody avait

remarqué que la mutation de ces résidus avait un effet délétère sur la réplication de réovirus; il en avait conclu que le NLS dans  $\mu 2$  était requis pour la réplication (Kobayashi *et al.*, 2009). Cependant, à la lumière de nos résultats, il est pertinent de se demander si les mutants qu'ils ont analysés sont repliés correctement; effectivement, si ces mutations induisent un défaut de repliement dans  $\mu 2$ , il est alors tout à fait normal qu'elles ne supportent pas la réplication du virus, et ce, sans aucune implication du NLS. Étant donné que  $\mu 2$  possède plusieurs séquences ressemblant à un NLS, il est possible que la fragmentation de la protéine en ses domaines isolés puisse permettre de mieux caractériser chacune de ces séquences indépendamment et leur implication potentielle comme NLS (Mbisa *et al.*, 2000). Aussi, aucun travail n'a été fait pour identifier la séquence d'export nucléaire (*Nuclear export signal*, NES) dans  $\mu 2$ . Il serait pertinent d'identifier cette séquence et de générer des mutants qui ne peuvent faire la navette entre le noyau et le cytoplasme. De cette manière, il serait possible d'étudier l'import de  $\mu 2$  sans effet confondant venant de son export.

De manière intéressante, la dynamique d'import/export de  $\mu 2$  n'est pas sans rappeler celle d'une autre protéine de réovirus, soit  $\sigma 3$ . Il a déjà été démontré que  $\sigma 3$ , en expression transitoire, se localise dans le noyau des cellules (Yue et Shatkin, 1996). Cependant, lorsque  $\mu 1$  est coexprimée avec  $\sigma 3$ , il y a perte de sa localisation nucléaire, probablement dû aux complexes formés avec  $\mu 1$  dans le cytoplasme qui l'empêche d'être importée au noyau. De plus, il n'y a pas à ma connaissance de résultats démontrant une localisation nucléaire de  $\sigma 3$  pendant l'infection avec réovirus dans la littérature. L'importance de la localisation nucléaire de  $\sigma 3$ , tout comme celle de  $\mu 2$ , est donc incertaine pendant l'infection. Il est à noter que  $\sigma 3$  est cependant plus petite que  $\mu 2$  (40 kDa versus 80 kDa);  $\sigma 3$  est donc suffisamment petite pour diffuser passivement dans le noyau, contrairement à  $\mu 2$  qui nécessite un mécanisme d'import actif. Les résultats dans la littérature, ainsi que de nombreux essais de ma part, n'ont pas permis d'observer la protéine  $\mu 2$  dans le noyau des cellules pendant l'infection, même en présence de leptomycine B (Kobayashi *et al.*,

2009). Une hypothèse intéressante serait qu'une protéine de réovirus, comme  $\mu 1$  pour  $\sigma 3$ , séquestre  $\mu 2$  dans le cytoplasme durant l'infection. J'ai testé rapidement si la co-expression de  $\mu 2$  avec  $\mu NS$ , avec laquelle elle interagit notamment pour former les VF, diminuait l'importation de  $\mu 2$  au noyau. Les résultats préliminaires en épifluorescence semblent suggérer que l'interaction de  $\mu 2$  avec  $\mu NS$  empêche l'accumulation de  $\mu 2$  dans le noyau, et devraient être répétés en microscopie confocale et validés par quantification (Figure 3). Finalement, il serait pertinent de générer des réovirus réassortants possédant des  $\mu 2$  n'ayant pas de NLS ou de NES. Il faut cependant s'assurer en amont que des mutations minimales sont effectuées, avant de conclure que l'impossibilité de récupérer de tels virus est liée à la fonction de la séquence mutée, et non pas seulement un défaut de structure dans  $\mu 2$  induit par cette mutation.

### *Ubiquitylation de $\mu 2$*

Il y a une vingtaine d'années, il a été démontré que le polymorphisme à 208 dans  $\mu 2$  influence sa capacité à être ubiquitylée (Miller *et al.*, 2004). L'ubiquitylation est une modification post-traductionnelle consistant en l'ajout d'une ubiquitine, une petite protéine de 26 kDa, sur les résidus lysines et menant la plupart du temps à la dégradation de la protéine marquée par le protéasome. Dans le cas de  $\mu 2$ , il a été démontré que la version P208 est moins ubiquitylée, alors que la version S208 l'est beaucoup plus, résultant en une dégradation accrue de la protéine lorsqu'une sérine est en position 208 (Miller *et al.*, 2004). Cependant, aucune étude subséquente n'est venue s'intéresser à cette différence d'ubiquitylation. Nous ne savons donc pas quelles lysines dans  $\mu 2$  sont ubiquitylées, ni pourquoi la position 208 influence ce phénomène. Cependant, nos résultats sont concordants avec cette hypothèse, puisque nous avons observé que les virus possédant la P208 ont des niveaux de  $\mu 2$  plus élevée que ceux possédant la S208 durant l'infection (Boudreault *et al.*, 2022). Nous avons donc voulu exploiter nos données d'IP-MS sur  $\mu 2$ -GFP et rechercher des lysines qui pourraient être potentiellement des sites d'ubiquitylation. Il est possible

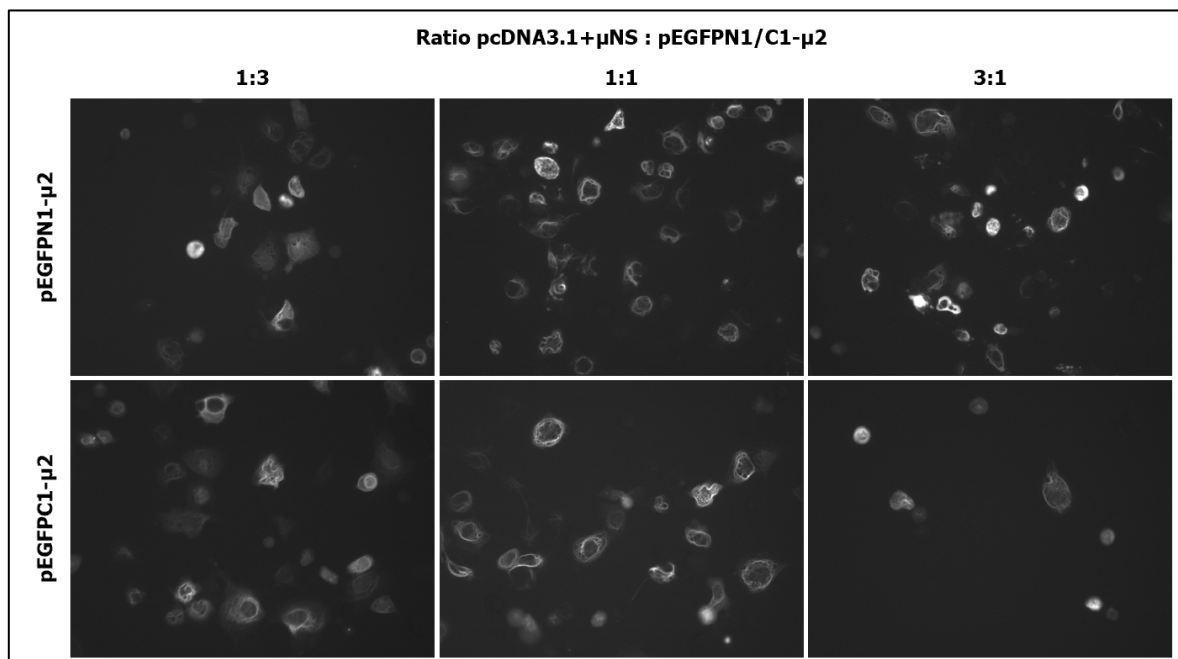


Figure 3. *Impact de la co-expression de  $\mu$ NS sur la localisation cellulaire de  $\mu$ 2.* Des cellules COS-7 ont été transfectées avec différents ratios de plasmide encodant pour  $\mu$ NS et  $\mu$ 2-GFP avec la lipofectamine LTX. Les cellules ont été observées 24 h après la transfection avec un microscope à épifluorescence Nikon TE2000E à 488 nm avec un objectif de 4 x pour visualiser la protéine  $\mu$ 2-GFP.

d'identifier ces lysines par spectrométrie de masse grâce à l'ajout de deux glycines de l'ubiquitine conjuguées à la lysine qui sont laissées suite à la digestion tryptique. Nous avons identifié un seul peptide potentiellement ubiquitinylé, couvrant la région 199-229, dont la lysine 214 serait la cible de l'ubiquitinylation (Figure 4A). Il est intéressant de noter la proximité de cette lysine avec la position 208, autant dans la séquence primaire que dans la structure publiée de  $\mu$ 2 (Figure 4B). Une hypothèse à investiguer serait que cette lysine est effectivement ubiquitinylée et que la position 208, de par sa proximité, influence l'accessibilité de la lysine 214 pour une E3 ubiquitine ligase. La proline 208 défavoriserait l'accès à ce résidu, alors que la sérine 208, dont la nature du résidu est beaucoup moins contraignante sur l'organisation de la structure tertiaire, permettrait un accès et une ubiquitinylation plus facile. Il serait alors de mise de générer des constructions  $\mu$ 2-GFP ayant le résidu 214 substitué par une arginine (K214R), un résidu aussi chargé positivement mais qui ne peut pas être ubiquitinylé. La substitution pour une alanine (K214A) pourrait aussi être investiguée, bien que plus risquée d'avoir un impact sur le repliement de

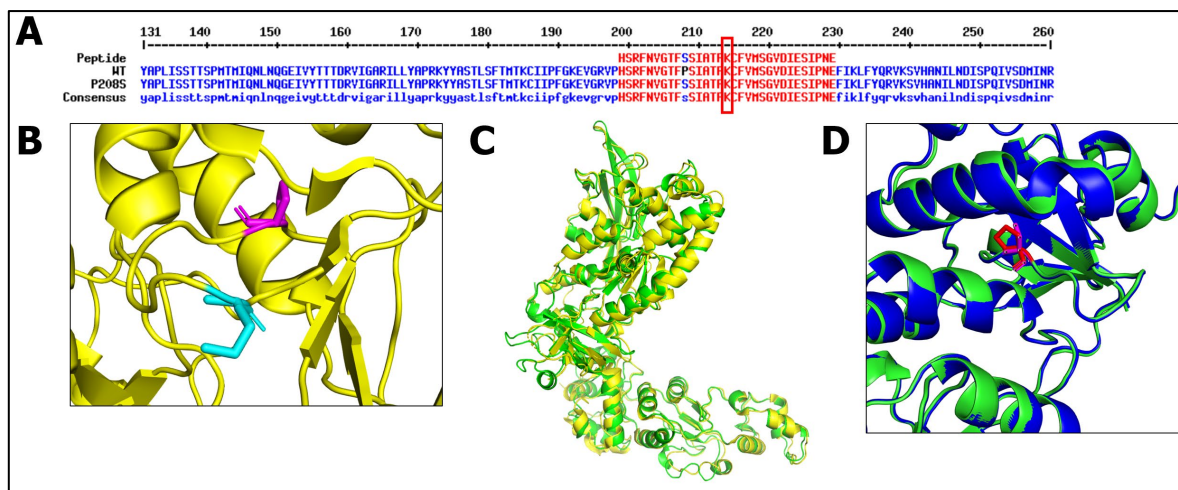


Figure 4. *Impact du polymorphisme P208S sur l'ubiquitinylation et la structure de  $\mu$ 2.* (A) Peptide potentiellement ubiquitinylé détecté dans l'immunoprécipitation de la protéine  $\mu$ 2-GFP. (B) Proximité de la proline 208 (en magenta) et de la lysine 214 (en turquoise) dans une région non-structurée du domaine de liaison à l'ARN de  $\mu$ 2 (en jaune). (C) Structure déterminée par cryomicroscopie électronique (7elh, en jaune) superposée à la prédiction de structure pour  $\mu$ 2 avec la proline à 208 par AlphaFold2 (en vert) (D) Superposition des prédictions d'AlphaFold2 pour  $\mu$ 2 avec la proline à 208 (en vert) ainsi que  $\mu$ 2 avec la sérine à 208 (en bleu). La sérine est en magenta, et la proline en rouge.

la protéine. Bien sûr, ces substitutions devraient être faites pour  $\mu$ 2-P208 et  $\mu$ 2-S208 afin d'étudier l'impact dans les deux contextes. Finalement, pour suivre l'ubiquitinylation, il est possible de transférer un plasmide contenant une ubiquitine marquée d'une étiquette HA fonctionnelle, qui permettra la détection avec un anti-HA. On peut alors répéter le même protocole d'immunoprécipitation anti-GFP que décrit au chapitre deux, et détecter dans l'immunoprécipitation le signal HA lié à l'ubiquitine. Il s'agit d'une hypothèse intéressante pour expliquer la différence d'ubiquitinylation de  $\mu$ 2 selon l'acide aminé à la position 208 qui mérite certainement de plus amples expériences.

### Structure

Étant donné que la structure de  $\mu$ 2 n'a été résolue que très récemment, et ce seulement pour la version possédant une proline à la position 208, nous n'avons que peu d'information structurale sur l'impact de cette substitution. Cependant, une percée majeure dans la biologie structurale a été récemment réussie et il est maintenant possible de faire des prédictions de structure tertiaire basées seulement

sur la séquence primaire. L'outil AlphaFold2 est certainement le plus avancé dans ce domaine (Jumper *et al.*, 2021; Tunyasuvunakool *et al.*, 2021). Nous avons donc, dans un premier temps, appliqué l'outil AlphaFold2 pour prédire la structure de  $\mu 2$  provenant de T3D<sup>S</sup> et possédant une proline à 208, et comparé cette prédiction à la structure *in situ* de  $\mu 2$  publiée récemment (Pan *et al.*, 2021). La structure globale de la prédiction est très similaire à la structure *in situ* expérimentale (Figure 4C). Subséquemment, nous avons aussi prédit la structure de cette même protéine pour laquelle la P208 était substituée par une sérine, et observé que le domaine de liaison à l'ARN, et notamment la région près de la position 208, est prédite par AlphaFold2 de manière identique (Figure 4D). Donc, s'il existe effectivement un défaut structural local induit par la sérine à la position 208, il sera nécessaire de déterminer la structure expérimentalement pour l'observer. Il est clair que l'approche par cristallographie et diffraction des rayons X ainsi que par RMN semble impossible, considérant que la plupart des protéines de réovirus, comme  $\sigma 1$ ,  $\mu 1$  et  $\lambda 3$ , ont vu leur structure résolues par ces techniques il y a une vingtaine d'années déjà (Chappell *et al.*, 2002; Liemann *et al.*, 2002; Tao *et al.*, 2002). L'approche utilisée récemment par Pan et collègues pour définir la seule structure de  $\mu 2$  que l'on possède, soit par cryomicroscopie électronique directement dans la particule virale, semble la plus prometteuse pour déterminer la structure du variant avec une sérine à 208 (Pan *et al.*, 2021). Cependant, au vue des prédictions d'AlphaFold2, il semble que la structure ne soit pas tellement affectée par la substitution P208S, et qu'une approche biochimique et de biologie moléculaire soit plus appropriée pour comprendre l'impact de ce changement d'acide aminé.

### ***Expression ectopique***

Un problème majeur que nous avons dû contourner pour étudier  $\mu 2$  est son expression ectopique. Effectivement, nous avons longtemps essayé d'exprimer  $\mu 2$  dans les L929, afin de pouvoir comparer directement l'impact de l'infection avec l'expression de  $\mu 2$  seule. Cependant, nous n'arrivions pas à exprimer  $\mu 2$ , ce qui était problématique pour la suite du projet. Avant de trouver que les cellules HEK 293T

convenaient à l'expression de  $\mu 2$ , nous avons tenté de comprendre ce qui empêchait son expression dans les L929. Nous avons tout d'abord regardé les niveaux d'ARNm produits à partir des plasmides codants pour GFP seul ou GFP- $\mu 2$ , et nous avons réalisé que nous détectons de 5 fois à 20 fois moins d'ARN lorsque  $\mu 2$  était en fusion avec GFP (Figure 5A). Ce résultat démontre que l'ARN de fusion  $\mu 2$ -GFP est beaucoup moins abondant que GFP seul, et suggère une possible instabilité au niveau de l'ARNm. Nous n'avons pas eu le temps d'investiguer la demi-vie de ces ARN, mais nous avons réussi à produire *in vitro* des ARNm, avec un analogue de la structure coiffe en 5' et une queue poly-A en 3', en tout point semblables à ceux produits par nos plasmides. En transfectant ces ARN directement dans les cellules, nous contournions la portion nucléaire (entrée du plasmide dans le noyau, transcription, stabilité nucléaire et export) et pouvions directement suivre nos ARN dans le cytoplasme. Cette approche ne nous a pas permis d'exprimer  $\mu 2$ , mais nous avons pu répliquer les résultats obtenus avec des plasmides (Figure 5B). Effectivement, même si nous avons transfecté la même quantité d'ARN pour chaque construction en nombre de moles, nous avons observé un niveau très faible des constructions contenant la région codante de  $\mu 2$  comparativement à GFP seul. Nous avons aussi testé l'ajout de la région 5' non-traduite (13 pb) ainsi que de la région 3' non traduite (80 pb) du segment M1 indépendamment, sans grand impact sur le niveau d'ARN des constructions contenant  $\mu 2$ . Ce résultat suggère que la portion codante de  $\mu 2$  est instable dans le cytoplasme et est rapidement dégradée.

En faisant de plus amples recherches, nous avons réalisé que certaines régions du segment M1 sont très riches en adénines et en thymines, ce qui se transcrit en régions riches en A et U dans l'ARNm. Ces régions AU-riches ont notamment été reliées à l'instabilité des ARNm (Ohme-Takagi *et al.*, 1993). De plus, la séquence la plus souvent reconnue par les protéines liant les régions AU-riches, AUUUA, se retrouve six fois dans la séquence codante de  $\mu 2$ ; il s'agit du segment de réovirus avec le plus de ces séquences (Gay et Babajko, 2000). Les motifs AUUUA sont principalement retrouvés dans deux régions, soit de 527 à 702 (positions calculées

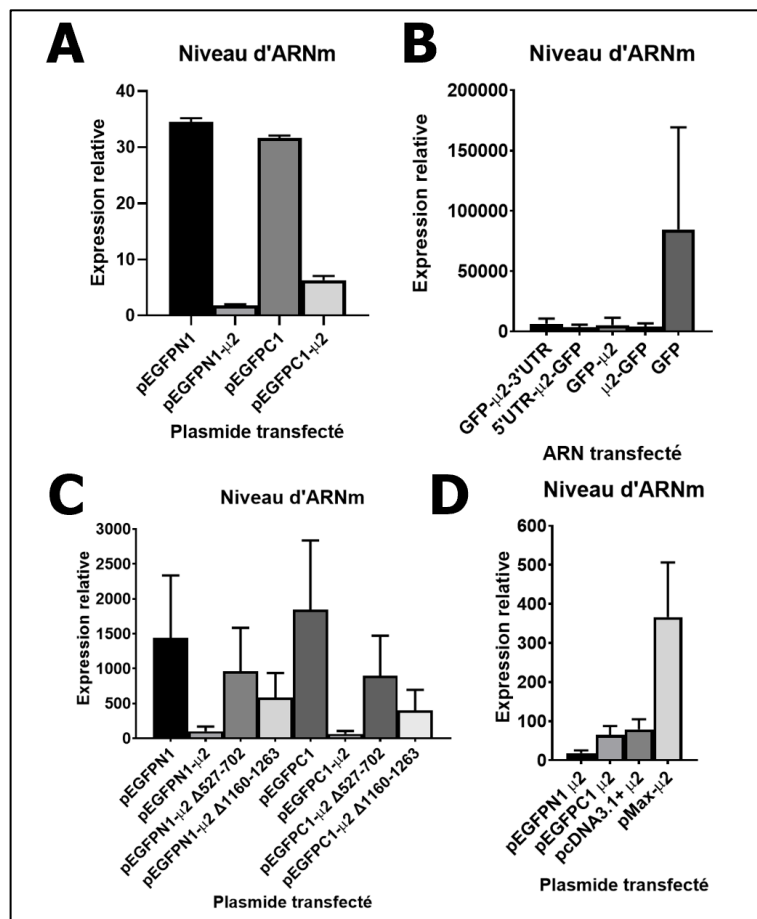


Figure 5. *Impact des séquences déstabilisatrices dans la région codante de  $\mu$ 2 sur le niveau d'ARNm.* (A) Des cellules L929 ont été transfectées avec du Transit2020 et l'ARN a été récolté à 24 h post transfection. Le niveau d'expression relative a été déterminé par ddPCR avec des amorces pour GFP. (B) Des cellules L929 ont été transfectées avec du Transit-mRNA et des ARN produits *in vitro* grâce au kit mMACHINE T7 Transcription kit et les ARN ont été récoltés à 24 h post transfection. Le niveau d'expression relative a été déterminé par ddPCR avec des amorces pour GFP. (C) Des cellules L929 ont été transfectées avec du Transit2020 et l'ARN a été récolté à 24 h post transfection. Le niveau d'expression relative a été déterminé par ddPCR avec des amorces pour GFP. (D) Des cellules L929 ont été transfectées avec du Transit2020 et l'ARN a été récolté à 24 h post transfection. Le niveau d'expression relative a été déterminé par ddPCR avec des amorces pour le segment M1.

à partir de l'ATG), qui contient trois AUUUA, et de 1160 à 1263, qui contient deux AUUUA. Nous avons donc retiré ces deux régions de nos plasmides de départ, et observé que les niveaux d'ARNm produits par ces plasmides étaient significativement augmentés (Figure 5C). Ces résultats suggèrent que ces deux régions participent à déstabiliser l'ARN de  $\mu$ 2, et peuvent expliquer en partie les difficultés que nous avons rencontrées pour exprimer  $\mu$ 2. Il serait intéressant de tester une construction avec la délétion des deux régions pour vérifier si leur effet peut être additif. Il serait aussi



pertinent d'y aller avec un modèle moins drastique que la délétion complète de ces régions, soit la délétion uniquement des séquences AUUUA ou leur perturbation grâce à des mutations silencieuses. Aussi, il serait pertinent de faire l'expérience inverse, et de greffer seulement ces régions à la séquence codante de GFP, pour vérifier si elles sont suffisantes pour induire la dégradation de l'ARN. De plus, ces découvertes pourraient avoir d'importantes retombées dans la biologie de réovirus. Effectivement, si le segment M1 est très instable, par quel mécanisme est-il protégé de la dégradation durant l'infection? Est-ce que la localisation de l'ARNm dans les VF est suffisante pour empêcher l'ARN du segment M1 d'être dégradé? Ou est-ce que réovirus détourne une protéine cellulaire liant le segment M1 et le déstabilisant, pour en faire une protéine stabilisant ce segment durant l'infection? Toutes ces hypothèses mériteraient certainement d'être poursuivies. Il serait aussi de mise de tester l'impact de la coexpression de  $\sigma$ NS sur le niveau d'ARN de ces constructions. Effectivement,  $\sigma$ NS agit comme une chaperone d'ARN, qui permet notamment la stabilisation des ARN de réovirus (Borodavka *et al.*, 2015; Bravo *et al.*, 2018, 2021; Zamora *et al.*, 2018). Bien qu'intéressants, ces résultats ne garantissent pas qu'il sera possible d'exprimer  $\mu$ 2 en stabilisant son ARNm. Effectivement, nous avons réussi à augmenter le niveau d'ARNm de  $\mu$ 2 en le faisant exprimer dans le plasmide pMax en fusion avec un intron chimérique, ce qui aide la maturation et l'export de l'ARN (Figure 5D). Pourtant, nous ne pouvons toujours pas détecter la protéine  $\mu$ 2 produite par ce plasmide, suggérant que la difficulté d'exprimer  $\mu$ 2 ne réside pas que dans l'instabilité de son ARNm, mais potentiellement aussi dans sa traduction ou son instabilité protéique.

### **Modulation et rôle de l'épissage alternatif dans la réplication virale**

Bien que mes travaux aient permis d'en apprendre beaucoup sur l'impact de réovirus et aussi de  $\mu$ 2 sur l'épissage alternatif cellulaire, il s'agit des premiers travaux s'intéressant en profondeur à ce phénomène. Il reste donc encore beaucoup d'expériences à réaliser et de questions en suspens auxquels des travaux futurs pourront répondre.

### ***Modulation de l'épissage alternatif par réovirus***

Nous avons utilisé la lignée de cellules fibroblastiques L929, lignée de référence pour l'étude de réovirus, afin de déterminer l'impact de ce virus sur l'épissage alternatif cellulaire. Cependant, puisque nous ne pouvions pas exprimer la protéine  $\mu 2$  dans ces mêmes cellules, nous avons dû utiliser les HEK 293T pour les expériences nécessitant l'expression ectopique de  $\mu 2$ . Ceci a considérablement compliqué les possibilités de comparer l'impact de  $\mu 2$  avec l'impact de l'infection complète sur l'épissage alternatif. Évidemment, s'il devient possible un jour d'exprimer  $\mu 2$  dans les L929 (voir section *Expression ectopique* de la présente discussion), il serait alors de mise de comparer l'impact de  $\mu 2$  à l'impact de l'infection, et d'analyser quel pourcentage des changements que l'on observe en infection est attribuable à  $\mu 2$ . Il est possible qu'une séquence codante conçue artificiellement, basée seulement sur la présence des bons codons pour exprimer  $\mu 2$ , ou bien optimisée par un programme tel que iCodon, puisse régler ce problème (Diez *et al.*, 2022).

Il semble cependant plus simple d'exploiter les HEK 293T, pour lesquelles l'expression de  $\mu 2$  fonctionne assez bien, et d'infecter ces cellules, ce qui est possible puisque nous l'avons déjà validé au laboratoire. Il serait alors très intéressant de comparer l'impact de nos constructions  $\mu 2$ -GFP, autant après 24 h que 48 h d'expression, à l'impact de l'infection avec réovirus dans les 293T. Cela permettrait de répondre à deux questions : (1) quelle est la proportion des changements qui sont observés suite à l'infection avec réovirus sont attribuables à la protéine  $\mu 2$ , et (2) quelle est l'importance de la réplication virale ainsi que des autres protéines virales dans l'activité de  $\mu 2$  sur l'épissage alternatif cellulaire? Tel que démontré dans le chapitre 2, il faudra faire très attention au temps choisi pour récolter les cellules suite à l'infection, puisque l'impact maximal sur l'épissage alternatif concorde avec le pic de réplication virale; nous ignorons pour l'instant la dynamique de réplication dans les 293T et si elle est semblable à celle qui est observée dans les L929. Aussi, la profondeur de notre séquençage du chapitre 1 n'était pas assez grande pour analyser l'épissage *de novo*. Plutôt que de pouvoir prédire de nouveaux

sites d'épissage, nous étions limités à regarder ce qui était décrit et connu dans les annotations. Étant donné l'impact de réovirus et  $\mu 2$  sur le complexe U5 du spliceosome, il est très possible que l'on observe des nouveaux sites d'épissage qui ne sont normalement pas utilisés en condition d'homéostasie. Il serait pertinent de pouvoir réanalyser l'épissage dans les L929 ou les 293T avec assez de profondeur pour prédire l'épissage *de novo*, ce qui pourrait permettre d'identifier de nouvelles modifications dans l'épissage alternatif passées jusque-là inaperçues.

Un autre aspect important qui pourrait être poursuivi serait de comparer l'impact de réovirus dans plusieurs lignées de cellules différentes. Bien qu'un peu compliqué puisqu'il faut correctement sélectionner le temps idéal suite à l'infection pour chacune de ces lignées, ces travaux permettrait de mieux comprendre l'importance de moduler l'épissage alternatif pour réovirus et l'impact du contexte cellulaire dans cette modulation. Une sous-question d'intérêt serait de mieux comprendre l'impact sur l'épissage alternatif de réovirus dans différents organismes. Le virus, ayant un très large tropisme pour les mammifères, infecte aussi bien l'humain que la souris. Cependant, chez l'humain, il n'est pas associé à des symptômes aigus, alors qu'il cause des myocardites ainsi que des complications neurologiques chez la souris. Étant donné que l'épissage alternatif est peu conservé entre différentes espèces proches dans l'arbre de la vie, il serait de mise de comprendre si certains aspects de la pathogénicité de réovirus sont liés à l'épissage chez ces différentes espèces (Yeo *et al.*, 2005). De plus, les chauve-souris constituent, comme pour les coronavirus, une espèce réservoir pour réovirus (Kohl et Kurth, 2015; Wang et Cowled, 2015). Il serait donc intéressant d'investiguer l'impact de réovirus sur l'épissage alternatif dans des cellules de chauve-souris, donc le niveau basal de réponse interféron est notamment beaucoup plus élevé (Sandekian *et al.*, 2013).

Un dernier aspect qui devrait être poursuivi est définitivement l'impact de ces changements transcriptomiques sur le protéome de la cellule infectée. Au chapitre 1, nous avons utilisé une approche de spectrométrie de masse pour identifier

certains peptides suggérant un impact de ces altérations de l'épissage alternatif sur le protéome (Figure 5, chapitre 1). Cependant, tous nos essais pour visualiser ces changements, notamment par WB, se sont avérés infructueux. Il n'y a, à ma connaissance, que très peu d'articles ayant été capable de mettre de l'avant des changements protéomiques découlant de la modulation de l'épissage alternatif d'origine virale. Il s'agit probablement de l'aspect le plus difficile de telles études. Une option intéressante serait d'effectuer des immunoprécipitations sur les protéines d'intérêt, plutôt que de faire un WB directement sur un lysat protéique. De cette manière, il est possible d'enrichir des isoformes de faible abondance, mais qui peuvent tout de même avoir une implication biologique. Il serait aussi probablement pertinent d'effectuer un séquençage de longue lecture sur des L929 contrôles et infectées avec réovirus. De cette manière, il serait possible d'observer les transcrits complets, plutôt que seulement des régions discrètes de l'ARNm qu'il faut recoller ensemble de manière bio-informatique. L'information supplémentaire des transcrits permettrait de compléter celle déjà acquise via notre séquençage de lectures courtes, et permettrait de prioriser les transcrits connus pour produire des isoformes protéiques dans nos analyses par WB.

### ***Rôle de la modulation de l'épissage alternatif par réovirus***

Bien que nous ayons investigué les rôles d'EFTUD2, de PRPF8 et de SNRNP200 dans la réplication de réovirus, nous n'avons pas examiné directement le rôle des changements d'épissage alternatif dans la biologie de réovirus. Pour ce faire, il serait de mise, dans un premier temps, de tester l'implication des gènes dont l'épissage est altéré en utilisant une approche de déplétion par siRNA, tel que déjà décrit dans la littérature (Thompson *et al.*, 2020). De cette manière, il est possible de retenir seulement les gènes ayant un impact pour maximiser les chances d'observer un phénotype en modulant l'épissage alternatif. Tel que décrit dans l'introduction et utilisé pour étudier le virus de l'influenza, il est possible d'utiliser des ASO pour favoriser la forme courte, en masquant le site d'épissage en 5' de la région à exclure (Thompson *et al.*, 2020). Cependant, cette approche ne peut que favoriser la forme

courte, et est donc plutôt limitée. L'utilisation des TOSS et des TOES, permettant de favoriser la forme longue ou la forme courte respectivement, est donc à préconiser, car elle permet autant de rétablir l'épissage vers le niveau des cellules non-infectées, que d'augmenter encore plus le changement causé par le virus. Idéalement, chaque événement d'épissage d'intérêt serait d'abord modulé dans les deux sens, et les événements ayant un impact seraient ensuite modulés tous ensemble, tel que décrit pour le virus de l'influenza (Thompson *et al.*, 2020). Cela permettrait de potentialiser encore plus les changements causés par réovirus lors de l'infection, et aussi de neutraliser le plus de changements possibles en même temps. L'effet observé peut se situer au niveau de la réplication virale, tel que démontré pour le virus de l'influenza (Thompson *et al.*, 2020). Cependant, considérant les résultats présents au chapitre 3, il serait extrêmement pertinent d'y aller plus large que seulement la réplication virale, et d'aussi surveiller de possibles impacts sur la survie, la mort cellulaire, ainsi que la réponse antivirale cellulaire via la voie de l'interféron.

### ***Implication dans l'activité oncolytique***

Un aspect intéressant de mes travaux à développer serait de se demander comment ces changements d'épissage alternatif médiés par réovirus sont impliqués dans l'activité oncolytique du virus. Il pourrait être intéressant de comparer l'impact sur l'épissage alternatif de réovirus dans des lignées de cellules saines et cancéreuses, et dans ces lignées cancéreuses, de comparer celles qui sont détruites par le virus à celles qui résistent à la destruction. Cela pourrait permettre de mettre en lumière des changements d'épissage alternatif nécessaires à la réplication de réovirus dans les cellules cancéreuses, et ceux requis pour la destruction de ces mêmes cellules. Les travaux portant sur EFTUD2, PRPF8 et SNRNP200 effectués au chapitre 3 pourraient aussi être répliqués dans des cellules normales et cancéreuses, par exemple le couple de cellules MCF7 (adénocarcinome mammaire métastatique) et MCF 10A (cellules épithéliales du sein), afin de mieux comprendre le rôle de ces protéines cellulaires dans la réplication de réovirus dans des cellules saines et transformées.

### ***Modulation et rôle de l'épissage alternatif dans la réplication d'autres virus***

Nos travaux se sont majoritairement concentrés sur réovirus et l'importance de la protéine  $\mu 2$  dans la modulation de l'épissage alternatif cellulaire. Cependant, de nombreuses protéines virales semblent en mesure d'induire de tels changements de l'épissage alternatif cellulaire et méritent plus d'investigations. Par exemple, je me suis aussi intéressé à l'impact d'une protéine de latence du VEB, la protéine EBNA1, pour laquelle nous avons aussi démontré la capacité à moduler l'épissage alternatif cellulaire, sans malheureusement avoir le temps de comprendre le mécanisme de fond en comble (Boudreault *et al.*, 2019 - Voir annexe 2). Parmi l'ensemble des protéines virales existantes, il y a présentement un manque flagrant de données sur la capacité des protéines ayant une activité oncogénique d'altérer l'épissage alternatif. Pourtant, il est bien connu que l'épissage alternatif est dérégulé pendant la carcinogenèse (voir introduction, section *Épissage alternatif et maladies*), et que des protéines virales peuvent déréguler l'épissage alternatif. L'hypothèse suivante s'impose donc par elle-même : est-il possible que des protéines virales oncogéniques induisent des changements dans l'épissage alternatif qui puissent, à leur tour, participer à la carcinogenèse? Un projet visant à répondre à cette question est présentement en cours dans le laboratoire. Ce projet comparera l'impact sur l'épissage alternatif de nombreuses oncoprotéines virales dans le même contexte cellulaire, et devrait nous permettre de mieux comprendre l'importance de l'épissage alternatif dans la carcinogenèse d'origine virale. De manière intéressante, il a récemment été démontré qu'une protéine du virus oncogénique HTLV-1, HBz, interagit avec de nombreuses protéines impliquées dans l'épissage et induit des altérations dans l'épissage alternatif cellulaire (Shallak *et al.*, 2022). De nombreuses protéines du complexe U5, comme EFTUD2, PRPF8, PRPF6, SNRNP40 et SNRNP200 sont parmi les interacteur de HBz, suggérant que l'étude de l'usurpation du complexe U5 pourrait aussi être d'intérêt dans la carcinogénèse d'origine virale (Shallak *et al.*, 2022).

## **Le complexe U5**

Mes travaux se sont essentiellement concentrés sur les protéines cellulaires EFTUD2, PRPF8 et SNRNP200, appartenant au complexe U5. Bien que nous ayons mis en évidence leur implication dans la modulation de l'épissage alternatif par réovirus, de nombreuses questions émergent de ces travaux et restent à être répondues.

### *Importance d'U5 dans la modulation de l'épissage alternatif par réovirus et $\mu 2$*

Mes travaux portant sur l'implication d'EFTUD2, de PRPF8 et de SNRNP200 dans la modulation de l'épissage alternatif (chapitre 2) ont été réalisés en regardant un nombre limité d'évènements d'épissage alternatif par AS-PCR. Il peut bien évidemment y avoir un biais dans la sélection des évènements, et il est difficile de tirer des conclusions globales avec seulement un sous-ensemble d'évènements aussi petit. Il serait de mise d'utiliser une approche non-biaisée, comme le RNA-Seq, pour étudier l'implication d'EFTUD2, de PRPF8 et de SNRNP200 dans la modulation de l'épissage alternatif par réovirus. L'approche décrite par siRNA au chapitre 2 est tout à fait applicable à cette démarche expérimentale. Des cellules L929 devraient être transfectées avec un siRNA contrôle ou des siRNA contre EFTUD2, PRPF8 et SNRNP200, puis soit infectées ou non avec réovirus avant de récolter l'ARN pour le séquençage. De cette manière, il est possible, dans la condition non-infectée, de déterminer l'impact de la déplétion d'EFTUD2, de PRPF8 et de SNRNP200 sur l'épissage alternatif cellulaire. Puis, dans la condition infectée, il est possible d'observer les évènements dont la modulation d'épissage est perdue lors de la déplétion d'EFTUD2, de PRPF8 et de SNRNP200 comparativement à la condition siRNA contrôle. Il serait aussi pertinent de faire la comparaison entre les cellules siRNA contrôle infectées (démontrant l'impact de réovirus sur l'épissage alternatif cellulaire) à la déplétion sans infection d'EFTUD2, de PRPF8 et de SNRNP200. Puisque nous avons observé une diminution des composantes du complexe U5 durant l'infection, les siRNA contre EFTUD2, PRPF8 et SNRNP200 devraient d'une certaine manière mimer l'effet de l'infection avec réovirus. Le résultat des

expériences précédentes devrait permettre de mieux comprendre le rôle respectif d'EFTUD2, de PRPF8 et de SNRNP20 dans la modulation de l'épissage alternatif par réovirus. Il serait aussi pertinent de tenter de rétablir les niveaux d'EFTUD2, de PRPF8 et de SNRNP200 individuellement par transfection durant l'infection et investiguer si l'apport en trans de ces protéines peut bloquer l'impact de réovirus sur l'épissage alternatif cellulaire.

Un autre aspect important serait de valider que lorsque l'on exprime  $\mu$ 2-GFP de manière ectopique, tel que décrit au chapitre 2, l'impact que nous avons observé sur l'épissage alternatif passe effectivement par les protéines du complexe U5. Ces résultats pourraient aller de pair avec l'analyse de l'impact de  $\mu$ 2 sur l'épissage alternatif cellulaire grâce au RNA-Seq décrite dans la section *Modulation de l'épissage alternatif par réovirus*. Nous avons cependant entrepris d'étudier l'impact des protéines du complexe U5 sur la modulation des minigènes d'épissage que nous avons utilisés au chapitre 2, ainsi que sur un évènement d'épissage alternatif endogène conservé, présenté et analysé dans le même chapitre, soit *CDKN2AIP*. En règle générale, la déplétion d'EFTUD2, de PRPF8 et de SNRNP200 agit de la même manière que vue au chapitre deux lors de l'infection virale dans les L929 : lorsque l'on déplete ces protéines dans les HEK 293T, l'impact des constructions  $\mu$ 2-GFP sur l'épissage alternatif est diminué de manière significative (Figure 6). L'effet semble moins important pour la déplétion de SNRNP200 et maximal pour la déplétion de PRPF8; il est possible que cela indique que  $\mu$ 2 exerce son impact sur l'épissage alternatif principalement via PRPF8, bien que de plus amples expériences seront nécessaires pour confirmer cette hypothèse. De manière intéressante, l'impact de  $\mu$ 2 sur le minigène de *HNRNPA2B1* n'est pas du tout affecté par la déplétion des protéines d'U5, alors que nous avons démontré dans le chapitre deux (Figure 6B) que cet évènement répondait de manière significative à la déplétion d'EFTUD2. Ce dernier résultat suggère qu'il est possible que pour cet évènement, des régions régulatrices en amont et en aval des exons ceinturant l'exon cassette puissent être requises pour observer une régulation par le complexe U5. De plus amples



expériences devraient être réalisées avec ce minigène ainsi que les autres afin de mieux comprendre le rôle des protéines d'U5 dans l'épissage alternatif de ces régions en présence et en absence de  $\mu 2$ .

Finalement, le dernier aspect qu'il serait important de clarifier est la nature de l'interaction entre  $\mu 2$  et les protéines du complexe U5. Premièrement, il serait pertinent de déterminer le domaine de  $\mu 2$  qui interagit avec ces protéines, basé sur la structure maintenant connue de  $\mu 2$  (Figure 3 de l'introduction). Deuxièmement, il

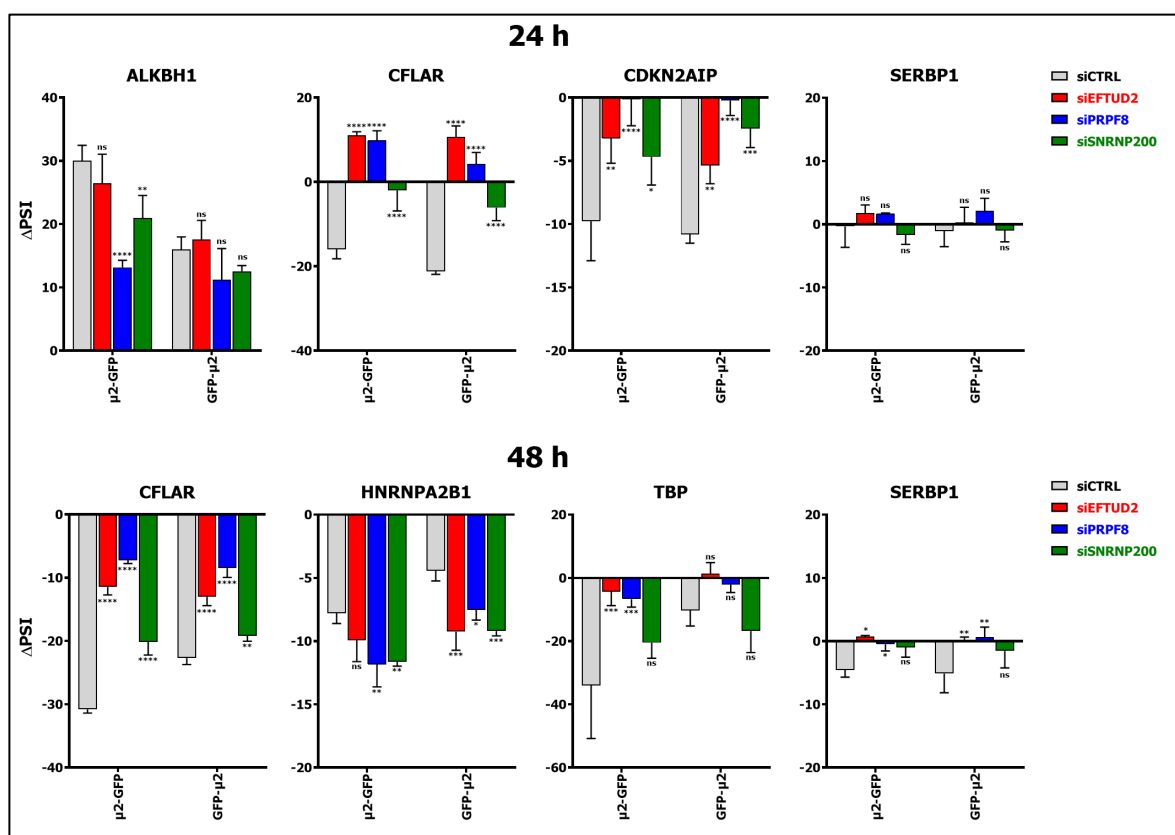


Figure 6. *Impact des constructions  $\mu 2$ -GFP sur l'épissage alternatif en absence des protéines EFTUD2, PRPF8 et SNRNP200.* Des cellules HEK 293T ont été transfectés avec des siRNA contre EFTUD2, PRPF8 et SNRNP200, puis 24 h plus tard, avec GFP,  $\mu 2$ -GFP et GFP- $\mu 2$  ainsi que les minigènes d'épissage avant que les ARN soient récoltés 48 h plus tard (pour la condition 48 h). Pour la condition 24 h, cette transfection a eu lieu 48 h après la transfection des siRNA et 24 h avant la récolte des ARN. Les différents évènements d'épissage ont été analysé par AS-PCR, et le  $\Delta$ PSI a été calculé en soustrayant le PSI de la condition  $\mu 2$  à la condition GFP seul. ANOVA à deux facteurs avec test de comparaisons multiples de Dunnett comparant à la condition siRNA contrôle; ns,  $P > 0.05$ ; \*,  $P \leq 0.05$ ; \*\*,  $P \leq 0.01$ ; \*\*\*,  $P \leq 0.001$ ; \*\*\*\*,  $P \leq 0.0001$ .

serait important de distinguer le ou les interacteurs directs des interacteurs indirects qui sont co-immunoprécipités par l'interaction directe de  $\mu 2$  avec EFTUD2, PRPF8

et/ou SNRNP200. Ce dernier point s'avère un véritable défi, de par la nature des protéines du complexe U5. Dans un premier temps, la taille considérable de ces protéines (250 kDa pour PRPF8 et SNRNP200, 135 kDa pour EFTUD2) rend très difficile l'approche *in vitro* pour déterminer les interactions directes. Il serait probablement plus sage de continuer le travail *in cellulo* d'abord, par exemple en découpant aussi les protéines du complexe U5 pour déterminer la région qui leur permet d'être immunoprécipitées par  $\mu 2$ . De cette manière, il serait peut-être possible d'exprimer seulement un domaine de ces protéines et de tester l'interaction directe avec  $\mu 2$  *in vitro* de ce domaine, étant donné la taille plus raisonnable d'un domaine isolé. Nous avons aussi considéré l'approche de double-hybride en levure, qui pourrait être poursuivie. Cependant, il faut rester prudent avec cette approche, dû à l'homologie de ces protéines entre les eucaryotes pluricellulaires et la levure (de 30 à 60% d'identité, et de 50 à 75% de similarité). Il est donc possible que lorsque l'on teste l'interaction de  $\mu 2$  avec une protéine du complexe U5, celle-ci puisse elle-même entrer en interaction avec le complexe U5 de la levure, et menant ainsi à valider une interaction indirecte plutôt que directe. Finalement, il serait possible de tenter l'approche inverse de celle décrite au chapitre 2 pour mieux comprendre l'interaction entre  $\mu 2$  et les protéines d'U5. Plutôt que d'immunoprécipiter  $\mu 2$  et de regarder pour les protéines d'U5, il serait intéressant d'immunoprécipiter les différentes protéines d'U5, que ce soit de manière endogène ou exprimées en trans, et de vérifier si  $\mu 2$  est détecté dans l'immunoprécipitation. Nous avons commencé à effectuer ce travail avec entre autres des constructions EFTUD2-FLAG et SNRNP200-FLAG, mais il semble que  $\mu 2$  bloque l'expression de ces protéines de manière dose dépendante. Il semble donc que l'approche avec des protéines exprimées à partir d'un plasmide s'avère difficile, et que l'approche endogène soit à préconiser. Dans tous les cas, il est vraisemblable qu'aucune des approches suggérées n'apporte une réponse claire et définitive à cette question, et qu'il faudra probablement une combinaison d'approche pour arriver à bien comprendre l'interaction entre  $\mu 2$  et les protéines du complexe U5.

### ***Rôle de protéines de complexe U5 dans la mort cellulaire programmée***

Au chapitre 3, nous avons observé de nouveaux rôles pour les protéines d'U5 EFTUD2, PRPF8 et SNRNP200 dans l'apoptose, la nécroptose et la réponse interféron. Des travaux subséquents seront nécessaires pour mieux comprendre comment ces protéines exercent leur rôle dans ces processus cellulaires. De manière intéressante, un des événements d'épissage que nous avons analysé puisque modulé par réovirus se situe dans le gène CFLAR. Ce gène produit la protéine c-FLIP qui possède notamment plusieurs isoformes (c-FLIP<sub>S</sub>, c-FLIP<sub>L</sub>, c-FLIP<sub>R</sub>) dont l'activité peut être inversée par épissage alternatif (Tsuchiya *et al.*, 2015). c-FLIP est impliquée dans la régulation de l'apoptose et de la nécroptose, et notamment la décision de la cellule de passer à l'un ou l'autre des programmes de mort, en interagissant avec la caspase-8 dans le DISC (Tsuchiya *et al.*, 2015). Étant donné l'impact de la déplétion d'EFTUD2 et de SNRNP200 sur l'apoptose et la nécroptose, il serait pertinent d'investiguer l'implication potentielle de c-FLIP dans ce mécanisme, ainsi que l'influence possible de son épissage. Nous avons déjà validé par qPCR qu'il est possible de dépléter CFLAR efficacement avec des siRNA (Figure 7A). Nous avons aussi observé que le siRNA #1 contre CFLAR sensibilise un peu les cellules à la mort médiée par réovirus, alors que le siRNA #2 possède plutôt un effet protecteur (Figure 7B). Ce résultat est plutôt surprenant, puisque l'effet des deux siRNA sur le niveau d'ARN de CFLAR est semblable. Nous avons donc vérifié si nos siRNA pouvaient influencer l'évènement d'épissage alternatif que nous avons précédemment analysé dans CFLAR. Malgré que nous n'eussions pas observé de changement statistiquement significatif, le siRNA #1 diminue quand même négativement l'épissage alternatif de cette région (Figure 7C). Ce résultat suggère qu'il serait de mise de regarder de manière plus globale l'épissage alternatif de CFLAR, et aussi d'aller directement moduler l'épissage de CFLAR pour potentiellement expliquer la différence d'impact de nos deux siRNA. Nous avons aussi mis de l'avant l'impact de la déplétion des protéines d'U5 sur l'épissage alternatif d'un site 5' alternatif dans MLKL (Chapitre 3, Figure 4D). L'étude de l'impact de ce site d'épissage dans l'activité

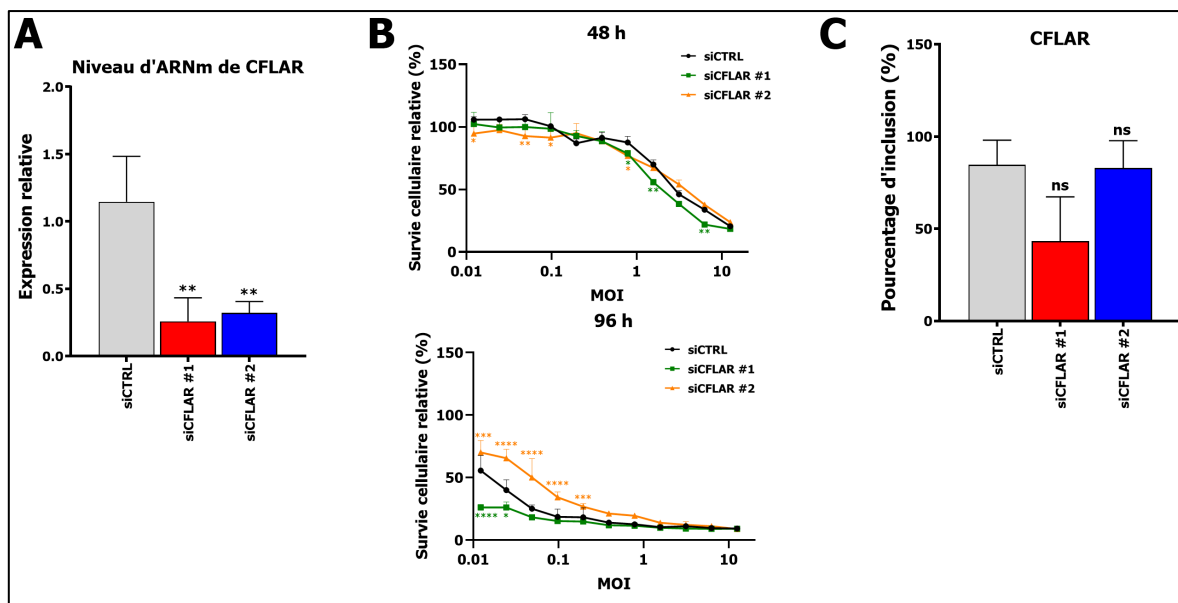


Figure 7. Impact de la déplétion de CFLAR sur la mort cellulaire médiée par réovirus. (A) Validation de la déplétion de CFLAR par qPCR. ANOVA à un facteur avec test de comparaisons multiples de Dunnett, chaque échantillon a été comparé à la condition siRNA contrôle; \*\*,  $P \leq 0.01$ . (B) Essai de survie au bleu de méthylène à 48 h ou 96 h avec des dilutions binaires de réovirus en condition siRNA contrôle ou siRNA contre CFLAR. ANOVA à deux facteurs avec test de comparaisons multiples de Dunnett comparant à la condition siRNA contrôle; \*,  $P \leq 0.05$ ; \*\*,  $P \leq 0.01$ ; \*\*\*,  $P \leq 0.001$ ; \*\*\*\*,  $P \leq 0.0001$ ; si rien n'est indiqué, les résultats ne sont pas statistiquement significatifs. (C) Analyse de l'épissage alternatif de l'exon 6 dans le gène CFLAR suite à la déplétion avec des siRNA. ANOVA à un facteur avec test de comparaisons multiples de Dunnett, chaque échantillon a été comparé à la condition siRNA contrôle; ns,  $P > 0.05$ .

de MLKL devrait être poursuivie, puisque ce site est associé à l'inclusion de huit acides aminés en phase dans la protéine MLKL. D'ailleurs, la régulation de l'activité par épissage alternatif de MLKL et de RIPK1 a déjà été démontrée (Arnež *et al.*, 2016; Yang *et al.*, 2005). De plus, il a été aussi démontré que certaines protéines impliquées dans le métabolisme des ARN était requises pour maintenir les niveaux protéiques de RIPK1 via son épissage alternatif (Callow *et al.*, 2018). Afin de déterminer l'impact des déplétions d'EFTUD2 et de SNRNP200 dans la nécroptose, il serait pertinent de remonter la cascade de signalisation (Introduction, Figure 1) et valider l'activation de chacune des protéines impliquées. Par exemple, il serait de mise de vérifier si RIPK3 et RIPK1 sont phosphorylées, marquant leur activation, et raffinant notre compréhension de l'endroit dans la cascade où EFTUD2 et SNRNP200 ont un effet (Galluzzi *et al.*, 2018). Il serait aussi possible de mener des expériences en surexprimant RIPK1, RIPK3 et MLKL, et valider si cette surexpression est

suffisante pour resensibiliser les cellules déplétées en EFTUD2 et SNRNP200 à la nécroptose. Finalement, un autre aspect à poursuivre serait de continuer à tester la capacité de la déplétion d'EFTUD2 et de SNRNP200 à protéger de la mort provenant de nouveaux stimuli apoptotiques et nécroptotiques. Par exemple, le virus Sendai élicite de la nécroptose médiée par la voie de l'interféron dans les cellules L929 lorsque les cellules infectées sont cultivées en présence de zVAD-fmk, un inhibiteur des caspases (Schock *et al.*, 2017). Nous avons déjà effectué des expériences préliminaires avec le virus Sendai qui ont semblé confirmer qu'EFTUD2 est requise pour la nécroptose dans ce contexte, ainsi que l'absence d'effet de la déplétion de SNRNP200. Ces résultats devraient être confirmés ainsi que poursuivis afin de mieux comprendre les mécanismes sous-jacents au rôle d'EFTUD2 et de SNRNP200 dans la nécroptose et l'apoptose.

Une autre piste d'investigation pour comprendre le rôle d'EFTUD2 et de SNRNP200 dans l'apoptose et la nécroptose serait d'investiguer l'impact de la déplétion de ces protéines sur le transcriptome. Par exemple, il existe des données publiques dans les cellules humaines HepG2 et K562 pour la déplétion d'EFTUD2, de PRPF8 et de SNRNP200 (Van Nostrand *et al.*, 2020). Il serait possible d'exploiter ces données pour trouver les impacts d'une réduction d'EFTUD2, de PRPF8 et de SNRNP200 sur le niveau d'ARN ainsi que l'épissage alternatif des protéines impliquées dans l'apoptose ainsi que la nécroptose. Évidemment, cette même expérience mais réalisée dans les L929, telle que suggérée dans la section *Importance d'U5 dans la modulation de l'épissage alternatif par réovirus et  $\mu 2$* , serait encore plus pertinente et permettrait de sonder à haut-débit le transcriptome pour identifier des gènes candidats qui peuvent expliquer le phénotype observé.

Finalement, il est pertinent de conclure sur l'importance de la signalisation du calcium dans la nécroptose (Galluzzi *et al.*, 2018). Par exemple, pour le virus Sendai la nécroptose requière l'activation des CAMKII et la signalisation du  $\text{Ca}^{2+}$  pour phosphoryler RIPK1 (Nomura *et al.*, 2014). Considérant l'interaction directe de  $\mu 2$

avec CAMK2D et CAMK2G, l'impact de  $\mu 2$  sur les niveaux des protéines d'U5, ainsi que les changements d'épissage détecté dans CAMK2D, il est possible que la signalisation du calcium soit impliquée dans le rôle d'EFTUD2 et de SNRNP200 dans la nécroptose, et nécessiterait d'être plus longuement investiguée.

## **CONCLUSION**

En conclusion, mes travaux permettent de mieux apprécier l'importance d'une régulation fine de l'épissage alternatif dans la cellule, ainsi que le bénéfice pour les virus d'induire de vastes perturbations de ce mécanisme durant l'infection. Mes travaux ont permis aussi de mettre de l'avant le rôle crucial du complexe U5 dans la régulation de l'épissage alternatif, et ont aussi identifié des nouveaux rôles des protéines de ce complexe dans l'apoptose, la nécroptose ainsi que dans la réponse antivirale cellulaire. Ces nouveaux rôles suggèrent un bénéfice important pour les virus de cibler le complexe U5 durant l'infection, établissant le complexe U5 comme un acteur important de la défense cellulaire contre les infections virales.

## REMERCIEMENTS

Dans un premier temps, j'aimerais remercier mes évaluateurs d'avoir pris le temps de lire et d'évaluer ma thèse. Merci aux professeurs Michelle Scott et Mannix Auger-Messier d'avoir fait partie de mon comité de mentorat. Vos conseils et votre enthousiasme étaient très appréciés. Merci aussi aux organismes subventionnaires qui ont supporté ce travail à travers des bourses et des subventions.

Dans un deuxième temps, j'aimerais remercier mes directeurs de recherche, les professeurs Martin Bisailon et Guy Lemay, pour leur encadrement exemplaire, leur disponibilité, leur confiance presque aveugle en mes capacités et mon jugement scientifique et leur soutien à travers toutes ces années. Merci à toi Martin pour ta bonne humeur et ton sac toujours rempli d'une nouvelle anecdote à nous raconter. Merci à vous Pr Lemay pour votre immense savoir; ce fut extrêmement agréable de discuter de réovirus et d'avoir votre perception basée sur tellement d'années d'expérience avec ce virus. Ce fut incroyablement enrichissant d'être supervisé par deux générations de chercheurs! J'aimerais aussi remercier l'équipe du laboratoire Perrailon de m'avoir supporté pendant mes études graduées. Un merci particulier à François Bolduc pour les gin'oclock et les nombreuses discussions scientifiques pendant lesquelles nos opinions divergeaient. Merci Chief de m'avoir challengé! Un merci à tous les stagiaires qui ont travaillé avec moi sur ces projets, et particulièrement à Patricia Roy. Merci Pat Patrouille d'être devenue beaucoup plus qu'une stagiaire et d'être encore présente dans ma vie! Finalement, j'aimerais aussi remercier Delphine Lanoie de m'avoir formé et appris la base sur réovirus pendant mon court séjour chez le Pr. Lemay à Montréal. Bien que je n'aie été que deux mois à Montréal, ce séjour a été très marquant, notamment grâce à toi.

Dans un troisième temps, j'aimerais remercier tous les gens qui ont fait de mon passage aux études graduées une période merveilleuse de ma vie. Merci à tous ceux qui se sont impliqués avec moi, que ce soit au RECMUS, à la Journée Phare, au



CERCUDS, etc. Un merci particulier à Hugo, Fanny, Ariane, Jean-Michel et Alexandra qui ont pris une place importante dans ce parcours. Aussi, je me dois de remercier tous les gens du département de biochimie, et aussi du PRAC, pour leur support et leur esprit collaboratif. Finalement, un merci particulier aux professionnels de la plateforme de RNomique (Mathieu Durand, qui a fait du travail colossal pour mes projets, Danny Bergeron, etc.) et de la plateforme de spectrométrie de masse (Dominique Lévesque), d'avoir épaulé mes projets et de m'avoir permis de devenir un meilleur scientifique.

Finalement, j'aimerais terminer en remerciant ma famille de leur support à travers ce parcours. Merci à mes parents, qui ne comprennent clairement pas ce que je fais dans le labo, mais qui sont tellement fiers de moi et de mes accomplissements. Vous avoir rendu fiers est une de mes plus grandes et belles réussites. Merci à mon frère pour son support à travers les années, et merci de suivre mes traces au doctorat. Finalement, un merci spécial à ma copine, Carole-Anne, d'avoir embelli ma vie au cours des deux dernières années. C'est l'heure de mon départ au laboratoire, mais je quitte en sachant que le labo est entre bonnes mains. Je te passe le flambeau et je te souhaite du succès dans tes études graduées!

## LISTE DES RÉFÉRENCES

- Abad, A. T. et Danthi, P. (2022) Early Events in Reovirus Infection Influence Induction of Innate Immune Response. *Journal of Virology*, vol. 96, n°14, p. e00917-22.
- Ajiro, M. et Zheng, Z.-M. (2014) Oncogenes and RNA splicing of human tumor viruses. *Emerging Microbes & Infections*, vol. 3, n°9, p. e63.
- Akusjarvi, G. (2008) Temporal regulation of adenovirus major late alternative RNA splicing. *Frontiers in Bioscience: A Journal and Virtual Library*, vol. 13, p. 5006-5015.
- Alamancos, G. P., Agirre, E. et Eyras, E. (2014) Methods to Study Splicing from High-Throughput RNA Sequencing Data. *In* K. J. Hertel (dir.), *Spliceosomal Pre-mRNA Splicing: Methods and Protocols*, *Methods in Molecular Biology* (p. 357-397). Totowa, NJ : Humana Press.
- Alkassar, M., Gärtner, B., Roemer, K., Graesser, F., Rommelaere, J., Kaestner, L., Haeckel, I. et Graf, N. (2011) The combined effects of oncolytic reovirus plus Newcastle disease virus and reovirus plus parvovirus on U87 and U373 cells in vitro and in vivo. *Journal of Neuro-Oncology*, vol. 104, n°3, p. 715-727.
- Alló, M., Buggiano, V., Fededa, J. P., Petrillo, E., Schor, I., Mata, M. de la, Agirre, E., Plass, M., Eyras, E., Elela, S. A., Klinck, R., Chabot, B. et Kornblihtt, A. R. (2009) Control of alternative splicing through siRNA-mediated transcriptional gene silencing. *Nature Structural & Molecular Biology*, vol. 16, n°7, p. 717-724.
- Anczuków, O., Rosenberg, A. Z., Akerman, M., Das, S., Zhan, L., Karni, R., Muthuswamy, S. K. et Krainer, A. R. (2012) The splicing factor SRSF1 regulates apoptosis and proliferation to promote mammary epithelial cell transformation. *Nature Structural & Molecular Biology*, vol. 19, n°2, p. 220-228.
- Andersen, K. G., Rambaut, A., Lipkin, W. I., Holmes, E. C. et Garry, R. F. (2020) The proximal origin of SARS-CoV-2. *Nature Medicine*, vol. 26, n°4, p. 450-452.
- Annunziata, C., Buonaguro, L., Buonaguro, F. M. et Tornesello, M. L. (2012) Characterization of the Human Papillomavirus (HPV) Integration Sites into Genital Cancers. *Pathology & Oncology Research*, vol. 18, n°4, p. 803-808.
- Aravamudhan, P., Guzman-Cardozo, C., Urbanek, K., Welsh, O. L., Konopka-Anstadt, J. L., Sutherland, D. M. et Dermody, T. S. (2022) The Murine Neuronal

Receptor NgR1 Is Dispensable for Reovirus Pathogenesis. *Journal of Virology*, vol. 96, n°8, p. e0005522.

- Armero, V. E. S., Tremblay, M.-P., Allaire, A., Boudreault, S., Martenon-Brodeur, C., Duval, C., Durand, M., Lapointe, E., Thibault, P., Tremblay-Létourneau, M., Perreault, J.-P., Scott, M. S. et Bisailon, M. (2017) Transcriptome-wide analysis of alternative RNA splicing events in Epstein-Barr virus-associated gastric carcinomas. *PLoS One*, vol. 12, n°5, p. e0176880.
- Arnež, K. H., Kindlova, M., Bokil, N. J., Murphy, J. M., Sweet, M. J. et Gunčar, G. (2016) Analysis of the N-terminal region of human MLKL, as well as two distinct MLKL isoforms, reveals new insights into necroptotic cell death. *Bioscience Reports*, vol. 36, n°1, p. e00291.
- Arnold, M. M., Murray, K. E. et Nibert, M. L. (2008) Formation of the factory matrix is an important, though not a sufficient function of nonstructural protein  $\mu$ NS during reovirus infection. *Virology*, vol. 375, n°2, p. 412-423.
- Arulanandam, R., Batenchuk, C., Varette, O., Zakaria, C., Garcia, V., Forbes, N. E., Davis, C., Krishnan, R., Karmacharya, R., Cox, J., Sinha, A., Babawy, A., Waite, K., Weinstein, E., Falls, T., Chen, A., Hamill, J., Silva, N. D., Conrad, D. P., Atkins, H., Garson, K., Ilkow, C., Kærn, M., Vanderhyden, B., Sonenberg, N., Alain, T., Boeuf, F. L., Bell, J. C. et Diallo, J.-S. (2015) Microtubule disruption synergizes with oncolytic virotherapy by inhibiting interferon translation and potentiating bystander killing. *Nature Communications*, vol. 6, n°1, p. 1-14.
- Ashraf, U., Benoit-Pilven, C., Lacroix, V., Navratil, V. et Naffakh, N. (2019) Advances in Analyzing Virus-Induced Alterations of Host Cell Splicing. *Trends in Microbiology*, vol. 27, n°3, p. 268-281.
- Barnhart, M. D., Moon, S. L., Emch, A. W., Wilusz, C. J. et Wilusz, J. (2013) Changes in cellular mRNA stability, splicing, and polyadenylation through HuR protein sequestration by a cytoplasmic RNA virus. *Cell Reports*, vol. 5, n°4, p. 909-917.
- Barton, E. S., Forrest, J. C., Connolly, J. L., Chappell, J. D., Liu, Y., Schnell, F. J., Nusrat, A., Parkos, C. A. et Dermody, T. S. (2001) Junction adhesion molecule is a receptor for reovirus. *Cell*, vol. 104, n°3, p. 441-451.
- Barton, E. S., Youree, B. E., Ebert, D. H., Forrest, J. C., Connolly, J. L., Valyi-Nagy, T., Washington, K., Wetzel, J. D. et Dermody, T. S. (2003) Utilization of sialic acid as a coreceptor is required for reovirus-induced biliary disease. *The Journal of Clinical Investigation*, vol. 111, n°12, p. 1823-1833.

- Benskey, M. J., Sandoval, I. M., Miller, K., Sellnow, R. L., Gezer, A., Kuhn, N. C., Vashon, R. et Manfredsson, F. P. (2019) Basic Concepts in Viral Vector-Mediated Gene Therapy. *In* F. P. Manfredsson et M. J. Benskey (dir.), *Viral Vectors for Gene Therapy: Methods and Protocols*, *Methods in Molecular Biology* (p. 3-26). New York, NY : Springer.
- Berger, A. K. et Danthi, P. (2013) Reovirus Activates a Caspase-Independent Cell Death Pathway. *mBio*, vol. 4, n°3, p. e00178-13.
- Berger, A. K., Hiller, B. E., Thete, D., Snyder, A. J., Perez, E., Upton, J. W. et Danthi, P. (2017) Viral RNA at Two Stages of Reovirus Infection Is Required for the Induction of Necroptosis. *Journal of Virology*, vol. 91, n°6, p. e02404-16.
- Berget, S. M. (1995) Exon Recognition in Vertebrate Splicing. *Journal of Biological Chemistry*, vol. 270, n°6, p. 2411-2414.
- Berget, S. M., Moore, C. et Sharp, P. A. (1977) Spliced segments at the 5' terminus of adenovirus 2 late mRNA. *Proceedings of the National Academy of Sciences of the United States of America*, vol. 74, n°8, p. 3171-3175.
- Best, S. A., Nwaobasi, A. N., Schmults, C. D. et Ramsey, M. R. (2017) CCAR2 Is Required for Proliferation and Tumor Maintenance in Human Squamous Cell Carcinoma. *Journal of Investigative Dermatology*, vol. 137, n°2, p. 506-512.
- Best, S. M. (2008) Viral Subversion of Apoptotic Enzymes: Escape from Death Row. *Annual review of microbiology*, vol. 62, p. 171-192.
- Beylerveld, G., Chin, D. J., Olmo, E. M. D., Carter, J., Najera, I., Cillóniz, C. et Shaw, M. L. (2018) Nucleolar Relocalization of RBM14 by Influenza A Virus NS1 Protein. *mSphere*, vol. 3, n°6.
- Bhowmick, R., Banik, G., Chanda, S., Chattopadhyay, S. et Chawla-Sarkar, M. (2014) Rotavirus infection induces G1 to S phase transition in MA104 cells via Ca<sup>2+</sup>/Calmodulin pathway. *Virology*, vol. 454-455, p. 270-279.
- Black, D. L. (1995) Finding splice sites within a wilderness of RNA. *RNA*, vol. 1, n°8, p. 763-771.
- Black, D. L. (2003) Mechanisms of alternative pre-messenger RNA splicing. *Annual Review of Biochemistry*, vol. 72, p. 291-336.
- Black, J. G. (2008) *Microbiology : principles and explorations* (7th ed.). J. Wiley & Sons.
- Boise, L. H., González-García, M., Postema, C. E., Ding, L., Lindsten, T., Turka, L. A., Mao, X., Nuñez, G. et Thompson, C. B. (1993) *bcl-x*, a *bcl-2*-related gene

that functions as a dominant regulator of apoptotic cell death. *Cell*, vol. 74, n°4, p. 597-608.

- Borodavka, A., Ault, J., Stockley, P. G. et Tuma, R. (2015) Evidence that avian reovirus  $\sigma$ NS is an RNA chaperone: implications for genome segment assortment. *Nucleic Acids Research*, vol. 43, n°14, p. 7044-7057.
- Boudreault, S., Armero, V. E. S., Scott, M. S., Perreault, J.-P. et Bisaillon, M. (2019) The Epstein-Barr virus EBNA1 protein modulates the alternative splicing of cellular genes. *Virology Journal*, vol. 16, n°1, p. 29.
- Boudreault, S., Durand, M., Martineau, C.-A., Perreault, J.-P., Lemay, G. et Bisaillon, M. (2022) Reovirus  $\mu$ 2 protein modulates host cell alternative splicing by reducing protein levels of U5 snRNP core components. *Nucleic Acids Research*, vol. 50, n°9, p. 5263-5281.
- Boudreault, S., Martenon-Brodeur, C., Caron, M., Garant, J.-M., Tremblay, M.-P., Armero, V. E. S., Durand, M., Lapointe, E., Thibault, P., Tremblay-Létourneau, M., Perreault, J.-P., Scott, M. S., Lemay, G. et Bisaillon, M. (2016) Global Profiling of the Cellular Alternative RNA Splicing Landscape during Virus-Host Interactions. *PLoS One*, vol. 11, n°9, p. e0161914.
- Boudreault, S., Roy, P., Lemay, G. et Bisaillon, M. (2019a) Viral modulation of cellular RNA alternative splicing: A new key player in virus–host interactions? *Wiley Interdisciplinary Reviews: RNA*, vol. 0, n°0, p. e1543.
- Boudreault, S., Roy, P., Lemay, G. et Bisaillon, M. (2019b) Viral modulation of cellular RNA alternative splicing: A new key player in virus–host interactions? *Wiley Interdisciplinary Reviews: RNA*, vol. 10, n°5, p. e1543.
- Boudreault, S., Tremblay, M.-P., Allaire, A., Armero, V. E. S. et Bisaillon, M. (2016) Viral oncoproteins involved in carcinogenesis. *Current Topics in Virology*, vol. 13, p. 18.
- Bourgeois-Daigneault, M.-C., St-Germain, L. E., Roy, D. G., Pelin, A., Aitken, A. S., Arulanandam, R., Falls, T., Garcia, V., Diallo, J.-S. et Bell, J. C. (2016) Combination of Paclitaxel and MG1 oncolytic virus as a successful strategy for breast cancer treatment. *Breast Cancer Research*, vol. 18, n°1, p. 83.
- Bourhill, T., Mori, Y., Rancourt, D. E., Shmulevitz, M. et Johnston, R. N. (2018) Going (Reo)Viral: Factors Promoting Successful Reoviral Oncolytic Infection. *Viruses*, vol. 10, n°8, p. 421.
- Bravo, J. P. K., Bartnik, K., Venditti, L., Acker, J., Gail, E. H., Colyer, A., Davidovich, C., Lamb, D. C., Tuma, R., Calabrese, A. N. et Borodavka, A. (2021) Structural basis of rotavirus RNA chaperone displacement and RNA annealing.

- Proceedings of the National Academy of Sciences of the United States of America, vol. 118, n°41, p. e2100198118.
- Bravo, J. P. K., Borodavka, A., Barth, A., Calabrese, A. N., Mojzes, P., Cockburn, J. J. B., Lamb, D. C. et Tuma, R. (2018) Stability of local secondary structure determines selectivity of viral RNA chaperones. *Nucleic Acids Research*, vol. 46, n°15, p. 7924-7937.
- Bray, N., Pimentel, H., Melsted, P. et Pachter, L. (2015) Near-optimal RNA-Seq quantification. *arXiv:1505.02710 [cs, q-bio]*.
- Brentano, L., Noah, D. L., Brown, E. G. et Sherry, B. (1998) The Reovirus Protein  $\mu 2$ , Encoded by the M1 Gene, Is an RNA-Binding Protein. *Journal of Virology*, vol. 72, n°10, p. 8354-8357.
- Brochu-Lafontaine, V. et Lemay, G. (2012) Addition of exogenous polypeptides on the mammalian reovirus outer capsid using reverse genetics. *Journal of Virological Methods*, vol. 179, n°2, p. 342-350.
- Broering, T. J., Kim, J., Miller, C. L., Piggott, C. D. S., Dinoso, J. B., Nibert, M. L. et Parker, J. S. L. (2004) Reovirus Nonstructural Protein  $\mu$ NS Recruits Viral Core Surface Proteins and Entering Core Particles to Factory-Like Inclusions. *Journal of Virology*, vol. 78, n°4, p. 1882-1892.
- Broering, T. J., Parker, J. S. L., Joyce, P. L., Kim, J. et Nibert, M. L. (2002) Mammalian Reovirus Nonstructural Protein  $\mu$ NS Forms Large Inclusions and Colocalizes with Reovirus Microtubule-Associated Protein  $\mu 2$  in Transfected Cells. *Journal of Virology*, vol. 76, n°16, p. 8285-8297.
- Brosseau, J.-P. (2018) Splicing isoform-specific functional genomic in cancer cells. *Applied Cancer Research*, vol. 38, n°1, p. 18.
- Brosseau, J.-P., Lucier, J.-F., Lamarche, A.-A., Shkreta, L., Gendron, D., Lapointe, E., Thibault, P., Paquet, É., Perreault, J.-P., Elela, S. A. et Chabot, B. (2014) Redirecting splicing with bifunctional oligonucleotides. *Nucleic Acids Research*, vol. 42, n°6, p. e40-e40.
- Brosseau, J.-P., Lucier, J.-F., Lapointe, E., Durand, M., Gendron, D., Gervais-Bird, J., Tremblay, K., Perreault, J.-P. et Elela, S. A. (2010) High-throughput quantification of splicing isoforms. *RNA*, vol. 16, n°2, p. 442-449.
- Brunetti, J. E., Scolaro, L. A. et Castilla, V. (2015) The heterogeneous nuclear ribonucleoprotein K (hnRNP K) is a host factor required for dengue virus and Junín virus multiplication. *Virus Research*, vol. 203, p. 84-91.

- Bryant, H. E., Wadd, S. E., Lamond, A. I., Silverstein, S. J. et Clements, J. B. (2001) Herpes Simplex Virus IE63 (ICP27) Protein Interacts with Spliceosome-Associated Protein 145 and Inhibits Splicing prior to the First Catalytic Step. *Journal of Virology*, vol. 75, n°9, p. 4376-4385.
- Buckley, P. T., Khaladkar, M., Kim, J. et Eberwine, J. (2014) Cytoplasmic intron retention, function, splicing, and the sentinel RNA hypothesis. *Wiley Interdisciplinary Reviews: RNA*, vol. 5, n°2, p. 223-230.
- Budhiraja, S., Liu, H., Couturier, J., Malovannaya, A., Qin, J., Lewis, D. E. et Rice, A. P. (2015) Mining the Human Complexome Database Identifies RBM14 as an XPO1-Associated Protein Involved in HIV-1 Rev Function. *Journal of Virology*, vol. 89, n°7, p. 3557-3567.
- Callow, M. G., Watanabe, C., Wickliffe, K. E., Bainer, R., Kummerfield, S., Weng, J., Cuellar, T., Janakiraman, V., Chen, H., Chih, B., Liang, Y., Haley, B., Newton, K. et Costa, M. R. (2018) CRISPR whole-genome screening identifies new necroptosis regulators and RIPK1 alternative splicing. *Cell Death & Disease*, vol. 9, n°3, p. 1-13.
- Campion, C. A., Soden, D. et Forde, P. F. (2016) Antitumour responses induced by a cell-based Reovirus vaccine in murine lung and melanoma models. *BMC Cancer*, vol. 16.
- Cesana, D., Sgualdino, J., Rudilosso, L., Merella, S., Naldini, L. et Montini, E. (2012) Whole transcriptome characterization of aberrant splicing events induced by lentiviral vector integrations. *The Journal of Clinical Investigation*, vol. 122, n°5, p. 1667-1676.
- Chakrabarty, R., Tran, H., Selvaggi, G., Hagerman, A., Thompson, B. et Coffey, M. (2015) The oncolytic virus, pelareorep, as a novel anticancer agent: a review. *Investigational New Drugs*, vol. 33, n°3, p. 761-774.
- Chang, S. T., Sova, P., Peng, X., Weiss, J., Law, G. L., Palermo, R. E. et Katze, M. G. (2011) Next-Generation Sequencing Reveals HIV-1-Mediated Suppression of T Cell Activation and RNA Processing and Regulation of Noncoding RNA Expression in a CD4+ T Cell Line. *mBio*, vol. 2, n°5, p. e00134-11.
- Chappell, J. D., Protta, A. E., Dermody, T. S. et Stehle, T. (2002) Crystal structure of reovirus attachment protein  $\sigma 1$  reveals evolutionary relationship to adenovirus fiber. *The EMBO Journal*, vol. 21, n°1-2, p. 1-11.
- Chauhan, K., Kalam, H., Dutt, R. et Kumar, D. (2019) RNA Splicing: A New Paradigm in Host-Pathogen Interactions. *Journal of Molecular Biology*, vol. 431, n°8, p. 1565-1575.

- Chellappan, S., Kraus, V. B., Kroger, B., Munger, K., Howley, P. M., Phelps, W. C. et Nevins, J. R. (1992) Adenovirus E1A, simian virus 40 tumor antigen, and human papillomavirus E7 protein share the capacity to disrupt the interaction between transcription factor E2F and the retinoblastoma gene product. *Proceedings of the National Academy of Sciences of the United States of America*, vol. 89, n°10, p. 4549-4553.
- Chen, H., Song, L., Li, G., Chen, W., Zhao, S., Zhou, R., Shi, X., Peng, Z. et Zhao, W. (2017) Human rotavirus strain Wa downregulates NHE1 and NHE6 expressions in rotavirus-infected Caco-2 cells. *Virus Genes*, vol. 53, n°3, p. 367-376.
- Chow, L. T., Gelinas, R. E., Broker, T. R. et Roberts, R. J. (1977) An amazing sequence arrangement at the 5' ends of adenovirus 2 messenger RNA. *Cell*, vol. 12, n°1, p. 1-8.
- Close, P., East, P., Dirac-Svejstrup, A. B., Hartmann, H., Heron, M., Maslen, S., Chariot, A., Söding, J., Skehel, M. et Svejstrup, J. Q. (2012) DBIRD complex integrates alternative mRNA splicing with RNA polymerase II transcript elongation. *Nature*, vol. 484, n°7394, p. 386-389.
- Coffey, M. C., Strong, J. E., Forsyth, P. A. et Lee, P. W. K. (1998) Reovirus Therapy of Tumors with Activated Ras Pathway. *Science*, vol. 282, n°5392, p. 1332-1334.
- Coombs, K. M. (1998) Stoichiometry of Reovirus Structural Proteins in Virus, ISVP, and Core Particles. *Virology*, vol. 243, n°1, p. 218-228.
- Crawford, S. E. et Estes, M. K. (2013) Viroporin-mediated calcium-activated autophagy. *Autophagy*, vol. 9, n°5, p. 797-798.
- Crawford, S. E., Hyser, J. M., Utama, B. et Estes, M. K. (2012) Autophagy hijacked through viroporin-activated calcium/calmodulin-dependent kinase kinase- $\beta$  signaling is required for rotavirus replication. *Proceedings of the National Academy of Sciences*, vol. 109, n°50, p. E3405-E3413.
- Cross, S. T., Michalski, D., Miller, M. R. et Wilusz, J. (2019) RNA regulatory processes in RNA virus biology. *Wiley Interdisciplinary Reviews: RNA*, vol. 10, n°5, p. e1536.
- Danthi, P. (2016) Viruses and the Diversity of Cell Death. *Annual Review of Virology*, vol. 3, n°1, p. 533-553.
- Danthi, P., Guglielmi, K. M., Kirchner, E., Mainou, B., Stehle, T. et Dermody, T. S. (2010) From Touchdown to Transcription: The Reovirus Cell Entry Pathway. *Current topics in microbiology and immunology*, vol. 343, p. 91-119.



- Danthi, P., Holm, G. H., Stehle, T. et Dermody, T. S. (2013) Reovirus receptors, cell entry, and proapoptotic signaling. *Advances in experimental medicine and biology*, vol. 790, p. 42-71.
- David, C. J. et Manley, J. L. (2010) Alternative pre-mRNA splicing regulation in cancer: pathways and programs unhinged. *Genes & Development*, vol. 24, n°21, p. 2343-2364.
- DeAntoneo, C., Danthi, P. et Balachandran, S. (2022) Reovirus Activated Cell Death Pathways. *Cells*, vol. 11, n°11, p. 1757.
- Dechtawewat, T., Songprakhon, P., Limjindaporn, T., Puttikhunt, C., Kasinrerak, W., Saitornuang, S., Yenchitsomanus, P. et Noisakran, S. (2015) Role of human heterogeneous nuclear ribonucleoprotein C1/C2 in dengue virus replication. *Virology Journal*, vol. 12, n°1, p. 14.
- Dermody, T. S., Parker, J. S. et Sherry, B. (2013) Orthoreoviruses. Dans David M. Knipe, Peter Howley (Éds). *Fields virology*. (6th edition.). Philadelphia : Lippincott Williams & Wilkins.
- Desmet, E. A., Anguish, L. J. et Parker, J. S. L. (2014) Virus-Mediated Compartmentalization of the Host Translational Machinery. *mBio*, vol. 5, n°5, p. e01463-14.
- Dhillon, P., Tandra, V. N., Chorghade, S. G., Namsa, N. D., Sahoo, L. et Rao, C. D. (2018) Cytoplasmic Relocalization and Colocalization with Viroplasms of Host Cell Proteins, and Their Role in Rotavirus Infection. *Journal of Virology*, vol. 92, n°15, p. e00612-18.
- Dickson, A. M., Anderson, J. R., Barnhart, M. D., Sokoloski, K. J., Oko, L., Opyrchal, M., Galanis, E., Wilusz, C. J., Morrison, T. E. et Wilusz, J. (2012) Dephosphorylation of HuR Protein during Alphavirus Infection Is Associated with HuR Relocalization to the Cytoplasm. *Journal of Biological Chemistry*, vol. 287, n°43, p. 36229-36238.
- Diez, M., Medina-Muñoz, S. G., Castellano, L. A., da Silva Pescador, G., Wu, Q. et Bazzini, A. A. (2022) iCodon customizes gene expression based on the codon composition. *Scientific Reports*, vol. 12, n°1, p. 12126.
- Dittmar, K. A., Jiang, P., Park, J. W., Amirikian, K., Wan, J., Shen, S., Xing, Y. et Carstens, R. P. (2012) Genome-Wide Determination of a Broad ESRP-Regulated Posttranscriptional Network by High-Throughput Sequencing. *Molecular and Cellular Biology*, vol. 32, n°8, p. 1468-1482.

- Dominski, Z. et Kole, R. (1993) Restoration of correct splicing in thalassemic pre-mRNA by antisense oligonucleotides. *Proceedings of the National Academy of Sciences*, vol. 90, n°18, p. 8673-8677.
- Dörner, A., Xiong, D., Couch, K., Yajima, T. et Knowlton, K. U. (2004) Alternatively Spliced Soluble Coxsackie-adenovirus Receptors Inhibit Coxsackievirus Infection. *Journal of Biological Chemistry*, vol. 279, n°18, p. 18497-18503.
- Dowling, D., Nasr-Esfahani, S., Tan, C. H., O'Brien, K., Howard, J. L., Jans, D. A., Purcell, D. F., Stoltzfus, C. M. et Sonza, S. (2008) HIV-1 infection induces changes in expression of cellular splicing factors that regulate alternative viral splicing and virus production in macrophages. *Retrovirology*, vol. 5, p. 18.
- Eichwald, C., Ackermann, M. et Nibert, M. L. (2018) The dynamics of both filamentous and globular mammalian reovirus viral factories rely on the microtubule network. *Virology*, vol. 518, p. 77-86.
- Eichwald, C., Kim, J. et Nibert, M. L. (2017) Dissection of mammalian orthoreovirus  $\mu 2$  reveals a self-associative domain required for binding to microtubules but not to factory matrix protein  $\mu$ NS. *PLoS One*, vol. 12, n°9, p. e0184356.
- Errington, F., Steele, L., Prestwich, R., Harrington, K. J., Pandha, H. S., Vidal, L., Bono, J. de, Selby, P., Coffey, M., Vile, R. et Melcher, A. (2008) Reovirus Activates Human Dendritic Cells to Promote Innate Antitumor Immunity. *The Journal of Immunology*, vol. 180, n°9, p. 6018-6026.
- Ewer, K. J., Lambe, T., Rollier, C. S., Spencer, A. J., Hill, A. V. et Dorrell, L. (2016) Viral vectors as vaccine platforms: from immunogenicity to impact. *Current Opinion in Immunology, Vaccines \* Special section: Cancer immunology: Genomics & biomarkers*, vol. 41, p. 47-54.
- Eymin, B. (2021) Targeting the spliceosome machinery: A new therapeutic axis in cancer? *Biochemical Pharmacology, RNA Therapeutics*, vol. 189, p. 114039.
- Fabozzi, G., Oler, A. J., Liu, P., Chen, Y., Mindaye, S., Dolan, M. A., Kenney, H., Gucek, M., Zhu, J., Rabin, R. L. et Subbarao, K. (2018) Strand-Specific Dual RNA Sequencing of Bronchial Epithelial Cells Infected with Influenza A/H3N2 Viruses Reveals Splicing of Gene Segment 6 and Novel Host-Virus Interactions. *Journal of Virology*, vol. 92, n°17, p. e00518-18.
- Fang, Z., Martin, J. et Wang, Z. (2012) Statistical methods for identifying differentially expressed genes in RNA-Seq experiments. *Cell & Bioscience*, vol. 2, n°1, p. 26.
- Fensterl, V., Chattopadhyay, S. et Sen, G. C. (2015) No Love Lost Between Viruses and Interferons. *Annual Review of Virology*, vol. 2, n°1, p. 549-572.

- Fensterl, V. et Sen, G. C. (2015) Interferon-Induced Ifit Proteins: Their Role in Viral Pathogenesis. *Journal of Virology*, vol. 89, n°5, p. 2462-2468.
- Fields, B. N., Knipe, D. M. et Howley, P. M. (2013) *Fields virology*. Books@Ovid (6th edition.). Lippincott Williams & Wilkins.
- Flather, D., Nguyen, J. H. C., Semler, B. L. et Gershon, P. D. (2018) Exploitation of nuclear functions by human rhinovirus, a cytoplasmic RNA virus. *PLOS Pathogens*, vol. 14, n°8, p. e1007277.
- Folegatti, P. M., Ewer, K. J., Aley, P. K., Angus, B., Becker, S., Belij-Rammerstorfer, S., Bellamy, D., Bibi, S., Bittaye, M., Clutterbuck, E. A., Dold, C., Faust, S. N., Finn, A., Flaxman, A. L., Hallis, B., Heath, P., Jenkin, D., Lazarus, R., Makinson, R., Minassian, A. M., Pollock, K. M., Ramasamy, M., Robinson, H., Snape, M., Tarrant, R., Voysey, M., Green, C., Douglas, A. D., Hill, A. V. S., Lambe, T., Gilbert, S. C., Pollard, A. J., Aboagye, J., Adams, K., Ali, A., Allen, E., Allison, J. L., Anslow, R., Arbe-Barnes, E. H., Babbage, G., Baillie, K., Baker, M., Baker, N., Baker, P., Baleanu, I., Ballaminut, J., Barnes, E., Barrett, J., Bates, L., Batten, A., Beadon, K., Beckley, R., Berrie, E., Berry, L., Beveridge, A., Bewley, K. R., Bijker, E. M., Bingham, T., Blackwell, L., Blundell, C. L., Bolam, E., Boland, E., Borthwick, N., Bower, T., Boyd, A., Brenner, T., Bright, P. D., Brown-O'Sullivan, C., Brunt, E., Burbage, J., Burge, S., Buttigieg, K. R., Byard, N., Cabera Puig, I., Calvert, A., Camara, S., Cao, M., Cappuccini, F., Carr, M., Carroll, M. W., Carter, V., Cathie, K., Challis, R. J., Charlton, S., Chelysheva, I., Cho, J.-S., Cicconi, P., Cifuentes, L., Clark, H., Clark, E., Cole, T., Colin-Jones, R., Conlon, C. P., Cook, A., Coombes, N. S., Cooper, R., Cosgrove, C. A., Coy, K., Crocker, W. E. M., Cunningham, C. J., Damratoski, B. E., Dando, L., Dattoo, M. S., Davies, H., De Graaf, H., Demissie, T., Di Maso, C., Dietrich, I., Dong, T., Donnellan, F. R., Douglas, N., Downing, C., Drake, J., Drake-Brockman, R., Drury, R. E., Dunachie, S. J., Edwards, N. J., Edwards, F. D. L., Edwards, C. J., Elias, S. C., Elmore, M. J., Emary, K. R. W., English, M. R., Fagerbrink, S., Felle, S., Feng, S., Field, S., Fixmer, C., Fletcher, C., Ford, K. J., Fowler, J., Fox, P., Francis, E., Frater, J., Furze, J., Fuskova, M., Galiza, E., Gbesemete, D., Gilbride, C., Godwin, K., Gorini, G., Goulston, L., Grabau, C., Gracie, L., Gray, Z., Guthrie, L. B., Hackett, M., Halwe, S., Hamilton, E., Hamlyn, J., Hanumunthadu, B., Harding, I., Harris, S. A., Harris, A., Harrison, D., Harrison, C., Hart, T. C., Haskell, L., Hawkins, S., Head, I., Henry, J. A., Hill, J., Hodgson, S. H. C., Hou, M. M., Howe, E., Howell, N., Hutlin, C., Ikram, S., Isitt, C., Iveson, P., Jackson, S., Jackson, F., James, S. W., Jenkins, M., Jones, E., Jones, K., Jones, C. E., Jones, B., Kailath, R., Karampatsas, K., Keen, J., Kelly, S., Kelly, D., Kerr, D., Kerridge, S., Khan, L., Khan, U., Killen, A., Kinch, J., King, T. B., King, L., King, J., Kingham-Page, L., Klenerman, P., Knapper, F., Knight, J. C., Knott, D., Koleva, S., Kupke, A., Larkworthy, C. W., Larwood, J. P. J., Laskey, A., Lawrie, A. M., Lee, A., Ngan Lee, K. Y., Lees, E. A., Legge, H., Lelliott, A., Lemm, N.-M., Lias, A. M., Linder,

A., Lipworth, S., Liu, X., Liu, S., Lopez Ramon, R., Lwin, M., Mabesa, F., Madhavan, M., Mallett, G., Mansatta, K., Marcal, I., Marinou, S., Marlow, E., Marshall, J. L., Martin, J., McEwan, J., McInroy, L., Meddaugh, G., Mentzer, A. J., Mirtorabi, N., Moore, M., Moran, E., Morey, E., Morgan, V., Morris, S. J., Morrison, H., Morshead, G., Morter, R., Mujadidi, Y. F., Muller, J., Munera-Huertas, T., Munro, C., Munro, A., Murphy, S., Munster, V. J., Mweu, P., Noé, A., Nugent, F. L., Nuthall, E., O'Brien, K., O'Connor, D., Oguti, B., Oliver, J. L., Oliveira, C., O'Reilly, P. J., Osborn, M., Osborne, P., Owen, C., Owens, D., Owino, N., Pacurar, M., Parker, K., Parracho, H., Patrick-Smith, M., Payne, V., Pearce, J., Peng, Y., Peralta Alvarez, M. P., Perring, J., Pfafferott, K., Pipini, D., Plested, E., Pluess-Hall, H., Pollock, K., Poulton, I., Presland, L., Provstgaard-Morys, S., Pulido, D., Radia, K., Ramos Lopez, F., Rand, J., Ratcliffe, H., Rawlinson, T., Rhead, S., Riddell, A., Ritchie, A. J., Roberts, H., Robson, J., Roche, S., Rohde, C., Rollier, C. S., Romani, R., Rudiansyah, I., Saich, S., Sajjad, S., Salvador, S., Sanchez Riera, L., Sanders, H., Sanders, K., Sapaun, S., Sayce, C., Schofield, E., Screatton, G., Selby, B., Semple, C., Sharpe, H. R., Shaik, I., Shea, A., Shelton, H., Silk, S., Silva-Reyes, L., Skelly, D. T., Smeeth, H., Smith, C. C., Smith, D. J., Song, R., Spencer, A. J., Stafford, E., Steele, A., Stefanova, E., Stockdale, L., Szigeti, A., Tahiri-Alaoui, A., Tait, M., Talbot, H., Tanner, R., Taylor, I. J., Taylor, V., Te Water Naude, R., Thakur, N., Themistocleous, Y., Themistocleous, A., Thomas, M., Thomas, T. M., Thompson, A., Thomson-Hill, S., Tomlins, J., Tonks, S., Towner, J., Tran, N., Tree, J. A., Truby, A., Turkentine, K., Turner, C., Turner, N., Turner, S., Tuthill, T., Ulaszewska, M., Varughese, R., Van Doremalen, N., Veighey, K., Verheul, M. K., Vichos, I., Vitale, E., Walker, L., Watson, M. E. E., Welham, B., Wheat, J., White, C., White, R., Worth, A. T., Wright, D., Wright, S., Yao, X. L. et Yau, Y. (2020) Safety and immunogenicity of the ChAdOx1 nCoV-19 vaccine against SARS-CoV-2: a preliminary report of a phase 1/2, single-blind, randomised controlled trial. *The Lancet*, vol. 396, n°10249, p. 467-478.

Friedrich, S., Schmidt, T., Geissler, R., Lilie, H., Chabierski, S., Ulbert, S., Liebert, U. G., Golbik, R. P. et Behrens, S.-E. (2014) AUF1 p45 Promotes West Nile Virus Replication by an RNA Chaperone Activity That Supports Cyclization of the Viral Genome. *Journal of Virology*, vol. 88, n°19, p. 11586-11599.

Fukuhara, T., Hosoya, T., Shimizu, S., Sumi, K., Oshiro, T., Yoshinaka, Y., Suzuki, M., Yamamoto, N., Herzenberg, Leonore A., Herzenberg, Leonard A. et Hagiwara, M. (2006) Utilization of host SR protein kinases and RNA-splicing machinery during viral replication. *Proceedings of the National Academy of Sciences*, vol. 103, n°30, p. 11329-11333.

Galganski, L., Urbanek, M. O. et Krzyzosiak, W. J. (2017) Nuclear speckles: molecular organization, biological function and role in disease. *Nucleic Acids Research*, vol. 45, n°18, p. 10350-10368.

Galluzzi, L., Vitale, I., Aaronson, S. A., Abrams, J. M., Adam, D., Agostinis, P., Alnemri, E. S., Altucci, L., Amelio, I., Andrews, D. W., Annicchiarico-Petruzzelli, M., Antonov, A. V., Arama, E., Baehrecke, E. H., Barlev, N. A., Bazan, N. G., Bernassola, F., Bertrand, M. J. M., Bianchi, K., Blagosklonny, M. V., Blomgren, K., Borner, C., Boya, P., Brenner, C., Campanella, M., Candi, E., Carmona-Gutierrez, D., Cecconi, F., Chan, F. K.-M., Chandel, N. S., Cheng, E. H., Chipuk, J. E., Cidlowski, J. A., Ciechanover, A., Cohen, G. M., Conrad, M., Cubillos-Ruiz, J. R., Czabotar, P. E., D'Angiolella, V., Dawson, T. M., Dawson, V. L., De Laurenzi, V., De Maria, R., Debatin, K.-M., DeBerardinis, R. J., Deshmukh, M., Di Daniele, N., Di Virgilio, F., Dixit, V. M., Dixon, S. J., Duckett, C. S., Dynlacht, B. D., El-Deiry, W. S., Elrod, J. W., Fimia, G. M., Fulda, S., García-Sáez, A. J., Garg, A. D., Garrido, C., Gavathiotis, E., Golstein, P., Gottlieb, E., Green, D. R., Greene, L. A., Gronemeyer, H., Gross, A., Hajnoczky, G., Hardwick, J. M., Harris, I. S., Hengartner, M. O., Hetz, C., Ichijo, H., Jäättelä, M., Joseph, B., Jost, P. J., Juin, P. P., Kaiser, W. J., Karin, M., Kaufmann, T., Kepp, O., Kimchi, A., Kitsis, R. N., Klionsky, D. J., Knight, R. A., Kumar, S., Lee, S. W., Lemasters, J. J., Levine, B., Linkermann, A., Lipton, S. A., Lockshin, R. A., López-Otín, C., Lowe, S. W., Luedde, T., Lugli, E., MacFarlane, M., Madeo, F., Malewicz, M., Malorni, W., Manic, G., Marine, J.-C., Martin, S. J., Martinou, J.-C., Medema, J. P., Mehlen, P., Meier, P., Melino, S., Miao, E. A., Molkenkin, J. D., Moll, U. M., Muñoz-Pinedo, C., Nagata, S., Nuñez, G., Oberst, A., Oren, M., Overholtzer, M., Pagano, M., Panaretakis, T., Pasparakis, M., Penninger, J. M., Pereira, D. M., Pervaiz, S., Peter, M. E., Piacentini, M., Pinton, P., Prehn, J. H. M., Puthalakath, H., Rabinovich, G. A., Rehm, M., Rizzuto, R., Rodrigues, C. M. P., Rubinsztein, D. C., Rudel, T., Ryan, K. M., Sayan, E., Scorrano, L., Shao, F., Shi, Y., Silke, J., Simon, H.-U., Sistigu, A., Stockwell, B. R., Strasser, A., Szabadkai, G., Tait, S. W. G., Tang, D., Tavernarakis, N., Thorburn, A., Tsujimoto, Y., Turk, B., Vanden Berghe, T., Vandenabeele, P., Vander Heiden, M. G., Villunger, A., Virgin, H. W., Vousden, K. H., Vucic, D., Wagner, E. F., Walczak, H., Wallach, D., Wang, Y., Wells, J. A., Wood, W., Yuan, J., Zakeri, Z., Zhivotovsky, B., Zitvogel, L., Melino, G. et Kroemer, G. (2018) Molecular mechanisms of cell death: recommendations of the Nomenclature Committee on Cell Death 2018. *Cell Death & Differentiation*, vol. 25, n°3, p. 486-541.

Gao, C., Zhai, J., Dang, S. et Zheng, S. (2018) Analysis of alternative splicing in chicken embryo fibroblasts in response to reticuloendotheliosis virus infection. *Avian Pathology*, vol. 47, n°6, p. 585-594.

Garcia-Blanco, M. A. (2006) Alternative splicing: therapeutic target and tool. *Progress in Molecular and Subcellular Biology*, vol. 44, p. 47-64.

Garrett, R. H., Grisham, C. M., Andreopoulos, S., Willmore, W. G. et Gallouzi, I. E. (2013) *Biochemistry*, 1st Canadian Edition (Nelson Education.). Toronto, ON, Canada.

- Gay, E. et Babajko, S. (2000) AUUUA Sequences Compromise Human Insulin-like Growth Factor Binding Protein-1 mRNA Stability. *Biochemical and Biophysical Research Communications*, vol. 267, n°2, p. 509-515.
- Gomatos, P. J. (1967) RNA synthesis in reovirus-infected L929 mouse fibroblasts. *Proceedings of the National Academy of Sciences of the United States of America*, vol. 58, n°4, p. 1798-1805.
- Gong, J. et Mita, M. M. (2014) Activated Ras signaling pathways and reovirus oncolysis: an update on the mechanism of preferential reovirus replication in cancer cells. *Molecular and Cellular Oncology*, vol. 4, p. 167.
- Gong, J., Sachdev, E., Mita, A. C. et Mita, M. M. (2016) Clinical development of reovirus for cancer therapy: An oncolytic virus with immune-mediated antitumor activity. *World Journal of Methodology*, vol. 6, n°1, p. 25.
- Gonzalez, S. L., Stremlau, M., He, X., Basile, J. R. et Münger, K. (2001) Degradation of the Retinoblastoma Tumor Suppressor by the Human Papillomavirus Type 16 E7 Oncoprotein Is Important for Functional Inactivation and Is Separable from Proteasomal Degradation of E7. *Journal of Virology*, vol. 75, n°16, p. 7583-7591.
- Gujar, S. A., Clements, D., Dielschneider, R., Helson, E., Marcato, P. et Lee, P. W. K. (2014) Gemcitabine enhances the efficacy of reovirus-based oncotherapy through anti-tumour immunological mechanisms. *British Journal of Cancer*, vol. 110, n°1, p. 83-93.
- Gujar, S. A., Marcato, P., Pan, D. et Lee, P. W. K. (2010) Reovirus Virotherapy Overrides Tumor Antigen Presentation Evasion and Promotes Protective Antitumor Immunity. *Molecular Cancer Therapeutics*, vol. 9, n°11, p. 2924-2933.
- Gujar, S. A., Pan, D., Marcato, P., Garant, K. A. et Lee, P. W. (2011) Oncolytic Virus-initiated Protective Immunity Against Prostate Cancer. *Molecular Therapy*, vol. 19, n°4, p. 797.
- Gujar, S., Dielschneider, R., Clements, D., Helson, E., Shmulevitz, M., Marcato, P., Pan, D., Pan, L., Ahn, D.-G., Alawadhi, A. et Lee, P. W. (2013) Multifaceted Therapeutic Targeting of Ovarian Peritoneal Carcinomatosis Through Virus-induced Immunomodulation. *Molecular Therapy*, vol. 21, n°2, p. 338.
- Hamano, S., Mori, Y., Aoyama, M., Kataoka, H., Tanaka, M., Ebi, M., Kubota, E., Mizoshita, T., Tanida, S., Johnston, R. N., Asai, K. et Joh, T. (2015) Oncolytic reovirus combined with trastuzumab enhances antitumor efficacy through TRAIL signaling in human HER2-positive gastric cancer cells. *Cancer Letters*, vol. 356, n°2 Pt B, p. 846-854.

- Han, L., Xin, X., Wang, H., Li, J., Hao, Y., Wang, M., Zheng, C. et Shen, C. (2018) Cellular response to persistent foot-and-mouth disease virus infection is linked to specific types of alterations in the host cell transcriptome. *Scientific Reports*, vol. 8, n°1, p. 5074.
- Hanahan, D. et Weinberg, R. A. (2011) Hallmarks of Cancer: The Next Generation. *Cell*, vol. 144, n°5, p. 646-674.
- Hardy, M. P. et O'Neill, L. A. J. (2004) The Murine Irak2 Gene Encodes Four Alternatively Spliced Isoforms, Two of Which Are Inhibitory. *Journal of Biological Chemistry*, vol. 279, n°26, p. 27699-27708.
- Hardy, W. R. et Sandri-Goldin, R. M. (1994) Herpes simplex virus inhibits host cell splicing, and regulatory protein ICP27 is required for this effect. *Journal of Virology*, vol. 68, n°12, p. 7790-7799.
- Hernandez-Lopez, H. R. et Graham, S. V. (2012) Alternative splicing in human tumour viruses: a therapeutic target? *Biochemical Journal*, vol. 445, n°2, p. 145-156.
- Hirose, T., Yamazaki, T. et Nakagawa, S. (2019) Molecular anatomy of the architectural NEAT1 noncoding RNA: The domains, interactors, and biogenesis pathway required to build phase-separated nuclear paraspeckles. *Wiley Interdisciplinary Reviews: RNA*, vol. 10, n°6, p. e1545.
- Homa, N. J., Salinas, R., Forte, E., Robinson, T. J., Garcia-Blanco, M. A. et Luftig, M. A. (2013) Epstein-Barr Virus Induces Global Changes in Cellular mRNA Isoform Usage That Are Important for the Maintenance of Latency. *Journal of Virology*, vol. 87, n°22, p. 12291-12301.
- Honda, K. et Taniguchi, T. (2006) IRFs: master regulators of signalling by Toll-like receptors and cytosolic pattern-recognition receptors. *Nature Reviews Immunology*, vol. 6, n°9, p. 644-658.
- Hsu, T. Y.-T., Simon, L. M., Neill, N. J., Marcotte, R., Sayad, A., Bland, C. S., Echeverria, G. V., Sun, T., Kurley, S. J., Tyagi, S., Karlin, K. L., Dominguez-Vidaña, R., Hartman, J. D., Renwick, A., Scorsone, K., Bernardi, R. J., Skinner, S. O., Jain, A., Orellana, M., Lagisetti, C., Golding, I., Jung, S. Y., Neilson, J. R., Zhang, X. H.-F., Cooper, T. A., Webb, T. R., Neel, B. G., Shaw, C. A. et Westbrook, T. F. (2015) The spliceosome is a therapeutic vulnerability in MYC-driven cancer. *Nature*, vol. 525, n°7569, p. 384-388.
- Hu, B., Huo, Y., Yang, L., Chen, G., Luo, M., Yang, J. et Zhou, J. (2017) ZIKV infection effects changes in gene splicing, isoform composition and lncRNA expression in human neural progenitor cells. *Virology Journal*, vol. 14, p. 217.

- Hu, B., Li, X., Huo, Y., Yu, Y., Zhang, Q., Chen, G., Zhang, Y., Fraser, N. W., Wu, D. et Zhou, J. (2016) Cellular responses to HSV-1 infection are linked to specific types of alterations in the host transcriptome. *Scientific Reports*, vol. 6, p. 28075.
- Huang, T., Nilsson, C. E., Punga, T. et Akusjärvi, G. (2002) Functional inactivation of the SR family of splicing factors during a vaccinia virus infection. *EMBO reports*, vol. 3, n°11, p. 1088-1093.
- Huang, W.-R., Li, J.-Y., Liao, T.-L., Yeh, C.-M., Wang, C.-Y., Wen, H.-W., Hu, N.-J., Wu, Y.-Y., Hsu, C.-Y., Chang, Y.-K., Chang, C.-D., Nielsen, B. L. et Liu, H.-J. (2022) Molecular chaperone TRiC governs avian reovirus replication by protecting outer-capsid protein  $\sigma$ C and inner core protein  $\sigma$ A and non-structural protein  $\sigma$ NS from ubiquitin- proteasome degradation. *Veterinary Microbiology*, vol. 264, p. 109277.
- Huh, K., Zhou, X., Hayakawa, H., Cho, J.-Y., Libermann, T. A., Jin, J., Harper, J. W. et Munger, K. (2007) Human Papillomavirus Type 16 E7 Oncoprotein Associates with the Cullin 2 Ubiquitin Ligase Complex, Which Contributes to Degradation of the Retinoblastoma Tumor Suppressor. *Journal of Virology*, vol. 81, n°18, p. 9737-9747.
- Huibregtse, J. M., Scheffner, M. et Howley, P. M. (1991) A cellular protein mediates association of p53 with the E6 oncoprotein of human papillomavirus types 16 or 18. *The EMBO Journal*, vol. 10, n°13, p. 4129-4135.
- Ilkow, C. S., Marguerie, M., Batenchuk, C., Mayer, J., Ben Neriah, D., Cousineau, S., Falls, T., Jennings, V. A., Boileau, M., Bellamy, D., Bastin, D., de Souza, C. T., Alkayyal, A., Zhang, J., Le Boeuf, F., Arulanandam, R., Stubbert, L., Sampath, P., Thorne, S. H., Paramanathan, P., Chatterjee, A., Strieter, R. M., Burdick, M., Addison, C. L., Stojdl, D. F., Atkins, H. L., Auer, R. C., Diallo, J.-S., Lichty, B. D. et Bell, J. C. (2015) Reciprocal cellular cross-talk within the tumor microenvironment promotes oncolytic virus activity. *Nature Medicine*, vol. 21, n°5, p. 530-536.
- Imbeault, M., Giguère, K., Ouellet, M. et Tremblay, M. J. (2012) Exon Level Transcriptomic Profiling of HIV-1-Infected CD4+ T Cells Reveals Virus-Induced Genes and Host Environment Favorable for Viral Replication. *PLOS Pathogens*, vol. 8, n°8, p. e1002861.
- Irvin, S. C., Zurney, J., Ooms, L. S., Chappell, J. D., Dermody, T. S. et Sherry, B. (2012) A Single-Amino-Acid Polymorphism in Reovirus Protein  $\mu$ 2 Determines Repression of Interferon Signaling and Modulates Myocarditis. *Journal of Virology*, vol. 86, n°4, p. 2302-2311.



- Ivanovic, T., Agosto, M. A., Chandran, K. et Nibert, M. L. (2007) A Role for Molecular Chaperone Hsc70 in Reovirus Outer Capsid Disassembly\*. *Journal of Biological Chemistry*, vol. 282, n°16, p. 12210-12219.
- Jagdeo, J. M., Dufour, A., Fung, G., Luo, H., Kleifeld, O., Overall, C. M. et Jan, E. (2015) Heterogeneous Nuclear Ribonucleoprotein M Facilitates Enterovirus Infection. *Journal of Virology*, vol. 89, n°14, p. 7064-7078.
- Jin, M., Liu, C., Han, W. et Cong, Y. (2019) TRiC/CCT Chaperonin: Structure and Function. *In* J. R. Harris et J. Marles-Wright (dir.), *Macromolecular Protein Complexes II: Structure and Function, Subcellular Biochemistry* (p. 625-654). Cham : Springer International Publishing.
- Johansson, C. et Schwartz, S. (2013) Regulation of human papillomavirus gene expression by splicing and polyadenylation. *Nature Reviews Microbiology*, vol. 11, n°4, p. 239-251.
- Jumper, J., Evans, R., Pritzel, A., Green, T., Figurnov, M., Ronneberger, O., Tunyasuvunakool, K., Bates, R., Žídek, A., Potapenko, A., Bridgland, A., Meyer, C., Kohl, S. A. A., Ballard, A. J., Cowie, A., Romera-Paredes, B., Nikolov, S., Jain, R., Adler, J., Back, T., Petersen, S., Reiman, D., Clancy, E., Zielinski, M., Steinegger, M., Pacholska, M., Berghammer, T., Bodenstein, S., Silver, D., Vinyals, O., Senior, A. W., Kavukcuoglu, K., Kohli, P. et Hassabis, D. (2021) Highly accurate protein structure prediction with AlphaFold. *Nature*, vol. 596, n°7873, p. 583-589.
- Kamta, J., Chaar, M., Ande, A., Altomare, D. A. et Ait-Oudhia, S. (2017) Advancing Cancer Therapy with Present and Emerging Immuno-Oncology Approaches. *Frontiers in Oncology*, vol. 7.
- Kanopka, A., Mühlemann, O., Petersen-Mahrt, S., Estmer, C., Öhrmalm, C. et Akusjärvi, G. (1998) Regulation of adenovirus alternative RNA splicing by dephosphorylation of SR proteins. *Nature*, vol. 393, n°6681, p. 185-187.
- Katz, Y., Wang, E. T., Airolidi, E. M. et Burge, C. B. (2010) Analysis and design of RNA sequencing experiments for identifying isoform regulation. *Nature Methods*, vol. 7, n°12, p. 1009-1015.
- Kelly, E. et Russell, S. J. (2007) History of Oncolytic Viruses: Genesis to Genetic Engineering. *Molecular Therapy*, vol. 15, n°4, p. 651-659.
- Keren, H., Lev-Maor, G. et Ast, G. (2010) Alternative splicing and evolution: diversification, exon definition and function. *Nature Reviews Genetics*, vol. 11, n°5, p. 345-355.

- Kim, E., Goren, A. et Ast, G. (2008) Alternative splicing: current perspectives. *BioEssays*, vol. 30, n°1, p. 38-47.
- Kim, J., Parker, J. S. L., Murray, K. E. et Nibert, M. L. (2004) Nucleoside and RNA Triphosphatase Activities of Orthoreovirus Transcriptase Cofactor  $\mu 2$ . *Journal of Biological Chemistry*, vol. 279, n°6, p. 4394-4403.
- Kim, M., Garant, K. A., Nieden, N. I. zur, Alain, T., Loken, S. D., Urbanski, S. J., Forsyth, P. A., Rancourt, D. E., Lee, P. W. K. et Johnston, R. N. (2011) Attenuated reovirus displays oncolysis with reduced host toxicity. *British Journal of Cancer*, vol. 104, n°2, p. 290-299.
- Klinck, R., Bramard, A., Inkel, L., Dufresne-Martin, G., Gervais-Bird, J., Madden, R., Paquet, É. R., Koh, C., Venables, J. P., Prinos, P., Jilaveanu-Pelms, M., Wellinger, R., Rancourt, C., Chabot, B. et Elela, S. A. (2008) Multiple Alternative Splicing Markers for Ovarian Cancer. *Cancer Research*, vol. 68, n°3, p. 657-663.
- Klymenko, T., Hernandez-Lopez, H., MacDonald, A. I., Bodily, J. M. et Graham, S. V. (2016) Human Papillomavirus E2 Regulates SRSF3 (SRp20) To Promote Capsid Protein Expression in Infected Differentiated Keratinocytes. *Journal of Virology*, vol. 90, n°10, p. 5047-5058.
- Knowlton, J. J., Castro, I. F. de, Ashbrook, A. W., Gestaut, D. R., Zamora, P. F., Bauer, J. A., Forrest, J. C., Frydman, J., Risco, C. et Dermody, T. S. (2018) The TRiC chaperonin controls reovirus replication through outer-capsid folding. *Nature Microbiology*, vol. 3, n°4, p. 481-493.
- Knowlton, J. J., Gestaut, D., Ma, B., Taylor, G., Seven, A. B., Leitner, A., Wilson, G. J., Shanker, S., Yates, N. A., Prasad, B. V. V., Aebersold, R., Chiu, W., Frydman, J. et Dermody, T. S. (2021) Structural and functional dissection of reovirus capsid folding and assembly by the prefoldin-TRiC/CCT chaperone network. *Proceedings of the National Academy of Sciences*, vol. 118, n°11, p. e2018127118.
- Kobayashi, T., Chappell, J. D., Danthi, P. et Dermody, T. S. (2006) Gene-Specific Inhibition of Reovirus Replication by RNA Interference. *Journal of Virology*, vol. 80, n°18, p. 9053-9063.
- Kobayashi, T., Ooms, L. S., Chappell, J. D. et Dermody, T. S. (2009) Identification of Functional Domains in Reovirus Replication Proteins  $\mu$ NS and  $\mu 2$ . *Journal of Virology*, vol. 83, n°7, p. 2892-2906.
- Koehler, H., Cotsmire, S., Langeland, J., Kibler, K. V., Kalman, D., Upton, J. W., Mocarski, E. S. et Jacobs, B. L. (2017) Inhibition of DAI-dependent necroptosis by the Z-DNA binding domain of the vaccinia virus innate immune

- evasion protein, E3. *Proceedings of the National Academy of Sciences*, vol. 114, n°43, p. 11506-11511.
- Koehler, H., Cotsmire, S., Zhang, T., Balachandran, S., Upton, J. W., Llangland, J., Kalman, D., Jacobs, B. L. et Mocarski, E. S. (2021) Vaccinia virus E3 prevents sensing of Z-RNA to block ZBP1-dependent necroptosis. *Cell Host & Microbe*, vol. 29, n°8, p. 1266- 1276.e5.
- Kohl, C. et Kurth, A. (2015) Bat Reoviruses. *Bats and Viruses* (p. 203-215). John Wiley & Sons, Ltd.
- Kole, R., Krainer, A. R. et Altman, S. (2012) RNA therapeutics: beyond RNA interference and antisense oligonucleotides. *Nature Reviews Drug Discovery*, vol. 11, n°2, p. 125-140.
- Konopka-Anstadt, J. L., Mainou, B. A., Sutherland, D. M., Sekine, Y., Strittmatter, S. M. et Dermody, T. S. (2014) The Nogo receptor NgR1 mediates infection by mammalian reovirus. *Cell Host & Microbe*, vol. 15, n°6, p. 681-691.
- Ku, C.-C., Che, X.-B., Reichelt, M., Rajamani, J., Schaap-Nutt, A., Huang, K.-J., Sommer, M. H., Chen, Y.-S., Chen, Y.-Y. et Arvin, A. M. (2011) Herpes simplex virus-1 induces expression of a novel MxA isoform that enhances viral replication. *Immunology and Cell Biology*, vol. 89, n°2, p. 173-182.
- Kuo, R.-L., Li, Z.-H., Li, L.-H., Lee, K.-M., Tam, E.-H., Liu, H. M., Liu, H.-P., Shih, S.-R. et Wu, C.-C. (2016) Interactome Analysis of the NS1 Protein Encoded by Influenza A H1N1 Virus Reveals a Positive Regulatory Role of Host Protein PRP19 in Viral Replication. *Journal of Proteome Research*, vol. 15, n°5, p. 1639-1648.
- Kuruppu, D. et Tanabe, K. K. (2005) Viral oncolysis by herpes simplex virus and other viruses. *Cancer Biology & Therapy*, vol. 4, n°5, p. 524-531.
- Kvam, V. M., Liu, P. et Si, Y. (2012) A comparison of statistical methods for detecting differentially expressed genes from RNA-seq data. *American Journal of Botany*, vol. 99, n°2, p. 248-256.
- Labbé, P., Faure, E., Lecointe, S., Le Scouarnec, S., Kyndt, F., Marrec, M., Le Tourneau, T., Offmann, B., Duplaà, C., Zaffran, S., Schott, J. J. et Merot, J. (2017) The alternatively spliced LRRFIP1 Isoform-1 is a key regulator of the Wnt/ $\beta$ -catenin transcription pathway. *Biochimica et Biophysica Acta (BBA) - Molecular Cell Research*, vol. 1864, n°7, p. 1142-1152.
- Laliberté, J.-F. et Zheng, H. (2014) Viral Manipulation of Plant Host Membranes. *Annual Review of Virology*, vol. 1, n°1, p. 237-259.

- Lanoie, D. et Lemay, G. (2018) Multiple proteins differing between laboratory stocks of mammalian orthoreoviruses affect both virus sensitivity to interferon and induction of interferon production during infection. *Virus Research*, vol. 247, p. 40-46.
- Lawrence, P., Schafer, E. A. et Rieder, E. (2012) The nuclear protein Sam68 is cleaved by the FMDV 3C protease redistributing Sam68 to the cytoplasm during FMDV infection of host cells. *Virology*, vol. 425, n°1, p. 40-52.
- Le Boeuf, F., Gebremeskel, S., McMullen, N., He, H., Greenshields, A. L., Hoskin, D. W., Bell, J. C., Johnston, B., Pan, C. et Duncan, R. (2017) Reovirus FAST Protein Enhances Vesicular Stomatitis Virus Oncolytic Virotherapy in Primary and Metastatic Tumor Models. *Molecular Therapy - Oncolytics*, vol. 6, p. 80-89.
- Lee, N., Pimienta, G. et Steitz, J. A. (2012) AUF1/hnRNP D is a novel protein partner of the EBER1 noncoding RNA of Epstein-Barr virus. *RNA*, vol. 18, n°11, p. 2073-2082.
- Lee, N., Yario, T. A., Gao, J. S. et Steitz, J. A. (2016) EBV noncoding RNA EBER2 interacts with host RNA-binding proteins to regulate viral gene expression. *Proceedings of the National Academy of Sciences of the United States of America*, vol. 113, n°12, p. 3221-3226.
- Lee, Y. et Rio, D. C. (2015) Mechanisms and Regulation of Alternative Pre-mRNA Splicing. *Annual Review of Biochemistry*, vol. 84, n°1, p. 291-323.
- Lehoux, M., D'Abramo, C. M. et Archambault, J. (2009) Molecular mechanisms of human papillomavirus-induced carcinogenesis. *Public Health Genomics*, vol. 12, n°5-6, p. 268-280.
- Lemay, G. (1988) Transcriptional and translational events during reovirus infection. *Biochemistry and Cell Biology = Biochimie Et Biologie Cellulaire*, vol. 66, n°8, p. 803-812.
- Lemay, G. (2018) Synthesis and Translation of Viral mRNA in Reovirus-Infected Cells: Progress and Remaining Questions. *Viruses*, vol. 10, n°12, p. 671.
- Leonardi, T. et Leger, A. (2021) Nanopore RNA Sequencing Analysis. *In* E. Picardi (dir.), *RNA Bioinformatics, Methods in Molecular Biology* (p. 569-578). New York, NY : Springer US.
- Lever, R. A. et Whitty, C. J. M. (2016) Ebola virus disease: emergence, outbreak and future directions. *British Medical Bulletin*.

- Li, B. et Dewey, C. N. (2011) RSEM: accurate transcript quantification from RNA-Seq data with or without a reference genome. *BMC Bioinformatics*, vol. 12, n°1, p. 323.
- Li, H., Qiu, J. et Fu, X.-D. (2012) RASL-seq for Massively Parallel and Quantitative Analysis of Gene Expression. *Current Protocols in Molecular Biology*, vol. 98, n°1, p. 4.13.1-4.13.9.
- Li, W., Dai, C., Kang, S. et Zhou, X. J. (2014) Integrative analysis of many RNA-seq datasets to study alternative splicing. *Methods, Systems Biology with Omics Data*, vol. 67, n°3, p. 313-324.
- Liemann, S., Chandran, K., Baker, T. S., Nibert, M. L. et Harrison, S. C. (2002) Structure of the Reovirus Membrane-Penetration Protein,  $\mu 1$ , in a Complex with Its Protector Protein,  $\sigma 3$ . *Cell*, vol. 108, n°2, p. 283-295.
- Lin, W., Zhu, C., Hong, J., Zhao, L., Jilg, N., Fusco, D. N., Schaefer, E. A., Brisac, C., Liu, X., Peng, L. F., Xu, Q. et Chung, R. T. (2015) The spliceosome factor SART1 exerts its anti-HCV action through mRNA splicing. *Journal of Hepatology*, vol. 62, n°5, p. 1024-1032.
- Lindberg, A. et Kreivi, J.-P. (2002) Splicing inhibition at the level of spliceosome assembly in the presence of herpes simplex virus protein ICP27. *Virology*, vol. 294, n°1, p. 189-198.
- Liu, Y.-C., Kuo, R.-L., Lin, J.-Y., Huang, P.-N., Huang, Y., Liu, H., Arnold, J. J., Chen, S.-J., Wang, R. Y.-L., Cameron, C. E. et Shih, S.-R. (2014) Cytoplasmic Viral RNA-Dependent RNA Polymerase Disrupts the Intracellular Splicing Machinery by Entering the Nucleus and Interfering with Prp8. *PLOS Pathogens*, vol. 10, n°6, p. e1004199.
- Mahalingam, D., Wilkinson, G. A., Eng, K. H., Fields, P., Raber, P., Moseley, J. L., Cheetham, K., Coffey, M., Nuovo, G., Kalinski, P., Zhang, B., Arora, S. P. et Fountzilias, C. (2020) Pembrolizumab in Combination with the Oncolytic Virus Pelareorep and Chemotherapy in Patients with Advanced Pancreatic Adenocarcinoma: A Phase Ib Study. *Clinical Cancer Research*, vol. 26, n°1, p. 71-81.
- Maio, F. A. D., Risso, G., Iglesias, N. G., Shah, P., Pozzi, B., Gebhard, L. G., Mammi, P., Mancini, E., Yanovsky, M. J., Andino, R., Krogan, N., Srebrow, A. et Gamarnik, A. V. (2016) The Dengue Virus NS5 Protein Intrudes in the Cellular Spliceosome and Modulates Splicing. *PLoS Pathogens*, vol. 12, n°8, p. e1005841.

- Mandadi, K. K. et Scholthof, K.-B. G. (2015) Genome-Wide Analysis of Alternative Splicing Landscapes Modulated during Plant-Virus Interactions in *Brachypodium distachyon*. *The Plant Cell*, vol. 27, n°1, p. 71-85.
- Marcato, P., Dean, C. A., Giacomantonio, C. A. et Lee, P. W. (2009) Oncolytic Reovirus Effectively Targets Breast Cancer Stem Cells. *Molecular Therapy: the Journal of the American Society of Gene Therapy*, vol. 17, n°6, p. 972.
- Marcato, P., Shmulevitz, M., Pan, D., Stoltz, D. et Lee, P. W. (2007) Ras Transformation Mediates Reovirus Oncolysis by Enhancing Virus Uncoating, Particle Infectivity, and Apoptosis-dependent Release. *Molecular Therapy*, vol. 15, n°8, p. 1522-1530.
- Martin, K., Singh, J., Hill, J. H., Whitham, S. A. et Cannon, S. B. (2016) Dynamic transcriptome profiling of Bean Common Mosaic Virus (BCMV) infection in Common Bean (*Phaseolus vulgaris* L.). *BMC Genomics*, vol. 17, n°1, p. 613.
- Martin, N. T., Roy, D. G., Workenhe, S. T., Wollenberg, D. J. M. van den, Hoeben, R. C., Mossman, K. L., Bell, J. C. et Bourgeois-Daigneault, M.-C. (2019) Pre-surgical neoadjuvant oncolytic virotherapy confers protection against rechallenge in a murine model of breast cancer. *Scientific Reports*, vol. 9, n°1, p. 1-6.
- Mbisa, J. L., Becker, M. M., Zou, S., Dermody, T. S. et Brown, E. G. (2000) Reovirus  $\mu 2$  Protein Determines Strain-Specific Differences in the Rate of Viral Inclusion Formation in L929 Cells. *Virology*, vol. 272, n°1, p. 16-26.
- McPhillips, M. G., Veerapraditsin, T., Cumming, S. A., Karali, D., Milligan, S. G., Boner, W., Morgan, I. M. et Graham, S. V. (2004) SF2/ASF Binds the Human Papillomavirus Type 16 Late RNA Control Element and Is Regulated during Differentiation of Virus-Infected Epithelial Cells. *Journal of Virology*, vol. 78, n°19, p. 10598-10605.
- Merkhofer, E. C., Hu, P. et Johnson, T. L. (2014) Introduction to Cotranscriptional RNA Splicing. *Methods in molecular biology* (Clifton, N.J.), vol. 1126, p. 83-96.
- Mertens, P. (2004) The dsRNA viruses. *Virus Research, Viral molecular machines: Replication systems within the inner cores of dsRNA viruses*, vol. 101, n°1, p. 3-13.
- Mesplède, T., Gagnon, D., Bergeron-Labrecque, F., Azar, I., Sénéchal, H., Coutlée, F. et Archambault, J. (2012) p53 Degradation Activity, Expression, and Subcellular Localization of E6 Proteins from 29 Human Papillomavirus Genotypes. *Journal of Virology*, vol. 86, n°1, p. 94-107.

- Metzker, M. L. (2010) Sequencing technologies — the next generation. *Nature Reviews Genetics*, vol. 11, n°1, p. 31-46.
- Meyer, F. (2016) Chapter Eight - Viral interactions with components of the splicing machinery. *In* M. San Francisco et B. San Francisco (dir.), *Progress in Molecular Biology and Translational Science, Host-Microbe Interactions* (Vol. 142, p. 241-268). Academic Press.
- Miller, C. L., Arnold, M. M., Broering, T. J., Eichwald, C., Kim, J., Dinoso, J. B. et Nibert, M. L. (2007) Virus-derived Platforms for Visualizing Protein Associations inside Cells. *Molecular & Cellular Proteomics*, vol. 6, n°6, p. 1027-1038.
- Miller, C. L., Arnold, M. M., Broering, T. J., Hastings, C. E. et Nibert, M. L. (2010) Localization of Mammalian Orthoreovirus Proteins to Cytoplasmic Factory-Like Structures via Nonoverlapping Regions of  $\mu$ NS. *Journal of Virology*, vol. 84, n°2, p. 867-882.
- Miller, C. L., Parker, J. S. L., Dinoso, J. B., Piggott, C. D. S., Perron, M. J. et Nibert, M. L. (2004) Increased Ubiquitination and Other Covariant Phenotypes Attributed to a Strain- and Temperature-Dependent Defect of Reovirus Core Protein  $\mu$ 2. *Journal of Virology*, vol. 78, n°19, p. 10291-10302.
- Modrek, B. et Lee, C. (2002) A genomic view of alternative splicing. *Nature Genetics*, vol. 30, n°1, p. 13-19.
- Mohamed, A., Clements, D. R., Gujar, S. A., Lee, P. W., Smiley, J. R. et Shmulevitz, M. (2020) Single Amino Acid Differences between Closely Related Reovirus T3D Lab Strains Alter Oncolytic Potency In Vitro and In Vivo. *Journal of Virology*, vol. 94, n°4.
- Mohamed, A., Johnston, R. N. et Shmulevitz, M. (2015) Potential for Improving Potency and Specificity of Reovirus Oncolysis with Next-Generation Reovirus Variants. *Viruses*, vol. 7, n°12, p. 6251-6278.
- Mohamed, A., Konda, P., Eaton, H. E., Gujar, S., Smiley, J. R. et Shmulevitz, M. (2020) Closely related reovirus lab strains induce opposite expression of RIG-I/IFN-dependent versus -independent host genes, via mechanisms of slow replication versus polymorphisms in dsRNA binding  $\sigma$ 3 respectively. *PLOS Pathogens*, vol. 16, n°9, p. e1008803.
- Mohamed, A., Smiley, J. R. et Shmulevitz, M. (2019) Polymorphisms in the most oncolytic reovirus strain confer enhanced cell attachment, transcription and single-step replication kinetics. *Journal of Virology*.

- Moiani, A., Paleari, Y., Sartori, D., Mezzadra, R., Miccio, A., Cattoglio, C., Cocchiarella, F., Lidonnici, M. R., Ferrari, G. et Mavilio, F. (2012) Lentiviral vector integration in the human genome induces alternative splicing and generates aberrant transcripts. *The Journal of Clinical Investigation*, vol. 122, n°5, p. 1653-1666.
- Mole, S., McFarlane, M., Chuen-Im, T., Milligan, S. G., Millan, D. et Graham, S. V. (2009) RNA splicing factors regulated by HPV16 during cervical tumour progression. *The Journal of Pathology*, vol. 219, n°3, p. 383-391.
- Mole, S., Milligan, S. G. et Graham, S. V. (2009) Human Papillomavirus Type 16 E2 Protein Transcriptionally Activates the Promoter of a Key Cellular Splicing Factor, SF2/ASF. *Journal of Virology*, vol. 83, n°1, p. 357-367.
- Morales-Sánchez, A. et Fuentes-Pananá, E. M. (2014) Human Viruses and Cancer. *Viruses*, vol. 6, n°10, p. 4047-4079.
- Morchikh, M., Cribier, A., Raffel, R., Amraoui, S., Cau, J., Severac, D., Dubois, E., Schwartz, O., Bennasser, Y. et Benkirane, M. (2017) HEXIM1 and NEAT1 Long Non-coding RNA Form a Multi-subunit Complex that Regulates DNA-Mediated Innate Immune Response. *Molecular Cell*, vol. 67, n°3, p. 387- 399.e5.
- Moreira, D. et López-García, P. (2009) Ten reasons to exclude viruses from the tree of life. *Nature Reviews Microbiology*, vol. 7, n°4, p. 306-311.
- Mukhopadhyay, U., Patra, U., Chandra, P., Saha, P., Gope, A., Dutta, M. et Chawla-Sarkar, M. (2022) Rotavirus activates MLKL-mediated host cellular necroptosis concomitantly with apoptosis to facilitate dissemination of viral progeny. *Molecular Microbiology*, vol. 117, n°4, p. 818-836.
- Newman, A. J. (1997) The role of U5 snRNP in pre-mRNA splicing. *The EMBO Journal*, vol. 16, n°19, p. 5797-5800.
- Niu, X., Wang, Y., Li, M., Zhang, X. et Wu, Y. (2017) Transcriptome analysis of avian reovirus-mediated changes in gene expression of normal chicken fibroblast DF-1 cells. *BMC Genomics*, vol. 18, n°1, p. 911.
- Noble, S. et Nibert, M. L. (1997) Core protein mu2 is a second determinant of nucleoside triphosphatase activities by reovirus cores. *Journal of Virology*, vol. 71, n°10, p. 7728-7735.
- Nomura, M., Ueno, A., Saga, K., Fukuzawa, M. et Kaneda, Y. (2014) Accumulation of Cytosolic Calcium Induces Necroptotic Cell Death in Human Neuroblastoma. *Cancer Research*, vol. 74, n°4, p. 1056-1066.



- Norman, K. L., Hirasawa, K., Yang, A.-D., Shields, M. A. et Lee, P. W. K. (2004) Reovirus oncolysis: The Ras/RalGEF/p38 pathway dictates host cell permissiveness to reovirus infection. *Proceedings of the National Academy of Sciences*, vol. 101, n°30, p. 11099-11104.
- Ohme-Takagi, M., Taylor, C. B., Newman, T. C. et Green, P. J. (1993) The effect of sequences with high AU content on mRNA stability in tobacco. *Proceedings of the National Academy of Sciences*, vol. 90, n°24, p. 11811-11815.
- Oltean, S. et Bates, D. O. (2014) Hallmarks of alternative splicing in cancer. *Oncogene*, vol. 33, n°46, p. 5311-5318.
- Pan, M., Alvarez-Cabrera, A. L., Kang, J. S., Wang, L., Fan, C. et Zhou, Z. H. (2021) Asymmetric reconstruction of mammalian reovirus reveals interactions among RNA, transcriptional factor  $\mu 2$  and capsid proteins. *Nature Communications*, vol. 12, n°1, p. 4176.
- Pan, Q., Shai, O., Lee, L. J., Frey, B. J. et Blencowe, B. J. (2008) Deep surveying of alternative splicing complexity in the human transcriptome by high-throughput sequencing. *Nature Genetics*, vol. 40, n°12, p. 1413-1415.
- Parker, J. S. L., Broering, T. J., Kim, J., Higgins, D. E. et Nibert, M. L. (2002) Reovirus Core Protein  $\mu 2$  Determines the Filamentous Morphology of Viral Inclusion Bodies by Interacting with and Stabilizing Microtubules. *Journal of Virology*, vol. 76, n°9, p. 4483-4496.
- Parkin, D. M. (2006) The global health burden of infection-associated cancers in the year 2002. *International Journal of Cancer*, vol. 118, n°12, p. 3030-3044.
- Perlmutter, J. D. et Hagan, M. F. (2015) Mechanisms of Virus Assembly. *Annual review of physical chemistry*, vol. 66, p. 217-239.
- Phelan, A., Carmo-Fonseca, M., McLaughlan, J., Lamond, A. I. et Clements, J. B. (1993) A herpes simplex virus type 1 immediate-early gene product, IE63, regulates small nuclear ribonucleoprotein distribution. *Proceedings of the National Academy of Sciences*, vol. 90, n°19, p. 9056-9060.
- Pikor, L. A., Bell, J. C. et Diallo, J.-S. (2015) Oncolytic Viruses: Exploiting Cancer's Deal with the Devil. *Trends in Cancer*, vol. 1, n°4, p. 266-277.
- Pimienta, G., Fok, V., Haslip, M., Nagy, M., Takyar, S. et Steitz, J. A. (2015) Proteomics and Transcriptomics of BJAB Cells Expressing the Epstein-Barr Virus Noncoding RNAs EBER1 and EBER2. *PLoS ONE*, vol. 10, n°6, p. e0124638.

- Prestwich, R. J., Errington, F., Ilett, E. J., Morgan, R. S. M., Scott, K. J., Kottke, T., Thompson, J., Morrison, E. E., Harrington, K. J., Pandha, H. S., Selby, P. J., Vile, R. G. et Melcher, A. A. (2008) Tumor Infection by Oncolytic Reovirus Primes Adaptive Antitumor Immunity. *Clinical Cancer Research*, vol. 14, n°22, p. 7358-7366.
- Prestwich, R. J., Ilett, E. J., Errington, F., Diaz, R. M., Steele, L. P., Kottke, T., Thompson, J., Galivo, F., Harrington, K. J., Pandha, H. S., Selby, P. J., Vile, R. G. et Melcher, A. A. (2009) Immune-Mediated Antitumor Activity of Reovirus Is Required for Therapy and Is Independent of Direct Viral Oncolysis and Replication. *Clinical Cancer Research*, vol. 15, n°13, p. 4374-4381.
- Prudencio, M., Belzil, V. V., Batra, R., Ross, C. A., Gendron, T. F., Pregent, L. J., Murray, M. E., Overstreet, K. K., Piazza-Johnston, A. E., Desaro, P., Bieniek, K. F., DeTure, M., Lee, W. C., Biendarra, S. M., Davis, M. D., Baker, M. C., Perkinson, R. B., Blitterswijk, M. van, Stetler, C. T., Rademakers, R., Link, C. D., Dickson, D. W., Boylan, K. B., Li, H. et Petrucelli, L. (2015) Distinct brain transcriptome profiles in C9orf72-associated and sporadic ALS. *Nature Neuroscience*, vol. 18, n°8, p. 1175-1182.
- Qu, T., Zhang, W., Qi, L., Cao, L., Liu, C., Huang, Q., Li, G., Li, L., Wang, Y., Guo, Q., Guo, Y., Ren, D., Gao, Y., Wang, J., Meng, B., Zhang, B. et Cao, W. (2020) ISG15 induces ESRP1 to inhibit lung adenocarcinoma progression. *Cell Death & Disease*, vol. 11, n°7, p. 1-16.
- Ran, F. A., Hsu, P. D., Wright, J., Agarwala, V., Scott, D. A. et Zhang, F. (2013) Genome engineering using the CRISPR-Cas9 system. *Nature Protocols*, vol. 8, n°11, p. 2281-2308.
- Rino, J., Martin, R. M., Carvalho, C., de Jesus, A. C. et Carmo-Fonseca, M. (2015) Chapter Nineteen - Single-Molecule Imaging of RNA Splicing in Live Cells. *In* S. A. Woodson et F. H. T. Allain (dir.), *Methods in Enzymology, Structures of Large RNA Molecules and Their Complexes* (Vol. 558, p. 571-585). Academic Press.
- Rivera-Serrano, E. E., Fritch, E. J., Scholl, E. H. et Sherry, B. (2017) A Cytoplasmic RNA Virus Alters the Function of the Cell Splicing Protein SRSF2. *Journal of Virology*, vol. 91, n°7, p. e02488-16.
- Rudd, P. et Lemay, G. (2005) Correlation between interferon sensitivity of reovirus isolates and ability to discriminate between normal and Ras-transformed cells. *Journal of General Virology*, vol. 86, n°5, p. 1489-1497.
- Salton, M. et Misteli, T. (2016) Small Molecule Modulators of Pre-mRNA Splicing in Cancer Therapy. *Trends in Molecular Medicine*, vol. 22, n°1, p. 28-37.

- Samarajiwa, S. A., Forster, S., Auchettl, K. et Hertzog, P. J. (2009) INTERFEROME: the database of interferon regulated genes. *Nucleic Acids Research*, vol. 37, n°suppl 1, p. D852-D857.
- Sandekian, V., Lim, D., Prud'homme, P. et Lemay, G. (2013) Transient high level mammalian reovirus replication in a bat epithelial cell line occurs without cytopathic effect. *Virus Research*, vol. 173, n°2, p. 327-335.
- Sandri-Goldin, R. M. (1994) Properties of an HSV-1 regulatory protein that appears to impair host cell splicing. *Infectious Agents and Disease*, vol. 3, n°2-3, p. 59-67.
- Sandri-Goldin, R. M. (1998) Interactions between a Herpes Simplex Virus Regulatory Protein and Cellular mRNA Processing Pathways. *Methods*, vol. 16, n°1, p. 95-104.
- Sandri-Goldin, R. M. (2008) The many roles of the regulatory protein ICP27 during herpes simplex virus infection. *Frontiers in Bioscience: A Journal and Virtual Library*, vol. 13, p. 5241-5256.
- Sandri-Goldin, R. M., Hibbard, M. K. et Hardwicke, M. A. (1995) The C-terminal repressor region of herpes simplex virus type 1 ICP27 is required for the redistribution of small nuclear ribonucleoprotein particles and splicing factor SC35; however, these alterations are not sufficient to inhibit host cell splicing. *Journal of Virology*, vol. 69, n°10, p. 6063-6076.
- Santiana, M., Ghosh, S., Ho, B. A., Rajasekaran, V., Du, W.-L., Mutsafi, Y., Jésus-Diaz, D. A. D., Sosnovtsev, S. V., Levenson, E. A., Parra, G. I., Takvorian, P. M., Cali, A., Bleck, C., Vlasova, A. N., Saif, L. J., Patton, J. T., Lopalco, P., Corcelli, A., Green, K. Y. et Altan-Bonnet, N. (2018) Vesicle-Cloaked Virus Clusters Are Optimal Units for Inter-organismal Viral Transmission. *Cell Host & Microbe*, vol. 24, n°2, p. 208- 220.e8.
- Saunders, L. R. et Barber, G. N. (2003) The dsRNA binding protein family: critical roles, diverse cellular functions. *The FASEB Journal*, vol. 17, n°9, p. 961-983.
- Saurav, S., Tanwar, J., Ahuja, K. et Motiani, R. K. (2021) Dysregulation of host cell calcium signaling during viral infections: Emerging paradigm with high clinical relevance. *Molecular Aspects of Medicine, Biology of Infections*, vol. 81, p. 101004.
- Scheffner, M., Huibregtse, J. M., Vierstra, R. D. et Howley, P. M. (1993) The HPV-16 E6 and E6-AP complex functions as a ubiquitin-protein ligase in the ubiquitination of p53. *Cell*, vol. 75, n°3, p. 495-505.

- Scheffner, M., Werness, B. A., Huibregtse, J. M., Levine, A. J. et Howley, P. M. (1990) The E6 oncoprotein encoded by human papillomavirus types 16 and 18 promotes the degradation of p53. *Cell*, vol. 63, n°6, p. 1129-1136.
- Schock, S. N., Chandra, N. V., Sun, Y., Irie, T., Kitagawa, Y., Gotoh, B., Coscoy, L. et Winoto, A. (2017) Induction of necroptotic cell death by viral activation of the RIG-I or STING pathway. *Cell Death & Differentiation*, vol. 24, n°4, p. 615-625.
- Sciabica, K. S., Dai, Q. J. et Sandri-Goldin, R. M. (2003) ICP27 interacts with SRPK1 to mediate HSV splicing inhibition by altering SR protein phosphorylation. *The EMBO Journal*, vol. 22, n°7, p. 1608-1619.
- Sen, G. C. et Sarkar, S. N. (2007) The interferon-stimulated genes: targets of direct signaling by interferons, double-stranded RNA, and viruses. *Current Topics in Microbiology and Immunology*, vol. 316, p. 233-250.
- Shallak, M., Alberio, T., Fasano, M., Monti, M., Iacobucci, I., Ladet, J., Mortreux, F., Accolla, R. S. et Forlani, G. (2022) The endogenous HBZ interactome in ATL leukemic cells reveals an unprecedented complexity of host interacting partners involved in RNA splicing. *Frontiers in Immunology*, vol. 13.
- Shen, S., Park, J. W., Lu, Z., Lin, L., Henry, M. D., Wu, Y. N., Zhou, Q. et Xing, Y. (2014) rMATS: Robust and flexible detection of differential alternative splicing from replicate RNA-Seq data. *Proceedings of the National Academy of Sciences*, vol. 111, n°51, p. E5593-E5601.
- Sherry, B. (1998) Pathogenesis of reovirus myocarditis. *Current Topics in Microbiology and Immunology*, vol. 233, n°Pt 2, p. 51-66.
- Sherry, B. (2009) Rotavirus and Reovirus Modulation of the Interferon Response. *Journal of Interferon & Cytokine Research*, vol. 29, n°9, p. 559-567.
- Shkreta, L., Bell, B., Revil, T., Venables, J. P., Prinos, P., Elela, S. A. et Chabot, B. (2013) Cancer-Associated Perturbations in Alternative Pre-messenger RNA Splicing. *In* J. Y. Wu (dir.), *RNA and Cancer, Cancer Treatment and Research* (p. 41-94). Springer Berlin Heidelberg.
- Shkreta, L., Blanchette, M., Toutant, J., Wilhelm, E., Bell, B., Story, B. A., Balachandran, A., Cochrane, A., Cheung, P. K., Harrigan, P. R., Grierson, D. S. et Chabot, B. (2017) Modulation of the splicing regulatory function of SRSF10 by a novel compound that impairs HIV-1 replication. *Nucleic Acids Research*, vol. 45, n°7, p. 4051-4067.
- Shmulevitz, M., Gujar, S. A., Ahn, D.-G., Mohamed, A. et Lee, P. W. K. (2012) Reovirus Variants with Mutations in Genome Segments S1 and L2 Exhibit

- Enhanced Virion Infectivity and Superior Oncolysis. *Journal of Virology*, vol. 86, n°13, p. 7403-7413.
- Shmulevitz, M., Marcato, P. et Lee, P. W. K. (2005) Unshackling the links between reovirus oncolysis, Ras signaling, translational control and cancer. *Oncogene*, vol. 24, n°52, p. 7720-7728.
- Shmulevitz, M., Pan, L.-Z., Garant, K., Pan, D. et Lee, P. W. K. (2010) Oncogenic Ras Promotes Reovirus Spread by Suppressing IFN- $\beta$  Production through Negative Regulation of RIG-I Signaling. *Cancer Research*, vol. 70, n°12, p. 4912-4921.
- Shwetha, S., Kumar, A., Mullick, R., Vasudevan, D., Mukherjee, N. et Das, S. (2015) HuR Displaces Polypyrimidine Tract Binding Protein To Facilitate La Binding to the 3' Untranslated Region and Enhances Hepatitis C Virus Replication. *Journal of Virology*, vol. 89, n°22, p. 11356-11371.
- Sinkovics, J. G. (2004) Progressive Development of Viral Therapy of Human Cancers: A Personal Narrative Account. *Viral Therapy of Human Cancers*. CRC Press.
- Smith, R. W. P., Malik, P. et Clements, J. B. (2005) The herpes simplex virus ICP27 protein: a multifunctional post-transcriptional regulator of gene expression. *Biochemical Society Transactions*, vol. 33, n°3, p. 499-501.
- Snyder, A. J. et Danthi, P. (2016) Lipid Membranes Facilitate Conformational Changes Required for Reovirus Cell Entry. *Journal of Virology*, vol. 90, n°5, p. 2628-2638.
- Sobotkova, E., Duskova, M., Eckschlager, T. et Vonka, V. (2008) Efficacy of reovirus therapy combined with cyclophosphamide and gene-modified cell vaccines on tumors induced in mice by HPV16-transformed cells. *International Journal of Oncology*, vol. 33, n°2, p. 421-426.
- Soliman, M., Seo, J.-Y., Baek, Y.-B., Park, J.-G., Kang, M.-I., Cho, K.-O. et Park, S.-I. (2022) Opposite Effects of Apoptotic and Necroptotic Cellular Pathways on Rotavirus Replication. *Journal of Virology*, vol. 96, n°1, p. e01222-21.
- Soreq, L., Guffanti, A., Salomonis, N., Simchovitz, A., Israel, Z., Bergman, H. et Soreq, H. (2014) Long Non-Coding RNA and Alternative Splicing Modulations in Parkinson's Leukocytes Identified by RNA Sequencing. *PLoS Comput Biol*, vol. 10, n°3, p. e1003517.
- Stanifer, M. L., Rippert, A., Kazakov, A., Willemsen, J., Bucher, D., Bender, S., Bartenschlager, R., Binder, M. et Boulant, S. (2016) Reovirus intermediate subviral particles constitute a strategy to infect intestinal epithelial cells by

- exploiting TGF- $\beta$  dependent pro-survival signaling. *Cellular Microbiology*, vol. 18, n°12, p. 1831-1845.
- Stojdl, D. F., Lichty, B. D., tenOever, B. R., Paterson, J. M., Power, A. T., Knowles, S., Marius, R., Reynard, J., Poliquin, L., Atkins, H., Brown, E. G., Durbin, R. K., Durbin, J. E., Hiscott, J. et Bell, J. C. (2003) VSV strains with defects in their ability to shutdown innate immunity are potent systemic anti-cancer agents. *Cancer Cell*, vol. 4, n°4, p. 263-275.
- Strong, J. E., Coffey, M. C., Tang, D., Sabinin, P. et Lee, P. W. K. (1998) The molecular basis of viral oncolysis: usurpation of the Ras signaling pathway by reovirus. *The EMBO Journal*, vol. 17, n°12, p. 3351-3362.
- Strong, J. E. et Lee, P. W. (1996) The v-erbB oncogene confers enhanced cellular susceptibility to reovirus infection. *Journal of Virology*, vol. 70, n°1, p. 612-616.
- Strong, J. E., Tang, D. et Lee, P. W. K. (1993) Evidence That the Epidermal Growth Factor Receptor on Host Cells Confers Reovirus Infection Efficiency. *Virology*, vol. 197, n°1, p. 405-411.
- Suttle, C. A. (2007) Marine viruses — major players in the global ecosystem. *Nature Reviews Microbiology*, vol. 5, n°10, p. 801-812.
- Tao, Y., Farsetta, D. L., Nibert, M. L. et Harrison, S. C. (2002) RNA Synthesis in a Cage—Structural Studies of Reovirus Polymerase  $\lambda 3$ . *Cell*, vol. 111, n°5, p. 733-745.
- Teijaro, J. R. (2016) Type I interferons in viral control and immune regulation. *Current Opinion in Virology, Emerging viruses* • *Viral immunology*, vol. 16, p. 31-40.
- Tempera, I., Leo, A. D., Kossenkov, A. V., Cesaroni, M., Song, H., Dawany, N., Showe, L., Lu, F., Wikramasinghe, P. et Lieberman, P. M. (2016) Identification of MEF2B, EBF1, and IL6R as Direct Gene Targets of Epstein-Barr Virus (EBV) Nuclear Antigen 1 Critical for EBV-Infected B-Lymphocyte Survival. *Journal of Virology*, vol. 90, n°1, p. 345-355.
- Tenorio, R., Fernández de Castro, I., Knowlton, J. J., Zamora, P. F., Sutherland, D. M., Risco, C. et Dermody, T. S. (2019) Function, Architecture, and Biogenesis of Reovirus Replication Neorganelles. *Viruses*, vol. 11, n°3, p. 288.
- Thirukkumaran, C. M., Shi, Z. Q., Luider, J., Kopciuk, K., Bahlis, N., Neri, P., Pho, M., Stewart, D., Mansoor, A. et Morris, D. G. (2014) Reovirus as a successful ex vivo purging modality for multiple myeloma. *Bone Marrow Transplantation*, vol. 49, n°1, p. 80-86.

- Thompson, M. G., Dittmar, M., Mallory, M. J., Bhat, P., Ferretti, M. B., Fontoura, B. M., Cherry, S. et Lynch, K. W. (2020) Viral-induced alternative splicing of host genes promotes influenza replication. (D. L. Black, J. L. Manley, et M. A. Garcia-Blanco, Dir.)eLife, vol. 9, p. e55500.
- Thompson, M. G., Muñoz-Moreno, R., Bhat, P., Roytenberg, R., Lindberg, J., Gazzara, M. R., Mallory, M. J., Zhang, K., García-Sastre, A., Fontoura, B. M. A. et Lynch, K. W. (2018) Co-regulatory activity of hnRNP K and NS1-BP in influenza and human mRNA splicing. *Nature Communications*, vol. 9, n°1, p. 2407.
- Trauernicht, A. M., Kim, S. J., Kim, N. H. et Boyer, T. G. (2007) Modulation of Estrogen Receptor  $\alpha$  Protein Level and Survival Function by DBC-1. *Molecular Endocrinology*, vol. 21, n°7, p. 1526-1536.
- Tremblay, M.-P., Armero, V. E. S., Allaire, A., Boudreault, S., Martenon-Brodeur, C., Durand, M., Lapointe, E., Thibault, P., Tremblay-Létourneau, M., Perreault, J.-P., Scott, M. S. et Bisailon, M. (2016) Global profiling of alternative RNA splicing events provides insights into molecular differences between various types of hepatocellular carcinoma. *BMC Genomics*, vol. 17, p. 683.
- Tsuchiya, Y., Nakabayashi, O. et Nakano, H. (2015) FLIP the Switch: Regulation of Apoptosis and Necroptosis by cFLIP. *International Journal of Molecular Sciences*, vol. 16, n°12, p. 30321-30341.
- Tunyasuvunakool, K., Adler, J., Wu, Z., Green, T., Zielinski, M., Židek, A., Bridgland, A., Cowie, A., Meyer, C., Laydon, A., Velankar, S., Kleywegt, G. J., Bateman, A., Evans, R., Pritzel, A., Figurnov, M., Ronneberger, O., Bates, R., Kohl, S. A. A., Potapenko, A., Ballard, A. J., Romera-Paredes, B., Nikolov, S., Jain, R., Clancy, E., Reiman, D., Petersen, S., Senior, A. W., Kavukcuoglu, K., Birney, E., Kohli, P., Jumper, J. et Hassabis, D. (2021) Highly accurate protein structure prediction for the human proteome. *Nature*, vol. 596, n°7873, p. 590-596.
- Turkkila, M., Andersson, K. M., Amu, S., Brisslert, M., Erlandsson, M. C., Silfverswärd, S. et Bokarewa, M. I. (2015) Suppressed diversity of survivin splicing in active rheumatoid arthritis. *Arthritis Research & Therapy*, vol. 17, n°1, p. 175.
- Twigger, K., Roulstone, V., Kyula, J., Karapanagiotou, E. M., Syrigos, K. N., Morgan, R., White, C., Bhide, S., Nuovo, G., Coffey, M., Thompson, B., Jebar, A., Errington, F., Melcher, A. A., Vile, R. G., Pandha, H. S. et Harrington, K. J. (2012) Reovirus exerts potent oncolytic effects in head and neck cancer cell lines that are independent of signalling in the EGFR pathway. *BMC Cancer*, vol. 12, p. 368.

- Twigger, K., Vidal, L., White, C. L., Bono, J. S. D., Bhide, S., Coffey, M., Thompson, B., Vile, R. G., Heinemann, L., Pandha, H. S., Errington, F., Melcher, A. A. et Harrington, K. J. (2008) Enhanced In vitro and In vivo Cytotoxicity of Combined Reovirus and Radiotherapy. *Clinical Cancer Research*, vol. 14, n°3, p. 912-923.
- Ule, J. et Blencowe, B. J. (2019) Alternative Splicing Regulatory Networks: Functions, Mechanisms, and Evolution. *Molecular Cell*, vol. 76, n°2, p. 329-345.
- Vadlamudi, Y., Dey, D. K. et Kang, S. C. (s.d.) Emerging Multi-cancer Regulatory Role of ESRP1: Orchestration of Alternative Splicing to Control EMT. *Current Cancer Drug Targets*, vol. 20, n°9, p. 654-665.
- Vadlamudi, Y. et Kang, S. C. (2022) Silencing ESRP1 expression promotes caspase-independent cell death via nuclear translocation of AIF in colon cancer cells. *Cellular Signalling*, vol. 91, p. 110237.
- Vairo, D., Tassone, L., Tabellini, G., Tamassia, N., Gasperini, S., Bazzoni, F., Plebani, A., Porta, F., Notarangelo, L. D., Parolini, S., Giliani, S. et Badolato, R. (2011) Severe impairment of IFN- $\gamma$  and IFN- $\alpha$  responses in cells of a patient with a novel STAT1 splicing mutation. *Blood*, vol. 118, n°7, p. 1806-1817.
- Van Nostrand, E. L., Freese, P., Pratt, G. A., Wang, X., Wei, X., Xiao, R., Blue, S. M., Chen, J.-Y., Cody, N. A. L., Dominguez, D., Olson, S., Sundararaman, B., Zhan, L., Bazile, C., Bouvrette, L. P. B., Bergalet, J., Duff, M. O., Garcia, K. E., Gelboin-Burkhart, C., Hochman, M., Lambert, N. J., Li, H., McGurk, M. P., Nguyen, T. B., Palden, T., Rabano, I., Sathe, S., Stanton, R., Su, A., Wang, R., Yee, B. A., Zhou, B., Louie, A. L., Aigner, S., Fu, X.-D., Lécuyer, E., Burge, C. B., Graveley, B. R. et Yeo, G. W. (2020) A large-scale binding and functional map of human RNA-binding proteins. *Nature*, vol. 583, n°7818, p. 711-719.
- van Eindhoven, W. G., Frank, D., Kalachikov, S., Cleary, A. M., Hong, D. I., Cho, E., Nasr, S., Perez, A. J., Mackus, W. J. M., Cayanis, E., Wellington, S., Fischer, S. G., Warburton, D. et Lederman, S. (1998) A single gene for human TRAF-3 at chromosome 14q32.3 encodes a variety of mRNA species by alternative polyadenylation, mRNA splicing and transcription initiation. *Molecular Immunology*, vol. 35, n°18, p. 1189-1206.
- van Eindhoven, W. G., Gamper, C. J., Cho, E., Mackus, W. J. M. et Lederman, S. (1999) TRAF-3 mRNA splice-deletion variants encode isoforms that induce NF- $\kappa$ B activation. *Molecular Immunology*, vol. 36, n°10, p. 647-658.
- Vaquero-Garcia, J., Barrera, A., Gazzara, M. R., González-Vallinas, J., Lahens, N. F., Hogenesch, J. B., Lynch, K. W. et Barash, Y. (2016) A new view of transcriptome complexity and regulation through the lens of local splicing variations. (*J. Valcárcel, Dir.*)*eLife*, vol. 5, p. e11752.



- Vargas, D. Y., Shah, K., Batish, M., Levandoski, M., Sinha, S., Marras, S. A. E., Schedl, P. et Tyagi, S. (2011) Single-Molecule Imaging of Transcriptionally Coupled and Uncoupled Splicing. *Cell*, vol. 147, n°5, p. 1054-1065.
- Venables, J. P., Klinck, R., Bramard, A., Inkel, L., Dufresne-Martin, G., Koh, C., Gervais-Bird, J., Lapointe, E., Froehlich, U., Durand, M., Gendron, D., Brosseau, J.-P., Thibault, P., Lucier, J.-F., Tremblay, K., Prinos, P., Wellinger, R. J., Chabot, B., Rancourt, C. et Elela, S. A. (2008) Identification of Alternative Splicing Markers for Breast Cancer. *Cancer Research*, vol. 68, n°22, p. 9525-9531.
- Venables, J. P., Klinck, R., Koh, C., Gervais-Bird, J., Bramard, A., Inkel, L., Durand, M., Couture, S., Froehlich, U., Lapointe, E., Lucier, J.-F., Thibault, P., Rancourt, C., Tremblay, K., Prinos, P., Chabot, B. et Elela, S. A. (2009) Cancer-associated regulation of alternative splicing. *Nature Structural & Molecular Biology*, vol. 16, n°6, p. 670-676.
- Venables, J. P., Koh, C.-S., Froehlich, U., Lapointe, E., Couture, S., Inkel, L., Bramard, A., Paquet, É. R., Watier, V., Durand, M., Lucier, J.-F., Gervais-Bird, J., Tremblay, K., Prinos, P., Klinck, R., Elela, S. A. et Chabot, B. (2008) Multiple and Specific mRNA Processing Targets for the Major Human hnRNP Proteins. *Molecular and Cellular Biology*, vol. 28, n°19, p. 6033-6043.
- Verma, D., Bais, S., Gaillard, M. et Swaminathan, S. (2010) Epstein-Barr Virus SM Protein Utilizes Cellular Splicing Factor SRp20 To Mediate Alternative Splicing. *Journal of Virology*, vol. 84, n°22, p. 11781-11789.
- Verma, D. et Swaminathan, S. (2008) Epstein-Barr Virus SM Protein Functions as an Alternative Splicing Factor. *Journal of Virology*, vol. 82, n°14, p. 7180-7188.
- Villemaire, J., Dion, I., Elela, S. A. et Chabot, B. (2003) Reprogramming Alternative Pre-messenger RNA Splicing through the Use of Protein-binding Antisense Oligonucleotides. *Journal of Biological Chemistry*, vol. 278, n°50, p. 50031-50039.
- Wahl, M. C., Will, C. L. et Lührmann, R. (2009) The Spliceosome: Design Principles of a Dynamic RNP Machine. *Cell*, vol. 136, n°4, p. 701-718.
- Waks, Z., Klein, A. M. et Silver, P. A. (2011) Cell-to-cell variability of alternative RNA splicing. *Molecular Systems Biology*, vol. 7, p. 506.
- Wang, E. T., Sandberg, R., Luo, S., Khrebtkova, I., Zhang, L., Mayr, C., Kingsmore, S. F., Schroth, G. P. et Burge, C. B. (2008) Alternative isoform regulation in human tissue transcriptomes. *Nature*, vol. 456, n°7221, p. 470-476.

- Wang, L.-F. et Cowled, C. (2015) *Bats and Viruses: A New Frontier of Emerging Infectious Diseases*. John Wiley & Sons.
- Wang, Y., Chen, D., Qian, H., Tsai, Y. S., Shao, S., Liu, Q., Dominguez, D. et Wang, Z. (2014) The splicing factor RBM4 controls apoptosis, proliferation, and migration to suppress tumor progression. *Cancer Cell*, vol. 26, n°3, p. 374-389.
- Wang, Y., Liu, J., Huang, B., Xu, Y.-M., Li, J., Huang, L.-F., Lin, J., Zhang, J., Min, Q.-H., Yang, W.-M. et Wang, X.-Z. (2015) Mechanism of alternative splicing and its regulation. *Biomedical Reports*, vol. 3, n°2, p. 152-158.
- Warzecha, C. C., Shen, S., Xing, Y. et Carstens, R. P. (2009) The epithelial splicing factors ESRP1 and ESRP2 positively and negatively regulate diverse types of alternative splicing events. *RNA biology*, vol. 6, n°5, p. 546.
- Watanabe, Y., Millward, S. et Graham, A. F. (1968) Regulation of transcription of the reovirus genome. *Journal of Molecular Biology*, vol. 36, n°1, p. 107-123.
- White, M. K., Pagano, J. S. et Khalili, K. (2014) *Viruses and Human Cancers: a Long Road of Discovery of Molecular Paradigms*. *Clinical Microbiology Reviews*, vol. 27, n°3, p. 463-481.
- Wilhelm, E., Pellay, F.-X., Benecke, A. et Bell, B. (2008) Determining the impact of alternative splicing events on transcriptome dynamics. *BMC Research Notes*, vol. 1, n°1, p. 94.
- Wollenberg, D. J. M. van den, Hengel, S. K. van den, Dautzenberg, I. J. C., Cramer, S. J., Kranenburg, O. et Hoeben, R. C. (2008) A strategy for genetic modification of the spike-encoding segment of human reovirus T3D for reovirus targeting. *Gene Therapy*, vol. 15, n°24, p. 1567-1578.
- Wood, K. A., Eadsforth, M. A., Newman, W. G. et O'Keefe, R. T. (2021) The Role of the U5 snRNP in Genetic Disorders and Cancer. *Frontiers in Genetics*, vol. 12, p. 636620.
- Woodley, L. et Valcárcel, J. (2002) Regulation of alternative pre-mRNA splicing. *Briefings in Functional Genomics & Proteomics*, vol. 1, n°3, p. 266-277.
- Workenhe, S. T., Ketela, T., Moffat, J., Cuddington, B. P. et Mossman, K. L. (2016) Genome-wide lentiviral shRNA screen identifies serine/arginine-rich splicing factor 2 as a determinant of oncolytic virus activity in breast cancer cells. *Oncogene*, vol. 35, n°19, p. 2465-2474.

- Wright, P. F., Neumann, G. et Kawaoka, Y. (2013) Orthomyxoviruses. Dans David M. Knipe, Peter Howley (Éds). *Fields virology*. (6th edition.). Philadelphia : Lippincott Williams & Wilkins.
- Xu, H., Fair, B. J., Dwyer, Z. W., Gildea, M. et Pleiss, J. A. (2019) Detection of splice isoforms and rare intermediates using multiplexed primer extension sequencing. *Nature Methods*, vol. 16, n°1, p. 55-58.
- Xu, J., Fang, Y., Qin, J., Chen, X., Liang, X., Xie, X. et Lu, W. (2016) A transcriptomic landscape of human papillomavirus 16 E6-regulated gene expression and splicing events. *FEBS letters*, vol. 590, n°24, p. 4594-4605.
- Yang, W. Q., Senger, D. L., Lun, X. Q., Muzik, H., Shi, Z. Q., Dyck, R. H., Norman, K., Brasher, P. M. A., Rewcastle, N. B., George, D., Stewart, D., Lee, P. W. K. et Forsyth, P. A. (2004) Reovirus as an experimental therapeutic for brain and leptomeningeal metastases from breast cancer. *Gene Therapy*, vol. 11, n°21, p. 1579-1589.
- Yang, Y. et Carstens, R. P. (2017) Alternative splicing regulates distinct subcellular localization of Epithelial splicing regulatory protein 1 (Esrp1) isoforms. *Scientific Reports*, vol. 7, n°1, p. 3848.
- Yang, Y., Hu, W., Feng, S., Ma, J. et Wu, M. (2005) RIP3  $\beta$  and RIP3  $\gamma$ , two novel splice variants of receptor-interacting protein 3 (RIP3), downregulate RIP3-induced apoptosis. *Biochemical and Biophysical Research Communications*, vol. 332, n°1, p. 181-187.
- Yeo, G. W., Nostrand, E. V., Holste, D., Poggio, T. et Burge, C. B. (2005) Identification and analysis of alternative splicing events conserved in human and mouse. *Proceedings of the National Academy of Sciences*, vol. 102, n°8, p. 2850-2855.
- Yin, P., Cheang, M. et Coombs, K. M. (1996) The M1 gene is associated with differences in the temperature optimum of the transcriptase activity in reovirus core particles. *Journal of Virology*, vol. 70, n°2, p. 1223-1227.
- Yin, P., Keirstead, N. D., Broering, T. J., Arnold, M. M., Parker, J. S., Nibert, M. L. et Coombs, K. M. (2004) Comparisons of the M1 genome segments and encoded  $\mu 2$  proteins of different reovirus isolates. *Virology Journal*, vol. 1, p. 6.
- Yoshida, H. (2007) Unconventional Splicing of XBP-1 mRNA in the Unfolded Protein Response. *Antioxidants & Redox Signaling*, vol. 9, n°12, p. 2323-2334.
- Yue, Z. et Shatkin, A. J. (1996) Regulated, stable expression and nuclear presence of reovirus double-stranded RNA-binding protein sigma3 in HeLa cells. *Journal of Virology*, vol. 70, n°6, p. 3497-3501.

- Zammarchi, F., de Stanchina, E., Bournazou, E., Supakorndej, T., Martires, K., Riedel, E., Corben, A. D., Bromberg, J. F. et Cartegni, L. (2011) Antitumorigenic potential of STAT3 alternative splicing modulation. *Proceedings of the National Academy of Sciences of the United States of America*, vol. 108, n°43, p. 17779-17784.
- Zamora, P. F., Hu, L., Knowlton, J. J., Lahr, R. M., Moreno, R. A., Berman, A. J., Prasad, B. V. V. et Dermody, T. S. (2018) Reovirus Nonstructural Protein  $\sigma$ NS Acts as an RNA Stability Factor Promoting Viral Genome Replication. *Journal of Virology*, vol. 92, n°15.
- Zhang, T., Yin, C., Boyd, D. F., Quarato, G., Ingram, J. P., Shubina, M., Ragan, K. B., Ishizuka, T., Crawford, J. C., Tummers, B., Rodriguez, D. A., Xue, J., Peri, S., Kaiser, W. J., López, C. B., Xu, Y., Upton, J. W., Thomas, P. G., Green, D. R. et Balachandran, S. (2020) Influenza Virus Z-RNAs Induce ZBP1-Mediated Necroptosis. *Cell*, vol. 180, n°6, p. 1115- 1129.e13.
- Zhao, H., Lin, W., Kumthip, K., Cheng, D., Fusco, D. N., Hofmann, O., Jilg, N., Tai, A. W., Goto, K., Zhang, L., Hide, W., Jang, J. Y., Peng, L. F. et Chung, R. T. (2012) A functional genomic screen reveals novel host genes that mediate interferon-alpha's effects against hepatitis C virus. *Journal of Hepatology*, vol. 56, n°2, p. 326-333.
- Zhu, C., Li, X. et Zheng, J. (2018) Transcriptome profiling using Illumina- and SMRT-based RNA-seq of hot pepper for in-depth understanding of genes involved in CMV infection. *Gene*, vol. 666, p. 123-133.
- Zhu, Z., Gorman, M. J., McKenzie, L. D., Chai, J. N., Hubert, C. G., Prager, B. C., Fernandez, E., Richner, J. M., Zhang, R., Shan, C., Tycksen, E., Wang, X., Shi, P.-Y., Diamond, M. S., Rich, J. N. et Chheda, M. G. (2017) Zika virus has oncolytic activity against glioblastoma stem cells. *Journal of Experimental Medicine*, vol. 214, n°10, p. 2843-2857.
- Zurney, J., Kobayashi, T., Holm, G. H., Dermody, T. S. et Sherry, B. (2009) Reovirus  $\mu$ 2 Protein Inhibits Interferon Signaling through a Novel Mechanism Involving Nuclear Accumulation of Interferon Regulatory Factor 9. *Journal of Virology*, vol. 83, n°5, p. 2178-2187.

## **ANNEXES**

### Liste des annexes

#### **Annexe 1**

Boudreault S, Roy P, Lemay G, Bisailon M. Viral modulation of cellular RNA alternative splicing: A new key player in virus–host interactions? *Wiley Interdiscip Rev RNA*. 2019 Apr 29;0(0):e1543.

#### **Annexe 2**

Boudreault S, Armero VES, Perreault JP, Scott MS, Bisailon M. (2019). The Epstein-Barr virus EBNA1 protein modulates the alternative splicing of cellular genes. *Virology Journal*, 16(1), 29, <https://doi.org/10.1186/s12985-019-1137-5>.

# Viral modulation of cellular RNA alternative splicing: A new key player in virus–host interactions?

Simon Boudreault<sup>1</sup> | Patricia Roy<sup>1</sup> | Guy Lemay<sup>2</sup> | Martin Bisailon<sup>1</sup> 

<sup>1</sup>Département de biochimie, Faculté de médecine et des sciences de la santé, Université de Sherbrooke, Sherbrooke, Québec, Canada

<sup>2</sup>Département de microbiologie, infectiologie et immunologie, Faculté de médecine, Université de Montréal, Montréal, Québec, Canada

## Correspondence

Martin Bisailon, Département de biochimie, Faculté de médecine et des sciences de la santé, Université de Sherbrooke, Sherbrooke, Québec, Canada J1E 4K8.  
Email: martin.bisailon@usherbrooke.ca

## Funding information

Natural Sciences and Engineering Research Council of Canada, Grant/Award Number: RGPIN-03736-2017, RGPIN-2016-03916; Canadian Institutes of Health Research

## Abstract

Upon viral infection, a tug of war is triggered between host cells and viruses to maintain/gain control of vital cellular functions, the result of which will ultimately dictate the fate of the host cell. Among these essential cellular functions, alternative splicing (AS) is an important RNA maturation step that allows exons, or parts of exons, and introns to be retained in mature transcripts, thereby expanding proteome diversity and function. AS is widespread in higher eukaryotes, as it is estimated that nearly all genes in humans are alternatively spliced. Recent evidence has shown that upon infection by numerous viruses, the AS landscape of host-cells is affected. In this review, we summarize recent advances in our understanding of how virus infection impacts the AS of cellular transcripts. We also present various molecular mechanisms allowing viruses to modulate cellular AS. Finally, the functional consequences of these changes in the RNA splicing signatures during virus–host interactions are discussed.

This article is categorized under:

RNA in Disease and Development > RNA in Disease

RNA Processing > Splicing Regulation/Alternative Splicing

## KEYWORDS

RNA alternative splicing, virus, virus–host interactions

## 1 | INTRODUCTION

The study of virus–host interaction has been a long and meticulous work to decipher both the impact of viral infection on the host cell, the response of the host cell to viral proteins and RNA, and the complex interplay and cross-talk between both. Upon infection, a race is established between the virus and its host cell to either gain control of cellular functions, vital for viral replication, or mount an efficient antiviral response to prevent viral spread. The result of this race is either replication for the virus or control of the infection and clearance for the host cell. Upon infection, viral determinants such as double-stranded RNA (dsRNA) are recognized by PRRs (pattern-recognition receptors) that trigger a signaling cascade that leads to the production of interferon (IFN). Upon secretion, IFN can act both in a paracrine fashion on uninfected cells to prepare them for infection, or in an autocrine manner to stimulate the infected cell. Upon binding and signaling, IFN leads to the expression of a plethora of interferon-stimulated genes (ISG) that are effectors of the cellular antiviral response against infection (Fensterl,

This is an open access article under the terms of the Creative Commons Attribution License, which permits use, distribution and reproduction in any medium, provided the original work is properly cited.

© 2019 The Authors. *WIREs RNA* published by Wiley Periodicals, Inc.

Chattopadhyay, & Sen, 2015; Sen & Sarkar, 2007). Hence, the transcriptome of the host cell is profoundly impacted by viral infection, with hundreds of genes being rapidly overexpressed in order of magnitude that can climb up to 10,000-fold.

Constitutive splicing is a vital RNA maturation step that allows the removal of introns, which are non-coding sequences, from the pre-mature transcript. To do so, the spliceosome, a large ribonucleoprotein made of multiple U spliceosomal RNAs and proteins, recognize the splice junction and catalyze two trans-esterification reactions to excise the intron (Figure 1a) (reviewed in Kim, Goren, & Ast, 2008; Y. Lee & Rio, 2015; Merkhofer, Hu, & Johnson, 2014). Briefly, the first step is the binding of U1 and U2 snRNP to the 5' splice site and the branch site, respectively. Then, the U4/U6.U5 tri-snRNP is recruited. Upon structural reorganization, U1 and U4 snRNP are released, leading to an activated B complex. The branch site becomes close in proximity to the 5' splice site through the new connection between U6 and U2 snRNP. In the first step, the 2' hydroxyl of the branch site performs a nucleophilic attack on the 5' phosphate of the first nucleotide of the intron (5' splice site), usually a guanosine. The reaction breaks the bond between the exon and the intron, forming a new one with the branch site and the intron. In the second catalytic reaction, the newly free 3' OH group attacks the last intronic nucleotide, also usually a guanosine. This links the two exons together, thereby releasing the intron lariat.

To complement this constitutive removal of introns, some exons, parts of exons, or introns can also be retained in the mature transcript by a process which is called alternative splicing (AS). AS arises from stimulatory and inhibitory signals coming from multiple splicing factors near weak splice sites, either helping the spliceosome to assemble at this location, or destabilizing it and giving rise to a mixed population of mature mRNAs (Figure 1b) (reviewed in Wang et al., 2015; Woodley & Valcárcel, 2002). Enhancing factors, such as SR proteins, bind to either intronic or exonic splicing enhancers (ISE and ESE respectively); inhibitory factors, such as hnRNP proteins, rather bind intronic or exonic splicing silencers (ISS and ESS respectively). AS is widespread in higher eukaryotes, as it is estimated that nearly all genes in humans are alternatively spliced (Wang et al., 2008). Many different types of AS events exist and are summarized in Figure 2a. Mainly, exon skipping, mutually exclusive exon, and tandem exon cassette all lead to different layouts of the same exons in the mature mRNA. Alternative 5' and 3' splice site selection can also lead to the removal of specific portions of exons. An intron might also not be properly recognized by the spliceosome and be kept in the mature RNA,

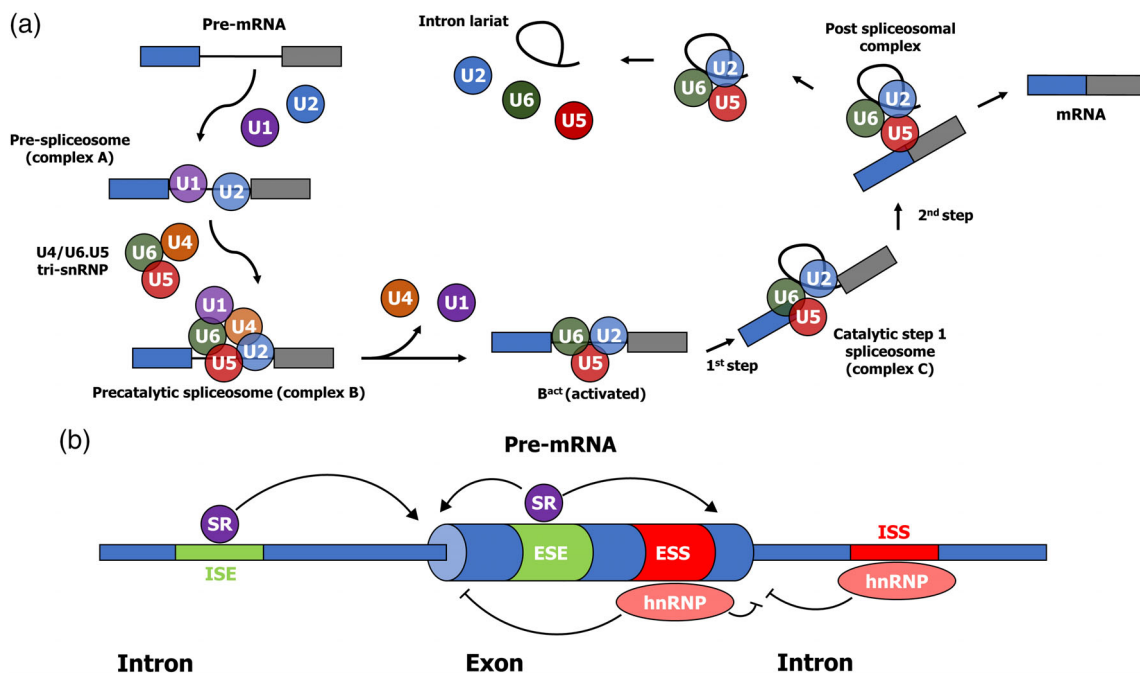


**FIGURE 1** Summary of the splicing reaction and regulatory signals/proteins involved. (a) The cycle of assembly and disassembly of the spliceosome throughout the splicing reaction. The stepwise interaction of the spliceosomal small ribonucleoprotein (snRNP) particles (U1, U2, U4, U4, U5, and U6; colored circles) in the excision of an intron from a pre-mature RNA (pre-mRNA) containing two exons (blue and gray) is depicted. The name of the spliceosomal complexes and the two catalytic steps of the reaction are indicated. (b) Positive and negative signals are stabilizing or destabilizing the assembly of the spliceosome on the pre-mRNA by *cis*-acting elements. The diagram represents a typical segment of eukaryotic precursor messenger RNA with one exon and the two surrounding introns. Intronic and exonic splicing enhancers (ISE and ESE; in green) are typically bound by factors promoting the splicing reaction from nearby splice sites, such as serine-arginine repeats (SR) proteins. Intronic and exonic splicing silencers (ISS and ESS; in red) are typically bound by factors inhibiting splicing from nearby splice sites, such as heterogeneous nuclear ribonucleoprotein particle (hnRNP) proteins

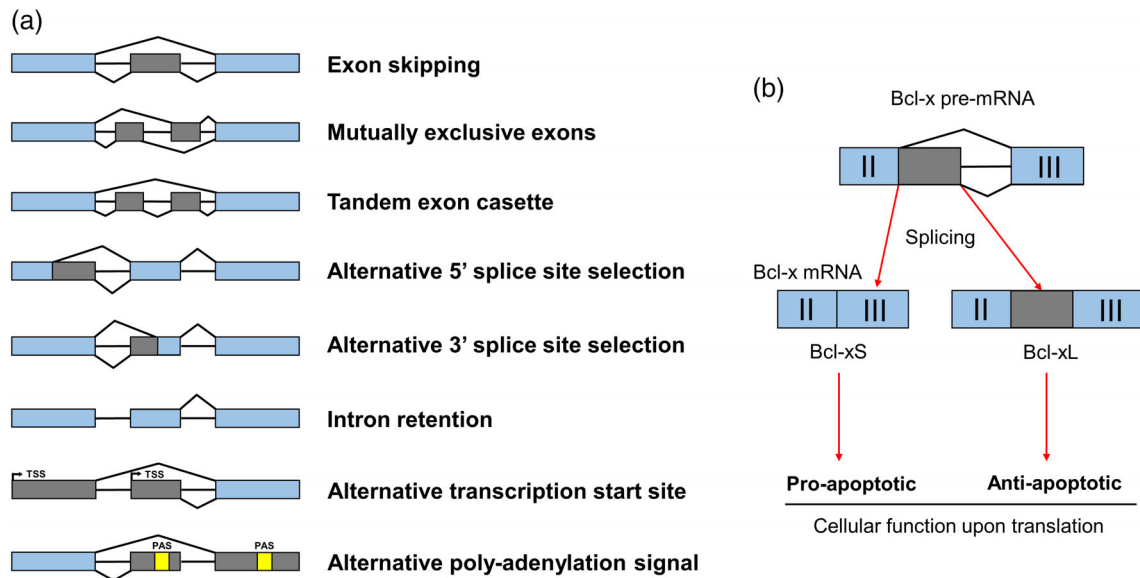


**FIGURE 2** Summary of the different types of AS events and the biological role of AS. (a) Exon skipping, mutually exclusive exon and tandem exon cassette allow selective removal of complete exons from the mature RNA. Alternative 5' and 3' splice site selection allows removal of a part of an exon, either in 5' or 3' using the intron as the reference. An intron might be kept in the mature RNA, leading to intron retention. Gray boxes represent regions that are alternatively spliced; blue boxes represent regions that are always conserved in the mature mRNA; yellow boxes represent poly-adenylation signals (PAS). TSS: Transcription start site. (b) The Bcl-x pre-mRNA is depicted, with the gray region (alternative 5' splice site) being spliced in or out to give rise to the short (Bcl-xS) or long (Bcl-xL) isoforms. The former produces a pro-apoptotic protein, and the latter an anti-apoptotic one, underlining the importance of AS for the regulation of biological activities of proteins

leading to intron retention. Furthermore, different transcription start sites (TSS) might be used to initiate transcription, leading to alternative 5' exons. Finally, poly-adenylation signals (PAS) might be differentially present in the spliced regions, promoting the use of different polyadenylation sites in isoforms from the same pre-mRNA. Functionally, AS allows a fine-tuning of the activity of encoded proteins by removing coding parts corresponding to domains, localization signals, or by introducing frameshifts and premature stop codons. A well-known example is the Bcl-x transcript, which upon splicing, can produce either a short pro-apoptotic protein or a longer anti-apoptotic protein upon differential usage of a 5' splice site (Wilhelm, Pelly, Benecke, & Bell, 2008) (Figure 2b). Other examples of alternatively spliced genes that are relevant to the replication of viruses are also well described, such as the Coxsackie virus and adenovirus receptor (CAR) gene. The *CXADR* gene produces a pre-mRNA that can be matured to generate the full-length CAR protein, and also a spliced isoform which lacks the transmembrane domain and is thus soluble. This isoform can prevent the binding of the virus to the complete receptor upon secretion (Dörner, Xiong, Couch, Yajima, & Knowlton, 2004). In another example, the murine *IRAK2* gene produces four well-described isoforms, including two isoforms which can stimulate the NF- $\kappa$ B pathway, and two other isoforms which act as dominant-negative forms (Hardy & O'Neill, 2004). Lastly, the *TRAF3* gene, involved in signal transduction of members of the tumor necrosis factor (TNF) family and vital for the activation of NF- $\kappa$ B and immune responses, possesses multiple alternatively spliced mRNA transcripts (van Eyndhoven et al., 1998). Full-length TRAF3 protein is unable to activate the NF- $\kappa$ B pathway but can potentiate the signaling induced by alternatively-spliced TRAF3 proteins (van Eyndhoven, Gamper, Cho, Mackus, & Lederman, 1999). These few examples only partially reflect the importance of AS in immune response and their potential involvement in virus–host interactions.

More than 40 years ago, the discovery of RNA sequences removed from mature RNA in adenovirus transcripts allowed the identification of splicing (Berget, Moore, & Sharp, 1977; Chow, Gelin, Broker, & Roberts, 1977). Since then, the importance of AS for some viruses, such as DNA viruses, has become well understood. Human papillomavirus (HPV), human immunodeficiency virus (HIV), and adenoviruses all necessitate the cellular splicing machinery to efficiently splice their mRNAs (for an exhaustive review on how viruses hijack the splicing machinery for their replication, see Meyer, 2016). For these viruses, splicing allows a relatively small genome to encode a broader range of functionally diverse proteins. However, the impact of viral infection on the cellular AS landscape was not studied thoroughly until very recently. The increased affordability and versatility of high-throughput sequencing technologies, such as RNA-sequencing, allowed scientists to probe the transcriptome of cells under specific conditions with a depth and width that was not possible using previous techniques. However, technical challenges linked to the study of these virus-induced changes in cellular AS have been reported (Ashraf,



Benoit-Pilven, Lacroix, Navratil, & Naffakh, 2019). In the present review, we examine the putative impact of these changes in AS on the interplay between viruses and host cells. A complete overview of known examples found in the literature and mechanisms allowing viruses to modulate cellular AS will be initially presented. Then, the impact of this modulation on virus–host interaction, and perspectives regarding the importance of studying this modulation will be discussed.

## 2 | CONTRIBUTION OF HIGH-THROUGHPUT APPROACHES

The advent of high-throughput sequencing approaches allowed scientists to probe the whole transcriptome of cells under different conditions, such as during viral infection. The initial aim of these studies was to depict the global portrait of the changes in gene expression triggered by infection. However, some of the studies performed also focused on the impact on mRNA maturation processes, such as AS. Although depicting the global portrait of all AS events being modulated during infection, transcriptomic studies alone are frequently only the starting point in assessing changes in AS. Subsequent validation of AS events using PCR-based technique and more in-depth mechanistic studies are needed to strengthen the conclusions. In the next sections, examples regarding DNA viruses will first be discussed, then RNA viruses will be addressed, and finally plant RNA viruses will be examined and are summarized in Table 1.

**TABLE 1** List of viruses shown to modulate AS in transcriptomic studies

Virus	Family	Genome	Validation of results	Additional details	References
<b>HCMV</b>	<i>Herpesviridae</i>	dsDNA	++	Validation using HSV-2	Batra et al. (2016)
<b>HSV-1</b>	<i>Herpesviridae</i>	dsDNA	–	Solely transcriptomic	Hu et al. (2016)
<b>EBV</b>	<i>Herpesviridae</i>	dsDNA	– + +	EBER1 and EBER2 expression EBNA1 expression; high-throughput RT-PCR Limited screen using microarray chips	Pimienta et al. (2015); Boudreault, Armero, Scott, Perreault, and Bisaillon (2019); Homa et al. (2013)
<b>HTLV-1</b>	<i>Herpesviridae</i>	dsDNA	++	Limited screen using microarray chips	Thénoz et al. (2014)
<b>HPV</b>	<i>Papillomaviridae</i>	dsDNA	+	Expression of E6	Xu et al. (2016)
<b>Mammalian reovirus</b>	<i>Reoviridae</i>	dsRNA	++ +	–	Boudreault et al. (2016); Rivera-Serrano, Fritch, Scholl, and Sherry (2017)
<b>Avian reovirus</b>	<i>Reoviridae</i>	dsRNA	–	Solely transcriptomic	Niu, Wang, Li, Zhang, and Wu (2017)
<b>FMDV</b>	<i>Picornaviridae</i>	(+)ssRNA	+	–	Han et al. (2018)
<b>Zika virus</b>	<i>Flaviviridae</i>	(+)ssRNA	–	Solely transcriptomic	Hu et al. (2017)
<b>Dengue virus</b>	<i>Flaviviridae</i>	(+)ssRNA	++	–	Sessions et al. (2013)
<b>Lentivirus</b>	<i>Retroviridae</i>	ssRNA-RT	++	–	Cesana et al. (2012); Moiani et al. (2012)
<b>Reticuloendotheliosis virus</b>	<i>Retroviridae</i>	ssRNA-RT	–	Solely transcriptomic	Gao, Zhai, Dang, and Zheng (2018)
<b>Influenza A virus</b>	<i>Orthomyxoviridae</i>	(–)ssRNA	+ +	–	Thompson et al. (2018); Fabozzi et al. (2018)
<b>Panicum mosaic virus</b>	<i>Tombusviridae</i>	(+)ssRNA	+	–	Mandadi and Scholthof (2015)
<b>Cucumber mosaic virus</b>	<i>Bromoviridae</i>	(+)ssRNA	–	Solely transcriptomic	Zhu, Li, and Zheng (2018)
<b>Bean common mosaic virus</b>	<i>Potyviridae</i>	(+)ssRNA	–	Solely transcriptomic	Martin, Singh, Hill, Whitham, and Cannon (2016)
<b>PSTVd</b>	<i>Pospiviroidae</i>	ssRNA	–	Viroid; solely transcriptomic	Zheng, Wang, Ding, and Fei (2017)

## 2.1 | DNA viruses

The *Herpesviridae* family, which possesses linear dsDNA genomes, has been the most studied for its ability to modulate AS. For example, the human cytomegalovirus (HCMV) infection triggers the overexpression of the RNA-binding protein CPEB1, which leads to a change in cellular AS (Batra et al., 2016). Overexpression of CPEB1 in non-infected cells mimicked the modifications seen in HCMV-infected cells, hence proving the involvement of CPEB1 in AS. Moreover, this change in AS was also observed following herpes simplex virus 2 (HSV-2) infection, further solidifying the results and pointing towards a possible conserved modulation of cellular AS for *Herpesviridae* members. A study focusing on transcriptomic changes during herpes simplex virus 1 (HSV-1) also showed modulation of cellular AS that mainly impacted genes involved in the cell cycle; this study included an RT-PCR validation of the changes in AS, although for only four genes (Hu et al., 2016). Moreover, the expression in cells of EBER1 and EBER2, two long non-coding RNAs localized to the nucleus from the Epstein-Barr virus (EBV), another *Herpesviridae*, induced changes in the AS profiles of transcripts linked to EBV oncogenic potential (Pimienta et al., 2015). This is quite interesting, as EBV is both a latent and oncogenic virus while EBER1 and EBER2 are expressed in all cellular contexts of EBV latency. Nonetheless, these results must be taken with caution, as no change in AS were validated in this study.

Oncogenic viruses have a special relationship with host-cell AS, as cancer cells present dysregulated AS profiles (David & Manley, 2010). In the context of cancer, it was demonstrated that EBV-positive gastric carcinomas showed specific alteration in AS compared to EBV-negative gastric carcinomas (Armero et al., 2017). The same conclusion was drawn with hepatitis B (HBV) and hepatitis C virus in hepatocellular carcinomas (Tremblay et al., 2016). In both cases, expression of a viral protein from those viruses possessing an oncogenic activity in cells (EBNA1 for EBV and HBx for HBV) induced changes in AS; nonetheless, high-throughput RT-PCR was used for validation on a limited number of AS events analyzed. Although these results seemed a little preliminary, a follow-up study showed that the impact of the EBNA1 protein on cellular splicing seemed indirect, as the binding of EBNA1 to cellular RNAs does not directly leads to modifications in AS (Boudreault et al., 2019). Interestingly, the expression of E6 from HPV in HEK293T, which is also a potent oncoprotein, leads to a modulation of splicing in cellular genes (Xu et al., 2016). Still, the experimental design used was not optimal, since this study used a transient expression of E6 in HEK293T cells; a more relevant cell line and the usage of stable cell lines to ensure reproducible expression of E6 between cells would have been more relevant. As cancer cells present dysregulated AS profiles, an exciting possibility would be that viral oncoproteins drive the modulation of cellular AS towards a cancer-like phenotype (David & Manley, 2010). To support this hypothesis, EBV-induced carcinogenesis was shown by microarray analyses to alter the AS profiles of many AS events (Homa et al., 2013); however, more studies are needed to prove this hypothesis.

## 2.2 | RNA viruses

Two recent studies have shown that mammalian reovirus, a member of the *Reoviridae* family of dsRNA viruses, can modulate the AS of the host-cell following viral infection. The first one demonstrated that upon infection of L929 cells with the reovirus serotype 3-Dearing strain (T3D) of reovirus, 240 AS events were modulated (Boudreault et al., 2016). The main strength of this study is that both AS-PCR and mass spectrometry were used to validate the results, giving additional weight to the findings. In contrast, a later study by another group showed a limited effect of the T3D virus compared to the reovirus serotype 1-Lang strain (T1L) (Rivera-Serrano et al., 2017). This apparent discrepancy is likely attributable to variations in the actual amino acid sequences of the T3D strain used in different laboratories (Sandekian & Lemay, 2015). Interestingly, the second study further suggests that the interaction of the viral protein  $\mu 2$  with the splicing factor SRSF2 in nuclear speckles is responsible for the modulation of cellular AS. The  $\mu 2$  protein is an important structural protein that is partially located to the nucleus during infection and can bind RNA (Brentano, Noah, Brown, & Sherry, 1998; Kobayashi, Ooms, Chappell, & Dermody, 2009). Nevertheless, there was no ectopic expression of  $\mu 2$  to demonstrate the ability of  $\mu 2$  to modulate AS by itself, and there was no loss-of-phenotype experiment to prove that SRSF2 is involved in these changes. Overall, these data do not rule out the possibility that other viral determinants and/or mechanisms might be at play. Nonetheless, supporting the idea that  $\mu 2$  is involved, the variant used in the first study possesses a proline at position 208 as in T1L, in contrast to the T3D variant of the second study that rather harbors a serine at this position (Sandekian & Lemay, 2015); this possibly explains the previously noted discrepancy in the effect on AS of T3D in the two studies. This proline to serine substitution in  $\mu 2$  is already known to be involved in differences of IFN sensitivity/induction and morphology of viral factories between T3D and T1L (Irvin et al., 2012; Lanoie & Lemay, 2018; Parker, Broering, Kim, Higgins, & Nibert, 2002; Rivera-Serrano et al., 2017; Zurney, Kobayashi, Holm, Dermody, & Sherry, 2009). In another study using a closely-related avian reovirus, RNA-sequencing of infected fibroblasts showed no change in cellular AS (Niu et al., 2017). It is still not clear if this avian strain is not able to

directly modulate cellular AS or if the experimental design precluded the observation of such changes. Finally, in another more distant member of the *Reoviridae* family, the pathogenic rotavirus, the cytoplasmic splicing of the stress-related factor XBP1 is altered following infection with some but not all of the rotaviral strains (Duarte et al., 2019). Interestingly, the NPS3 protein was identified as the primary determinant, but the splicing of XBP1 was always studied in the context of infection; ectopic expression of NSP3 should be tested to better understand all the determinants necessary to modulate splicing. Surprisingly, this is the only example of cytoplasmic splicing being modulated by viral infection, which is a relatively rare phenomenon and happens only in fewer than 30 genes (Buckley, Khaladkar, Kim, & Eberwine, 2014). Further studies will help to understand if modulation of nuclear splicing is conserved in the *Reoviridae* family, if other *Reoviridae* also modulates cytoplasmic splicing, and what are the molecular determinants behind those changes.

Studies have shown that RNA viruses from numerous other families are also able to trigger the modulation of host-cell AS, which seems to indicate that viral modulation of cellular AS is a somewhat widespread phenomenon during virus–host interactions. Foot-and-mouth disease virus (FMDV), a *Picornaviridae*, often leads to persistence in infected cloven-footed animals, but the molecular mechanisms allowing persistence of the virus remain unclear. Interestingly, cells that were adapted to enable persistent FMDV infection showed changes in cellular AS compared to non-adapted cells (Han et al., 2018). For example, adapted cells presented changes in the AS of the splicing factor hnRNP A2B1, and this suggests that cellular AS could have a functional role in virus replication and persistence mechanisms. However, their validation was limited to 4 genes in RT-PCR, and AS profiles in cultured cells can vary with passaging, which restrains the conclusion one can emit from this study. The recent outburst of interest in Zika virus, a *Flaviviridae* causing microcephaly in newborns and the Guillain-Barré syndrome, spawned interest in changes induced by this virus following viral infection. Although it is solely transcriptomic, a study showed dysregulated AS following infection with this virus using RNA-Seq (Hu et al., 2017). Similar results were shown following Dengue virus (DV) infection; in this case, an extensive PCR validation screen confirmed 32 AS events modulated by DV (Sessions et al., 2013). The demonstration about the ability of the NS5 protein of DV to modulate AS (see Section 3.4) and the transcriptomic studies altogether suggest that other *Flaviviridae* could have the same impact on cellular AS. It was recently concluded that reticuloendotheliosis virus, a retrovirus causing immunosuppression and cancer in avian species, trigger changes in AS of 859 cellular AS events (Gao et al., 2018). Nevertheless, the implications of these findings are limited since the authors focused their analyses on genes with AS that were differentially expressed following infection and never analyzed the modulation of AS per se, which is a major drawback of their study. Retroviruses, which integrate their genomes into the host cell DNA, present a particular case since they have a special relationship with host-cell AS: the introduction of exogenous viral sequences containing splicing-regulating signals could drive the production of aberrantly spliced transcripts. Integration of the viral genome of lentiviruses inside the genetic material of the host cell was demonstrated to induce aberrant splicing at the integration site, by bringing newly transcribed splice sites in pre-mature RNAs (Cesana et al., 2012; Moiani et al., 2012). Another study, based on microarray chips, which are less efficient than RNA-Sequencing for quantifying AS, showed that normal and malignant CD4<sup>+</sup> T-cells infected with HTLV-1, an oncogenic retrovirus, display multiple alternate exon usage events as compared to non-infected CD4<sup>+</sup> T-cells (Thénoz et al., 2014). Finally, in the case of influenza A virus (IAV), infection was also recently demonstrated to modulate the AS of 4 AS events which are co-regulated by hnRNP K and NS1-BP (Thompson et al., 2018). Moreover, laboratory and seasonal strains differ in the splicing modulation they induce (Fabozzi et al., 2018). Although the validation of this study was limited to three AS events (*TBK1*, *IFI35*, and *DDIT3*), it is reminiscent of the case of reovirus in which different strains have different impacts on AS, as discussed above.

## 2.3 | Plant viruses

Although less studied, evidence for the involvement of plant viruses in the modulation of AS during virus–host interactions are emerging. For example, the Panicum mosaic virus and its satellite virus both trigger changes in AS in *Brachypodium distachyon* following infection (Mandadi & Scholthof, 2015). Interestingly, novel intron-retaining variants of *SCL33*, a serine/arginine-rich splicing factor, were identified and modulated by these two viruses. Moreover, infection of the hot pepper (*Capsicum annuum* L., an increasingly important crop worldwide) with cucumber mosaic virus leads to changes in the host AS (Zhu et al., 2018), and the bean common mosaic virus is also able to trigger alterations in host AS that seems to be strain-specific (Martin et al., 2016). Except for *SCL33*, all these studies were solely transcriptomic and were limited by the annotations of AS in plants, which are still incomplete. Although the goal of the current review is to focus on viruses, it should be noted that dysregulation of AS was also observed in a tomato model of infection by the Potato Spindle Tuber Viroid (PSTVd), which is a self-replicating RNA molecule (Zheng et al., 2017). As viroids do not encode for any proteins, it is quite intriguing how PSTVd infection alters AS. Although there was no RT-PCR validation of changes in AS, recent studies

showed that PSTVd can interact with RPL5 to modulate the splicing of TFIIIA, enhancing the levels of TFIIIA-7ZF, an isoform essential for PSTVd replication, which suggests a potential mechanism for the modulation of AS (reviewed in Disanayaka Mudiyansele, Qu, Tian, Jiang, & Wang, 2018). In conclusion, novel high-throughput approaches such as RNA-Seq have allowed scientists to probe the transcriptome of infected cells extensively. These experiments have revealed the first hints at changes in cellular AS following infection with numerous virus from different families, a concept that scientists have only started to grasp.

### 3 | MECHANISM-DRIVEN APPROACHES

Although interesting, these transcriptomic studies only depict the global portrait of the changes in cellular AS, with little insights into the mechanistic operating behind those changes. However, other studies have delved deeply into the characterization of viral products that are potent modulators of AS and their mechanism of action. The viral protein that has been the most studied is probably ICP27, an HSV protein which is well-known as a potent AS inhibitor. Other examples that will be presented for DNA viruses include the EBV SM and EBER1 proteins. Then RNA viruses will be addressed, by discussing the RNA-dependent RNA polymerase (RdRp) NS5 and 3Dpol from DV and picornavirus, the influenza virus NS1, poliovirus 2A<sup>PRO</sup> and HIV-1 Vpr. A summary of their mechanisms of action on cellular AS is depicted in Figure 3. and relevant information about this section is outlined in Table 2.

#### 3.1 | ICP27

The immediate-early infected cell protein 27 (ICP27, also known as EI63) from the double-stranded DNA virus HSV-1 is known to be an important regulatory protein required for productive viral infection and expression of late viral genes (Sacks, Greene, Aschman, & Schaffer, 1985; Sandri-Goldin & Mendoza, 1992). Moreover, this protein also inhibits splicing in the host cell during infection at early stages of spliceosome assembly (Hardy & Sandri-Goldin, 1994; Lindberg & Kreivi, 2002). Interestingly, these results were obtained through *in vitro* splicing assays and thus might not adequately represent *in cellulo* conditions. ICP27 causes redistribution of small nuclear ribonucleoprotein particles (snRNP) to a more punctuate distribution (Phelan et al., 1993). Nonetheless, it was later shown that this redistribution and the interaction with SRSF2, requiring the C-terminal repressor region of ICP27, correlates with the splicing inhibition but is not sufficient to induce this phenotype (Sandri-Goldin et al., 1995). In this case, the splicing was studied *in cellulo*, further confirming the ability of ICP27 to inhibit splicing. The redistribution of the splicing factor SRSF2 seems to be conserved, as it also occurs with the ICP27 protein of *herpesvirus saimiri* (HVS; Cooper et al., 1999). ICP27 modulation of splicing was later demonstrated to require its interaction

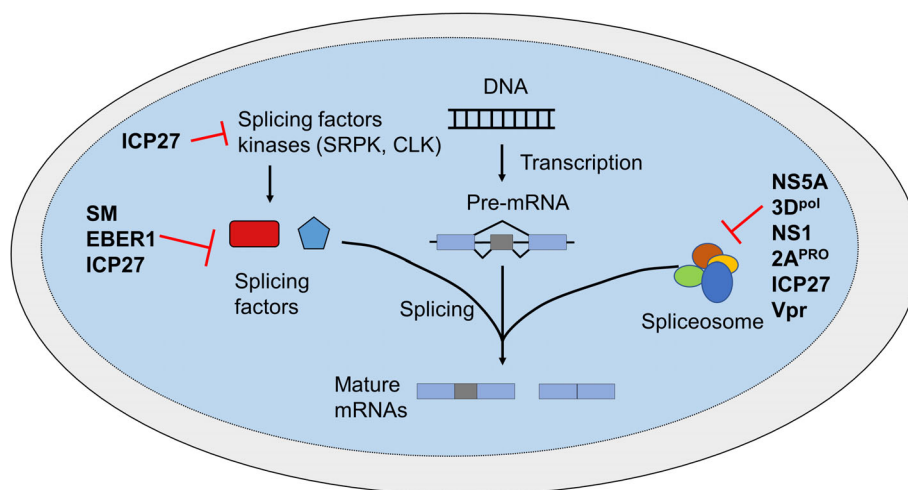


**FIGURE 3** Schematic representation of the mechanisms of action for viral products that are potent modulators of cellular AS. NS5 from dengue virus, 3D<sup>POL</sup> from picornavirus, NS1 from influenza virus, 2A<sup>PRO</sup> from poliovirus, Vpr from HIV-1 and ICP27 from *Herpesviridae* were all shown to interact with the spliceosome and inhibits the splicing reaction. SM and EBER1 from Epstein–Barr virus and ICP27 from herpes-simplex virus 1 interact with splicing factors, and ICP27 is also able to interact with kinases that phosphorylate splicing factors. In the case of ICP27 which appears at numerous places in this figure, the mechanism of action sufficient to trigger a change in cellular AS is still not clear

**TABLE 2** Viral proteins involved in modulating the splicing machinery

Viral determinant	Virus	Family	Genome	Mechanism	Cellular genes with alternative splicing modification	References
<b>ICP27</b>	HSV-I	Herpesviridae	dsDNA	Redistribution of snRNP Interaction with SRSF2, SRSF3 ICP27 interaction with SF3B2 Interaction with SRPK1 leading to hypophosphorylation of SR proteins	–	Hardy and Sandri-Goldin (1994); Lindberg and Kreivi (2002); Phelan, Carmo-Fonseca, McLaughlan, Lamond, and Clements (1993); Sandri-Goldin, Hibbard, and Hardwicke (1995); Bryant, Wadd, Lamond, Silverstein, and Clements (2001); Sciabica (2003)
	HSV-II			Direct interaction of ICP27 with PML pre-mRNA	PML	Nojima et al. (2009)
	Herpesvirus saimiri			Redistribution of SRSF2	–	Cooper et al. (1999)
	Marek's disease virus			Interaction with SR proteins	chTERT	Amor et al. (2011)
<b>ORF57</b>	KSHV	Herpesviridae	dsDNA	Interaction with spliceosomal snRNP	–	Majerciak et al. (2008)
<b>SM</b>	Epstein–Barr virus	Herpesviridae	dsDNA	SM interaction with STAT1 pre-mRNA; displacement of SRSF1 and recruitment of SRSF3	STAT1	Verma and Swaminathan (2008), Verma, Bais, Gaillard, and Swaminathan (2010)
<b>EBER1</b>	Epstein–Barr virus	Herpesviridae	dsDNA	Interaction with AUF1/hnRNP D	–	Lee, Pimienta, and Steitz (2012)
<b>NS5</b>	Dengue virus	Flaviviridae	(+)ssRNA	NS5 interaction with CD2BP2 and DDX23 from the U5 snRNP particle	ZNF35, CASP8, MXA, etc.	Maio et al. (2016)
<b>3D<sup>POL</sup></b>	EV71	Picornaviridae	(+)ssRNA	3D <sup>POL</sup> interacts with Prp8 to block the second catalytic step of the splicing reaction	PIP85a, $\beta$ -globin, NCL	Liu et al. (2014)
<b>NS1A</b>	IAV	Orthomyxoviridae	(–)ssRNA	Binding to U6 snRNP, thus blocking the U6-U4 interaction. SRSF2 relocalization in the nucleus Interaction with UAP56	TP53	Fortes, Beloso, and Ortín (1994); Fortes, Lamond, and Ortín (1995); Lu, Qian, and Krug (1994); Qiu, Nemeroff, and Krug (1995); Chiba, Hill-Batorski, Neumann, and Kawaoka (2018); Dubois et al. (2019)
<b>2A<sup>pro</sup></b>	Poliovirus	Picornaviridae	(+)ssRNA	2A <sup>pro</sup> blocks the second catalytic step of the splicing reaction	FAS, FGFR2 and MINX	Álvarez, Castelló, Carrasco, and Izquierdo (2011)
<b>Vpr</b>	HIV	Retroviridae	ssRNA-RT	Vpr interaction with SF3B2 which block SF3B2-SF3B4 interaction	–	Kuramitsu et al. (2005); Hashizume et al. (2007)

with SF3B2, an essential pre-mRNA splicing factor, through its C-terminal region (Bryant et al., 2001). In contrast, another study showed that ICP27 interacts with SR proteins such as SRSF3 and decreases their phosphorylation status (Sciabica, 2003). This under-phosphorylation of SR proteins necessitates the ICP27 interaction with the SR protein kinase 1 (SRPK1), leading to its relocalization to the nucleus, and was shown to be sufficient to inhibit splicing. Caution must be taken regarding these results, as the experiments conducted to investigate the modulation of splicing were solely *in vitro* splicing experiments that might not completely recapitulate the complexity of the regulation *in cellulo*. To this date, the precise molecular determinants of ICP27 inhibition of splicing are still not precise, although the protein has been the subject of multiple reviews (Sandri-Goldin, 1994; Sandri-Goldin, 1998, 2008; Smith, Malik, & Clements, 2005). Many ICP27 homologs share biological features reminiscent of ICP27. In herpes simplex virus type 2 (HSV-2), ICP27 changes the AS of the promyelocytic leukemia (*PML*) gene by inducing the retention of the intron 7a in the pre-mRNA, leading to a switch from isoform PML-II to PML-V (Nojima et al., 2009). Interestingly, PML-II favors viral replication as opposed to PML-V which limits viral replication, suggesting that ICP27 might modulate cellular AS to restrict viral replication. In Marek's disease virus (MDV-1), ICP27 interacts with SR proteins and inhibits the splicing of the *chTERT* gene (Amor et al., 2011). Finally, the ORF57 of the Kaposi's Sarcoma-Associated Herpesvirus (KSHV) encodes a homolog of ICP27 which colocalizes with SRSF2 in nuclear speckles and interacts with the five spliceosomal snRNPs (U1, U2, U4, U5, and U6); this interaction might be indirect, as ORF57 seems to interact with nascent RNA, and RNase treatments were not performed in the ORF57 pulldowns (Majerciak et al., 2008).

### 3.2 | SM

The SM protein from EBV is a nuclear protein essential for EBV lytic replication through its RNA-binding activity, allowing enhanced EBV gene expression by increasing EBV transcripts stability and nuclear export. It is a homolog of the previously discussed ICP27. Moreover, it also acts as a splicing factor on cellular transcripts through direct interaction, leading to the displacement of SRSF1 from the pre-mRNA and the recruitment of SRSF3. This activity impacts the splicing of *STAT1*, for which SM favors a novel STAT1 $\beta$  isoform producing a protein acting as a dominant negative of the canonical STAT1 $\alpha$  (Verma et al., 2010; Verma & Swaminathan, 2008). Because STAT1 has a vital role in the IFN signal transduction pathway, this modulation of *STAT1* splicing is presumed to impact the antiviral response, although it was not experimentally verified. The splicing of *STAT1* was the only example of SM-mediated change in cellular AS.

### 3.3 | EBER1

As previously discussed, the expression of EBER1 and EBER2 from EBV in cells lead to significant changes in the expression and the splicing of cellular genes (Pimienta et al., 2015, p. 1). Although the molecular mechanism for EBER2 is not known, evidence for EBER1 points towards its capacity to interact mainly with the p40 isoform of the AUF1/hnRNP D splicing factor (Lee et al., 2012). Nevertheless, no study directly looked at the ability of EBER1 alone to modulate cellular AS nor the involvement of AUF1/hnRNP D in this probable modulation of AS.

### 3.4 | NS5

For the *Flaviviridae* family, the NS5 protein harbors the catalytic sites of RdRp, guanylyltransferase, and methyltransferase, allowing the production of fully-capped mRNA during replication. Moreover, it is the only one of two proteins possessing enzymatic activity for this family of viruses, the other one being NS3 (Brand, Bisailon, & Geiss, 2017). Recently, in an extensive study, it was demonstrated that NS5 from DV interacts with core components of the spliceosome, more precisely CD2BP2 and DDX23 from the U5 snRNP particle (Maio et al., 2016). This interaction led to a modulation of the splicing of cellular genes such as *ZNF35*, *CASP8*, and *MXA*. In the context of viral infection, increased intron retention was demonstrated during DV infection in cells and silencing specific U5 component also improved viral replication. The authors hypothesized that hijacking of the spliceosome by NS5 could allow a more favorable cellular environment for viral replication.

### 3.5 | 3D<sup>POL</sup>

As described for DV, the RdRp from picornavirus, more precisely Enterovirus 71 (EV71), is also able to localize to the nucleus. Once in the nucleus, it interacts with Prp8, one of the main components of the spliceosome, leading to the

accumulation of the lariat form of the splicing intermediate due to a blockade of the second catalytic step (Liu et al., 2014). Genes that have their splicing modulated belongs to cell growth, proliferation, and differentiation pathways. It is interesting to underline that as previously discussed, persistently infected cells with another member of the *picornaviridae* family, MFDV, display AS modulation (Han et al., 2018). It will be interesting to know if the RdRp from MFDV is involved in those changes. Another mechanism involving the cleavage of Sam68 will be discussed in Section 4.1.

### 3.6 | NS1

The NS1 protein from IAV is a crucial multifunctional protein for viral replication that suppresses the innate antiviral response. Moreover, NS1 is also a potent inhibitor of splicing. NS1 interacts with the spliceosome through its RNA-binding domain, with the consequence of inhibiting the catalytic steps required for adequate splicing (Fortes et al., 1994; Lu et al., 1994). It was later shown that NS1 binds to specific regions of U6 snRNA. This binding blocks the interaction of U6 to both U2 and U4 snRNP and thus explains the inhibition of splicing (Qiu et al., 1995). These findings are somewhat surprising, as IAV necessitate the host splicing machinery to splice some of its RNA, notably the M1 segment coding for NS1. However, the M1 gene segment is still spliced in presence of NS1 despite the blockade on splicing, which suggests that the inhibition in splicing is specific for cellular RNA; further studies are required to confirm this and explain the observed phenomenon (Fortes et al., 1994; Lu et al., 1994). NS1 expression also changes the nuclear localization pattern of splicing factor SRSF2, both in the context of ectopic expression and of viral infection (Fortes et al., 1995). Recently, mass spectrometry analysis of protein–protein interaction of NS1 from both strains H1N1 and H7N9 showed enrichment in interacting partners involved in mRNA splicing and RNA processing (Kuo et al., 2018, 2016). Interestingly, the two proteins did not interact with the same cellular partners, which suggests that there might exist species-specific modulation of AS, or that the identified proteins are the result of artificial noise from the experimental design. Moreover, it was also shown that NS1 interacts with UAP56, an helicase involved in pre-mRNA splicing; the impact of this interaction is still not known (Chiba et al., 2018). As previously discussed, IAV-infected cells present modulation in their AS, which make the NS1 protein an interesting model to study viral modulation of AS (Thompson et al., 2018). Finally, it was recently demonstrated that NS1 modulates the splicing of TP53 towards  $\beta$  and  $\gamma$  isoforms, which are pro-viral factors in IAV infection (Dubois et al., 2019).

### 3.7 | 2A<sup>PRO</sup>

Poliovirus genome produces a single transcript that is translated into a long polyprotein that is processed by viral protease 2A<sup>PRO</sup> and 3C<sup>PRO</sup>. Moreover, those proteins also cleave cellular proteins, leading to their degradation in infected cells. Surprisingly, the 2A<sup>PRO</sup> protease is also an inhibitor of splicing, which was demonstrated for the *FAS*, *FGFR2* and *MINX* genes (Álvarez et al., 2011). Since *in vitro* splicing assay of the *MINX* gene showed accumulation of the first exon and the lariat product containing the unspliced second exon, it was concluded that 2A<sup>PRO</sup> blocks the second catalytic step of the splicing reaction. Again, caution must be taken regarding *in vitro* experiments, as their results cannot be directly transferred *in cellulo*.

### 3.8 | Vpr

Vpr, a small 96 amino acid protein from HIV-1, was shown to inhibit the splicing reaction both *in vitro* and *in cellulo* (Kuramitsu et al., 2005). Later studies proved that this inhibition is dependent on the interaction with SF3B2, which blocks the essential interaction of SF3B2 with SF3B4 (Hashizume et al., 2007). Nonetheless, these results are difficult to reconcile with the biology of HIV replication, as this virus needs the cellular machinery to splice its RNA. Still, the authors have shown that some introns were not affected by this inhibition. If Vpr can mediate a blockade of splicing only on cellular RNA, as it might be the case for NS1, then further studies should eventually explain how this cellular-specific blockade is possible.

## 4 | MODULATION OF SPLICING FACTORS LOCALIZATION, LEVELS AND POST-TRANSLATIONAL MODIFICATIONS BY VIRUSES

Other mechanisms can be at play during viral infections that do not necessitate direct interaction with the cellular splicing machinery but can also have an impact on cellular splicing. Cellular localization, post-translational modifications, and levels of splicing factors can all affect the outcome of the splicing reaction (David & Manley, 2010; Shin & Manley, 2004; Twyffels, Gueydan, & Krays, 2011). This strongly suggests that viruses could modulate cellular AS through these indirect mechanisms,

**TABLE 3** List of viruses having a potential indirect effect on alternative splicing

Virus	Family	Genome	Splicing factors impacted	References
<b>Modulation of splicing factor localization</b>				
<b>EBV</b>	<i>Herpesviridae</i>	dsDNA	SRSF2, SRSF3, SON	Park and Miller (2018)
<b>Vesicular stomatitis virus</b>	<i>Rhabdoviridae</i>	(-)ssRNA	hnRNP A1, K and C1/C2 hnRNP M	Kneller, Connor, and Lyles (2009) Redondo, Madan, Alvarez, and Carrasco (2015)
<b>Poliovirus</b>	<i>Picornaviridae</i>	(+)ssRNA	HuR, TIA1/TIAR SRSF3 hnRNP M	Álvarez, Castelló, Carrasco, and Izquierdo (2013) Fitzgerald, Chase, Cathcart, Tran, and Semler (2013) Jagdeo et al. (2015)
<b>Coxsackievirus B3</b>	<i>Picornaviridae</i>	(+)ssRNA	SRSF3 hnRNP M	Fitzgerald et al. (2013) Jagdeo et al. (2015)
<b>Rhinovirus</b>	<i>Picornaviridae</i>	(+)ssRNA	SFPQ	Flather, Nguyen, Semler, and Gershon (2018)
<b>Sindbis virus</b>	<i>Togaviridae</i>	(+)ssRNA	HuR, hnRNP K	Barnhart, Moon, Emch, Wilusz, and Wilusz (2013)
<b>HIV</b>	<i>Retroviridae</i>	ssRNA-RT	hnRNP A1	Monette, Ajamian, López-Lastra, and Mouland (2009)
<b>Junin/DV</b>	<i>Flaviviridae</i>	(+)ssRNA	hnRNP A2, K	Brunetti, Scolaro, and Castilla (2015)
<b>MFDV</b>	<i>Picornaviridae</i>	(+)ssRNA	Sam68	Lawrence, Schafer, and Rieder (2012)
<b>HCV</b>	<i>Flaviviridae</i>	(+)ssRNA	HuR	Shwetha et al. (2015)
<b>Rotavirus</b>	<i>Reoviridae</i>	dsRNA	HuR, hnRNP C1	Dhillon et al. (2018)
<b>Modulation of splicing factor levels</b>				
<b>HCMV</b>	<i>Herpesviridae</i>	dsDNA	CstF-64, PTB	Adair, Liebisch, Su, and Colberg-Poley (2004)
<b>HPV</b>	<i>Papillomaviridae</i>	dsDNA	SRSF1, SRSF2, SRSF3, SRSF4	Klymenko, Hernandez-Lopez, MacDonald, Bodily, and Graham (2016), McPhillips et al. (2004); Mole et al. (2009); Mole, Milligan, and Graham (2009)
<b>HIV</b>	<i>Retroviridae</i>	ssRNA-RT	SRSF2, hnRNP A/B, hnRNP H SR proteins	Dowling et al. (2008) Fukuhara et al. (2006)
<b>Modulation of splicing factor post-translational modifications</b>				
<b>HSV-1</b>	<i>Herpesviridae</i>	dsDNA	SRSF3, SRSF5 (hyperphosphorylated)	Sciabica (2003)
<b>Adenovirus</b>	<i>Adenoviridae</i>	dsDNA	SR proteins (hypophosphorylated)	Kanopka et al. (1998)
<b>Vaccinia virus</b>	<i>Poxviridae</i>	dsDNA	SR proteins (hypophosphorylated)	Huang, Nilsson, Punga, and Akusjärvi (2002)
<b>HIV-1</b>	<i>Retroviridae</i>	ssRNA-RT	SRSF2 (hyperphosphorylated)	Kadri et al. (2015)
<b>Sindbis virus</b>	<i>Togaviridae</i>	(+)ssRNA	HuR (hypophosphorylated)	Dickson et al. (2012)

and the following section will look further into the known examples for each of these mechanisms. An overview of viruses and splicing factors discussed is available in Table 3.

#### 4.1 | Modulation of splicing factors localization

Several viruses modulate the localization of splicing factors during infection. For example, vesicular stomatitis virus (VSV) infection leads to cytoplasmic accumulation of hnRNP A1, hnRNP K, and hnRNP C1/C2 through a mechanism that is dependent on the mRNA export factor RAE1 (Kneller et al., 2009). A study suggested that the Vesicular stomatitis virus M proteins are involved in this relocalization, at least for the splicing factor hnRNP H (Redondo et al., 2015). Moreover, the poliovirus



2A<sup>pro</sup>, besides being an inhibitor of splicing as seen in the previous section, also induces a selective nucleo-cytoplasmic translocation of the splicing factors and RNA-binding proteins HuR and TIA1/TIAR (Álvarez et al., 2013). This redistribution leads to the modulation of the splicing of the exon 6 of the *FAS* gene. SRSF3 and hnRNP M localization were also shown to be impacted by infection from *Picornaviridae* (Fitzgerald et al., 2013; Jagdeo et al., 2015). Recently, an MS-based approach was used to look broadly at proteins re-equilibrating from the nucleus to the cytoplasm during infection with a rhinovirus, which is another member of the *Picornaviridae* family (Flather et al., 2018). This study identified SFPQ, a splicing factor, as a pro-viral factor that is relocalized to the cytoplasm following cleavage by the viral proteinase 3CD/3C. Furthermore, Sindbis virus also induces the relocalization of HuR and hnRNP K from the nucleus to the cytoplasm of infected cells (Barnhart et al., 2013; Burnham, Gong, & Hardy, 2007; Dickson et al., 2012). Interestingly, the mechanism for HuR depends on the viral RNAs, which contains HuR binding-site in their 3' UTR, and the phosphorylation of HuR (discussed in Section 4.3). This relocalization also induces changes in the splicing of known targets of HuR, such as *PCBP2* and *DST*. HuR seems to be a target of choice for viruses to affect relocalization, as HCV and rotavirus (later discussed) also induce its accumulation in the cytoplasm (Dhillon et al., 2018; Shwetha et al., 2015). More examples of splicing factors relocalization during viral infection have been described, such as hnRNP A1 during HIV infection (Monette et al., 2009), hnRNP A2 and hnRNP K during DV and Junin virus infection (Brunetti et al., 2015), and Sam68 during MFDV infection (Lawrence et al., 2012). Finally, many viruses rely heavily on replication structure built by viral proteins for their replication cycle. In the case of rotavirus, a segmented dsRNA virus solely replicating in the cytoplasm, these structures are named viroplasm and have been shown to sequester hnRNPs and AU-rich element-binding proteins (ARE-BPs) independently of RNA (Dhillon et al., 2018). The proteins sequestered, such as HuR and hnRNP C1, act as positive or negative regulator in viral progeny production. During lytic EBV infection, novel nodular structures composed of viral and cellular RNA splicing and export factors, termed VINORCs (for virus-induced nodular structures), were recently discovered and were shown to colocalize with splicing factors such as SRSF2, SRSF3, SON, and NXF1 (Park & Miller, 2018). These examples underline the capacity of viruses to modulate AS by changing the cellular localization of splicing factors, and in cases where cellular splicing was not analyzed, suggest an impact at this level in the host cell. It also stresses the crucial importance not only to look at the cellular localization of splicing factors but also to monitor the impact of this localization (or relocalization) on cellular AS.

## 4.2 | Modulation of splicing factors levels

Viral infections also trigger massive changes in the gene expression program of infected cells, and several viruses have been shown to modulate the levels of expression of splicing factors. For example, HCMV infection increases the expression of the cleavage stimulation factor 64 (CstF-64) and PTB (Adair et al., 2004). Moreover, in the case of HIV, macrophages are an important viral reservoir, and it was found that HIV infection leads to an upregulation of the SR protein SRSF2 and a down-regulation of hnRNP A/B and hnRNP H in the macrophages during the first weeks of infection. Around the peak of virus production, the trend is inverted: the level of SRSF2 decreases and the level hnRNP A/B and hnRNP H increases (Dowling et al., 2008). HIV infection of HEK293 cells also decreases the overall level/activity of SR proteins (Fukuhara et al., 2006). HPV replication is heavily dependent on the expression of some specific splicing factors, such as SRSF2 and SRSF3, at different times during infection. It appears that the virus has evolved to modulate the expression of these proteins (Klymenko et al., 2016; McPhillips et al., 2004; Mole, McFarlane, et al., 2009; Mole, Milligan, & Graham, 2009); this subject was reviewed extensively (Klymenko & Graham, 2012; McFarlane & Graham, 2010; Mole, Veerapraditsin, McPhillips, & Graham, 2006). Lastly, it was demonstrated that reovirus infection leads to transcriptional changes in the expression levels of splicing factors, with ESRP1 which has an epithelium-specific role being the most overexpressed following infection (Boudreault et al., 2016). Although the impact on cellular AS may be limited, these studies underline that viruses can alter the expression levels of splicing factors throughout infection.

## 4.3 | Modulation of splicing factors post-translational modifications

Post-translational modifications, such as phosphorylation, have been known to influence the activity of splicing factors. Various studies have demonstrated that viral infection can also induce changes in the post-translational modification profiles of splicing factors. For example, SR proteins from adenovirus-infected cells are hypophosphorylated, which renders them inactive as enhancers or splicing repressors. This dephosphorylation requires the interaction of the adenovirus protein E4-ORF4 with the protein phosphatase 2A (PP2A) and impacts SRSF1, SRSF2, SRSF4, SRSF5, and SRSF6 (Kanopka et al., 1998). Moreover, E4-ORF4 also interacts directly with SRSF2 and SRSF9, mainly with the hyperphosphorylated forms (Nilsson et al., 2001). The same group observed a similar hypophosphorylation and inactivation of SR proteins in vaccinia virus-

infected cells, with possible involvement of the viral dual-specificity protein phosphatase VH1 (Huang et al., 2002). Interestingly, the extent of dephosphorylation was greater in vaccinia infection than in adenovirus infection, which seems to correlate with the absence of introns in vaccinia genes compared to adenoviral genes. In this case, as seen before with the studies on the expression of splicing factors during infection, the biological impact on cellular AS was not assessed. The HIV-1 Tat protein was shown to modulate *Tau* AS, by upregulating DYRK1A kinase which leads to increased phosphorylated SRSF2 (Kadri et al., 2015). As previously discussed, infection with Sindbis virus causes relocalization of HuR to the cytoplasm; this relocalization is dependent on the dephosphorylation of the protein (Dickson et al., 2012). Moreover, ICP27 also interacts with SRPK1, leading to hypophosphorylation of splicing factors (Sciabica, 2003). A similar activity was demonstrated for the HPV protein E1 E4 (Prescott et al., 2014). Although only Tat was shown to influence cellular AS, acting on the phosphorylation level of splicing factors is another exciting mechanism by which viruses could potentially modulate the cellular splicing machinery.

## 5 | BIOLOGICAL RELEVANCE OF CELLULAR AS MODULATION

Upon viral infection, a tug of war between the virus and the cell is triggered with the ultimate consequence of allowing or restricting viral replication. On the one hand, viruses try to hijack essential cellular components such as DNA polymerases and ribosomes, to replicate and block the innate immune response triggered by the IFN pathway. On the other hand, the cells try to mount an effective antiviral response and limit virus replication, for example by shutting down translation. During viral infection, modulation of cellular AS could be directly caused by viral proteins or RNA, and/or could be triggered by the cell as a self-defense mechanism to counteract the virus. Moreover, this response could also be driven through the IFN pathway and could be triggered in non-infected cells by soluble antiviral factors to prime these cells before viral infection. To this date, the functional importance of viral modulation of AS during viral infection is still not evident. However, the examples of NS5A from DV, 3D<sup>pol</sup> from EV71, and 2A<sup>pro</sup> from poliovirus seem to point towards viruses being able to modulate cellular

**TABLE 4** List of viruses that modulate cellular AS with a known mechanism, and the cellular genes impacted

Virus	Family	Genome	Cellular genes with alternative splicing modification	Mechanism of modulation/determinant	References
Herpes-simplex virus II	<i>Herpesviridae</i>	dsDNA	PML	ICP27	Nojima et al. (2009)
Marek's disease virus	<i>Herpesviridae</i>	dsDNA	chTERT	Probable interaction of ICP27 with SRSF3	Amor et al. (2011)
Epstein-Barr virus	<i>Herpesviridae</i>	dsDNA	STAT1	SM protein displaces SRSF1 from pre-mRNA and recruits SRSF3	Verma et al. (2008) Verma et al. (2010)
Human cytomegalovirus	<i>Herpesviridae</i>	dsDNA	CAST, MYO18A	Overexpression of CPEB1 following infection	Batra et al. (2016)
Sindbis virus	<i>Togaviridae</i>	(+)ssRNA	PCBP2 DST	Viral RNAs containing HuR binding-site in their 3' UTR induces the relocalization of HuR to the cytoplasm	Barnhart et al. (2013)
Dengue virus	<i>Flaviviridae</i>	(+)ssRNA	ZNF35, CASP8, MXA, etc.	NS5 interacts with CD2BP2 and DDX23 from the U5 snRNP particle	Maio et al. (2016)
EV71	<i>Picornaviridae</i>	(+)ssRNA	PIP85a, $\beta$ -globin, NCL	3D <sup>pol</sup> interacts with Prp8 to block the second catalytic step of the splicing reaction	Liu et al. (2014)
Poliovirus	<i>Picornaviridae</i>	(+)ssRNA	FAS, FGFR2 and MINX	2A <sup>pro</sup> blocks the second catalytic step of the splicing reaction.	Álvarez et al. (2011)
			FAS	2A <sup>pro</sup> induces a selective nucleo-cytoplasmic translocation of HuR and TIA1/TIAR	Álvarez et al. (2013)
Influenza virus A	<i>Orthomyxoviridae</i>	(-)ssRNA	TP53	Interaction of NS1 with CPSF4	Dubois et al. (2019)

AS directly, probably as ways to favor their replication (Table 4) (Álvarez et al., 2011, 2013; Liu et al., 2014; Maio et al., 2016). Interestingly, splicing factors often act as host factors enhancing or restricting viral replication, underlining their important role in virus biology. For example, hnRNP C1/C2 during DV infection (Dechtawewat et al., 2015), hnRNP K during DV/Junin virus infections (Brunetti et al., 2015), hnRNP D during West Nile virus infection (Friedrich et al., 2014), hnRNP M during picornaviruses infections (Jagdeo et al., 2015), SART1 and HuR during HCV infection (Lin et al., 2015, p. 1; Shwetha et al., 2015; Zhao et al., 2012), PRP19 during IAV H1N1 infection (Kuo et al., 2016, p. 19) and Sam68 during FMDV infection (Lawrence et al., 2012, p. 68) all acts as positive regulators of viral replication. The opposite effect can also be seen, as in the context of reovirus replication, gene silencing of SRSF2, an important splicing factor that interacts with the reovirus protein  $\mu 2$ , enhances the replication of this virus (Rivera-Serrano et al., 2017). However, the involvement of splicing factors in virus replication does not necessarily indicate that AS modulation of the host cell transcriptome directly stimulates or inhibits viral replication, and further studies will help our understanding of this potential dual role of splicing factors. Nevertheless, infection of cells with HSV-1 favors a spliced variant of MxA, a potent antiviral factor, that enhances HSV-1 replication instead of limiting it, and this is perhaps the best evidence of a virus benefiting from modulating cellular AS (Ku et al., 2011). The potential of abrogating the IFN response and IFN-stimulated effector through AS is important and could serve as another mechanism for viruses to evade the antiviral state triggered by infection (Chauhan, Kalam, Dutt, & Kumar, 2019). Still, a study that looked at both the expression and AS following infection revealed that alterations in AS are not happening preferentially in overexpressed genes, which are usually ISG linked to the cellular antiviral state (Boudreault et al., 2016). In a study about new therapies directed against HIV-1 and respiratory syncytial virus, specific inhibition using a morpholino oligonucleotide against the long isoform of the molecular chaperone MRJ leads to a decreased replication of these two viruses (Ko et al., 2019). Another biological relevant example for virus–host interaction is ICP27 of HSV-2, as previously discussed; the expression of this protein leads to a switch from a PML isoform favoring viral replication to one which is limiting the replication of HSV-2 (Nojima et al., 2009). Although minimal, examples about MxA, MRJ, and PML point towards a potential direct benefit for viruses to modulate the AS landscape of the host cell to better replicate, or to limit their replication under a certain threshold. It is also noteworthy to underline that transcriptomic studies reveal the global portrait of the RNA splicing landscape of the host cell independently of the cause of these changes, and the possibility that the cell could trigger AS change to defend itself should still be considered. In fact, it is highly possible that transcriptomic studies describe modulations that are caused both by viruses and the host cell. Lastly, it is important to remember that if the modulation of cellular AS presents an advantage for viruses, infected cells might have evolved a countermeasure to restrict this mechanism, which emphasizes the complexity of adequately mapping the specific cellular and viral determinants of these changes in the context of virus–host interaction.

The state of knowledge is still too sparse to identify common cellular mRNA targets which have their AS modulated by numerous viruses. Nonetheless, a common theme is starting to emerge in which cellular genes involved in mRNA processing, including genes linked to mRNA maturation, degradation, and notably, splicing appear to have changes in AS following viral infection (Boudreault et al., 2016; Fabozzi et al., 2018; Han et al., 2018; Hu et al., 2017, 2016; Rivera-Serrano et al., 2017). Whether this indeed constitutes a targeted modulation of AS still remains to be established. Nonetheless, an attractive hypothesis would be that viruses could preferentially target the AS of genes involved in splicing, which would ultimately lead to abnormal mRNA isoform expression for those genes. This would further dysregulate cellular splicing by altering the normal balance of protein isoforms, changing their finely regulated activity and disturbing the splicing machinery.

## 6 | CONCLUSIONS AND PERSPECTIVES

The advent of affordable high throughput sequencing techniques has allowed scientists to delve deeply into the transcriptomic changes happening during virus–host interactions. These studies, combined with mechanistic ones, have allowed the discovery and characterization of AS changes following viral infections in different contexts. Although this field of study is still relatively recent, the accumulating evidence point towards widespread changes in cellular AS following infections by viruses. A better understanding of how and why viruses modulate cellular AS will surely help to gain a better global understanding of virus–host interaction and the role of cellular AS in this interplay. Recently, it was shown that the splicing factor SRSF2 limits HSV-1 oncolysis in breast cancer cells, and it also negatively regulates the replication of other promising oncolytic viruses such as reovirus (Rivera-Serrano et al., 2017; Workenhe, Ketela, Moffat, Cuddington, & Mossman, 2015). Understanding of the role of cellular AS in viral replication could thus help the design of better oncolytic viruses exploiting the dysregulated AS landscape typical of cancer cells (David & Manley, 2010). Moreover, as previously discussed, numerous splicing factors are involved in viral replication, either as positive or negative factors. Potential new antiviral drugs targeting host cell splicing

factors have emerged, and a better understanding of the role of cellular AS could help the design of more potent or safer anti-virals (Fukuhara et al., 2006; Shkreta et al., 2017). All these fields will benefit from a better understanding of the role of cellular AS modification during viral infection, a phenomenon we have only just begun to investigate.

## ACKNOWLEDGMENTS

This work was supported by a Vanier Canada graduate scholarship from the Canadian Institutes of Health Research (CIHR) to S.B., a grant from the Natural Sciences and Engineering Research Council of Canada (RGPIN/03736–2017) to G.L. and (RGPIN-2016-03916) to M.B.

## CONFLICT OF INTEREST

The authors have declared no conflicts of interest for this article.

## RELATED WIREs ARTICLE

[Unconventional RNA-binding proteins step into the virus–host battlefield](#)

## ORCID

Martin Bisailleon  <https://orcid.org/0000-0001-7822-0933>

## FURTHER READING

- Damania, P., Sen, B., Dar, S. B., Kumar, S., Kumari, A., Gupta, E., ... Venugopal, S. K. (2014). Hepatitis B virus induces cell proliferation via HBx-induced microRNA-21 in hepatocellular carcinoma by targeting programmed cell death protein4 (PDCD4) and phosphatase and tensin homologue (PTEN). *PLoS One*, *9*(3), e91745. <https://doi.org/10.1371/journal.pone.0091745>
- Meyer, F. (2016). Viral interactions with components of the splicing machinery. *Progress in Molecular Biology and Translational Science*, *142*, 241–268.
- Prakash, O., Swamy, O. R., Peng, X., Tang, Z.-Y., Li, L., Larson, J. E., ... Samaniego, F. (2005). Activation of Src kinase Lyn by the Kaposi sarcoma-associated herpesvirus K1 protein: Implications for lymphomagenesis. *Blood*, *105*(10), 3987–3994. <https://doi.org/10.1182/blood-2004-07-2781>
- Sekimoto, T., & Yoneda, Y. (2012). Intrinsic and extrinsic negative regulators of nuclear protein transport processes. *Genes to Cells*, *17*(7), 525–535. <https://doi.org/10.1111/j.1365-2443.2012.01609.x>

## REFERENCES

- Adair, R., Liebisch, G. W., Su, Y., & Colberg-Poley, A. M. (2004). Alteration of cellular RNA splicing and polyadenylation machineries during productive human cytomegalovirus infection. *Journal of General Virology*, *85*(12), 3541–3553. <https://doi.org/10.1099/vir.0.80450-0>
- Álvarez, E., Castelló, A., Carrasco, L., & Izquierdo, J. M. (2011). Alternative splicing, a new target to block cellular gene expression by poliovirus 2A protease. *Biochemical and Biophysical Research Communications*, *414*(1), 142–147. <https://doi.org/10.1016/j.bbrc.2011.09.040>
- Álvarez, E., Castelló, A., Carrasco, L., & Izquierdo, J. M. (2013). Poliovirus 2A protease triggers a selective nucleo-cytoplasmic redistribution of splicing factors to regulate alternative pre-mRNA splicing. *PLoS One*, *8*(9), e73723. <https://doi.org/10.1371/journal.pone.0073723>
- Amor, S., Strassheim, S., Dambrine, G., Remy, S., Rasschaert, D., & Laurent, S. (2011). ICP27 protein of Marek's disease virus interacts with SR proteins and inhibits the splicing of cellular telomerase chTERT and viral vIL8 transcripts. *Journal of General Virology*, *92*(6), 1273–1278. <https://doi.org/10.1099/vir.0.028969-0>
- Armero, V. E. S., Tremblay, M.-P., Allaire, A., Boudreault, S., Martenon-Brodeur, C., Duval, C., ... Bisailleon, M. (2017). Transcriptome-wide analysis of alternative RNA splicing events in Epstein-Barr virus-associated gastric carcinomas. *PLoS One*, *12*(5), e0176880. <https://doi.org/10.1371/journal.pone.0176880>
- Ashraf, U., Benoit-Pilven, C., Lacroix, V., Navratil, V., & Naffakh, N. (2019). Advances in analyzing virus-induced alterations of host cell splicing. *Trends in Microbiology*, *27*(3), 268–281. <https://doi.org/10.1016/j.tim.2018.11.004>
- Barnhart, M. D., Moon, S. L., Emch, A. W., Wilusz, C. J., & Wilusz, J. (2013). Changes in cellular mRNA stability, splicing, and polyadenylation through HuR protein sequestration by a cytoplasmic RNA virus. *Cell Reports*, *5*(4), 909–917. <https://doi.org/10.1016/j.celrep.2013.10.012>
- Batra, R., Stark, T. J., Clark, E., Belzile, J.-P., Wheeler, E. C., Yee, B. A., ... Yeo, G. W. (2016). RNA-binding protein CPEB1 remodels host and viral RNA landscapes. *Nature Structural & Molecular Biology*, *23*(12), 1101–1110. <https://doi.org/10.1038/nsmb.3310>

- Berget, S. M., Moore, C., & Sharp, P. A. (1977). Spliced segments at the 5' terminus of adenovirus 2 late mRNA. *Proceedings of the National Academy of Sciences of the United States of America*, 74(8), 3171–3175.
- Boudreau, S., Armero, V. E. S., Scott, M. S., Perreault, J.-P., & Bisaille, M. (2019). The Epstein-Barr virus EBNA1 protein modulates the alternative splicing of cellular genes. *Virology Journal*, 16(1), 29. <https://doi.org/10.1186/s12985-019-1137-5>
- Boudreau, S., Martenon-Brodeur, C., Caron, M., Garant, J.-M., Tremblay, M.-P., Armero, V. E. S., ... Bisaille, M. (2016). Global profiling of the cellular alternative RNA splicing landscape during virus-host interactions. *PLoS One*, 11(9), e0161914. <https://doi.org/10.1371/journal.pone.0161914>
- Brand, C., Bisaille, M., & Geiss, B. J. (2017). Organization of the Flavivirus RNA replicase complex. *WIREs RNA*, 8(6). <https://doi.org/10.1002/wrna.1437>
- Brentano, L., Noah, D. L., Brown, E. G., & Sherry, B. (1998). The Reovirus protein  $\mu 2$ , encoded by the M1 gene, is an RNA-binding protein. *Journal of Virology*, 72(10), 8354–8357.
- Brunetti, J. E., Scolaro, L. A., & Castilla, V. (2015). The heterogeneous nuclear ribonucleoprotein K (hnRNP K) is a host factor required for dengue virus and Junin virus multiplication. *Virus Research*, 203, 84–91. <https://doi.org/10.1016/j.virusres.2015.04.001>
- Bryant, H. E., Wadd, S. E., Lamond, A. I., Silverstein, S. J., & Clements, J. B. (2001). Herpes simplex virus IE63 (ICP27) protein interacts with spliceosome-associated protein 145 and inhibits splicing prior to the first catalytic step. *Journal of Virology*, 75(9), 4376–4385. <https://doi.org/10.1128/JVI.75.9.4376-4385.2001>
- Buckley, P. T., Khaladkar, M., Kim, J., & Eberwine, J. (2014). Cytoplasmic intron retention, function, splicing, and the sentinel RNA hypothesis. *WIREs RNA*, 5(2), 223–230. <https://doi.org/10.1002/wrna.1203>
- Burnham, A. J., Gong, L., & Hardy, R. W. (2007). Heterogeneous nuclear ribonucleoprotein K interacts with Sindbis virus nonstructural proteins and viral subgenomic mRNA. *Virology*, 367(1), 212–221. <https://doi.org/10.1016/j.virol.2007.05.008>
- Cesana, D., Sgualdino, J., Rudilosso, L., Merella, S., Naldini, L., & Montini, E. (2012). Whole transcriptome characterization of aberrant splicing events induced by lentiviral vector integrations. *The Journal of Clinical Investigation*, 122(5), 1667–1676. <https://doi.org/10.1172/JCI62189>
- Chauhan, K., Kalam, H., Dutt, R., & Kumar, D. (2019). RNA splicing: A new paradigm in host-pathogen interactions. *Journal of Molecular Biology*, 431, 1565–1575. <https://doi.org/10.1016/j.jmb.2019.03.001>
- Chiba, S., Hill-Batorski, L., Neumann, G., & Kawaoka, Y. (2018). The cellular DEXD/H-box RNA helicase UAP56 co-localizes with the influenza A virus NS1 protein. *Frontiers in Microbiology*, 9. <https://doi.org/10.3389/fmicb.2018.02192>
- Chow, L. T., Gelinis, R. E., Broker, T. R., & Roberts, R. J. (1977). An amazing sequence arrangement at the 5' ends of adenovirus 2 messenger RNA. *Cell*, 12(1), 1–8. [https://doi.org/10.1016/0092-8674\(77\)90180-5](https://doi.org/10.1016/0092-8674(77)90180-5)
- Cooper, M., Goodwin, D. J., Hall, K. T., Stevenson, A. J., Meredith, D. M., Markham, A. F., & Whitehouse, A. (1999). The gene product encoded by ORF 57 of herpesvirus saimiri regulates the redistribution of the splicing factor SC-35. *Journal of General Virology*, 80(5), 1311–1316. <https://doi.org/10.1099/0022-1317-80-5-1311>
- David, C. J., & Manley, J. L. (2010). Alternative pre-mRNA splicing regulation in cancer: Pathways and programs unhinged. *Genes & Development*, 24(21), 2343–2364. <https://doi.org/10.1101/gad.1973010>
- Dechtawawat, T., Songprakhon, P., Limjindaporn, T., Puttikhunt, C., Kasinrer, W., Saitornuang, S., ... Noisakran, S. (2015). Role of human heterogeneous nuclear ribonucleoprotein C1/C2 in dengue virus replication. *Virology Journal*, 12(1), 14. <https://doi.org/10.1186/s12985-014-0219-7>
- Dhillon, P., Tandra, V. N., Chorghade, S. G., Namsa, N. D., Sahoo, L., & Rao, C. D. (2018). Cytoplasmic relocation and colocalization with viroplasm of host cell proteins, and their role in rotavirus infection. *Journal of Virology*, 92(15), e00612–e00618. <https://doi.org/10.1128/JVI.00612-18>
- Dickson, A. M., Anderson, J. R., Barnhart, M. D., Sokoloski, K. J., Oko, L., Opyrchal, M., ... Wilusz, J. (2012). Dephosphorylation of HuR protein during Alphavirus infection is associated with HuR relocalization to the cytoplasm. *Journal of Biological Chemistry*, 287(43), 36229–36238. <https://doi.org/10.1074/jbc.M112.371203>
- Dissanayaka Mudiyanselage, S. D., Qu, J., Tian, N., Jiang, J., & Wang, Y. (2018). Potato spindle tuber viroid RNA-templated transcription: Factors and regulation. *Viruses*, 10(9), 503. <https://doi.org/10.3390/v10090503>
- Dörmer, A., Xiong, D., Couch, K., Yajima, T., & Knowlton, K. U. (2004). Alternatively spliced soluble coxsackie-adenovirus receptors inhibit coxsackievirus infection. *Journal of Biological Chemistry*, 279(18), 18497–18503. <https://doi.org/10.1074/jbc.M311754200>
- Dowling, D., Nasr-Esfahani, S., Tan, C. H., O'Brien, K., Howard, J. L., Jans, D. A., ... Sonza, S. (2008). HIV-1 infection induces changes in expression of cellular splicing factors that regulate alternative viral splicing and virus production in macrophages. *Retrovirology*, 5, 18. <https://doi.org/10.1186/1742-4690-5-18>
- Duarte, M., Vende, P., Charpilienne, A., Gratia, M., Laroche, C., & Poncet, D. (2019). Rotavirus infection alters splicing of the stress-related transcription factor XBP1. *Journal of Virology*, 93(5), e01739–e01718. <https://doi.org/10.1128/JVI.01739-18>
- Dubois, J., Traversier, A., Julien, T., Padey, B., Lina, B., Bourdon, J.-C., ... Terrier, O. (2019). The non-structural NS1 protein of influenza viruses modulates TP53 splicing through the host factor CPSF4. *Journal of Virology*, 93(7), e02168–18. <https://doi.org/10.1128/JVI.02168-18>
- Fabozzi, G., Oler, A. J., Liu, P., Chen, Y., Mindaye, S., Dolan, M. A., ... Subbarao, K. (2018). Strand-specific dual RNA sequencing of bronchial epithelial cells infected with influenza A/H3N2 viruses reveals splicing of gene segment 6 and novel host-virus interactions. *Journal of Virology*, 92(17), e00518–e00518. <https://doi.org/10.1128/JVI.00518-18>
- Fensterl, V., Chattopadhyay, S., & Sen, G. C. (2015). No love lost between viruses and interferons. *Annual Review of Virology*, 2(1), 549–572. <https://doi.org/10.1146/annurev-virology-100114-055249>

- Fitzgerald, K. D., Chase, A. J., Cathcart, A. L., Tran, G. P., & Semler, B. L. (2013). Viral proteinase requirements for the nucleocytoplasmic relocation of cellular splicing factor SRp20 during Picornavirus infections. *Journal of Virology*, *87*(5), 2390–2400. <https://doi.org/10.1128/JVI.02396-12>
- Flather, D., Nguyen, J. H. C., Semler, B. L., & Gershon, P. D. (2018). Exploitation of nuclear functions by human rhinovirus, a cytoplasmic RNA virus. *PLoS Pathogens*, *14*(8), e1007277. <https://doi.org/10.1371/journal.ppat.1007277>
- Fortes, P., Beloso, A., & Ortín, J. (1994). Influenza virus NS1 protein inhibits pre-mRNA splicing and blocks mRNA nucleocytoplasmic transport. *The EMBO Journal*, *13*(3), 704–712.
- Fortes, P., Lamond, A. I., & Ortín, J. (1995). Influenza virus NS1 protein alters the subnuclear localization of cellular splicing components. *Journal of General Virology*, *76*(4), 1001–1007. <https://doi.org/10.1099/0022-1317-76-4-1001>
- Friedrich, S., Schmidt, T., Geissler, R., Lilie, H., Chabierski, S., Ulbert, S., ... Behrens, S.-E. (2014). AUF1 p45 promotes West Nile virus replication by an RNA chaperone activity that supports cyclization of the viral genome. *Journal of Virology*, *88*(19), 11586–11599. <https://doi.org/10.1128/JVI.01283-14>
- Fukuhara, T., Hosoya, T., Shimizu, S., Sumi, K., Oshiro, T., Yoshinaka, Y., ... Hagiwara, M. (2006). Utilization of host SR protein kinases and RNA-splicing machinery during viral replication. *Proceedings of the National Academy of Sciences*, *103*(30), 11329–11333. <https://doi.org/10.1073/pnas.0604616103>
- Gao, C., Zhai, J., Dang, S., & Zheng, S. (2018). Analysis of alternative splicing in chicken embryo fibroblasts in response to reticuloendotheliosis virus infection. *Avian Pathology*, *47*(6), 585–594. <https://doi.org/10.1080/03079457.2018.1511047>
- Han, L., Xin, X., Wang, H., Li, J., Hao, Y., Wang, M., ... Shen, C. (2018). Cellular response to persistent foot-and-mouth disease virus infection is linked to specific types of alterations in the host cell transcriptome. *Scientific Reports*, *8*(1), 5074. <https://doi.org/10.1038/s41598-018-23478-0>
- Hardy, M. P., & O'Neill, L. A. J. (2004). The murine Irak2 gene encodes four alternatively spliced isoforms, two of which are inhibitory. *Journal of Biological Chemistry*, *279*(26), 27699–27708. <https://doi.org/10.1074/jbc.M403068200>
- Hardy, W. R., & Sandri-Goldin, R. M. (1994). Herpes simplex virus inhibits host cell splicing, and regulatory protein ICP27 is required for this effect. *Journal of Virology*, *68*(12), 7790–7799.
- Hashizume, C., Kuramitsu, M., Zhang, X., Kurosawa, T., Kamata, M., & Aida, Y. (2007). Human immunodeficiency virus type 1 Vpr interacts with spliceosomal protein SAP145 to mediate cellular pre-mRNA splicing inhibition. *Microbes and Infection*, *9*(4), 490–497. <https://doi.org/10.1016/j.micinf.2007.01.013>
- Homa, N. J., Salinas, R., Forte, E., Robinson, T. J., Garcia-Blanco, M. A., & Luftig, M. A. (2013). Epstein-Barr virus induces global changes in cellular mRNA isoform usage that are important for the maintenance of latency. *Journal of Virology*, *87*(22), 12291–12301. <https://doi.org/10.1128/JVI.02464-13>
- Hu, B., Huo, Y., Yang, L., Chen, G., Luo, M., Yang, J., & Zhou, J. (2017). ZIKV infection effects changes in gene splicing, isoform composition and lncRNA expression in human neural progenitor cells. *Virology Journal*, *14*(217), 217. <https://doi.org/10.1186/s12985-017-0882-6>
- Hu, B., Li, X., Huo, Y., Yu, Y., Zhang, Q., Chen, G., ... Zhou, J. (2016). Cellular responses to HSV-1 infection are linked to specific types of alterations in the host transcriptome. *Scientific Reports*, *6*, 28075. <https://doi.org/10.1038/srep28075>
- Huang, T., Nilsson, C. E., Punga, T., & Akusjärvi, G. (2002). Functional inactivation of the SR family of splicing factors during a vaccinia virus infection. *EMBO Reports*, *3*(11), 1088–1093. <https://doi.org/10.1093/embo-reports/kvf217>
- Irvin, S. C., Zurney, J., Ooms, L. S., Chappell, J. D., Dermody, T. S., & Sherry, B. (2012). A single-amino-acid polymorphism in reovirus protein  $\mu$ 2 determines repression of interferon signaling and modulates myocarditis. *Journal of Virology*, *86*(4), 2302–2311. <https://doi.org/10.1128/JVI.06236-11>
- Jagdeo, J. M., Dufour, A., Fung, G., Luo, H., Kleifeld, O., Overall, C. M., & Jan, E. (2015). Heterogeneous nuclear Ribonucleoprotein M facilitates Enterovirus infection. *Journal of Virology*, *89*(14), 7064–7078. <https://doi.org/10.1128/JVI.02977-14>
- Kadri, F., Pacifici, M., Wilk, A., Parker-Struckhoff, A., Valle, L. D., Hauser, K. F., ... Peruzzi, F. (2015). HIV-1-tat protein inhibits SC35-mediated tau exon 10 inclusion through up-regulation of DYRK1A kinase. *Journal of Biological Chemistry*, *290*(52), 30931–30946. <https://doi.org/10.1074/jbc.M115.675751>
- Kanopka, A., Mühlemann, O., Petersen-Mahrt, S., Estmer, C., Öhrmalm, C., & Akusjärvi, G. (1998). Regulation of adenovirus alternative RNA splicing by dephosphorylation of SR proteins. *Nature*, *393*(6681), 185–187. <https://doi.org/10.1038/30277>
- Kim, E., Goren, A., & Ast, G. (2008). Alternative splicing: Current perspectives. *BioEssays*, *30*(1), 38–47. <https://doi.org/10.1002/bies.20692>
- Klymenko, T., Hernandez-Lopez, H., MacDonald, A. I., Bodily, J. M., & Graham, S. V. (2016). Human papillomavirus E2 regulates SRSF3 (SRp20) to promote capsid protein expression in infected differentiated keratinocytes. *Journal of Virology*, *90*(10), 5047–5058. <https://doi.org/10.1128/JVI.03073-15>
- Klymenko, T., & Graham, S. V. (2012). Human papillomavirus gene expression is controlled by host cell splicing factors. *Biochemical Society Transactions*, *40*(4), 773–777. <https://doi.org/10.1042/BST20120079>
- Kneller, E. L. P., Connor, J. H., & Lyles, D. S. (2009). hnRNPs relocate to the cytoplasm following infection with vesicular stomatitis virus. *Journal of Virology*, *83*(2), 770–780. <https://doi.org/10.1128/JVI.01279-08>
- Ko, S.-H., Liao, Y.-J., Chi, Y.-H., Lai, M.-J., Chiang, Y.-P., Lu, C.-Y., ... Huang, L.-M. (2019). Interference of DNAJB6/MRJ isoform switch by Morpholino inhibits replication of HIV-1 and RSV. *Molecular Therapy--Nucleic Acids*, *14*, 251–261. <https://doi.org/10.1016/j.omtn.2018.12.001>
- Kobayashi, T., Ooms, L. S., Chappell, J. D., & Dermody, T. S. (2009). Identification of functional domains in Reovirus replication proteins  $\mu$ NS and  $\mu$ 2. *Journal of Virology*, *83*(7), 2892–2906. <https://doi.org/10.1128/JVI.01495-08>

- Ku, C.-C., Che, X.-B., Reichelt, M., Rajamani, J., Schaap-Nutt, A., Huang, K.-J., ... Arvin, A. M. (2011). Herpes simplex virus-1 induces expression of a novel MxA isoform that enhances viral replication. *Immunology and Cell Biology*, 89(2), 173–182. <https://doi.org/10.1038/icb.2010.83>
- Kuo, R.-L., Chen, C.-J., Tam, E.-H., Huang, C.-G., Li, L.-H., Li, Z.-H., ... Wu, C.-C. (2018). Interactome analysis of NS1 protein encoded by influenza A H7N9 virus reveals an inhibitory role of NS1 in host mRNA maturation. *Journal of Proteome Research*, 17(4), 1474–1484. <https://doi.org/10.1021/acs.jproteome.7b00815>
- Kuo, R.-L., Li, Z.-H., Li, L.-H., Lee, K.-M., Tam, E.-H., Liu, H. M., ... Wu, C.-C. (2016). Interactome analysis of the NS1 protein encoded by influenza A H1N1 virus reveals a positive regulatory role of host protein PRP19 in viral replication. *Journal of Proteome Research*, 15(5), 1639–1648. <https://doi.org/10.1021/acs.jproteome.6b00103>
- Kuramitsu, M., Hashizume, C., Yamamoto, N., Azuma, A., Kamata, M., Yamamoto, N., ... Aida, Y. (2005). A novel role for Vpr of human immunodeficiency virus type 1 as a regulator of the splicing of cellular pre-mRNA. *Microbes and Infection*, 7(9), 1150–1160. <https://doi.org/10.1016/j.micinf.2005.03.022>
- Lanoie, D., & Lemay, G. (2018). Multiple proteins differing between laboratory stocks of mammalian orthoreoviruses affect both virus sensitivity to interferon and induction of interferon production during infection. *Virus Research*, 247, 40–46. <https://doi.org/10.1016/j.virusres.2018.01.009>
- Lawrence, P., Schafer, E. A., & Rieder, E. (2012). The nuclear protein Sam68 is cleaved by the FMDV 3C protease redistributing Sam68 to the cytoplasm during FMDV infection of host cells. *Virology*, 425(1), 40–52. <https://doi.org/10.1016/j.viro.2011.12.019>
- Lee, N., Pimienta, G., & Steitz, J. A. (2012). AUF1/hnRNP D is a novel protein partner of the EBER1 noncoding RNA of Epstein-Barr virus. *RNA*, 18(11), 2073–2082. <https://doi.org/10.1261/rna.034900.112>
- Lee, Y., & Rio, D. C. (2015). Mechanisms and regulation of alternative Pre-mRNA splicing. *Annual Review of Biochemistry*, 84(1), 291–323. <https://doi.org/10.1146/annurev-biochem-060614-034316>
- Lin, W., Zhu, C., Hong, J., Zhao, L., Jilg, N., Fusco, D. N., ... Chung, R. T. (2015). The spliceosome factor SART1 exerts its anti-HCV action through mRNA splicing. *Journal of Hepatology*, 62(5), 1024–1032. <https://doi.org/10.1016/j.jhep.2014.11.038>
- Lindberg, A., & Kreivi, J.-P. (2002). Splicing inhibition at the level of spliceosome assembly in the presence of herpes simplex virus protein ICP27. *Virology*, 294(1), 189–198. <https://doi.org/10.1006/viro.2001.1301>
- Liu, Y.-C., Kuo, R.-L., Lin, J.-Y., Huang, P.-N., Huang, Y., Liu, H., ... Shih, S.-R. (2014). Cytoplasmic viral RNA-dependent RNA polymerase disrupts the intracellular splicing machinery by entering the nucleus and interfering with Prp8. *PLoS Pathogens*, 10(6), e1004199. <https://doi.org/10.1371/journal.ppat.1004199>
- Lu, Y., Qian, X. Y., & Krug, R. M. (1994). The influenza virus NS1 protein: A novel inhibitor of pre-mRNA splicing. *Genes & Development*, 8(15), 1817–1828. <https://doi.org/10.1101/gad.8.15.1817>
- Maio, F. A. D., Risso, G., Iglesias, N. G., Shah, P., Pozzi, B., Gebhard, L. G., ... Gamarnik, A. V. (2016). The dengue virus NS5 protein intrudes in the cellular spliceosome and modulates splicing. *PLoS Pathogens*, 12(8), e1005841. <https://doi.org/10.1371/journal.ppat.1005841>
- Majerciak, V., Yamanegi, K., Allemand, E., Kruhlak, M., Krainer, A. R., & Zheng, Z.-M. (2008). Kaposi's sarcoma-associated Herpesvirus ORF57 functions as a viral splicing factor and promotes expression of intron-containing viral lytic genes in spliceosome-mediated RNA splicing. *Journal of Virology*, 82(6), 2792–2801. <https://doi.org/10.1128/JVI.01856-07>
- Mandadi, K. K., & Scholthof, K.-B. G. (2015). Genome-wide analysis of alternative splicing landscapes modulated during plant-virus interactions in *Brachypodium distachyon*. *The Plant Cell*, 27(1), 71–85. <https://doi.org/10.1105/tpc.114.133991>
- Martin, K., Singh, J., Hill, J. H., Whitham, S. A., & Cannon, S. B. (2016). Dynamic transcriptome profiling of bean common mosaic virus (BCMV) infection in common bean (*Phaseolus vulgaris* L.). *BMC Genomics*, 17(1), 613. <https://doi.org/10.1186/s12864-016-2976-8>
- McFarlane, M., & Graham, S. V. (2010). Human papillomavirus regulation of SR proteins. *Biochemical Society Transactions*, 38(4), 1116–1121. <https://doi.org/10.1042/BST0381116>
- McPhillips, M. G., Veerapraditsin, T., Cumming, S. A., Karali, D., Milligan, S. G., Boner, W., ... Graham, S. V. (2004). SF2/ASF binds the human papillomavirus type 16 late RNA control element and is regulated during differentiation of virus-infected epithelial cells. *Journal of Virology*, 78(19), 10598–10605. <https://doi.org/10.1128/JVI.78.19.10598-10605.2004>
- Merkhofer, E. C., Hu, P., & Johnson, T. L. (2014). Introduction to cotranscriptional RNA splicing. *Methods in Molecular Biology*, 1126, 83–96. [https://doi.org/10.1007/978-1-62703-980-2\\_6](https://doi.org/10.1007/978-1-62703-980-2_6)
- Meyer, F. (2016). Chapter eight - viral interactions with components of the splicing machinery. In M. San Francisco & B. San Francisco (Eds.), *Progress in molecular biology and translational science* (Vol. 142, pp. 241–268). San Francisco, US: Academic Press. <https://doi.org/10.1016/bs.pmbts.2016.05.008>
- Moiani, A., Paleari, Y., Sartori, D., Mezzadra, R., Miccio, A., Cattoglio, C., ... Mavilio, F. (2012). Lentiviral vector integration in the human genome induces alternative splicing and generates aberrant transcripts. *The Journal of Clinical Investigation*, 122(5), 1653–1666. <https://doi.org/10.1172/JCI61852>
- Mole, S., Veerapraditsin, T., McPhillips, M. G., & Graham, S. V. (2006). Regulation of splicing-associated SR proteins by HPV-16. *Biochemical Society Transactions*, 34(6), 1145–1147. <https://doi.org/10.1042/BST0341145>
- Mole, S., McFarlane, M., Chuen-Im, T., Milligan, S. G., Millan, D., & Graham, S. V. (2009). RNA splicing factors regulated by HPV16 during cervical tumour progression. *The Journal of Pathology*, 219(3), 383–391. <https://doi.org/10.1002/path.2608>
- Mole, S., Milligan, S. G., & Graham, S. V. (2009). Human papillomavirus type 16 E2 protein transcriptionally activates the promoter of a key cellular splicing factor, SF2/ASF. *Journal of Virology*, 83(1), 357–367. <https://doi.org/10.1128/JVI.01414-08>
- Monette, A., Ajamian, L., López-Lastra, M., & Mouland, A. J. (2009). Human immunodeficiency virus type 1 (HIV-1) induces the cytoplasmic retention of heterogeneous nuclear ribonucleoprotein A1 by disrupting nuclear import implications for HIV-1 gene expression. *Journal of Biological Chemistry*, 284(45), 31350–31362. <https://doi.org/10.1074/jbc.M109.048736>

- Nilsson, C. E., Petersen-Mahrt, S., Durot, C., Shtrichman, R., Krainer, A. R., Kleinberger, T., & Akusjärvi, G. (2001). The adenovirus E4-ORF4 splicing enhancer protein interacts with a subset of phosphorylated SR proteins. *The EMBO Journal*, 20(4), 864–871. <https://doi.org/10.1093/emboj/20.4.864>
- Niu, X., Wang, Y., Li, M., Zhang, X., & Wu, Y. (2017). Transcriptome analysis of avian reovirus-mediated changes in gene expression of normal chicken fibroblast DF-1 cells. *BMC Genomics*, 18(1), 911. <https://doi.org/10.1186/s12864-017-4310-5>
- Nojima, T., Oshiro-Ideue, T., Nakanoya, H., Kawamura, H., Morimoto, T., Kawaguchi, Y., ... Hagiwara, M. (2009). Herpesvirus protein ICP27 switches PML isoform by altering mRNA splicing. *Nucleic Acids Research*, 37(19), 6515–6527. <https://doi.org/10.1093/nar/gkp633>
- Park, R., & Miller, G. (2018). Epstein-Barr virus-induced nodules on viral replication compartments contain RNA processing proteins and a viral long noncoding RNA. *Journal of Virology*, 92(20), e01254–e01218. <https://doi.org/10.1128/JVI.01254-18>
- Parker, J. S. L., Broering, T. J., Kim, J., Higgins, D. E., & Nibert, M. L. (2002). Reovirus Core protein  $\mu$ 2 determines the filamentous morphology of viral inclusion bodies by interacting with and stabilizing microtubules. *Journal of Virology*, 76(9), 4483–4496. <https://doi.org/10.1128/JVI.76.9.4483-4496.2002>
- Phelan, A., Carmo-Fonseca, M., McLaughlan, J., Lamond, A. I., & Clements, J. B. (1993). A herpes simplex virus type 1 immediate-early gene product, IE63, regulates small nuclear ribonucleoprotein distribution. *Proceedings of the National Academy of Sciences*, 90(19), 9056–9060. <https://doi.org/10.1073/pnas.90.19.9056>
- Pimienta, G., Fok, V., Haslip, M., Nagy, M., Takyar, S., & Steitz, J. A. (2015). Proteomics and transcriptomics of BJAB cells expressing the Epstein-Barr virus noncoding RNAs EBER1 and EBER2. *PLoS One*, 10(6), e0124638. <https://doi.org/10.1371/journal.pone.0124638>
- Prescott, E. L., Brimacombe, C. L., Hartley, M., Bell, I., Graham, S., & Roberts, S. (2014). Human papillomavirus type 1 E1 E4 protein is a potent inhibitor of the serine-arginine (SR) protein kinase SRPK1 and inhibits phosphorylation of host SR proteins and of the viral transcription and replication regulator E2. *Journal of Virology*, 88(21), 12599–12611. <https://doi.org/10.1128/JVI.02029-14>
- Qiu, Y., Nemeroff, M., & Krug, R. M. (1995). The influenza virus NS1 protein binds to a specific region in human U6 snRNA and inhibits U6-U2 and U6-U4 snRNA interactions during splicing. *RNA*, 1(3), 304–316.
- Redondo, N., Madan, V., Alvarez, E., & Carrasco, L. (2015). Impact of vesicular stomatitis virus M proteins on different cellular functions. *PLoS One*, 10(6), e0131137. <https://doi.org/10.1371/journal.pone.0131137>
- Rivera-Serrano, E. E., Fritch, E. J., Scholl, E. H., & Sherry, B. (2017). A cytoplasmic RNA virus alters the function of the cell splicing protein SRSF2. *Journal of Virology*, 91(7), e02488–e02416. <https://doi.org/10.1128/JVI.02488-16>
- Sacks, W. R., Greene, C. C., Aschman, D. P., & Schaffer, P. A. (1985). Herpes simplex virus type 1 ICP27 is an essential regulatory protein. *Journal of Virology*, 55(3), 796–805.
- Sandekian, V., & Lemay, G. (2015). A single amino acid substitution in the mRNA capping enzyme  $\lambda$ 2 of a mammalian orthoreovirus mutant increases interferon sensitivity. *Virology*, 483, 229–235. <https://doi.org/10.1016/j.virol.2015.04.020>
- Sandri-Goldin, R. M. (1994). Properties of an HSV-1 regulatory protein that appears to impair host cell splicing. *Infectious Agents and Disease*, 3(2–3), 59–67.
- Sandri-Goldin, R. M., Hibbard, M. K., & Hardwicke, M. A. (1995). The C-terminal repressor region of herpes simplex virus type 1 ICP27 is required for the redistribution of small nuclear ribonucleoprotein particles and splicing factor SC35; however, these alterations are not sufficient to inhibit host cell splicing. *Journal of Virology*, 69(10), 6063–6076.
- Sandri-Goldin, R. M., & Mendoza, G. E. (1992). A herpesvirus regulatory protein appears to act post-transcriptionally by affecting mRNA processing. *Genes & Development*, 6(5), 848–863. <https://doi.org/10.1101/gad.6.5.848>
- Sandri-Goldin, R. M. (1998). Interactions between a herpes simplex virus regulatory protein and cellular mRNA processing pathways. *Methods*, 16(1), 95–104. <https://doi.org/10.1006/meth.1998.0647>
- Sandri-Goldin, R. M. (2008). The many roles of the regulatory protein ICP27 during herpes simplex virus infection. *Frontiers in Bioscience: A Journal and Virtual Library*, 13, 5241–5256.
- Sciabica, K. S. (2003). ICP27 interacts with SRPK1 to mediate HSV splicing inhibition by altering SR protein phosphorylation. *The EMBO Journal*, 22(7), 1608–1619. <https://doi.org/10.1093/emboj/cdg166>
- Sen, G. C., & Sarkar, S. N. (2007). The interferon-stimulated genes: Targets of direct signaling by interferons, double-stranded RNA, and viruses. *Current Topics in Microbiology and Immunology*, 316, 233–250.
- Sessions, O. M., Tan, Y., Goh, K. C., Liu, Y., Tan, P., Rozen, S., & Ooi, E. E. (2013). Host cell transcriptome profile during wild-type and attenuated dengue virus infection. *PLoS Neglected Tropical Diseases*, 7(3), e2107. <https://doi.org/10.1371/journal.pntd.0002107>
- Shin, C., & Manley, J. L. (2004). Cell signalling and the control of pre-mRNA splicing. *Nature Reviews Molecular Cell Biology*, 5(9), 727–738. <https://doi.org/10.1038/nrm1467>
- Shkreta, L., Blanchette, M., Toutant, J., Wilhelm, E., Bell, B., Story, B. A., ... Chabot, B. (2017). Modulation of the splicing regulatory function of SRSF10 by a novel compound that impairs HIV-1 replication. *Nucleic Acids Research*, 45(7), 4051–4067. <https://doi.org/10.1093/nar/gkw1223>
- Shwetha, S., Kumar, A., Mullick, R., Vasudevan, D., Mukherjee, N., & Das, S. (2015). HuR displaces polypyrimidine tract binding protein to facilitate La binding to the 3' untranslated region and enhances hepatitis C virus replication. *Journal of Virology*, 89(22), 11356–11371. <https://doi.org/10.1128/JVI.01714-15>
- Smith, R. W. P., Malik, P., & Clements, J. B. (2005). The herpes simplex virus ICP27 protein: A multifunctional post-transcriptional regulator of gene expression. *Biochemical Society Transactions*, 33(3), 499–501. <https://doi.org/10.1042/BST0330499>
- Thénoz, M., Vermin, C., Mortada, H., Karam, M., Pinatel, C., Gessain, A., ... Mortreux, F. (2014). HTLV-1-infected CD4+ T-cells display alternative exon usages that culminate in adult T-cell leukemia. *Retrovirology*, 11(119), 119. <https://doi.org/10.1186/s12977-014-0119-3>



- Thompson, M. G., Muñoz-Moreno, R., Bhat, P., Roytenberg, R., Lindberg, J., Gazzara, M. R., ... Lynch, K. W. (2018). Co-regulatory activity of hnRNP K and NS1-BP in influenza and human mRNA splicing. *Nature Communications*, 9(1), 2407. <https://doi.org/10.1038/s41467-018-04779-4>
- Tremblay, M.-P., Armero, V. E. S., Allaire, A., Boudreault, S., Martenon-Brodeur, C., Durand, M., ... Bisailon, M. (2016). Global profiling of alternative RNA splicing events provides insights into molecular differences between various types of hepatocellular carcinoma. *BMC Genomics*, 17(683), 683. <https://doi.org/10.1186/s12864-016-3029-z>
- Twyffels, L., Gueydan, C., & Kruijs, V. (2011). Shuttling SR proteins: More than splicing factors. *The FEBS Journal*, 278(18), 3246–3255. <https://doi.org/10.1111/j.1742-4658.2011.08274.x>
- van Eindhoven, W. G., Frank, D., Kalachikov, S., Cleary, A. M., Hong, D. I., Cho, E., ... Lederman, S. (1998). A single gene for human TRAF-3 at chromosome 14q32.3 encodes a variety of mRNA species by alternative polyadenylation, mRNA splicing and transcription initiation. *Molecular Immunology*, 35(18), 1189–1206. [https://doi.org/10.1016/S0161-5890\(98\)00099-6](https://doi.org/10.1016/S0161-5890(98)00099-6)
- van Eindhoven, W. G., Gamper, C. J., Cho, E., Mackus, W. J. M., & Lederman, S. (1999). TRAF-3 mRNA splice-deletion variants encode isoforms that induce NF- $\kappa$ B activation. *Molecular Immunology*, 36(10), 647–658. [https://doi.org/10.1016/S0161-5890\(99\)00079-6](https://doi.org/10.1016/S0161-5890(99)00079-6)
- Verma, D., Bais, S., Gaillard, M., & Swaminathan, S. (2010). Epstein-Barr virus SM protein utilizes cellular Splicing factor SRp20 to mediate alternative splicing. *Journal of Virology*, 84(22), 11781–11789. <https://doi.org/10.1128/JVI.01359-10>
- Verma, D., & Swaminathan, S. (2008). Epstein-Barr virus SM protein functions as an alternative splicing factor. *Journal of Virology*, 82(14), 7180–7188. <https://doi.org/10.1128/JVI.00344-08>
- Wang, E. T., Sandberg, R., Luo, S., Khrebukova, I., Zhang, L., Mayr, C., ... Burge, C. B. (2008). Alternative isoform regulation in human tissue transcriptomes. *Nature*, 456(7221), 470–476. <https://doi.org/10.1038/nature07509>
- Wang, Y., Liu, J., Huang, B., Xu, Y.-M., Li, J., Huang, L.-F., ... Wang, X.-Z. (2015). Mechanism of alternative splicing and its regulation. *Biomedical Reports*, 3(2), 152–158. <https://doi.org/10.3892/br.2014.407>
- Wilhelm, E., Pellay, F.-X., Benecke, A., & Bell, B. (2008). Determining the impact of alternative splicing events on transcriptome dynamics. *BMC Research Notes*, 1(1), 94. <https://doi.org/10.1186/1756-0500-1-94>
- Woodley, L., & Valcárcel, J. (2002). Regulation of alternative pre-mRNA splicing. *Briefings in Functional Genomics & Proteomics*, 1(3), 266–277. <https://doi.org/10.1093/bfpg/1.3.266>
- Workenhe, S. T., Ketela, T., Moffat, J., Cuddington, B. P., & Mossman, K. L. (2015). Genome-wide lentiviral shRNA screen identifies serine/arginine-rich splicing factor 2 as a determinant of oncolytic virus activity in breast cancer cells. *Oncogene*, 35, 2465–2474. <https://doi.org/10.1038/onc.2015.303>
- Xu, J., Fang, Y., Qin, J., Chen, X., Liang, X., Xie, X., & Lu, W. (2016). A transcriptomic landscape of human papillomavirus 16 E6-regulated gene expression and splicing events. *FEBS Letters*, 590(24), 4594–4605. <https://doi.org/10.1002/1873-3468.12486>
- Zhao, H., Lin, W., Kumthip, K., Cheng, D., Fusco, D. N., Hofmann, O., ... Chung, R. T. (2012). A functional genomic screen reveals novel host genes that mediate interferon-alpha's effects against hepatitis C virus. *Journal of Hepatology*, 56(2), 326–333. <https://doi.org/10.1016/j.jhep.2011.07.026>
- Zheng, Y., Wang, Y., Ding, B., & Fei, Z. (2017). Comprehensive transcriptome analyses reveal that potato spindle tuber viroid triggers genome-wide changes in alternative Splicing, inducible trans-acting activity of phased secondary small interfering RNAs, and immune responses. *Journal of Virology*, 91(11), e00247–17. <https://doi.org/10.1128/JVI.00247-17>
- Zhu, C., Li, X., & Zheng, J. (2018). Transcriptome profiling using Illumina- and SMRT-based RNA-seq of hot pepper for in-depth understanding of genes involved in CMV infection. *Gene*, 666, 123–133. <https://doi.org/10.1016/j.gene.2018.05.004>
- Zurney, J., Kobayashi, T., Holm, G. H., Dermody, T. S., & Sherry, B. (2009). Reovirus  $\mu$ 2 protein inhibits interferon signaling through a novel mechanism involving nuclear accumulation of interferon regulatory factor 9. *Journal of Virology*, 83(5), 2178–2187. <https://doi.org/10.1128/JVI.01787-08>


**How to cite this article:** Boudreault S, Roy P, Lemay G, Bisailon M. Viral modulation of cellular RNA alternative splicing: A new key player in virus–host interactions? *WIREs RNA*. 2019;10:e1543. <https://doi.org/10.1002/wrna.1543>

RESEARCH

Open Access



# The Epstein-Barr virus EBNA1 protein modulates the alternative splicing of cellular genes

Simon Boudreault, Victoria E. S. Armero, Michelle S. Scott, Jean-Pierre Perreault and Martin Bisailon\* 

## Abstract

**Background:** Alternative splicing (AS) is an important mRNA maturation step that allows increased variability and diversity of proteins in eukaryotes. AS is dysregulated in numerous diseases, and its implication in the carcinogenic process is well known. However, progress in understanding how oncogenic viruses modulate splicing, and how this modulation is involved in viral oncogenicity has been limited. Epstein-Barr virus (EBV) is involved in various cancers, and its EBNA1 oncoprotein is the only viral protein expressed in all EBV malignancies.

**Methods:** In the present study, the ability of EBNA1 to modulate the AS of cellular genes was assessed using a high-throughput RT-PCR approach to examine AS in 1238 cancer-associated genes. RNA immunoprecipitation coupled to RNA sequencing (RIP-Seq) assays were also performed to identify cellular mRNAs bound by EBNA1.

**Results:** Upon EBNA1 expression, we detected modifications to the AS profiles of 89 genes involved in cancer. Moreover, we show that EBNA1 modulates the expression levels of various splicing factors such as hnRNPA1, FOX-2, and SF1. Finally, RNA immunoprecipitation coupled to RIP-Seq assays demonstrate that EBNA1 immunoprecipitates specific cellular mRNAs, but not the ones that are spliced differently in EBNA1-expressing cells.

**Conclusion:** The EBNA1 protein can modulate the AS profiles of numerous cellular genes. Interestingly, this modulation protein does not require the RNA binding activity of EBNA1. Overall, these findings underline the novel role of EBNA1 as a cellular splicing modulator.

**Keywords:** Alternative splicing, Epstein-Barr virus, Virus-host interaction, High-throughput RT-PCR, RIP-sequencing, EBNA1, Splicing factors

## Background

Alternative splicing (AS) is an important mechanism allowing higher proteome diversity in eukaryotes. In *Homo sapiens*, AS is nearly ubiquitous, as more than 90% of human genes undergo AS [1]. AS, as opposed to constitutive splicing, leads to different arrangement of exons, retained introns, and splice-sites for the same pre-messenger RNA (pre-mRNA). This allows the same pre-mRNA to be processed into different isoform-coding mature mRNAs, sometimes even with opposing functions at the protein level. The regulatory aspect of AS is becoming increasingly known, and changes in AS are linked with various diseases

such as cancer, Parkinson's disease, amyotrophic lateral sclerosis, and rheumatoid arthritis [2–5].

Recently obtained evidence show that viruses can disrupt the AS of cellular transcripts, although functional consequences on viral infection are still sparse. A number of studies have shown different mechanisms allowing viruses from various families to alter host-cell AS. For example, Sindbis virus sequestration of HuR protein in the cytoplasm through multiple HuR 3'-UTR binding sequences in viral genomic and subgenomic RNAs modifies the splicing of *PCBP2* and *DST* transcripts (a complete list of all gene names used in this manuscript and their official complete name is included in Additional file 1: Table S1) [6]. Similarly, the poliovirus protease 2A (2Apro) is able to change the cellular localization of HuR, TIA1 and TIAR, thereby impacting the splicing of the apoptotic gene *FAS* [7].

\* Correspondence: [Martin.Bisailon@usherbrooke.ca](mailto:Martin.Bisailon@usherbrooke.ca)

Département de biochimie, Faculté de médecine et des sciences de la santé, Université de Sherbrooke, Sherbrooke, Québec J1E 4K8, Canada



Moreover, Vesicular stomatitis virus (VSV) infection triggers relocalization of splicing factors, such as hnRNPA1, hnRNPC1/C2, and hnRNPKM from the nucleus to the cytoplasm with functional consequences on splicing still unknown [8]. Finally, several transcriptomics studies have shown dysregulation of AS in different cell models following viral infection [9–11]. How the course of viral infection is affected by these AS modifications remains to be investigated.

Studies about the impact of *herpesviridae* on cellular splicing have mainly focused on Herpes simplex virus 1 (HSV-1) and its immediate early ICP27 protein. ICP27 interferes with the splicing machinery and thus contributes to host protein synthesis shut-off during HSV-1 infection [12, 13]. The interaction of ICP27 with components of the splicing machinery and the redistribution of splicing factors are involved in this phenomenon [14, 15]. However, RNA-sequencing studies performed on HSV-1 infected cells found no evidence of disruption of AS upon viral infection [16]. New evidence on the modulation of AS by Epstein-Barr virus (EBV), another virus from the *herpesviridae* family involved in numerous cancers (such as Burkitt's and Hodgkin's lymphomas, gastric carcinoma, and nasopharyngeal cancer), is emerging and suggests potential roles for the EBV SM protein and EBER1/2 non-coding RNAs in this modulation of AS. The viral SM protein was shown to alter the splicing of *STAT1* gene, resulting in a transcript coding for a dominant-negative STAT1 protein [17, 18]. Because of the role of STAT1 in the interferon signal transduction pathways, the impact of the altered splicing on infectivity is presumably important. Moreover, the two non-coding RNAs (EBER1 and EBER2), which accumulate in the nucleus during latent infection can alter cellular AS. EBER1 was shown to interact with the AUF1/hnRNP D splicing factor, and expression of both EBERs in cultured cell line leads to significant changes in the AS landscape of the host-cell [19, 20].

Aside from EBERs and various mi-RNAs, EBNA1 is the only protein expressed in all forms of latency during EBV infection [21]. It localizes to the nucleus and has multiple roles including binding to cellular and viral genomes, regulation of signaling pathways, and gene transcription [22, 23]. EBNA1 is also thought to act as an oncoprotein and links EBV infection to carcinogenesis. For example, EBNA1 can bind USP7, a ubiquitin protease stabilizing both p53 and MDM2. This competitive binding destabilizes both p53 and MDM2, thus promoting cell survival [24]. Furthermore, EBNA1 increases the levels of STAT1, the turnover of SMAD2, and inhibits the activity and DNA binding properties of NF- $\kappa$ B; all of these proteins have well-known roles in tumorigenesis [25, 26]. The oncogenic properties of the EBNA1 have been discussed elsewhere [27].

Recently, we demonstrated that EBNA1 expression modulates the AS of various cellular genes which are

also dysregulated in EBV-positive gastric carcinomas [28]. In the present study, we present the mechanistic investigation behind those changes and possible causes underlying this modulation. The ability of EBNA1 to modify the AS of 1238 cellular genes involved in cancer was investigated using a high-throughput RT-PCR platform. Our results highlight viral modulation of AS as a potential key player in tumorigenesis.

## Methods

### Generation of stable EBNA1 HEK293T cells

Stable HEK293T cells expressing the EBNA1-FLAG-HA protein were generated using MSCV-N EBNA1 plasmid. MSCV-N EBNA1 was a gift from Karl Munger (Addgene plasmid # 37954) [29]. Upon transfection, cells were selected using 5  $\mu$ g/mL puromycin for 20 days. To maintain the selection, cells were kept in 3  $\mu$ g/ml puromycin-DMEM-10% fetal bovine serum.

### Validation of EBNA1 expression by Western blot

HEK293T cells and HEK293T stable cells expressing EBNA1-FLAG-HA were grown upon confluency in T-75 flasks, trypsinized and pelleted at 1500 rpm, 5 min. Cell were resuspended in RIPA Buffer (1% Triton X-100, 1% sodium deoxycholate, 0.1% SDS, 1 mM EDTA, 50 mM Tris-HCl pH 7.5 and complete protease inhibitor (ROCHE)) and lysed using ultrasound on ice at 13% amplitude, 5 s for two times. Cellular debris were then pelleted at 13000 RPM, 4  $^{\circ}$ C, 10 min. If chromosomal DNA was still floating after centrifugation, the ultrasound and centrifugation process was carried out a second time. Lysates were dosed for total protein in triplicate using standard Bradford assay (Thermo Scientific Coomassie Protein Assay). The appropriate quantity of protein was diluted to ten microliters in water, completed with Laemmli buffer at 1x (final concentration) and heated 5 min at 95  $^{\circ}$ C. Sample were loaded on 10% SDS-polyacrylamide gels and electrophoresis on was carried out at 150 V. Gels were transferred onto a polyvinylidene difluoride (PVDF) membrane at 4  $^{\circ}$ C, 1 h15, 100 V. The membrane was blocked in 5% milk in TBS-T (10 mM Tris-HCl pH 8.0, 220 mM NaCl, 0.1% Tween 20), 1 h at room temperature. Upon washing in TBS-T (3x, 5 min each), mouse anti-Flag antibody (Sigma Aldrich), anti-HA or anti-EBNA1 antibody (Santa Cruz Biotechnology) diluted 1:1000 (Flag, HA) or 1:100 (EBNA1) in 2.5% milk/PBS were incubated overnight with the membrane in humid chamber at 4  $^{\circ}$ C. The membrane was washed 3 times in TBS-T and incubated with a sheep anti mouse-HRP secondary antibody 1:5000 (Amersham Biosciences) during 1 h in a humid chamber at room temperature. Membrane was washed 3 times with TBS-T and one time with PBS. Bound antibodies were revealed using an enhanced chemiluminescence (ECL) kit (Perkin

Elmer) and scanned on ImageQuant LAS4000 (GE Healthcare Life Science). Mouse anti- $\beta$ -actin loading control (Sigma) was done on the same membrane after stripping the membrane by boiling it in PBS for 1 min. The procedure was then the same from the blocking upon revelation using the anti- $\beta$ -actin antibody diluted 1:2000 (in 2.5% milk/PBS) and the secondary anti-mouse (1:5000) antibody from Amersham.

#### **Immunofluorescence of stably expressing EBNA1 HEK293T**

The day before, HEK293T cells stably expressing the EBNA1-FLAG-HA protein were seeded at a density of  $5 \times 10^4$  cells/well in 24-well plates. Cells were washed twice with PBS and fixed 20 min using 4% paraformaldehyde and 4% sucrose in PBS at room temperature. Cells were then permeabilized with 0.15% triton X-100 in PBS for 5 min at room temperature and blocked in 10% normal goat serum (Wisent). Anti-HA antibody (Santa Cruz Biotechnologies) was incubated 4 h at room temperature to allow detection of EBNA1-FLAG-HA protein. Cells were washed and incubated 1 h in the dark with DyLight 488-labelled goat anti-mouse secondary antibody (ThermoFisher Scientific). Nucleus staining was performed using 1  $\mu$ g/ml Hoechst, 15 min at room temperature. Cover glasses were mounted on slides with SlowFadeGold mounting medium (Life Technologies), then epifluorescence microscopy was conducted using a Nikon Eclipse TE2000-E visible/epifluorescence inverted microscope using bandpass filters for Hoechst and DyLight 488.

#### **High throughput RT-PCR screening of AS events**

HEK293T and HEK293T cells expressing EBNA1-FLAG-HA were grown upon confluency and pelleted. Total RNA extractions were performed on cell pellets using TRIzol (Invitrogen) with chloroform, following the manufacturer's protocol. The aqueous layer was recovered, mixed with one volume of 70% ethanol and applied directly to a RNeasy Mini Kit column (Qiagen). DNase treatment on the column and total RNA recovery were performed as per the manufacturer's protocol. RNA integrity was assessed with an Agilent 2100 Bioanalyzer (Agilent Technologies). Reverse transcription was performed on 2.2  $\mu$ g total RNA with Transcriptor reverse transcriptase, random hexamers, dNTPs (Roche Diagnostics), and 10 units of RNase OUT (Invitrogen) following the manufacturer's protocol in a total volume of 20  $\mu$ l. All forward and reverse primers were individually resuspended to 20–100  $\mu$ M stock solution in Tris-EDTA buffer (IDT) and diluted as a primer pair to 1.2  $\mu$ M in RNase DNase-free water (IDT). End-point PCR reactions were done on 10 ng cDNA in 10  $\mu$ l final volume containing 0.2 mmol/L each dNTP, 1.5 mmol/L MgCl<sub>2</sub>, 0.6  $\mu$ mol/L each primer, and 0.2 units of

Platinum Taq DNA polymerase (Invitrogen). An initial incubation of 2 min at 95 °C was followed by 35 cycles at 94 °C 30 s, 55 °C 30 s, and 72 °C 60 s. The amplification was completed by a 2 min incubation at 72 °C. PCR reactions were carried on thermocyclers GeneAmp PCR System 9700 (ABI), and the amplified products were analyzed by automated chip-based microcapillary electrophoresis on Caliper LC-90 instruments (Caliper Life-Sciences). Amplicon sizing and relative quantitation was performed by the manufacturer's software, before being uploaded to the LIMS database.

#### **String network**

Using the STRING database [30] version 10.0, genes were submitted for generation of protein-protein interaction network from the *Homo sapiens* interactome. *P*-value for the protein-protein interaction enrichment was directly recovered from the STRING analysis.

#### **Gene ontology analysis**

The Database for Annotation, Visualization and Integrated Discovery (DAVID) [31] version 6.8 with Bonferroni correction was used. Reference background was composed of all genes analysed in the high-throughput RT-PCR assay in order to take into account the bias from cancer-related genes.

#### **Protein levels of splicing factors**

As described before, HEK293T cells and HEK293T stable cells expressing EBNA1-FLAG-HA were grown upon confluency, trypsinized and lysed in RIPA buffer. Lysates were dosed and loaded on 10% acrylamide gel. Antibodies were diluted 1:1000 for SF1 (Abgent), Rbm23 (Abgent); hnRNPA1 (Rabbit polyclonal against the ASASSQRGR peptide, see [32]), Fox-2 (Abcam), and 1:100 for SRSF3 (Santa Cruz Biotechnologies). Secondary anti rabbit antibody (Cell Signaling Technology) diluted 1:5000 was used for the first 4 antibodies and an anti mouse (Cell Signaling Technology) diluted 1:5000 for the SRSF3 antibody. Results shown in this paper are representative results of two to three independent experiments.

#### **RNA immunoprecipitation**

HEK293T cells and HEK293T stable cells expressing EBNA1-FLAG-HA were grown upon confluency in P150 dishes, harvested and pelleted. They were then washed twice in cold PBS, and resuspended in the same volume as the pellet of polysome lysis buffer (10 mM Hepes pH 7.0, 100 mM KCl, 5 mM MgCl<sub>2</sub>, 0.5% NP-40, 1 mM DTT, 100 u/mL RNase inhibitor and complete protease inhibitor (Roche)). After an incubation of 5 min on ice, they were frozen at –80 °C to complete the lysis. After a rapid thaw, tubes were centrifuged 20 min at 4 °

C, 13000 g. The supernatant was dosed using the Bradford assay (Thermo Scientific Coomassie Protein Assay) in triplicate. For each IP, 50  $\mu$ L of Anti-Ha matrix (Roche) was centrifuged 1 min at 13,400 rpm and the supernatant was discarded. Beads were washed with 1 mL of NT2 buffer (50 mM Tris-HCl, pH 7.4, 150 mM NaCl, 1 mM MgCl<sub>2</sub>, 0.05% NP-40) followed by 1 min centrifugation at 13,400 rpm for 5 times. They were then resuspended in 900  $\mu$ L of NET-2 buffer (NT2 buffer supplemented with 20 mM EDTA, pH 8.0, 1 mM DTT and 100 U/mL RNase inhibitor) and 100  $\mu$ L (adjusted with NT-2 buffer to a total protein quantity of 2.5 mg) of lysate from either control or EBNA1 expressing cells was added. Tubes were inverted a couple of times, centrifuged 1 min at 13,400 rpm, 4 °C and 100  $\mu$ L was removed as the input to evaluate RNA degradation. All tubes were incubated on a rotating wheel at 4 °C overnight. Beads were precipitated at 5000 g for 5 min, 4 °C and washed five times with ice-cold NT2 buffer. Upon the last washing, beads were resuspended in 90  $\mu$ L of NT-2 buffer and 10  $\mu$ L of RQ1 DNase and incubated at 37 °C for 30 min. Input tubes were directly added 10  $\mu$ L of RQ1 DNase. DNase-treated IP were diluted with 1 mL NT-2 buffer, centrifuged and supernatant was discarded. Beads were resuspended in 150  $\mu$ L of proteinase K buffer (1% SDS, 1.2 mg/mL proteinase K from Boehringer Mannheim), and input tubes were directly added SDS and proteinase K to the same volume. Tubes were incubated at 55 °C during 30 min with inversion at every 10 min. RNA was then extracted with phenol-chloroform, followed by a second chloroform extraction step. Precipitation of RNA using 272 mM ammonium acetate, 122 mM LiCl and 27  $\mu$ g/mL glycogen in ice-cold ethanol was carried out during 2 h at -80 °C and followed by high-speed centrifugation. Pellets were washed in 75% ethanol, ethanol was thoroughly removed, and RNA was resuspended in water.

#### RIP-Seq library preparation

Quality (input) and quantity (input and IP) assessments were performed on Agilent Nano Chip (Catalog number 5067–1511). Inputs from both control and EBNA1 expressing cells both showed good RNA integrity (RIN = 8.9 and 9.2, respectively), thus underlining RNA was not degraded due to experimental procedures. RNA was ribodepleted using Illumina Ribo-Zero rRNA Removal Kit as per manufacturer's protocol. The RNA-seq library was then built using Illumina SSV21106 kit from 9  $\mu$ L ribo-depleted RNA. Library quality was assessed using Agilent DNA HS Chip (Catalog number 5067–4626). Library quantification was performed by qPCR following Illumina Kappa library quantification protocol. HEK293T and HEK293T-EBNA1 libraries were multiplexed and sequencing was done using Illumina HiSeq 4000 at 100

bp paired-end reads at McGill University and Génome Québec Innovation Centre Sequencing Service.

#### RIP-Seq analysis

Upon sequencing, 22,887,816 and 21,858,499 reads were obtained for control and EBNA1 RIP libraries, with respective average quality score of 39 and 38. Reads corresponding to both conditions were first trimmed and adaptors were removed using Trimmomatic (Galaxy Tool Version 0.32.2). STAR (version 2.5.1b) was used to align reads to hg38 human genome with annotation release 89 from the ENSEMBL database. Reads were sorted by names via samtools (version 1.3.2) and the rmdup function was used to remove PCR and sequencing duplicates. Reads unmapped or mapped to the scaffolds and their respective ID in the header were then removed using samtools (version 1.3.2) and the custom following awk command, because they are unsuitable for the analysis with RIPSeeker:

```
samtools view -h file.bam | awk '((NR <= 197 && length($2) < 10) || (NR >= 198 && length($3) < 5 && $3! ~ /* */) ) {print $0}' > file.out.sam.
```

The output file was then converted to the bam format using samtools and analyzed using the R package RIPSeeker (version 1.10.0). The RIPSeeker package was chosen as it is one of the only programs specifically designed to assign peaks in RIP experiments [33]. RIPSeeker was used on both HEK293T-EBNA1 and HEK293T using HEK293T as a control to determine the reliability of assigned peaks.

#### Data availability

The data discussed in this publication have been deposited in NCBI's Gene Expression Omnibus [34] and are accessible through GEO Series accession number GSE107808 (<https://www.ncbi.nlm.nih.gov/geo/query/acc.cgi?acc=GSE107808>).

#### qPCR

Reverse transcription was performed on 1.7  $\mu$ g RNA (qPCR on splicing factors), 600 ng and 300 ng (RIP-qPCR, replicate 1 and 2–3, respectively) with Transcriptor reverse transcriptase, random hexamers, dNTPs (Roche Diagnostics), and 10 units of RNase OUT (Invitrogen) following the manufacturer's protocol in a total volume of 10  $\mu$ L. All forward and reverse primers were individually resuspended to 20–100  $\mu$ M stock solution in Tris-EDTA buffer (IDT) and diluted as a primer pair to 1  $\mu$ M in RNase DNase-free water (IDT). Quantitative PCR (qPCR) reactions were performed in 10  $\mu$ L in 96 well plates on a CFX-96 thermocycler (BioRad) with 5  $\mu$ L of 2X iTaq Universal SYBR Green Supermix (BioRad), 10 ng (3  $\mu$ L) cDNA (qPCR on splicing factors) or 5 ng (3  $\mu$ L) cDNA

(RIP-qPCR), and 200 nM final (2  $\mu$ l) primer pair solutions. The following cycling conditions were used: 3 min at 95 °C; 50 cycles: 15 s at 95 °C, 30 s at 60 °C, 30 s at 72 °C. Relative expression levels were calculated using the qBASE framework. For every PCR run, control reactions performed in the absence of template were performed for each primer pair and these were consistently negative.

#### As-PCR

Total RNA was extracted from cells using Qiazol (Qiagen) and following the manufacturer's protocol. Reverse transcription was carried out using 1  $\mu$ g of RNA and 4  $\mu$ l of iScript Reverse Transcription Supermix (BIO-RAD) in a final volume of 20  $\mu$ l using the following PCR program: 5 min at 25 °C; 20 min at 46 °C; 1 min at 95 °C. AS specific primer (IDT) were designed to amplify only one ASE and were resuspended together at 1  $\mu$ M. Primers used and predicted amplicon are available in Additional file 1: Table S2. Each reaction was composed of ThermoPol buffer (NEB), dNTPs, primers, cDNA and TAQ (NEB) and were incubated using the following program: 2 min at 94 °C; 34 cycles: 30 s at 94 °C; 30 s at 55 °C; 1 min at 72 °C; 2 min at 72 °C (final elongation). PCR products were resolved using a Caliper

LC-90 capillary electrophoresis (Caliper LifeSciences).

## Results

### Expression of EBNA1 in HEK293T

The EBNA1 protein is particularly interesting in regards to viral carcinogenesis as it is the only EBV protein expressed in all EBV-positive cancers [21]. Its constant expression in EBV-malignancies points toward a strong causative role. In the current study, the role of EBNA1 on cellular AS was investigated. Figure 1a outlines the global workflow used to study the impact of EBNA1 on AS. To decipher the role of EBNA1 on cellular AS, the HEK293T cell line was chosen since most of the mechanistic studies on EBNA1 have been performed in this cell line [23, 35–37]. A stable HEK293T cell line expressing the EBNA1 protein tagged with both HA/FLAG peptides was established using transfection. Upon antibiotic selection, EBNA1 expression was validated by Western blot using antibodies against both the HA the FLAG tag, and using an EBNA1-specific antibody (Fig. 1b). This led to the detection of a major EBNA1 band at 80 kDa, consistent with previous reports [38–41]. EBNA1 expression was further validated in immunofluorescence, demonstrating a

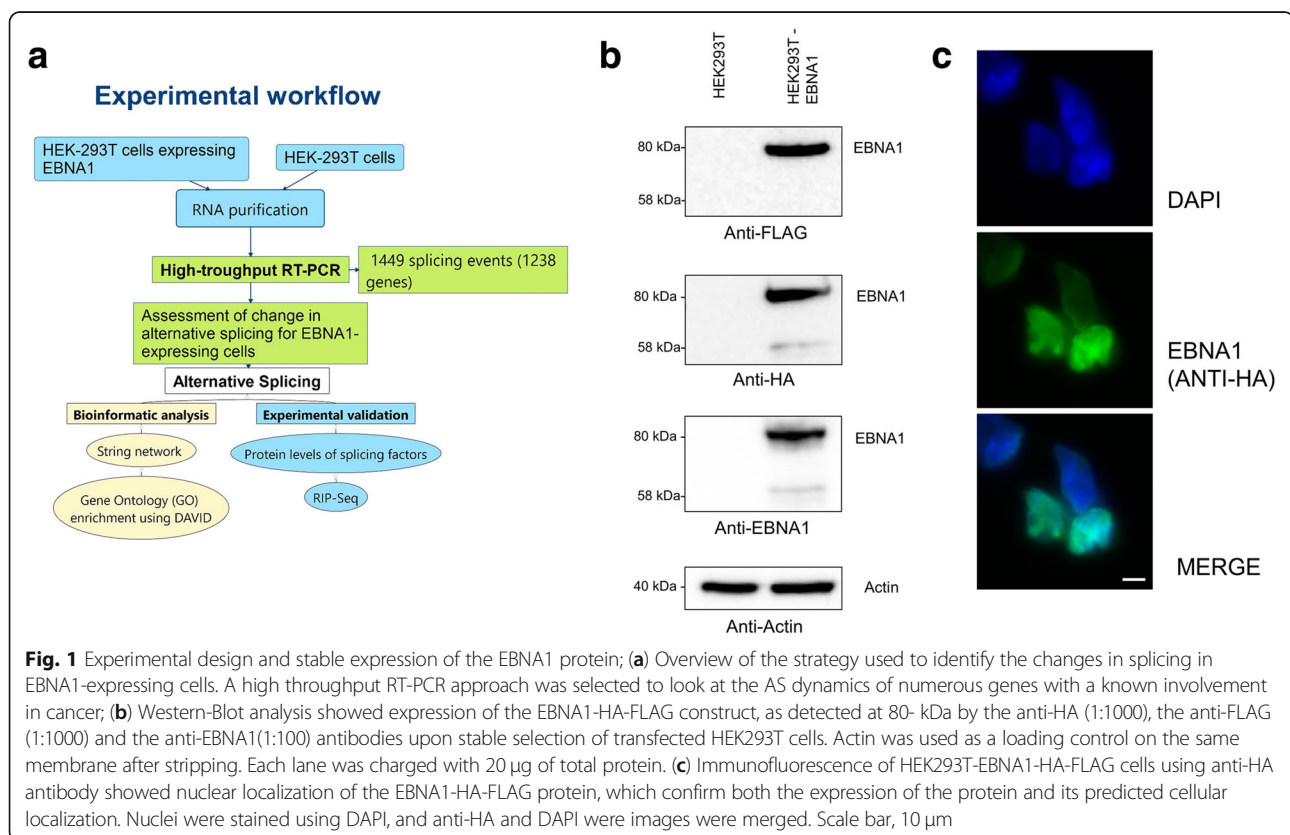


**Fig. 1** Experimental design and stable expression of the EBNA1 protein; **(a)** Overview of the strategy used to identify the changes in splicing in EBNA1-expressing cells. A high throughput RT-PCR approach was selected to look at the AS dynamics of numerous genes with a known involvement in cancer; **(b)** Western-Blot analysis showed expression of the EBNA1-HA-FLAG construct, as detected at 80- kDa by the anti-HA (1:1000), the anti-FLAG (1:1000) and the anti-EBNA1(1:100) antibodies upon stable selection of transfected HEK293T cells. Actin was used as a loading control on the same membrane after stripping. Each lane was charged with 20  $\mu$ g of total protein. **(c)** Immunofluorescence of HEK293T-EBNA1-HA-FLAG cells using anti-HA antibody showed nuclear localization of the EBNA1-HA-FLAG protein, which confirm both the expression of the protein and its predicted cellular localization. Nuclei were stained using DAPI, and anti-HA and DAPI were images were merged. Scale bar, 10  $\mu$ m

nuclear localization of the EBNA1-FLAG-HA construct, which is consistent with previous reports [22] (Fig. 1c).

**EBNA1 modulation of AS events**

Evaluation of the ability of EBNA1 to modify the AS of cellular genes involved in cancer was performed by extracting total RNA from both control and EBNA1-expressing HEK293T cells. Following confirmation of the high quality of recovered RNA, it was subjected to a high-throughput RT-PCR platform designed to assess changes in AS. This assay has been developed to probe 1449 AS events affecting 1238 genes which are either suspected or have been confirmed to be involved in carcinogenesis [42]. Oligonucleotide primer pairs were designed to amplify specific AS events (ASEs), which generate amplicons of various lengths (either short or long depending on the status of the AS event). Following RT-PCR amplification, the products were resolved using capillary electrophoresis, detected, and quantified. The percent-spliced-in (PSI) metric was used to compare ASEs in both conditions (i.e. control cells and cells expressing EBNA1). ASEs with a high  $|\Delta\text{PSI}|$  correspond to a significant modification of their splicing status when EBNA1 is expressed. Only ASEs with  $|\Delta\text{PSI}| \geq 10$  were considered as being modified by EBNA1 expression. To ensure the right isoform choice from the electrophoregrams,

all ASEs with high  $|\Delta\text{PSI}|$  were manually curated. Upon visual inspection of electrophoregrams for accurate peak assignments, 89 ASEs had significant modifications to their splicing patterns attributable to the presence of EBNA1 (Fig. 2a; complete list in Table 1). For example, transcripts encoded by *CCDC62*, a nuclear receptor coactivator, and *LPPR5*, a membrane-bound signaling protein, both showed important shifts from the long form of the ASE to the short one in EBNA1-expressing cells (Fig. 2b). However, *NTRK2*, a tyrosine receptor kinase involved in the MAPK signaling pathway, shows a shift from the short to the long form in EBNA1-expressing cells. Additional representative electrophoregrams are depicted in supplementary data (Additional file 1: Figure S1). Finally, it should also be noted that using HEK293T cells transfected with an empty MSCV-N vector yielded similar results than using the control cell line (Additional file 1: Figure S2).

**Characterization of changes in AS**

Genes for which the AS profiles were modified in EBNA1-expressing cells belong to numerous families and have widespread activities. For example, transcripts encoding ATP binding cassette transporters (*ATP11A*, *ATP6VIC2*), immune responses effectors (*IL37*, *IRF7*), transcription factors (*PAX2*, *ZNF493*), RNA splicing factors and their regulators (*CLK1*, *CLK2*, *ZRANB2*),

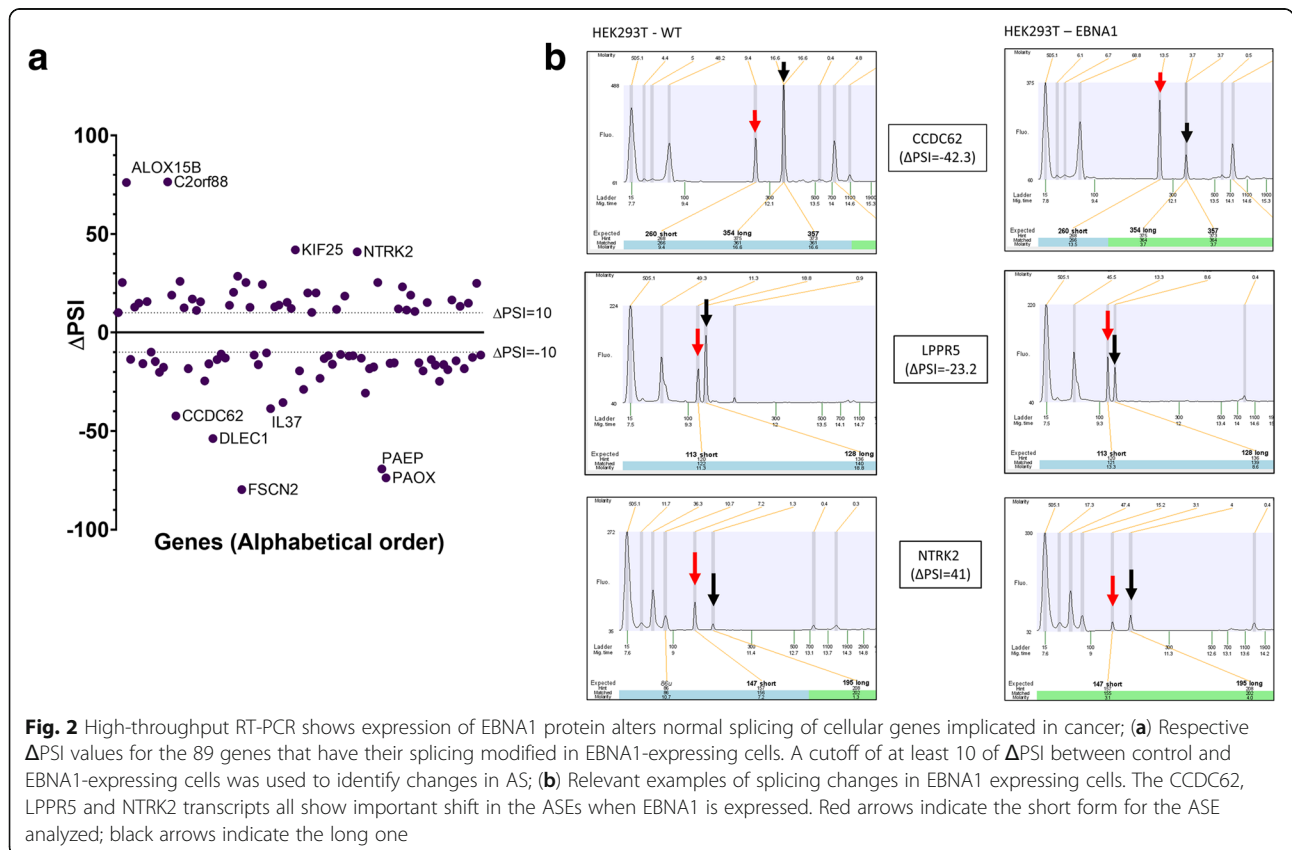


**Table 1** List of genes that have their splicing modulated following EBNA1 expression with the respective  $\Delta$ PSI for these AS events

Gene	$\Delta$ PSI	Gene	$\Delta$ PSI	Gene	$\Delta$ PSI
<i>ABTB1</i>	10.1	<i>FSCN2</i>	-79.8	<i>OPRL1</i>	-30.7
<i>ADAMTSL1</i>	25.4	<i>GCNT1</i>	25.4	<i>OSBPL9</i>	-18.3
<i>ALOX15B</i>	76.1	<i>GEM</i>	12.8	<i>OSCAR</i>	-17.5
<i>ANKMY1</i>	-13.7	<i>GIGYF2</i>	-11.5	<i>P2RX5</i>	25.4
<i>AOC2</i>	12.9	<i>GK</i>	-16.3	<i>PAEP</i>	-69.3
<i>ASAH2B</i>	14.9	<i>HGF</i>	24.4	<i>PAOX</i>	-73.8
<i>ATG16L1</i>	-15.8	<i>ICA1L</i>	-10.4	<i>PAX2</i>	-15.6
<i>ATP11A</i>	15.7	<i>IL37</i>	-38.6	<i>PAXBP1</i>	-15.4
<i>ATP6V1C2</i>	-10.0	<i>IRF7</i>	13.0	<i>PCDH9</i>	12.0
<i>BMP4</i>	-14.7	<i>ITGA6</i>	13.9	<i>PHKB</i>	23.2
<i>BRD8</i>	-20.1	<i>ITGB1</i>	-35.5	<i>PITX2</i>	11.4
<i>C16orf13</i>	-17.7	<i>ITPR1</i>	15.3	<i>PKD1L2</i>	19.0
<i>C2orf88</i>	76.4	<i>IZUMO4</i>	12.2	<i>PLOD2</i>	10.7
<i>CAPN9</i>	19.0	<i>KIF25</i>	42.0	<i>PRC1</i>	-15.4
<i>CCDC62</i>	-42.3	<i>KIF9</i>	-19.4	<i>PTP4A3</i>	-19.4
<i>CD37</i>	26.0	<i>KL</i>	-28.8	<i>PTPN13</i>	15.2
<i>CLK1</i>	12.5	<i>L3MBTL1</i>	20.1	<i>RBBP6</i>	-13.8
<i>CLK2</i>	-18.3	<i>LAMA4</i>	10.2	<i>RLN2</i>	-16.5
<i>COL13A1</i>	17.0	<i>LETMD1</i>	20.1	<i>RNF135</i>	-24.7
<i>COL8A1</i>	11.2	<i>LPPR5</i>	-23.2	<i>RUNX2</i>	-16.3
<i>CSPP1</i>	15.6	<i>MTMR3</i>	-13.3	<i>SLC3A2</i>	-18.8
<i>CTSB</i>	-24.5	<i>MYH11</i>	-11.8	<i>SYK</i>	16.5
<i>DCLRE1C</i>	-15.9	<i>MYO18A</i>	-16.1	<i>TM2D2</i>	-14.4
<i>DLEC1</i>	-53.8	<i>NAA60</i>	11.7	<i>TMTC4</i>	13.3
<i>DMBX1</i>	-13.8	<i>NDEL1</i>	-11.2	<i>TRPV4</i>	-18.3
<i>DTX2</i>	-11.0	<i>NFATC2</i>	18.5	<i>TSGA10</i>	14.9
<i>EFNA1</i>	-13.0	<i>NFU1</i>	-12.0	<i>TTC23</i>	-12.7
<i>EPS8L3</i>	13.8	<i>NRXN2</i>	-11.8	<i>ZNF493</i>	25.0
<i>FAM13B</i>	20.4	<i>NTRK2</i>	41.0	<i>ZRANB2</i>	-11.5
<i>FAM86A</i>	28.6	<i>ODF2L</i>	-13.1		

proteases (*CAPN9*), and signaling proteins (*BMP4*, *CD37*) have their AS modified in EBNA1-expressing cells. Analysis of protein classes using PANTHER revealed the wide diversity of protein activity encoded by these genes, with hydrolase and nucleic acid binding being the most abundant ones (Fig. 3a). Next, the possibility that genes which have their splicing modulated by EBNA1 belongs to a specific network or pathway was assessed using STRING Network. Protein-protein interactions showed a small significant network ( $p = 0.03$ ) involving RUNX2, PAX2, SYK, BMP4, and ITGB1 amongst others (Fig. 3b). Interestingly, many of these proteins are transcription factors or have known roles in morphogenesis and cellular differentiation. To determine if a specific

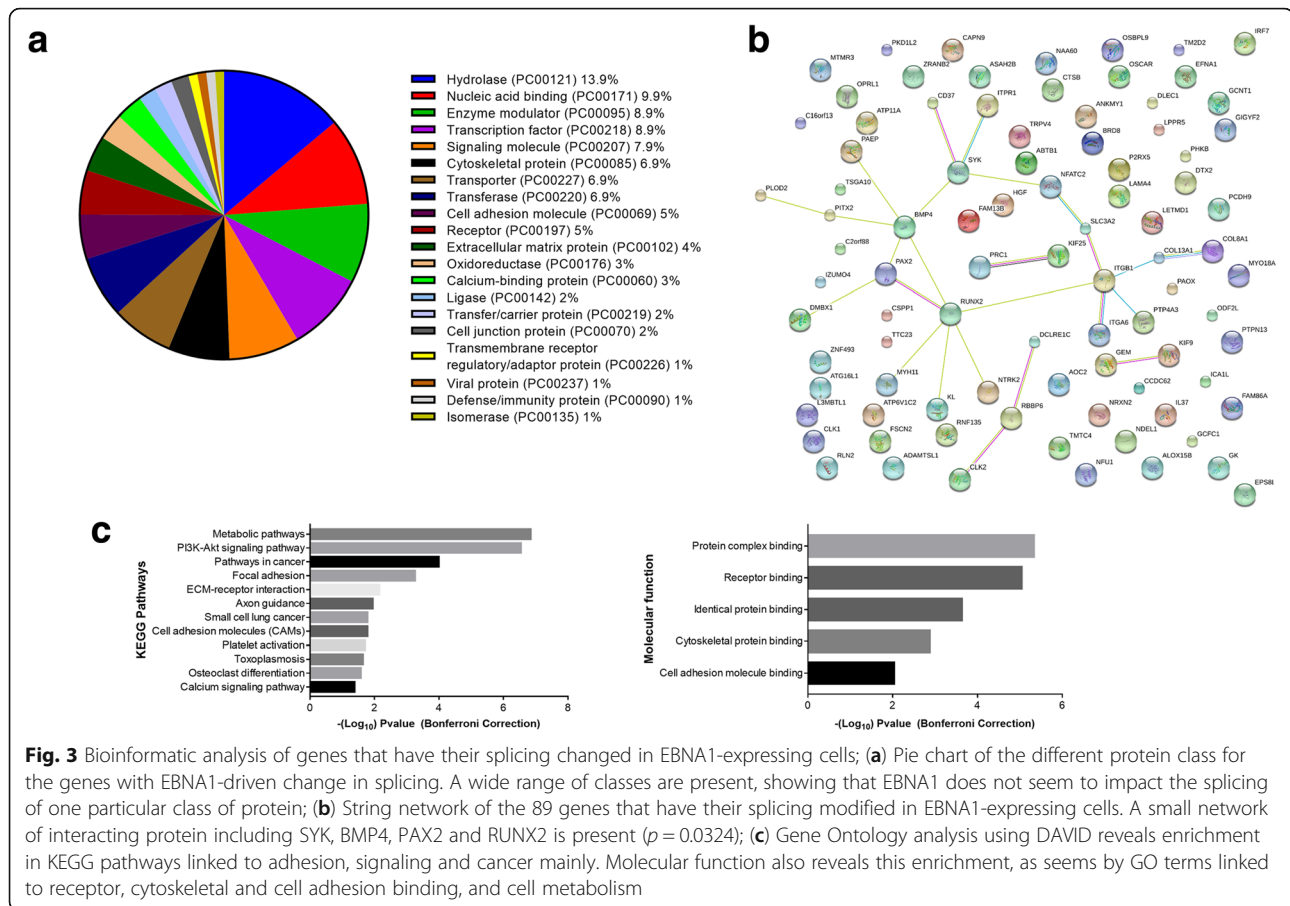
biological role was targeted by EBNA1, gene ontology analysis was carried using DAVID for the KEGG pathways and molecular functions. As predicted, many pathways involved in cancers, such as the PI3K-AKT pathway, are enriched, since the assay focused on genes involved in cancer (Fig. 3c). Interestingly, many terms linked to adhesion, such as focal adhesion, ECM-receptor interaction, cell adhesion molecules (CAMs), and cell adhesion molecule binding are enriched, which could indicate preferential modulation of AS for genes involved in adhesion.

### Deciphering EBNA1 modulation of AS

High-throughput studies reveal global portraits of what is happening in a particular condition/circumstance in a cell and thus can simultaneously reveal various molecular mechanisms leading to the global picture observed. Dissecting those mechanisms and their contributions to the observed outcomes is the primary challenge of this type of study. In the current case, many different mechanisms might explain how the EBNA1 protein is able to achieve modulation of AS, as outlined in Fig. 4a. First, EBNA1 could bind to splicing factors through direct protein-protein interaction, thus impacting either their activity and/or their binding to nascent pre-mRNAs. Second, EBNA1 expression could lead to a change in the expression of splicing factors, thus disturbing the ratio of enhancing and silencing splicing factors on pre-mRNA. Finally, EBNA1 could bind to nascent pre-mRNA in the nucleus, thus preventing the binding of splicing factors and/or acting itself as a splicing enhancer or inhibitor. It should be noted that EBNA1 interaction with splicing factors has been previously demonstrated as EBNA1 is able to bind to the hnRNPH1 splicing factor [28]. Since the first possibility has already been demonstrated, we focused on the latter two possibilities.

In a previous study, we had shown that in EBV-positive gastric carcinomas, several splicing factors had their expression changed compared to healthy tissues [28]. To study the possibility that EBNA1 disrupts the expression of splicing factors, protein levels of splicing factors (SF) were assessed in HEK293T and HEK293T-EBNA1 cells. We probed various SF from the hnRNP family (hnRNPA1 and hnRNPH1), the SR family (SRSF2, phosphorylated-SRSF2, SRSF3, SRSF6, SRSF9 and SRSF10), as well as general SF (ESRP1, FOX-2, RBM23, and SF1). Analysis of proteins level by Western blotting clearly showed that EBNA1 decreases the abundance of SF1, RBM23, hnRNPA1, and FOX-2 by 1.5 to 4-fold (Fig. 4b). However, the protein levels of hnRNPH1, p-SRSF2, SRSF3, SRSF6, and SRSF10 remained constant following EBNA1 expression. A representative Western blot for SRSF3 is shown in Fig. 4b. Note that Western blots against ESRP1, SRSF2 and SRSF9 were inconclusive. Gene expression levels for these splicing factors (SF1, RBM23, hnRNPA1, and FOX-2) were also





quantified using qPCR and failed to detect any statistically significant transcriptional effect of EBNA1 on these genes (Fig. 4c), suggesting that the expression of EBNA1 can alter the expression of specific splicing factors at the protein level, either by affecting their translation or their stability.

#### RIP-sequencing of EBNA1-bound RNA

The last possibility to explain EBNA1 modulation of AS involves EBNA1 binding directly to mRNAs. Interestingly, it was previously demonstrated that EBNA1 is able to bind RNA and RNA G-quadruplex (G4) structures (i.e. guanine-rich secondary structure formed of stacked guanine quartet) [35, 43, 44]. Moreover, the EBNA1 mRNA harbors such G4 structures, leading to the hypothesis that EBNA1 could bind its own mRNA [35]. This raised the possibility that EBNA1 might bind to nascent pre-mRNAs in the nucleus in a sequence- or structure-dependent manner, potentially altering the splicing of cellular transcripts. To seek out if EBNA1 was bound to mRNAs which have their splicing modulated, RIP-seq was carried out from both HEK293T and HEK293T cells expressing EBNA1. A flowchart summarizing the RIP-Seq protocol is outlined in Additional file 1: Figure S3. Numerous experimental controls were performed to ensure recovery of

high-quality RNA for sequencing. First, immunoprecipitations were validated by Western-Blotting and showed efficient immunoprecipitation of the EBNA1 protein only in EBNA1-expressing cells (Additional file 1: Figure S4). Total lysates were also processed as IP fractions and then assessed on Agilent Nano Chip to evaluate RNA degradation through ribosomal 28S/18S ratio. Satisfactory RNA integrity numbers were obtained (9.2 for EBNA1 cells; 8.9 for control cells), hence revealing very limited RNA degradation resulting from the experimental procedure (Additional file 1: Figure S5). Immunoprecipitation fractions also showed strong peaks from the 28S and 18S ribosomal RNAs, probably due to carry over of highly abundant rRNA during the immunoprecipitation procedure (Additional file 1: Figure S5). To ensure appropriate depth of sequencing, those rRNAs were depleted using Illumina Ribo-Zero. Upon depletion, samples were completely free of rRNA, as seen from the results of the Agilent Nano Chip analysis (Additional file 1: Figure S6). Libraries were built and then quality was assessed; results are shown in Additional file 1: Figure S7. Upon sequencing, more than 20 million high quality reads were obtained from both conditions. To determine enriched peaks in the RIP data, reads were processed using a

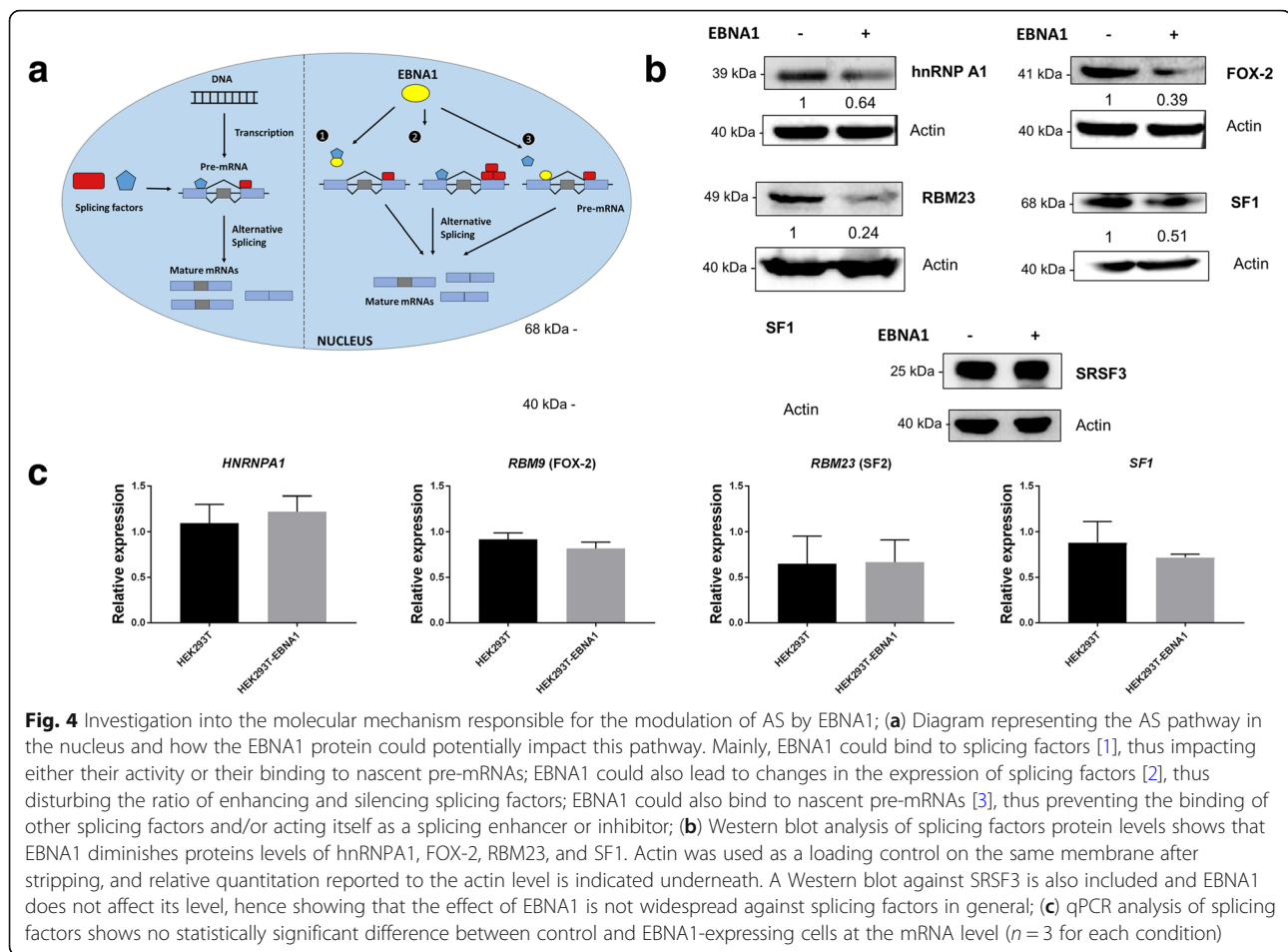
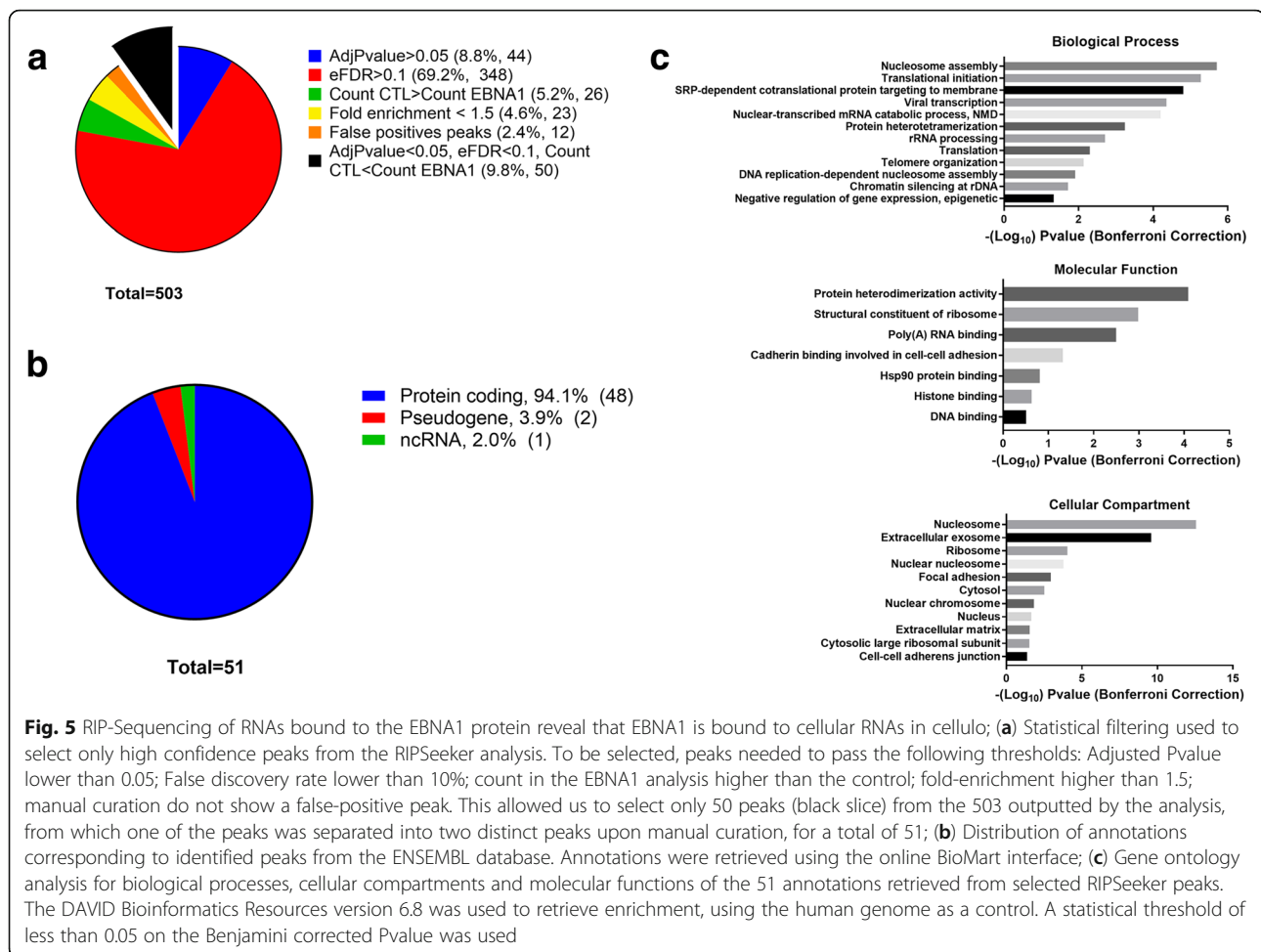


**Fig. 4** Investigation into the molecular mechanism responsible for the modulation of AS by EBNA1; **(a)** Diagram representing the AS pathway in the nucleus and how the EBNA1 protein could potentially impact this pathway. Mainly, EBNA1 could bind to splicing factors [1], thus impacting either their activity or their binding to nascent pre-mRNAs; EBNA1 could also lead to changes in the expression of splicing factors [2], thus disturbing the ratio of enhancing and silencing splicing factors; EBNA1 could also bind to nascent pre-mRNAs [3], thus preventing the binding of other splicing factors and/or acting itself as a splicing enhancer or inhibitor; **(b)** Western blot analysis of splicing factors protein levels shows that EBNA1 diminishes protein levels of hnRNP A1, FOX-2, RBM23, and SF1. Actin was used as a loading control on the same membrane after stripping, and relative quantitation reported to the actin level is indicated underneath. A Western blot against SRSF3 is also included and EBNA1 does not affect its level, hence showing that the effect of EBNA1 is not widespread against splicing factors in general; **(c)** qPCR analysis of splicing factors shows no statistically significant difference between control and EBNA1-expressing cells at the mRNA level ( $n = 3$  for each condition)

standard bioinformatic protocol (trimming using Trimmomatic, alignment using STAR on the hg38 genome, PCR and sequencing duplicates removal using samtools rmdup, peak calling with RIPSeeker). The analysis yielded 503 peaks corresponding to 527 unique annotations; results are available online with the raw reads (GEO Series accession number GSE107808). To ensure sufficient stringency, data were filtered using strict statistical thresholds: Benjamini-corrected  $P$ -values under 0.05; false discovery rate under 0.1; count numbers from the EBNA1 dataset higher than in the control dataset, and a fold-enrichment relative to the control greater than 1.5 (Fig. 5a). Further manual curation using the read coverage over these regions identified 12 false positive peaks, narrowing down the list of probable EBNA1-bound RNAs to 50. Manual curation also allowed to validate the real positioning of the peaks, and to further separate a peak overlapping histones *HIST1H2AC* and *HIST1H2BC* into two separate peaks. The complete list of manually curated peaks can be visualized in Table S3. Interestingly, the vast majority of these annotations correspond to protein-coding genes (94%), with the rest being two pseudogenes and one non-coding RNA (Fig. 5b). Gene ontology analysis using

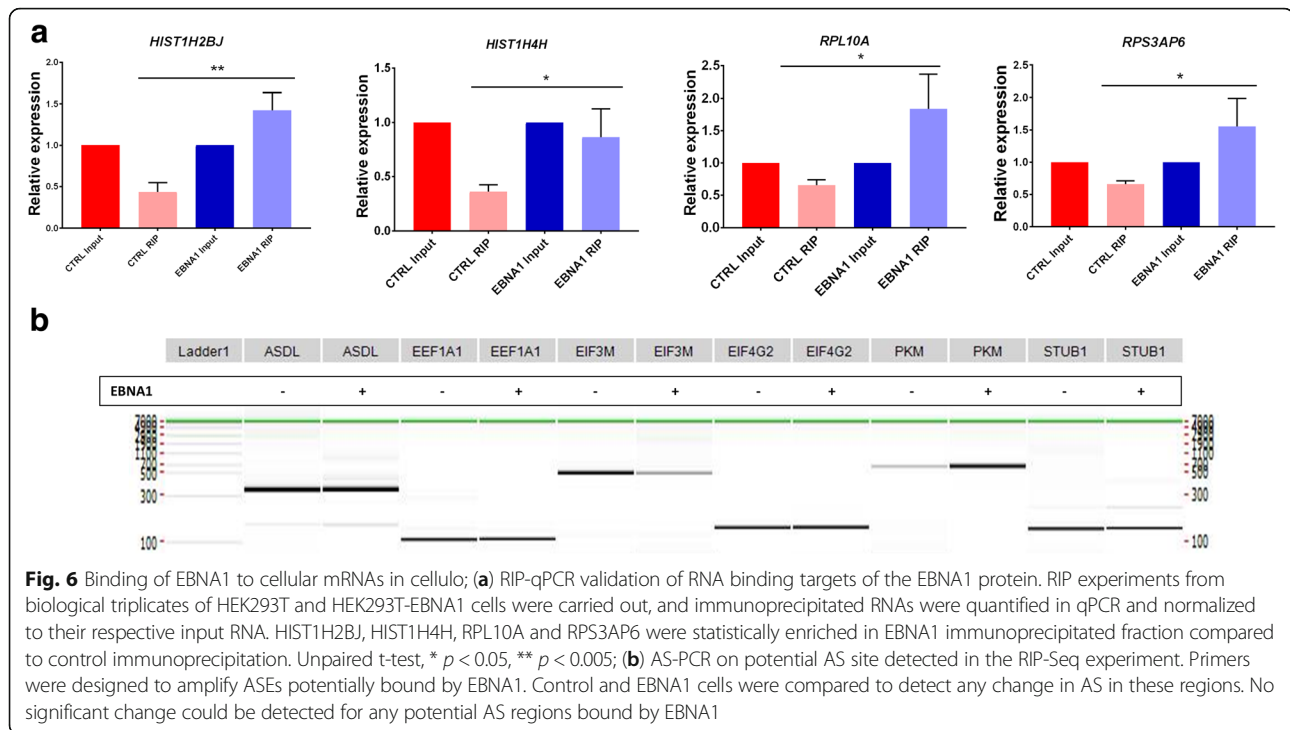
the DAVID bioinformatic database showed enrichment in biological processes linked to ribosome biogenesis, translation, and chromatin organization (Fig. 5c, Bonferroni adjusted  $p$ -value < 0.05). Cellular compartment and molecular function analysis confirmed enrichment in EBNA1 bound transcripts for genes encoding proteins from the nucleosome and ribosome and with functions such as structural constituent of ribosome and poly(A) RNA binding. Interestingly, the term adhesion is also enriched as previously seen in EBNA1 modulation of AS (Fig. 3). This might suggest that EBNA1 could target this pathway both through AS modulation and direct RNA binding. To further validate these results, RIP experiments were carried out in biological triplicates from HEK293T and HEK293T-EBNA1 cells, and levels of immunoprecipitated RNAs were quantified using qPCR. Each immunoprecipitation was normalized to its input RNA, and relative expression from EBNA1-expressing cells and control cells were compared for 11 EBNA1 interactors as predicted by our RIP-Seq experiment. Levels of immunoprecipitated RNAs were statistically higher when EBNA1 was present for *HIST1H2BJ*, *HIST1H4H*, *RPL10A*, and *RPS3AP6* (Fig. 6a), hence showing that EBNA1 is able to interact with



cellular RNAs such as mRNA (*HIST1H2BJ*, *HIST1H4H*, *RPL10A*) and non-coding RNA (*RPS3AP6*). It was not possible to prove a conclusive statistical enrichment for the 7 other predicted EBNA1 targets as predicted by the RIP-Seq. However, none of the EBNA1-bound targets predicted by RIP-Seq belonged to identified genes that had their splicing modulated following EBNA1 expression (Table 1 and Additional file 1: Table S3). Since we only focused previously on approximately 1500 ASEs, one possibility would be that the transcripts bound by EBNA1 were not part of our initial AS screening. To assess the possibility that EBNA1-bound transcripts have their splicing modulated through EBNA1 interaction, the 51 regions of interaction determined by RIP-Seq were analyzed for potential ASE regions. Three of these regions covered an exon cassette and 3 others spanned the intron between two exons (possible intron retention) (Table S2). RT-PCR designed on these potential ASEs bound by EBNA1 failed to validate any change in the splicing outcome in these regions (Fig. 6b). Therefore, these findings suggest that EBNA1 does not modulate AS through direct binding to cellular mRNAs but provide clear evidence that EBNA1 binds to cellular mRNAs *in cellulo*.

## Discussion

Previous studies had already shown that EBV can disturb the splicing of cellular genes using few different mechanisms. For instance, the viral SM protein acts as a splicing factor, recruits SRSF3 to modulate splicing and competes with SRSF1 for RNA-binding. The only known gene to have its splicing impacted by SM is *STAT1*, for which SM is able to favor the STAT1 $\beta$  isoform, which is a dominant negative suppressor of STAT1 $\alpha$  [17, 18]. Moreover, EBV expresses EBEB1 and EBEB2, two long non-coding RNAs accumulating in the nucleus during latent infection. EBEB1 was not demonstrated to impact the splicing of cellular genes, but it is likely since it interacts with AUF1/hnRNP D splicing factor [19]. Expression of both EBEBs in cells lead to significant changes in the expression and the splicing of cellular genes, but the effect of EBEB1 and EBEB2 alone were not investigated [20]. The current study is the first to look at modifications of AS using a high-throughput approach aimed at understanding how a single EBV molecule (protein or RNA) is impacting the AS patterns in the host cell. However, such experiments should ultimately be repeated in different cellular



contexts, such as B cells and epithelial cells, to have a better understanding of the changes that are cell-type specific from those that are ubiquitous. Such studies would also give significant insight into the mechanistic behind these changes, and a more precise role in EBV infection. Moreover, this paper focused on genes involved in cancer, but a broader approach looking at the whole cellular AS using RNA-Seq, as it was recently used in the context of viral infection, could have identified more ASEs modulated by EBNA1, which is one of the drawback of the current approach [9, 10]. Nevertheless, although our results are limited, they establish sufficient evidences to justify follow-up studies using high-throughput sequencing technique, knock-down assays to confirm a reverse phenotype, and expression of EBNA1 in additional cell lines to further validate these findings.

Some of the genes with splicing change in EBNA1-expressing cells are particularly interesting in regards to viral carcinogenesis and replication. For example, the calpain CAPN9 was showed to be downregulated in gastric cancer [45, 46], leading to the hypothesis that this protein may act as a tumor suppressor. EBNA1 modulation of *CAPN9* splicing ( $\Delta$ PSI = 19) could impact the level of the expressed protein or its isoform ratio. Since EBV is known to be implicated in gastric cancer, splicing modification could be another way of diminishing the level of CAPN9 protein, but at the post-transcriptional level. Further studies in this field have great potential regarding a better understanding of viral carcinogenesis. On the other hand, EBNA1 also modulates the splicing of genes previously known to have

potential implication in its replicating cycle. The binding of IRF7, a known key player of antiviral immunity, to the BamHI Q promoter (Qp) of EBV was previously demonstrated [47]. This interaction represses transcription of EBNA1 gene downstream of Qp. However, the Qp promoter is only used in type-1 latency, which is characterized by exclusive expression of EBNA1 and low levels of IRF7 protein. IRF7 is upregulated by another EBV protein, LMP-1 during type III latency, which leads to the IRF7 inactivation of Qp. In this type of latency, other promoters are used to transcribe EBNA1. This led to the hypothesis that IRF7 might be involved in the regulation of EBV latency. EBNA1 modification of *IRF7* splicing ( $\Delta$ PSI = 13) could be another way of regulating EBV promoter usage through IRF-7 post-transcriptional modulation.

The current study also investigated the nature of the cellular RNAs bound to EBNA1 using high-throughput sequencing. Our analysis showed a relatively low number of cellular RNAs potentially bound by EBNA1. This is in part due to the high stringency of statistical filters used to select data. It might also be attributable to the background noise of the experiment and the transcriptional effect of the EBNA1 protein, i.e. some genes seemed to be over-expressed in EBNA1-expressing cells, hence leading potentially to more non-specifically immunoprecipitated RNA transcripts. Nevertheless, we validated four different RNAs enriched during EBNA1 immunoprecipitation (Fig. 6a) that belong mainly to enriched GO terms from the RIP-Seq analysis, i.e. genes that are either histones or ribosomal proteins (Fig. 5c), demonstrating

that the RIP-Seq data are representative of the biological role of EBNA1 in binding to cellular RNAs. Interestingly, the enrichment of these RNAs in EBNA1 RIP are relatively low. This finding might suggest that the binding of EBNA1 to cellular RNA is either transitory or of low affinity. An interesting hypothesis would be that a tight binding of EBNA1 to cellular RNAs would likely sequester the protein away from its main role in replication and segregation of the EBV episome during latency, and therefore be deleterious for viral latency [36, 44]. It will be interesting to study the role of EBNA1 binding to cellular RNAs when EBNA1 is not needed for the maintenance of the viral episome (i.e. not during cellular division). Since the potential binding of EBNA1 to its own mRNA was previously suggested [35, 48], we also looked at the RIP-Seq data to question if such binding occurs in cells. Our result indicated that nearly 7000 reads originated from the EBNA1 mRNA in the HEK293T-EBNA1, and no read was detectable in the control HEK293T (Additional file 1: Figure S8). This suggests that EBNA1 interacts with its own mRNA in a cellular context. A previous study suggested that EBNA1 could potentially bind to G-quadruplex (G4) located in the coding sequence for the glycine-alanine repeats (GAR) domain, i.e. between nucleotides 270 and 984 of the EBNA1 coding sequence [35]. To verify if EBNA1 indeed pulled down a specific region of its own mRNA, the same approach as previously used to validate EBNA1-bound mRNA (RIP-qPCR) was used. Primers were designed to amplify regions in the beginning (37–131), the middle (1137–1278) and the end (1752–1837) of the EBNA1 coding sequence (shown in red in Additional file 1: Figure S8). However, this experiment failed to validate an enrichment in any region of the coding sequence (Additional file 1: Figure S8). Clearly, further studies will be needed to have a clear understanding of the binding of EBNA1 to its own mRNA. The investigation of the dynamics of EBNA1 interaction with cellular RNAs and with its own mRNA will be interesting to better understand the impact of EBNA1 in EBV-positive latent cells.

Surprisingly, EBNA1-bound RNAs are not spliced differentially, either by comparing the genes determined by high throughput RT-PCR (Table 1) with the RIP-Seq peaks (Table S3) or by doing AS-PCR on ASE regions where EBNA1 is predicted to bind by RIP-Seq (Fig. 6b). As stated in Fig. 4a (third hypothesis), modulation of AS through direct interaction with cellular RNAs was a possible manner by which EBNA1 could potentially change the AS of cellular genes. However, our results do not support this hypothesis, and point toward the two other proposed mechanisms (modulation of expression of splicing factors and interaction with splicing factors) as the ones used by EBNA1 to modulate AS (Fig. 4a). The ability of EBNA1 to modulate the expression of splicing factors such as SF1, SF2, hnRNPA1 and FOX-2 (Figs. 4b and c) corroborates the

second hypothesis. However, differential motif enrichment analyses using DREME [49] on the sequences located between the primer pairs used for RT-PCR, as compared to 89 unchanged ASEs randomly selected, yielded no significant enrichment in a sequence that could be linked to the changes in AS. Indeed, it is probable that the sum of all these changes in expression of SF is leading to the change in alternative splicing, and thus for every ASEs that we have analysed there is a specific combination of some of the splicing factors that have their expression changed that are responsible for the change in AS. This probably explain why no specific motif could be identified by enrichment analysis. As previously demonstrated, EBNA1 interacts with splicing factor hnRNPH1 [28] (first hypothesis). Further studies will be needed to decipher the role of changes in splicing factor expression and direct interaction with splicing factors on the AS of cellular gene and how the EBNA1 protein exploits these characteristics during EBV infection, latency and carcinogenesis.

Both in the context of viral infection and carcinogenesis, it is tempting to speculate that the development of splice-switching oligonucleotides specific to virally-induced splicing modifications could help both the prevention and the treatment against diseases arising from viral infection. The development of such tools is already accelerating, and the identification of splicing events modulated by viruses that could have impact on viral replication or carcinogenesis is likely the first step towards their usage in this context.

## Conclusion

This study demonstrates that the expression of the EBV EBNA1 protein in cells induces changes in the AS pattern of numerous cellular genes previously shown or suspected to be implicated in cancer. These modifications could have drastic implication in viral carcinogenesis and EBV latency, since they are likely to change the proteome diversity in EBNA1-expressing cells. Overall, these data pave the way to a better understanding of virus-host interaction, latency of herpesviruses, viral carcinogenesis, and the implication of splicing in these phenomena.

## Additional files

**Additional file 1:** The following are available online at [www.mdpi.com/xxx/s1](http://www.mdpi.com/xxx/s1), **Table S1** List of gene names and their respective official full names **Table S2** AS-PCR primers used to analyze the AS of potential ASEs bound by EBNA1 **Table S3** List of the 51 peaks identified in EBNA1 RIP-Seq **Figure S1** Supplemental electrophoregrams of genes that have their splicing modulated upon EBNA1 expression, **Figure S2** Effect of transient MSCV-N transfection on cellular AS. **Figure S3** Flowchart summarizing the RIP-Seq protocol and controls used, **Figure S4** Western-Blotting of immunoprecipitation of EBNA1, **Figure S5** Quality assessment of input RNA and immunoprecipitated RNA for the RIP-Seq experiment, **Figure S6** Quality assessment of control and EBNA1 RIP following ribo-depletion, **Figure S7** Quality assessment of library for the RIP-Seq,

**Figure S8** Read distribution on the EBNA1 coding sequence in the EBNA1 RIP-Seq and qPCR measurement of immunoprecipitated EBNA1 mRNA. (PDF 2818 kb)

### Acknowledgments

We would like to thank Mathieu Durand, Elvy Lapointe and Philippe Thibeault for their help in RT-PCR and AS-PCR analysis, qPCR analysis, library preparation and bioinformatic processing of the data. We would also like to thank both Benoit Chabot and Johanne Toutant for kindly giving antibodies against FOX-2 and hnRNPA1, and Sonia Couture and Sherif Abou Elela for antibodies against SRSF2. We also acknowledge the help of Vincent Boivin, Jean-Michel Garant, and the other members of the Scott laboratory for their help with bioinformatic analyses.

### Funding

This work was supported by a grant from the Natural Sciences and Engineering Research Council of Canada (NSERC) (MB). SB holds a Vanier Canada graduate scholarship from the Canadian Institutes of Health Research (CIHR).

### Authors' contributions

Conceptualization, MB, SB, JPP, and MSS; methodology, MB and SB; validation, SB; investigation, SB and VESA; resources, MB; data curation, SB and VESA; writing—original draft preparation, SB and MB; writing—review and editing, SB, MB, JPP, and MSS; visualization, SB; funding acquisition, MB, JPP, and MSS. All authors read and approved the final manuscript.

### Competing interests

The authors declare no conflict of interest. The funders had no role in the design of the study; in the collection, analyses, or interpretation of data; in the writing of the manuscript, or in the decision to publish the results.

### Publisher's Note

Springer Nature remains neutral with regard to jurisdictional claims in published maps and institutional affiliations.

Received: 22 November 2018 Accepted: 25 February 2019

Published online: 04 March 2019

### References

- Wang ET, Sandberg R, Luo S, Khrebukova I, Zhang L, Mayr C, et al. Alternative isoform regulation in human tissue transcriptomes. *Nature*. 2008;456(7221):470–6.
- David CJ, Manley JL. Alternative pre-mRNA splicing regulation in cancer: pathways and programs unhinged. *Genes Dev*. 2010;24(21):2343–64.
- Prudencio M, Belzil VV, Batra R, Ross CA, Gendron TF, Pregent LJ, et al. Distinct brain transcriptome profiles in C9orf72-associated and sporadic ALS. *Nat Neurosci*. 2015;18(8):1175–82.
- Soreq L, Guffanti A, Salomonis N, Simchovitz A, Israel Z, Bergman H, et al. Long non-coding RNA and alternative splicing modulations in Parkinson's leukocytes identified by RNA sequencing. *PLoS Comput Biol*. 2014;10(3):e1003517.
- Turkkila M, Andersson KM, Amu S, Brisslert M, Erlandsson MC, Silfverswärd S, et al. Suppressed diversity of survivin splicing in active rheumatoid arthritis. *Arthritis Research & Therapy*. 2015;17(1):175.
- Barnhart MD, Moon SL, Emch AW, Wilusz CJ, Wilusz J. Changes in cellular mRNA stability, splicing, and polyadenylation through HuR protein sequestration by a cytoplasmic RNA virus. *Cell Rep*. 2013;5(4):909–17.
- Álvarez E, Castelló A, Carrasco L, Izquierdo JM. Poliovirus 2A protease triggers a selective Nucleo-cytoplasmic redistribution of splicing factors to regulate alternative pre-mRNA splicing. *PLoS One*. 2013;8(9):e73723.
- Kneller ELP, Connor JH, Lyles DS. hnRNPs Relocalize to the cytoplasm following infection with vesicular stomatitis virus. *J Virol*. 2009;83(2):770–80.
- Boudreault S, Martenon-Brodeur C, Caron M, Garant J-M, Tremblay M-P, Armero VES, et al. Global profiling of the cellular alternative RNA splicing landscape during virus-host interactions. *PLoS One*. 2016;11(9):e0161914.
- Hu B, Huo Y, Yang L, Chen G, Luo M, Yang J, et al. ZIKV infection effects changes in gene splicing, isoform composition and lncRNA expression in human neural progenitor cells. *Virology*. 2017;14:217.
- Rivera-Serrano EE, Fritch EJ, Scholl EH, Sherry BA. Cytoplasmic RNA virus alters the function of the cell splicing protein SRSF2. *J Virol*. 2017;91(7):e02488–16.
- Lindberg A, Kreivi J-P. Splicing inhibition at the level of spliceosome assembly in the presence of herpes simplex virus protein ICP27. *Virology*. 2002;294(1):189–98.
- Sciabica KS. ICP27 interacts with SRPK1 to mediate HSV splicing inhibition by altering SR protein phosphorylation. *EMBO J*. 2003;22(7):1608–19.
- Bryant HE, Wadd SE, Lamond AI, Silverstein SJ, Clements JB. Herpes simplex virus IE63 (ICP27) protein interacts with spliceosome-associated protein 145 and inhibits splicing prior to the first catalytic step. *J Virol*. 2001;75(9):4376–85.
- Sandri-Goldin RM, Hibbard MK, Hardwicke MA. The C-terminal repressor region of herpes simplex virus type 1 ICP27 is required for the redistribution of small nuclear ribonucleoprotein particles and splicing factor SC35; however, these alterations are not sufficient to inhibit host cell splicing. *J Virol*. 1995;69(10):6063–76.
- Rutkowski AJ, Erhard F, L'Hernault A, Bonfert T, Schilhabel M, Crump C, et al. Widespread disruption of host transcription termination in HSV-1 infection. *Nat Commun*. 2015;6:7126.
- Verma D, Bais S, Gaillard M, Swaminathan S. Epstein-Barr virus SM protein utilizes cellular splicing factor SRp20 to mediate alternative splicing. *J Virol*. 2010;84(22):11781–9.
- Verma D, Swaminathan S. Epstein-Barr virus SM protein functions as an alternative splicing factor. *J Virol*. 2008;82(14):7180–8.
- Lee N, Pimienta G, Steitz JA. AUF1/hnRNP D is a novel protein partner of the EBER1 noncoding RNA of Epstein-Barr virus. *RNA*. 2012;18(11):2073–82.
- Pimienta G, Fok V, Haslip M, Nagy M, Takyar S, Steitz JA. Proteomics and transcriptomics of BJAB cells expressing the Epstein-Barr virus noncoding RNAs EBER1 and EBER2. *PLoS One*. 2015;10(6):e0124638.
- Frappier L. The Epstein-Barr Virus EBNA1 Protein. *Scientifica (Cairo)*. 2012;438204.
- Fischer N, Voß MD, Mueller-Lantzsch N, Grässer FA. A potential NES of the Epstein-Barr virus nuclear antigen 1 (EBNA1) does not confer shuttling. *FEBS Lett*. 1999;447(2–3):311–4.
- Lu F, Wikramasinghe P, Norseen J, Tsai K, Wang P, Showe L, et al. Genome-wide analysis of host-chromosome binding sites for Epstein-Barr virus nuclear antigen 1 (EBNA1). *Virology*. 2010;7:262.
- Saridakis V, Sheng Y, Sarkari F, Holowaty MN, Shire K, Nguyen T, et al. Structure of the p53 binding domain of HAU5P/USP7 bound to Epstein-Barr nuclear antigen 1 implications for EBV-mediated immortalization. *Mol Cell*. 2005;18(1):25–36.
- Valentine R, Dawson CW, Hu C, Shah KM, Owen TJ, Date KL, et al. Epstein-Barr virus-encoded EBNA1 inhibits the canonical NF-kappaB pathway in carcinoma cells by inhibiting IKK phosphorylation. *Mol Cancer*. 2010;9:1.
- Wood VHJ, O'Neil JD, Wei W, Stewart SE, Dawson CW, Young LS. Epstein-Barr virus-encoded EBNA1 regulates cellular gene transcription and modulates the STAT1 and TGFbeta signaling pathways. *Oncogene*. 2007;26(28):4135–47.
- Schulz TF, Cordes S. Is the Epstein-Barr virus EBNA-1 protein an oncogen? *PNAS*. 2009;106(7):2091–2.
- Armero VES, Tremblay M-P, Allaire A, Boudreault S, Martenon-Brodeur C, Duval C, et al. Transcriptome-wide analysis of alternative RNA splicing events in Epstein-Barr virus-associated gastric carcinomas. *PLoS One*. 2017;12(5):e0176880.
- Rozenblatt-Rosen O, Deo RC, Padi M, Adelmant G, Calderwood MA, Rolland T, et al. Interpreting cancer genomes using systematic host network perturbations by tumour virus proteins. *Nature*. 2012;487(7408):491–5.
- Szklarczyk D, Franceschini A, Wyder S, Forslund K, Heller D, Huerta-Cepas J, et al. STRING v10: protein–protein interaction networks, integrated over the tree of life. *Nucl Acids Res*. 2015;43(D1):D447–52.
- Jiao X, Sherman BT, Huang DW, Stephens R, Baseler MW, Lane HC, et al. DAVID-WS: a stateful web service to facilitate gene/protein list analysis. *Bioinformatics*. 2012;28(13):1805–6.
- Patry C, Bouchard L, Labrecque P, Gendron D, Lemieux B, Toutant J, et al. Small interfering RNA-mediated reduction in heterogeneous nuclear Ribonucleoparticule A1/A2 proteins induces apoptosis in human Cancer cells but not in Normal mortal cell lines. *Cancer Res*. 2003;63(22):7679–88.
- Edgar R, Domrachev M, Lash AE. Gene expression omnibus: NCBI gene expression and hybridization array data repository. *Nucl Acids Res*. 2002;30(1):207–10.

34. Murat P, Zhong J, Lekieffre L, Cowieson NP, Clancy JL, Preiss T, et al. G-quadruplexes regulate Epstein-Barr virus–encoded nuclear antigen 1 mRNA translation. *Nat Chem Biol*. 2014;10(5):358–64.
35. Dheekollu J, Wiedmer A, Sentana-Lledo D, Cassel J, Messick T, Lieberman PM. HCF1 and OCT2 cooperate with EBNA1 to enhance OriP-dependent transcription and Episome maintenance of latent Epstein-Barr virus. *J Virol*. 2016;90(11):5353–67.
36. Ayoubian H, Fröhlich T, Pogodski D, Flatley A, Kremmer E, Schepers A, et al. Antibodies against the mono-methylated arginine-glycine repeat (MMA-RG) of the Epstein-Barr virus nuclear antigen 2 (EBNA2) identify potential cellular proteins targeted in viral transformation. *J Gen Virol*. 2017;98(8):2128–42.
37. Wang SC, Hammarskjöld ML, Klein G. Immunoprecipitation of Epstein-Barr virus EBNA1 protein using human polyclonal serum. *J Virol Methods*. 1986;13(4):323–32.
38. Hammarskjöld M-L, Shih-Chung W, Klein G. High-level expression of the Epstein-Barr virus EBNA1 protein in CV1 cells and human lymphoid cells using a SV40 late replacement vector. *Gene*. 1986;43(1):41–50.
39. Hennessy K, Kieff E. One of two Epstein-Barr virus nuclear antigens contains a glycine-alanine copolymer domain. *Proc Natl Acad Sci U S A*. 1983;80(18):5665–9.
40. Sculley TB, Sculley DG, Pope JH, Bornkamm GW, Lenoir GM, Rickinson AB. Epstein-Barr virus nuclear antigens 1 and 2 in Burkitt lymphoma cell lines containing either 'a'- or 'b'-type virus. *Intervirology*. 1988;29(2):77–85.
41. Klinck R, Bramard A, Inkel L, Dufresne-Martin G, Gervais-Bird J, Madden R, et al. Multiple alternative splicing markers for ovarian Cancer. *Cancer Res*. 2008;68(3):657–63.
42. Lu C-C, Wu C-W, Chang SC, Chen T-Y, Hu C-R, Yeh M-Y, et al. Epstein-Barr virus nuclear antigen 1 is a DNA-binding protein with strong RNA-binding activity. *J Gen Virol*. 2004;85(10):2755–65.
43. Norseen J, Johnson FB, Lieberman PM. Role for G-Quadruplex RNA binding by Epstein-Barr virus nuclear antigen 1 in DNA replication and metaphase chromosome attachment. *J Virol*. 2009;83(20):10336–46.
44. Li Y, Zhao DY, Greenblatt JF, Zhang Z. RIPSeeker: a statistical package for identifying protein-associated transcripts from RIP-seq experiments. *Nucleic Acids Res* 2013;41(8):e94–e94.
45. Snudden DK, Hearing J, Smith PR, Grässer FA, Griffin BE. EBNA-1, the major nuclear antigen of Epstein-Barr virus, resembles « RGG » RNA binding proteins. *EMBO J*. 1994;13(20):4840–7.
46. Lee H-J, Tomioka S, Kinbara K, Masumoto H, Jeong S-Y, Sorimachi H, et al. Characterization of a human digestive tract-specific Calpain, nCL-4, expressed in the Baculovirus system. *Arch Biochem Biophys*. 1999;362(1):22–31.
47. Yoshikawa Y, Mukai H, Hino F, Asada K, Kato I. Isolation of two novel genes, Down-regulated in gastric Cancer. *Jpn J Cancer Res*. 2000;91(5):459–63.
48. Zhang L, Pagano JS. Interferon regulatory factor 7 is induced by Epstein-Barr virus latent membrane protein 1. *J Virol*. 2000;74(3):1061–8.
49. Bailey TL. DREME: motif discovery in transcription factor ChIP-seq data. *Bioinformatics*. 2011;27(12):1653–9.

**Ready to submit your research? Choose BMC and benefit from:**

- fast, convenient online submission
- thorough peer review by experienced researchers in your field
- rapid publication on acceptance
- support for research data, including large and complex data types
- gold Open Access which fosters wider collaboration and increased citations
- maximum visibility for your research: over 100M website views per year

**At BMC, research is always in progress.**

Learn more [biomedcentral.com/submissions](https://biomedcentral.com/submissions)

